University of Alberta

In-situ Testing for Liquefaction Evaluation of Sandy Soils

by

Catherine Elizabeth Fear ©

A thesis submitted to the Faculty of Graduate Studies and Research
in partial fulfillment of the requirements for the degree of
Doctor of Philosophy

in

Geotechnical Engineering

Department of Civil Engineering

Edmonton, Alberta

Spring 1996

National Library
of Canada

Acquisitions and
Bibliographic Services Branch

395 Wellington Street
Ottawa, Ontario
K1A 0N4

Bibliothèque nationale
du Canada

Direction des acquisitions et
des services bibliographiques

395, rue Wellington
Ottawa (Ontario)
K1A 0N4

Your file Votre référence

Our file Notre référence

The author has granted an irrevocable non-exclusive licence allowing the National Library of Canada to reproduce, loan, distribute or sell copies of his/her thesis by any means and in any form or format, making this thesis available to interested persons.

L'auteur a accordé une licence irrévocable et non exclusive permettant à la Bibliothèque nationale du Canada de reproduire, prêter, distribuer ou vendre des copies de sa thèse de quelque manière et sous quelque forme que ce soit pour mettre des exemplaires de cette thèse à la disposition des personnes intéressées.

The author retains ownership of the copyright in his/her thesis. Neither the thesis nor substantial extracts from it may be printed or otherwise reproduced without his/her permission.

L'auteur conserve la propriété du droit d'auteur qui protège sa thèse. Ni la thèse ni des extraits substantiels de celle-ci ne doivent être imprimés ou autrement reproduits sans son autorisation.

ISBN 0-612-10586-5

Canadä

University of Alberta

Faculty of Graduate Studies and Research

The undersigned certify that they have read, and recommend to the Faculty of Graduate Studies and Research for acceptance, a thesis entitled **In-situ Testing for Liquefaction Evaluation of Sandy Soils** submitted by **Catherine Elizabeth Fear** in partial fulfillment of the requirements for the degree of Doctor of Philosophy in Geotechnical Engineering.

PK Robertson

Dr. P.K. Robertson (Supervisor)

Dr. N.R. Morgenstern

D C Sego

Dr. D.C. Sego

FE Hicks

Dr. F.E. Hicks

AW Lipsett

Dr. A.W. Lipsett

T. Leslie Youd

Dr. T.L. Youd (External Examiner)

April 11 1996

Date of Approval by Committee

University of Alberta
Edmonton

Department of Civil Engineering

Canada T6G 2G7

220 Civil/Electrical Engineering Building
Telephone (403) 492-4235
Fax (403) 492-0249

To: Catherine Fear

From: Gerry Cyre

Date: April 19, 1996

As co-author, I give you my permission to use the following material in your Ph.D. thesis:

Fear, C.E., Cyre, G., Robertson, P.K., and Morgenstern, N.R. 1996. Proceedings of the 49th Canadian Geotechnical Conference, St. John's, Newfoundland, September 23-25.

Gerry Cyre

Gerry Cyre
Specialist Technologist (Geotechnical)

University of Alberta
Edmonton

Canada T6G 2G7

Department of Civil Engineering

220 Civil/Electrical Engineering Building
Telephone (403) 492-4235
Fax (403) 492-0249

To: Catherine Fear

From: Dr. N.R. Morgenstern

Date: April 19, 1996

As co-author, I give you my permission to use the following material in your Ph.D. thesis:

Fear, C.E., Cyre, G., Robertson, P.K., and Morgenstern, N.R. 1996. Proceedings of the 49th Canadian Geotechnical Conference, St. John's, Newfoundland, September 23-25.

Dr. N.R. Morgenstern
University Professor

University of Alberta
Edmonton

Department of Civil Engineering

Canada T6G 2G7

220 Civil/Electrical Engineering Building
Telephone (403) 492-4235
Fax (403) 492-0249

To: Catherine Fear

From: Dr. P.K. Robertson
(Thesis Supervisor)

Date: April 19, 1996

As co-author and Principal Investigator of the Canadian Liquefaction Experiment (CANLEX) Project, I give you my permission to use the following papers or CANLEX reports in your Ph.D. thesis:

Robertson, P.K. and Fear, C.E. 1995. Liquefaction of sands and its evaluation, Proceedings of IS Tokyo '95, First International Conference on Earthquake Geotechnical Engineering, Keynote Lecture.

Robertson, P.K. and Fear, C.E. 1995. Application of CPT to evaluate liquefaction potential, Proceedings of the International Symposium on Cone Penetration Testing, CPT'95, Linkoping, Sweden.

Robertson, P.K. and Fear, C.E. 1996. Soil liquefaction and its evaluation based on SPT and CPT, Proceedings of the 1996 NCEER Workshop on Liquefaction.

Fear, C.E., Robertson, P.K., Hofmann, B.A., Sego, D.C., Campanella, R.G., Byrne, P.M., Davies, M.P., Konrad, J.-M., Küpper, A., List, B.R., and Youd, L. 1995. Summary of CANLEX Phase I Site Characterization, Proc. of the 48th Canadian Geotechnical Conference, Vancouver, B.C., 331-340.

Fear, C.E. and Robertson, P.K. 1995. Estimating the undrained strength of sand: a theoretical framework. Canadian Geotechnical Journal, 32(5): 859-870.

Fear, C.E., Cyre, G., Robertson, P.K., and Morgenstern, N.R. 1996. Proceedings of the 49th Canadian Geotechnical Conference, St. John's, Newfoundland, September 23-25.

Fear, C.E. and Robertson, P.K. 1996. CANLEX Phase II data review report.

Dr. P.K. Robertson
Professor and CANLEX Principal Investigator

AGRA Earth & Environmental Limited

FACSIMILE TRANSMITTAL

4810 - 93 Street
EDMONTON, ALBERTA T6E 5M4
Phone No. (403) 436-2152
Fax No. (403) 435-8425

TO: Dr. C. Fear

COMPANY: U. Of A. - Dept. Of Civil Eng.

FAX NO.: 492-8198

SENDER: Dr. E. McRoberts, Ph.D.,P.Eng.

FILE NO.: 2210

NO. OF PAGES (INCLUDING THIS PAGE): 1

DATE: April 15, 1996

ORIGINAL TO BE SENT BY MAIL: YES NO x

This transmission is intended only for the Addressee. It may contain privileged or confidential information. Any unauthorized disclosure is strictly prohibited. If you have received this transmission in error, please notify us immediately (collect) so that we may correct our transmission. Please then destroy the original. Thank you.

RE: ASCE "A RE-CONSIDERATION OF THE INITIATION OF LIQUEFACTION IN SANDY SOILS" VOL. 121, ISSUE 3, PAGES 249-261; BY CATHERINE E. FEAR AND EDWARD C. McROBERTS

As co-author I give my permission to use this material in your thesis.

E.C. McRoberts, Ph.D., P. Eng.
Senior Vice President
Chief Technical Officer

University of Alberta

Library Release Form

Name of Author: Catherine Elizabeth Fear

Title of Thesis: In-situ Testing for Liquefaction Evaluation of Sandy Soils

Degree: Doctor of Philosophy

Year this Degree Granted: 1996

Permission is hereby granted to the University of Alberta Library to reproduce single copies of this thesis and to lend or sell such copies for private, scholarly, or scientific research purposes only.

The author reserves all other publication and other rights in association with the copyright in the thesis, and except as hereinbefore provided, neither the thesis nor any substantial portion thereof may be printed or otherwise reproduced in any material form whatever without the author's prior written permission.

Catherine Fear.

20 Haddington Avenue
Toronto, Ontario
Canada, M5M 2N7

April 19, 1996

Date submitted to the Faculty of
Graduate Studies and Research

Dedicated to my mom,
Elizabeth Carlisle Fear,
for all her love and encouragement.

ABSTRACT

Liquefaction of sandy soils can have significant financial, environmental and human impacts, with observable ground surface features ranging from sand boils to catastrophic flow failures, depending on the type and extent of liquefaction that occurs. Liquefaction phenomena have been divided into two main types: cyclic softening and flow liquefaction. Cyclic softening (liquefaction) generally occurs in level to gently sloping ground in which shear stress reversal can occur, but may also occur in and around soil structures and buildings. Deformations associated with cyclic softening occur only during cyclic loading and accumulate with additional cycles of loading as a consequence of a loss in soil stiffness. Flow liquefaction occurs only in strain-softening soil, provided that a trigger mechanism (static or cyclic) causes the soil to strain-soften. Flow liquefaction generally occurs in sloping ground in which the driving stresses are larger than the resulting undrained shear strength of the soil. Deformations can be catastrophic if the soil structure contains sufficient strain-softening material and if the geometry is such that a kinematically admissible mechanism can develop. In-situ testing can provide a useful tool for evaluating liquefaction potential and any consequences. Conventional standard penetration test (SPT) based methods and cone penetration test (CPT) based methods for evaluating liquefaction potential and resulting undrained shear strengths are reviewed. An integrated CPT based method for evaluating cyclic softening (liquefaction) potential is proposed. In addition, a comprehensive framework for evaluating flow liquefaction potential, linking in-situ testing to undrained laboratory response is developed. Other methods for estimating the undrained strength of sand susceptible to flow liquefaction are investigated, including critical state soil mechanics concepts applied to in-situ testing results and an experimental program of rapid downhole plate load tests in loose sand. Finally, a family of solutions is recommended for evaluating either cyclic softening (liquefaction) or flow liquefaction potential in sandy soils from in-situ testing, based on the level of risk associated with a particular project.

ACKNOWLEDGEMENTS

To my supervisor, Dr. Peter K. Robertson, thank-you for your expert guidance and countless hours discussing various new ideas. Your never-ending enthusiasm provided me with a constant source of motivation. The opportunities you provided me with, such as being an active participant in the CANLEX project, co-authoring various papers with you and presenting papers at conferences, have all benefitted me greatly. I could have never picked a better supervisor!

To Dr. Ed McRoberts, Chief Technical Officer of AGRA Earth and Environmental Ltd., Edmonton, it was a privilege to be able to work with you and learn so much from a practitioner's point of view. Your initial ideas for research projects (see Chapters 2 and 7) and the great amounts of your own time that you spent working with me were truly appreciated. You helped teach me to have a questioning mind and think about new concepts to greater depths.

To other staff members in the Department of Civil Engineering, particularly Dr. Norbert R. Morgenstern and Dr. Dave C. Sego (both in the Geotechnical Group), thank-you for your valuable input and review of my work as it progressed. To Gerry Cyre, Specialist Technologist (Geotechnical), thank-you for your ingenuity and inventiveness with respect to field testing and particularly for your assistance with Chapter 6. To Prof. Peter Dozzi, Dr. Sieman AbouRizk and Dr. A.E. Elwi, thank-you for recruiting me to the University of Alberta in the first place!

I gratefully appreciate the funding that I received from various organizations throughout my time at the University of Alberta, as follows: a 1967 Science and Engineering Scholarship (1991-1995) from the Natural Sciences and Engineering Research Council of Canada (NSERC), a Ralph Steinhauer Award of Distinction (1992-1994) from the Alberta Heritage Fund, and a Karl A. Clark Memorial Scholarship (1995-1996) from the Alberta Research Council. I am also grateful to the University of Alberta for providing me with a Walter H. Johns Graduate Fellowship (1991-1995) and a J. Gordin Kaplan Graduate Student Award (1994). In addition, in 1993, I was honoured to receive a Leonard E. Gads Teaching Assistant Award from the Faculty of Engineering and a Graduate Student Teaching Award from University Teaching Services.

This work was also partly supported by CANLEX (Canadian Liquefaction Experiment), which is a project funded through a Collaborative Research and Development Grant from the Natural Science and Engineering Research Council of Canada (NSERC), Syncrude Canada Ltd, Suncor Inc., B.C. Hydro, Hydro Québec, and Kennecott Corporation. The collaboration includes the geotechnical consultants, AGRA Earth and Environmental Ltd., EBA Engineering Consultants Ltd., Golder Associates, Klohn-Crippen Consultants Ltd. and Thurber Engineering Ltd, as well as faculty and students from the Universities of Alberta, British Columbia, Laval, Carleton and Sherbrooke. I was lucky to be an active participant in the CANLEX project from start to finish.

To my Mom (Elizabeth), Dad (Gordon), and sister (Susan), thank-you for always taking an interest in my work and providing me with encouragement. To my Grampa (P.Eng.) and Granny (Jim and Connie Boyd), you are a constant source of inspiration. To my friends, many of whom I met while living in Pembina Hall for the duration of my Ph.D. and others who were fellow graduate students, thanks for all the fun times and breaks away from my work!

Finally, but most importantly, to my financé and soon-to-be husband, Michael Wride, thank-you so much for all your love and support while you were completing your own Ph.D. in the Department of Physiology (Faculty of Medicine). Together, we have made, and will continue to make, a solid team. Here's to accomplishing our goal of graduating together in the Spring of 1996!

TABLE OF CONTENTS

Page

LIST OF TABLES

LIST OF FIGURES

LIST OF SYMBOLS

CHAPTER 1: INTRODUCTION

1.1 Overview 1
1.2 Terminology 3
  1.2.1 An historical perspective 3
    a) Hazen (1920) 4
    b) Terzaghi (1925) 5
    c) Casagrande (1936) 5
    d) Terzaghi and Peck (1948) 5
    e) Mogami and Kubo (1953) 5
    f) Seed and Lee (1966) 5
    g) Casagrande (1969) 6
    h) Casagrande (1975a) 7
    i) Casagrande (1975b) 7
    j) Committee on Soil Dynamics of the Geotechnical Engineering Division (1978) 8
    k) Seed (1979) 10
    l) Castro et al. (1982) 11
    m) National Research Council (1985) 11
    n) Castro (1987) 13
    o) Seed (1987) 14
    p) Hutchinson (1988) 16
    q) Poulos (1988) 16
    r) Davis, Castro and Poulos (1988) 18
    s) Seed and Harder (1990) 19
    t) Morgenstern (1992) 19

u) McRoberts and Sladen (1992) ... 19
v) Ishihara (1993) ... 20
w) Morgenstern (1994) ... 21
x) Robertson (1994) ... 21
y) Yoshida et al. (1994) ... 22
z) Yasuda et al. (1994) ... 23
aa) McRoberts (1994) ... 24
1.2.2 Definitions adopted in this thesis ... 24
a) Flow liquefaction ... 25
b) Cyclic softening ... 26
(i) Cyclic liquefaction ... 26
(ii) Cyclic mobility ... 27
1.3 Current Practice ... 28
1.3.1 Evaluation of liquefaction potential ... 28
1.3.2 Evaluation of undrained shear strength ... 29
1.3.3 Problems with current practice ... 29
1.4 Thesis Objectives ... 31
1.4.1 Cyclic softening ... 31
1.4.2 Flow Liquefaction ... 32
1.4.3 Practical applications ... 33
References ... 37

CHAPTER 2: REASSESSMENT OF CURRENT PRACTICE USED FOR EVALUATING CYCLIC LIQUEFACTION POTENTIAL BASED ON THE STANDARD PENETRATION TEST (SPT)

2.1 Introduction ... 40
2.2 Methodology ... 42
2.3 Example Case Records ... 46
2.3.1 Critical liquefied case records ... 46
2.3.2 Non-liquefied case records ... 50
2.4 Discussion ... 51
2.4.1 Revised plots of CSR versus $(N_1)_{60}$ ... 52
2.4.2 Impeded drainage ... 54
2.4.3 Additional data from recent studies ... 54
2.4.4 Interpretation and significance of results ... 55

2.5 Conclusions 58
References 76

CHAPTER 3: AN INTEGRATED METHOD FOR EVALUATING CYCLIC LIQUEFACTION POTENTIAL BASED ON THE CONE PENETRATION TEST (CPT)

3.1 Introduction 80
3.2 Estimation of Cyclic Resistance Ratio (CRR) 81
3.3 Estimation of Soil Behaviour Type 84
3.4 Estimation of Fines Content 85
3.5 Laboratory Methods for Estimating CRR 85
3.6 Linking the In-Situ Method to Laboratory Testing 87
3.7 Application of the Integrated CPT Approach 88
3.8 Other Methods of Estimating CRR 90
3.9 Correction for Thin Sand Layers 92
3.10 Conclusions and Recommendations 93
References 115

CHAPTER 4: A FRAMEWORK FOR EVALUATING FLOW LIQUEFACTION POTENTIAL AND UNDRAINED RESPONSE BASED ON BOTH LABORATORY AND IN-SITU TESTING

4.1 Introduction 118
4.2 Void Ratio Interpretations from In-Situ Testing 119
    4.2.1 Conventional methods 119
        a) CPT 120
        b) SPT 120
        c) Shear wave velocity 121
        d) Geophysical logging 122
    4.2.2 Correlations between in-situ tests 123
    4.2.3 Shear wave velocity based method 125
4.3 General Concepts of the Proposed Framework 126
    4.3.1 Critical state soil mechanics 126

4.3.2 Methods of interpreting state 128
a) Sladen and Hewitt (1989) 128
b) Been and Jefferies (1992) 129
c) Plewes et al. (1992) 130
4.3.3 Reference stress ratio (RSR) approach 130
4.4 Application of the Proposed Framework 132
4.4.1 Field determination of RSR 132
4.4.2 Laboratory determination of RSR 133
4.4.3 Laboratory response 134
4.4.4 Linking in-situ characterization and laboratory response 137
4.4.5 Selecting a reference ultimate state line (USL) 138
4.5 Conclusions and Recommendations 139
References 159

CHAPTER 5: A FRAMEWORK FOR ESTIMATING UNDRAINED SHEAR STRENGTH BASED ON IN-SITU TESTING

5.1 Introduction 162
5.2 Current Methods for Estimating S_u using Penetration Tests 163
5.3 Framework for Estimating S_u from Shear Wave Velocity Measurements 164
5.3.1 Determining S_u from critical state soil mechanics 164
5.3.2 Estimating soil state from shear wave velocity measurements 167
5.3.3 Estimating S_u from shear wave velocity measurements 167
5.4 Application of the Proposed Approach to Two Sands 168
5.4.1 Test program 168
5.4.2 Results 170
5.4.3 Conversion of V_{s1} to SPT $(N_1)_{60}$ and CPT q_{c1} 172
5.4.4 The effect of compressibility on V_{s1}-$(N_1)_{60}$ and V_{s1}-q_{c1} correlations 173
5.4.5 Sensitivity of the proposed method to the input parameters 174
5.5 Other Considerations 175
5.6 Comparison with the Current Methods of Estimating S_u 175
5.7 Comparison with Laboratory Testing Results 179
5.8 Conclusions 180
References 200

CHAPTER 6: EMPIRICAL ESTIMATION OF UNDRAINED SHEAR STRENGTH BASED ON DOWNHOLE PLATE LOAD TESTS

6.1 Introduction 203
6.2 Test Program and Equipment 204
    6.2.1 Basic equipment for initial 4" diameter plate load tests 204
    6.2.2 Advanced equipment for 6", 7" or 8" diameter plate load tests 205
6.3 General Plate Load Test Theory 207
6.4 Interpretation of Results 210
    6.4.1 Four inch diameter plate load tests 211
    6.4.2 Six inch diameter plate load tests 212
        a) Raw field data versus time 212
        b) Bearing stress profiles 214
        c) Processed field data versus depth 214
        d) Estimated undrained strength profiles 215
6.5 Comparison with Other Measures of Undrained Shear Strength 217
6.6 Conclusions and Recommendations 219
References 253

CHAPTER 7: A RECONSIDERATION OF CASE HISTORIES USED TO EMPIRICALLY ESTIMATE UNDRAINED SHEAR STRENGTH

7.1 Introduction 254
7.2 Historical Information about the Case Histories 256
    7.2.1 Calaveras Dam 256
    7.2.2 Sheffield Dam 257
    7.2.3 Fort Peck Dam 258
    7.2.4 Solfatara Canal Dike 259
    7.2.5 Lake Merced Bank 260
    7.2.6 Kawagishi-Cho Building 261
    7.2.7 Uetsu Railway Embankment 262
    7.2.8 Snow River Bridge Fill 263
    7.2.9 Koda Numa Railway Embankment 265
    7.2.10 San Fernando Juvenile Hall 266

7.2.11 Lower San Fernando Dam 268
7.2.12 Upper San Fernando Dam 271
7.2.13 Mochi-Koshi Tailings 273
7.2.14 Whiskey Springs Fan 274
7.2.15 La Marquesa Dam - Upstream Slope 276
7.2.16 La Marquesa Dam - Downstream Slope 277
7.2.17 La Palma Dam 278
7.2.18 Lake Ackerman 279
7.2.19 Nerlerk Embankment 280
7.2.20 Heber Road 282
7.2.21 Duncan Dam 283

7.3 Classification of the Case Histories 285
7.3.1 Summary of case history statistics 285
7.3.2 Comparison of initial conditions 285
7.3.3 Comparison of observed deformations 286
7.3.4 Classification based on deformation characteristics 288

7.4 Flow Liquefaction versus Cyclic Softening 289
7.4.1 Statically triggered slope failures 289
7.4.2 Cyclically loaded case histories 290
a) Lateral spreads 290
b) Flow failures 290
c) Slump failures 291
7.4.3 S_u versus $(N_1)_{60}$ for flow liquefaction case histories 292

7.5 Representative Values of $(N_1)_{60}$ and S_u 293
7.5.1 Range of data reported in the literature 293
7.5.2 A minimum $(N_1)_{60}$ approach 294
7.5.3 Uncertainty with S_u 295

7.6 Conclusions 296

References 318

CHAPTER 8: WORKED EXAMPLE

8.1 Introduction 323
8.2 Soil Parameters for the Massey Site 323
8.2.1 Index parameters 323
8.2.2 Choice of reference ultimate state line (USL) 324

8.2.3 Grain characteristic parameters 325

8.3 Review of Field Data and Void Ratio Interpretations.......... 326

8.3.1 In-situ testing results.......... 327

8.3.2 Conventional void ratio interpretations 327

8.3.3 Correlations between in-situ tests 329

8.3.4 Shear wave velocity based estimations of void ratio 330

8.3.5 Soil behaviour type.......... 331

8.4 Interpretations of State.......... 332

8.4.1 Sladen and Hewitt (1989) 332

8.4.2 Been and Jefferies (1992) 333

8.4.3 Plewes et al. (1992).......... 334

8.5 Review of Laboratory Data.......... 334

8.5.1 Flow liquefaction response.......... 335

a) Undisturbed samples.......... 335

(i) Initial state 335

(ii) Stress-strain response 336

b) Reconstituted samples.......... 337

(i) Initial conditions 337

(ii) Stress-strain response 337

c) Link between RSR and response 338

8.5.2 Cyclic softening response.......... 342

a) Undisturbed samples.......... 342

8.6 Link between Field and Laboratory Data 343

8.6.1 Flow liquefaction.......... 343

a) Estimated in-situ profiles of reference stress ratio (RSR).......... 343

b) Estimated in-situ profiles of response to undrained monotonic loading 344

(i) Comparison of void ratio and RSR in the laboratory and in the field.......... 345

(ii) CPT-based average estimated response profiles 346

8.6.2 Cyclic softening 350

a) Estimated in-situ profiles of CRR.......... 350

8.7 Discussion.......... 353

8.7.1 Data review results compared with other CANLEX sites 353

8.7.2 Estimated response.......... 355

a) Flow liquefaction 355

b) Cyclic softening 357
8.8 Summary and Conclusions 358
References 387

CHAPTER 9: GENERAL DISCUSSION AND CONCLUSIONS

9.1 Overview 389
9.2 Evaluation of Cyclic Softening Potential 389
  9.2.1 Simplified "Seed" methodology 390
  9.2.2 Integrated CPT approach 391
9.3 Evaluation of Flow Liquefaction Potential and Subsequent Response 393
  9.3.1 Empirical approach 393
  9.3.2 Simplified reference stress ratio (RSR) approach 394
  9.3.3 Site specific approach 395
9.4 Risk Assessment: A Family of Solutions 396
  9.4.1 Low risk projects 398
  9.4.2 Moderate risk projects 398
  9.4.3 High risk projects 399
9.5 Cautionary Notes and Limitations of the Proposed Methods 400
  9.5.1 Cyclic softening evaluation 400
    a) Loose clean sand versus sand with fines 400
    b) Minimum versus average design approach 400
  9.5.2 Flow liquefaction evaluation 401
    a) Grain characteristic and site specific input parameters 401
    b) Total void ratio versus skeletal void ratio effects on response 401
    c) Using undisturbed samples as a reference 401
9.6 Recommendations for Future Work 402
  9.6.1 Investigating proposed methods of evaluation at other sites 402
    a) Cyclic softening 402
    b) Flow liquefaction 403
  9.6.2 Development of a continuous seismic CPT 404
  9.6.3 Further testing of downhole plate load tests in loose sand 405
9.7 Final Remarks 405
References 411

LIST OF TABLES

Page

CHAPTER 2

2-1 Composition of 125 case records in the original Berkeley catalogue.............. 61

2-2 Summary of changes in $(N_1)_{60}$ for critical liquefied case records in the original Berkeley study.. 62

2-3 Summary of Berkeley case records for which the original assessment was the same as in this study.. 63

2-4 Classification of drainage conditions for all case records.......................... 64

CHAPTER 3

3-1 Boundaries of soil behaviour type.. 95

3-2 Correction factors for influence of earthquake magnitude on cyclic resistance ratio (after Seed et al., 1985).. 96

CHAPTER 5

5-1 Material properties for (a) Ottawa and Alaska sand (Cunning, 1994); Ottawa sand with added kaolinite fines (Skirrow, 1995) and (b) other sands (Sasitharan et al., 1994)... 182

CHAPTER 6

6-1 Summary of 4" (10 cm) plate load testing.. 220

6-2 Summary of 6" (15 cm) plate load testing.. 221

CHAPTER 7

7-1 Summary of data by Seed and Harder (1990).. 299

7-2 Summary of case history statistics... 300

7-3 Summary of deformation analysis... 301

7-4 Summary of range in data reported by various authors............................ 302

7-5 Duncan Dam results (Byrne et al., 1994)..303

7-6 Summary of minimum $(N_1)_{60}$ approach..304

CHAPTER 8

8-1 Index parameters for CANLEX sites. 360

8-2 Grain characteristic parameters for CANLEX sites. 361

8-3 Summary of data for Massey frozen samples tested to date..362

8-4 Summary of undrained monotonic test results for Massey site..363

8-5 Summary of undrained cyclic simple shear test results for Massey site. 364

8-6 Summarized results of data review: average values of soil parameters in the target zone at CANLEX sites. 365

8-7 Predicted average representative response at the Massey site based on average values of soil parameters in the target zone..366

LIST OF FIGURES

Page

CHAPTER 1

1-1 Flowchart for evaluating soil liquefaction (modified from Robertson, 1994) 34

1-2 Schematic of undrained monotonic behaviour of sand in triaxial compression (modified from Robertson, 1994) 35

1-3 Schematic of undrained cyclic behaviour of sand illustrating cyclic liquefaction (modified from Robertson, 1994) 36

CHAPTER 2

2-1 Plots of CSR versus $(N_1)_{60}$ in original Berkeley catalogue 65

2-2 Summary strip logs for all critical liquefied case records except Luan Nan (case record 56) 66

2-3 Comparison of original summary strip log for Luan Nan (case record 56) with additional logs obtained in this study 67

2-4 Summary strip logs for five sample nonliquefied case records 68

2-5 Plot of CSR versus $(N_1)_{60}$ from this study for nonliquefied case records 69

2-6 Plot of CSR versus $(N_1)_{60}$ from this study for liquefied and pressure relief case records 70

2-7 Plot of all liquefied and pressure relief case records from this study, showing upper bound state lines 71

2-8 Summary of state boundary lines from this study compared with the original Berkeley interpretations 72

2-9 Plots of CSR versus $(N_1)_{60}$ to investigate effects of site drainage conditions 73

2-10 Comparison of recent data with the results of this study (labels refer to fines contents) 74

2-11 Plot of CSR versus $(N_1)_{60}$ with limiting strain lines for clean sand (modified from Seed et al., 1985) 75

CHAPTER 3

3-1 Schematic of undrained cyclic behaviour of sand illustrating cyclic liquefaction (modified from Robertson, 1994). 97

3-2 Comparison between various CPT based charts for estimating cyclic resistance ratio (CRR) for clean sands (modified from Robertson and Fear, 1995) 98

3-3 Comparison of CPT based methods for clean sands proposed by Robertson and Campanella (1985) and NCEER (1996) with recent field performance data from Stark and Olson (1995) and Suzuki et al. (1995) 99

3-4 Summary of variation of cyclic resistance ratio with fines content based on CPT field performance data (modified from Stark and Olson, 1995). 100

3-5 Suggested correction for fines content to corrected cone tip resistance based on field performance data. 101

3-6 CPT soil behaviour type chart (modified from Robertson, 1990) 102

3-7 Variation of fines content with CPT friction ratio (modified from Suzuki et al., 1995). 103

3-8 Variation of soil behaviour type index (I_c) with fines content 104

3-9 Correlation between earthquake magnitude (M) and number of representative cycles at 0.65 τ_{max} (N), based on recommendations by Seed et al. (1985) 105

3-10 Post cyclic liquefaction volumetric and horizontal strain curves using CPT or SPT results (modified from Ishihara, 1993) 106

3-11 Plan of the detailed test site area at the CANLEX Phase III site (J-pit) (modified from Iravani et al., 1995). 107

3-12 Comparison between measured fines contents (from SPT sampler) and those predicted using the CPT for three profiles at the CANLEX Phase III site (J-pit) 108

3-13 Example of applying the integrated CPT method to estimate cyclic resistance ratio (CRR) and comparison with the results of cyclic simple shear tests on in-situ frozen samples from the CANLEX Phase II Massey site 109

3-14 Soil behaviour type chart to estimate cyclic resistance ratio (CRR) (modified from Olsen and Koester, 1995). 110

3-15 Soil behaviour type chart to estimate cyclic resistance ratio (CRR) (modified from Suzuki et al., 1995). 111

3-16 Cyclic resistance ratio predicted from Robertson's (1990) soil behaviour type chart based on the integrated CPT method 112

3-17 Predicting cyclic resistance ratio (CRR) from shear wave velocity measurements; (a) modified from Robertson et al. (1992) and (b) NCEER Workshop (1996) (modified from Andrus and Stokoe, 1996) 113

3-18 Suggested correction (K_c) to CPT penetration resistance in thin sand layers (based on results by Vreugdenhil et al., 1994) 114

CHAPTER 4

4-1 Schematic of undrained monotonic behaviour of sand in triaxial compression (modified from Robertson, 1994) 141

4-2 Flowchart for interpreting void ratio from in-situ testing 142

4-3 Conventional void ratio interpretation from CPT (modified from Baldi et al., 1986) 143

4-4 Variation of corrected shear wave velocity with void ratio for a range of sands (based on results from Sasitharan, 1994; Cunning, 1994; Chillarige, 1995; and Skirrow, 1996) 144

4-5 Change in corrected shear wave velocity with age for uncemented sands (modified from Robertson et al., 1995) 145

4-6 Proposed correlation between shear wave velocity and CPT tip resistance and slope (λ_{ln}) of the ultimate state line (USL) (modified from Robertson et al., 1995) 146

4-7 Critical state soil mechanics concepts illustrated by (a) an e-p'-q diagram with (b) projections onto the e-ln(p') plane 147

4-8 Factors influencing response of sandy soils in undrained monotonic testing 148

4-9 CPT liquefaction/nonliquefaction dividing line based on field observations (modified from Sladen and Hewitt, 1989) 149

4-10 Unified relationship of $Q_p(1-B_q)$ to state parameter and critical state parameters M and λ_{log} (modified from Been and Jefferies, 1992) 150

4-11 Contours of estimated state parameter on soil type behaviour classification chart (modified from Plewes et al., 1992) 151

4-12 Effects of λ_{ln} on undrained response for the same value of state parameter 152

4-13 Flowchart for estimating RSR from in-situ testing 153

4-14 Flowchart for measuring undrained response from laboratory testing............. 154

4-15 Components of undrained response for triaxial compression loading............. 155

4-16 Components of undrained response for triaxial extension loading................. 156

4-17 Suggested interaction between field characterization and in-situ response from laboratory testing.. 157

4-18 Ultimate state lines (USLs) for a variety of sands (based on data tabulated by Sasitharan et al., 1994); also shown are selected reference USLs for Sand Heads sand (after Chillarige et al., 1995) and Fraser River sand... 158

CHAPTER 5

5-1 Relationship between clean sand equivalent SPT blowcount, $(N_1)_{60}$-cs, and undrained residual strength (S_u) from case studies (modified from Seed and Harder, 1990)... 183

5-2 Relationship between clean sand equivalent SPT blowcount, $(N_1)_{60}$-cs and undrained strength ratio, S_u/σ_v' (modified from Stark and Mesri, 1992).. 184

5-3 Correlations between residual strength and normalized CPT penetration resistance based on relative density (modified from Robertson, 1990)............ 185

5-4 Correlations between residual strength ratio and normalized CPT penetration resistance based on state parameter (modified from Robertson, 1990).. 186

5-5 Critical state soil mechanics concepts illustrated by (a) e-p'-q diagram with (b) projections onto the e-ln(p') plane. 187

5-6 Steady state lines for Ottawa sand and Alaska sand compared with (a) other sands and (b) Ottawa sand with fines and kaolin. 188

5-7 Relationship between S_u/p' and (a) state parameter (Ψ) and (b) reference stress ratio (RSR) in triaxial compression for Ottawa sand and Alaska sand. 189

5-8 Contractant-dilatant boundary (RSR=1 or Ψ=0) compared with contours of V_{s1} (or S_u in triaxial compression) for (a) Ottawa sand and (b) Alaska sand.. 190

5-9 Relationship between S_u in triaxial compression and V_{s1} for Ottawa sand and Alaska sand for a range in K_o. 191

5-10 Relationship between S_u in triaxial compression and V_{s1} for other sands compared with Ottawa sand and Alaska sand.. 192

5-11 Relationship between S_u in triaxial compression and V_{s1} for Ottawa sand with fines and kaolin compared with Ottawa sand and Alaska sand. 193

5-12 Illustration of the sensitivity of S_u-V_{s1} relationship in triaxial compression associated with the range in possible values for the parameter A for Ottawa sand and Alaska sand and K_o=0.4. 194

5-13 Relationship between S_u in triaxial compression and $(N_1)_{60}$ for Ottawa sand and Alaska sand compared with data from Duncan Dam and results from Seed and Harder (1990). 195

5-14 Relationship between S_u/σ_v' in triaxial compression and $(N_1)_{60}$ for Ottawa sand and Alaska sand compared with results from Stark and Mesri (1992). 196

5-15 Relationship between S_u in triaxial compression and q_{c1} for Ottawa sand and Alaska sand compared with results from Robertson (1990). 197

5-16 Relationship between S_u/p' in triaxial compression and $(q_c-p)/p'$ for Ottawa sand and Alaska sand compared with results from Robertson (1990). 198

5-17 Contractant-dilatant boundary lines for Ottawa sand and Alaska sand compared with results from Baziar and Dobry (1995). 199

CHAPTER 6

6-1 Plan of the detailed test site area at the CANLEX Phase III site (J-pit) (modified from Iravani et al., 1995). 222

6-2 Configuration of the 4" (10 cm) diameter downhole plate load test setup. 223

6-3 Schematic outlining the details of the 4" (10 cm) diameter downhole plate assembly. 224

6-4 Calibration charts for the 4" (10 cm) plate load tests for (a) the load cell and (b) the displacement cell. 225

6-5 Configuration of the large diameter downhole plate load test setup, with downhole load cell and pore pressure transducer. 226

6-6 Schematic outlining the details of the large diameter downhole plate assembly, with built-in load cell and pore pressure transducer. 227

6-7 Calibration charts for the large diameter plate load tests for (a) the load cell and (b) the displacement cell. 228

6-8 Calibration chart for the large diameter plate load tests for the pore pressure transducer. 229

6-9 Recommended values of N_c for undrained loading in saturated clays (modified from Skempton, 1951)........230

6-10 Typical CPT results (CPT-21) in the detailed test site area at the CANLEX Phase III site (J-pit) (modified from ConeTec, 1995)........231

6-11 Summary of corrected CPT cone tip resistance profiles from all CPTs in and near the detailed test site area at the CANLEX Phase III site (J-pit); test site target zone for testing and sampling located from 3 m to 7 m, as indicated........232

6-12 Plot of the CPT data in the target zone at CANLEX Phase III site (J-pit) on the soil behaviour type classification chart by Robertson (1990)........233

6-13 Bearing stress versus depth measured during 4" (10 cm) diameter plate load tests in borehole PL1........234

6-14 Bearing stress versus depth measured during 4" (10 cm) diameter plate load tests in borehole PL2........235

6-15 Bearing stress versus depth measured during 4" (10 cm) diameter plate load tests in borehole FS52........236

6-16 Bearing stress versus depth measured during 4" (10 cm) diameter plate load tests in borehole FS5........237

6-17 Results of 7" (18 cm) plate load test PL4-1 in terms of (a) displacement versus time, (b) pore pressure measurements versus time and (c).bearing stress measurements versus time........238

6-18 Results of 6" (15 cm) plate load test PL4-2 in terms of (a) displacement versus time, (b) pore pressure measurements versus time and (c) bearing stress measurements versus time........239

6-19 Results of 6" (15 cm) plate load test PL4-3 in terms of (a) displacement versus time, (b) pore pressure measurements versus time and (c) bearing stress measurements versus time........240

6-20 Results of 6" (15 cm) plate load test PL5-1 in terms of (a) displacement versus time, (b) pore pressure measurements versus time and (c) bearing stress measurements versus time........241

6-21 Results of 6" (15 cm) plate load test PL6-1 in terms of (a) displacement versus time, (b) pore pressure measurements versus time and (c) bearing stress measurements versus time........242

6-22 Bearing stress versus depth measured during 6" (15 cm) diameter plate load tests in borehole PL4; note the first test used a 7" (18 cm) diameter plate........243

6-23 Bearing stress versus depth measured during 6" (15 cm) diameter plate load tests in borehole PL5........244

6-24 Bearing stress versus depth measured during 6" (15 cm) diameter plate load tests in borehole PL6 245

6-25 Summary of bearing stress versus depth measured during 6" (15 cm) diameter plate load tests in boreholes PL4, PL5 and PL6 246

6-26 Profiles of 6" (15 cm) plate load test results versus depth in borehole PL4 in terms of (a) bearing stress, (b) pore pressure compared to hydrostatic, (c) time, and (d) estimated undrained shear strength (S_u) based on N_c=9 247

6-27 Profiles of 6" (15 cm) plate load test results versus depth in borehole PL5 in terms of (a) bearing stress, (b) pore pressure compared to hydrostatic, (c) time, and (d) estimated undrained shear strength (S_u) based on N_c=9 248

6-28 Profiles of 6" (15 cm) plate load test results versus depth in borehole PL6 in terms of (a) bearing stress, (b) pore pressure compared to hydrostatic, (c) time, and (d) estimated undrained shear strength (S_u) based on N_c=9 249

6-29 Summary of profiles of estimated undrained shear strength (S_u) based on N_c=9 for boreholes PL4, PL5 and PL6 250

6-30 Summary of profiles of estimated ratio of undrained shear strength to vertical effective stress (S_u/σ_v') based on N_c=9 for boreholes PL4, PL5 and PL6 251

6-31 Summary of profiles of estimated ratio of undrained shear strength to mean normal effective stress (S_u/p') based on N_c=9 and K_o=0.5 for boreholes PL4, PL5 and PL6 252

CHAPTER 7

7-1 Relationship between clean sand equivalent SPT blowcount, $(N_1)_{60}$-cs, and undrained residual strength (S_u) from case histories (after Seed and Harder, 1990) 305

7-2 Relationship between field SPT blowcount, $(N_1)_{60}$ in-situ, and undrained residual strength (S_u) from case histories (after Seed and Harder, 1990) 306

7-3 Case histories from Seed and Harder (1990) and Stark and Mesri (1992) plotted in terms of initial slope height and initial slope angle 307

7-4 Case histories from Seed and Harder (1990) and Stark and Mesri (1992) plotted in terms of relative runout (runout/initial height) and slope angle ratio (ratio of post-failure slope angle to initial slope angle) 308

7-5 Case histories from Seed and Harder (1990) and Stark and Mesri (1992) plotted in terms of brittleness index (see Equation 7-3) and approximate RSR; the relationship suggested by Sladen et al. (1985) is also shown 309

7-6 Example of a flow failure: cross-section of pre-failure and post-failure geometry of Calaveras Dam (case record 1), modified from Hazen (1918) 310

7-7 Example of a lateral spread: cross-section of pre-failure and post-failure geometry of Whiskey Springs Fan (case record 14), modified from Harder (1988) 311

7-8 Example of a slump failure: cross-section of pre-failure and post-failure geometry of La Marquesa Dam Upstream and Downstream (case records 15 and 16), modified from De Alba et al. (1988) 312

7-9 Plot of S_u versus clean sand equivalent SPT blowcount, $(N_1)_{60}$-cs, after Seed and Harder (1990) for those case histories classified as flow failures; theoretical clean Ottawa sand lines (see Chapter 5) shown for comparison 313

7-10 Plot of S_u versus field SPT blowcount, $(N_1)_{60}$ in-situ, after Seed and Harder (1990) for those case histories classified as flow failures; theoretical clean Ottawa sand lines (see Chapter 5) and Duncan Dam (21) results shown for comparison 314

7-11 Range in S_u and $(N_1)_{60}$ in-situ reported by various authors (see Table 7-4) for the case histories in the Seed and Harder (1990) and Stark and Mesri (1992) database. 315

7-12 Plot of S_u versus minimum clean sand equivalent SPT blowcount, $(N_1)_{60}$-cs, for those case histories classified as flow failures; Seed and Harder (1990) lines and theoretical clean Ottawa sand line (see Chapter 5) shown for comparison 316

7-13 Plot of S_u versus minimum field SPT blowcount, $(N_1)_{60}$ in-situ, for those case histories classified as flow failures; Seed and Harder (1990) lines and theoretical clean Ottawa sand and Alaska sand lines (see Chapter 5) shown for comparison 317

CHAPTER 8

8-1 Location of CANLEX Phase II Massey and Kidd sites in the Fraser River Delta, B.C. (modified from Lawrence et al., 1995). 367

8-2 End of test conditions for all Fraser River reconstituted and undisturbed triaxial samples; selected reference ultimate state line (USL) for Fraser River sand is indicated 368

8-3 Quasi-steady state (QSS) conditions for any of the Fraser River samples in Figure 8-2 that had a QSS; selected approximate QSS line (QSSL) is indicated; selected reference USL is shown for comparison. 369

8-4 Plan of the detailed test site at the CANLEX Phase II Massey site (modified from Campanella, 1995). 370

8-5 Corrected profiles of (a) shear wave velocity, V_{s1}, (b) CPT cone tip resistance, q_{c1}, and (c) SPT blowcount, $(N_1)_{60}$, at the Massey site; test site target zone for testing and sampling located from 8 m to 13 m, as indicated. 371

8-6 Conventional void ratio interpretations for (a) CPT, (b) SPT, (c) V_s measurements, and (d) geophysical logging; void ratios of frozen samples and Laval sampler samples are shown for comparison; RSR=1 line based on selected reference Fraser River USL is also shown 372

8-7 Correlations between in-situ tests: (a) comparison of CPT and SPT in terms of $q_{c1}/(N_1)_{60}$, (b) comparison of CPT and V_s in terms of Y, (c) comparison of SPT and shear wave velocity in terms of X. 373

8-8 Direct void ratio interpretations for (a) CPT, (b) SPT, (c) V_s measurements, and (d) geophysical logging; void ratios of frozen samples and Laval sampler samples are shown for comparison; RSR=1 line based on selected reference Fraser River USL is also shown 374

8-9 Plot of the CPT data in the target zone at the Massey site (8 m to 13 m) on the soil behaviour type classification chart by Robertson (1990). 375

8-10 Comparison at the Massey site of the state parameter method by Been and Jefferies (1992) and the field observation method by Sladen and Hewitt (1989) for estimating flow liquefaction potential based on CPT results 376

8-11 Estimation of state parameter in the target zone at the Massey site using the method by Plewes et al. (1992) based on estimated contours of state parameter on a soil behaviour type classification chart 377

8-12 Enlarged plot of shear wave velocity based interpretation of void ratio from the CPT from Figure 8-8(a) illustrating the types of laboratory tests that were conducted on frozen samples from the Massey site (D=drained test). 378

8-13 Undrained monotonic laboratory response of anisotropically consolidated Massey triaxial samples: (a) initial conditions, (b) brittleness index, I_B, (c) minimum strength ratio, S_{min}/p'_i, and (d) axial strain (ε_a) at S_{min}. 379

8-14 Undrained monotonic laboratory response of anisotropically consolidated Massey triaxial samples: (a) end-of-test conditions, (b) end-of-test strength ratio, S_f/p'_i, (c) peak stress ratio, M_p, and (d) end-of test stress ratio, M_f 380

8-15 Profiles of estimated RSR in-situ at the Massey site relative to the reference Fraser River USL for (a) CPT, (b) SPT, (c) Vs, and (d) geophysical logging 381

8-16 Comparison between laboratory conditions (termed lab) and estimated in-situ conditions (termed field) for frozen samples from the Massey site: (a) comparison of e_{lab} and e_{field}, (b) comparison of RSR_{lab} and RSR_{field} 382

8-17 Estimated average profiles of undrained triaxial compression and extension response in-situ at the Massey site based on interpretation of the CPT compared with results of testing frozen samples: (a) brittleness index, I_B, (b) axial strain (e_a) at minimum strength, and (c) minimum strength ratio, S_{min}/p'_i 383

8-18 Estimated average profiles of undrained triaxial compression and extension response in-situ at the Massey site based on interpretation of the CPT compared with results of testing frozen samples: (a)-end-of-test strength ratio, S_f/p'_i, (b) peak stress ratio, M_p, and (c) end-of-test stress ratio, M_f 384

8-19 Application of the integrated CPT method to the Massey site: (a) CPT q_{c1} results, (b) interpreted soil behaviour type index, I_c, (c) estimated fines contents (FC), (d) recommended fines content based correction to q_{c1} to obtain clean sand equivalent value, and (e) estimated cyclic resistance ratio (CRR) profile compared with results of testing frozen samples. 385

8-20 Illustration of how typical undrained triaxial compression and triaxial extension (a) stress paths and (b) stress strain curves can be estimated by combining individual estimated components of response corresponding to the average estimated RSR in the Massey site target zone (see Table 8-7) 386

CHAPTER 9

9-1 Schematic illustrating the concept of dividing lines in terms of CPT penetration resistance, q_c, for both flow liquefaction potential and cyclic softening (liquefaction) potential. 407

9-2 General flowchart for evaluating liquefaction potential at a site 408

9-3 Recommended family of solutions for evaluating cyclic softening (liquefaction) potential based on the risk level (i.e. consequences of failure) associated with a particular project 409

9-4 Recommended family of solutions for evaluating flow liquefaction potential based on the risk level (i.e. consequences of failure) associated with a particular project 410

LIST OF SYMBOLS, NOMENCLATURE AND ABBREVIATIONS

$(\varepsilon_a)_f$ = axial strain from beginning of test to end-of-test
$(\varepsilon_a)_i$ = initial axial strain
$(\varepsilon_a)_{min}$ = axial strain from beginning of test to S_{min}
$(\varepsilon_a)_p$ = axial strain from beginning of test to S_p
$(M_f)_C$ = M_f in triaxial compression
$(M_f)_E$ = M_f in triaxial extension
$(M_p)_C$ = M_p in triaxial compression
$(M_p)_E$ = M_p in triaxial extension
$(N_1)_{60}$ = SPT blowcount corrected for overburden effects and energy effects
$(N_1)_{60}$-cs = clean sand equivalent $(N_1)_{60}$
$(N_1)_{60}$-in-situ = in-situ $(N_1)_{60}$
$(q_{c1})_{cs}$ = equivalent clean sand q_{c1}
A = intercept of V_{s1}-axis at $e = 0$ on a V_{s1}-e plot, in m/s
a_{max} = maximum earthquake acceleration at the ground surface
B = slope of V_{s1}-e plot, in m/s
B = width of plate in plate load test (=diameter of circular plate)
β_f = post-failure slope angle
BH = borehole
β_i = initial slope angle
BPT = Becker penetration test
B_q = dynamic pore pressure ratio
C_0, C_1, C_2 = material constants linking relative density to CPT measurements
CANLEX = Canadian Liquefaction Experiment
ClS = clayey sand
C_N = SPT overburden correction factor
CPT = cone penetration test
CRR = cyclic resistance ratio
CSR = cyclic stress ratio
CSS = cyclic simple shear
C_u = coefficient of uniformity (= D_{60}/D_{10})
D = depth of footing for bearing capacity calculations
$\Delta(N_1)_{60}$ = fines content correction to SPT $(N_1)_{60}$ to obtain $(N_1)_{60}$-cs
D.A. = double amplitude

ΔN_1 = fines content correction to SPT N_1 to obtain equivalent clean sand N_1
Δq_{c1} = correction to q_{c1} for fines content to obtain clean sand equivalent q_{c1}
D_r = relative density
ΔRSR = horizontal shift on e-ln p' plot between USL and QSSL for a soil deposit
$\Delta\tau$ = cyclic loading shear stresses
D_x = soil particle size such than x% are smaller than that size
e = void ratio
ε_a = axial strain; axial strain that occurs while at minimum strength
e_c = void ratio of frozen sample after thaw and consolidation
e_{field} = estimated in-situ void ratio of frozen sample
e_{lab} = void ratio of frozen sample in laboratory immediately prior to testing ($=e_c$)
e_{max} = maximum void ratio
e_{min} = minimum void ratio
EQ = earthquake
ER = energy ratio, in percent, for the specific SPT setup used
e_{us} = void ratio on the reference USL at the same value of p'
e_{us} = void ratio on the USL for the same p' as the initial state
F = normalized friction ratio, in percent = $[f_s/(q_c - \sigma_{vo})] \times 100\%$
ϕ'_{us} = ultimate state friction angle
FC = fines content, % passing the No. 200 sieve
FS = fine sand
FS = frozen sample
f_s = CPT sleeve friction
FSx = frozen sampling borehole No. x
Γ = intercept of the USL in e-ln p' or e-log p' space at p'=1.0 kPa
g = gravitational acceleration = 9.81 m/s^2
γ = unit weight of soil
G_s = specific gravity
GWT = groundwater table
H = thin sand layer thickness
I_B = brittleness index
I_c = soil behaviour type index
I_p = plasticity index
k^* = soil constant = $M (3 + 0.85/\lambda_{log})$
K_c = correction factor to cone resistance in thin sand layers embedded in clay
K_o = ratio of σ_h' to σ_v'

Λ = critical state plastic hardening ratio
L = length of footing for bearing capacity calculations
Laval = Université Laval
λ_{ln} = slope of the USL in e-ln p' space
λ_{log} = slope of the USL in e-log p' space
LSS = limited strain softening
M = earthquake magnitude, on the Richter scale
M = ratio of q to p' along the USL = q_{us}/p'_{us}
m^* = soil constant = $11.9 - 13.3\lambda_{log}$
M_C = triaxial compression stress ratio at ultimate state $(=q_{us}/p'_{us})_C$
M_E = triaxial extension stress ratio at ultimate state $(=q_{us}/p'_{us})_E$
M_f = end-of-test stress ratio = $(q/p')_f$
M_{min} = stress ratio at S_{min} = ratio of q to p' at S_{min}
M_p = peak stress ratio = $(q/p')_p$
N = number of uniform cycles of cyclic loading
N = raw SPT blowcount
N_1 = SPT blowcount corrected for overburden effects
na = stress exponent, typically = 0.125
nb = stress exponent, typically = 0.125
N_c = bearing capacity factor
N_k = empirical cone bearing factor
OCR = overconsolidation ratio
p = mean normal total stress = $\frac{1}{3}(\sigma_1 + 2\sigma_3)$
π = pi
p' = mean normal effective stress = $\frac{1}{3}(\sigma_1' + 2\sigma_3')$
p'_f = magnitude of the end-of-test p'
p'_i = initial mean normal effective stress
p'_{min} = magnitude of p' at S_{min}
p'_p = magnitude of p' at S_p
p'_s = stress on the QSSL
P_a = atmospheric or reference pressure; generally taken to be 100 kPa
p_o' = initial mean normal effective stress
p_{us}' = mean normal effective stress at ultimate state
Q = normalized CPT penetration resistance = $(q_c - \sigma_{vo})/\sigma_{vo}'$
q = deviator stress = $\sigma_1' - \sigma_3'$

q^* = normalized cone tip resistance = $Q_p/(1 - B_q)$

q_c = raw CPT cone tip resistance

q_{c1} = CPT cone tip resistance corrected for overburden effects

q_{cA} = tip resistance in a thin sand layer

q_{cB} = tip resistance in fine grained soil surrounding a thin sand layer

q_f = end-of-test deviator stress

q_f = ultimate bearing capacity of a footing or plate

q_i = initial deviator stress (= zero for isotropic tests)

q_{min} = minimum deviator stress

Q_p = normalized cone tip resistance = $(q_c - p_o)/p'_o$

q_p = peak deviator stress

QSS = quasi steady state

QSSL = quasi steady state line

q_{us} = deviator stress at ultimate state

r = spacing between the USL and the virgin consolidation line

ρ_b = soil bulk density

r_c = initial state ratio

r_d = a factor to account for the variation in earthquake acceleration with depth

r_m = a factor to convert between an equivalent CSR for an earthquake of magnitude 7.5 and a CSR for an earthquake of magnitude, M

RSR = reference stress ratio $(=p'_i/p'_{us})$

RSR_{field} = estimated in-situ RSR of frozen sample

RSR_{lab} = RSR of frozen sample in laboratory immediately prior to testing

r_u = pore pressure ratio

S = sand

σ' = effective stress

σ'_{hi} = initial effective confining stress placed on frozen sample prior to testing

σ'_{vi} = initial effective vertical stress placed on frozen sample prior to testing

σ_1 = major principal total stress

σ_1' = major principal effective stress

σ_3 = minor principal total stress

σ_3' = minor principal effective stress

SD = standard deviation

S_f = magnitude of the end-of-test strength

σ_h' = horizontal effective stress

S_i = magnitude of the initial static shear stress

Si = silt
SiS = silty sand
S_{min} = magnitude of the minimum shear strength
σ_o = initial total vertical stress
σ_o' = initial effective vertical stress
S_p = magnitude of the peak shear strength
S_p = peak shear stress
SPT = standard penetration test
SS = simple shear
S_u = undrained shear strength of sand
S_{us} = ultimate undrained shear strength of sand
σ_v = total vertical stress
σ_v' = effective vertical stress
τ_{av} = average cyclic shear stress
τ_{cyc}/σ_{vo}' = cyclic resistance ratio
τ_d = average driving stress
TE = triaxial compression
TE = triaxial extension
τ_{max} = maximum shear stress
τ_o = shear stresses due to gravity
U. of A. = University of Alberta
UBC = University of British Columbia
US = ultimate state
USL = ultimate state line
V_s = raw shear wave velocity measurements
V_s = shear wave velocity
V_{s1} = shear wave velocity measurements corrected for overburden effects
X = conversion factor between SPT and V_s, in $1/(MPa)^{0.25}$
Y = conversion factor between CPT and V_s, in $(m/s)/(MPa)^{0.25}$
Ψ = state parameter = e - ess
z = depth

CHAPTER 1

INTRODUCTION[1]

1.1 Overview

Liquefaction is a broad term used by geotechnical engineers to describe a variety of phenomena that occur when loose sand is loaded quickly in an undrained manner, such that the porewater pressure within the sand increases rapidly. The resulting phenomena can range from sand boils (mini "volcanoes" on the ground surface which erupt sand/water mixtures to relieve pore pressure) to catastrophic flow slides. Different mechanisms (static or dynamic) can induce liquefaction and different physical processes can occur as a sand liquefies, depending on its initial state, the nature of the loading and the geometry of the site. Regardless of the trigger or the process that occurs, the consequences of liquefaction can be enormous, with significant financial and environmental implications and risk to human safety.

One of the most well known recent cases of liquefaction occurred as a result of the January 17, 1995 Hanshin-Awaji earthquake, which caused massive damage to the city of Kobe, Japan. Holzer (1995) reported that "the earthquake killed 5378 people, damaged or destroyed about 152 000 buildings, and incinerated the equivalent of 70 U.S. city blocks", resulting in about $100 billion U.S. in property losses. Liquefaction primarily occurred in the form of lateral spreading in reclaimed port facilities. These facilities included a large area along the shoreline (reclaimed from 1953 to 1970) as well as two large reclaimed islands, Port Island (with reclamation beginning in 1966) and Rokko Island (reclaimed from 1973 to 1992) (Holzer, 1995). In the reclaimed areas, Holzer (1995) reported that "fill was dumped into standing water that had an average water depth of 12 m. No significant effort was made during reclamation to compact the sandy fill to increase its liquefaction resistance." Liquefaction related deformations consisted of up to 2 m of permanent horizontal displacement from lateral spreading and settlements that generally ranged from 30 to 50 cm (Holzer, 1995). One of the most significant impacts was that the area affected by liquefaction was extensive and differential deformations were large enough to put most of the harbour cranes out of commission. Structures that have low tolerances for differential movements can suffer large damage as a result of this type of liquefaction phenomenon. In addition, "more than 95% of the shipping berths were inoperable after the earthquake. Approximately 24 km of wharf was damaged" (Holzer, 1995). This had a significant financial implication for Japan. As an article regarding risk management and earthquake engineering in the April 22nd issue of The Economist wisely stated, "the economic costs of an earthquake to a business do not stop with repairing and replacing damaged buildings; interrupted trading and increased unemployment must be added on top". The port at Kobe is "the largest foreign-trade port in Japan and the third busiest port in the world" (Holzer, 1995). Repairing the physical damage caused by earthquake-induced liquefaction and returning such a large port to an operable state would be costly. However, in addition, the interruption to trade and shipping would result in significant financial repercussions.

---

[1] *A version of part of this chapter has been published. Robertson, P.K. and Fear, C.E. 1995. Liquefaction of sands and its evaluation, Proceedings of IS Tokyo '95, First International Conference on Earthquake Geotechnical Engineering, Keynote Lecture.*

The failure of the Stava tailings dam in northern Italy, which experienced a major flowslide in 1985 (D'Appolonia and Morgenstern, 1988), is another case history illustrating the type of damage that can be caused by liquefaction. The Stava tailings dam was located at the head of a narrow valley, above the resort town of Stava. NBC presented a television documentary about the case history, as part of their series entitled "Disaster Chronicles". The program emphasized the human impact of the failure: 268 people were killed as approximately 600 000 m^3 of "mud" rushed down the steep and narrow Stava valley, sweeping through two towns. The people who were killed had essentially no warning of the imminent disaster. Even if they had been able to recognize a warning sign, they would likely not have had enough time to flee to safety, as the tailings dam failed essentially spontaneously and massive amounts of material flowed rapidly down the valley. The tailings dam consisted of two stages, the first constructed by the upstream method of construction and the second constructed first by the centreline method and then the upstream method (D'Appolonia and Morgenstern, 1988). The upper stage failed first; subsequently, the lower stage could not hold back the failed material from the upper stage. The mine changed owners more than once during the life of the dam and unfortunately, this resulted in poor engineering management and design. The failure was attributed to statically triggered liquefaction, as a result of a slow rising water table in the loose sand shell of the tailings dam. Once the material "liquefied", it suffered a severe reduction in strength, such that it could not longer resist the large driving stresses and the sudden failure occurred. This case history differs from the Kobe case history in that, at this site, the potential for liquefaction directly posed an unacceptable risk to human safety. Consequently, when the liquefaction failure occurred, many people were killed. The failure also had large financial implications. Depending on the nature of the tailings, the failure of such a tailings dam could also have significant environmental implications in addition to the scar on the landscape. Potentially toxic substances (e.g. heavy metals, radioactive isotopes, various chemicals) could flow out over large distances downstream.

The two case histories presented above illustrate the types of mechanisms that can trigger liquefaction (i.e. from earthquake loading to static loading) and the range of consequences that can result, with deformations ranging from a few metres to hundreds of metres. Financial, environmental and human implications can be significant depending on the nature of the failure. Until fairly recently, both case histories would be referred to as liquefaction failures. However, although both cases involved rapid undrained loading of loose sand, the physics that drove the two failures were very different, due to the type of loading, the nature of the site geometry, and the state of the soil. Consequently, it is important to address the terminology used to describe various undrained failure mechanisms in sand before proceeding any further with discussions of liquefaction analysis and design.

1.2 Terminology

1.2.1 An historical perspective

Whether a sand is subjected to static or cyclic undrained loading, its response will be governed by **physics**. What different responses are called is a matter of **terminology**. Of course, in order to decide what terminology to use, the physics must be understood first. Adapting appropriate terminology is important as it allows us to communicate with each other such that if a certain term is used, everyone understands what physical processes that term implies. The following excerpts from the geotechnical literature provide a chronological sampling of the terminology and explanations of the corresponding physics that various authors have chosen to use to describe the range of phenomena broadly known as "liquefaction". It will soon become clear to the reader that, as Poulos (1988) pointed out, "there are different schools of thought with respect to the mechanism causing liquefaction and the appropriate methods for analyzing and designing to prevent liquefaction". Casagrande (1969) tried to sort out these differences with an "ad hoc committee", but, nevertheless, some confusion continues to linger in the geotechnical engineering community.

a) Hazen (1920)

One of the earliest examples of a slope failure caused by liquefaction of sand was the failure of the Calaveras Dam. Calaveras Dam was a hydraulic fill dam constructed early this century near San Francisco. The upstream shell of the dam failed on March 24, 1918, while the dam was under construction (Hazen and Metcalf, 1918; Hazen, 1918), having reached a height of approximately 61 m, with a upstream slope angle of 18.4°. The failure was not associated with any earthquake loading. Upstream movements extended 183 m beyond the original toe of the upstream slope and resulted in a post-failure slope angle of approximately 5.7° (for more details, see Chapter 7). Hazen (1920) recognized the process of liquefaction in his comments regarding the failure, as follows:

"An extra pressure in the water in the pores of such a material may be produced by a sudden blow or shock which tends to compress the solid material by crushing the edges and points where they bear, or by causing a re-arrangement of particles with smaller voids. An illustration of this can be seen in the sand on the seashore. Such sand, comparable to dune sand in size, is usually found to be saturated with water for a certain distance above the water level. This condition is maintained by capillarity. If a weight is slowly placed on this saturated sand, there is a slight settlement, the grains of sand coming to firmer bearings, and the weight is carried. A sharp blow, as with the foot, however, liquefies a certain volume and makes quicksand. The condition of quicksand lasts only for a few seconds until the surplus water can find its way out. When this happens the grains again come to solid bearings and stability is restored. During a few seconds after the sand is struck, however, it is almost liquid, and is capable of moving or flowing or of transmitting pressure in the same measure as a liquid."

"As the dam is built higher, pressure increases; there is compression and reduction in porosity. Each additional increment of loading and compression means that a certain quantity of water representing the difference between the old voids and the new voids must be expelled. As long as the material remains sufficiently pervious to carry off this excluded water, the process of compression is harmless. The surplus water is pushed back into the reservoir and stability is retained. There may come a time, however, when the compression goes forward so rapidly that the surplus water cannot be carried off fast enough. When that point is reached (if it is reached), there will tend to be an excess of water in the interstices and that excess will transmit some of the pressure that was before carried only by the bearings of solid particles, and the frictional resistance of the material will be less, and perhaps much less, than it was before."

"The thought has occurred to the writer, in looking at the material that slid in the Calaveras Dam, that something of this kind may have happened on a large scale - 800, 000 cu yd of fill flowed for a brief space, and then became solid. It was, in fact, so solid that in examining it afterward, by samples and by borings, it was difficult to see how the material could have flowed - as it certainly did flow."

b) Terzaghi (1925)

Terzaghi used a German expression which translates directly into English as "settlement-flow" to describe the flow of saturated sands.

c) Casagrande (1936), as reported by Morgenstern (1994)

"A serious disturbance, for example, an earthquake, or possibly even large seepage pressures, may result in a tendency to reduce the volume due to an adjustment in the structure, reducing the shearing resistance to such a point that the whole mass can flow like a liquid under the effect of the seepage pressures."

d) Terzaghi and Peck (1948), as reported by Ishihara (1993)

"Spontaneous liquefaction" was used "to indicate the sudden change of loose deposits of sand into flows much like viscous fluid, triggered by a slight disturbance".

e) Mogami and Kubo (1953), as reported by Ishihara (1993)

"A similar phenomenon was recognized by Mogami and Kubo to take place during earthquakes and addressed under the name of liquefaction as an issue of engineering significance".

f) Seed and Lee (1966), as reported by Casagrande (1975b)

Following the major 1964 Niigata earthquake, the geotechnical community was alerted to the serious effects of earthquake-induced liquefaction of soil. For example, buildings that were structurally sound tipped over in bearing capacity type failures as the soil beneath them liquefied. Consequently, researchers at Berkeley in California began conducting undrained cyclic triaxial tests on sand to study this phenomenon. "Initial liquefaction" was defined as the point at which the pore pressure equalled the confining pressure for the first time. "Failure" was defined in terms of the number of cycles when the strain amplitude in one complete cycle reached a certain magnitude. Seed and Lee also concluded the following, according to Casagrande (1975b):

- "Initial liquefaction can be produced by cyclic loading also in medium dense and dense sands and is not limited to loose sands."
- "The liquefaction potential decreases with increasing confining pressure."
- "The liquefaction potential decreases with increasing initial principal stress ratio and, therefore, sand adjacent to a slope is less susceptible to liquefaction than beneath a horizontal surface."

g) Casagrande (1969)

Casagrande addressed a letter dated April 30, 1969 to Bjerrum, Peck, Richart, H.B. Seed, Whitman and Wilson[2], suggesting an "ad hoc committee" to discuss what terminology should be used to describe the phenomena that occur when saturated sands are subjected to H.B. Seed's type of cyclic loading tests and noted the following:

H.B. Seed had initially suggested "cyclic liquefaction". Bjerrum objected to "cyclic liquefaction" and proposed "cyclic softening". Whitman agreed with "cyclic softening". Poulos and Castro agreed that "cyclic softening" conveyed a better concept of what is happening in cyclic tests than the term "cyclic mobility" (which Casagrande had been provisionally using). Casagrande himself was "at first startled by Bjerrum's suggestion", but decided that "the more (he) thought about it, the more (he) liked it because it describes what is happening, without the necessity of knowing whether or not redistribution of water content is occurring". He also noted that "in the British Report on the Aberfan Disaster, Alan Bishop stated that the terms 'flow slide' and 'liquefaction slide' are synonymous" and that, as he remembered, Terzaghi "also did not consider these terms to mean different phenomena".

---

[2] *The series of letters referred to in the following section were kindly provided by Dr. E.C. McRoberts of AGRA Earth and Environmental, Ltd., Edmonton, from the collections of the late Dr. R.M. Hardy.*

The replies to Casagrande's letter were as follows:

Peck first liked "cyclic strain softening", but then voted for "cyclic mobility". Wilson liked "cyclic mobility" better than "cyclic softening" or "cyclic strain softening", associated "softening" with cohesive or thixotropic materials only, not with sand, felt that adding the word "strain" helped relate the phenomenon to sands, but still did not convey the correct meaning to him, and agreed that "partial liquefaction" is not correct and that "liquefaction" must be left out of the term. H.B. Seed very much preferred "cyclic mobility" to "cyclic softening" or "cyclic strain softening" to describe the loss of strength of saturated sands under cyclic loading conditions and agreed with Wilson "that softening is more readily associated with a weakening of clays whereas the loss of stability in saturated sands is often complete and sudden with the soil not only softening but going beyond this and becoming mobile". In the end, a majority, including H.B. Seed, agreed on the term "cyclic mobility" to describe the effects observed in the cyclic triaxial tests. However, as noted by Casagrande, the term liquefaction continued to be used in the literature in connection with the cyclic triaxial tests.

h) Casagrande (1975a)

"The term 'liquefaction' as used in conjunction with cyclic triaxial tests refers to the development of pore pressures equal to the confining pressure in the moment when the shear stresses disappear. The number of cycles to produce this phenomenon, or to achieve a specified axial strain, is defined as 'failure by liquefaction'. This so-called liquefaction has not the slightest similarity with the liquefaction that produces flow. Because entirely different phenomena are involved, it should not be surprising that the number of cycles to achieve this so-called liquefaction decreases with increasing confining pressure and also with increasing principal stress ratio; in other words, these variables have exactly the opposite effects from those which exist for true liquefaction." In addition, Casagrande felt that "pore pressures equal to the confining pressure are the product of 1) redistribution of water content produced by boundary effects and 2) of the unrealistic cycling through the hydrostatic state of stress".

i) Casagrande (1975b)

Recognizing the differences between what had historically been known as liquefaction and the liquefaction associated with cyclic triaxial tests, Casagrande (1975b) proposed two terms, "actual liquefaction" and "cyclic liquefaction". He defined actual liquefaction as "what was simply called 'liquefaction' before the development of cyclic laboratory tests. It is the response of loose, saturated sand when subjected to strains or shocks that results in substantial loss of strength and in extreme cases leads to flow slides". He defined cyclic liquefaction as "the response of a test specimen of dilative sand to cyclic loading in a triaxial test when the peak pore pressure rises momentarily in each cycle to the confining pressure".

As Casagrande explained, "until 1966, the term liquefaction was used in literature for the response of saturated loose sand to strains or shocks that resulted in flow slides. With the development of the cyclic triaxial tests in connection with research on the response of sand under earthquake loading, the same term began to be used for a specific response of sand in cyclic triaxial tests. In an effort to prevent confusion by the use of the same term for entirely different phenomena, an informal committee of several colleagues and myself tried in 1969 to find another term for the cyclic response phenomena in laboratory tests. Finally, we agreed on the term 'cyclic mobility'. However, by then the term liquefaction was already so well entrenched in literature for use with the cyclic triaxial tests that it proved impractical to adhere to this agreement; and the confusion continued. While I would much prefer not to use the term 'liquefaction' for a phenomenon that truly is not liquefaction, I decided reluctantly to use it for both phenomena in this paper, but to differentiate between them with appropriate adjectives..."

When referring to the conclusions made by Seed and Lee (1966), Casagrande remarked that "at that time I did not realize that the term 'liquefaction' in their paper had an entirely different meaning than the phenomenon that I had always associated with that term. Therefore, these three conclusions appeared to contradict all my past experience and also the results of Castro's investigations."

j) Committee on Soil Dynamics of the Geotechnical Engineering Division (1978)

Committee Members: D. Anderson, J.M. Bell, R.E. Brown, W.F. Brumund, Y.S. Chae, J.T. Christian, V.P. Drnevich, L.W. Heller, R.N. Hwang, I.M. Idriss, J. Lysmer, J.P. Mulilis, R. Pyke, M.L. Silver, H. Singh, S. Singh, K. Stokoe, G.E. Triandafilidis, A.S. Veletsos, T.S. Vinson, R.N. Yong, T.L. Youd, and W.F.M. Marcuson III (Chairman).

In 1978, the Committee on Soil Dynamics of the Geotechnical Engineering Division (herein referred to as the 1978 Committee) recognized that "some important variations, discrepancies, and ambiguities have developed in terminology used to describe the liquefaction phenomenon and its effects". Consequently, the 1978 Committee recommended a list of definitions after reviewing various terms used in the past. Some of the recommended definitions are outlined below.

The term liquefaction was recognized as "the act or process of transforming any substance into a liquid" and that this occurs in sandy soils as a result of "increased pore pressure and reduced effective stress". The 1978 Committee went on to define liquefaction as "a changing of state that is independent of the initiating disturbance that could be a static, vibratory, sea wave or shock loading, or a change in the ground-water pressure. The definition is also independent of deformation or ground failure movements that might follow the transformation. Liquefaction always produces a transient loss of shear resistance, but does not always produce a longer-term reduction of shear strength". The 1978 Committee recommended that adjectives describing the type of liquefaction (e.g. "initial", "cyclic" or "true") should not be used because the terms often got dropped in practice and this led to confusion.

The 1978 Committee defined "cyclic strain softening" as "a stress-strain behaviour under cyclic loading conditions in which the ratio of strains to differential shear stresses increases with each stress or strain cyclic" and that "in saturated undrained cohesionless soils, cyclic strain softening is caused by increased pore-water pressure". The 1978 Committee went on to say that "continued cyclic loading usually leads to increasing axial strains and increasing pore-water pressures, but does not necessarily lead to loss of ultimate shear strength if the material is dilative". The 1978 Committee also suggested that the term "full or 100% pore pressure ratio" (i.e. when the change in pore pressure equals the initial effective minor principal stress or the initial vertical effective overburden stress, depending on the pore pressure ratio definition being used) replace the older term "initial liquefaction".

The term "limited flow strain" or "limited flow deformation" was defined by the 1978 Committee as "flow strains or deformations that commence following liquefaction but are arrested after a finite displacement, usually as a consequence of a dilatancy caused pore pressure drop and accompanying increase of effective stress" and which "are accompanied by a transient loss of shear resistance rather than permanent loss of shear strength". However, "unlimited flow strain" or unlimited flow deformation" was defined by the 1978

Committee as "flow strains or deformations that commence following liquefaction and continue unabated under undrained constant total stress conditions" and are "accompanied by permanent loss of shear strength". The 1978 Committee remarked that this phenomenon was formerly called "true liquefaction" by some engineers.

k) Seed (1979)

With respect to loading saturated sands of medium to high densities with a series of cyclic stress applications of relatively low magnitude, Seed noted that this "could build up high pore water pressures and induce significant deformations in samples that exhibited dilatant behaviour under static loading conditions." Seed also noted that "this is a different type of liquefaction than that induced by static stresses, since samples that develop pore pressures equal to the applied confining pressures at some stages of a loading cycle will also usually dilate and thereby mobilize sufficient resistance to limit the strains produced by the peak cyclic stresses at other stages of the loading cycle. It has recently been proposed that such a condition be called 'initial liquefaction with limited strain potential' or 'cyclic mobility'."

Seed (1979) stated that "'liquefaction' denotes a condition where a soil will undergo continued deformation at a constant low residual stress or with low residual resistance, due to the buildup and maintenance of high pore water pressures, which reduce the effective confining pressure to a very low value; pore pressure buildup leading to liquefaction may be due either to static or cyclic stress applications and the possibility of its occurrence will depend on the void ratio or relative density of a sand and the confining pressure; it may also be caused by a critical hydraulic gradient during an upward flow of water in a sand deposit."

Seed (1979) also stated that a" 'peak cyclic pore pressure ratio of 100%' denotes a condition where, during the course of cyclic stress applications, the residual pore water pressure on completion of any full stress cycle becomes equal to the applied confining pressure; the development of a peak cyclic pore pressure ratio of 100% has no implications concerning the magnitude of the deformations that the soil might subsequently undergo; however, it defines a condition that is a useful basis for assessing various possible forms of subsequent soil behaviour."

Seed (1979) also proposed that a "'peak cyclic pore pressure ratio of 100% with limited strain potential' or 'cyclic mobility' denotes a condition in which the cyclic stress applications develop a peak cyclic pore pressure ratio of 100% and subsequent cyclic stress applications cause limited strains to develop either because of the remaining resistance of the soil to deformation or because the soil dilates, the pore pressure drops, and the soil stabilizes under the applied loads. Cyclic mobility may also be used in a broader sense to describe the cyclic straining that may occur even with pore pressure ratios less that 100% in which case the actual peak value of pore pressure ratio may simply be stated."

l) Castro et al. (1982), as reported by McRoberts and Sladen (1992)

"Liquefaction is a phenomenon wherein a mass of soil loses a large percentage of its shear resistance, when subjected to undrained monotonic, cyclic or shock loading, and flows in a manner resembling a liquid until the shear stresses acting on the mass are as low as the reduced shear resistance."

m) National Research Council (1985)

The NRC Committee on Earthquake Engineering produced a book summarizing current practice by 1985 with respect to designing against earthquake-induced liquefaction. The book states that "during earthquakes the shaking of the ground may cause a loss of strength or stiffness that results in the settlement of buildings, landslides, the failure of earth dams, or other hazards. The process leading to such loss of strength or stiffness is called *soil liquefaction*. It is a phenomenon associated primarily, but not exclusively, with saturated cohesionless soils." The book goes on to say that "knowledge concerning liquefaction and its effects has come mainly from three distinct efforts. These are (1) field observations during and following earthquakes, (2) experiments in the laboratory on saturated soil samples and models of foundations and earth structures, and (3) theoretical studies." The book concludes that, for earthquake-induced liquefaction, "the most commonly observed manifestation of liquefaction is the occurrence of 'sand boils' on the ground surface."

The NRC book states that "the density of a cohesionless soil also is a very important factor, because pore pressures build up rapidly in a loose sand, and a point may be reached where the sand loses much of its initial resistance to shear. Pore pressure buildup occurs even in a dense sand, but at a slower rate; although significant cyclic and permanent strains may develop, the soil can retain its shear resistance." In addition, "laboratory tests have also shown that a soil has a value of undrained steady-state strength that is only a function of its void ratio and is independent of its stress history, including any pore pressure buildup that may have occurred under earthquake loading. Thus, for a soil to be capable of losing strength and flowing, it must be subjected in the field to shear stresses that exceed its steady-state shear strength."

The NRC book concludes that "the word *liquefaction*, as generally used, includes all phenomena involving excessive deformations or movements as a result of transient or repeated disturbance of saturated cohesionless soils (footnote: "This broad usage of the word *liquefaction* is endorsed by the great majority of engineers, although some would restrict use of the word to flow failures."). Thus, both flow failures and deformation failures are said to be liquefaction failures." Flow failures were defined as "the condition where a soil mass can deform continuously under a shear stress less than or equal to the static shear stress applied to it. Such a condition will cause slope instability or bearing capacity failure." Deformation failures were defined as "unacceptably large permanent displacements or settlements during (and/or immediately after) shaking, but the earth mass remains stable following shaking without great changes in geometry. Examples are settlements of oil tanks and the slumping and cracking of earth dams ... and the destruction of roadways and pipelines by large ground oscillations."

The book goes on to say that "if large increases in pore pressure occur within an earth mass as a result of an earthquake, significant cyclic or permanent deformations can occur. In some cases, these deformations may be large enough to constitute a failure. In other cases, a flow failure of the earth mass may develop. Of particular concern is a situation where the pore pressures rise to equal (or nearly equal) the total overburden stress; this is named the $\sigma' \approx 0$ condition (also sometimes called initial liquefaction)." Failure will occur if there is "both a prior susceptibility to loss of strength in the soil mass and a triggering mechanism (such as an increase in pore pressure). The two combine to initiate the progressive loss of strength within the soil." In evaluating level ground conditions, "the primary goal is to identify the conditions for reaching the $\sigma' \approx 0$ condition in the soil profile, which triggers the development of liquefaction effects at the ground surface." However, in sloping ground, "zones where the $\sigma' \approx 0$ condition occurs are identified, and a residual strength is assigned to those zones using correlations of observed residual strengths with in-situ penetration resistance. A static stability analysis is then performed." The book then concludes that "the word liquefaction, as used by engineers and nonexperts, does not refer to a single well-defined phenomenon, but rather to a complex set of interrelated phenomena that can contribute to the occurrence of unacceptable damage to a building or other facility during an earthquake."

Under the topic "liquefaction failure mechanisms for horizontal ground", the NRC book states that "...essentially all of the stress within the soil stems from the self-weight of the soil. Any static shear stresses that may be present in the ground are from the depositional process and subsequent loading history. However, these shear stresses are not needed for equilibrium of the mass, and the shear stresses can therefore change as a result of shaking and even become zero." Sand boils, subsidence and settlement and differential transient motions (due to reductions in soil stiffness) can result from excess pore pressures.

Under the topic "flow failures of slopes and embankments", the NRC book talks about type I and type II stress-strain behaviour of a sand, which refers to strain-softening and strain-hardening behaviour, respectively. It goes on to say that "with a soil having type I stress-strain behaviour, a progressive failure can occur with no volume change (i.e. truly undrained conditions) at any point within the earth mass", but that "on the other had, if the sand within the slope has a stress-strain curve of type II under truly undrained conditions, there cannot be a flow failure". It goes on to say that "cyclic loading may cause some permanent strain and some permanent downhill movement, but it cannot change the value of the undrained steady-state (residual) strength. Thus, at the end of the transient loading, the ever-present static stress is still less that the peak shear resistance and downslope movement will be arrested."

The NRC book also discussions the mechanism of redistribution of pore water and density within a soil causing loosening of a sand. This can also lead to failure as the steady state strength will be lower than for the original void ratio of the sand. It is also suggested that high pore pressures in a sand can cause cracking in surrounding soil, reduce its shear resistance and also lead to failure.

n) Castro (1987)

Castro (1987) was a supporter of critical state soil mechanics to explain flow liquefaction failures. He conducted undrained monotonic tests to establish the steady state line of a sand. In table form, Castro (1987) proposed that if a soil had no driving shear stresses on it and volume decreases occurred, they could lead to ground settlement, while if pore pressure increases occurred they could lead to sand boils and ground settlement. However, if driving shear stresses were present, Castro (1987) proposed that if loss of stability (i.e. liquefaction) occurred, it could lead to flow slides, sinking of heavy buildings and floating of light structures. On the other hand, if limited shear distortion occurred (i.e. the soil mass remains stable), Castro (1987) proposed that slopes could slump, buildings could settle and lateral spreads could occur.

Castro stated that "the term 'driving' refers to those shear stresses that are required for static equilibrium and, therefore, are available to drive the mass should the soil lose sufficient strength. The 'driving' shear stresses are not the shear stresses resulting from placement or consolidation of the soil, but rather are the minimum shear stresses which are necessary to maintain equilibrium of the soil mass under external or gravity loads (e.g. static foundation loads or weight of sloping ground or embankment). ... In a soil deposit with level ground and not supporting any structure, the driving shear stresses are zero. There are shear stresses in the soil due to the fact that $K_o \neq 1$ [K_o = ratio of horizontal to vertical effective stresses]; however, they are not required for equilibrium and may be referred to as 'locked-in' shear stresses. As an earthquake shakes the ground, small shear deformations may occur due to the 'locked-in' shear stress. However, with very small shear deformations, the stresses are redistributed and the 'locked-in' shear stresses disappear." Castro concluded that "it is important to note ... that the term liquefaction is often used to refer to all of the above phenomena, even though ... their physical mechanisms are quite different. In the subsequent discussion, the term liquefaction will only be used to describe the cases in which the soil mass loses stability (e.g. in flow slides) and will be defined in that context."

o) Seed (1987)

Seed (1987) stated that "...ensuring that liquefaction can not be triggered is a legitimate means of avoiding undesirable consequences. This can be achieved by designing on the principle of keeping the induced pore pressure ratio, r_u, well below 100%; achievement of this condition ensures that liquefaction will not occur, and thus it generally provides a stable and minimally deforming structure." He also felt that "...dense cohesionless soils do not normally present problems in the design of dams or embankments, because they rarely, if ever, develop conditions where $r_u \approx 100\%$, and, if they do, it will usually have no practical consequences."

Seed (1987) concluded that "...within a reasonable range of embankment heights and slopes often found in practice, larger embankments with somewhat steeper slopes, which create higher effective confining pressures and higher initial shear stresses, may make it more difficult (in terms of the required level of applied shear stresses) to build up pore pressures in sand deposits, and therefore more difficult to trigger liquefaction by inducing a condition of $r_u \approx 100\%$, than would lower dams with flatter slopes. Since higher and steeper embankments may make it more difficult to build up pore pressure and trigger liquefaction, it would appear that these embankments can sometimes be constructed on sands with lower N_1 values and still not cause liquefaction to be triggered, than can embankments with lesser heights and flatter slopes. However, changing the height and slope of an embankment will also change the embankment response, thereby changing the level of applied shear stresses, and thus it is difficult to reach general conclusions concerning the relative effects of higher embankments and steeper slope conditions. There is no field evidence to indicate, however, that flattening the slopes or lowering the height of an embankment will reduce the possibility of triggering liquefaction, while there is limited evidence to suggest that the reverse may be true."

However, Seed (1987) also stated that "on the other hand, if liquefaction occurs and the liquefied soil develops a residual strength that is independent of confining pressure, then the larger the driving shear stresses in a soil structure, the more likely it is that either sliding or large deformations will develop. Thus, for high embankments and embankments with steeper slopes, higher residual strengths and thus higher N_1 values are required to prevent sliding than for smaller dams or embankments with flatter slopes." "Thus, if the problem of embankment stability on potentially liquefiable soils is approached from the point of view of evaluating what happens after the soil liquefies, it is concluded that steeper slopes and higher dams are more dangerous that flatter slopes and lower dams, or that a higher N_1 value is needed in the foundation soil for a high dam than for a low dam. This is a correct and logical conclusion, *if the soil in or below the dam is to be allowed to liquefy.*"

Seed (1987) also stated that "experience shows, for example, that reducing the driving stresses and ensuring a high factor of safety against liquefaction-type (flow) sliding does not necessarily prevent large deformations from developing if a soil liquefies. In fact, large deformations (5-10 ft) have occurred on slopes as flat as 2% (1 on 50), where the driving stress was as low as 60 psf and the post-earthquake factor of safety against sliding was probably greater than 2.0. Examples are the Juvenile Hall landslide in the San Fernando earthquake of 1971, and bridge foundation movements, such as those at the Snow River Bridge, in the Alaska earthquake of 1964. Furthermore, very low dams, with heights of 20 and 30 ft, are known to have failed and deformed excessively as a result of liquefaction, under relatively low levels of earthquake shaking (0.2-0.3g). Thus, determining a residual strength, even if it is done reliably, is not necessarily a solution to the whole problem of embankment stability on potentially liquefiable soils; it is a potential solution in some cases (depending on the choice of residual strength values) to the flow slide evaluation problem, but it contributes little to the deformation evaluation problem.

p) Hutchinson (1988), reported by Morgenstern (1994)

A liquefaction flow slide is "characterized by the sudden collapse and extensive, very to extremely rapid run-out of a mass of granular material or debris, following some disturbance. An essential feature is that the material involved has a meta-stable, loose or high porosity structure. As a result of the disturbance this collapses transferring the overburden load wholly or partly onto the pore fluid, in which excess pressures are generated. The consequent loss of strength gives the failing material, briefly a semi-fluid character and allows a flow slide to develop."

q) Poulos (1988)

"Currently there is a sense among members of the geotechnical profession in civil engineering that there are different schools of thought with respect to the mechanism causing liquefaction and the appropriate methods for analyzing and designing to prevent liquefaction. Two of these schools can be traced to differences between the use of the term liquefaction by Professor Arthur Casagrande and his students at Harvard University, of which the author is one, and the use of the same term by Professor H. Bolton Seed, himself a former student of Professor Casagrande, and his students at Berkeley."

Poulos (1988) pointed out that "...'liquefaction' as observed by Seed and Lee in undrained cyclic load tests and 'liquefaction' as it was observed by Castro in undrained monotonic tests were two different phenomena. One was a phenomenon of excessive deformation and the other was a stability failure." Poulos (1988) went on to propose two terms, "liquefaction" and the "Z-condition" to distinguish between the two types of "liquefaction". The definitions of the two terms, as given by Poulos (1988) are as follows:

Liquefaction

- "a stability failure due to undrained shear of highly contractive, fully saturated masses of soil"

- "the driving shear stresses are greater than the undrained steady state strengths such that the failure involves an acceleration of the mass"
- "the mass comes to rest as the driving shear stresses are reduced, and the inertia of the accelerated mass is overcome by the undrained steady state shear strength"

Z-condition

- "that stage during seismic, blast-induced or other shaking when the effective stress within the soil momentarily becomes zero"
- "it can occur only if the shear stresses in the soil are reversed in sign so that adjacent particles are sheared in opposite directions"
- "if shear stresses are reversed a sufficient number of times, the effective stress can momentarily pass through zero; in laboratory triaxial and direct simple shear tests, this condition results in a rapid increase in strain for contractive specimens; it has been postulated to occur in-situ"
- "the undrained steady state shear strength is not affected by the shaking, that is, by the fact that the Z-condition occurred, as long as the void ratio of the specimen remains constant; if shear stress is reapplied, the state point moves to the right toward the steady state line"
- "the moment when the Z-condition first occurs during a cyclic load test has been referred to as 'initial liquefaction'
- "subsequently, it was pointed out that the Z-condition does not imply zero shear strength. Also, Casagrande suggested that the Z-condition probably occurs only, or much more severely, in the laboratory than in situ. To date, the writer knows of no cases for which the Z-condition has been observed in the field."

Poulos concluded that "Liquefaction is a catastrophic failure; the Z-condition implies that large deformations may occur that may or may not be critical to a particular structure." In addition, he stated that "the conventional cyclic load test does not model in-situ seismic loading for two important reasons. First, the inertia of the mass in-situ is not modeled. ... Second, there are test errors in the undrained cyclic triaxial test that, to date, have not been well evaluated. ... Because of the cycling, the water in the specimen can redistribute ... with the result that the strains are larger than would occur if redistribution did not occur. ... The question arises of whether the same kind of redistribution occurs in situ during the one-minute or so duration of an earthquake. To date there is no information available to enable direct comparison between cyclic load test results and in-situ deformation."

r) Davis, Castro and Poulos (1988)

"The seismic behaviour of an embankment consisting of a loose, saturated soil depends on whether the average driving shear stress (τ_d) in the mass due to gravity forces is larger or smaller than the undrained steady state shear strength (S_{us}) (Poulos, Castro and France, 1985). If the driving shear stress due to gravity loading is smaller than the undrained steady state strength, then the case is analyzed as a deformation problem. Permanent deformation can occur each time the sum of the dynamic shear stress plus the driving shear stresses exceeds the resistance mobilizable at that time ("yield strength"). The lowest value that the yield strength can have in a highly contractive soil is the undrained steady state strength (S_{us}). Thus, for this case, when shaking stops, there is no further accumulation of permanent deformation, except that, as excess pore pressure dissipates, consolidation (settlement) occurs."

"If, on the other hand, the driving shear stress due to gravity loading is greater than the undrained steady state strength, a metastable condition exists. The earthquake shaking can then induce sufficient strain so that the mobilizable strength drops from undrained peak to undrained steady state. Now a condition of instability exists, and the mass accelerates down the critical failure surface, like a block down a curved surface. Movement stops when the inertia of the sliding mass is overcome by the undrained steady state strength. This type of stability failure appears as a liquefaction or "flow" slide. The initial and final driving shear stresses will bracket the mobilized shear strength."

Therefore, Davis et al.(1988) distinguish between liquefaction case histories and deformation case histories. The Lower San Fernando Dam is cited as an example of a liquefaction case history whereas the Heber Road lateral spread is cited as an example of a deformation case history. A different method of analysis is used for each type of case history to estimate the mobilized undrained shear strength. For a liquefaction case history, they suggest that Newton's law can be used together with the observed magnitudes and duration of movement. For a deformation case history, they suggest that a Newmark-type of analysis can be used. The authors go on to say that "with the exception of Lower San Fernando Dam and Heber Road case histories there are few case histories with sufficient information to develop a reliable estimate of the mobilized shear strength. It also will be shown that soils having zero or very low measured blowcounts have backfigured mobilized shear strengths greater than zero."

s) Seed and Harder (1990)

Seed and Harder (1990) concluded that "...'triggering' or initiation of potential liquefaction failure (is) defined as sufficient pore pressure or strain accumulation to bring the material to a condition at which undrained residual (or 'steady state') strength will control further behaviour."

t) Morgenstern (1992)

"The question of liquefaction has attracted an enormous amount of attention, most of it related to earthquake effects. However, ..., there are numerous examples of static liquefaction and earthquake loading is only one of several potential initiating mechanisms. For major instability to occur, the post-earthquake follower stresses must exceed the available resistance. Earthquake considerations are important in assessing the triggering of liquefaction. They are less so for the consideration of post-trigger stability. In addition to earthquakes, liquefaction of loose materials can be triggered by foundation movements, rapid construction, a rise in seepage pressures and possibly other processes such as long term deterioration of strength."

"The formulation of steady-state concepts of shear strength (Poulos, 1981) was an important contribution to clarify the distinction between liquefaction and what is now known as cyclic mobility. It also provides a framework for evaluating the ultimate stability of a loose cohesionless material in the flowing state. In practice, there remains many difficulties to be resolved in order to determine the steady state strength with adequate precision."

"Steady state concepts do not deal with the onset of liquefaction. They only provide information on strength in the flow state. This may be adequate in some instances, particularly if the Factor of Safety in the liquefied state is in excess of unity. In this case, there is little need to assess triggering. When triggering, either by dynamic or static agencies, is of interest, the collapse surface concept advocated by Sladen et al. (1985) appears productive."

u) McRoberts and Sladen (1992)

McRoberts and Sladen (1992) agreed with Castro's (1987) conclusions, stating that "the greater part of the literature on the liquefaction of sand fosters separate methodologies: that is, the cyclic mobility or Berkeley approach versus the steady state approach to describe the same range of field phenomena. That divergent opinions exist is not new and while it would be unreasonable to attempt to resolve all aspects of controversies that have existed for over twenty years, there is scope for stating elements of the arguments and exploring common ground." McRoberts and Sladen agreed with the definition of liquefaction as stated by Castro et al. (1982).

McRoberts and Sladen followed Castro et al. (1982) in their definition that "cyclic mobility is the progressive softening of a saturated sand when subjected to cyclic loading at constant void ratio. The softening is accompanied by high pore pressures, increasing cyclic deformation, and in some cases, permanent deformations, but it does not lead to loss in shear strength nor to continuous deformation, both of which are essential aspects of liquefaction."

v) Ishihara (1993)

Ishihara made a clear distinction between level ground conditions and sloping ground conditions in terms of the liquefaction phenomena that can occur. For conditions of level ground, he concluded that the "phenomenon of cyclic softening or liquefaction is of prime concern" and that the result of this phenomenon is that "the ground starts to move back and forth with a large amplitude". On the other hand, for sloping ground conditions, Ishihara (1993) concluded that "flow failure or large lateral displacement is of major issue in addition to cyclic softening" and that if cyclic softening or liquefaction is triggered, "the ground will at least undergo large-amplitude motions causing settlements or breakage of overlying structures, as in the case of level ground". Finally, he stated that "in the worst case, the ground will start to move largely in one horizontal direction, driven even by a slightly persisting gravity-induced force, bringing about an intolerable amount of lateral deformation or flow type failure".

With respect to cyclic laboratory testing, Ishihara made the following comments:

- cyclic triaxial loading "creates stress conditions on a plane at 45° through the sample which is analogous to those produced on the horizontal plane in the ground during earthquakes"
- "it is generally observed (in such a test) that the pore water pressure builds up steadily as the cyclic axial stress is applied"

- "initial liquefaction" or simply "liquefaction" = in a cyclic triaxial test when the pore water pressure "eventually approaches a value equal to the initially applied confining pressure, thereby producing an axial strain of about 5% in double amplitude (D.A.)"
- "for loose sand, the initial liquefaction can certainly be taken as a state of softening, because infinitely large deformation is produced suddenly with complete loss of strength during or immediately following the 100% pore water pressure buildup"
- "for medium dense to dense sand, a state of softening is also produced with a nearly 100% pore water pressure buildup, accompanied by about 5% D.A. axial strain. However, the deformation thereafter does not grow indefinitely large and complete loss of strength does not take place in the sample even after the onset of initial liquefaction. Nonetheless, some degree of softening takes place in the sample accompanied by a sizable amount of cyclic strain..."
- "the onset condition of liquefaction or cyclic softening will be specified in terms of the magnitude of cyclic stress ratio required to produce 5% D.A. axial strain in 20 cycles of uniform load application. This cyclic stress ratio is sometimes referred to simply as cyclic strength."

w) Morgenstern (1994)

"The reduction to almost zero effective stress by induced pore pressures is commonly termed liquefaction. The elements of liquefaction have been understood for a long time and from the earliest works in soil mechanics, the relationship between flow slide mechanics and liquefaction has been recognized."

x) Robertson (1994)

Robertson (1994) proposed that depending on whether a sand is strain-hardening or strain-softening, as defined by state parameter, Ψ, a measure of the in-situ state relative to the steady state line, it may experience "flow liquefaction" or "cyclic liquefaction". Strain-softening material ($\Psi>0$) can experience either "flow liquefaction" or "cyclic liquefaction". However, strain-hardening material ($\Psi<0$) can only experience "cyclic liquefaction".

Robertson (1994) proposed that flow liquefaction occurs when a strain-softening material is triggered either monotonically or cyclically to "hit" the collapse surface, in terms of critical state soil mechanics, and the stress path travels towards the steady state line. The residual ultimate undrained shear strength (S_u) is determined by the conditions at steady state. Once the gravitational stresses pick up again, if the gravitational stresses are greater than S_u, flow liquefaction will occur and the nature of the deformations depend on the boundary conditions. Progressive failure can occur and the deformations can continue after the trigger event.

However, cyclic liquefaction occurs, according to Robertson (1994), when cyclic loading is large enough to cause shear stress reversal to occur. Provided that the duration of loading is long enough, the sand will eventually pass through a condition of zero effective stress with every loading cycle. This will result in a large loss of stiffness. The stress-strain curves for such sand will become "banana-shaped". Even in denser sands, although any subsequent loading will result in dilative behaviour, the loss in stiffness will affect the stress-strain response and deformations will occur. The looser the sand, the bigger the effect. The deformations will essentially stop after cyclic loading, as most of the deformation can be attributed to the accumulation of deformation during each cycle of loading which takes the sand through the condition of zero effective stress. The deformation does not occur at the point of zero effective stress, as the driving stresses at this point will also be zero; however, as load is put back on the sand as the cyclic loading continues, the sand will strain due to the loss of stiffness.

Robertson (1994) also proposed that cyclic mobility is similar to cyclic liquefaction in that it is caused by cyclic loading; however, the cyclic loading is not large enough to cause shear stress reversal. If shear stress reversal does not occur, then the condition of zero effective stress is not reached. As a result, the soil will not experience the dramatic loss of stiffness that is seen during cyclic liquefaction and the deformations will also be smaller. The deformations essentially stop after cyclic loading.

y) Yoshida et al. (1994)

"Several new features are presented ... from the point of view to predict the behaviour of sand after liquefaction. The biggest one is the appearance of low stiffness region whose size depends on the amount of cyclic loading. The stiffness of this region is very small, and the strain range is as large as several ten percents, which is a sufficient order of shear strain to cause large amount of liquefaction-induced permanent deformation. It may be recognized that this region occurs because soil particle configuration is very unstable, possible floating up in the pore water or just close to that. The phase change from low stiffness region to high stiffness region occurs because the soil particle come to a new stable configuration. This concept explains the change of material property due to cyclic loading. Therefore, the mechanism of liquefaction-induced lateral spreading is quite different [from] the ordinary discussion on residual strength or steady state under monotonic loading without cyclic loading before it." It appears that the cyclic loading in the laboratory testing by Yoshida et al. (1994) involved shear stress reversal.

z) Yasuda et al. (1994)

Abstract: "The stress-strain relationships of sand after liquefaction were studied by conducting torsional shear and triaxial compression tests under several conditions. A prescribed number of cyclic loadings were applied first, then a monotonic loading was applied in undrained condition. The stress-strain relationships during the monotonic loading are discussed. The stress-strain curves [of the subsequent monotonic loading] were affected by the accumulated excess pore pressure ratio and by the severity of liquefaction. The shear and secant modulus decreased to less than 1/1000 due to liquefaction. The shear strain increased more than 10% with very low stress in the liquefied specimen. And, there exists a so called 'reference strain at resistance transformation, γ_L' which increases with decreases in soil density, severity of liquefaction and fines content and with increase with confining pressure."

"In triaxial compression tests, the number of cycles of cyclic loading was fixed for 20 cycles in all specimens. The amplitude of the cyclic loading was controlled to accumulate a prescribed value of excess pore pressure. Therefore, in case of fully-liquefied condition, $F_L=1$ and $\Delta u/\sigma_o'=1.0$, the cyclic shear stress ratio which produce liquefaction in 20 cycles, $R_{L,20}$, was applied. If the amplitude of cyclic loading was smaller than $R_{L,20}$, liquefaction did not occur and the accumulated excess pore pressure ratio was less than 1.0" (i.e. the definition of "liquefaction" appears to be zero effective stress)

"...the distribution of the estimated permanent ground displacement " in "a model ground with gentle slope" shows that "the displacement increases from the bottom of the liquefied layer to the ground surface."

aa) McRoberts (1994)

A sand can experience a trigger, whether it is cyclic or static and its response is determined by whether it is loose or dense.

A loose sand will experience an increase in pore pressure, shear strain and, ultimately, flow since the driving stresses (cyclic or static) will be greater than its steady state strength. Level ground loose sand will experience significant settlement.

Under cyclic loading, a dense sand will not flow if its steady state strength (S_u) is greater than the driving stresses (the combined effects due to gravity, τ_o, and the cyclic loading, $\pm \Delta\tau$). However, it can experience any of the following: a reduction in stiffness; a volume strain in dry sand; or increased pore pressures due to volume strain in a saturated sand with subsequent settlement. Pore pressure generation during cyclic tests on dense materials is a consequence of the volume change that would occur during a drained test and result in settlement, but is prevented from occurring by the undrained conditions of the test. Under static loading, a dense sand will not flow if S_u is greater than the driving stresses (the combined effects due to gravity and the additional static loads).

Case histories that flow in the field should be called "liquefaction" case histories. The flow occurred due to the loss of strength in loose sand. Very loose sands have essentially no strength and thus, the steady state strength condition is essentially the same as the condition of zero effective stress. Zero strength in a cyclic test is momentarily observed because a zero effective stress condition is momentarily imposed on the soil sample. Thus, the temporary condition of zero strength occurs purely because of the loading conditions and should not be confused with "liquefaction". When dense samples are monotonically sheared after the zero effective stress condition is reached, dilation occurs and high strengths are reached that are not conducive to the development of liquefaction. The resulting deformation is not dependant on whether or not shear stress reversal occurred; it simply depends on the steady state strength. Post-earthquake surface phenomena in dense sands should not be called "liquefaction" as the sand did not experience a loss in strength.

1.2.2 Definitions adopted in this thesis

As the above section has clearly indicated, there has definitely been confusion over the years, even amongst the most well-known leaders of soil mechanics, as to what terminology should be used to describe the observed deformations that occur when a saturated sand is subjected to undrained static or cyclic loading. Liquefaction has been a broad term used to describe a large range of field response phenomena ranging from sand boils to catastrophic flowslides. Liquefaction has also be used as a generic term to describe laboratory response phenomena consisting of the increase of pore pressures and shear strains to particular levels. However, it is beginning to be clear that different responses in the field are controlled by different physics. The physics that control are a function of the state of the soil (i.e. strain-softening versus strain-hardening), the geometry of the site (i.e. level ground versus sloping ground) and the nature of the rapid undrained loading. It seems that some case histories of liquefaction failure consist of a loss in strength, while others consist primarily of a loss in stiffness, although all result in some degree of deformation. Different physics would therefore be expected to control the response of each of the two types of liquefaction. However, after failure has occurred, it can often be difficult to distinguish which type of physics controlled, based on observations of deformation alone.

Figure 1-1, presents a flowchart similar to that proposed by Robertson (1994), which proposes classifying the broad definition of liquefaction into two main categories: flow liquefaction and cyclic softening. Flow liquefaction is a phenomenon that can be triggered by either monotonic or cyclic loading, but only in strain softening material. If sufficient material strain softens and the driving stresses are greater than the undrained shear strength, a flow failure can occur. Cyclic softening (cyclic liquefaction), however, can occur in either strain softening or strain hardening material and the nature of the resulting deformations is dependent on the size and duration of cyclic loading. Following the work by Robertson (1994) and Robertson and Fear (1995), the following definitions of liquefaction are adopted in this thesis:

a) Flow liquefaction

Applies to strain softening soils only.

- Requires a strain softening response in undrained loading resulting in constant shear stress and effective stress (see Figure 1-2 which presents a schematic of a typical strain-softening response triggered by monotonic undrained loading).
- Requires in-situ shear stresses greater than ultimate or minimum undrained shear strength

- Flow liquefaction can be triggered by either monotonic or cyclic loading.
- For failure of a soil structure to occur, such as a slope, a sufficient volume of material must strain soften. The resulting failure can be a slide or a flow depending on the material characteristics and ground geometry. The resulting movements are due to internal causes and can occur after the trigger mechanism occurs.
- Can occur in any metastable saturated soil, such as very loose granular deposits, very sensitive clays and loess (silt) deposits.

This type of liquefaction is that supported by Casagrande, Castro, Poulos etc as being "true liquefaction". Examples of flow liquefaction failures include the Fort Peck Dam (Casagrande, 1965), Aberfan flowslide (Bishop, 1973), Zealand flowslide (Koppejan et al., 1948) and the Stava Tailings Dam, which has been described at the beginning of this chapter. Flow liquefaction failures are not common, but when they do occur, they take place rapidly, with little warning, and are usually catastrophic.

b) Cyclic softening

Two terms can be used to define cyclic softening. Applies to both strain softening and strain hardening soils.

(i) Cyclic liquefaction

- Requires undrained cyclic loading during which shear stress reversal occurs or zero shear stress can develop (i.e. occurs when in-situ static shear stresses are low compared to cyclic shear stresses), as illustrated in Figure 1-3.
- Requires sufficient undrained cyclic loading to allow effective stress to reach essentially zero.
- At the point of zero effective stress, no shear stress exists. When shear stress is applied, pore pressure drops as the material tends to dilate, but a very soft initial stress strain response can develop resulting in large deformations.
- Deformations during cyclic loading can accumulate to large values, but generally stabilize when cyclic loading stops. The resulting movements are due to external causes and occur only during the cyclic loading.
- Can occur in almost all sands provided that the cyclic loading is sufficiently large in size and duration.
- Clayey soils can experience cyclic liquefaction but deformations are generally small due

to the cohesive strength at zero effective stress. Deformations in clay soils are often controlled by rate effects (creep).

(ii) Cyclic mobility

- Requires undrained cyclic loading during which shear stresses are always greater than zero; i.e. no shear stress reversal develops.
- Zero effective stress will not develop.
- Deformations during cyclic loading will stabilize, unless the soil is very loose and flow liquefaction is triggered. The resulting movements are due to external causes and occur only during the cyclic loading.
- Can occur in almost any sand provided that the cyclic liquefaction is sufficiently large in size and duration, but no shear stress reversal occurs.
- Clays can experience cyclic mobility but deformations are usually controlled by rate effects (creep).

This type of liquefaction is the type studied by the H.B. Seed and the Berkeley group of researchers. Examples of cyclic softening could be seen after the major earthquakes in Niigata in 1964 and in Kobe in 1995 (as described earlier in this chapter), in the form of sand boils, damaged lifelines (pipelines, etc.), lateral spreads, slumping of small embankments and ground surface cracks. It is important to note that site specific conditions, such as overlying less permeable layers that can restrict drainage paths, can lead to flow liquefaction after cyclic liquefaction, as a result of loosening of a sand due to pore water redistribution, given the right geometry.

Further details regarding the definitions of flow liquefaction and cyclic softening can be found in Robertson and Fear (1995). Flow liquefaction and cyclic softening can both result in large deformations. However, flow liquefaction is generally characterized by a loss in soil strength leading to "spontaneous" flow failures if sufficient material strain-softens (as a result of either a monotonic or cyclic trigger) and a kinematically admissible mechanism develops. Cyclic softening, on the other hand, generally involves deformations which accumulate during cyclic loading (e.g. earthquake loading) as a result of a loss in soil stiffness. Flow liquefaction potential is controlled by soil state (density and stresses) and grain characteristics. Cyclic softening potential is controlled by soil state and the size and duration of cyclic loading. Flow liquefaction failures generally occur in sloping ground in which a kinematically admissible mechanism can develop. Cyclic softening failures generally occur in level or gently sloping ground in which shear stress reversal can occur (i.e. cyclic liquefaction occurs). Different physics control the two phenomena and, therefore, a different framework is necessary to link laboratory and field data for each case.

1.3 Current Practice

Current practice does not always distinguish between flow liquefaction and cyclic softening, as defined above. The traditional empirical methods of design against earthquake-induced liquefaction have often been applied to both level ground and sloping ground conditions, with empirical correction factors applied to the case of sloping ground. However, these methods do not work for designing against statically-induced liquefaction, because they involve the calculation of a cyclic stress ratio induced by an earthquake. As a result, steady state concepts were developed to explain statically triggered flowslides. Similar methods should also be applied when designing against cyclically triggered flow liquefaction, as it is not the nature of the trigger that matters with flow liquefaction, but whether or not the material is strain-softening and the relative magnitudes of the driving stresses and the undrained shear strength of the sand.

1.3.1 Evaluation of liquefaction potential

The most widely used method for estimating cyclic softening (liquefaction) potential is the simplified method by Seed et al. (1985), based on a large database of case histories for which an earthquake-induced cyclic stress ratio (CSR) could be calculated and standard penetration test (SPT) data were available. The standard penetration test (SPT) is the most commonly used method to investigate in-situ liquefaction potential. The measured blowcounts per foot, N, as the SPT sampler is driven into the ground give an indication of the density of the soil. In general, the higher the measured blowcount, the denser the soil. However, it is extremely important to correct the measured blowcount for overburden stresses and energy effects (Seed et al., 1985; Robertson and Fear , 1995). Overburden stresses have the effect of increasing the measured blowcount, for the same density of soil. Different SPT setups impart different amounts of energy to the sampler; a higher imparted energy has the effect of decreasing the measured blowcount, for the same density of soil. Once the measured blowcounts have been corrected for both overburden and energy effects, the corrected blowcount, $(N_1)_{60}$, can be used to estimate liquefaction potential at a site using the simplified method by Seed et al. (1985). This method and other current methods of evaluating liquefaction potential will be presented in greater detail in subsequent chapters.

Various methods have been developed to estimate flow liquefaction potential based on steady state concepts. These include field observations of statically triggered failures and non-failures in the Beaufort Sea by Sladen and Hewitt (1989) and estimations of state parameter from the CPT by Been and Jefferies (1992) and Plewes et al. (1992). The state parameter approach was based on previous studies by Been and Jefferies (1985) and Been et al. (1987), based on calibration chamber testing of the CPT. These methods will be presented in greater detail in subsequent chapters.

1.3.2 Evaluation of undrained shear strength

Once a sand is evaluated as having the potential for flow liquefaction, given a suitable trigger mechanism, one of the most commonly used methods of estimating the undrained shear strength of a sand is a correlation between undrained shear strength (S_u) and equivalent clean sand $(N_1)_{60}$ by Seed and Harder (1990) which draws on earlier work by Seed (1987). This correlation is based on 17 case histories, ranging from lateral spreads to major flowslides, for which SPT data was available. This method and other current methods of estimating undrained strength will be presented in greater detail in subsequent chapters.

1.3.3 Problems with current practice

The Seed et al. (1985) methodology for evaluating cyclic softening (liquefaction) potential was based on extensive field performance data from essentially level ground sites which either had or had not experienced cyclic softening (liquefaction) due to earthquake loading. Liquefaction was assumed to have occurred based on the presence of observable surface features such as sand boils and ground cracks. The field observation data used to compile these curves are apparently based on the following:

Holocene age deposits
Level or gently sloping ground
Magnitude M=7.5 earthquakes
Depth range from 1 to 14 m (3 to 47 ft)
  N.B. 90% of data is for depths < 10 m (32ft)
Representative average SPT N values for the layer that was considered to have experienced cyclic liquefaction

Hence, caution should be exercised when extrapolating the correlation to conditions outside of the range. Applying the method to sloping ground conditions is not appropriate, even with the empirical correction factors suggested by Seed and Harder (1990). Most steeply sloping ground will be more likely to suffer from flow liquefaction (from a cyclic or static trigger) than cyclic softening (liquefaction). Therefore, extrapolating the correlations based on cyclic liquefaction in level ground conditions to evaluating flow liquefaction potential in sloping ground is not appropriate. In addition, the Seed methodology has many uncertainties. The correlations are empirical and there is some uncertainty over the degree of conservatism in the correlations as a result of the methods used to select representative values of penetration resistance within the layers assumed to have liquefied. The detailed investigation at Duncan Dam (Byrne et al., 1994) which consisted of both in-situ testing and laboratory testing of undisturbed samples, raised some of these issues.

The evaluation of flow liquefaction potential differs depending on the method that is used. The field observation based method by Sladen and Hewitt (1989) appears to disagree with the CPT inferred state parameter methods by Been and Jefferies (1992) and Plewes et al. (1992). The method by Been and Jefferies (1992) appears to be much more unconservative than the method by Sladen and Hewitt (1989). This poses a dilemma to the geotechnical engineer: at a particular site, it would not be surprising if the method by Sladen and Hewitt (1989) predicts that flow liquefaction will occur, given a suitable trigger, while the method by Been and Jefferies (1992) predicts that the material is sufficiently resistant and cannot be triggered.

Once a material is considered to be susceptible to flow liquefaction, the relationship by Seed and Harder (1990) for estimating the undrained strength of liquefied sand presents another dilemma to the geotechnical engineer, as it consists of upper and lower bound lines. It is not uncommon to find that the upper bound line will result in an acceptable factor of safety whereas the lower bound line will suggest a potentially unstable condition. Conservative practice often leads engineers to use the lower bound line which may result in unnecessary expenditures.

In addition, the relationship by Seed and Harder (1990) combines case histories which are likely examples of cyclic softening (liquefaction) with those that are examples of flow liquefaction. Estimating an undrained shear strength for evaluating stability once a zone of material in a slope is predicted to be susceptible to flow liquefaction, given a suitable trigger, is logical. However, estimating an undrained shear strength for cases of cyclic (softening) liquefaction may give erroneous results. Deformations that occur will take place and accumulate only during cyclic loading as a result of the temporary loss in soil stiffness. Therefore, a stability analysis based on an estimated undrained shear strength does not model the correct physics. Other methods are more suitable for evaluating the magnitude of deformations as a result of cyclic liquefaction.

1.4 Thesis Objectives

The examples of damage to the Kobe port and failure of the Stava tailings dam, given at the beginning of this chapter, indicate the range of consequences that can arise from liquefaction. Liquefaction-induced failures can have major financial implications, pose a serious threat to human safety and may have a significant impact on the environment. It is obvious that minimizing these hazards is the goal of the geotechnical engineer. However, many of the approaches used in current practice are empirical and some are potentially unduly conservative.

The overall goal of this research is to distinguish between flow liquefaction and cyclic softening and develop a framework for evaluating the potential for either type of liquefaction at a given site. The framework will combine in-situ testing with laboratory results from testing undisturbed samples.

1.4.1 Cyclic softening

Since the most commonly used method of evaluating cyclic softening (liquefaction) is the method by Seed et al. (1985), it is logical to first reassess the suggested correlations between cyclic resistance ratio (CRR) and SPT $(N_1)_{60}$ by reviewing the corresponding database of case histories. Chapter 2 presents the results of such a study, using a consistent weak-link-in-the-chain approach to selecting the representative $(N_1)_{60}$ for each case record.

The SPT, however, can often be unreliable. The CPT is preferable because of its continuous nature and greater repeatability and reliability. Therefore, Chapter 3 presents an integrated CPT method for evaluating cyclic softening (liquefaction) potential. The proposed framework allows for a comparison with results from cyclic tests on undisturbed samples in the laboratory such that site specific corrections to the individual components of the framework can be made.

1.4.2 Flow Liquefaction

Chapter 4 presents a framework to evaluate whether a soil is strain-softening and, therefore, susceptible to flow liquefaction. The framework links in-situ test signatures from the SPT, CPT, shear wave velocity measurements and geophysical logs to the response observed in the laboratory when undisturbed samples are tested under different directions of loading. The goal of the chapter is to propose a method for developing a site-specific correlation between estimated response and in-situ testing such that flow liquefaction potential can be evaluated across the site based on limited localized undisturbed sampling and testing. If the site-specific correlations appear general in nature, they would be useful for interpreting in-situ testing for a low risk project (for which undisturbed sampling is beyond the project scope) or preliminary site screening for a high risk project.

For flow liquefaction considerations, one of the most important components of response is the resulting undrained strength of the sand. Chapter 5 presents a method of estimating the undrained strength from in-situ testing, based on critical state soil mechanics and an empirical relationship between measured shear wave velocity and void ratio. The method is extended to estimate undrained strengths from the SPT and CPT using site-specific correlations between shear wave velocity and SPT or CPT penetration resistance. Comparisons are then made with the current methods of estimating undrained strengths from in-situ testing.

Chapter 6 summarizes an experimental field testing program that was undertaken to investigate the potential of downhole plate load tests as an alternative method for estimating the undrained strength of sand. The program was preliminary in nature and only a limited amount of data are available. The results of analyzing the data are presented, illustrating that the findings appeared promising. The chapter recommends how further testing could be performed to further investigate the potential of downhole plate load tests as an alternative in-situ test.

The most commonly used method of estimating the undrained strength of sand is the empirical, SPT-based method proposed by Seed and Harder (1990). However, the type of case history incorporated in the method ranges from a lateral spread to a major flowslide.

This suggests that the empirical chart combines cases of cyclic softening (liquefaction) and flow liquefaction. Undrained shear strength is only truly meaningful for flow liquefaction, when a material strain-softens. Cases of cyclic liquefaction deform primarily as a result of loss in stiffness; an undrained shear strength is not relevant. Therefore, Chapter 7 reviews these case histories from this point of view, trying to distinguish between the two types of case histories. The choice of the representative $(N_1)_{60}$ for each case history is also briefly discussed.

1.4.3 Practical applications

Chapter 8 presents a worked example illustrating how both the framework for evaluation of cyclic softening (liquefaction) potential and the framework for evaluation of flow liquefaction potential and subsequent response can be applied at a given site. The worked example is the Massey Tunnel site in the Fraser River Delta of British Columbia. The site was one of the Canadian Liquefaction Experiment (CANLEX) sites at which substantial in-situ testing, undisturbed sampling and laboratory testing was performed.

Chapter 9 provides a general discussion and conclusions regarding the application of the proposed methods for evaluating both cyclic softening (liquefaction) and flow liquefaction potential. The chapter recommends a family of solutions, based on the level of risk of the specific project. Cautionary notes and limitations of the proposed methods of liquefaction are also given. Finally, recommendations for future studies are given.

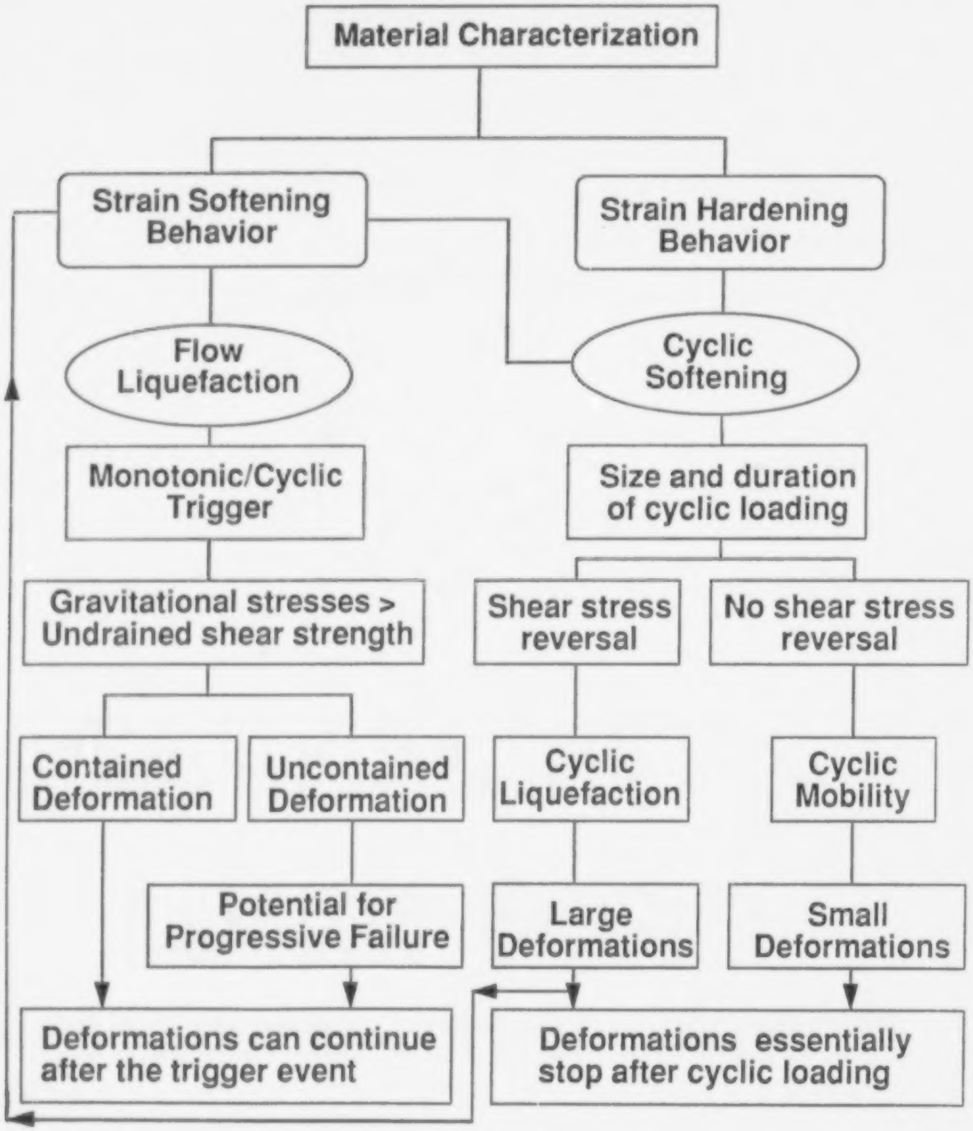
Material Characterization
Strain Softening Behavior
Strain Hardening Behavior
Flow Liquefaction
Cyclic Softening
Monotonic/Cyclic Trigger
Size and duration of cyclic loading
Gravitational stresses > Undrained shear strength
Shear stress reversal
No shear stress reversal
Contained Deformation
Uncontained Deformation
Cyclic Liquefaction
Cyclic Mobility
Potential for Progressive Failure
Large Deformations
Small Deformations
Deformations can continue after the trigger event
Deformations essentially stop after cyclic loading

Figure 1-1 Flowchart for evaluating soil liquefaction (modified from Robertson, 1994).

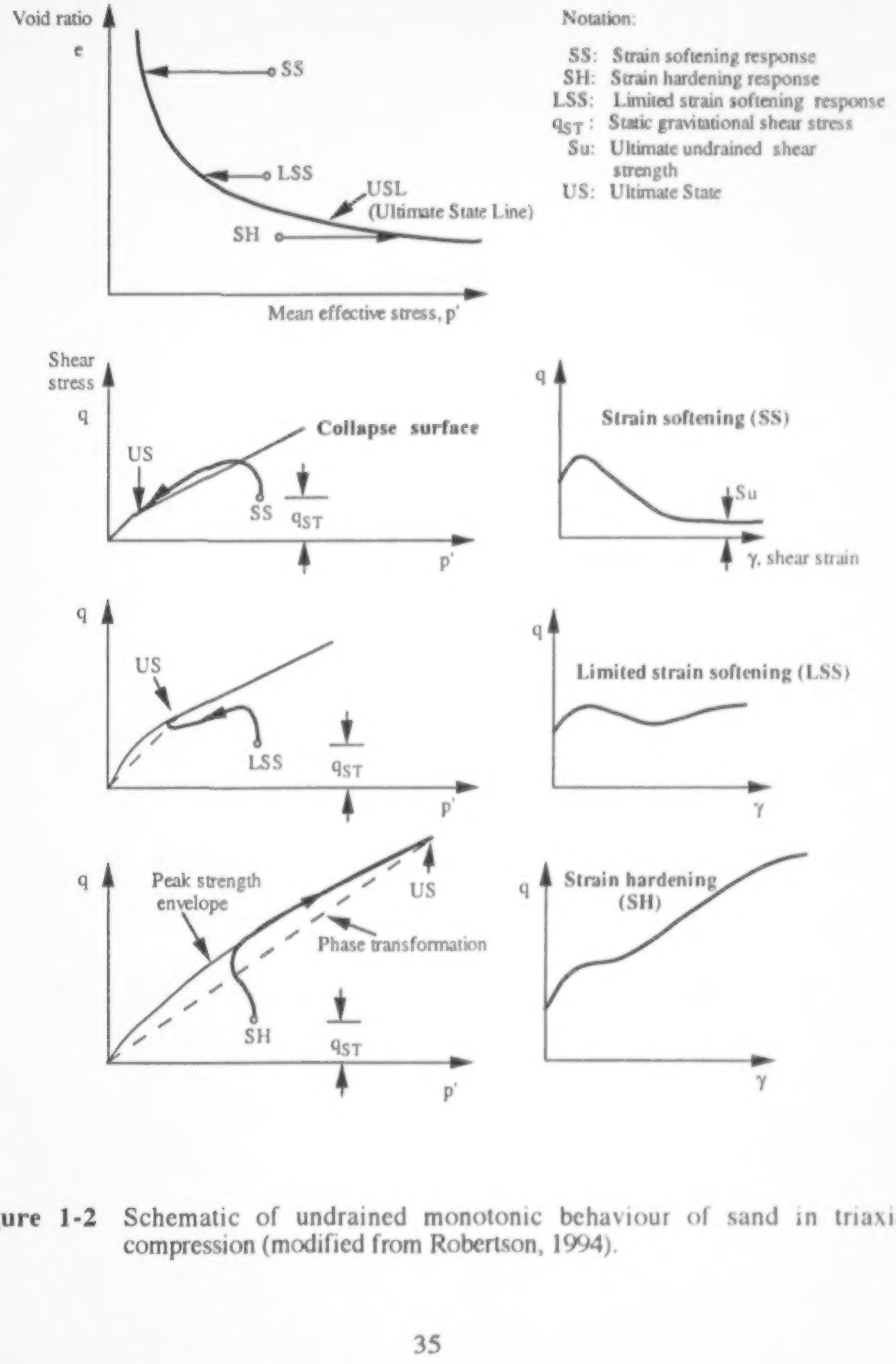
Void ratio
e
SS
LSS
USL
(Ultimate State Line)
SH
Mean effective stress, p'
Notation:
SS: Strain softening response
SH: Strain hardening response
LSS: Limited strain softening response
q_{ST}: Static gravitational shear stress
Su: Ultimate undrained shear strength
US: Ultimate State
Shear stress
q
Collapse surface
US
SS
q_{ST}
p'
q
Strain softening (SS)
Su
γ, shear strain
q
US
LSS
q_{ST}
p'
q
Limited strain softening (LSS)
γ
q
Peak strength envelope
US
Phase transformation
SH
q_{ST}
p'
q
Strain hardening (SH)
γ

Figure 1-2 Schematic of undrained monotonic behaviour of sand in triaxial compression (modified from Robertson, 1994).

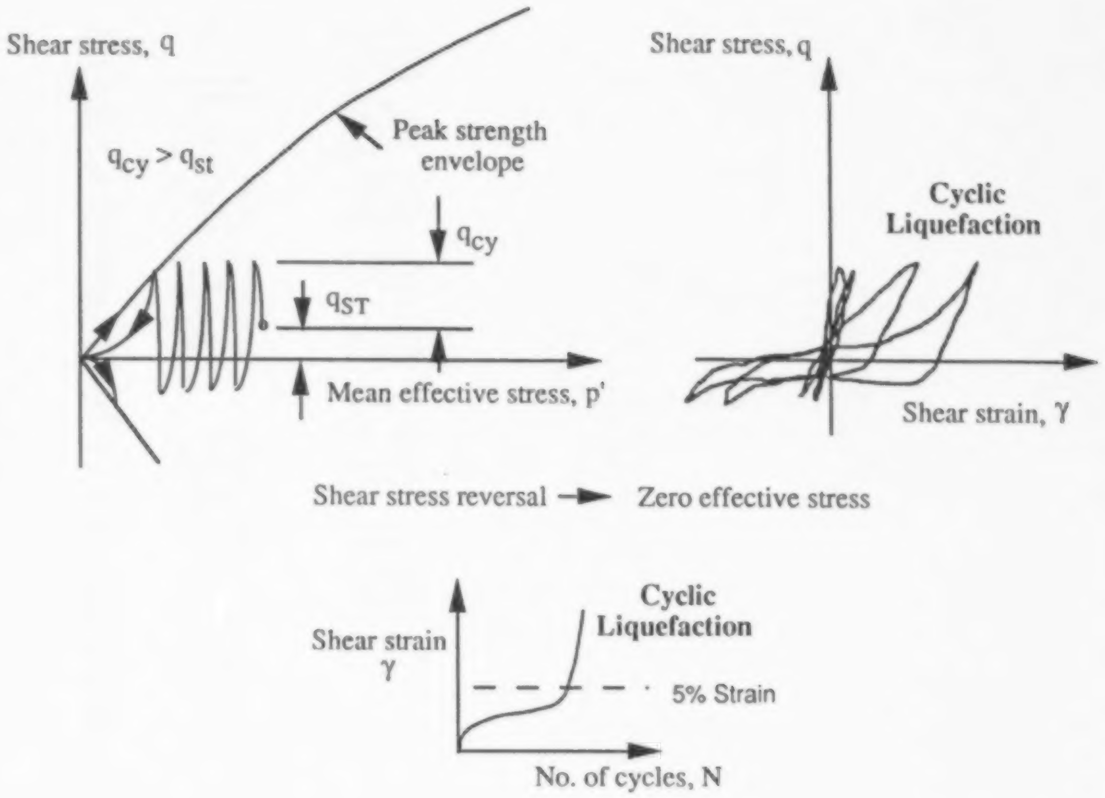
Shear stress, q
$q_{cy} > q_{st}$
Peak strength envelope
q_{cy}
q_{ST}
Mean effective stress, p'
Shear stress, q
Cyclic Liquefaction
Shear strain, γ
Shear stress reversal → Zero effective stress
Shear strain γ
Cyclic Liquefaction
5% Strain
No. of cycles, N

Figure 1-3 Schematic of undrained cyclic behaviour of sand illustrating cyclic liquefaction (modified from Robertson, 1994).

References

Been, K., and Jefferies, M.G. 1985. A state parameter for sands. *Géotechnique*, 35(2): 99-112.

Been, K., and Jefferies, M.G. 1992. Towards systematic CPT interpretation. *Proceedings of the Wroth Symposium*, 44-55.

Been, K., Jefferies, M.B., Crooks, J.H.A., and Rothenburg, L., 1987. The cone penetration test in sands, Part 2: General inference of state, *Géotechnique*, 37(3): 285-299.

Bishop, A.W. 1973. The stability of tips and spoil heaps. *Quarterly Journal of Engineering Geology*, 6: 335-376.

Byrne, P.M., Imrie, A.S., and Morgenstern, N.R. 1994. Results and implications of seismic performance studies for Duncan Dam. *Canadian Geotechnical Journal*, 31(6): 979-988.

Casagrande, A. 1936. Characteristics of cohesionless soils affecting the stability of earth fills. *J. Boston Society of Civil Engineers*, 23, 257-276.

Casagrande, A. 1965. Role of the 'calculated risk' in earthwork and foundation engineering. The Terzaghi Lecture, *J. of Soil Mech. and Found. Div.*, ASCE 91(SM4), 1-40.

Casagrande, A. 1969. Personal communication to Bjerrum, Peck, Richart, Seed, Whitman and Wilson, attached to Casagrande (1975a).

Casagrande, A. 1975a. Personal communication to R.M. Hardy.

Casagrande, A. 1975b. Liquefaction and cyclic deformation of sands - a critical review. *Proc. 5th Pan-American Conference*, Argentina, 81-133.

Castro, G. 1987. On the behaviour of soils during earthquakes - liquefaction. *Proc. 3rd International Conference on Soil Dynamics and Earthquake Engineering*.

Castro, G., Enos, J.L., France, J.W. and Poulos, S.J. 1982. Liquefaction induced by cyclic loading. *Report to National Science Foundation*, Washington, D.C., No. NSF/CEE-82018.

Committee on Soil Dynamics of the Geotechnical Engineering Division 1978. Definition of terms related to liquefaction. *Journal of the Geotechnical Engineering Division*, ASCE 104(GT9): 1197-1200.

D'Appolonia, E., and Morgenstern, N.R. 1988. Evaluation of the cause of failure of the Stava Embankment. *Private report to Montedison S.A.*.

Davis, A.P. Jr., Castro, G. and Poulos, S.J. 1988. Strengths backfigured from liquefaction case histories. *Proceedings, 2nd International Conference on Case Histories in Geotechnical Engineering*, St. Louis, Paper No. 4.35, 1693-1701.

Hazen, A. 1918. A study of the slip in the Calaveras Dam. *Engineering News-Record*, 81, 26, 1158-1164.

Hazen, A. 1920. Hydraulic fill dams. *Transactions*, ASCE 83, 1713-1745.

Hazen, A. and Metcalf, L. 1918. Middle section of upstream side of Calaveras Dam slips into reservoir. *Engineering News-Record*, 80, 14, 679-681.

Holzer, T.L. 1995. The 1995 Hanshin-Awaji (Kobe), Japan, earthquake. GSA Today, *A publication of the Geological Society of America*, 5(8).

Hutchinson, J.N. 1988. Morphological and geotechnical parameters of landslides in relation to geology and hydrogeology. *Proc. 5th In. Symp. on Landslides*, 1, 3-35, Lausanne.

Ishihara, K. 1993. Liquefaction and flow failure during earthquakes. The 33rd Rankine Lecture, *Géotechnique*, 43(3), 351-415.

Koppejan, A.W., Van Wamelen, B.M., and Weinberg, L.J.H. 1948. Coastal landslides in the Dutch province of Zealand. *Proceedings of the 2nd International Conference on Soil Mechanics and Foundation Engineering*, Rotterdam, Holland, 89-96.

McRoberts, E.C. (1994). Personal discussions.

McRoberts, E.C. and Sladen, J.A. 1992. Observations of static and cyclic sand liquefaction methodologies. *Canadian Geotechnical Journal*, 29, 4.

Mogami, T. and Kubo, K. 1953. The behaviour of soil during vibration. *Proc. 3rd International Conference on Soil Mechanics and Foundation Engineering*, 1, 152-153.

Morgenstern, N.R. 1992. The evaluation of slope stability - a 25 year perspective. *Stability and Performance of Slopes and Embankments - II*, 1, 1-25.

Morgenstern, N.R. 1994. Observations on the collapse of granular materials. The Kersten Lecture, *42nd Annual Geotechnical Engineering Conference*, Minneapolis, Minnesota.

National Research Council 1985. *Liquefaction of soils during earthquakes*. Committee on Earthquake Engineering, G.W. Housner (Chairman), National Academy Press.

Plewes, H.D., Davies, M.P, and Jefferies, M.G. 1992. CPT based screening procedure for evaluating liquefaction susceptibility. *Proceedings of the 45th Canadian Geotechnical Conference*, Toronto, Ontario, 4:1-4:9.

Poulos, S.J. 1981. The steady state of deformations. *J. Geotech. Eng. Div.*, ASCE 107: 553-562.

Poulos, S.J. 1988. Liquefaction and related phenomena. *Advanced Dam Engineering for Design, Construction and Rehabilitation*, R. B. Jansen (ed.), 292-320.

Poulos, S.J., Castro, G., and France, J.W. 1985. Liquefaction evaluation procedure. *J. of Geotech. Engrg.*, ASCE 111(GT6), 772-795.

Robertson, P.K. 1994. Suggested terminology for liquefaction. *Proceedings of the 47th Canadian Geotechnical Conference*, Halifax, Nova Scotia, 277-286.

Robertson, P.K. and Fear, C.E. 1995. Liquefaction of sands and its evaluation. *IS Tokyo '95, First International Conference on Earthquake Geotechnical Engineering*, Keynote Lecture, 3.

Seed, H.B. 1979. Soil liquefaction and cyclic mobility evaluation for level ground during earthquakes. *J. Geotech. Eng. Div.*, ASCE 105(GT2), 201-255.

Seed, H.B. 1987. Design problems in soil liquefaction. *J. Geotech. Engrg.*, ASCE 113(8), 827-845.

Seed, H.B. and Lee, K.L. 1966. Liquefaction of saturated sands during cyclic loading. *J. of the Soil Mech. and Found. Div.*, ASCE, November.

Seed, H.B., Tokimatsu, K., Harder, L.F., and Chung, R. 1985. Influence of SPT procedures in soil liquefaction resistance evaluations. *Journal of Geotechnical Engineering*, ASCE 111(12): 1425-1445.

Seed, R.B. and Harder, L.F. 1990. SPT-based analysis of cyclic pore pressure generation and undrained residual strength. *H. Bolton Seed Memorial Symposium Proceedings*, 2, 351-376.

Sladen, J.A., D'Hollander, R.D., and Krahn, J. 1985. The liquefaction of sands, a collapse surface approach. *Canadian Geotechnical Journal*, 22: 564-578.

Sladen, J.A., and Hewitt, K.J. 1989. Influence of placement method on the in situ density of hydraulic sand fills. *Canadian Geotechnical Journal*, 26: 453-466.

Terzaghi , K. 1925 *Erdbaumechanik*. Franz Deuticke, Vienna.

Terzaghi, K. and Peck, R.B. 1948. *Soil mechanics in engineering practice*, p. 108 in the second edition, John Wiley and Sons, Inc.

Yasuda, S., Masuda, T., Yoshida, N., Nagase, H., Kiku, H., Itafuji, S., Mine, K., and Sato, K. 1994. Torsional shear and triaxial compression tests on deformation characters of sands before and after liquefaction. *US-Japan Workshop*.

Yoshida, N., Yasuda, S., Kiku, M., Masuda, T., and Finn, W.D. 1994. A fundamental study for predicting the behavior of sand after liquefaction. *US-Japan Workshop*.

CHAPTER 2

REASSESSMENT OF CURRENT PRACTICE USED FOR EVALUATING CYCLIC LIQUEFACTION POTENTIAL BASED ON THE STANDARD PENETRATION TEST (SPT)[1]

2.1 Introduction

In earthquake design of saturated sandy soils, a fundamental issue is whether or not the design earthquake could initiate phenomena such as lateral spreading, cracking, settlement, sand boils, flow slides, buoyancy, and loss of bearing capacity. These phenomena taken together are often referred to as liquefaction. Figure 2-1 presents the primary source of current practice for predicting the initiation of what is called liquefaction, based on the well known work of Seed et al. (1984) who presented a catalogue of 125 case records referred to here as the Berkeley catalogue. These plots define an empirical state line between case records that were designated as having liquefied and those that did not. The case records embraced by the Berkeley catalogue are cited as being for level ground and the extension of these data to the design of sloping ground, dams and other structures has been presented by Seed (1983) and Rollins and Seed (1990). Professional and regulatory practice often adopts this work as a design method and to a significant extent, it also forms a standard against which other theories and methods of liquefaction assessment are judged.

The most significant aspect of the Berkeley catalogue is the assignment of a single Standard Penetration Test (SPT) $(N_1)_{60}$ value to describe the state of the sand for a given case record. The objective of this study was to reconsider the Berkeley catalogue selection of $(N_1)_{60}$ data. While much use has been made of the original work, many of the case records are difficult to obtain, and the raw data is not available in the original catalogue. Fear and McRoberts (1993) have recently summarized all of the original data in catalogue form[2], including all of the borehole logs that could be located. The objective of this chapter is to summarize the major findings of this work.

---

[1] *A version of this chapter has been published. Fear, C.E. and McRoberts, E.C. 1995. Reconsideration of Initiation of Liquefaction in Sandy Soils. Journal of Geotechnical Engineering, ASCE 121(3): 249-261.*

[2] *Fear, C.E. and McRoberts, E.C. 1993. Report on liquefaction potential and catalogue of case records, Internal Research Report, Geotechnical Engineering Library, Department of Civil Engineering, University of Alberta. The report is available from the Geotechnical Engineering Group at the University of Alberta.*

This study has adopted the approach of characterizing liquefaction or non-liquefaction with a single $(N_1)_{60}$ value. However, it is argued, in agreement with general design practice that, all else being equal, the layer with the lowest $(N_1)_{60}$ would have the least resistance against liquefaction. Hence, a "weakest-link-in-the-chain" approach was consistently used in this study. This is, in general, a different approach than was used in the original work and is considered to be a justifiable method for reconsidering the data. This study primarily restricts itself to a reconsideration of the $(N_1)_{60}$ data component of the case records. The state of the sand, as measured by the $(N_1)_{60}$ value, is, of course, not the only factor affecting liquefaction potential. Clearly, the magnitude and acceleration of the earthquake, depth of the weak layer and depth of the groundwater table, as embraced by the average cyclic stress ratio (CSR) are key parameters. This study adopts the original methodology for calculating this ratio, but reassigns the CSR and fines content data as appropriate for the new selection of $(N_1)_{60}$ representing the weakest state of the sand. Case records in clean sands (percent passing the No. 200 sieve $\leq 5\%$) and those in silty sands are kept separate as they were in the original work.

As discussed in the National Research Council (NRC, 1985) summary, there are many other factors which also influence the response of a particular site to ground motion. Site topography can be a factor and, while the original catalogue was for level ground, there are cases where some modest slopes or additional loading were present. Site drainage and, in particular, the influence exerted by impedance of seepage, potentially further complicated by both hydraulic fracturing and density changes (water content redistribution), clearly exert possible influences. Other soil factors such as aging, grain size distribution, gravel content effects, in-situ stresses and so on will all exert effects as well. It might be said that there are so many other factors in addition to the triad of major factors considered here (CSR, $(N_1)_{60}$, fines content) that it is imprudent to base any consideration of liquefaction on such restricted grounds. Certainly the experienced designer will not rely solely on such a simplistic approach, but the predictions offered can be useful at a screening level. While some of the other factors that influence liquefaction may have been subjectively considered in the Berkeley work, there are no records available to indicate what may have been done.

This study finds that, in many cases, the Berkeley catalogue did not select a minimum value of $(N_1)_{60}$. From a design perspective, this can be a particularly significant issue as practice tends to focus on identifying the loosest zone and then applying the Seed et al. (1984) criterion to this layer. A conservatively-biased criterion that is accepted in practice makes it exceptionally difficult to introduce alternative technologies and design methodologies, especially in terms of regulatory opinions and design precedents in high risk design environments. It can be argued, given the implications of liquefaction failure and the variety of difficulties and unknowns associated with the case records, that a conservative assessment is justified. However, it should be explicitly understood that this is the case. In many other situations, on a site specific basis, more economical designs justified by investigation and testing may be appropriate.

2.2 Methodology

The approach of the Berkeley catalogue was simple and straightforward in that either there were or were not surface manifestations during or after an earthquake and, hence, it was concluded that liquefaction either had or had not occurred. It is recognized, following the concerns that were first raised by Casagrande (1976) and were recently reviewed by McRoberts and Sladen (1992), Ishihara (1993), Youd (1993), and Robertson (1994), that definitions of what does or does not constitute liquefaction is being actively discussed in the geotechnical community. This study adopted the original definitions of liquefaction used by the Berkeley catalogue. If surface features such as sand boils, cracking, lateral spreading or settlement were seen, the case record was classified as "liquefied" (indicated by the solid symbols in Figure 2-1). However, if no surface features were visible, either during or after the earthquake, the case record was classified as "non-liquefied" (indicated by the open symbols in Figure 2-1). In addition, a few case records in the Berkeley catalogue were classified as having "marginal liquefaction" (indicated by the cross symbols in Figure 2-1). Another category entitled "pressure relief" was added in this study for case records for which sand boils were the only surface feature observed at the site. This "pressure relief" category was added in order to explore the possible differences between sand boils and other liquefaction responses to seismic actions. This study used the same symbols in subsequent plots for case records that were reclassified as pressure relief and for those for which the classification was left as marginal liquefaction, as given in the Berkeley catalogue, as it was felt that they likely represented similar phenomena.

Following Ambraseys' (1988) numbering system, the Berkeley catalogue of 125 case records was expressed as 123 case records (four case records were merged into two). The reference papers cited by Seed et al. (1984) were obtained for each of these case records with a few exceptions (Cluff (1973), Dames and Moore (1975), Seed (1973), and Tsuchida (1979)). Information summary sheets and borehole logs for all of the case records and the complete reference list are contained in Fear and McRoberts (1993).

In the Berkeley catalogue, each case record was reduced to a single pair of SPT $(N_1)_{60}$ and CSR, reflecting state and loading, respectively. The in-situ relative density is reflected by $(N_1)_{60}$, which is the SPT blowcount typically corrected to a vertical effective stress of 1 tsf using a correction, C_N, and an applied energy ratio (ER) of 60%, as summarized below:

$$[2\text{-}1] \qquad (N_1)_{60} = C_N\left(\frac{ER}{60}\right)N$$

where:
$(N_1)_{60}$ = corrected SPT blowcount
C_N = correction for vertical effective stress (see Equation 2-3, later in the chapter)
N = raw SPT blowcount
ER = energy ratio applied to the SPT hammer, in percent.

The CSR is a measure of the amount of shear stress induced by the earthquake at a level ground site, relative to the initial vertical effective stress, and can be calculated using the following formula (after Seed et al., 1984):

$$[2\text{-}2] \qquad CSR = 0.65\,\frac{a_{max}}{g}\,\frac{\sigma_o}{\sigma'_o}\,\frac{r_d}{r_m}$$

where:
a_{max} = maximum earthquake acceleration at the ground surface
g = gravitational acceleration = 9.81 m/s^2
σ_o = initial vertical total stress
σ'_o = initial vertical effective stress
r_d = factor to account for variation in earthquake acceleration with depth
= 1 - 0.010z in this study, where z is the critical depth, in metres
(N.B. this equation for r_d was selected to match the correlation proposed by Seed and Idriss (1982) and used in the Berkeley catalogue as closely as possible)
r_m = factor to convert between equivalent CSR for earthquake of Magnitude 7.5 and CSR for earthquake of magnitude M (Table 5 in Seed et al., 1984).

All else being equal, the layer with the lowest $(N_1)_{60}$ will have the least resistance against liquefaction. Thus, this study focused on the selection of the minimum $(N_1)_{60}$ for each case record and the CSR was recalculated if necessary. Selection of the minimum $(N_1)_{60}$ value is open to the criticism that the lowest value may actually be a testing error. In this study, all data were accepted at face value. In addition, variations in CSR occur with depth and are further complicated by the level of the groundwater table. It would therefore seem possible to have a combination of state and loading at another depth in a borehole which might have less resistance against liquefaction than the minimum $(N_1)_{60}$ and the corresponding CSR. However, the magnitude of the CSR is dominated by the earthquake acceleration at a specific site. As a result, the variations in CSR with depth over the depths under consideration in this study (generally less than 13.0 m, the maximum depth in the Berkeley catalogue, with only 9 case records between 13.0 m and a maximum depth of 19.5 m) are relatively small compared to the large variations in $(N_1)_{60}$ with depth. Therefore, following the logic outlined by Liao and Whitman (1986) by selecting the minimum $(N_1)_{60}$ and then calculating the corresponding CSR seems to be a reasonable way of characterizing the liquefaction resistance of a particular borehole.

The basis for the selection of N in the Berkeley catalogue is not clear and, as expressed by Liao and Whitman (1986), who presented a recent summary of previous liquefaction catalogues, the methodology used in the Berkeley catalogue was not explicitly stated nor consistently followed. The only specific citation as to the methodology followed that has been located is a table in both Seed and Peacock (1971) and Seed and Idriss (1971) which presented an early version of the Berkeley catalogue and included a column labelled as the "average penetration resistance at critical depth, N". Liao and Whitman (1986) considered that a close inspection of Seed et al. (1975, 1984) shows that choosing the minimum N_1-value in each boring or profile is in most cases equivalent to the Berkeley characterization. However, this study found that the $(N_1)_{60}$ in the Berkeley catalogue was a minimum value only for some cases; for many other cases, it could be considered to be an average value over some portion of the borehole and, for a few cases, it was a high value.

The question of site characterization with more than one borehole must also be considered. As noted by Liao and Whitman (1986), sites tend to be characterized by a single value of SPT N. They also commented that how this value is selected as being representative of a single boring profile or of the entire site is often not very clear or consistent. Liao and Whitman (1986) argued that it is best to consider each individual boring as a case study and to select the minimum $(N_1)_{60}$ from each boring to represent the soil conditions for the case study. This would be preferable to either considering all of the borings in the liquefied zone of a site as one case study and the borings in the non-liquefied zone as a second case study (resulting in two case records) or considering each blowcount in each boring as a case study (resulting in numerous case records). According to Liao and Whitman (1986), the former would result in problems with site characterization and the latter would result in a lack of statistical independence between case records. This study considered each borehole as an individual case record, where possible, and, in particular, when extra boreholes were obtained from a particular site in addition to a typical log. This was the case for the Luan Nan (case record 56) and Le Ting (case record 57) sites in the original database. It appears that the study conducted by Seed et al. (1984) may have only been able to obtain typical logs for some sites.

The borehole log for each case record was reviewed, the SPT N which would yield the lowest $(N_1)_{60}$ was selected and the corresponding depth and fines content (percent passing the No. 200 sieve) of the soil were noted. No blowcounts were selected from above the groundwater table or within clay layers (selections were restricted to sands and occasionally silts), except for one case record in clayey sand (case record 55) which was considered to be potentially interbedded. No blowcounts were selected at depths of less than 2 m since SPT blow counts and the C_N correction factors at these depths were considered to be unreliable. For each case record, in order to calculate $(N_1)_{60}$, the C_N correction was determined as follows, in order to match the C_N correction proposed by Seed and Idriss (1982) and used in the Berkeley catalogue as closely as possible:

[2-3a] $$C_N = \frac{2}{1 + \sigma'_v} \quad \text{for } \sigma'_v < 1 \text{ tsf}$$ (after Skempton, 1986)

[2-3b] $$C_N = \left(\frac{1}{\sigma'_v}\right)^{0.56} \quad \text{for } \sigma'_v \geq 1 \text{ tsf}$$ (after Jamiolkowski, 1985)

where:

σ'_v = vertical effective stress (N.B. $\sigma'_v = \sigma'_o$ in this study).

In addition, the specific SPT hammer energy ratio for each case record given in the Berkeley catalogue was adopted at face value.

For two case records (7 and 16), the original case record was in clean sand, but was replaced by a case record in sand with fines. For seven case records (1, 2, 4, 15, 17, 63 and 64) originally in clean sand in the Berkeley catalogue, each original case record was replaced by two case records in this study, consisting of the minimum $(N_1)_{60}$ in clean sand and the minimum $(N_1)_{60}$ in sand with fines. It was not clear which of the two was the critical $(N_1)_{60}$; therefore, both values were selected and used on the appropriate subsequent plots. These pairs of case records, together with the additional information from the borehole logs that were obtained for the Luan Nan and Le Ting sites, as described earlier, resulted in expanding the original Berkeley catalogue database to a total of 155 case records.

2.3 Example Case Records

Table 2-1 provides statistics regarding the composition of the original database of 125 case records in the Berkeley catalogue and the changes that were made during the reconsideration in this study. Some of these statistics are primarily for interest; the effects of others will be discussed later. Strip logs and detailed data sheets for all of the sites are given in the research report by Fear and McRoberts (1993); selected strip logs are presented in Figures 2-2 to 2-4.

The non-liquefied case records are important points for defining the liquefaction trigger line and many of them had large reductions with the new selections of representative values of $(N_1)_{60}$. However, although all case records (liquefied and non-liquefied) were re-evaluated where possible, it was felt that case records in the Berkeley catalogue that were said to have liquefied with values of $(N_1)_{60}$ greater than 15 were especially pivotal to this study. As will be presented later in this chapter, it was primarily the result of moving these case records that produced significant differences with the Berkeley catalogue in terms of upper bound lines to the liquefied data. At lower values of $(N_1)_{60}$, the effects were less significant. These important case records are highlighted on Figure 2-1 (case records 1, 3, 4, 7, 8, 17, 56 and 87 on the clean sand plot and 55, 90 and 111 on the plot for sand with fines). Table 2-2 provides a summary of these case records by comparing the original interpretations with the results of this study and providing some additional comments of importance. Detailed consideration of these critical case records and some of the nonliquefied case records and further discussion of the relevant factors are provided below. The reader is also referred to the research report by Fear and McRoberts (1993).

2.3.1 Critical liquefied case records

The following section discusses the critical liquefied case records outlined above. Summary strip logs for all of these critical case records are presented in Figures 2-2 and 2-3; detailed data sheets can be found in Fear and McRoberts (1993).

Case records 1, 3 and 4 as well as case record 2 (see Figure 2-2 and Table 2-2) are located in close proximity in what appears to be the same geological environment. They were all investigated in the late sixties by Kishida (1969). These sites were affected by the 1891

Mino-Owari (M=7.9) earthquake. Case record 1 admits to considerably lower values of $(N_1)_{60}$ than the Berkeley catalogue $(N_1)_{60}$ of 25.5 (FC=0%) and two choices of 6.7 (FC=0%) and 10.7 (FC=8%) were picked and used in this study, as indicated in Table 2-2. The Berkeley catalogue placed case record 2 at an $(N_1)_{60}$ of 12.5 (FC=5%) and this study selected values of 6.3 and 10.6 in sand with fines contents of 8% and 4%, respectively. Only sand boils were reported for case records 1 and 2 and were reclassified in this study as cases of pressure relief. Sand boils and some cracking were reported for case records 3 and 4. For case record 3, the site investigation (Kishida, 1969) missed a pumice layer at shallow depth which may or may not be significant since a white mixture of sand and water was observed erupting from the ground at the site. Case records 3 and 4 were both reported as having gravel contents greater than 20% and this may also be a reason why the values of $(N_1)_{60}$ for these case records are high. Of considerable significance for case record 1 and especially for case records 3 and 4 which are located nearby, Kishida (1969) states that "it is not clear whether the eruptions of water resulted from a liquefied condition or from the artesian conditions". Kishida reports that the area was in an artesian condition (artesian wells were used until 1940) and that case records 3 and 4 are located near small hills. The reassigned values of $(N_1)_{60}$ for case records 3 and 4 are given in Table 2-2. This study considers that there is sufficient doubt about case records 3 and 4 having truly liquefied such that placing them in the pressure relief category is justified, although a case could be made for removing them from this study. In addition, it should be kept in mind that these case records are not based on a recent earthquake, but on an event that occurred in 1891.

For case record 7 (see Figure 2-2 and Table 2-2), taken from Kodera (1964), the Berkeley catalogue gave an N of 16 (FC=1%), at a depth of 8.23 m, producing an $(N_1)_{60}$ of 20.5. The N in the log for this site at this depth has a value of 3 (FC=10%), resulting in a reassessed $(N_1)_{60}$ of 3.9. The basis for the original interpretation is unknown. For case record 8 (see Figure 2-2 and Table 2-2), the original N of 12 (FC=5%) was selected at a depth of 5.18, producing an $(N_1)_{60}$ of 16.5. The N in the log for this site at approximately this depth has a value of 8 (FC=5%), resulting in a reassessed $(N_1)_{60}$ of 11.1. Case records 7 and 8 are, Piers 21 and 30 of the Arakawa Bridge, respectively, that were affected by the 1923 Kanto (M=7.9) earthquake. Of further interest is the fact that Piers 7 and 12 of the Arakawa Bridge (case records 5 and 6, respectively) which were also said to have liquefied have Berkeley interpretations of $(N_1)_{60}$ of 11.0 (FC=10%) and 2.5 (FC=22%) versus reassessments of 1.1 (FC=20%) and 2.7 (FC=22%) in this study, respectively. Pier 49 of the Arakawa Bridge (case record 9) was said to have had marginal liquefaction and have a Berkeley interpretation of $(N_1)_{60}$ of 7.0 (FC=20%) versus a reassessment of 2.2 (FC=30-40%). These case records are in the same geological environment as case records 7 and 8 and there does not seems to be any justification for assigning values of $(N_1)_{60}$ of 20.5 to Site 7 or 16.5 to Site 8. In addition, the fact that these case records consist of liquefaction damage to the Arakawa Bridge piers and site investigations which were carried out nearby raises questions about the case records. The bridge piers, which were partly founded on piles, and the loading from the bridge may have provided driving stresses such that the case records could be considered to consist of other than truly level ground conditions.

Site 17, taken from Kishida (1969) was affected by the 1948 Fukui (M=7.3) earthquake and was reassessed as shown in the corresponding strip log (see Figure 2-2) and Table 2-2.

Sites 55 and 56 are from China and along with Site 57 were apparently interpreted in the Berkeley catalogue using "typical" logs from the original reference (Shengcong et al., 1983). Sites 55, 56 and 57 were all affected by the 1976 Tangshan (M=7.6) earthquake and are also reported by the Beijing Municipal Bureau of City Planning (1982). Many logs were obtained in this study from this report for sites 56 and 57 and each log containing sufficient information was included in the database as an additional case record. For site 56, named Luan Nan, 7 boreholes were obtained (see Figure 2-3 and Table 2-2). The original $(N_1)_{60}$ was 22.0 in clean sand and the site was said to have liquefied. As shown in Table 2-2, four of the seven boreholes were said to have liquefied with $(N_1)_{60}$ ranging from 7.7 to 21.4, also in clean sand. Three of these case records had minimum values of $(N_1)_{60}$ substantially less than the original selection of 22.0. However, one borehole, 56-L6, had a high $(N_1)_{60}$ of 21.4. In view of the fact that there were also three non-liquefied case records in the same geological environment with $(N_1)_{60}$ ranging from 12.3 to 22.0, the original interpretation is considered highly conservative. It is not unreasonable to question both the original Berkeley interpretation of the Luan Nan site and the applicability of case record 56-L6, which was introduced in this study. Moreover, the failure modes for case record 56-L6 and any of the other liquefied case records are not specified in either the Berkeley catalogue or the additional information that was obtained from China and may well consist of only pressure relief phenomena. As a result, in subsequent plots in this study, case record 56-L6 will be assigned a question mark to indicate that it can be considered as a questionable liquefied case record. For the Luan Nan case records, with the exception of 56-L6, the dividing line between liquefied and non-liquefied case records is at an $(N_1)_{60}$ between 12.3 and 14.0.

Although not listed in Table 2-2, it is of interest to note that 20 additional boreholes with sufficient information to be considered as individual case records were obtained from the Beijing Municipal Bureau of City Planning (1982) for case record 57 (Le Ting), in sand with fines. These consisted of 7 non-liquefied case records with $(N_1)_{60}$ ranging from 8.4 to 19.8 (average of 13.0) and 13 liquefied case records with $(N_1)_{60}$ ranging from 6.5 to 12.6 (average of 9.2). Thus the dividing line between liquefied and non-liquefied case records is at an $(N_1)_{60}$ between 9.2 and 13.0, less than that for the Luan Nan case records which were in clean sand.

Case record 55 was assessed using a typical log (see Figure 2-2 and Table 2-2) rather than a specific log as no other logs were obtained by this study or, apparently, for the Berkeley interpretation. As can be seen in Table 2-2, the original interpretation of 21.5 was in a sand with a fines content of 20%. For this typical log, an $(N_1)_{60}$ of 6.2 in clayey sand has been adopted in this study, although an intermediate value of 14.8 in silt could be assigned to this case record. The clayey sand layer could be interbedded sand and clay.

Case record 87 (see Figure 2-2 and Table 2-2), taken from Iwasaki et al. (1978), was affected by the June 1978 Miyagiken-Oki (M=7.4) earthquake and was alternatively assessed at a lower $(N_1)_{60}$ level, as indicated in Table 2-2.

Case record 90 (see Figure 2-2 and Table 2-2) at the Yuriage Bridge is also taken from Iwasaki et al. (1978), was also affected by the June 1978 Miyagiken-Oki earthquake. However, although it was in the Berkeley catalogue with an $(N_1)_{60}$ of 21.5 (FC=7%), it was not included in the Seed et al. (1984) plot for sand with fines, possibly because the case record had greater than 20% gravel. This same site did not liquefy during an earthquake of smaller magnitude and was used as case record 73 in the Berkeley catalogue; however, it was also not included on the Seed et al. (1984) plot for sand with fines. Three other case records (89, 91 and 92) were also located at Yuriage Bridge in the same geological environment. Case records 89 and 91 which liquefied were originally interpreted with values of $(N_1)_{60}$ of 5.0 (FC=10%) and 12.0 (FC=12%) were reassessed with values of $(N_1)_{60}$ of 2.7 (FC=10%) and 11.2 (FC=12%), respectively. Case record 92 (see Figure 2-4) which did not liquefy had an original interpreted $(N_1)_{60}$ of 21.0 (FC=17%) and a reassessed $(N_1)_{60}$ of 11.5 (FC=17%). The fines contents did vary between the case records, but not enough to explain the differences outlined here. In view of the facts that another pier with a low $(N_1)_{60}$ did not liquefy, lower values of $(N_1)_{60}$ were found in other units which did liquefy, and the borehole for case record 90 had a high gravel content, case record 90 will be shown with a question mark on subsequent plots in this paper. In addition, although the nature of the bridge foundations is unclear, the piers and the loading from the bridge may have provided driving stresses, like the Arakawa Bridge, such that all of the case records for the Yuriage Bridge could be considered to consist of other than truly level ground conditions.

Case record 111 (see Table 2-2) which was affected by the 1979 Imperial Valley (M=6.6) earthquake, was originally interpreted as having an $(N_1)_{60}$ of 16 based on an N of 11 (FC=18%) in soil unit C at a site named River Park (Youd and Bennett, 1983, Figures 10 and 11), which was affected by the 1979 Imperial Valley (M=6.6) earthquake. Referencing Youd and Bennett (1983), an N of 11 appears to be an average value in soil unit C for the boreholes drilled at this site. An N of as low as 7, resulting in an $(N_1)_{60}$ of 10.6 (FC=18%) can be assigned to this case record, from one of the boreholes, BH4, at the site. This can be seen on the strip log for case record 120 (see Figure 2-4), the same site which did not liquefy during the 1981 Westmorland (M=5.6) event.

2.3.2 Non-liquefied case records

The following discussion presents five non-liquefied case records in order to illustrate the types of reductions in $(N_1)_{60}$ that were made. Summary strip logs for all of these critical case records are presented in Figure 2-4; corresponding data sheets can be found in Fear and McRoberts (1993).

Case record 16 (see Figure 2-4), taken from Kishida (1969), represents the Takaya 2 site in Japan which did not liquefy during the 1948 Fukui (M=7.3) earthquake. The Berkeley catalogue selected an N of 29 at a depth of 8.23m, resulting in an $(N_1)_{60}$ of 40.5 (FC=2%). This study selected an N of 10 at 15.0 m, resulting in an $(N_1)_{60}$ of 10.4 (FC=15%).

Case record 19 (see Figure 2-4), also taken from Kishida (1969), represents the Agricultural Union site in Japan which also did not liquefy during the 1948 Fukui earthquake. The Berkeley catalogue selected an N of 20 at a depth of 7.62 m, resulting in an $(N_1)_{60}$ of 29 (FC=0%). This study selected an N of 5 at 5.0 m, resulting in an $(N_1)_{60}$ of 8.5 (FC=0%). It should also be noted that in an earlier catalogue of liquefaction case histories, Seed and Idriss (1971) picked an N of 5 at 6.10 m, a value much less than the N of 20 given in the Berkeley catalogue and closer to that selected in this study.

Case record 96 (see Figure 2-4), taken from Iwasaki et al. (1981), represents the Kitawabuchi 3 site in Japan which did not liquefy during the June 1978 Miyagiken-Oki (M=7.4) earthquake. The Berkeley catalogue selected an N of 23 at a depth of 6.10 m, resulting in an $(N_1)_{60}$ of 29 (FC=0%). This study selected an N of 12 at a depth of 4.10 m, resulting in an $(N_1)_{60}$ of 17.1 (FC=0%).

The soil profile for case record 120 (see Figure 2-4) is taken from Youd and Bennett (1983) and is the same as for case record 111 (see Table 2-2), one of the critical liquefied case records. The site liquefied during the 1979 Imperial Valley (M=6.6) earthquake (case record 111), but did not liquefy during the 1981 Westmorland (M=5.6) earthquake (case record 120). As outlined earlier, for case record 111, this site had an $(N_1)_{60}$ of 16 in the Berkeley catalogue versus a reassessed $(N_1)_{60}$ of 10.6 in this study.

As explained previously, case record 92 (see Figure 2-4) is located at the Yuriage Bridge site in Japan (Iwasaki et al., 1978) and did not liquefy during the June 1978 Miyagiken-Oki (M=7.4) earthquake. The Berkeley catalogue selected an N of 17 at a depth of 7.32 m, resulting in an $(N_1)_{60}$ of 21 (FC=17%). The fines content given by the Berkeley catalogue for this depth was 17%. An N of 14 at 17.0 m was selected, resulting in an $(N_1)_{60}$ of 11.5 (FC=17%).

2.4 Discussion

As outlined in Table 2-1, for 94 of the case records, either a new assessment was made (58 case records) or this study agreed with the original Berkeley catalogue interpretation (36 case records). For the 58 case records for which a new assessment was made, the Berkeley catalogue selection appears to be often representative of the average $(N_1)_{60}$ over some portion of the borehole and in some cases was a high value. For the remaining 36 case records, the Berkeley catalogue appears to have selected the minimum $(N_1)_{60}$, thus agreeing with the results of this study.

For these 36 case records, this study produced slightly higher or lower values of $(N_1)_{60}$ than given in the Berkeley catalogue, even for sites for which this study used the same selection of raw blowcount and critical depth. This was primarily due to small differences in the calculation of the correction factors, such as C_N and r_d. For a few sites, this study did not quite agree with the level of the groundwater table or the value of N as given in the Berkeley catalogue. Table 2-3 presents statistics for these 36 case records and for the 31 case records for which data were not found. For the latter, either the reference papers cited by Seed et al. (1984) were not found or they did not contain borehole logs for the case records; the Berkeley catalogue interpretations for these case records were accepted at face value in this study. In several cases, it appears that the original interpretations may have been based on data presented in tabular form or quoted as average values. All of the case records in Table 2-3 possess low to intermediate values of $(N_1)_{60}$ and, hence, are not crucial to the shape or location of the upper and lower bound state lines, which are discussed later.

2.4.1 Revised plots of CSR versus $(N_1)_{60}$

Figure 2-5 presents the case records from this study that did not liquefy, with the $(N_1)_{60}$ axis expanded from the proportion considered in the Berkeley catalogue. The number next to each case record represents the fines content. Details of the notation are given at the beginning of this thesis. With the exception of case record 19, a lower bound state line can be established on the plot for clean sands (fines content ≤ 5%). When this line is superimposed on the plot for sand with fines, there are 14 case records which have fines contents greater than clean sand and plot above or to the left of the line. At the same level of earthquake intensity, as expressed by CSR, a case record in sand with fines may have a lower value of $(N_1)_{60}$ than that in clean sand without liquefying. This supports the view that finer grained soils are more resistant to liquefaction for the same penetration resistance. A lower bound state line for sands with fines is also shown and can be seen to have a different shape as well as location than the lower bound state line for clean sand.

Figure 2-6 presents the interpretation for liquefied and pressure relief sites from this study, also with an expanded $(N_1)_{60}$ axis. The number next to each case record represents the fines content. Considering sands with fines and with the exception of case record 90 (which as previously discussed could be influenced by gravel and is questionable), an upper bound state line for liquefied case records is established. This state boundary is transferred to the clean sand plot and it can be seen that an essentially subparallel line forms a reasonable state boundary to all of the liquefied clean sand case records. Case record 56-L6 on the clean sand plot is considered to be questionable as explained earlier and case record 17 is considered questionable as will be explained later. This also supports the general observation that sands with fines are more resistant to liquefaction than clean sands at the same value of $(N_1)_{60}$. It is difficult to support a further discrimination based on the percentage of fines. In fact, a close inspection of the original Berkeley plot (Seed et al., 1984) also supports this conclusion.

All of the liquefied and pressure relief case records from this study are combined in Figure 2-7, also with an expanded $(N_1)_{60}$ axis. The two upper bound state lines from Figure 2-6 for liquefied case records in sand with fines and for liquefied case records in clean sands are shown on Figure 2-7. A conservative upper bound line is also shown, extending to a $(N_1)_{60}$ of 22 and encompassing all of the pressure relief case records as well as three questionable case records. Case records 56-L6 and 90 have been discussed earlier. Case record 17, which is presented in Table 2-2, had two selections for minimum values of $(N_1)_{60}$, 16.6 in clean sand and 6.5 in sand with fines. Both selections are more critical than the original Berkeley interpretation of 24.0 in clean sand. The new selection in sand with fines is probably more crucial than the new selection in clean sand. Thus, in Figure 2-7, of the two data points shown for case record 17, the one in clean sand with the higher $(N_1)_{60}$ can be considered to be questionable.

All of the interpretations from this study have been combined in Figure 2-8, for comparison with the lines from the Berkeley catalogue, and the $(N_1)_{60}$ axis has been returned to the proportion used in the original catalogue. Unlike the representation found in the Berkeley catalogue, there is no distinct line between liquefied and non-liquefied sites in either clean sands or sands with fines. The upper bound state lines from this study for liquefied case records in both clean sands (fines contents ≤ 5%) and sands with fines are at substantially lower values of $(N_1)_{60}$ than the trigger lines from the Berkeley catalogue interpretations, particularly at higher values of CSR. At values of CSR less than about 0.140, the upper bound state line for clean sand is similar to the Berkeley catalogue line for clean sands. At values of CSR less than about 0.18, the upper bound state line for sand with fines is similar to the Berkeley catalogue line for sands with fines contents of 15%. The lower bound state line encompassing all of the non-liquefied case records is substantially less than the upper bound state line for all liquefied case records in sand with fines. In clean sand, this is valid up to a CSR of about 0.25. Although not shown on Figure 2-8, it appears that there may be a horizontal cutoff for each of the upper bound lines, representing a threshold CSR required to cause liquefaction. For clean sand, this would be at a CSR of about 0.07.

2.4.2 Impeded drainage

Andrus et al. (1991) and Yegian et al. (1994) have postulated that an impermeable soil cap may play a crucial role in preventing the upward dissipation of excess pore water pressure. This may influence the sand state that is or is not susceptible to liquefaction at a given $(N_1)_{60}$. The 155 case records in this study were considered in terms of the potential for open seepage versus impeded drainage, in terms of the available stratigraphic information. Table 2-4 summarizes the results of the classification for each case record. Some case records appear twice for each of the new datapoints selected in this study. In each case, the drainage condition for the datapoint in clean sand is given first, followed by the drainage condition for the datapoint in sand with fines. The drainage potential was classified as open seepage if no soil above the minimum $(N_1)_{60}$ was less permeable in terms of soil classification (classification 1 in Table 2-4). However, if a layer of less permeable soil was present at some point above the minimum $(N_1)_{60}$, the drainage potential was classified as impeded drainage (classifications 1*, 2 or 3 in Table 2-4). It is recognized that thin impermeable layers that were not observed in the investigations or reported may exist. For 32 of the 155 case records, the drainage conditions could be considered to be open seepage. For 92 of the case records, there was some type of drainage impedance. The remaining 31 case records had drainage conditions which were unknown (classification 4 in Table 2-4). Figure 2-9 presents a summary of the data, combining together clean sands and sands with fines. Interpretation of the drainage conditions will be discussed later in this chapter.

2.4.3 Additional data from recent studies

Additional data from Ambraseys (1988; 1992), Kayen et al. (1992) and Kayen (1993) were also obtained and reconsidered. These 25 case records are summarized in the catalogue compiled by Fear and McRoberts (1993) and the results in terms of CSR and $(N_1)_{60}$ are plotted in Figure 2-10. The equivalent CSR for an earthquake of magnitude 7.5 was calculated for all case records in this study, including those by Ambraseys (1988), for the purpose of comparing the results with the plots in the Berkeley catalogue. Case record A11 is the same as case record 17 in the Berkeley catalogue, except that the values of $(N_1)_{60}$ and CSR are slightly different since Ambraseys (1988) gave different values for the unit weight and the level of the groundwater table for this site than Seed et al. (1984). Therefore, of the two selections of $(N_1)_{60}$ for case record A11, the higher one can be considered to be questionable, as explained previously for case record 17. The additional case records appear to support the conclusions drawn from the reconsideration of the Berkeley database, especially in terms of the location of the upper bound state lines for liquefied case records. However, since the additional case records were predominantly cases of liquefaction, there were not enough non-liquefied case records to make any definite conclusions as to their location with respect to the location of the lower bound state lines, particularly the lower bound state line for clean sand. It would be desirable and of interest to obtain some more non-liquefied case records from recent earthquakes for comparison with the conclusions of this study.

2.4.4 Interpretation and significance of results

The Berkeley interpretations are generally more conservative than the interpretations made here, particularly at higher values of CSR and it is clear that they constitute a conservative assessment of the potential for triggering earthquake-induced phenomena in sandy soils, based on $(N_1)_{60}$, CSR and fines content. Even the conservative upper bound state line (encompassing all of the questionable liquefied case records and pressure relief case records), although similar to the Berkeley line for clean sand up to a CSR of about 0.25, is not as conservative as the Berkeley line at higher values of CSR. Furthermore, the results of this study indicate a zone in which liquefaction may or may not occur, whereas, the more conservative Berkeley plot indicates no such zone.

From a design perspective, a site located at a combination of CSR and $(N_1)_{60}$ plotting to the left of the lower bound state line for all non-liquefied case records would clearly be at risk for the initiation of a wide range of earthquake-induced phenomena. Some differences between clean sands and sands with fines is apparent in making such a determination. Secondly, there is a transition zone between the lower bound state boundary for non-liquefied case records and the upper bound state boundary for liquefied case records where liquefaction phenomena may or may not occur. In addition, between the upper bound and the conservatively assessed upper bound state lines for liquefied case records, there is a potential for pressure relief phenomena such as sand boils and, by inference, subsequent settlement.

The above results and discussion are based on using a "weakest-link-in-the-chain" approach, assuming that all of the case histories are level ground conditions and accepting the definition of liquefaction based on field observations as given by the Berkeley catalogue. The ideal level ground condition consists of ground that is completely level and in which an element of soil has, initially, no horizontal or vertical shear stresses acting on it. If the ground is actually sloping or if the soil in question is close to or beneath structures such as buildings or bridges, these initial driving shear stresses acting on the soil may not be equal to zero. As outlined in Table 2-1, if only the sites for which the conditions were known are considered, about half could be called "level ground"; the other half may have had higher initial driving shear stresses than a truly level ground condition due to their proximity to such things as building foundations, bridge piers and slopes of various kinds. In addition, it was observed that there was little difference between values of $(N_1)_{60}$ for case records in the sloping ground and structure categories and values of $(N_1)_{60}$ for the case records which could truly be considered to be level ground. None of these case records consisted of steeply sloping ground and the trigger plots presented here are not considered to be applicable to such slopes. Case records with significant slopes are considered by Seed (1987).

Drainage conditions, as summarized in Table 2-4 and Figure 2-9 may exert an effect on the interpretation of the case records. It appears that the liquefied case records at higher values of $(N_1)_{60}$ tend to be classified as cases of impeded drainage. Indeed, the maximum $(N_1)_{60}$ for open drainage liquefied case records appears to be approximately 11, with the exception of one case record at 14.3. This case record was classified as open drainage based on some general borehole logs from the site, rather than the specific log for the case record. The non-liquefied data tends to be randomly distributed with the possible suggestion that there is more impeded drainage than open seepage at values of $(N_1)_{60}$ less than 10. The interpretation of this data is complicated by post-seismic effects (most site investigations were conducted some time after the earthquake) and missing stratigraphic data. There does appear to be some suggestion for support of the conclusions which were drawn by Andrus et al. (1991) and Yegian et al. (1994) and discussed earlier.

The upper bound state lines determined in this study are asymptotic to values of $(N_1)_{60}$ in the region of 13 to 15. This is consistent with observations made by Robertson et al. (1992) and McRoberts and Sladen (1992) that, for screening purposes, the state boundary between contractant and dilatant sandy material falls within this range. For earthquakes with $M<8$, Bartlett and Youd (1992) considered an $(N_1)_{60}$ of 15 to represent the dividing line as to whether or not significant lateral spreading would occur and, hence, whether or not the design analysis should include an evaluation of ground displacements. Ishihara (1993, Figure 99) suggested a boundary line for liquefaction which can be interpreted to range from an $(N_1)_{60}$ of 19 to 24, and a dividing line between flow and no flow at an average $(N_1)_{60}$ of 10. Ishihara's flow-no flow boundary line could be considered to be low compared with the results discussed above. The conservative upper bound line in Figure 2-8 is asymptotic to an $(N_1)_{60}$ of 22 and is consistent with Ishihara's (1993, Figure 99) boundary line for liquefaction. Ishihara is understood to define liquefaction as any earthquake-induced phenomenon or 5% double amplitude strain. Within this context, the interpretation considered in this study could be viewed as follows: the upper bound state line would describe a state boundary line for all earthquake-induced phenomena except sand boils or settlement and the conservative upper bound line would represent an upper bound to sand boil activity or substantial settlement. It is considered that limited settlement could still occur beyond the conservative upper bound line.

The upper and lower bound state lines presented in this study are meant to be envelopes which encompass all of the data. Thus, they are lines of zero exceedance based on the interpretation method used and the data available. Applying probabilistic techniques to the data, as was performed by Liao (1986) on the original Berkeley database, may prove to be useful, but is beyond the scope of this paper. In addition, there appears to be insufficient data at this time to, for example, interpolate curves of probabilities of exceedance between the upper bound state line for clean sand and the conservative upper bound state line. These data consist of 5 case records which have been classified as pressure relief/marginal liquefaction and 3 case records which are considered to be questionable. Clearly, it would be of great interest to North American practice to focus some research on the few case histories, particularly the questionable ones, which fall between the upper bound state line and the conservative upper bound state line. Limited information has been obtained regarding these eight case records, which are from Japan (7 case records) or China (1 case record). Further study may be able to help resolve whether these case records are valid or truly questionable.

The observation, in this study, of various state boundary lines and zones in which different earthquake-induced phenomena will occur appears to be consistent with the conclusions which Seed himself was beginning to make. Seed et al. (1985) presented a "tentative relationship between cyclic stress ratio, N_1-values and limiting strains for natural deposits of clean sand", as shown in Figure 2-11. This figure suggested that at values of $(N_1)_{60}$ lower than the most conservative liquefaction-no liquefaction boundary line for clean sand, the consequences of cyclic loading, the forms of liquefaction and the amount of strain that would occur depend on the magnitude of $(N_1)_{60}$. However, many do not make use of the strain lines that were proposed by Seed et al. (1985), but rely solely on the most conservative trigger line for liquefaction trigger analyses.

A final note of interest is that participants in the recent NCEER Workshop (1996) came to the consensus of recommending a conservative average-based $(N_1)_{60}$ correlation to estimate CRR. The recommended correlation, as indicated by the thick line in Figure 2-11, follows the conservative 3% shear strain line for clean sand proposed by Seed et al. (1985), except at low values of $(N_1)_{60}$. At values of $(N_1)_{60}$ less than approximately 10, the NCEER Workshop (1996) recommendation deviates from the Seed et al. (1985) line (which heads towards zero CRR, as indicated by the dashed line), in order to be more consistent with the recommended CPT-based correlation (see Chapter 3) and indicate a potential threshold CRR. This study also suggested a potential threshold CRR. It is important to note that both this study and the NCEER Workshop (1996) recommendation imply the following:

Holocene age deposits
Level or gently sloping ground
Magnitude M=7.5 earthquakes
Depth range from 1 to 14 m (3 to 47 ft)
  N.B. 90% of data is for depths < 10 m (32ft)

Hence, caution should be exercised when extrapolating the correlations to conditions outside of the range. However, the NCEER Workshop (1996) recommendation also implies representative average SPT N values for the layer that was considered to have experienced cyclic liquefaction and incorporates all types of cyclically induced observed surface features into the definition of cyclic liquefaction. The results of this study would suggest that the NCEER Workshop (1996) recommendation is conservative and should be applied with caution.

2.5 Conclusions

In general, it must be noted that this study, in itself, does not seek to produce a new design methodology for liquefaction. Rather, it offers an alternative way of considering the original database and this may be useful as a component of the overall design process. It must be cautioned that neither the present study nor the original interpretations should be used by itself as a design method. The data presented here may be complementary to other design findings, especially if these are found to be difficult to implement due to the precedents offered by the original work. The original Berkeley work permitted a clear yes/no type of choice in assessing the potential for triggering of liquefaction. This original work has unfortunately evolved into a design method which, if coupled with lower bound site data, may well be overly conservative and either embody a poor use of resource allocation for risk reduction, or unnecessary costs. Alternatively, there may well be instances where the original method, if combined with average site data in the zone of interest, may not be sufficiently conservative depending on factors that were unquantified in both the original and present studies. Resolution of these factors is clearly a matter for design. This study, by introducing a different interpretation of the case records and the wide transition zones, introduces the potential for design domains in which there is substantial scope to demonstrate possible economic benefits of more detailed site investigations and analyses, such as those reported by Byrne et al. (1994).

This study found, especially for higher $(N_1)_{60}$ liquefied case records, that a safe state line defined at a given earthquake intensity (i.e. CSR) could be established considerably lower than the original Berkeley recommendation. This upper bound line is based on minimum $(N_1)_{60}$ interpretations and is more consistent with the design practice of selecting the lowest, more critical, in-situ data. This practice is becoming increasingly prevalent as cone penetrometer testing (CPT) allows for a more detailed record of soil variations than is generally possible with SPT testing. A conservative design boundary line, which encompasses case records for which only sand boils were reported and three case records of doubtful provenance, was also established. This conservative line is similar to the original Berkeley line for clean sand at values of CSR up to about 0.25, but is significantly less than the Berkeley line at higher values of CSR. The upper bound line is therefore viewed as being transitional between all case records for which strong evidence of seismically induced phenomena, other than sand boils, is reported, and a domain, defined by the conservative design boundary line, in which only sand boils and three questionable case records are found. A transition zone, within which liquefaction may or may not occur, also clearly exists. For clean sands, this represents a range of $(N_1)_{60}$ from 5 to 13 for a CSR of 0.16. The study did not recover the unique line between the upper bound liquefied state and the lower bound non-liquefied state as represented in the Berkeley catalogue. Rather, there is a broad zone in which either state is possible. At a given earthquake intensity, as measured by the CSR, there is a lower bound state line below which liquefaction is highly probable.

Analyzing numerous case studies to produce a trigger plot for liquefaction is not a simple task. There are many variable factors which serve to complicate the process. No matter how the study is performed or how consistent one tries to be in assigning a single valued combination of $(N_1)_{60}$ and CSR to a case record, one must always exercise a certain amount of judgement. It is clear that the original Berkeley interpretations involved judgement and were directed toward a conservative assessment of the database. In addition, $(N_1)_{60}$ and CSR are not the only factors affecting the potential for liquefaction at a particular site. Other factors such as fines content, gravel content, cementation, age, fabric, thickness of the liquefied layer, thickness or nature of any overlying non-liquefied layer, impeded seepage and topography may affect both the potential for liquefaction and the extent of the effects once liquefaction has been triggered. These factors and others likely add uncertainty to the database and may account for the transition zones that have been observed in this study. However, based on the available data, it was difficult to further distinguish between the data on the basis of any of these factors, except for fines content and possible impeded seepage. While an effect of fines content was found, the study does not support the broader range reported in the original work. Some trends have been suggested regarding the effects of impeded drainage; however, further investigation and research is needed to determine specific effects on liquefaction potential. The application of statistical techniques to the revised database using the methods and procedures followed by Liao (1986) would constitute a logical extension of this study.

Table 2-1: Composition of 125 case records in the original Berkeley catalogue

	Number of Case Records
A. Classification of the Original 125 Case Records	
(i) Berkeley catalogue	
Liquefied	67
Marginal Liquefaction	7
Non-liquefied	51
(ii) This study	
Liquefied	56
Pressure relief/marginal liquefaction	15
Non-liquefied	52
Liquefied or non-liquefied depending on location at the site	2
B. Case Records repeated twice in the Database (each pair of points reflects one site investigation, but two different earthquakes, usually one which did not cause liquefaction and a larger one which did)	21
C. Availability of Reference Papers	
Original reference papers were located	112
Related papers found when original reference was not found	12
No reference paper found	1
D. Site conditions	
Level ground	49
On or near sloping ground (dyke, dam, slope, river embankment, lakeside or riverside)	25
Under or near a structure (e.g. bridge, building)	22
Site conditions unknown	29
E. Re-evaluation of case records	
(i) No re-evaluation could be made	31
Original reference paper did not contain a BH log	18
Original reference paper was not found; any alternates that were found did not contain BH logs	13
(ii) A re-evaluation was made	94
Same $(N_1)_{60}$ selected as in the Berkeley catalogue	36
Lower $(N_1)_{60}$ selected than in the Berkeley catalogue	58

Table 2-2: Summary of changes in $(N_1)_{60}$ for critical liquefied case records in the original Berkeley study

	Case Record				Original Data					New Data					
	No.	Name	Earthquake	Reference	Liquefied?	$(N_1)_{60}$	Depth (m)	CSR	FC (%)	Liquefied?	$(N_1)_{60}$	Depth (m)	CSR	FC (%)	Comments
Case Records Originally in Clean Sands	1	Ogaki	1891 Mino-Owari	Kishida (1969)	yes	25.5	10.05	0.375	0	pressure relief pressure relief	6.7 10.7	5.00 17.00	0.371 0.362	0 8	•sand boils only • investigated in late sixties by Kishida (1969) • area in artesian condition (artesian wells used until 1940) • "not clear whether the eruptions of water resulted from a liquefied condition or from the artesian conditions" (Kishida, 1969) • located in what appears to be the same geological environment as case records 3 and 4
	3	Unuma	1891 Mino-Owari	Kishida (1969)	yes	25.0	6.10	0.330	3	pressure relief	20.0	9.35	0.339	4	• sand boils and some cracking • investigated in late sixties by Kishida (1969) • site investigation missed a pumice layer at shallow depth which may or may not be significant since a white mixture of sand and water was observed erupting from the ground • gravel contents greater than 20% • similar concerns re: artesian conditions as for case record 1
	4	Ogase	1891 Mino-Owari	Kishida (1969)	yes	17.0	5.18	0.290	4	pressure relief pressure relief	15.8 17.5	4.00 5.18	0.264 0.287	10 4	• sand boils and some cracking • investigated in late sixties by Kishida (1969) • gravel contents greater than 20% • similar concerns re: artesian conditions as for case record 1
	7	Arakawa 21	1923 Kanto	Kodera (1964)	yes	20.5	8.23	0.240	1	yes	3.9	8.25	0.237	10	• Pier 21 of the Arakawa Bridge • Piers 7 and 12 (case records 5 and 6) of the bridge which liquefied and Pier 49 which had marginal liquefaction were in the same geological environment and were re-assigned lower values of $(N_1)_{60}$ as well • site conditions may be considered to be other than truly level ground due to bridge piers and bridge loading
	8	Arakawa 30	1923 Kanto	Kodera (1964)	yes	16.5	5.18	0.230	5	yes	11.1	5.00	0.225	5	• Pier 30 of the Arakawa Bridge • same comments apply as for case record 7
	17	Takaya 45	1948 Fukui	Kishida (1969)	yes	24.0	7.01	0.280	4	yes yes	6.5 16.6	15.00 10.00	0.306 0.293	30 4	
	56	Luan Nan	1976 Tangshan	Shengcong et al. (1983)	yes	22.0	5.36	0.175	3	yes (56-L2) yes (56-L3) yes (56-L6) yes (56-L7) no (56-L1) no (56-L4) no (56-L5)	7.7 13.2 21.4 14.0 12.3 22.0 17.8	5.30 10.30 8.30 8.30 11.30 9.30 4.30	0.252 0.210 0.281 0.255 0.228 0.264 0.171	3 3 3 3 3 3 3	• apparently interpreted in the Berkeley catalogue using a "typical log" from Shengcong et al. (1983) • this study obtained additional logs from the Beijing Municipal Bureau of City Planning (1982), both liquefied and non-liquefied • failure modes not specified in either report
	87	Yuriagekami 2	June 1978 Miyagiken-Oki	Iwasaki et al. (1978)	yes	15.0	4.27	0.250	0	yes	5.6	3.50	0.243	0	
Case Records Originally in Silty Sands	55	Qing Yin	1976 Tangshan	Shengcong et al. (1983)	yes	21.5	5.30	0.395	20	yes	6.2	11.75	0.394	clayey sand	• apparently interpreted in the Berkeley catalogue using a "typical log" from Shengcong et al. (1983) • no additional logs were obtained • clayey sand layer could be interbedded sand and clay • failure mode not specified in Shengcong et al. (1983)
	90	Yuriage Bridge 2	June 1978 Miyagiken Oki	Iwasaki et al. (1978)	yes	21.5	3.35	0.225	7	yes	20.1	3.35	0.216	7	• from the Yuriage Bridge (Iwasaki, 1978) • listed in the Berkeley catalogue, but not included in the Seed et al. (1984) plot for sand with fines, possibly because it had a gravel content > 20% • this same site did not liquefy in an smaller earlier EQ (case record 73 - also listed in the Berkeley catalogue, but not included in the plot for sand with fines) • another pier with a lower $(N_1)_{60}$ did not liquefy and lower $(N_1)_{60}$'s were found in other units which did liquefy
	111	River Park C	1979 Imperial Valley	Youd et al. (1983)	yes	16.0	4.27	0.240	18	yes	10.6	3.50	0.239	18	• soil unit C at the site was said to have liquefied • Berkeley catalogue $(N_1)_{60}$ seems to be based on the average N in soil unit C for boreholes drilled at the site

Table 2-3: Summary of Berkeley case records for which the original assessment was the same as in this study

Response	Number of Case Records	(N1)60		
		Mean	Standard deviation	Range
A. 36 case records for which borehole logs were found				
liquefied	14	7.4	5.1	1.4 to 13.6 (1)
pressure relief	10	5.8	4.3	2.8 to 17.0
non-liquefied	12	10.6	5.7	2.4 to 20.1
B. 31 case records for which borehole logs were not found (2,3)				
liquefied	16	8.3	3.4	1.5 to 14.5
non-liquefied	15	13.0	5.4	8.0 to 26.5

Notes:

(1) Except for case record 90 (see Table 1) which liquefied with an (N1)60 of 20.1.
(2) Case records with no borehole logs in references cited by Seed et al. (1984) = 18.
(3) 10 case records are based on 5 sites, each affected by two earthquakes.

Table 2-4: Classification of drainage conditions for all case records

Case Record	Drainage Condition	Case Record	Drainage Condition	Case Record	Drainage Condition	Case Record	Drainage Condition	Case Record	Drainage Condition
1	3	29	2	56 (L7)	1*	68	2	101	1
1	1*	30	1*	57 (BH1)	3	69	2	102	1
2	1	31	4	57 (BH10)	1	70	2	103	4
2	1	32	2	57 (BH11)	1*	71	2	104	4
3	2	33	1	57 (BH12)	3	72	2	105	1*
4	3	34	1	57 (BH13)	3	73	4	106	1*
4	3	35	1	57 (BH14)	3	74	1	107	1
5	3	36	4	57 (BH15)	3	75	4	108	1
6	1	37	4	57 (BH19)	3	76	4	109	1
7	1	38	4	57 (BH2)	3	77	3	110	1
8	1	39	4	57 (BH21)	3	78	1	111	3
9	1*	40	4	57 (BH22)	3	79	1	112	3
10	4	41	4	57 (BH23)	3	80	1	113	3
11	4	42	4	57 (BH24)	3	81	1	114	1*
12	2	43	4	57 (BH25)	3	82	1	115	1*
13	2	44	3	57 (BH26)	3	83	4	116	3
14	2	45	3	57 (BH4)	3	84	2	117	2
15	1	46	3	57 (BH5)	3	85	2	118	2
15	1	47	3	57 (BH7)	3	86	2	119	1
16	2	48	1	57 (BH8)	3	87	2	120	3
17	1*	49	2	57 (BH9)	3	88	2	121	3
17	1*	50	2	58	3	89	2	122	3
18	2	51	3	59	4	90	4	123	1*
19	3	52	4	60	4	91	1		
20	1	53	4	61	4	92	4		
21	1*	54	3	62	3	93	4		
22	4	55	3	63	3	94	4		
23	4	56 (L1)	3	63	3	95	3		
24	4	56 (L2)	2	64	1*	96	3		
25	4	56 (L3)	3	64	3	97	1		
26	4	56 (L4)	3	65	2	98	1		
27	1	56 (L5)	2	66	3	99	1		
28	3	56 (L6)	1*	67	2	100	1		

Notes:

1 = open drainage = perm. above ≥ perm. of layer of interest (e.g. gravel over sand)
1* = indicates that open drainage exists for some thickness above the layer of interest, although there is a less permeable layer well above the layer of interest
2 = shut drainage A = perm. above slightly less than in layer of interest (e.g. silt over sand)
3 = shut drainage B = perm. above much less than in layer of interest (e.g. clay over sand)
4 = drainage conditions unknown

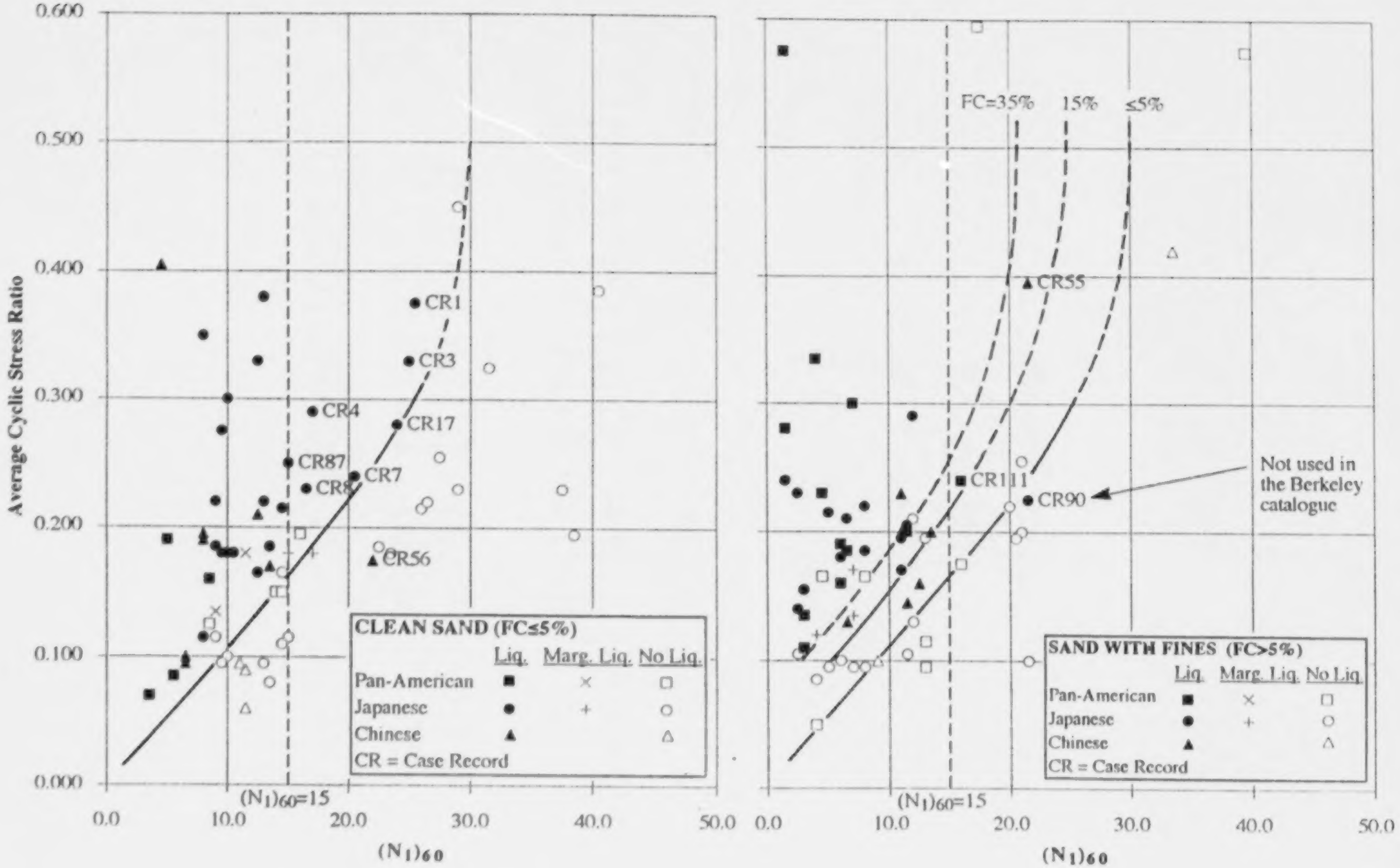

Figure 2-1 Plots of CSR versus $(N_1)_{60}$ in original Berkeley catalogue.

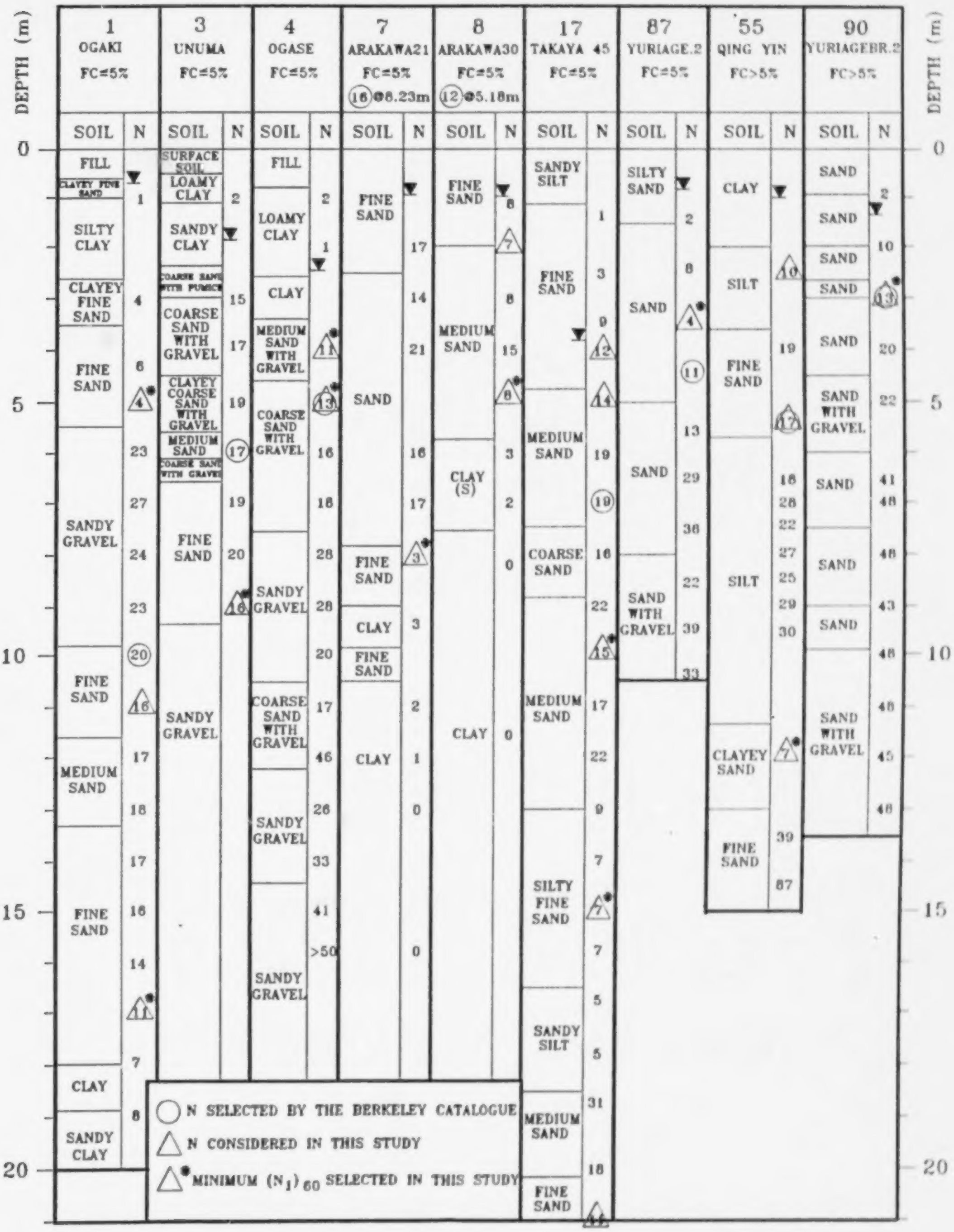
DEPTH (m)
1 OGAKI FC≤5%
3 UNUMA FC≤5%
4 OGASE FC≤5%
7 ARAKAWA21 FC≤5% (16)@8.23m
8 ARAKAWA30 FC≤5% (12)@5.18m
17 TAKAYA 45 FC≤5%
87 YURIAGE.2 FC≤5%
55 QING YIN FC>5%
90 YURIAGEBR.2 FC>5%
SOIL
N
0
5
10
15
20
FILL
CLAYEY FINE SAND
SILTY CLAY
CLAYEY FINE SAND
FINE SAND
SANDY GRAVEL
FINE SAND
MEDIUM SAND
FINE SAND
CLAY
SANDY CLAY
SURFACE SOIL
LOAMY CLAY
SANDY CLAY
COARSE SAND WITH PUMICE
COARSE SAND WITH GRAVEL
CLAYEY COARSE SAND WITH GRAVEL
MEDIUM SAND
COARSE SAND WITH GRAVEL
FINE SAND
SANDY GRAVEL
LOAMY CLAY
CLAY
MEDIUM SAND WITH GRAVEL
COARSE SAND WITH GRAVEL
SANDY GRAVEL
COARSE SAND WITH GRAVEL
SANDY GRAVEL
SANDY GRAVEL
FINE SAND
SAND
FINE SAND
CLAY
FINE SAND
CLAY
MEDIUM SAND
CLAY (S)
CLAY
SANDY SILT
FINE SAND
MEDIUM SAND
COARSE SAND
MEDIUM SAND
SILTY FINE SAND
SANDY SILT
MEDIUM SAND
FINE SAND
SILTY SAND
SAND
SAND
SAND WITH GRAVEL
CLAY
SILT
FINE SAND
SILT
CLAYEY SAND
FINE SAND
SAND
SAND WITH GRAVEL
SAND WITH GRAVEL
1
4
6
4
23
27
24
23
20
16
17
18
17
16
14
11
7
8
2
15
17
19
17
19
20
16
2
1
11
13
16
18
28
28
20
17
46
26
33
41
>50
17
14
21
16
17
3
3
2
1
0
0
8
7
8
15
8
3
2
0
0
1
3
9
12
14
19
19
16
22
15
17
22
9
7
7
7
5
5
31
18
11
2
8
4
11
13
29
36
22
39
33
10
19
17
18
28
22
27
25
29
30
7
39
87
2
10
13
20
22
41
48
48
43
48
48
45
48
N SELECTED BY THE BERKELEY CATALOGUE
N CONSIDERED IN THIS STUDY
MINIMUM $(N_1)_{60}$ SELECTED IN THIS STUDY

Figure 2-2 Summary strip logs for all critical liquefied case records except Luan Nan (case record 56).

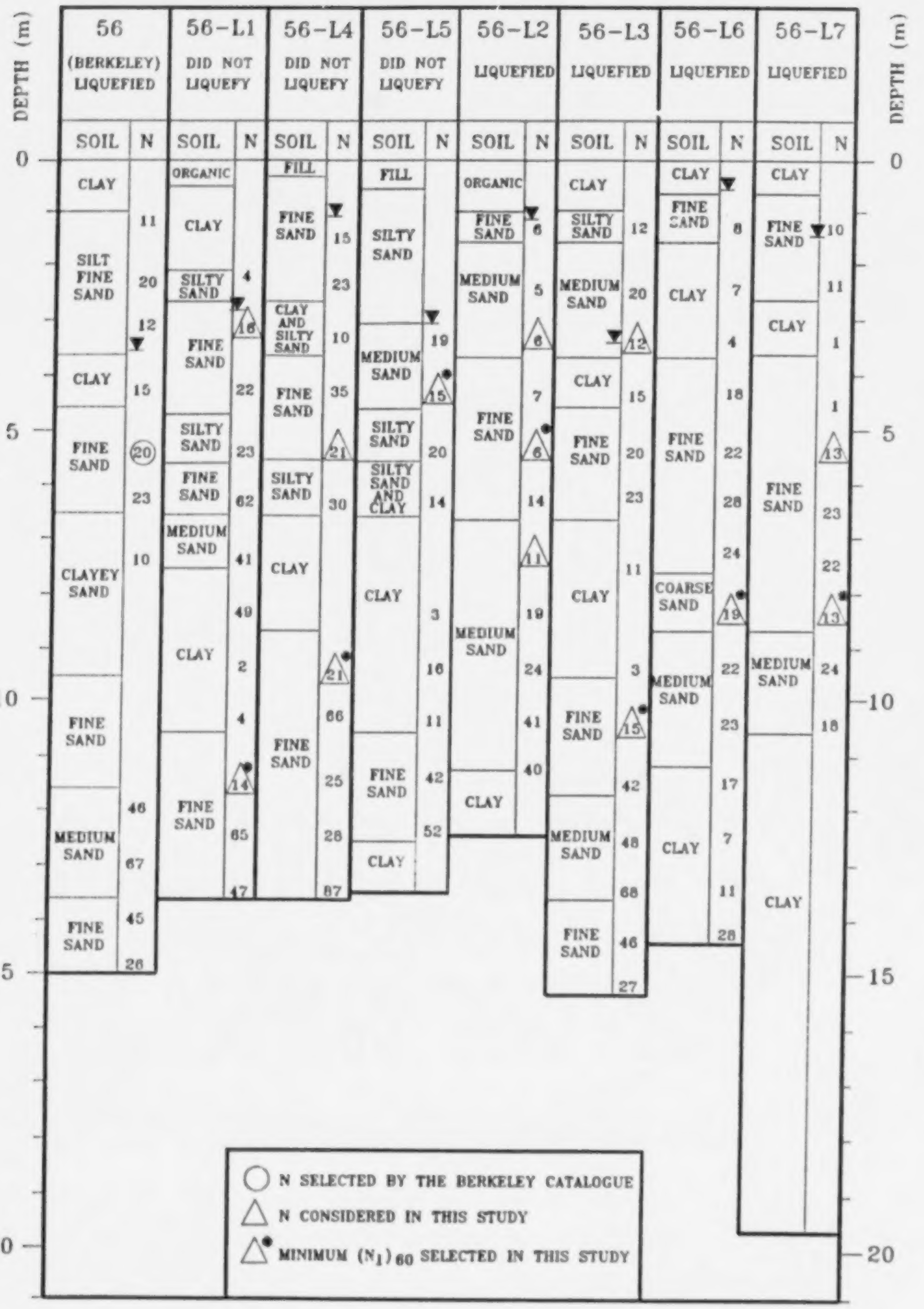
DEPTH (m)
56 (BERKELEY) LIQUEFIED
56-L1 DID NOT LIQUEFY
56-L4 DID NOT LIQUEFY
56-L5 DID NOT LIQUEFY
56-L2 LIQUEFIED
56-L3 LIQUEFIED
56-L6 LIQUEFIED
56-L7 LIQUEFIED
SOIL
N
0
5
10
15
20
CLAY
SILT FINE SAND
FINE SAND
CLAYEY SAND
MEDIUM SAND
ORGANIC
SILTY SAND
FILL
CLAY AND SILTY SAND
SILTY SAND AND CLAY
COARSE SAND
N SELECTED BY THE BERKELEY CATALOGUE
N CONSIDERED IN THIS STUDY
MINIMUM $(N_1)_{60}$ SELECTED IN THIS STUDY

Figure 2-3 Comparison of original summary strip log for Luan Nan (case record 56) with additional logs obtained in this study.

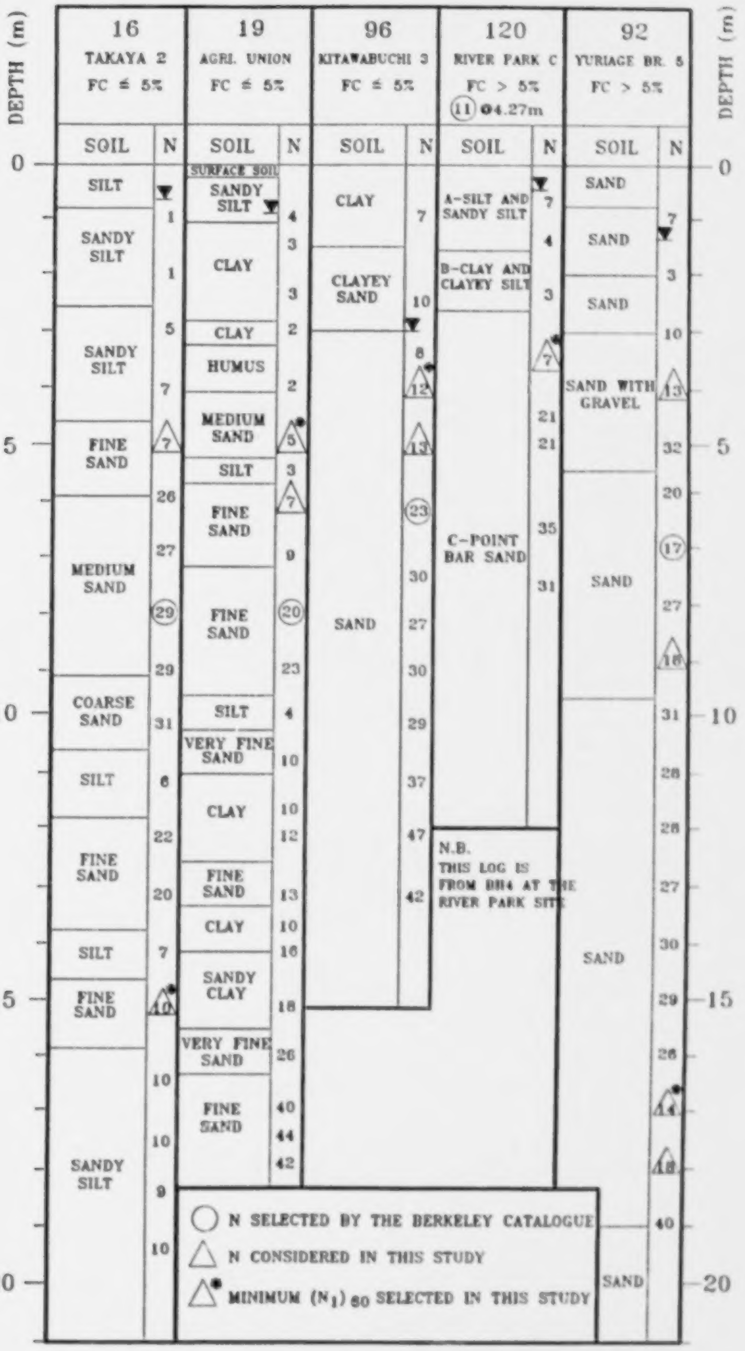
DEPTH (m)
16
TAKAYA 2
FC ≤ 5%
19
AGRI. UNION
FC ≤ 5%
96
KITAWABUCHI 3
FC ≤ 5%
120
RIVER PARK C
FC > 5%
⑪ @4.27m
92
YURIAGE BR. 5
FC > 5%
SOIL
N
0
5
10
15
20
SILT
SANDY SILT
SANDY SILT
FINE SAND
MEDIUM SAND
COARSE SAND
SILT
FINE SAND
SILT
FINE SAND
SANDY SILT
1
1
5
7
7
26
27
29
29
31
6
22
20
7
10
10
10
9
10
SURFACE SOIL
SANDY SILT
CLAY
CLAY
HUMUS
MEDIUM SAND
SILT
FINE SAND
FINE SAND
SILT
VERY FINE SAND
CLAY
FINE SAND
CLAY
SANDY CLAY
VERY FINE SAND
FINE SAND
4
3
3
2
2
5
3
7
9
20
23
4
10
10
12
13
10
16
18
26
40
44
42
CLAY
CLAYEY SAND
SAND
7
10
8
12
13
23
30
27
30
29
37
47
42
A-SILT AND SANDY SILT
B-CLAY AND CLAYEY SILT
C-POINT BAR SAND
7
4
3
7
21
21
35
31
N.B.
THIS LOG IS FROM BH4 AT THE RIVER PARK SITE
SAND
SAND
SAND
SAND WITH GRAVEL
SAND
SAND
SAND
7
3
10
13
32
20
17
27
16
31
28
28
27
30
29
26
14
18
40
○ N SELECTED BY THE BERKELEY CATALOGUE
△ N CONSIDERED IN THIS STUDY
△ MINIMUM $(N_1)_{60}$ SELECTED IN THIS STUDY

Figure 2-4 Summary strip logs for five sample nonliquefied case records.

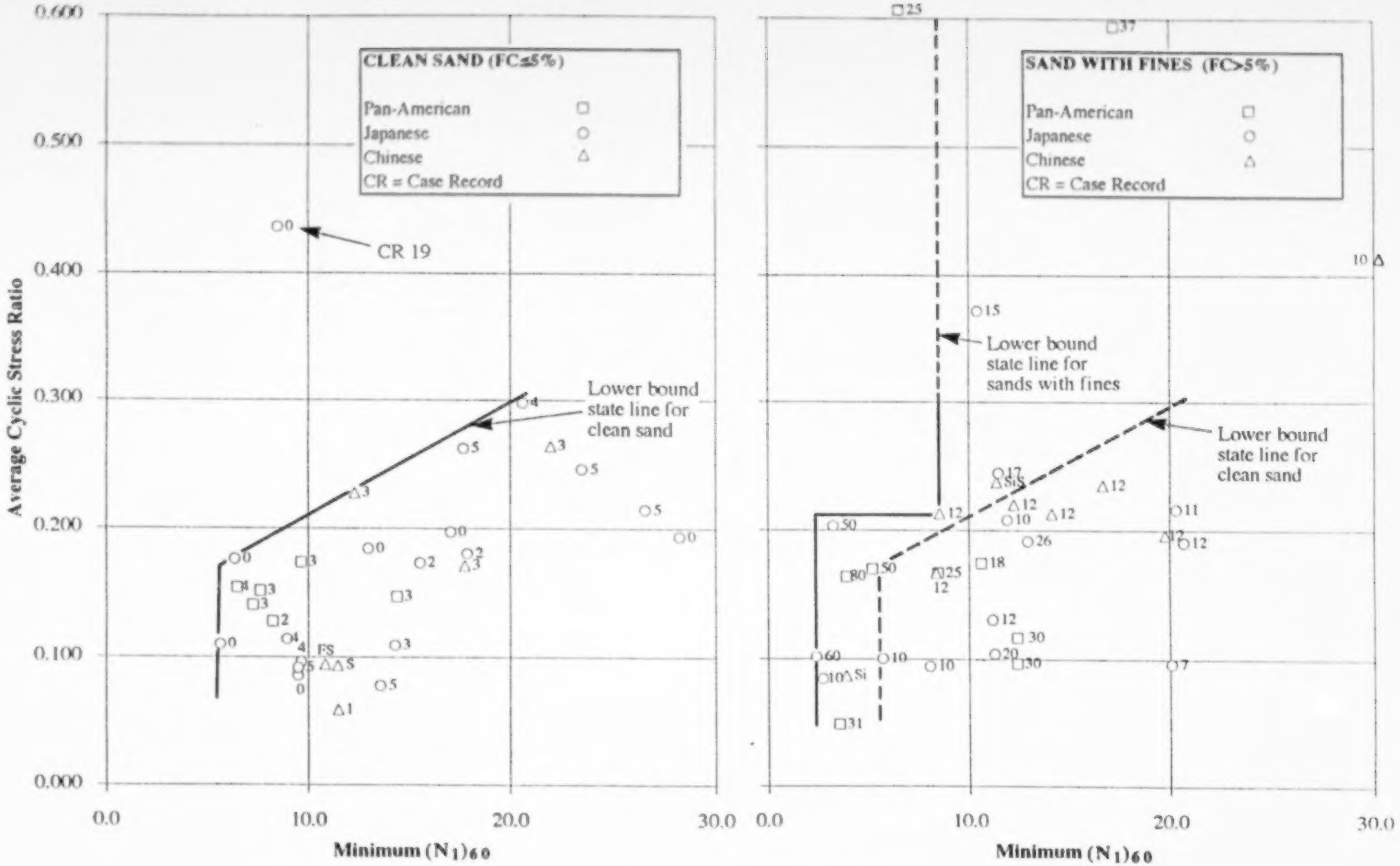

Figure 2-5 Plot of CSR versus $(N_1)_{60}$ from this study for nonliquefied case records.

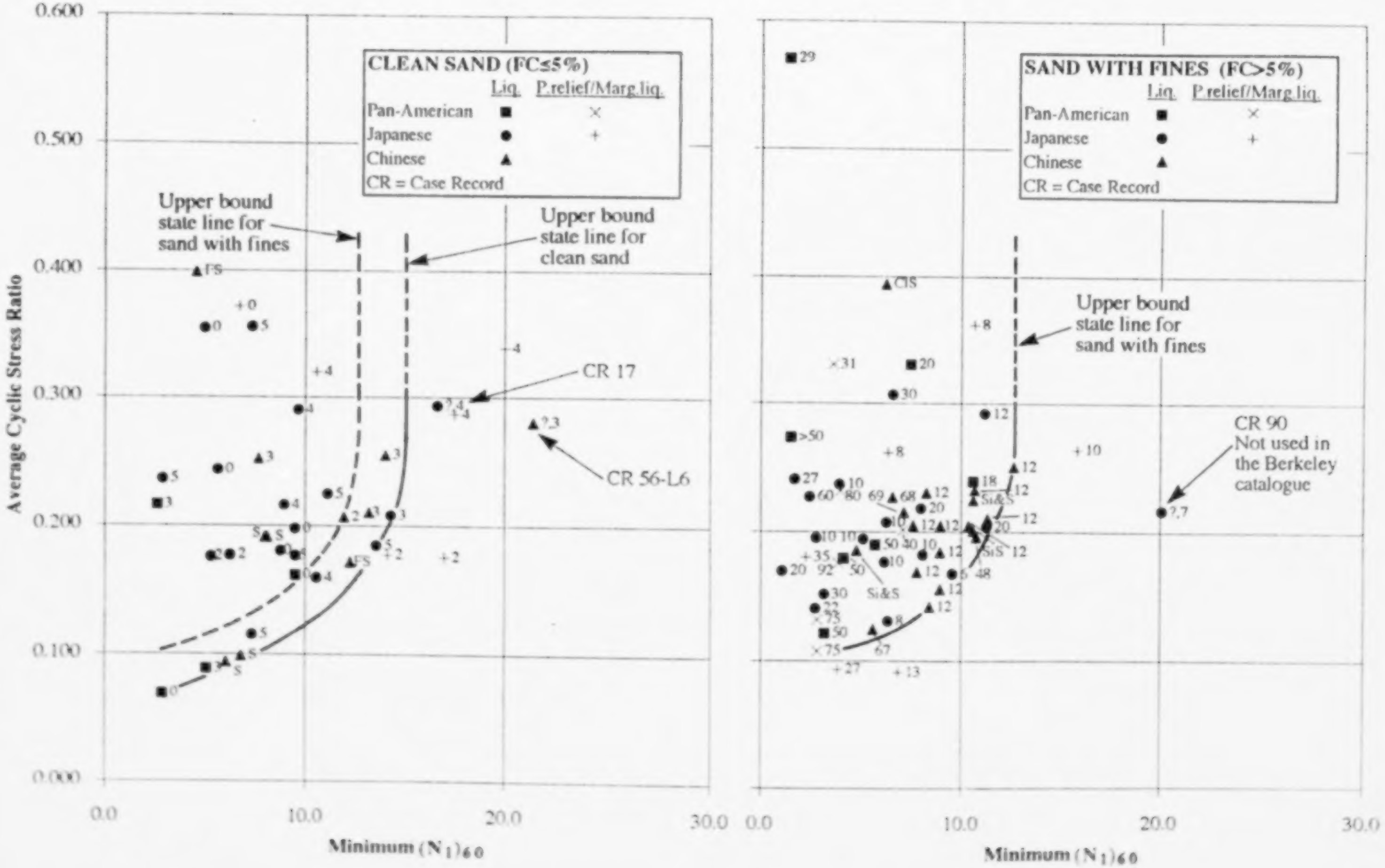

Figure 2-6 Plot of CSR versus $(N_1)_{60}$ from this study for liquefied and pressure relief case records.

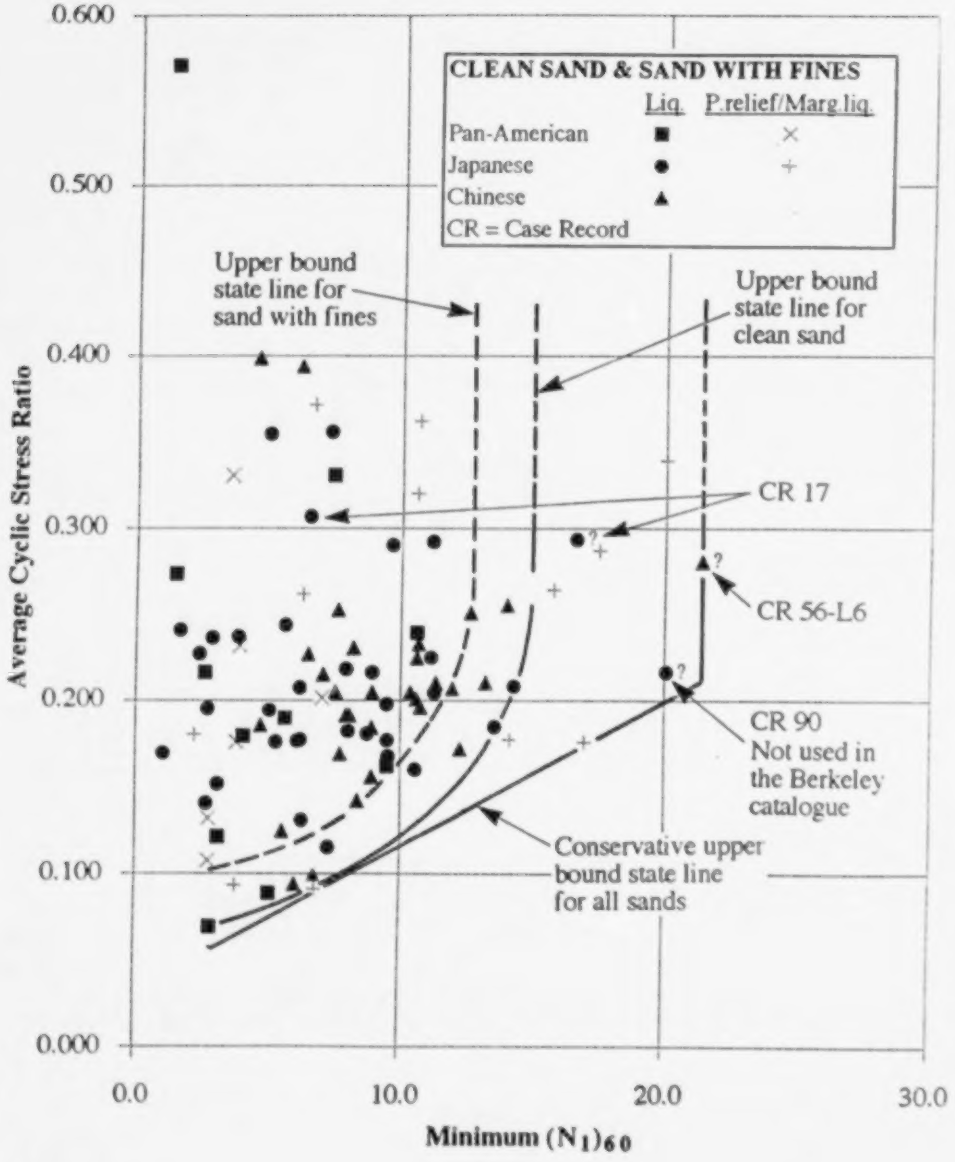

Figure 2-7 Plot of all liquefied and pressure relief case records from this study, showing upper bound state lines.

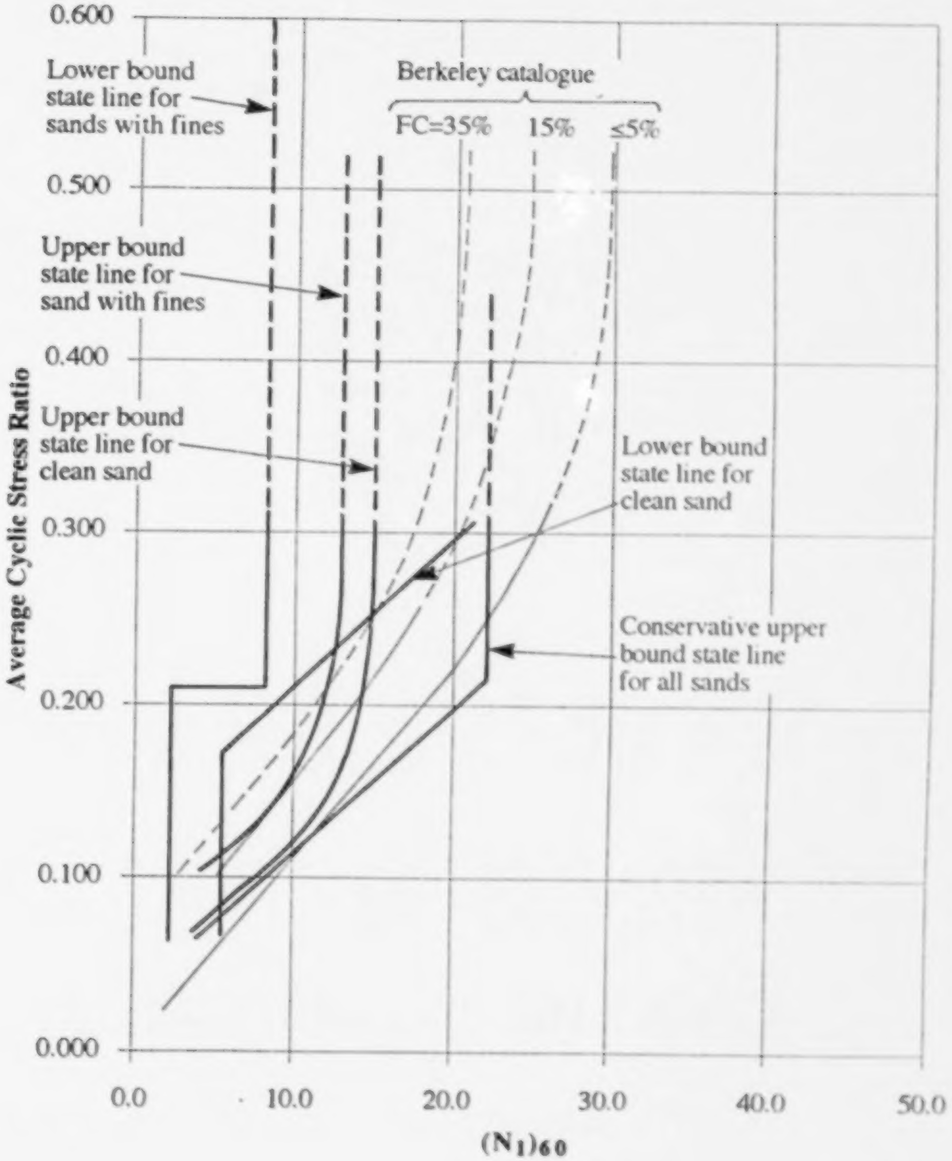

Figure 2-8 Summary of state boundary lines from this study compared with the original Berkeley interpretations.

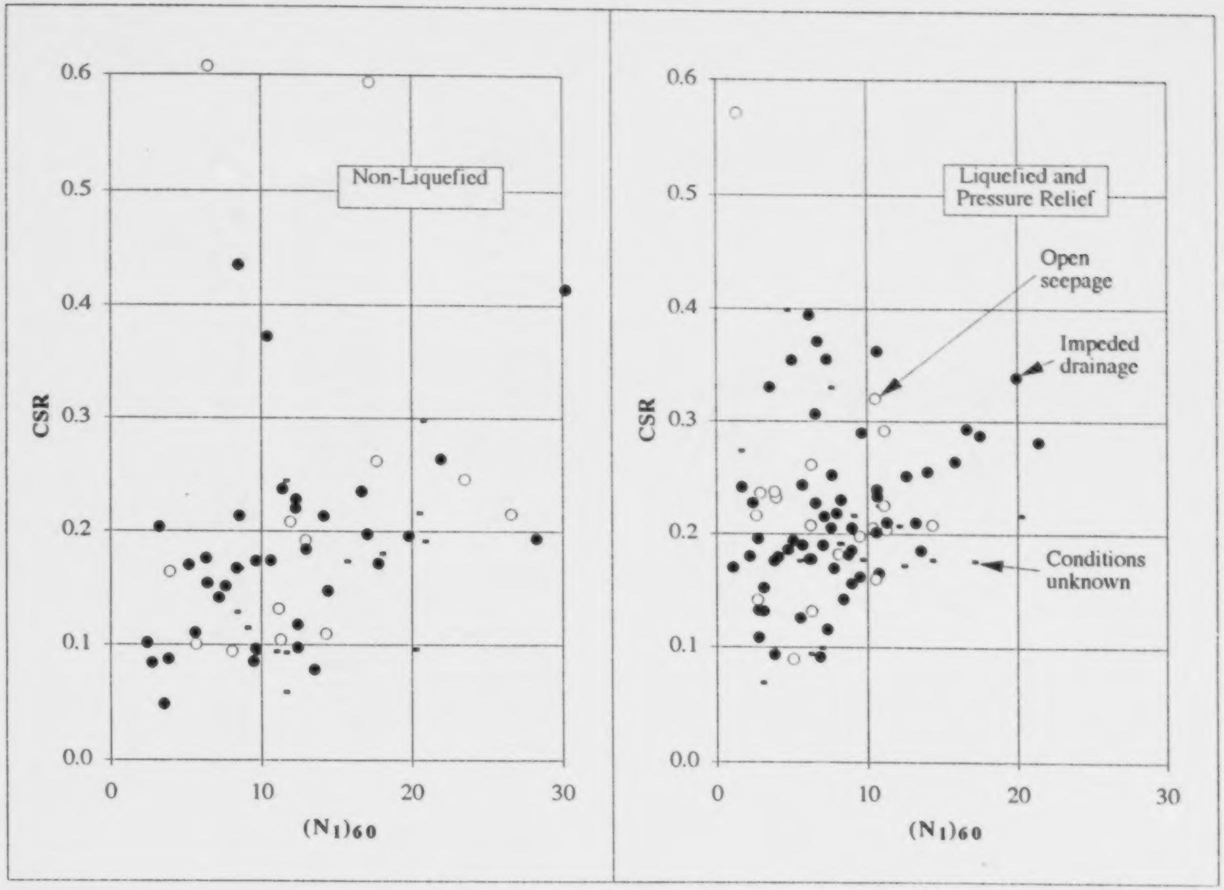

Figure 2-9 Plots of CSR versus $(N_1)_{60}$ to investigate effects of site drainage conditions.

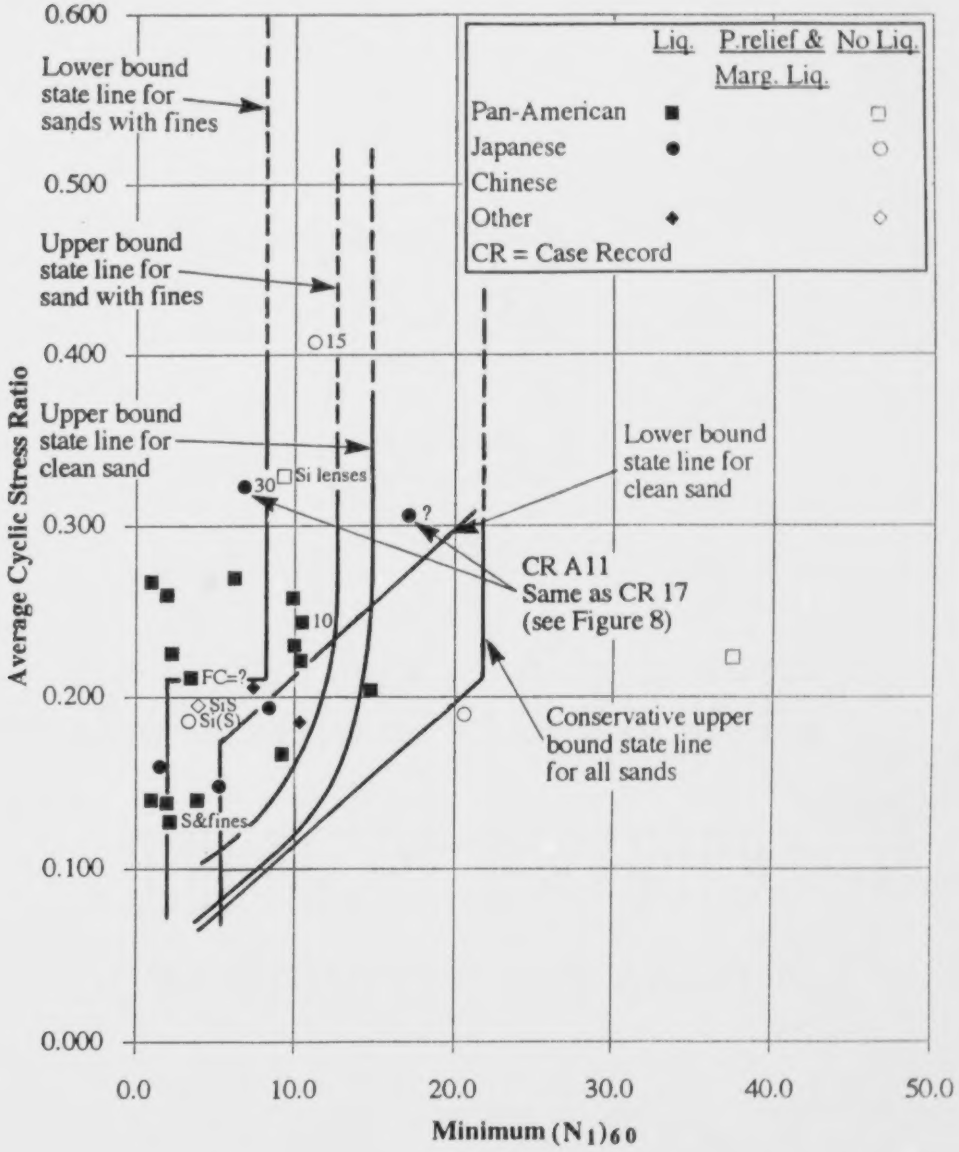

Figure 2-10 Comparison of recent data with the results of this study (labels refer to fines contents).

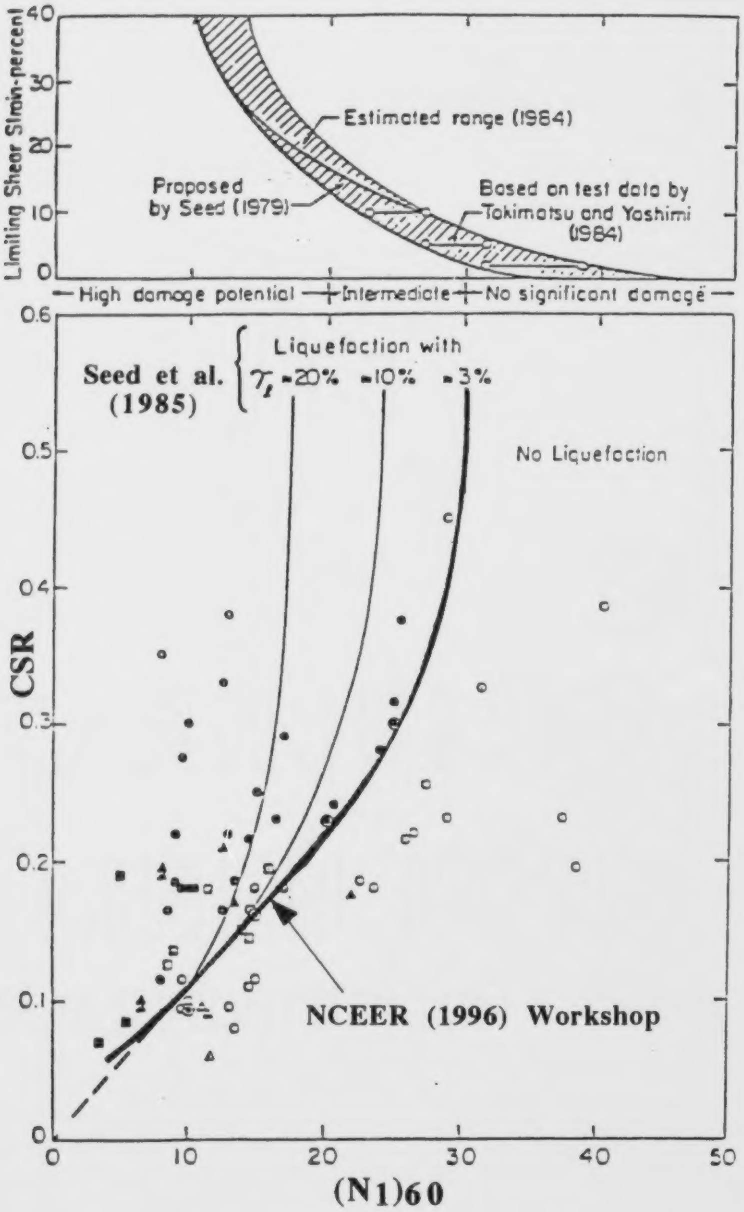

Figure 2-11 Plot of CSR versus $(N_1)_{60}$ with limiting strain lines for clean sand and line from NCEER (1996) Workshop (modified from Seed et al., 1985).

References

Ambraseys, N.N. 1992. Personal communication containing the list of references for the additional sites added to the Berkeley catalogue by Ambraseys (1988).

Ambraseys, N.N. 1988. Engineering seismology. *Earthquake Engineering and Structural Dynamics*, 17(1): 1-105.

Andrus, R.D., Stokoe, K.H., and Roesset, J.M. 1991. Liquefaction of gravelly soil at Pence Ranch during the 1983 Borah Peak earthquake. *Proc., Soil Dyn. and Earthq. Engrg.*, V, Computational Mech. Publ., Southampton, U.K., 251-262.

Bartlett, S.F. and Youd, T.L. 1992. Empirical analysis of horizontal ground displacements generated by liquefaction-induced lateral spreads. *National Center for Earthquake Engineering Research (NCEER), Technical Report NCEER-92-0021.*

Beijing Municipal Bureau of City Planning, Department of Geotechnical Exploration et al. 1982. *Research report of sand liquefaction during the Tangshan earthquake.* (in Chinese).

Byrne, P.M., Imrie, A.S., and Morgenstern, N.R. 1994. Results and implications of seismic performance studies for Duncan Dam. *Canadian Geotechnical Journal*, 31(6): 979-988.

Casagrande, A. 1976. Liquefaction and cyclic deformation of sands, a critical review. *Harvard Soil Mechanics Series No. 88*, Harvard University, Cambridge, Massachusetts.

Cluff, L.S. 1973. Personal communication cited by Seed et al. (1984).

Dames and Moore 1975. Offshore soils investigation, Los Angeles Harbor, LNG Ship Terminal. *Report to Western LNG Terminal Company.*

Fear, C.E., and McRoberts, E.C. 1993. Report on liquefaction potential and catalogue of case records, *Internal Research Report, Geotechnical Engineering Library*, Department of Civil Engineering, University of Alberta, Edmonton, Alberta, Canada.

Ishihara, K. 1993. Liquefaction and flow failure during earthquakes. *The 33rd Rankine Lecture, Géotechnique*, 43(3): 351-415.

Iwasaki, T. 1981. Studies on aseismic stability of river dykes considering ground liquefaction. *Proc. of the 16th Annual Meeting, JSSMFE*, 637-640 (in Japanese).

Iwasaki, T., Kawashima, K., and Tokida K. 1978. Report of the Miyagiken-Oki earthquake of June, 1978. *Public Works Research Institute, Ministry of Construction, Japan, Report No. 1422* (in Japanese).

Jamiolkowski, M., Baldi, G., Bellotti, R., Ghionna, V., and Pasqualini, E. 1986. Penetration resistance and liquefaction of sands. *Proceedings of the 11th International Conference of Soil Mechanics and Foundation Engineering*, San Francisco, 4: 1891-1896.

Kayen, R.E. 1993. Personal communication containing several borehole logs referred to, but not contained in Kayen et al. (1992).

Kayen, R.E., Mitchell, J.K., Lodge, A., Seed, R.B., Nishio, S., and Coutinho, R. 1992. Evaluation of SPT-, CPT-, and shear wave-based methods for liquefaction potential assessment using Loma Prieta data. *Proceedings of the Fourth Japan-U.S. Workshop on Earthquake Resistant Design of Lifeline Facilities and Countermeasures for Soil Liquefaction, Technical Report NCEER-92-0019*, 1, M. Hamada, and T. D. O'Rouke, eds., 177-204.

Kishida, H. 1969. Characteristics of liquefied sands during Mino-Owari, Tohnankai and Fukui earthquakes. *Soils Found.*, 9(1): 75-92.

Kodera, J. 1964. Earthquake damage and the ground of pier foundations, Part 1. *Tsuchi-To-Kiso*, 12(3): 11-18 (in Japanese).

Liao, S.S.C. 1986. Statistical modeling of earthquake-induced liquefaction. *Ph.D. Dissertation*, Department of Civil Engineering, Massachusetts Institute of Technology, 470 p.

Liao, S.S.C., and Whitman, R.V. 1986. A catalog of liquefaction and non-liquefaction occurrences during earthquakes. *Research Report*, Department of Civil Engineering, M.I.T., Cambridge, Massachusetts.

McRoberts, E.C., and Sladen, J.A. 1992. Observations on static and cyclic sand liquefaction methodologies. *Can. Geotech. J.*, 29(4): 650-665.

National Research Council 1985. Liquefaction of soils during earthquakes. Committee on Earthquake Engineering, Commission on Engineering and Technical Systems, G.W. Housner (Chairman), National Academy Press, 240 p.

NCEER Workshop 1996. Proceedings to be published at a subsequent date by Youd et al. (1996).

Robertson, P.K. 1994. Suggested terminology for liquefaction. *Proceedings of the 47th Canadian Geotechnical Conference, Halifax, Nova Scotia*, Canadian Geotechnical Society, Ottawa, Canada, 277-286.

Robertson, P.K., Woeller, D.J., and Finn, W.D.L. 1992. Seismic cone penetration test for evaluating liquefaction potential under cyclic loading. *Can. Geotech. J.*, 29(4): 686-695.

Rollins, K.M., and Seed, H.B. 1990. Influence of buildings on potential liquefaction damage. *J. Geotech. Engrg*., ASCE 116(2): 165-185.

Seed, H.B. 1987. Design problems in soil liquefaction. *J. Geotech. Engrg*., ASCE 113(8): 827-845.

Seed, H.B. 1983. Earthquake-resistant design of earth dams. *Proc. Symp. on Seismic Design of Embankments and Caverns*, ASCE, 41-64.

Seed, H.B. 1973. Cited in text, but missing from reference list in Seed et al. (1984).

Seed, H.B., Arango, I., and Chan, C. 1975. Evaluation of soil liquefaction potential during earthquakes. *Report No. EERC 75-28*, University of California, Berkeley.

Seed, H.B., and Idriss, I.M. 1971. Simplified procedure for evaluating soil liquefaction potential. *J. Soil Mech. Found. Div*., ASCE 97(9): 1249-1273.

Seed, H.B., and Idriss, I.M. 1982. *Ground motions and soil liquefaction during earthquakes.* The Earthquake Engineering Research Institute, University of California, Berkeley.

Seed, H.B., and Peacock, W.H. 1971. Test procedures for measuring soil liquefaction characteristics. *J. Soil Mech. Found. Div*., 97(8): 1099-1119.

Seed, H.B., Tokimatsu, K., Harder, L.F., and Chung, R.M. 1985. Influence of SPT procedures in soil liquefaction resistance evaluations. *J. Geotech. Engrg*., ASCE 111(12): 1425-1445.

Seed H.B., Tokimatsu K., Harder L.F., and Chung R.M. 1984. The influence of SPT procedures in soil liquefaction resistance evaluations. *Earthquake Engineering Research Center Report No. UCB/EERC-84/15*, College of Engineering, University of California, Berkeley, California.

Shengcong, F., and Tatsuoka, F. 1983. *Report of Japan-China Cooperative Research on Engineering Lessons from Recent Chinese Earthquakes, Including the 1976 Tangshan Earthquake (Part 1)*. C. Tamura, T. Katayama, and F. Tatsuoka, eds., Institute of Industrial Science, University of Tokyo.

Skempton, A. W. 1986. Standard penetration test procedures and the effects in sands of overburden pressure, relative density, particle size, ageing and overconsolidation." *Geotechnique*, 36(3): 425-447.

Tsuchida, H. 1979. The damage to port structures by the 1978 Miyagiken-Oki earthquake. *Technical Note, The Port and Harbour Research Institute, Ministry of Transport, Japan, No. 325* (in Japanese).

Yegian, M.K., Ghahraman, V.G., and Hrutiunyan, R.N. 1994. Liquefaction and embankment failure case histories, 1988 Armenian earthquake. *J. Geotech. Engrg. Div*., ASCE 120(3): 581-596.

Youd, T.L. 1993. Liquefaction-induced lateral spread displacement. *Technical Note N-1862*, Naval Civil Engineering Laboratory, Port Hueneme, California.

Youd, T.L., and Bennett, M.J. 1983. Liquefaction Sites, Imperial Valley, California. *J. Geotech. Engrg. Div.*, ASCE 109(3): 440-457.

CHAPTER 3

AN INTEGRATED METHOD FOR EVALUATING CYCLIC LIQUEFACTION POTENTIAL BASED ON THE CONE PENETRATION TEST (CPT)[1,2,3]

3.1 Introduction

Cyclic softening commonly occurs in the field as a result of earthquake loading, resulting in observable features such as sand boils, lateral spreading, and ground cracks. The largest deformations occur when in-situ shear stresses are low and the earthquake causes shear stress reversal in the ground (see Figure 3-1). This process results in essentially zero effective stress and subsequent large reductions in soil stiffness leading to deformations which accumulate with additional cycles of loading. Cyclic softening potential is a function of the density of the soil as well as the duration and size of the cyclic loading.

The previous chapter dealt with the SPT-based method of evaluating cyclic softening (liquefaction) potential at a site. The SPT based method, although it is the most commonly used method in practice, has many problems, primarily due to the unreliable nature of the SPT. Many factors can affect the SPT, including inadequate cleaning of the hole, failure to maintain an adequate head of water in the borehole, careless measure of hammer drop, inaccurate weight of the hammer, hammer striking the drill rod collar eccentrically, lack of hammer free fall, sampler driven above the bottom of the casing, careless blow count, use of a non-standard sampler, coarse gravel or cobbles in the soil and the use of bent drill rods (Kulhawy and Mayne, 1990). However, the most important factor affecting SPT results is the energy delivered to the SPT sampler. It is extremely important to measure the rod energy ratio delivered to the sampler during the actual site investigation (rather than relying on global correction values) and correct the measured blowcount to a reference energy ratio (generally accepted as 60%), in order to improve the level of reliability of the SPT. In

---

[1] *A version of part of this chapter has been published. Robertson, P.K. and Fear, C.E. 1995. Application of CPT to evaluate liquefaction potential, Proceedings of the International Symposium on Cone Penetration Testing, CPT'95, Linkoping, Sweden.*

[2] *A version of part of this chapter has been published. Robertson, P.K. and Fear, C.E. 1995. Liquefaction of sands and its evaluation, Proceedings of IS Tokyo '95, First International Conference on Earthquake Geotechnical Engineering, Keynote Lecture.*

[3] *A version of part of this chapter is in the process of being published. Robertson, P.K. and Fear, C.E. 1996. Soil liquefaction and its evaluation based on SPT and CPT, Proceedings of the 1996 NCEER Workshop on Liquefaction.*

addition, the SPT is typically conducted at five foot depth intervals. It is therefore possible to miss important ground features. The cone penetration test (CPT), being continuous in nature, can provide a more detailed profile of the ground. In addition, the CPT is generally more repeatable and reliable.

3.2 Estimation of Cyclic Resistance Ratio (CRR)

Cyclic softening is predicted to occur when the cyclic stress ratio (CSR) induced by the earthquake exceeds the cyclic resistance ratio (CRR), τ_{cyc}/σ_{vo}', available in the ground. Seed et al. (1985) developed a simplified method to estimate CSR (see Chapter 2); this approach can be summarized as follows (after Tokimatsu and Yoshimi, 1983):

$$\text{[3-1]} \qquad CSR = \frac{\tau_{av}}{\sigma_{vo}'} = 0.1\,(M - 1)\,(\frac{a_{max}}{g})(\frac{\sigma_{vo}}{\sigma_{vo}'})(1 - 0.015z)$$

where:
τ_{av} = average cyclic shear stress
M = earthquake magnitude, commonly 7.5
a_{max} = maximum horizontal acceleration at ground surface
g = acceleration due to gravity = 9.81 m/s^2
σ_{vo} = total vertical overburden stress
σ_{vo}' = effective vertical overburden stress
z = depth in meters (for $z < 25$m).

CRR can be estimated in the field using the SPT (see Chapter 2), CPT or V_s measurements or estimated in the laboratory using cyclic triaxial or cyclic simple shear testing.

Correlations between CRR and CPT q_{c1} for both clean sand and silty sands were developed by Robertson and Campanella (1985), by converting the Seed et al. (1985) SPT-based correlation for clean sand (see Chapter 2) using general $q_{c1}/(N_1)_{60}$ ratios. Similar CPT-based charts were developed by Seed and de Alba (1986), Shibata and Teparaska (1988) and Mitchell and Tseng (1990). Figure 3-2 illustrates the differences between the most commonly used CPT-based charts. Based on recent discussions at the NCEER Workshop (1996), the curve by Robertson and Campanella (1985) has been modified slightly to be more consistent with the SPT curve (see Figure 3-3: solid line represents relationship proposed by Robertson and Campanella, 1985; dashed line represents modification based on NCEER Workshop, 1996). The resulting modified CPT clean sand correlation can be approximated by the following equation:

$$[3\text{-}2] \qquad CRR = 93\left(\frac{(q_{c1})_{cs}}{100}\right)^3 + 0.08$$

where:
$(q_{c1})_{cs}$ is the equivalent clean sand q_{c1}, in MPa
3 MPa $< (q_{c1})_{cs} <$ 16 MPa.

Until recently, the database of cyclic softening (liquefaction) case histories having SPT data available (see Chapter 2) was much larger than the databases of case histories having CPT or shear wave velocity data available; consequently, the SPT-based method has been the most commonly used method in practice. However, the amount of available CPT field performance data is increasing (Ishihara, 1993; Kayen et al., 1992; Stark and Olson, 1995; Suzuki et al., 1995) and the combined database is now larger than the SPT database. The recent CPT data seem to confirm that the existing CPT-based correlations for estimating CRR are generally good for both clean sands and silty sands. Figure 3-3 compares the recent field performance data from Stark and Olson (1995) and Suzuki et al. (1995) for clean sands to the Robertson and Campanella (1985) clean sand correlation. In general, the correlation by Robertson and Campanella (1985) gives a dividing line between liquefaction case records and non-liquefaction case records that matches the field performance data well. The slight modification to the Robertson and Campanella (1985) correlation, based on the NCEER Workshop (1996) discussions and as approximated by Equation 3-2, is also shown in Figure 3-3.

The field observation data in the Stark and Olson (1995) and Suzuki et al. (1995) databases are apparently based on the following:

Holocene age, clean sand deposits
Level or gently sloping ground
Magnitude M=7.5 earthquakes
Depth range from 1 to 15 m (3 to 45 ft)
  (84% is for depths < 10 m (30 ft))
Representative average CPT q_{c1} values for the layer that was considered to have experienced cyclic liquefaction.

Therefore, caution should be exercised when extrapolating the CPT correlation given in Equation 3-2 to conditions outside of the above range. Since this CPT method is based on the Seed methodology, similar limitations apply as to when the correlation is applicable and similar uncertainty exists over degree of conservatism contained within the correlation. An important feature to recognize is that the correlation appears to be based on average values for the liquefied layers. However, due to the continuous nature of the CPT, the correlation is often applied to all measured CPT values, including low values below the average. Having the continuous soil profile is useful, but caution should be taken when applying the average based CPT methodology to variable deposits in which a small part of the CPT data predicts that cyclic liquefaction could occur. The possible conservatism of the method when applied to such cases as well as the consequences of liquefaction of individual layers should be considered as part of the design process. A detailed review of the CPT data, similar to that carried out by Fear and McRoberts (1995) on SPT data (see Chapter 2) would be required to investigate the degree of conservatism contained in Figure 3-3.

The correlation given in Equation 3-2 is for clean sands. In general, for the same CRR, the penetration resistance in silty sands is smaller. This is likely due to the greater compressibility and decreased permeability of silty sands, which reduces penetration resistance and moves the penetration process toward an undrained penetration, respectively. Based on their database of 180 CPT case records (some in clean sands, as shown in Figure 3-3, and some in silty sands), Stark and Olson (1995) were able to develop a set of correlations between CRR and q_{c1} for various sandy soils, based on fines content and mean grain size, as shown in Figure 3-4.

Based on the work by Stark and Olson (1995), fines content based corrections to tip resistance can be estimated to allow measurements of q_{c1} in silty sands to be converted to clean sand equivalent values. The range in potential corrections (Δq_{c1}) are illustrated in Figure 3-5; the recommended correction can be expressed by the following:

$$[3\text{-}3] \qquad \begin{aligned} &\Delta q_{c1} = 6 \text{ MPa} && \text{if FC} \geq 35\% \\ &\Delta q_{c1} = 0 && \text{if FC} \leq 5\% \\ &\Delta q_{c1} = 0.2\,(\text{FC} - 5)\ \text{MPa} && \text{if } 5\% < \text{FC} < 35\% \end{aligned}$$

where:
FC = fines content, in percent.

Note that Figure 3-5 also indicates the corresponding suggested corrections, $\Delta(N_1)_{60}$, for the SPT, as a function of fines content. Although the corrections given by Figure 3-5 and Equation 3-3 are based on fines content, it is clear that the CRR of a soil is a function of many factors, including plasticity of the fines, grain characteristics (mineralogy, grain shape etc.) as well as fines content. Hence, the corrections should be applied with caution. When a soil is fine-grained or contains some amount of fines, some cohesion or adhesion can develop between the fine particles making the soil more resistant at essentially zero effective confining stress. A greater CRR is generally exhibited by sandy soils containing some fines. However, this tendency depends on the type of fines (Ishihara, 1993). Laboratory testing has shown that the most important index property distinguishing which type of fines have this effect is plasticity index, I_p (Ishihara and Koseki, 1989). Cyclic triaxial tests reported by Ishihara (1993) suggested that $I_p=10$ is the point below which the presence of fines has little effect on CRR, but above which, CRR increases with increasing values of I_p.

3.3 Estimation of Soil Behaviour Type

Since the corrections suggested in Equation 3-3 are based on fines content, a profile of fines content with depth must be determined. One reason for the continued use of the SPT has been the need to obtain a soil sample for determining the fines content of the soil in order to apply the Seed methodology (see Chapter 2). Although the CPT has the advantage that it produces a continuous profile, unlike the SPT, it does not provide samples for which grain size distributions can be produced. However, in recent years, various charts have been developed to estimate soil type from the CPT (Olsen and Malone, 1988; Robertson and Campanella, 1988; Robertson, 1990). Since fines content is obviously some function of soil type, it seems logical to try to estimate fines content from the CPT predictions of soil behaviour type. It is possible to combine the CPT results (cone tip resistance and sleeve friction) with soil classification charts, such as that by Robertson (1990) shown in Figure 3-6 to estimate soil behaviour type. The boundaries between soil behaviour type zones 2 to 7 can be approximated as concentric circles about a common point (Jefferies and Davies, 1993). The radius of each circle can then be used as a soil behaviour type index. This index, I_c, based on the CPT chart by Robertson (1990), is defined as follows:

$$[3\text{-}4] \qquad I_c = [\,(3.47 - \log Q)^2 + (\log F + 1.22)^2\,]^{0.5}$$

where:
Q = normalized CPT penetration resistance = $(q_c - \sigma_{vo})/\sigma_{vo}'$
F = normalized friction ratio, in percent = $[f_s/(q_c - \sigma_{vo})] \times 100\%$
f_s = CPT sleeve friction.

The boundaries of soil behaviour type are then given in terms of the index, Ic, as shown in Table 3-1. The soil behaviour type index does not apply to zones 1, 8 or 9.

3.4 Estimation of Fines Content

Experience has shown that the CPT friction ratio (ratio of the CPT sleeve friction to the cone tip resistance) increases with increasing fines content and soil plasticity. Figure 3-7 from Suzuki et al. (1995) illustrates the relationship between friction ratio and fines content. Many soils fall in the normally consolidated region of the soil behaviour type chart shown in Figure 3-6. Therefore, as soil behaviour type changes from a clean sand to a sandy silt (I_c increases from 1.31 to 2.60), friction ratio increases and a range in fines content can be estimated according to the soil behaviour type index, I_c, as shown in Figure 3-8. The recommended relationship shown in Figure 3-8 can be approximated by the following equation:

[3-5] $$\text{Fines Content, FC (\%)} = 1.75\, I_c^3 - 3.7$$

In combination, Equations 3-2 to 3-5 provide an integrated CPT approach to estimating the potential for cyclic liquefaction in a sandy deposit. By considering this integrated approach in terms of its individual components, it is possible to modify the equations to account for site specific conditions. For example, the profile of estimated fines content with depth can be compared with actual measured fines contents from samples and the relationship in Equation 3-5 can be modified to best fit the site specific data. The final profile of estimated CRR with depth can be compared with laboratory testing on undisturbed samples.

3.5 Laboratory Methods for Estimating CRR

Resistance to cyclic loading (CRR) is a primarily a function of the state of a soil (i.e. void ratio, effective confining stresses and soil structure) and the intensity and duration of the cyclic loading (i.e. cyclic shear stress and number of cycles), as well as the grain characteristics of the soil. Soil structure incorporates factors such as fabric, age and cementation. Grain characteristics incorporate factors such as grain size distribution, grain shape and morphology. Void ratio (i.e. relative density) is recognized as a dominant factor affecting the CRR of sands. However, studies by Ladd (1974), Mulilis et al. (1977) and Tatsuoka et al. (1986) have clearly shown that sample preparation (i.e. soil fabric) is important. Therefore, reconstituted samples may have a different resistance to cyclic loading than undisturbed samples, since it can be difficult to simulate the in-situ fabric when preparing reconstituted samples. Tokimatsu and Hosaka (1986) suggested that shear wave velocity measurements or the small strain shear modulus could be used to improve the value of testing reconstituted samples in the laboratory. Ideally, testing undisturbed samples is the best method of determining the appropriate values of in-situ CRR.

In the laboratory, when testing undisturbed samples of sand, CRR can be estimated by conducting either cyclic triaxial or cyclic simple shear tests. The latter are generally considered to more closely represent earthquake loading for level ground conditions. Cyclic simple shear tests can be interpreted in terms of the applied cyclic stress ratio (CSR) which results in "liquefaction" of a sample. This value of CSR is equal to the cyclic resistance of the soil (i.e. CRR) to the applied loading. Typically, a sample is loaded in undrained cyclic shear under a constant CSR and the number of uniform cycles (N) that must be applied to cause "liquefaction" is recorded.

It is important to define the onset of "liquefaction" as the point at which the soil experiences large uncontrolled deformations, rather than the point at which 5% double amplitude axial strain is reached (a common definition in historical laboratory testing). For loose sand, the 5% double amplitude strain criterion is often met close to the point at which the effective confining stress is essentially zero and deformations develop rapidly; hence, the definition is the same as that for cyclic liquefaction. However, for denser sand samples, the 5% double amplitude strain criterion can occur well before sufficient pore pressure has developed to take the sample to the state of essentially zero effective stress. Hence, if that definition of liquefaction is adopted, it may well be unduly conservative since deformations may actually be progressing rather slowly.

Since different samples will "liquefy" under different numbers of cycles, the results can be normalized to estimate the equivalent values of CRR that would liquefy the same samples under 15 cycles of undrained loading. Based on the work by Seed et al. (1985), the equivalent CSR at N=15 (equivalent to earthquake magnitude, M = 7.5) can be determined by multiplying the applied CSR by a correction factor ($1/r_m$), where r_m is dependent upon the measured N (or the equivalent earthquake magnitude, M), as given in Table 3-2. Tokimatsu and Yoshimi (1983) suggested that the correction factor ($1/r_m$) could be approximated by the following equation:

$$\frac{1}{r_m} = \frac{0.1(M-1)}{0.65} \qquad [3\text{-}6]$$

A best fit curve through the M and N data in Table 3-2, is shown in Figure 3-9 and indicates that M can be approximated from N using the following equation:

$$M = -0.0038N^2 + 0.2442N + 4.7034 \qquad (R^2 = 0.9989) \qquad [3\text{-}7]$$

Equations 3-6 and 3-7 can be combined in order to correct the applied CSR to an equivalent CSR at N=15 cycles. This can be taken as the CRR of the soil for a Magnitude M=7.5 earthquake with 15 cycles of equivalent uniform loading.

For high risk projects, a limited amount of laboratory testing on high quality undisturbed samples of sand should be considered. The method of in-situ ground freezing has been successful in obtaining undisturbed samples of sandy soils at several sites (Yoshimi et al., 1978; Yoshimi et al., 1989; Yoshimi et al., 1994; Sego et al., 1994; Hofmann et al., 1994 and 1995). In general, cyclic simple shear tests are the most appropriate tests to perform.

3.6 Linking the In-Situ Method to Laboratory Testing

On a site specific basis, predictions of CRR based on any of the three in-situ tests (SPT, CPT or V_s) and measurements of CRR by laboratory testing of undisturbed samples can be compared. The integrated CPT approach is the most straightforward and comprehensive method to apply. However, if data from more than one in-situ testing method are available, evaluating CRR based on each of the methods is useful for providing independent evaluations of cyclic softening (liquefaction) potential. The formulae given for the integrated CPT approach are general in nature and may not apply on a site specific basis. It is recommended that for low risk projects, the integrated CPT approach be applied directly. However, for moderate to high risk projects, a site specific approach with a link to laboratory testing should be taken in order to modify the individual components of the method if necessary. This will allow for estimates of CRR to be extrapolated beyond the zone of undisturbed sampling, based on the results of in-situ testing alone. Thus, laboratory testing and field testing can be linked in a framework for investigating the potential for cyclic softening. The profile of CRR can then be compared with the predicted CSR profile for the design earthquake in order to estimate liquefaction potential at the site in question.

The primary concern for cases of cyclic liquefaction is the amount of deformation that occurs during and after the earthquake. Catastrophic flowslides will generally not occur, since cyclic liquefaction tends to occur in level or gently sloping ground in which shear stress reversal occurs (although if cyclic liquefaction occurs at the toe of a slope, the slope may fail in a slumping fashion). However, cyclic liquefaction will result in horizontal displacements, lateral spreading and surface settlements. These movements can affect the integrity of structures if the deformations are significant. Post cyclic liquefaction shear strains (resulting in horizontal displacements) and post cyclic liquefaction volumetric strains (resulting in settlements) can be estimated using methods suggested by Ishihara (1993), as shown in Figure 3-10. These methods are suitable to the integrated CPT approach because they are based on the factor of safety against liquefaction (i.e. the ratio of CRR to CSR) and incorporate values of CPT q_{c1}. In the case of slightly sloping ground, methods such as those proposed by Bartlett and Youd (1995) can be used to estimate deformations associated with lateral spreading.

3.7 Application of the Integrated CPT Approach

Phase III of the Canadian Liquefaction Experiment (CANLEX) Project consisted of filling an old borrow pit (J-pit) at Syncrude, in Ft. McMurray, Alberta, with tailings to create a relatively loose sand deposit with a groundwater table at a depth of approximately 0.5 m. Figure 3-11 presents a plan of the area of detailed test site at which in-situ testing and in-situ freezing and sampling were performed. Both SPT and CPT testing was conducted in the detailed test site area.

Grain size distributions were performed on samples from the SPT sampler, giving estimates of fines content with depth at the site. Each SPT was paired up with the closest CPT in order to compare the measured fines contents with the fines content profiles predicted using the integrated CPT method. Thus, CPT-20 and SPT-1 were paired together, CPT-22 and SPT-2 were paired together, and CPT-23 and SPT-3 were paired together. Figure 3-12 compares the profiles of predicted fines content for each CPT with the measured fines contents from the corresponding SPT. In general, the predicted fines content is close to the measured values, although there is some scatter, which may be due, in part, to the averaging effect of the sampling as well as the approximate nature of the correlation. It appears that the method may overestimate fines content when the actual fines content is low (e.g. see the CPT22-SPT2 comparison). However, it is interesting to note the rapid variation in fines content with depth at this particular site and how the interpretations of fines content using the integrated CPT method appears to track this variation.

Figure 3-13 illustrates how each component of the integrated CPT approach can be applied to a CPT profile. In this case, the CPT profile is one of several CPTs performed in the detailed test site at the Massey Tunnel site (CPT M9406), as part of Phase II of the CANLEX project. Detailed testing and in-situ freezing and sampling was concentrated in a target zone located from 8 m to 13 m. Additional details regarding the interpretation of the Massey Tunnel site are given in Chapter 8. Figure 3-13 first presents the profile of corrected cone tip resistance, q_{c1}, for the particular CPT. The profile of soil behaviour type index, I_c, was estimated by combining the cone tip resistance and sleeve friction from the CPT with Equation 3-4. The soil above 5 m depth is quite variable with the estimated I_c ranging from approximately 1 to 3. However, below 5 m, the soil becomes fairly uniform, with an average estimated I_c of approximately 1.8. Based on Table 3-1, this value of I_c corresponds to a sand, ranging from a clean sand to a silty sand.

The profile of fines content was estimated by combining the profile of I_c with Equation 3-5. The estimated fines content is quite variable above 5 m, but below 5 m, it is fairly constant with an average value of approximately 6%. Superimposed on the CPT estimated profile of fines content is a range of measured fines contents in the target zone (8 m to 13 m). The CPT estimated profile appears to overestimate fines content in this region; however, the indicated range of measured values are presently based on very limited data. Further testing is required at this site to produce a clear profile of measured fines contents with depth. The profile of the recommended correction to cone tip resistance, Δq_{c1}, was estimated by combining the profile of fines content with Equation 3-3. Above 5 m, Δq_{c1} is quite variable, ranging from zero to large values, corresponding to the variety in the estimated fines content. Below 5 m, Δq_{c1} is fairly uniform and rather small because the estimated fines content in this region is fairly constant and generally not much greater than 5% (see Equation 3-3).

Adding the Δq_{c1} profile to the measured q_{c1} profile and combining the resulting equivalent clean sand profile of corrected tip resistance, $(q_{c1})_{cs}$, with Equation 3-2 produces the final profile of CRR. As for the profiles of the individual components of the integrated CPT method, the estimated CRR is quite variable above 5 m. However, below 5 m, it is fairly constant with an average value of approximately 0.1. Superimposed on the CRR profile are the results of testing undisturbed samples of sand from the Massey site in the laboratory. Cyclic simple shear tests were performed and the measured cyclic resistance for each test was corrected to equivalent Magnitude M=7.5 (N=15 cycles) values of CRR using Equations 3-6 and 3-7. The CPT estimated profile of CRR compares well with the laboratory results. However, since the average fines content was generally less than 10% in the region in which the samples were tested, the corrections to CPT tip resistance for fines content were very small. Further laboratory testing of undisturbed samples from sites at which the fines content is greater and would lead to more significant corrections to cone tip resistance would be useful to confirm how well the integrated CPT method estimates CRR in siltier sands.

3.8 Other Methods of Estimating CRR

Olsen and Malone (1988), Olsen and Koester (1995) and Suzuki et al. (1995) have also suggested integrated methods to estimate the CRR of sandy soils directly from the CPT. The correlations are presented in the form of soil type behaviour charts with contours of CRR. The Olsen and Koester (1995) method (see Figure 3-14) is based on SPT-CPT conversions plus some laboratory CRR data. The Suzuki et al. (1995) method (see Figure 3-15) is based on field observation data. Note that the Olsen and Koester (1995) method has truly normalized the corrected q_{c1} by dividing it by atmospheric pressure (typically taken as 100 kPa = 0.1 MPa), resulting in a dimensionless term, whereas Suzuki et al (1995) presented results in MPa. When q_{c1} is expressed in units of MPa, the normalized value is therefore approximately ten times larger in magnitude.

The method described here is based on field observations and is similar to those of Olsen and Koester (1995) and Suzuki et al. (1995), but has the advantage that the process has been broken down into its individual components (see Equations 3-2 to 3-5). This allows for the incorporation of site specific correlations when applying the method. Figure 3-16 summarizes the components of the integrated CPT method recommended here by presenting contours of estimated CRR on the soil classification chart by Robertson (1990). Note that the cone tip resistance in Figure 3-16 is expressed as Q (see Equation 3-4); for vertical effective stresses close to 100 kPa, the value of Q is essentially the same as the normalized q_{c1} used by Olsen and Koester (1995). The contours of estimated CRR were determined by combining Equations 3-2 to 3-5. Note that the contours of estimated CRR are generally cut off in zone 4 (silt mixtures). Beyond this zone, soil plasticity can have a significant effect on cyclic resistance. For CPT data falling within zone 4, soil plasticity should be evaluated in order to determine its effect on CRR. The integrated CPT method proposed here does not incorporate the effects of soil plasticity. Consequently, it does not apply to zone 3 (clays) where the effects of soil plasticity can be significant. Contours of estimated fines content are also presented, based on combining Equations 3-4 and 3-5. Comparing Figure 3-16 to Figures 3-14 and 3-15 illustrates that, in general, the predictions of CRR using the method proposed here are more conservative than either the Olsen and Koester (1995) method or the Suzuki et al. (1995) method, particularly for sandy soils with fines. The chart in Figure 3-16 is primarily shown for illustrative purposes.

CRR can also be estimated from shear wave velocity measurements. Figure 3-17a presents a correlation between corrected shear wave velocity, V_{s1}, and CRR developed by Robertson et al. (1992), based on limited field performance data. Tokimatsu et al. (1991) suggested a similar chart based on laboratory results. Kayen et al. (1992) and Lodge (1994) modified the chart proposed by Robertson et al. (1992), based on additional field data. A comparison of the methods by Robertson et al. (1992), Kayen et al. (1992) and Lodge (1994) is presented in Figure 3-17b. Based on discussions at the recent NCEER Workshop (1996), use of a relationship between V_{s1} and CRR similar to that by Lodge (1994) has been recommended. Note that the correlations in Figure 3-17b have been shown down to a CRR of only about 0.1. It would be expected that below CRR=0.1, the relationships would become much flatter. The correlations are empirical and, again, there is uncertainty over the degree of conservatism that they contain because of the methods used to select the representative values of shear wave velocity for the various case histories. A detailed review of the shear wave velocity data, similar to that carried out by Fear and McRoberts (1995) on SPT data would be required to investigate the degree of conservatism contained in Figure 3-17. The same limitations as to the applicability of the correlation apply as for the SPT and CPT, due to the type of the case records contained in the database. At present, the integrated CPT approach is more reliable than the shear wave velocity method. The shear wave velocity database is limited and the profiles of shear wave velocity, although they are step functions, are not truly continuous in nature. Shear wave velocity intervals are typically in the order of 1 m which may average out some of the low shear wave velocity regions associated with looser sand.

3.9 Correction for Thin Sand Layers

Interpretation of the CPT tip resistance can be difficult in thin sand layers embedded in softer (e.g. clay) deposits. As the CPT cone penetrates the ground, it is influenced both by the soil ahead of it and behind it. Therefore, the measured cone resistance will start to change before it reaches a new soil, as the cone begins to sense a soil ahead of itself. The cone will also continue to sense the original soil for a certain distance into a new soil. The result is that, in thinly interbedded soils, the measured cone resistance may not reach the true value that would be measured in a given layer if the layer were thicker. The cone can respond more fully in thin soft layers than in thin stiff layers because, in soft soils, the diameter of the sphere of influence is as small as 2 to 3 cone diameters, whereas, in stiff soils, it can be up to 20 cone diameters. The measured cone resistance in thin sand layers embedded in soft clay may underpredict the true resistance of the sand. This can have a significant impact on the estimated CRR and, thus, the cyclic liquefaction potential of the layer.

Vreugdenhil et al. (1994) have shown that the error in the measured cone resistance in a thin stiff layer (soil A, a sand) is a function of the thickness of the layer as well as the stiffness of the layer relative to the surrounding softer soil (soil B, a fine grained soil). The relative stiffness of soil A to soil B is related to the relative measured cone resistance (q_{cA}/q_{cB}). Figure 3-18 presents a suggested correction factor to cone resistance (K_c) as a function of the layer thickness. The corrections have a reasonable trend, but are large. The recommended conservative correction indicated in Figure 3-18 corresponds to $q_{cA}/q_{cB}=2$ and is given by the following equation:

[3-8] $$K_c = 0.5\left(\frac{H}{1000} - 1.45\right)^2 + 1.0$$

where:
q_{cA}/q_{cB} =2
H = layer thickness, in mm
q_{cA} = tip resistance in the sand layer
q_{cB} = tip resistance in the fine grained soil surrounding the layer.

When CPT data are plotted on a soil classification chart such as that by Robertson (1990) shown in Figure 3-6, thin sand layers embedded in soft clay deposits are often incorrectly classified as silty sands as a result of the measured cone tip resistance being lower than the actual full value for the sand if it were a thicker layer. Classification of such soil layers can be improved if a correction such as K_c is applied to the cone resistance before the soil classification charts are applied.

It is interesting to note, however, that the drainage conditions for a thin sand layer embedded in a soft clay are quite different than a thicker deposit of the very same sand. Further studies could be conducted to investigate the effect of restricted drainage conditions on the CRR of a thin sand layer embedded in a soft clay, as compared to the CRR of similar, but thicker, sand deposits. Such studies could help investigate the applicability of the Robertson and Campanella (1985) correlation between CRR and $(q_{c1})_{cs}$, as given in Equation 3-2, to thin sand layers after the cone tip resistance is corrected as suggested in Equation 3-8.

3.10 Conclusions and Recommendations

A framework has been proposed for estimating the CRR directly from the CPT, by first estimating soil behaviour type (as represented by I_c), then estimating fines content, next estimating the required correction to tip resistance to obtain an equivalent clean sand tip resistance and finally, estimating CRR using the relationship proposed by Robertson and Campanella (1985). Recent field performance data summarized by Stark and Olson (1995) and Suzuki et al. (1995) have confirmed this relationship. Corrections should be made to thin sand layers embedded in thick surrounding clay layers. If undisturbed sampling and testing are within the scope of the project (i.e. for a high risk project), the test results can be compared with the estimated CRR profile for the site, in order to modify the individual components of the CPT method to suit site-specific conditions. If the project is low risk in nature, or for initial site screening of a high risk project site, the integrated CPT method, as proposed here, can be applied directly. For moderate risk projects, the correction for fines content can be modified on a site specific basis.

Cyclic softening (liquefaction) potential can then be estimated by comparing the CRR profile with the CSR profile corresponding to the design earthquake, estimated using Equation 3-1. Zones in which CRR<CSR are predicted to be susceptible to cyclic softening (liquefaction). As discussed above, the Robertson and Campanella (1985) may

contain some degree of conservatism, based on the methods used to select representative values of q_{c1} for the case records (i.e. generally average values). Therefore, if only limited thin layers (of minimum q_{c1}) are predicted to liquefy, the site should be investigated more carefully. Finally, in regions in which cyclic softening (liquefaction) is predicted, methods such as those proposed by Ishihara (1993), as shown in Figure 3-10, can be used to estimate volumetric and shear strains at the site. These can be integrated to estimate permanent post-liquefaction settlements and horizontal displacements. In the case of slightly sloping ground, methods such as those proposed by Bartlett and Youd (1995) can be used to estimate deformations associated with lateral spreading.

Table 3-1: Boundaries of soil behaviour type

Soil Behaviour Type Index, Ic	Zone	Soil Behaviour Type (see Figure I-27)
Ic < 1.31	7	Gravelly sand
1.31 < Ic < 2.05	6	Sands: clean sand to silty sand
2.05 < Ic < 2.60	5	Sand Mixtures: silty sand to sandy silt
2.60 < Ic < 2.95	4	Silt Mixtures: clayey silt to silty clay
2.95 < Ic < 3.60	3	Clays
Ic > 3.60	2	Organic soils: peats

Table 3-2: Correction factors for influence of earthquake magnitude on cyclic resistance ratio (after Seed et al., 1985)

Earthquake Magnitude, M	No. of representative cycles at 0.65 τ_{max}	$r_m = \frac{\text{CRR for M=M}}{\text{CRR for M=7.5}}$
8.5	26	0.89
7.5	15	1.0
6.75	10	1.13
6	5 to 6	1.32
5.25	2 to 3	1.5

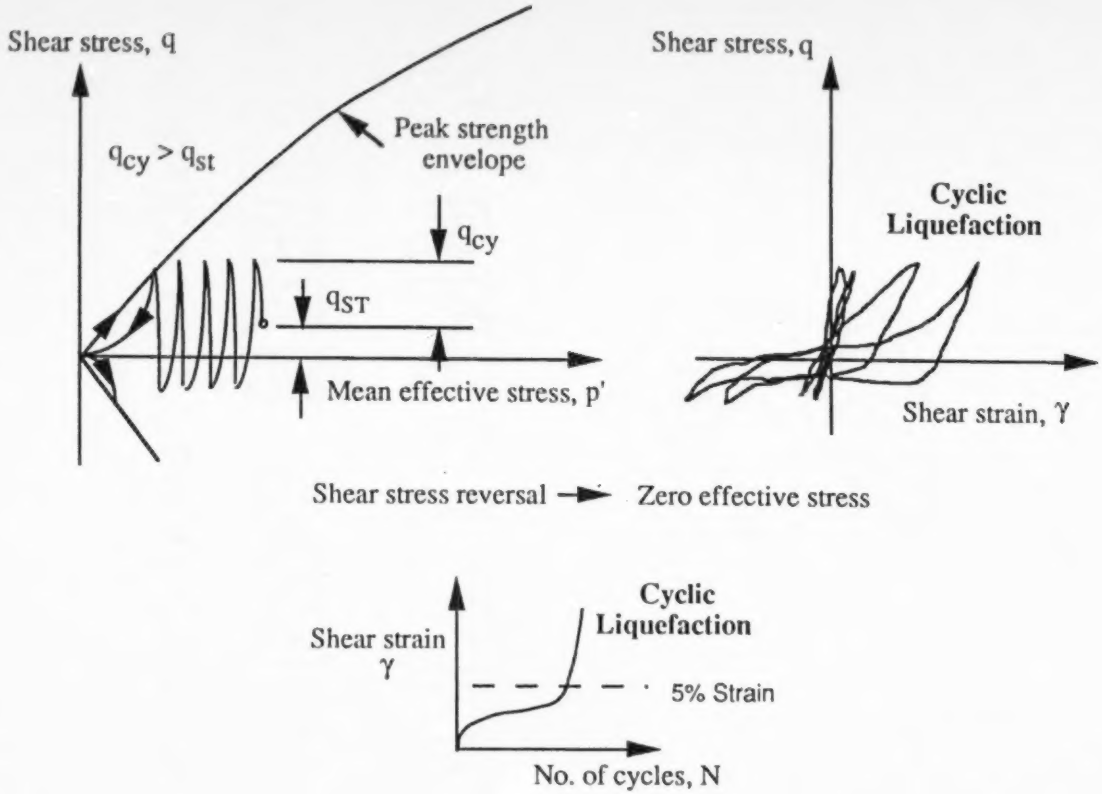
Shear stress, q
$q_{cy} > q_{st}$
Peak strength envelope
q_{cy}
q_{ST}
Mean effective stress, p'
Shear stress, q
Cyclic Liquefaction
Shear strain, γ
Shear stress reversal → Zero effective stress
Shear strain γ
Cyclic Liquefaction
5% Strain
No. of cycles, N

Figure 3-1 Schematic of undrained cyclic behaviour of sand illustrating cyclic liquefaction (modified from Robertson, 1994).

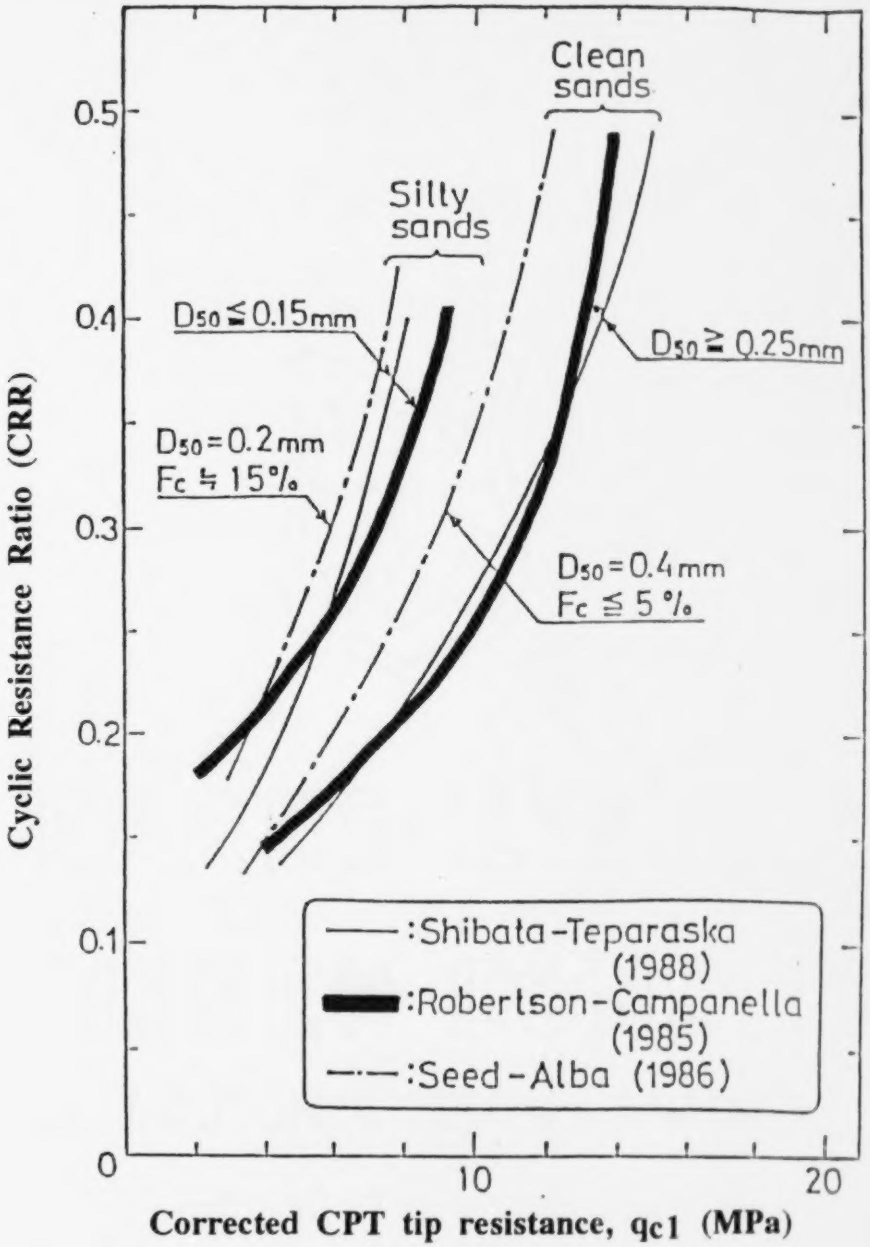

Figure 3-2 Comparison between various CPT based charts for estimating cyclic resistance ratio (CRR) for clean sands (modified from Robertson and Fear, 1995).

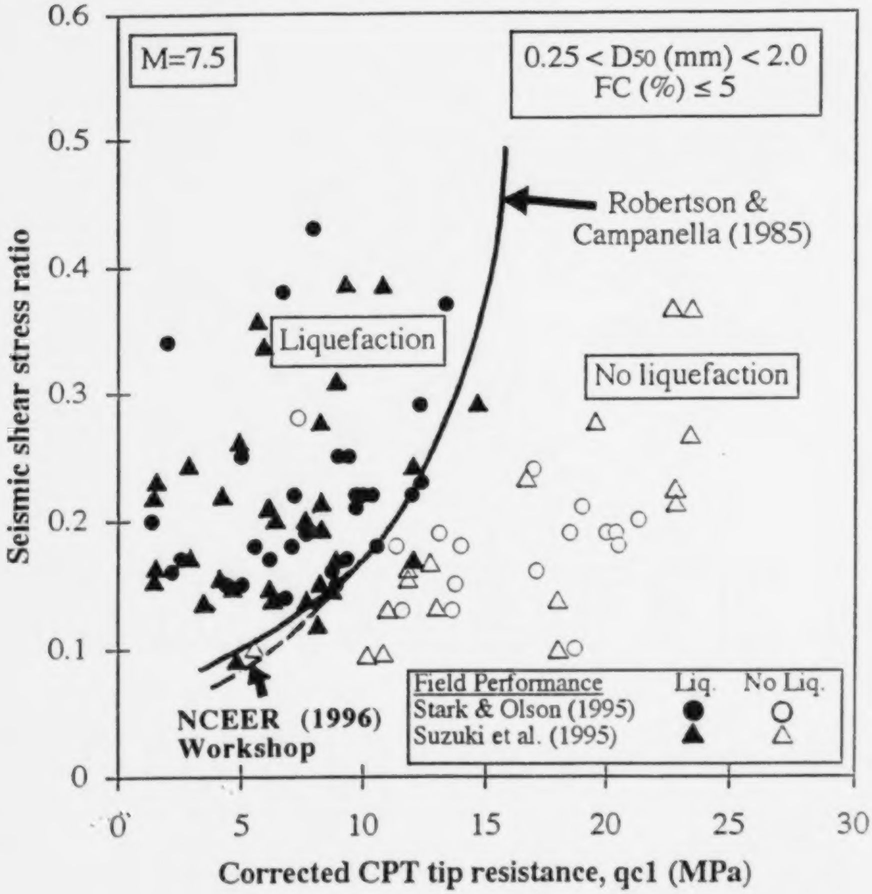

Figure 3-3 Comparison of CPT based methods for clean sands proposed by Robertson and Campanella (1985) and NCEER (1996) with recent field performance data from Stark and Olson (1995) and Suzuki et al. (1995).

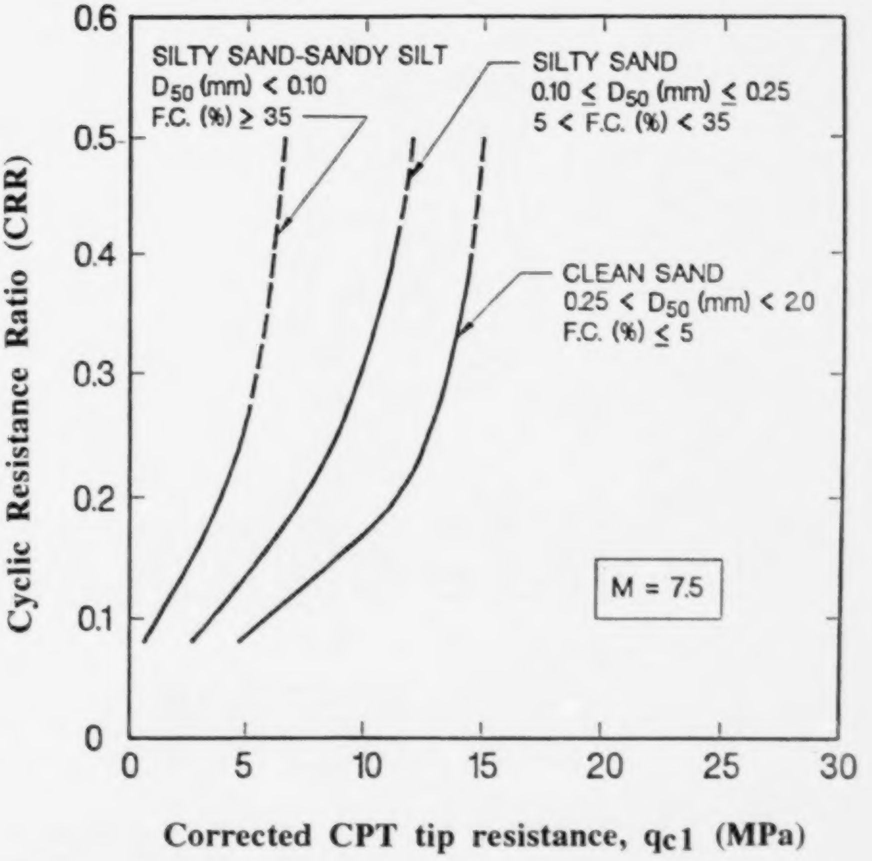

Figure 3-4 Summary of variation of cyclic resistance ratio with fines content based on CPT field performance data (modified from Stark and Olson, 1995).

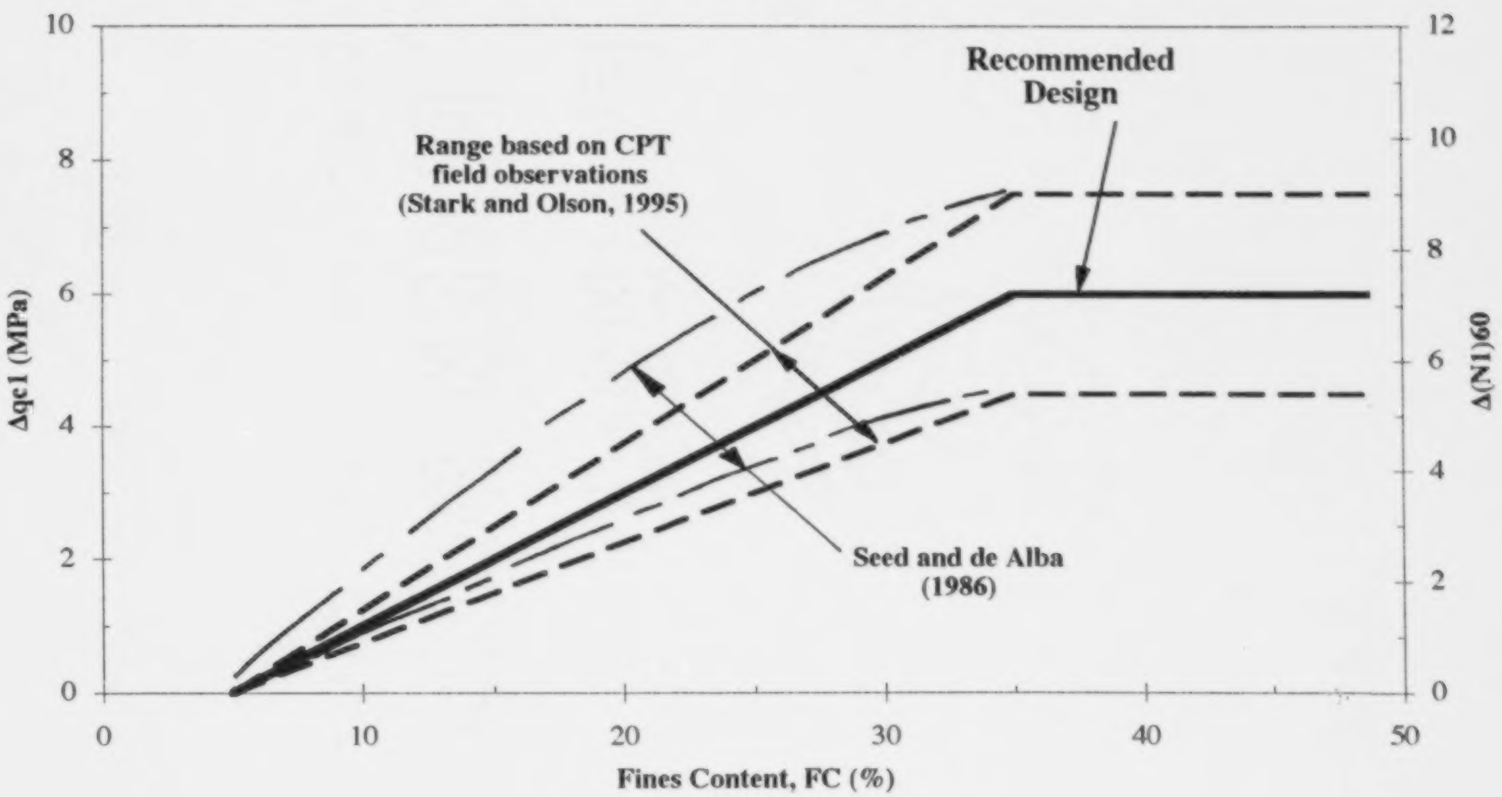

Figure 3-5 Suggested correction for fines content to corrected cone tip resistance based on field performance data.

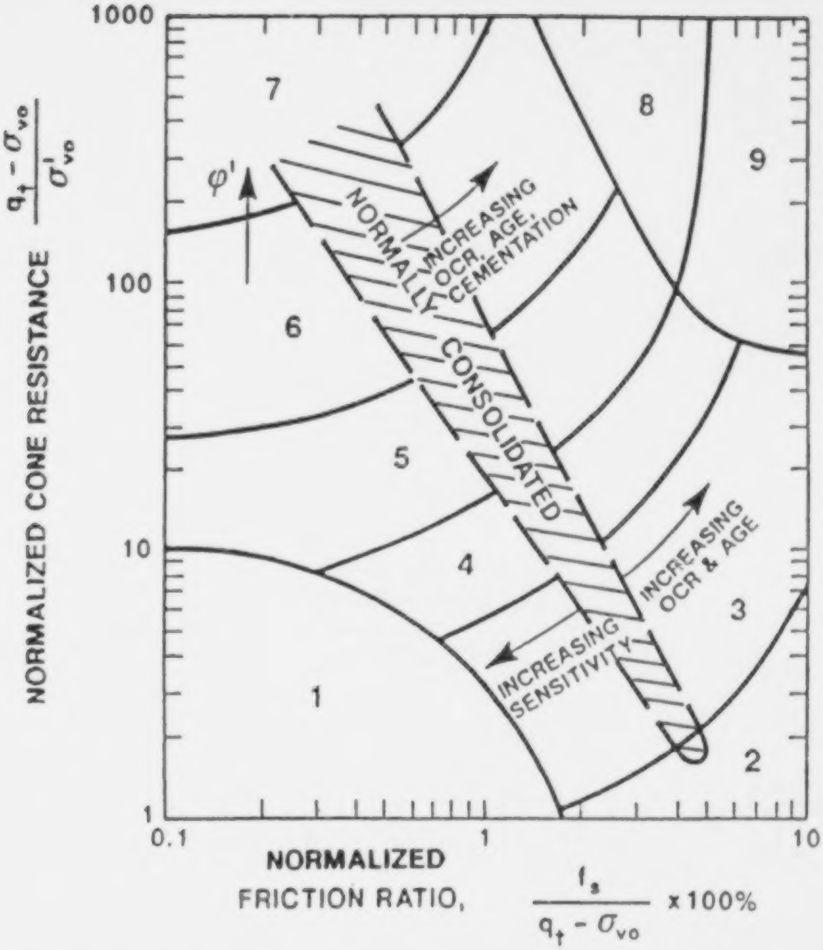

1. SENSITIVE, FINE GRAINED
2. ORGANIC SOILS – PEATS
3. CLAYS – CLAY TO SILTY CLAY
4. SILT MIXTURES – CLAYEY SILT TO SILTY CLAY
5. SAND MIXTURES – SILTY SAND TO SANDY SILT
6. SANDS – CLEAN SAND TO SILTY SAND
7. GRAVELLY SAND TO SAND
8. VERY STIFF SAND TO CLAYEY* SAND
9. VERY STIFF, FINE GRAINED*

(*) HEAVILY OVERCONSOLIDATED OR CEMENTED

Figure 3-6 CPT soil behaviour type chart (modified from Robertson, 1990).

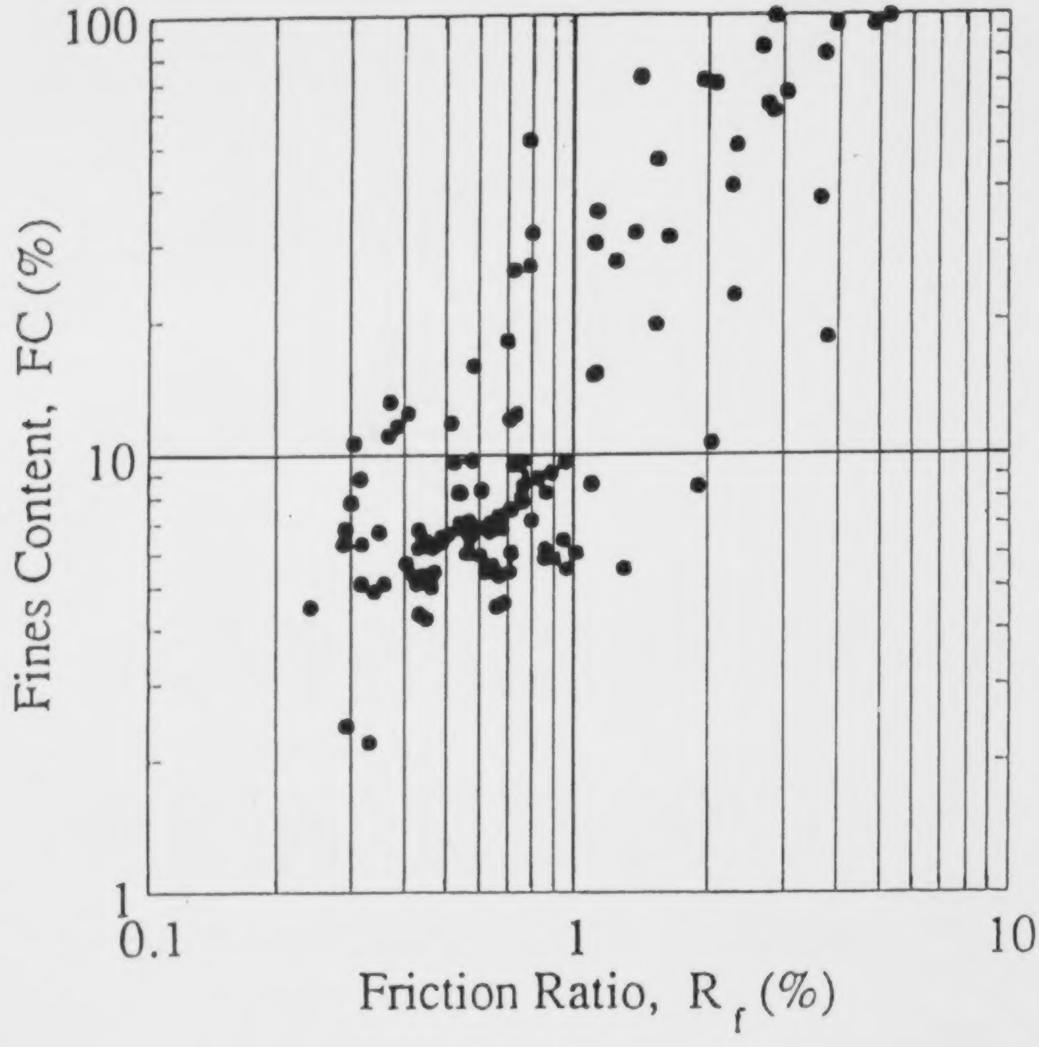

Figure 3-7 Variation of fines content with increasing CPT friction ratio (modified from Suzuki et al., 1995).

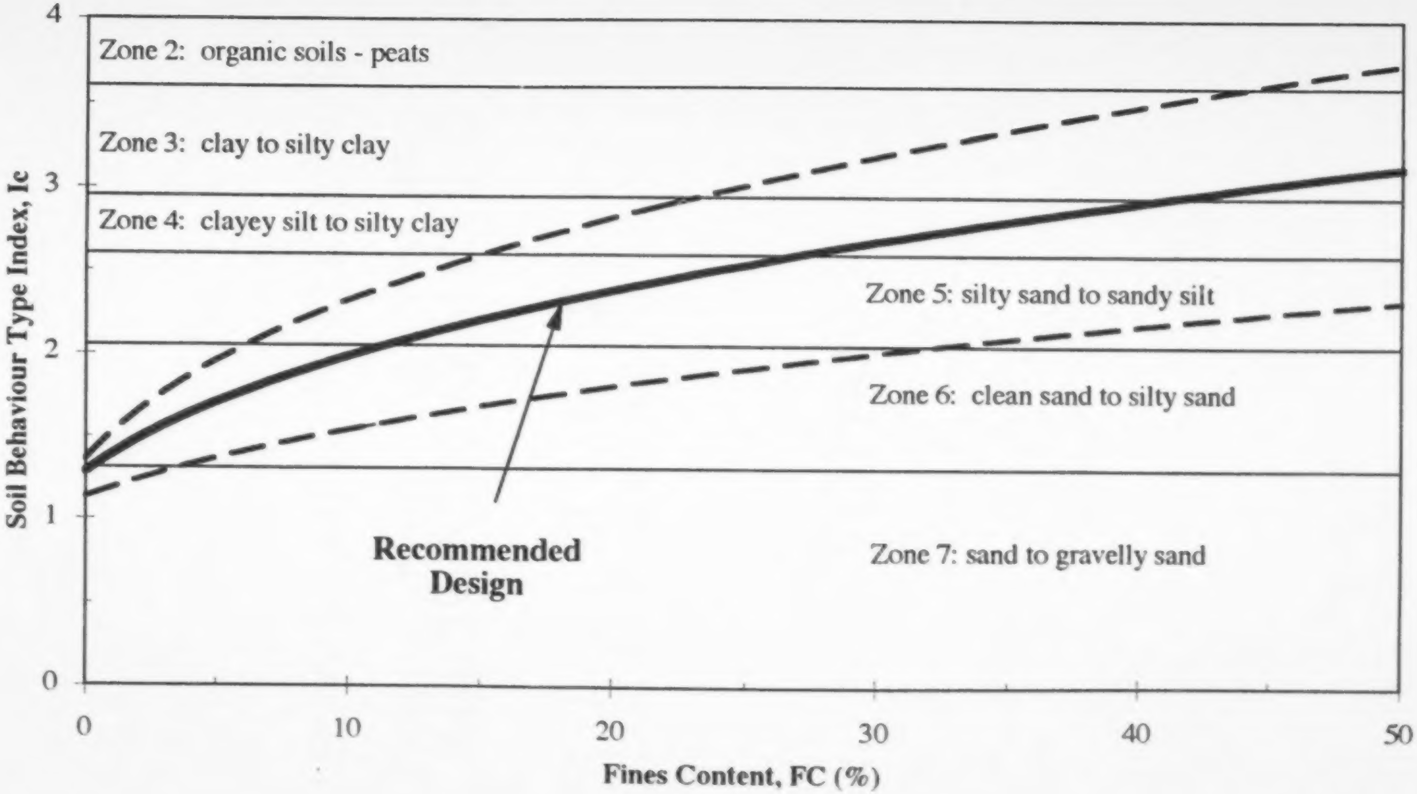

Figure 3-8 Variation of soil behaviour type index (I_c) with fines content.

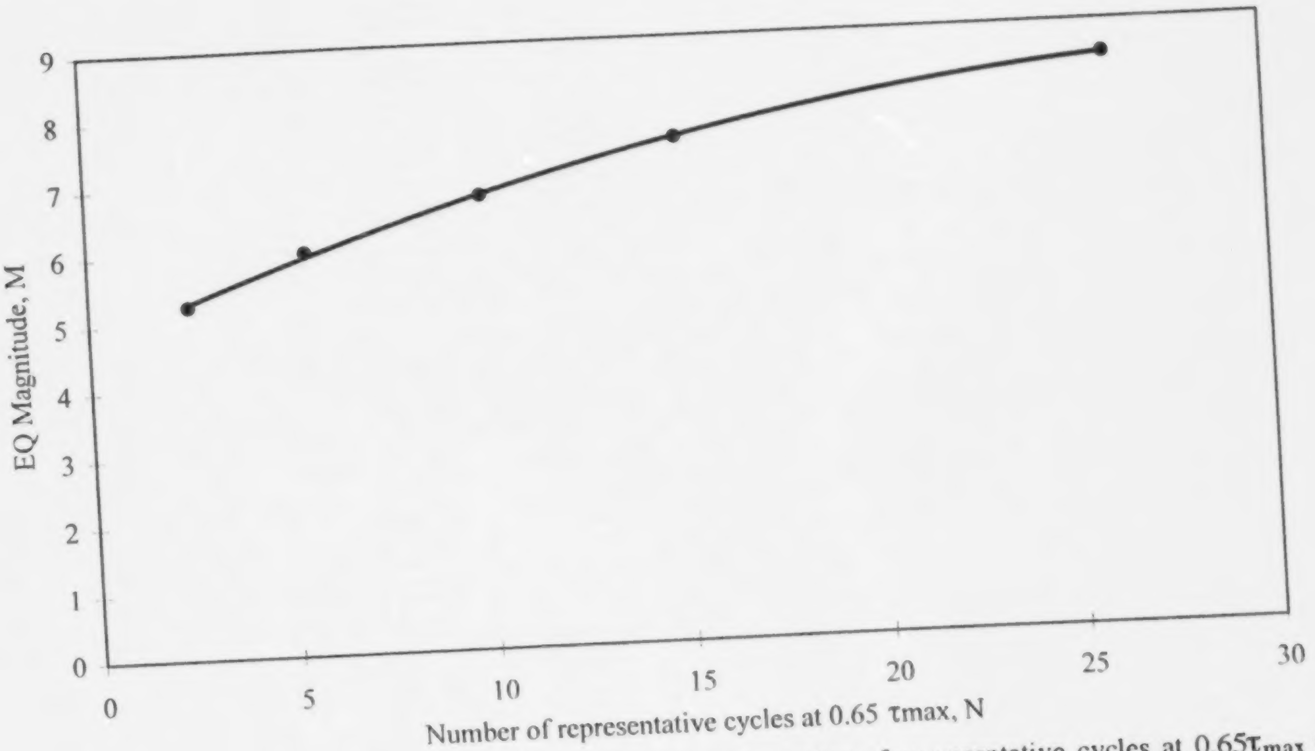

Figure 3-9 Correlation between earthquake magnitude (M) and number of representative cycles at $0.65\tau_{max}$ (N), based on recommendations by Seed et al. (1985).

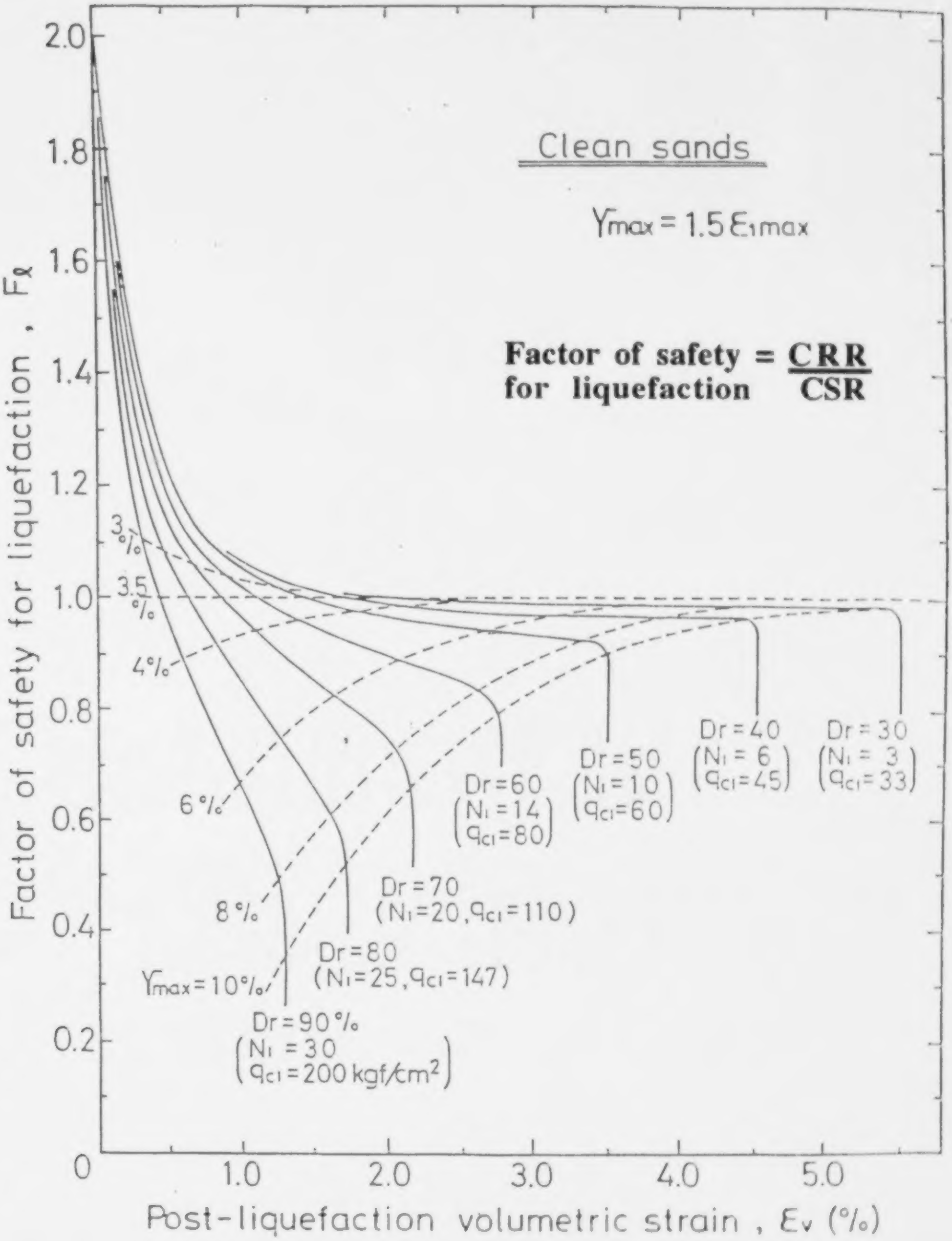

Figure 3-10 Post cyclic liquefaction volumetric and horizontal strain curves using CPT or SPT results (modified from Ishihara, 1993).

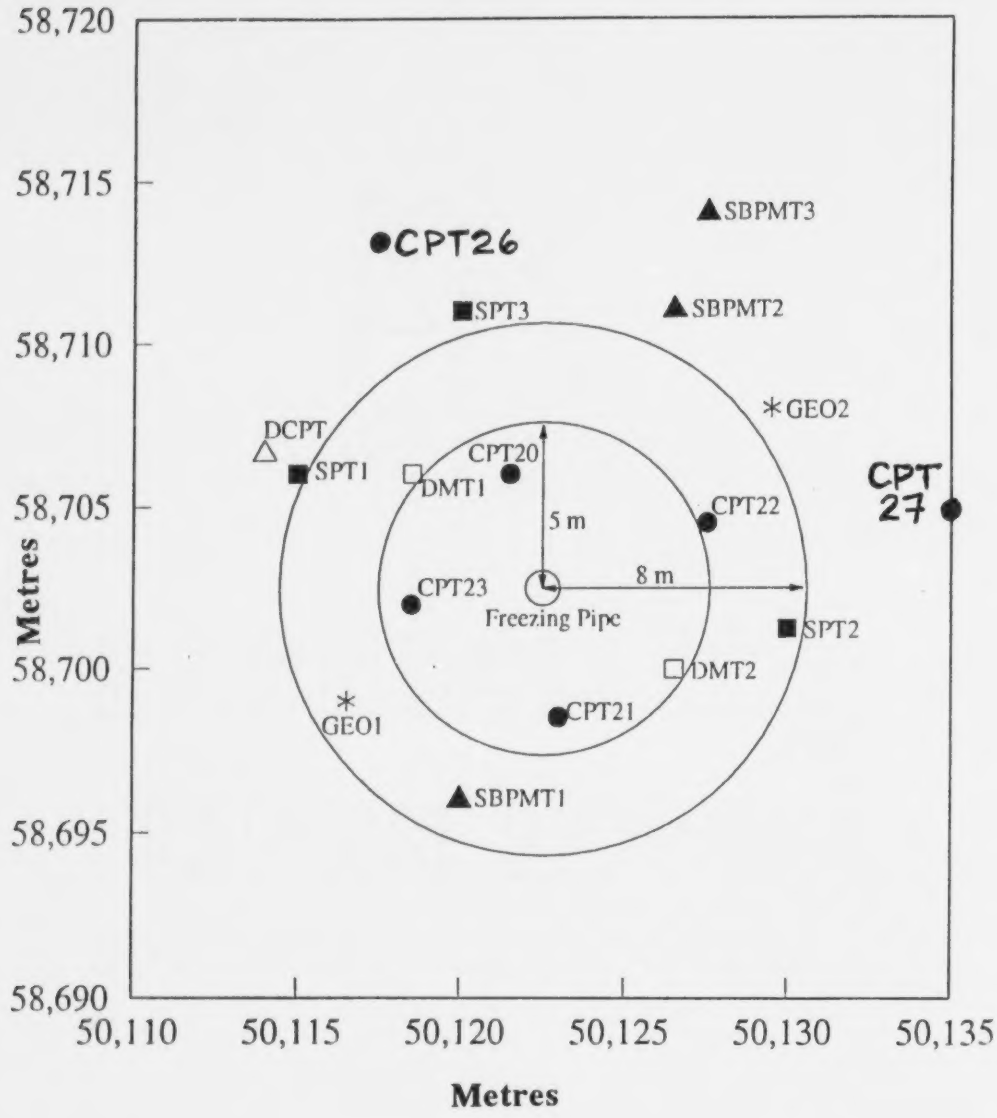

58,720
58,715
58,710
58,705
58,700
58,695
58,690
50,110
50,115
50,120
50,125
50,130
50,135
Metres
Metres
CPT26
SBPMT3
SPT3
SBPMT2
GEO2
DCPT
SPT1
DMT1
CPT20
CPT 27
CPT22
5 m
8 m
CPT23
Freezing Pipe
SPT2
DMT2
GEO1
CPT21
SBPMT1

Figure 3-11 Plan of the detailed test site area at the CANLEX Phase III site (J-pit) (modified from Iravani et al., 1996).

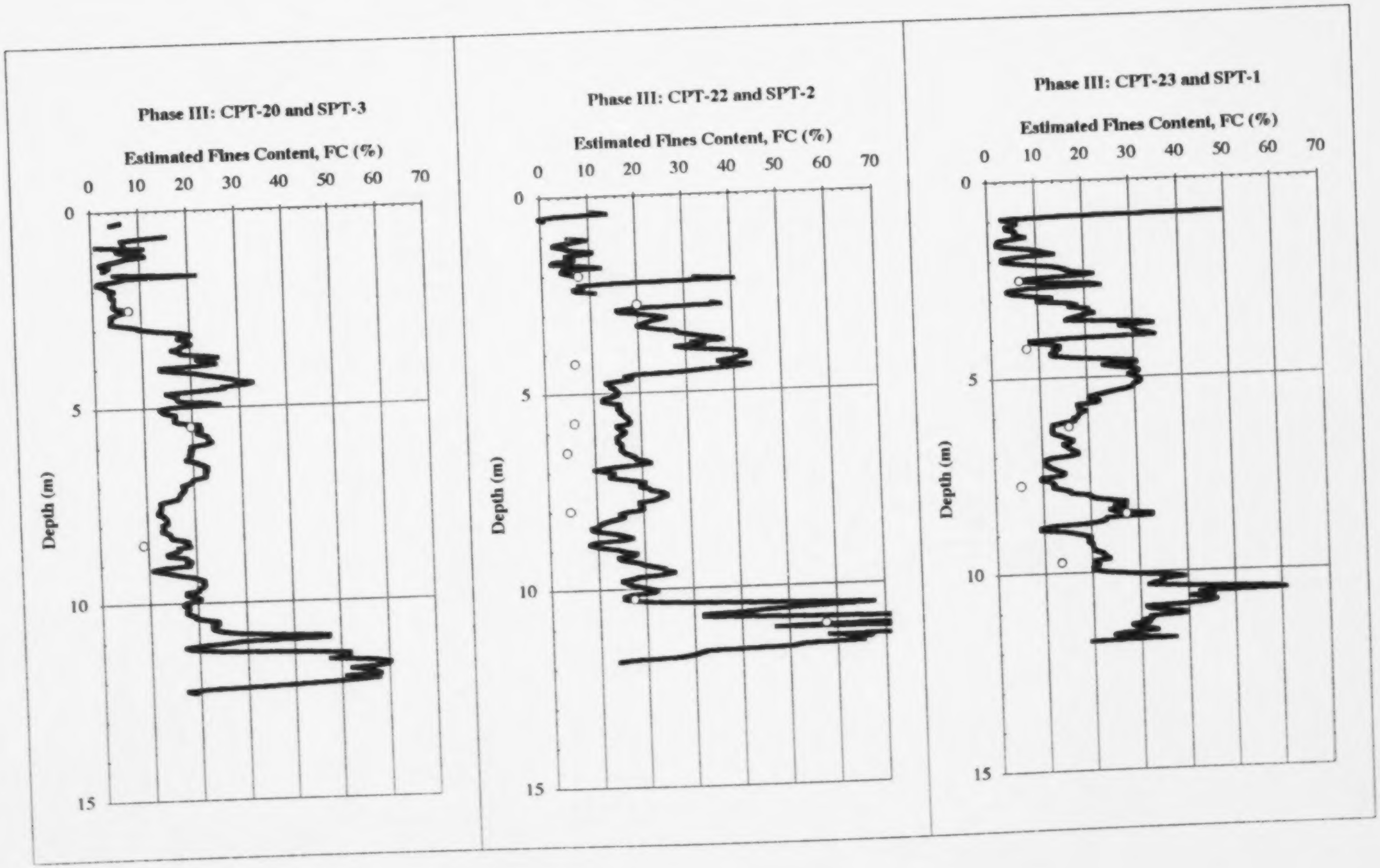

Figure 3-12 Comparison between measured fines contents (from SPT sampler) and those predicted using the CPT for three profiles at the CANLEX Phase III site (J-pit).

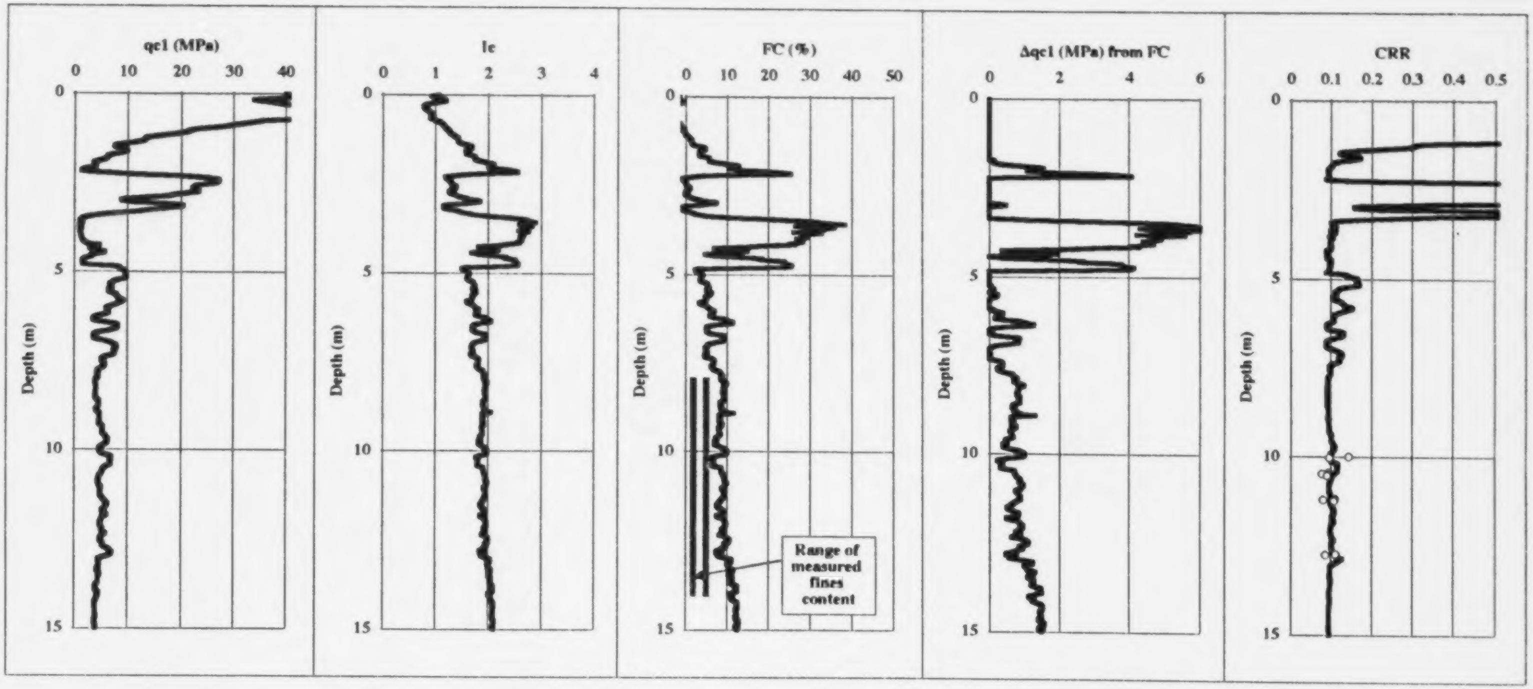

Figure 3-13 Example of applying the integrated CPT method to estimate cyclic resistance ratio (CRR) and comparison with the results of cyclic simple shear tests on in-situ frozen samples from the CANLEX Phase II Massey site.

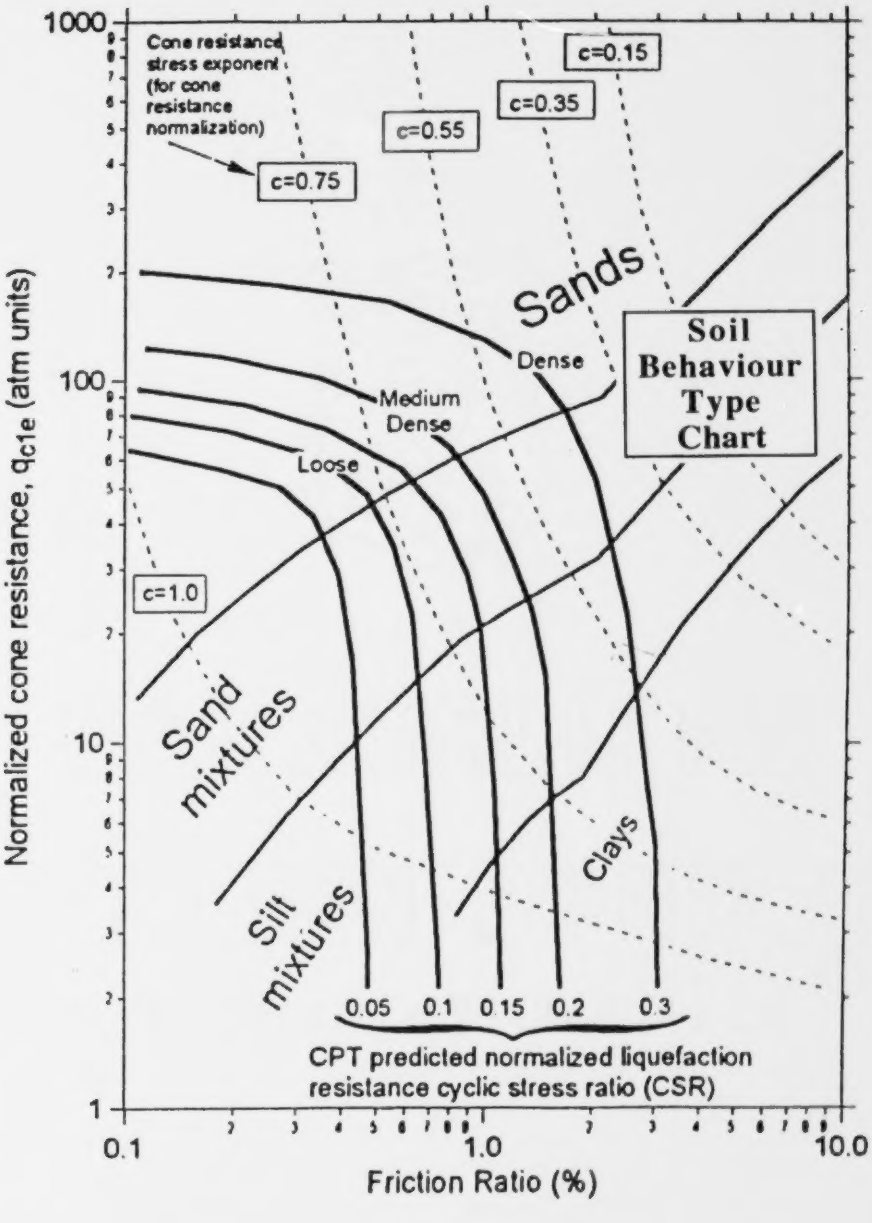

Figure 3-14 Soil behaviour type chart to estimate cyclic resistance ratio (CRR) (modified from Olsen and Koester, 1995).

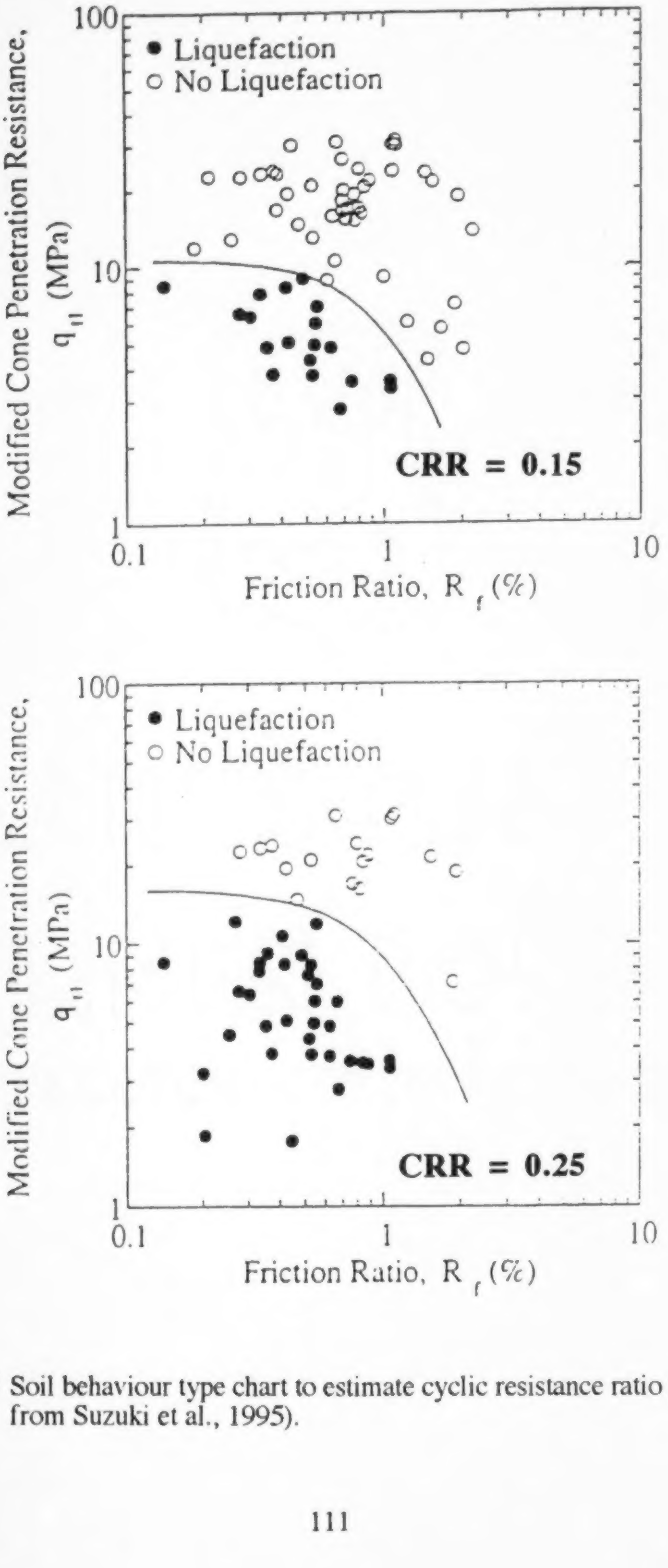

Figure 3-15 Soil behaviour type chart to estimate cyclic resistance ratio (CRR) (modified from Suzuki et al., 1995).

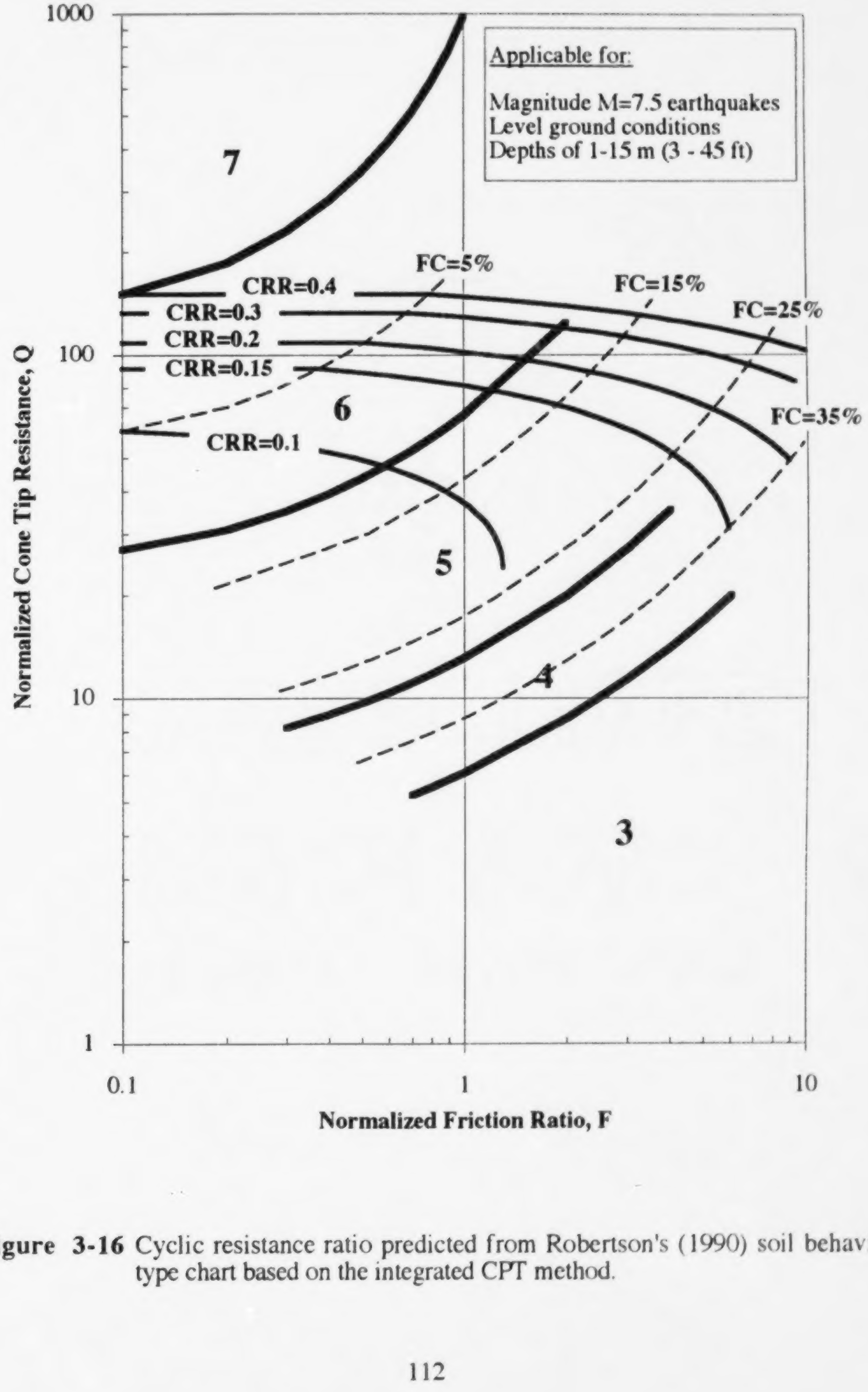

Figure 3-16 Cyclic resistance ratio predicted from Robertson's (1990) soil behaviour type chart based on the integrated CPT method.

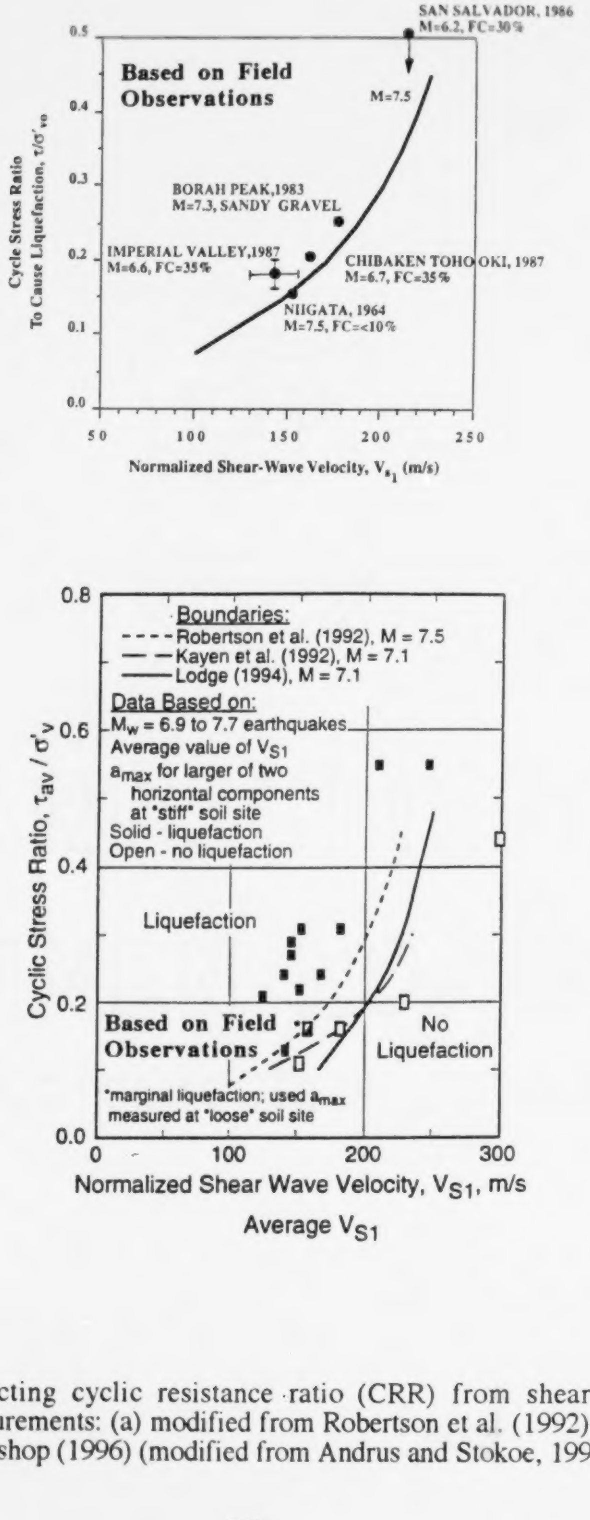

Figure 3-17 Predicting cyclic resistance ratio (CRR) from shear wave velocity measurements: (a) modified from Robertson et al. (1992) and (b) NCEER Workshop (1996) (modified from Andrus and Stokoe, 1996).

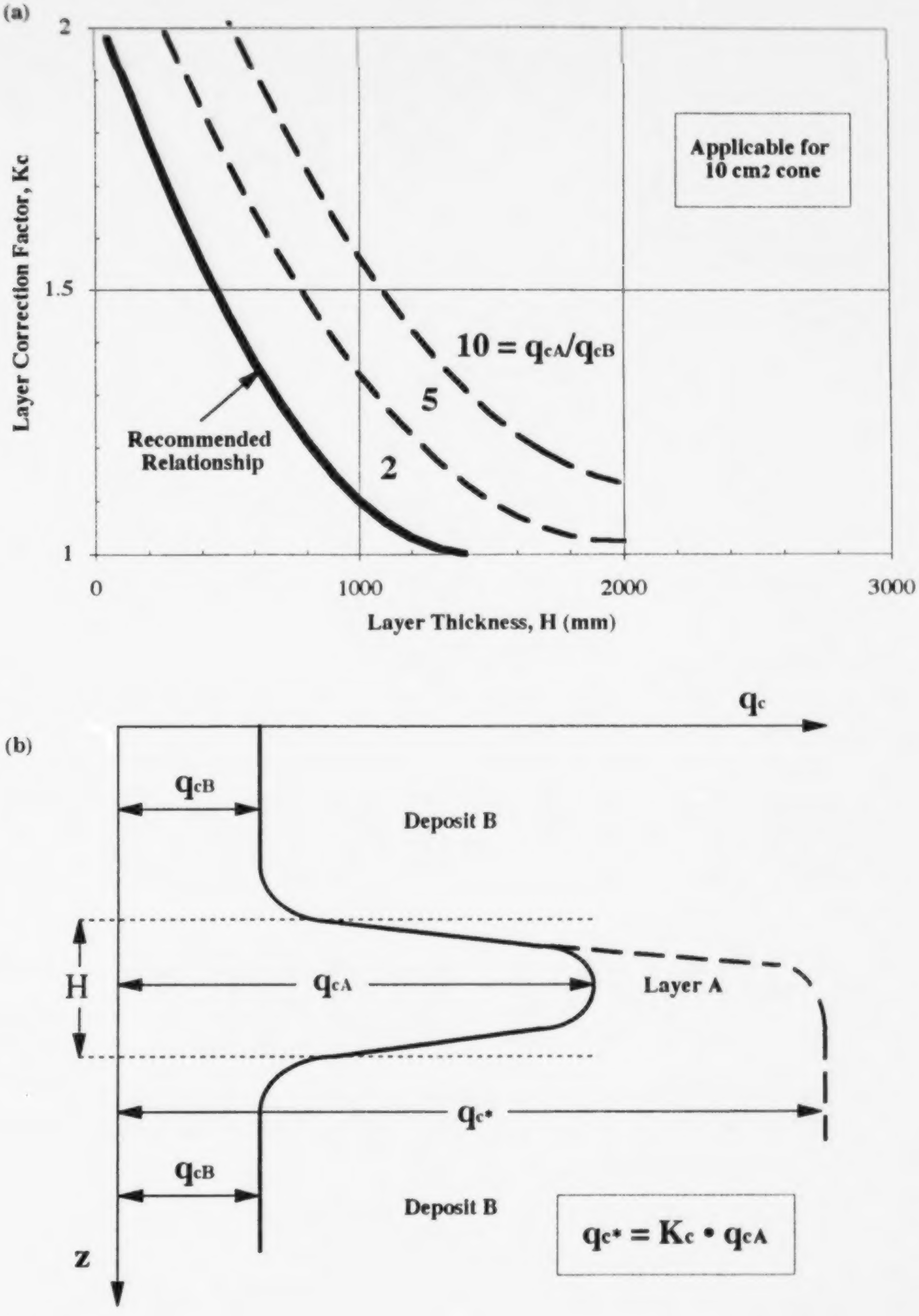

Figure 3-18 Suggested correction (K_c) to CPT penetration resistance in thin sand layers (based on results by Vreugdenhil et al., 1994).

References

Andrus, R.D. and Stokoe, K.H. 1996. Guidelines for evaluation of liquefaction resistance using shear wave velocity. *Submission to 1996 NCEER Workshop*.

Bartlett S.F., and Youd, T.L. 1995. Empirical prediction of liquefaction induced lateral spread. *Journal of Geotechnical Engineering*, ASCE 121(4): 316-329.

Fear, C.E. and McRoberts, E.C. 1995. Reconsideration of Initiation of Liquefaction in Sandy Soils. *Journal of Geotechnical Engineering*, ASCE 121(3): 249-261.

Hofmann, B.A., Sego, D.C., and Robertson, P.K. 1994. Undisturbed sampling of a deep loose sand deposit using ground freezing. *Proceedings of the 47th Canadian Geotechnical Conference*, Halifax, Nova Scotia, 287-296.

Hofmann, B.A., and Sego, D.C. 1995. In-situ ground freezing for undisturbed samples of loose sand - Phase II. *Proceedings of the 48th Canadian Geotechnical Conference, Vancouver*, B.C., 197-212.

Iravani, S., Hofmann, B.A., Fear, C., Cyre, G., Lefebvre, M.E., Natarajan, S., Stahl, R., and Robertson, P.K. 1995. General Site Characterization of J-pit Site - Syncrude Canada Ltd., *CANLEX Phase III Activity 3A (General Site Characterization)*, University of Alberta.

Ishihara, K. 1993. Liquefaction and flow failure during earthquakes. The 33rd Rankine Lecture, *Géotechnique*, 43(3), 351-415.

Ishihara, K., and Koseki, J. 1989. Cyclic shear strength of fines-containing sands. Earthquake Geotechnical Engineering. *Proceedings of the Discussion Session on Influence of Local Conditions on Seismic Response, 12th ICSMFE*, Rio de Janeiro, 101-106.

Jefferies M.G. and Davies, M.P. 1993. Use of CPTu to estimate equivalent SPT N_{60}. *ASTM Geotechnical Testing Journal*, 16(4): 458-467.

Kayen, R. E., Mitchell, J. K., Lodge, A., Seed, R. B., Nishio, S., and Coutinho, R. 1992. Evaluation of SPT-, CPT-, and shear wave-based methods for liquefaction potential assessment using Loma Prieta data. *Proceedings of the Fourth Japan-U.S. Workshop on Earthquake Resistant Design of Lifeline Facilities and Countermeasures for Soil Liquefaction, Technical Report NCEER-92-0019*, 1, M. Hamada, and T. D. O'Rouke, eds., 177-204.

Kulhawy, F.M., and Mayne, P.W. 1990. Manual on estimating soil properties for foundation design. Cornell University, EL-6800, *Research Project 1493-6*, prepared for Electric Power Research Institute.

Ladd, R.S. 1974. Specimen preparation and liquefaction of sands. *Journal of ASCE*, 110(GT10): 1180-1184.

Lodge, A.L. 1994. Shear wave velocity measurements for subsurface characterization. Ph.D. Dissertation, University of California at Berkeley.

Mitchell, J.K., and Tseng, D.-J. 1990. Assessment of liquefaction potential by cone penetration resistance. *Proceedings, H. Bolton Seed Memorial Symposium*, Berkeley, California, 2, J.M. Duncan (ed.), 335-350.

Mulilis, J.P., Seed, H.B., Chan, C.K., Mitchell, J.K., and Arulanandan, K. 1977. Effects of sample preparation on sand liquefaction. *Journal of ASCE*, 103(GT2): 99-108.

NCEER Workshop 1996. Proceedings to be published at a subsequent date by Youd et al. (1996).

Olsen, R.S., and Koester, J.P. 1995. Prediction of liquefaction resistance using the CPT. *Proceedings of the International Symposium on Cone Penetration Testing, CPT '95*, Linkoping, Sweden.

Olsen, R.S., and Malone, P.G. 1988. Soil classification and site characterization using the cone penetrometer test. *Penetration Testing 1988, ISOPT-1*, De Ruiter (ed.), Balkema, Rotterdam, 2: 887-893.

Robertson, P.K. 1990. Soil classification using the CPT. *Canadian Geotechnical Journal*, 27(1): 151-158.

Robertson, P.K. and Campanella, R.G. 1985. Liquefaction potential of sands using the cone penetration test. *Journal of Geotechnical Division of ASCE*, 22(3): 298-307.

Robertson, P.K. and Campanella, R.G. 1988. *Design manual for use of CPT and CPTu*. Pennsylvania Department of Transportation, (PennDot), 200 p.

Robertson, P.K. and Fear, C.E. 1995. Liquefaction of sands and its evaluation. *IS Tokyo '95, First International Conference on Earthquake Geotechnical Engineering*, Keynote Lecture, 3.

Robertson, P.K., Woeller, D.J., and Finn, W.D.L. 1992. Seismic cone penetration test for evaluating liquefaction potential under cyclic loading. *Canadian Geotechnical Journal*, 29: 686-695.

Seed, H.B., and de Alba, P. 1986. Use of SPT and CPT tests for evaluating the liquefaction resistance of sands. *Use of In-situ Tests in Geotechnical Engineering*, ASCE, Geotechnical Special Publication, 6: 281-302.

Seed, H. B., Tokimatsu, K., Harder, L. F., and Chung, R. 1985. Influence of SPT procedures in soil liquefaction resistance evaluations. *J. Geotech. Engrg.*, ASCE 111(12), 1425-1445.

Sego, D.C., Robertson, P.K., Sasitharan, S., Kilpatrick, B.L., and Pillai, V.S. 1994. Ground freezing and sampling of foundation soils at Duncan Dam. *Canadian Geotechnical Journal*, 31(6): 939-950.

Shibata, T., and Teparaska, W. 1988. Evaluation of liquefaction potentials of soils using cone penetration tests. *Soils and Foundations*, 28(2): 49-60.

Stark, T.D., and Olson, S.M. 1995. Liquefaction resistance using CPT and field case histories, *Journal of Geotechnical Engineering*, ASCE 121(12): 856-869.

Suzuki, Y., Tokimatsu, K., Taye, Y. and Kubota, Y. 1995. Correlation between CPT data and dynamic properties of in-situ frozen samples. *Proceedings of the 3rd International Conference on Recent Advances in Geotechnical Earthquake Engineering and Soil Dynamics*, 1, St. Louis, U.S.A..

Tatsuoka, F., Ochi, K., Fujii, S., and Okamoto, M. 1986. Cyclic undrained triaxial and torsional shear strength of sands for different sample preparation methods. *Soils and Foundations*, 26(3): 23-41.

Tokimatsu, K., and Hosaka, Y. 1986. Effects of sample disturbance on dynamic properties of sand. *Soils and Foundations*, 26(1): 53-64.

Tokimatsu, K., and Yoshimi, Y. 1983. Empirical correlation of soil liquefaction based on SPT N-value and fines content. *Soils and Foundations*, 23(4): 56-74.

Tokimatsu, K., Kuwayama, S., and Tamura, S. 1991. Liquefaction potential evaluation based on Rayleigh wave investigation and its comparison with field behaviour. *Proceedings of the 2nd International Conference on Recent Advances in Geotechnical Earthquake Engineering and Soil Dynamics*, St. Louis, Mo., 1: 357-364.

Vreugdenhil, R., Davis, R., and Berrill, J. 1994. Interpretation of cone penetration results in multilayered soils. *International Journal for Numerical Methods in Geomechanics*, 18: 585-599.

Yoshimi, Y., Hatanaka, M., and Oh-Oka, H. 1978. Undisturbed sampling of saturated sands by freezing. *Soils and Foundations*, 18(3): 105-111.

Yoshimi, Y., Tokimatsu, K., and Hosaka, Y. 1989. Evaluation of liquefaction resistance of clean sands based on high-quality undisturbed samples. *Soils and Foundations*, 29(1): 93-104.

Yoshimi, Y., Tokimatsu, K., and Ohara, J. 1994. In situ liquefaction resistance of clean sands over a wide density range. *Géotechnique*, 44(3): 479-494.

CHAPTER 4

A FRAMEWORK FOR EVALUATING FLOW LIQUEFACTION POTENTIAL AND UNDRAINED RESPONSE BASED ON BOTH LABORATORY AND IN-SITU TESTING[1,2]

4.1 Introduction

Flow liquefaction can occur only in strain-softening soils. If sufficient material strain-softens and the driving stresses are greater than the ultimate undrained strength, flow liquefaction can lead to large deformations. Figure 4-1 illustrates how the response of a sand under undrained monotonic loading is a function of the initial state of the material relative to the ultimate state line (USL). If the initial state of the sand is sufficiently loose, the material will strain-soften directly to ultimate state; this is the definition of flow liquefaction. If the initial state of the sand is sufficiently dense, the material will strain-harden directly to ultimate state; such material cannot experience flow liquefaction, but may be susceptible to cyclic softening (liquefaction) depending on the size and duration of cyclic loading. Limited strain-softening (LSS) can occur when the initial state of the sand is close to the ultimate state line. Such material will experience a temporary loss in strength as it strain-softens to a quasi-steady state (QSS) before strain-hardening to ultimate state. As long as the strains that occur while the material is passing through the QSS (minimum strength) point are small, this type of soil response would be expected to result in only limited deformations, not catastrophic flowslides. However, this is an area of continuing research; further studies are required to investigate the in-situ importance of the QSS point observed in the laboratory. From studies on Toyoura sand, Ishihara (1993) concluded that every type of sand has a unique ultimate state (in terms of void ratio and mean normal effective stress) at large strains, which is independent of drainage conditions and initial soil fabric, but that the QSS is a function of both the initial state and soil fabric.

Figure 4-1 illustrates how a strain-softening response can be triggered by monotonic undrained loading. However, this is only one type of trigger than can lead to such a

---

[1] *A version of part of this chapter has been published. Fear, C.E., Robertson, P.K., Hofmann, B.A., Sego, D.C., Campanella, R.G., Byrne, P.M., Davies, M.P., Konrad, J.-M., Küpper, A., List, B.R., and Youd, L. 1995. Summary of CANLEX Phase 1 Site Characterization, Proc. of the 48th Canadian Geotechnical Conference, Vancouver, B.C., 331-340.*

[2] *A version of part of this chapter has been published. Robertson, P.K. and Fear, C.E. 1995. Liquefaction of sands and its evaluation, Proceedings of IS Tokyo '95, First International Conference on Earthquake Geotechnical Engineering, Keynote Lecture.*

response if the state of the soil is sufficiently loose. A strain-softening response can also be triggered by undrained cyclic loading, a q=constant stress path and even drained loading, as long as the stress path leads to the collapse surface, as indicated in Figure 4-1. Once the collapse surface is reached, the material will strain-soften to ultimate state. This chapter examines methods for determining flow liquefaction potential based on in-situ testing and presents a framework for linking the in-situ state with the estimated response. Undrained monotonic loading is examined in particular, because undrained monotonic triaxial tests (compression and extension) were performed at each of the Canadian Liquefaction Experiment (CANLEX) sites. Additional details regarding one of the CANLEX sites illustrating the link between laboratory response and field predictions will be presented in Chapter 8.

4.2 Void Ratio Interpretations from In-Situ Testing

The first step in any liquefaction analysis should be to estimate the in-situ state of the soil to determine if flow liquefaction is possible (i.e. if the soil is strain-softening in undrained shear). Void ratio is an important component of soil state and is a key factor that affects the response of a sand to either undrained monotonic or cyclic loading. When truly undisturbed samples of sand are obtained from the field (e.g. using ground freezing techniques), it is possible to measure the total void ratio of each sample in the laboratory. However, it is not always possible to obtain undisturbed samples and interpreting void ratio profiles from in-situ testing provides an alternative approach. The CANLEX sites are unique in that the interpreted void ratio profiles can be compared directly with the measured void ratios of the frozen samples. Additional details will be given in Chapter 8.

4.2.1 Conventional methods

Figure 4-2 presents a flowchart outlining the various in-situ tests and the conventional methods of estimating in-situ void ratio from the CPT, SPT, V_s measurements and geophysical logging. Methods for interpreting the CPT and SPT are conventionally based on estimating relative density using empirical formulae and then estimating void ratio using e_{max} and e_{min}. The shear wave velocity and geophysical methods estimate void ratio directly.

a) CPT

The conventional interpretation of void ratio from the CPT for unaged, uncemented sands follows the work by Baldi et al. (1986), as shown in Figure 4-3. This method consists of first estimating profiles of relative density (D_r) using the following relationship:

[4-1] $$D_r = \left(\frac{1}{C_2}\right) \ln\left(\frac{q_c}{C_0(\sigma_v')^{C_1}}\right)$$

where:
q_c = measured cone tip resistance
σ_v'= vertical effective stress
C_0, C_1 and C_2 = material constants

The relationship given by Equation 4-1 was developed for Ticino sand, based on calibration chamber studies by Baldi et al. (1986). Ticino sand consists of approximately 95% quartz and 5% feldspar, with an average fines content of less than 5%. Index parameters for Ticino sand are as follows: e_{max}=0.89, e_{min}=0.52, G_s=2.67, and C_u = 1.13 (D_{60}/D_{10} = 0.65/0.40). If the sand to be analyzed has grain characteristics similar to those of Ticino sand, the values of material constants given in Figure 4-3 can be selected, as follows: C_0=157, C_1=0.55 and C_2=2.41 (applicable for K_o=0.45). Void ratio profiles can then be estimated, based on the estimated profiles of D_r, the values of e_{max} and e_{min}, and the following equation:

[4-2] $$e = e_{max} - D_r\,(e_{max} - e_{min})$$

b) SPT

The conventional interpretation of void ratio from the SPT for unaged, uncemented sands follows the work by Skempton (1986). This method consists of first estimating profiles of D_r using the following relationship:

[4-3] $$\frac{(N_1)_{60}}{D_r^{\;2}} = \text{constant}$$

Most sites at which flow liquefaction is an issue consist of loose young sands. When applying Equation 4-3 to such sites, a constant of 40 can be selected as being representative of loose, young sands. Void ratio profiles can then be estimated, based on the estimated profiles of D_r, the values of e_{max} and e_{min}, and Equation 4-2.

c) Shear wave velocity

Cunning et al. (1995) found that the primary factors controlling values of measured shear wave velocity for unaged, uncemented sands was void ratio and stress level. When shear wave velocity measurements were corrected for effective overburden pressure (i.e. V_{s1}), Cunning et al. (1995) found that V_{s1} and void ratio were related as illustrated in Figure 4-4 and given by the following equation:

$$V_{s1} = (A - Be)\, K_o^{\,0.125} \tag{4-4}$$

where:
A and B = constants for a given sand
e = void ratio
K_o = coefficient of earth pressure at rest (from self-boring pressuremeter interpretation)
V_{s1} is in m/s and given by the following equation:

$$V_{s1} = V_s \left(\frac{P_a}{\sigma_v'}\right)^{0.25} \tag{4-5}$$

where:
V_{s1} = corrected shear wave velocity
V_s = measured shear wave velocity
P_a = atmospheric pressure, typically 100 kPa
σ_v' = vertical effective stress, in kPa.

The shear wave velocity method is attractive because, for a given K_o, it estimates void ratio directly, rather than first estimating D_r; however, there is scatter in the correlation (see Figure 4-4) as the data tend to fall within a band. Global values of A and B can be used to describe this band; alternatively, specific values of A and B can be estimated for each individual sand. The D_r-based methods of interpreting the CPT and SPT depend on e_{min} and e_{max} to estimate void ratio. The validity of these terms are sometimes questionable, particularly in silty sands, which can result in difficulties in interpreting void ratio. In addition, the correlations based on penetration resistance from the SPT and CPT are affected by other factors such as soil compressibility. Shear wave velocity, on the other hand, is little influenced by factors such as soil compressibility.

Figure 4-4 was prepared by measuring shear wave velocity in the laboratory using bender elements during different stages of isotropic consolidation (i.e. K_o=1.0) of reconstituted samples. The data all fit within a band, suggesting that global values of A and B apply to all sands. However, for an individual sand, the parameters A and B are estimated by fitting a line to the data for the particular sand. It is important to note that because A and B are estimated from laboratory testing of reconstituted samples, the relationship given in Equation 4-4 is applicable only to young, recently deposited uncemented sands. However, many real deposits of sand are old and have experienced aging effects. Superimposed on Figure 4-4 are values of V_{s1}, as measured in the field, and corresponding average values of void ratio for the Phase I and Phase II CANLEX sites. It is not completely correct to directly compare the field ($K_o \approx 0.5$) and laboratory data (K_o=1) on the same plot because of the difference in K_o conditions (see Equation 4-4). However, the resulting error is typically less than 10%.

Based on Figure 4-4, Robertson et al. (1995) suggested that aging has the effect of increasing the measured shear wave velocity for a given void ratio and proposed a correlation between aging and the difference in V_{s1} measured in the field as compared to laboratory values for unaged sand. This correlation is shown in Figure 4-5; the relationship is tentative and, as additional data becomes available, could be modified. Since the relationship between V_{s1} and void ratio (as given in Equation 4-4) is approximately linear for a given K_o over typical ranges of void ratio, the change in measured V_{s1} in the field due to aging can be incorporated as a correction added to the parameter A (as determined in the laboratory) in Equation 4-4. This, in essence, shifts the relationship between V_{s1} and void ratio upwards on the plot in Figure 4-4, so that for a measured V_{s1}, void ratio in the field is not underpredicted. Aging also has a small effect on penetration resistance from the CPT and SPT (Skempton, 1986; Kulhawy and Mayne, 1990).

d) Geophysical logging

Geophysical logging can also be used to directly estimate void ratio. In simple terms, the following relationship can be used:

[4-6] $$e = \frac{(G_s - \rho_b)}{(\rho_b - 1)}$$

where:
G_s = specific gravity of the soil
ρ_b = corrected bulk density of the soil.

The corrected bulk density of the soil can be determined from the results of geophysical logging using modified geophysical interpretations proposed by Plewes et al. (1988).

4.2.2 Correlations between in-situ tests

Comparisons between in-situ test methods are useful for examining for consistency between test signatures. Conversion factors between in-situ tests can also be used to convert one type of in-situ test signature to the equivalent signature of another type of in-situ test. This can allow for estimation of void ratios from the SPT or CPT using a direct void ratio method rather than a conventional D_r-method. Comparisons between the CPT, SPT and V_s profiles in the target zone were made and the appropriate conversion factors between in-situ tests were estimated.

In order to compare the various in-situ test signatures, the results should first be corrected for effective overburden pressure. The measured shear wave velocity, V_s, should be corrected to V_{s1} using Equation 4-5. The measured CPT tip resistance, q_c, should be corrected for effective overburden stress using the following equation:

$$[4\text{-}7] \qquad q_{c1} = q_c \left(\frac{P_a}{\sigma_v'}\right)^{0.5}$$

where:
q_{c1} = corrected tip resistance
q_c = measured tip resistance
P_a = atmospheric pressure, typically 100 kPa
σ_v' = vertical effective stress, in kPa.

The measured SPT N-value should be corrected for effective overburden stress and energy effects using the following equation:

$$[4\text{-}8] \qquad (N_1)_{60} = N \left(\frac{P_a}{\sigma_v'}\right)^{0.5} \left(\frac{ER}{60}\right)$$

where:
$(N_1)_{60}$ = corrected tip resistance
N = measured tip resistance
P_a = atmospheric pressure, typically 100 kPa
σ_v' = vertical effective stress, in kPa
ER = measured energy ratio, in percent.

The conventional conversion between corrected SPT and corrected CPT is in terms of the ratio $q_{c1}/(N_1)_{60}$. This ratio is a function of the soil type and typically has values ranging from 0.3 to 0.6 (when q_{c1} is in MPa), corresponding to soil types ranging from sandy silts to gravelly sands, respectively.

Based on earlier work by Robertson et al. (1992), the relationship between corrected shear wave velocity and corrected CPT tip resistance can be approximated by the following equation (see Chapter 5 as well):

$$[4\text{-}9] \qquad q_{c1} = \left(\frac{V_{s1}}{Y}\right)^4$$

where:

q_{c1} = corrected tip resistance, as given in Equation 4-7, in MPa
V_{s1} = corrected shear wave velocity, as given in Equation 4-5, in m/s
Y = conversion factor between CPT and V_s, in $(m/s)/(MPa)^{0.25}$.

Robertson et al. (1995) looked at various sands, including Fraser River sand, and investigated the effects of compressibility (represented by the slope of the ultimate state line (USL), λ_{ln}) on the value of Y, as indicated in Figure 4-6. There appears to be a relationship (which is influenced by aging) between Y and λ_{ln}. Increasing the compressibility of a sand decreases the measured q_{c1}, while having little effect on the measured V_{s1}. Values of Y appear to range from approximately 90 for relatively incompressible sands to 140 for compressible sands. Aging appears to have a greater effect on the measured V_{s1}, but little effect on the measured q_{c1}, with the result being that Y increases with age (Robertson et al., 1995).

Based on a modified version of the work by Yoshida et al (1988), a similar relationship can be developed between corrected shear wave velocity and corrected SPT blowcount as follows (see Chapter 5 as well):

$$[4\text{-}10] \qquad (N_1)_{60} = \left(\frac{V_{s1}}{X}\right)^4$$

where:

$(N_1)_{60}$ = corrected SPT blowcount, as given in Equation 4-8
V_{s1} = corrected shear wave velocity, as given in Equation 4-5, in m/s
X = conversion factor between SPT and V_s, in $1/(MPa)^{0.25}$.

Note that, theoretically, the ratio $(X/Y)^4$ should equal to the ratio $q_{c1}/(N_1)_{60}$. Small differences between the field estimated average $(X/Y)^4$ and average $q_{c1}/(N_1)_{60}$ in a soil deposit at a given site would be expected due to the different intervals over which the various terms are estimated and averaged. Shear wave velocity measurements are typically step functions averaged over 1 m intervals, SPT measurements reflect a 1 foot (30 cm) interval and are usually measured at a depth of every 5 feet, while CPT measurements provide an essentially continuous profile, with measurements typically taken every few centimetres.

4.2.3 Shear wave velocity based method

As discussed previously, the shear wave velocity method provides a direct estimate of void ratio. The conventional CPT or SPT methods are indirect and are sensitive to the values of e_{min} and e_{max} as well as soil compressibility. However, combining Equation 4-4 (which links V_{s1} and void ratio) with the conversion factors Y and X (as defined in Equations 4-9 and 4-10) allows for more direct methods of interpreting void ratio from the CPT and SPT, respectively. The advantage of using the CPT is that its continuous nature allows for a more detailed profile of estimated void ratio within a given soil deposit.

Combining Equations 4-4 and 4-9 results in the following equation which allows for direct estimates of void ratio to be made based on profiles of CPT q_{c1} without having to first estimate D_r:

$$[4\text{-}11] \qquad q_{c1} = \left(\frac{(A - Be)\, K_o^{0.125}}{Y}\right)^4$$

Likewise, combining Equations 4-4 and 4-10 results in the following equation which allows for direct estimates of void ratio to be made based on profiles of SPT $(N_1)_{60}$ without having to first estimate D_r:

$$[4\text{-}12] \qquad (N_1)_{60} = \left(\frac{(A - Be)K_o^{0.125}}{X}\right)^4$$

Both the conventional and shear-wave velocity methods of interpreting void ratio from the CPT and SPT will be applied to one of the CANLEX sites and the results will be compared in Chapter 8. Void ratio can also be estimated from the CPT based on state parameter, Ψ' (Been and Jefferies, 1992). However, a knowledge of the ultimate state line is required to convert state parameter to void ratio. Details of this approach are given in the next section.

4.3 General Concepts of the Proposed Framework

4.3.1 Critical state soil mechanics

Considerable evidence suggests that the response of sands can be described within a critical state framework similar to that applied to clay soils (e.g. Atkinson, 1993; Coop et al., 1995). The collapse surface approach (Sladen et al., 1985a) to flow liquefaction analysis resides within a critical state soil mechanics framework. The ultimate state line (USL) for a given sand and a given direction of loading (e.g. triaxial compression or triaxial extension) can be plotted in p'-q-e space (see Figure 4-7a), where e is void ratio and p' (mean normal effective stress) and q (deviator stress) are defined as follows:

[4-13] $$p' = \frac{1}{3}(\sigma_1' + 2\,\sigma_3')$$

[4-14] $$q = \sigma_1' - \sigma_3'$$

The USL is controlled by the grain characteristics of the soil. Along the USL, q and p' are related by M, which is a function of friction angle and direction of loading. Theoretical values of M for triaxial compression (M_C) and triaxial extension (M_E) are given by the following equations (Wood, 1990):

[4-15] $$M_C = (q_{us}/p'_{us})_C = \frac{6\sin\phi'_{us}}{3 - \sin\phi'_{us}}$$

[4-16] $$M_E = (q_{us}/p'_{us})_E = \frac{6\sin\phi'_{us}}{3 + \sin\phi'_{us}}$$

where:
ϕ'_{us} = ultimate state friction angle.

When the USL in p'-q-e space is projected onto the e-p' plane and the p' axis is plotted on a logarithmic scale, the USL can be approximated as a straight line over a given stress range (see Figure 4-7b). Been et al. (1991) showed that, in the e-p' plane, steady state and critical state are the same condition and are independent of the stress path followed to reach this ultimate state. Therefore, the various USLs in p'-q-e space project onto a single USL in the e-p' plane. In theory, the USL in the e-p' plane can be defined over a given stress range by two parameters, Γ and λ_{ln}. Γ is the void ratio on the USL at p'=1 kPa and λ_{ln} is the slope of the USL when the p' axis is plotted on a natural logarithm scale. The USL in the e-ln p' plane is therefore defined as follows:

[4-17] $e = \Gamma - \lambda_{ln} \ln (p')$

However, p' may not be the correct stress invariant to use. Eventually, it may be more suitable to simply use the Mohr-Coulomb failure criterion (which is independent of the intermediate principal stress), as previously suggested by Casagrande (e.g. Casagrande, 1975). Nevertheless, proceeding with the use of p', in e-p' space, soils with void ratios loose of the USL could strain soften at large strains, while soils dense of the USL could strain harden at large strains. Soils that have initial void ratios close to the USL can have a limited strain softening (LSS) response to monotonic loading, in that they will strain soften to a quasi-steady-state (QSS) before eventually, at large strains, dilating to ultimate state (US) (see Figure 4-1). For some sands, very large strains are required to reach US and, in some cases, conventional triaxial equipment may not reach these large strains ($\varepsilon_a > 20\%$).

The response of a sand in undrained monotonic loading is a function of many factors. Figure 4-8 illustrates that, in addition to void ratio (e) and initial mean normal effective stress (p'_i), several other factors will also influence the response of a sand, including direction of loading (e.g. triaxial compression versus triaxial extension), soil structure (i.e. fabric, aging, cementation), soil compressibility, and initial deviator stress (q_i). It is desirable to eliminate one or more of the factors in order to observe the effects of the other major factors. Void ratio and p'_i can be combined in terms of state parameter, Ψ, as proposed by Been and Jefferies (1985), based on earlier work by Wroth and Bassett (1965), relative to a reference ultimate state line (USL) in e-ln p' space. Ψ is the difference between the initial void ratio of the sample and the void ratio on the reference USL at the same value of p', e_{us} (see Figure 4-7b), as given by the following equation:

[4-18] $\Psi = e - e_{us} = e - [\Gamma - \lambda_{ln} \ln (p')]$

When Ψ=0, the initial state of the soil falls on the USL, in e-p' space. Soils with Ψ>0 are loose of the USL; soils with $\Psi<0$ are dense of the USL. Therefore, it was originally proposed by Been and Jefferies (1985) that estimating state parameter could be used as a method of predicting the liquefaction potential of a soil deposit. The following sections present various methods of estimating state.

4.3.2 Methods of interpreting state

a) Sladen and Hewitt (1989)

As a result of site investigations and field observations of both flow failures and no failures in Nerlerk and Ukalerk sand during placement of hydraulic fill, Sladen and Hewitt (1989) developed an empirical dividing line between liquefaction and no liquefaction, based on the CPT. Sladen et al. (1985b) reported that Nerlerk sand was found to have a mean grain size, D_{50}, of 0.22 mm and an average fines content of about 10% and that Ukalerk sand had a D_{50} of 0.31 mm and a fines content of 2%. Sladen and Hewitt (1989) reported that Ukalerk sand had a uniformity coefficient, $C_u=D_{60}/D_{10}=1.5$ to 1.8, $e_{max}=0.80$, $e_{min}=0.50$, and $G_s=2.66$. The dividing line to determine liquefaction potential, in terms of q_c versus mean normal effective stress, p', as developed by Sladen and Hewitt (1989) is shown in Figure 4-9. This relationship shown in Figure 4-9 was based on an assumed K_o of approximately 0.40. Therefore, the dividing line can be converted back to a relationship between q_c and σ'_{vo} and expressed by the following equation (Robertson et al., 1992):

$$[4\text{-}19] \qquad q_c \left(\frac{P_a}{\sigma'_{vo}}\right)^{0.6} = 6.7 \text{ MPa}$$

The relationship given in Equation 4-19 could be transposed into a dividing line of q_c versus depth, given a site specific water table and unit weights of soil. This relationship can be superimposed over field CPT data from a given site in order to estimate flow liquefaction potential (provided that the sand deposit is considered to be similar to those deposits for which the relationship was determined). The best method of estimating if two sands may respond in a similar manner is probably to compare their ultimate state lines. Soil with values of q_c greater than the dividing line can be considered as having states that will not liquefy. Soil with values of q_c less than the dividing line can be considered as having states that can liquefy, given a suitable trigger mechanism. In Chapter 8, this dividing line is applied to the CPT data at one of the CANLEX sites, for comparison with other methods of evaluating state.

b) Been and Jefferies (1992)

Based on critical state soil mechanics theory outlined above, state parameter (Ψ) could be a useful indicator of flow liquefaction potential, provided there is a reliable method of predicting its value within a soil deposit. Been and Jefferies (1992) developed a method, based on earlier work by Been and Jefferies (1985) and Been et al. (1987), for estimating the state parameter of a soil deposit, directly from the CPT, based on calibration chamber testing. Some uncertainty exists over the corrections made for chamber size effects. In particular, since the correlations were determined mostly by testing relatively dense sand, for which large corrections had to be made, and the resulting correlations were extrapolated into the range of loose sands, there is uncertainty in the resulting correlations for loose sands. In addition, Sladen (1989) questioned the uniqueness of the relationship between Ψ and normalized CPT penetration resistance proposed by Been and Jefferies (1987) and suggested that stress effects had not been properly accounted for in the proposed relationship.

Nevertheless, different soil types were examined by Been and Jefferies (1992) and the estimation of Ψ was found to be a function of the friction angle (i.e. M) and the slope of the USL (λ_{log}) of the sand deposit, as shown in Figure 4-10. The following equation was proposed to estimate Ψ:

[4-20] $q^* = k^* \exp(-m^* \Psi)$

where:

[4-21] $q^* = Q_p/(1 - B_q)$

[4-22] $Q_p = (q_c - p_o)/p'_o$

[4-23] $k^* = M\,(3 + 0.85/\lambda_{log})$

[4-24] $m^* = 11.9 - 13.3\lambda_{log}$

Note that λ_{log} is the slope of the USL in e-p' space, when the p' axis is plotted on a logarithm base 10 scale; $\lambda_{log} = 2.302\lambda_{ln}$. It is very important, when comparing values of λ for various sands to be consistent in how λ is defined. The value of B_q is typically very close to zero in sandy soils. Therefore, q^* and Q_p can be considered to be equal in sandy soils, without significant error. The work was based on consideration of loading in triaxial compression; therefore M can be taken as equal to M_C.

In Chapter 8, this set of equations is applied to the CPT data at one of the CANLEX sites, for comparison with other methods of evaluating state. Been and Jefferies (1992) proposed that $\Psi=0$ represented the dividing line between material that could liquefy and that which could not.

c) Plewes et al. (1992)

Plewes et al. (1992) expanded upon the work by Been et al. (1987) by estimating contours of state parameter directly on the CPT soil classification chart as proposed by Jefferies and Davies (1991), as shown in Figure 4-11. Note that this soil classification chart normalizes cone tip resistance in a linear manner using mean normal stresses (p and p') rather than vertical stresses (σ_v and σ_v') as in the soil classification chart by Robertson (1990) that was used for the integrated CPT method in Chapter 3; i.e. Q_p (see Equation 4-22) rather than Q. CPT field data (in terms of normalized cone tip resistance and sleeve friction) can be superimposed on this figure in order to estimate the in-situ state of a sandy deposit. Soils with $\Psi>0$ are considered to be susceptible to liquefaction, given a suitable trigger mechanism.

4.3.3 Reference stress ratio (RSR) approach

State parameter, if estimated accurately, is one method for estimating the potential for flow liquefaction. However, the applicability of Ψ is limited predominantly to estimating the dividing line between states which are susceptible to flow liquefaction (i.e. $\Psi>0$) and those which are not (i.e. $\Psi<0$), over a limited stress range in a single sand deposit. The actual value of Ψ can not be correlated to response of a sand to monotonic undrained loading when dealing with either a large stress range in one sand or when trying to compare different sands. For a single straight reference USL in e-ln p' space (i.e. constant λ_{ln}), samples with constant values of Ψ would have similar undrained responses. However, in general, the USL for any given sand is curved (Ishihara, 1993; Sasitharan et al. 1994) and the slope, λ_{ln}, increases with increasing p'. Even in the same stress range, different sands have different USLs with different values of λ_{ln}. As shown in Figure 4-12, two sands may have the same state parameter relative to their individual USLs, but behave very differently in undrained shear, as a result of the different λ_{ln} value associated with each USL. The sand with the flatter USL will respond in a more brittle manner and will have a lower ultimate shear strength. Therefore, a constant value of Ψ does not imply similar responses in undrained loading for a given stress path due to the changing value of λ_{ln}.

An alternative measure of the initial state of a sample, which encompasses the effects of λ_{ln}, is the ratio p'_i/p'_{us} (see Figure 4-12) where p'_i is the initial mean normal effective stress of the sample and p'_{us} is the value of p' on the reference USL at the same void ratio. In e-ln p' space, Ψ and p'_i/p'_{us} are related by the slope of the USL, λ_{ln}, as follows:

$$[4\text{-}25] \qquad \frac{p'_i}{p'_{us}} = \exp\left(\frac{\Psi}{\lambda_{ln}}\right) = \text{Reference Stress Ratio (RSR)}$$

Note that when RSR=1, Ψ=0. The slope of the USL, λ_{ln}, is related to the grain characteristics of the material. The grain characteristics influence the compressibility of the sand skeleton. Thus, by combining e, p' and compressibility, the impact of the other factors such as direction of loading, structure and stress anisotropy can be examined more easily. Under a given direction of undrained monotonic loading, samples with the same soil structure and consolidation stress state and with the same value of RSR would be expected to respond in the same way (Sladen et al. 1985a). Identifying initial state by RSR relative to a selected reference USL provides a consistent framework that can be extended to other sands which have different USLs with different values of λ_{ln}. In Chapter 8, this ratio is used at one of the CANLEX sites to characterize Fraser River sand. In general, as RSR increases, a material is weaker and more brittle in response, when loaded undrained.

The concepts introduced here are not new, but rather, draw on the ideas of other researchers, as reported in the literature. Based on Mohr-Coulomb failure criteria, Casagrande (e.g. Casagrande, 1975) suggested characterizing a sand by a ratio between the initial effective confining pressure (σ'_3) and that at the liquefied state. Sladen et al. (1985a) proposed a relationship between brittleness index (one aspect of response) and RSR for Nerlerk sand with various fines contents and Leighton Buzzard sand, suggesting that "brittleness index is a reasonably unique function of initial p'/p'us for all sands and hence of state parameter for a given sand". McRoberts and Sladen (1992) suggested plotting laboratory stress path results in terms of q/p'_{us} and p'/p'_{us} to compare different tests. Cuccovillo and Coop (1993) plotted stress paths for triaxial compression tests on intact calcarenite in this manner. The ratio p'/p'_{us} represented a measure of the state of the soil relative to its ultimate state. Ishihara (1993) proposed a similar type of reference stress ratio, which he termed "initial state ratio" (r_c), relating the initial state of a soil to the quasi steady state (QSS) line in terms of the initial consolidation p' and the stress on the QSS line (p'_s), at the same void ratio. Ishihara (1993) noted that "this ratio is a parameter of prime importance for characterizing the undrained behaviour of sand".

It is interesting to note that the RSR concept for characterizing the state of sand is not unlike the method used to define state for clay. Overconsolidation ratio (OCR) can be expressed as the stress ratio relating the current p' to the maximum past p'. The only difference between RSR and OCR is that the latter is referenced to the virgin consolidation line, while the former is referenced to the USL because individual sands do not have unique consolidation lines. With increasing OCR, a clay becomes stronger and responds in a less brittle manner, when loaded undrained. Two samples of clay with the same OCR are expected to respond in a similar manner. OCR for a clay can be converted to RSR, based on the relationship between isotropic OCR and state parameter proposed by Plewes et al. (1992), as follows:

[4-26] $$\log(\mathrm{RSR}) = \frac{\Psi'}{\lambda_{log}} = \log(r) - \Lambda\log(\mathrm{OCR})$$

The term r represents the spacing between the USL and the virgin consolidation line and Λ is the critical state plastic hardening ratio. For most clays, $r \approx 2.3$ and $\Lambda = 0.8$ (Plewes et al., 1992). The RSR concept is, therefore, a global approach that could be applied to both sands and clays.

4.4 Application of the Proposed Framework

4.4.1 Field determination of RSR

Figure 4-13 (a modified version of Figure 4-2) outlines the various in-situ tests and the direct methods of estimating void ratio from the CPT, SPT, shear wave velocity measurements and geophysical logs, as explained earlier in this report. Note that the method of estimating void ratio for the SPT and CPT shown in Figure 4-13, is the V_s-based method. However, any reliable method of estimating void ratio from in-situ testing could be used. Once in-situ void ratios and stress conditions are estimated, in-situ profiles of RSR relative to the reference USL can be estimated. Following the flowchart in reverse, profiles of CPT, SPT, V_s or geophysical void ratios that represent an RSR of 1 could be back-calculated and superimposed over raw field logs. In-situ state (as estimated by in-situ testing) could then be compared to the reference USL (which, by definition, corresponds to RSR=1).

4.4.2 Laboratory determination of RSR

Figure 4-14 presents a flowchart outlining the various methods of preparing reconstituted samples and testing in the laboratory. Moist tamped samples tend to be looser for the same stress conditions and thus have higher values of RSR than water pluviated samples. Air pluviated samples have intermediate values of RSR. The magnitude of RSR, consolidation state (hydrostatic or K_o), soil structure and direction of loading govern the observed stress-strain response in terms of brittleness, strength, strain and stress ratio. The same factors govern the response of undisturbed samples. Triaxial and simple shear tests were performed at the CANLEX sites (further details for one of the sites are given in Chapter 8); only methods for interpreting triaxial data are presented here, due to the complexity and uncertainty of interpretation of simple shear test results. It is felt, based on the results of hollow cylinder testing on samples of Syncrude sand, that triaxial compression and triaxial extension represent the two loading condition extremes (Vaid et al., 1995). Vaid et al. (1995) concluded that the response in simple shear would therefore be predicted to fall between that in triaxial compression and that in triaxial extension.

Previous tests on Syncrude sand as part of Phase I of the CANLEX project (Vaid et al., 1995) have shown that anisotropically consolidated samples have a different stress-strain response to undrained loading than do isotropically consolidated samples. The results illustrated the importance of testing samples (reconstituted or undisturbed) under the in-situ K_o conditions. Studies reported by Georgiannou et al. (1990) resulted in similar conclusions. Anisotropic stress states that model in-situ conditions in loose sand ($Ko \approx 0.5$, based on the CANLEX test sites) have the effect of preloading a sample in compression. Therefore, less additional load is required for failure in compression that in extension. In extensional loading, the sample has to first be unloaded from the initial stress state before any strain-softening can possibly occur.

Reconstituted samples, even when tested anisotropically, may have different responses to undrained loading due to different methods of sample preparation. As a result, testing undisturbed samples that capture the in-situ state not only in terms of density and stress, but also in terms of soil structure is important. Direction of loading also has an effect on the response to undrained loading. Thus, it is also important to test samples under the direction(s) of loading appropriate to the in-situ conditions. Tests presented in Chapter 8 for one of the CANLEX sites are triaxial compression and extension tests predominantly on undisturbed samples under anisotropic initial stress conditions corresponding to K_o=0.5. However, a few tests were performed on reconstituted samples.

4.4.3 Laboratory response

In order to model in-situ sand behaviour, stress-strain relations are required. The undrained stress-strain response of any sample, when tested in the laboratory, can be characterized by various components. The key components identified here are: brittleness, minimum strength, strain that occurs while at minimum strength, strength at the end of the test (generally represents the ultimate strength), stress ratio (M=q/p') at peak and at the end of the test. Figures 4-15 and 4-16 illustrate the method of quantifying the various components of response for triaxial compression and extension, respectively.

Brittleness is defined in terms of the parameter termed brittleness index (I_B) which is defined as follows:

[4-27a] $$I_B = \frac{S_p - S_{min}}{S_p - S_i}$$ for triaxial compression

[4-27b] $$I_B = \frac{S_p - S_{min}}{S_p + S_i}$$ for triaxial extension

where:
S_p = magnitude of the peak shear strength
S_{min} = magnitude of the minimum shear strength
S_i = magnitude of the initial static shear stress.

Note that the formulae for brittleness index are slightly different for triaxial compression and extension for anisotropic samples ($S_i > 0$) and relate to the incremental stresses required to trigger failure from the initial stress state. For isotropic tests ($S_i = 0$), the two formulae become identical and simplify to the conventional definition of brittleness index (Bishop, 1971) which was based on isotropic testing. If sufficient straining occurs during the test, the end of the test represents the ultimate state (US) conditions. If the test does not experience a QSS, then the minimum strength and the end of test strength are assumed to be the same. A brittleness index of zero indicates a material that is strain-hardening.

Strain-hardening materials have equal peak, minimum and end-of-test strengths. A brittleness index greater than zero indicates a material that either strain-softens directly to US or experiences limited strain softening to a quasi-steady state (QSS) before dilating to US. The latter will generally have a smaller brittleness index than the former.

Based on critical state soil mechanics, a theoretical method for estimating the ultimate undrained shear strength for soils that are susceptible to flow liquefaction was proposed by Fear and Robertson (1995). Details are given in Chapter 5. However, the basic concept was that for a soil with a given void ratio, assuming no pore pressure redistribution and therefore no change in void ratio, the ultimate undrained shear strength (S_{us}) could be calculated within the critical state soil mechanics framework. An element of soil will travel along a stress path in an undrained plane with constant void ratio until it reaches the USL (see Figures 4-1 and 4-7). The value of p' on the USL (p'_{us}) at the given void ratio can be determined from the parameters Γ and λ_{ln}, using Equation 4-17. The ultimate undrained shear strength ($S_{us}=0.5\ q_{us}$) at this point is related to p'_{us} by M. Fear and Robertson (1995) expressed the equation for S_{us} in terms of state parameter (Ψ) and λ_{ln}, assuming a single straight USL for a given sand over a given stress range (see Chapter 5). A more global approach, as explained previously, is to make use of RSR which is a function of Ψ and λ_{ln} (see Equation 4-25). Combining all of these relationships gives the following equation for theoretically estimating the ultimate undrained strength ratio of an element of soil:

$$\frac{S_{us}}{p'_i} = \frac{M}{2} \bullet \frac{1}{RSR} \qquad [4\text{-}28]$$

Note that M has different values in compression and extension (see Equations 4-15 and 4-16). Dividing Equation 4-15 by Equation 4-16, it can be concluded that for typical friction angles, ϕ'_{us}, ranging from 30° to 40°, the value of M_C ranges from 1.40 to 1.54 times the value of M_E. Therefore, this theoretical method would predict approximately 40% to 50% higher ultimate undrained shear strengths in compression than in extension, for the same RSR. Actual differences between the undrained response in triaxial compression and extension may also be partially due to the inherent material anisotropy of sands (Arthur and Menzies, 1972). If pore pressure redistribution occurs in the field, loosening a sand deposit from its original conditions, this method may overpredict the ultimate undrained strength.

For sands that are very loose and strain-soften immediately to ultimate state, the ultimate undrained strength is the key to estimating the consequences of flow liquefaction in terms of slope stability and predicting resulting deformations. However, it appears that many sandy soils, while not being sufficiently loose to be completely strain-softening, do demonstrate limited strain-softening. When loaded undrained, these soils strain-soften temporarily to a quasi-steady-state (QSS) before dilating to ultimate state. The undrained strength associated with the QSS point (S_{min}) can be significantly smaller than the ultimate undrained strength. Provided that the strains associated with passing through the point of QSS are small, it could be argued that it is only the final ultimate strength which is of concern and which is generally large for these soils relative to completely strain-softening soils. However, the issue of QSS and whether or how to incorporate it into design analysis are areas of continuing debate.

For the one CANLEX site given as a worked example in Chapter 8, both S_{min}/p'_o and S_f/p'_o are shown for all tests. S_f is the end-of-test strength, which is generally less than or equal to the ultimate strength (as the stress path may be still moving towards ultimate state at the end of the test). For tests with a QSS, S_{min} is less than S_f; for tests with no QSS, S_{min} and S_f are taken to be the same, the end-of-test strength. Based on limited laboratory results from Phase II of the CANLEX project, it was found that, on an e-ln p' plot, the QSS points appear to fall approximately along a parallel line to the USL (details are given in Chapter 8). As a result, assuming that q and p' are still related by M along the QSS line (QSSL), Equation 4-28 can be modified to theoretically estimate the undrained strength ratio at QSS (S_{min}/p'_i), as follows:

$$\text{[4-29]} \qquad \frac{S_{us}}{p'_i} = \frac{M}{2} \bullet \frac{1}{(RSR + \Delta RSR)}$$

The term ΔRSR corresponds to the horizontal shift on the e-ln p' plot between the USL and the QSSL. ΔRSR is computed as the ratio of p' on the USL to p' on the QSSL, at the same void ratio. Ishihara (1993), based on work on Toyoura sand, stated that a given sand will have a unique USL, because the soil is completely remoulded by the time US is reached, but may have several different QSSLs which are a function of soil fabric and which may or may not be completely parallel to the USL. Therefore, it can be expected that the QSS points for reconstituted samples of a given sand may plot differently than those for undisturbed samples. Conversely, if the QSS points for undisturbed samples from similar sands at different sites plot similarly, it could be concluded that the two sites have a similar soil fabric. It is logical that within any one uniform soil deposit, there could be one soil fabric and, hence, a unique QSSL.

The theoretical predictions of ultimate undrained strength and strength at QSS will be compared to the actual values measured in the laboratory on undisturbed and reconstituted samples at one of the CANLEX sites in Chapter 8.

4.4.4 Linking in-situ characterization and laboratory response

Figure 4-17 outlines the interaction between field characterization of a deposit and the response of samples of sand in the laboratory. Ideally, one would like to characterize a deposit using in-situ tests such as CPT, SPT, V_S, geophysical logging or pressuremeter testing, and be able to predict the in-situ response to loading. Undisturbed samples, when tested undrained in the laboratory, will produce a certain response, in terms of brittleness, strength, strain and stress ratio. The key to linking the observed laboratory response to the in-situ response is to be able to correlate a particular signature from an in-situ test with laboratory results for certain initial conditions and thus be able to estimate the in-situ response. It is postulated that this objective can be achieved by determining the RSR for each sample, relative to a reference USL in e-ln p' space, prior to subjecting the sample to undrained loading and observing its response. Likewise, the signatures from the CPT, SPT, V_S or geophysical logging can be converted into profiles of RSR relative to the same reference USL, using methods outlined in Cunning et al. (1995) and Fear and Robertson (1995). Therefore, RSR, defined relative to a reference USL, can serve to link field characterization to laboratory response, for a particular sand.

Chapter 8 compares the observed relationship between the minimum and end-of-test strength ratio components of response and RSR for undisturbed samples tested in the laboratory with the theoretical relationships presented in Equations 4-28 and 4-29. In addition, tentative relationships between the other components of response (brittleness, axial strain at minimum strength, etc.) and RSR are proposed in Chapter 8 for one of the CANLEX sites. When laboratory testing for all of the CANLEX sites is completed, it will be possible to confirm if these relationships between the various components of response and RSR are general in nature and applicable to a variety of sands. Careful selection of the reference USL is important if different sands are to be compared.

4.4.5 Selecting a reference ultimate state line (USL)

There may be significant scatter to data resulting from monotonic triaxial laboratory tests under different directions of loading (Vaid et al., 1990) and drawing a unique USL for all of the tested samples may be difficult. However, testing on both Syncrude sand and Fraser River sand, as part of the CANLEX project, has shown that the data at ultimate state for a given sand fall within a band. Therefore, the reference USL can be selected as any line parallel to this band. The critical issue is to use the same reference USL when interpreting both field and laboratory data in order to provide a consistent link between in-situ test signatures and response.

Generally, if monotonic tests on loose sands are taken to large enough strains, the end of each test represents the US condition; however, in some cases, tests may appear to have been stopped before they had strained sufficiently to reach US. Samples that do reach US in undrained loading are generally very loose and strain soften without experiencing a QSS (e.g. reconstituted samples prepared by moist tamping and therefore having high values of RSR). Samples that are denser and experience a QSS are ultimately dilating towards US when the tests are stopped. Samples that are dilating have a high propensity for pore water redistribution (i.e. changing void ratio) and/or shear band development. Hence, interpretation of stress, strains and void ratio become uncertain. In some cases, tests cannot be strained any further due to equipment limitations. The mixture of samples that reach US and those which are still moving towards US may partially explain the apparent observation of a band of data for the end-of-test conditions on an e-ln p' plot. It is advisable to select the reference USL based on the loosest samples which clearly reach US, in order to have a reference line that is as close as possible to the true USL (Castro, 1969).

Figure 4-18 presents USLs for a variety of sands as reported in the literature and tabulated by Sasitharan et al. (1994). It is clear from Figure 4-18 that the USL for most sands curves at high stresses. Ishihara (1993) also indicated that the USL is curved in nature. Approximating a curved USL by a bi-linear relationship is convenient in that the USL can be broken down into straight line portions over various stress ranges (corresponding to various void ratio ranges), with each portion having an associated Γ and λ_n. In order to estimate RSR for a particular element of soil, the portion of the USL which has a void ratio range that includes the void ratio of the element must be used as the reference USL. In other words, the mean normal effective stress of the element, p'_i, must be divided by the mean normal effective stress at the same void ratio on this portion of the USL, p'_{us}, to estimate RSR. To determine p'_{us}, the value of Γ and λ_{ln} corresponding to the appropriate portion of the USL must be used.

4.5 Conclusions and Recommendations

This chapter has outlined both existing and new methods of estimating the void ratio and state of a sandy soil deposit. Conventional methods of estimating state (i.e the method by Sladen and Hewitt (1989) versus the method by Been and Jefferies (1992)) often give different conclusions regarding liquefaction potential. In addition, the conventional methods, although they may give reasonable dividing lines for liquefaction potential, are not good for estimating the response of a soil to undrained monotonic loading. The RSR-based framework suggested here allows for a direct estimation of soil response by linking in-situ characterization with the laboratory response of undisturbed samples. The framework can be applied on a site-specific basis, but as additional data becomes available, the ultimate goal of future studies would be to develop a global method of estimating in-situ response directly from in-situ testing without the need for undisturbed samples. This would be useful for low risk projects for which obtaining undisturbed samples is beyond the project scope and budget or for initial site screening of high risk projects.

Chapter 8 presents a worked example, based on detailed field and laboratory studies at one of the CANLEX sites, illustrating the step-by-step application of the framework outlined here and comparing the resulting predictions of void ratio and soil state with the predictions using existing methods. As will be seen in Chapter 8, the individual components of response clearly appear to be a function of the magnitude of RSR. Tentative relationships are given for the CANLEX site presented in the worked example and specific details regarding the proposed framework and how to apply it are discussed further.

The framework proposed here is capable of estimating flow liquefaction potential and the subsequent elements of response of a deposit of sand. However, whether a slope or soil structure will fail and slide depends on a number of factors, including the amount of strain-softening soil relative to strain-hardening soil, the brittleness of the strain-softening ground, drainage conditions and the geometry of the ground. Even if a catastrophic failure can not occur, the magnitude of any deformations that may occur depend on the same factors. Applying the framework proposed in this chapter is only the first step in a complete liquefaction analysis. If some material is found to be strain-softening with a brittle response to undrained loading, the slope or soil structure must be examined in detail as a whole, using numerical methods, for example, to estimate the overall stability and potential deformations that may occur. The most dangerous soils are those which have a sufficiently loose state to strain-soften directly to ultimate state in a brittle manner. In general, slope failures as a result of flow liquefaction are not common; however, when they do occur, they can take place rapidly, with little warning, and often catastrophic results. Consequently, it is important to proceed cautiously when designing against flow liquefaction, particularly in the case of high risk projects for which the consequences of failure can be enormous.

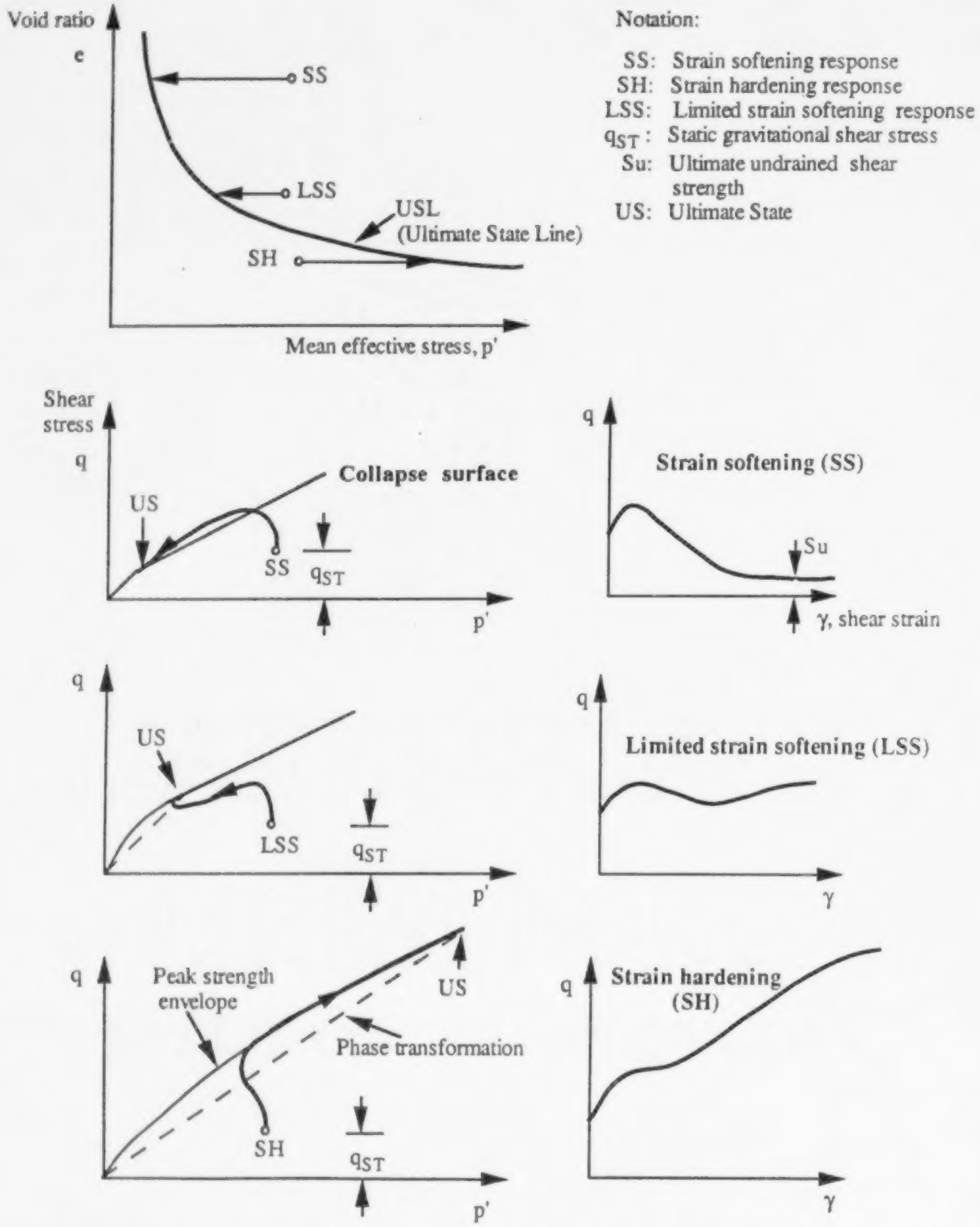
Void ratio
e
SS
LSS
USL
(Ultimate State Line)
SH
Mean effective stress, p'
Notation:
SS: Strain softening response
SH: Strain hardening response
LSS: Limited strain softening response
q_ST: Static gravitational shear stress
Su: Ultimate undrained shear strength
US: Ultimate State
Shear stress
q
Collapse surface
US
SS
q_ST
p'
q
Strain softening (SS)
Su
γ, shear strain
q
US
LSS
q_ST
p'
q
Limited strain softening (LSS)
γ
q
Peak strength envelope
US
Phase transformation
SH
q_ST
p'
q
Strain hardening (SH)
γ

Figure 4-1 Schematic of undrained monotonic behaviour of sand in triaxial compression (modified from Robertson, 1994).

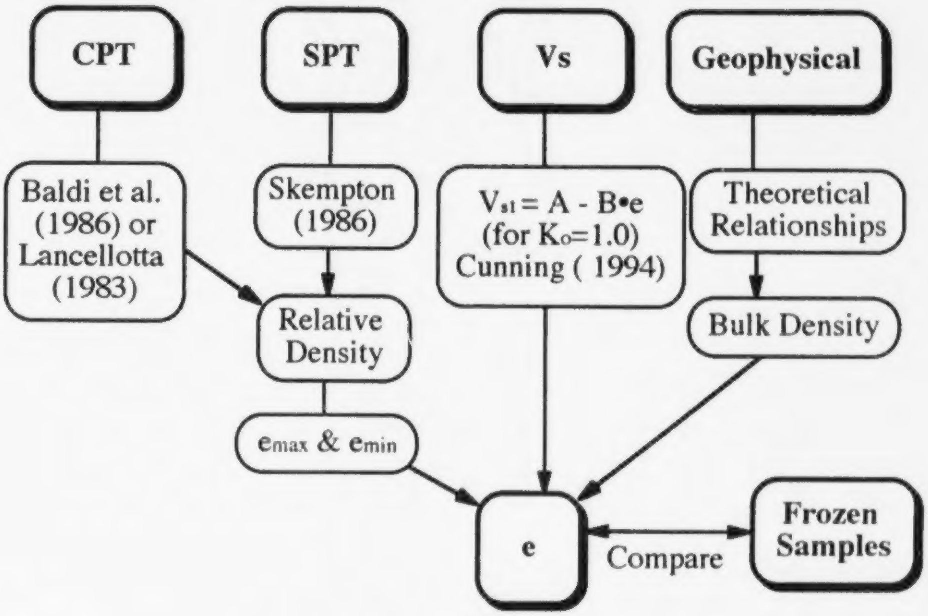
CPT
SPT
Vs
Geophysical
Baldi et al. (1986) or Lancellotta (1983)
Skempton (1986)
Vs1 = A - B•e (for Ko=1.0) Cunning (1994)
Theoretical Relationships
Relative Density
Bulk Density
emax & emin
e
Compare
Frozen Samples

Figure 4-2 Flowchart for interpreting void ratio from in-situ testing.

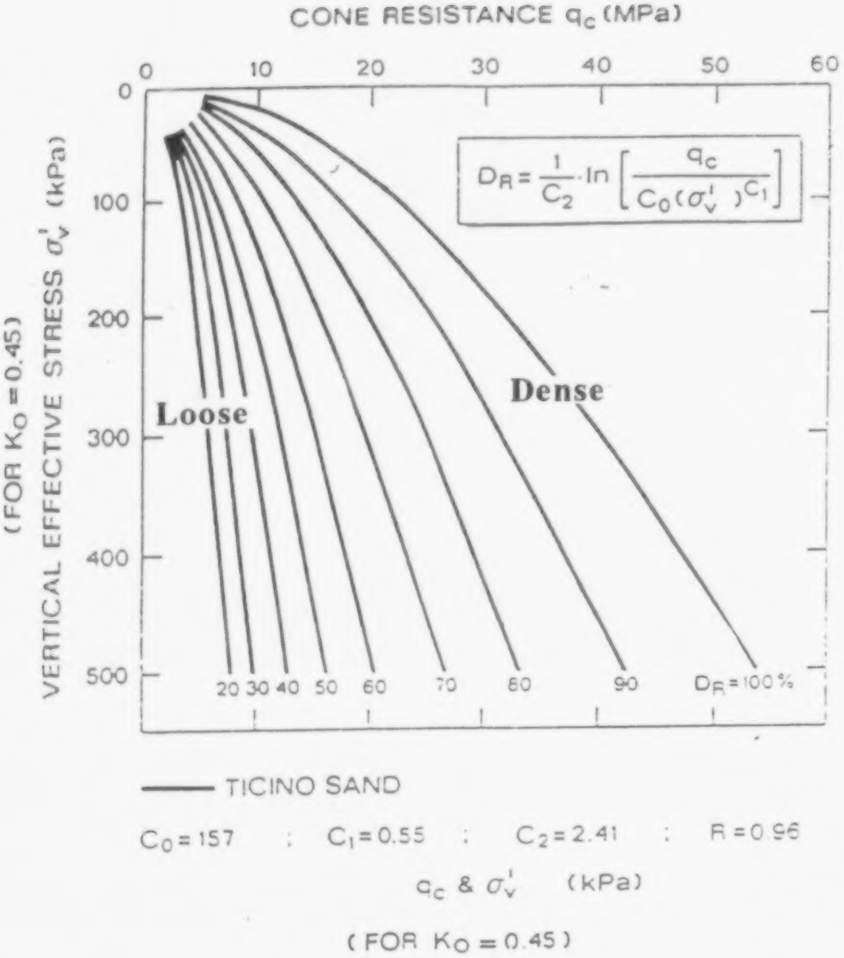

Figure 4-3 Conventional void ratio interpretation from CPT (modified from Baldi et al., 1986).

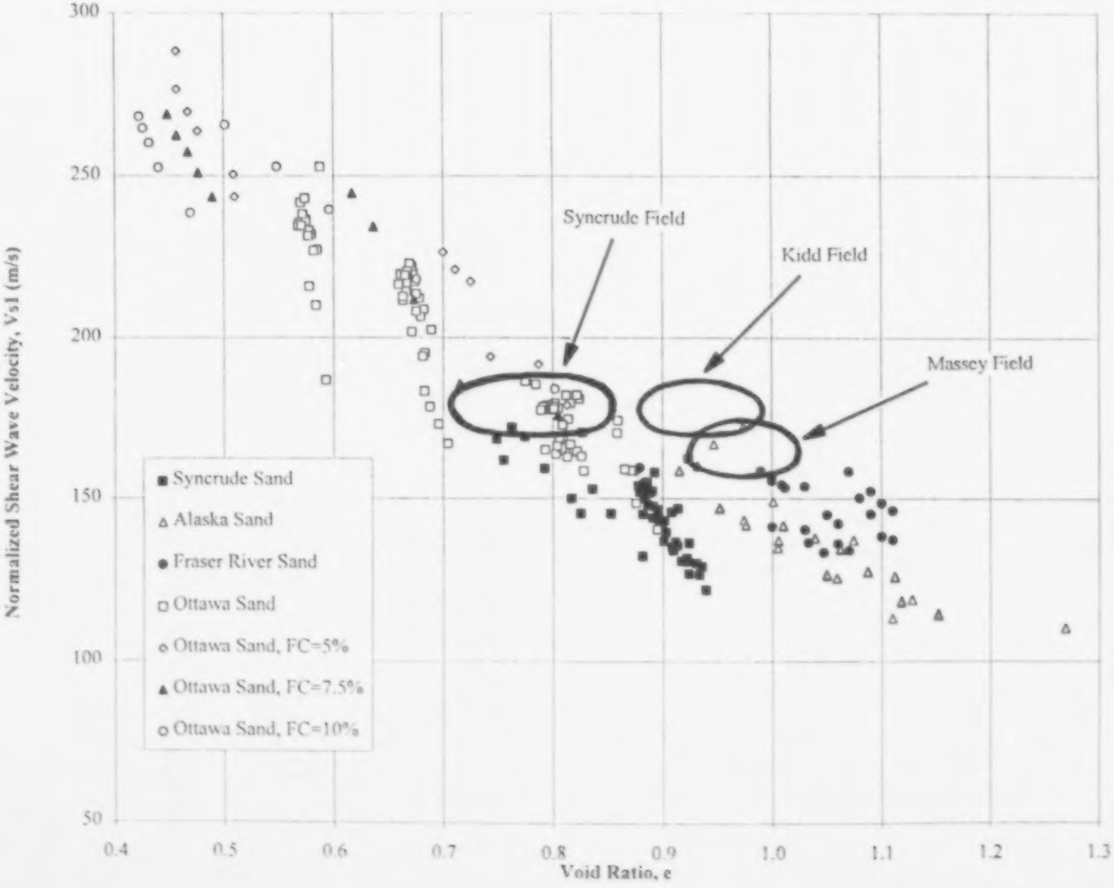

Figure 4-4 Variation of corrected shear wave velocity with void ratio for a range of sands (based on results from Sasitharan, 1994; Cunning, 1994; Chillarige, 1995; and Skirrow, 1996).

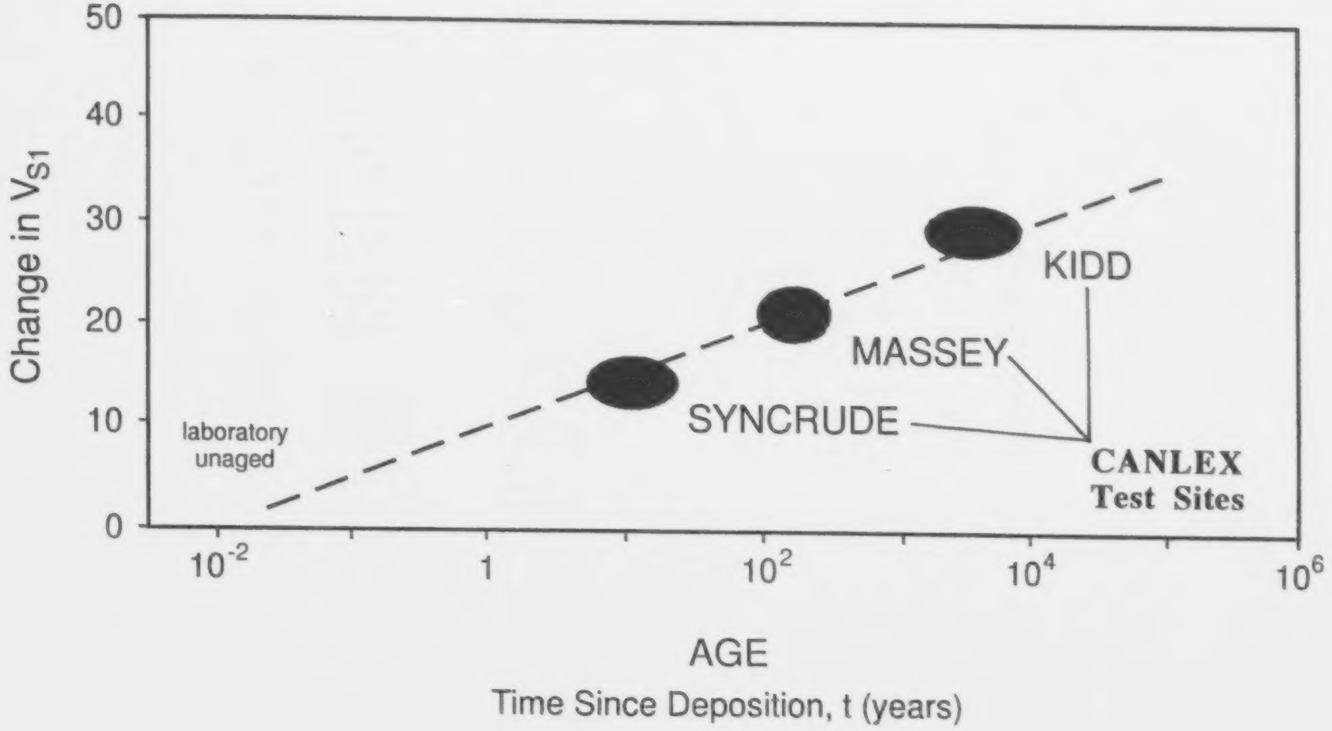

Figure 4-5 Change in corrected shear wave velocity with age for uncemented sands (modified from Robertson et al., 1995).

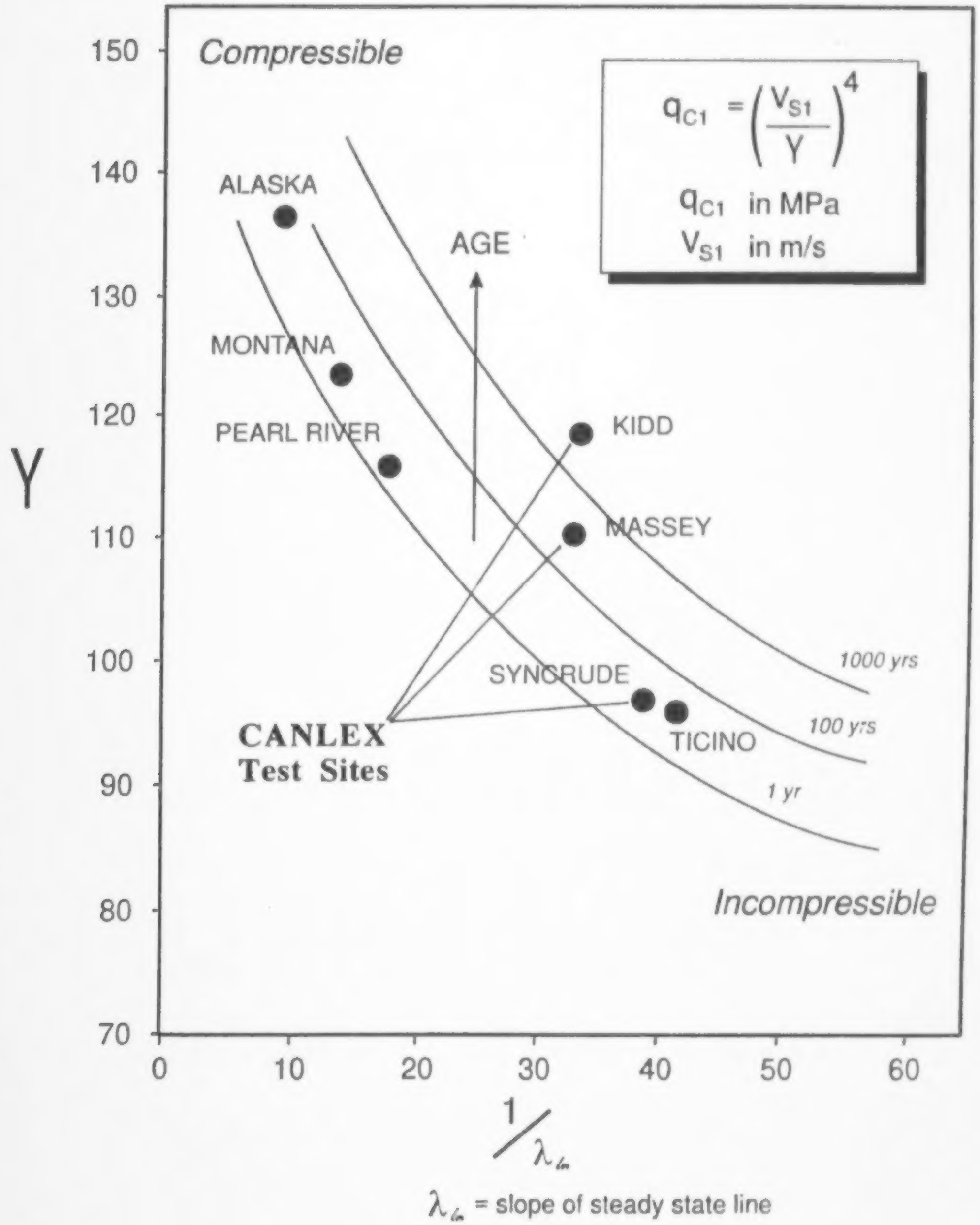

Figure 4-6 Proposed correlation between shear wave velocity and CPT tip resistance and slope (λ_{ln}) of the ultimate state line (USL) (modified from Robertson et al., 1995).

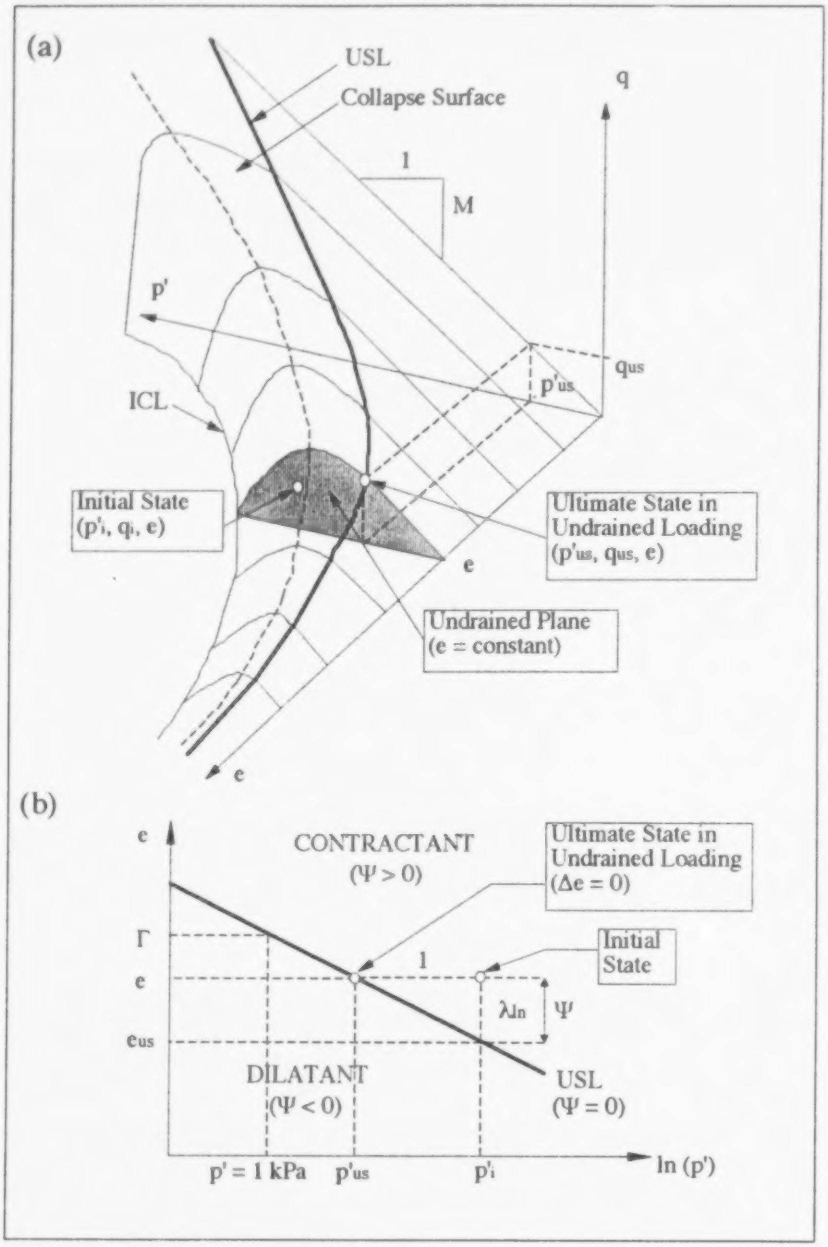
(a)
USL
Collapse Surface
q
1
M
p'
q_us
p'_us
ICL
Initial State (p'i, qi, e)
Ultimate State in Undrained Loading (p'us, qus, e)
e
Undrained Plane (e = constant)
e
(b)
e
CONTRACTANT (Ψ > 0)
Ultimate State in Undrained Loading (Δe = 0)
Γ
1
Initial State
e
λln
Ψ
e_us
DILATANT (Ψ < 0)
USL (Ψ = 0)
p' = 1 kPa
p'us
p'i
ln (p')

Figure 4-7 Critical state soil mechanics concepts illustrated by (a) an e-p'-q diagram with (b) projections onto the e-ln(p') plane.

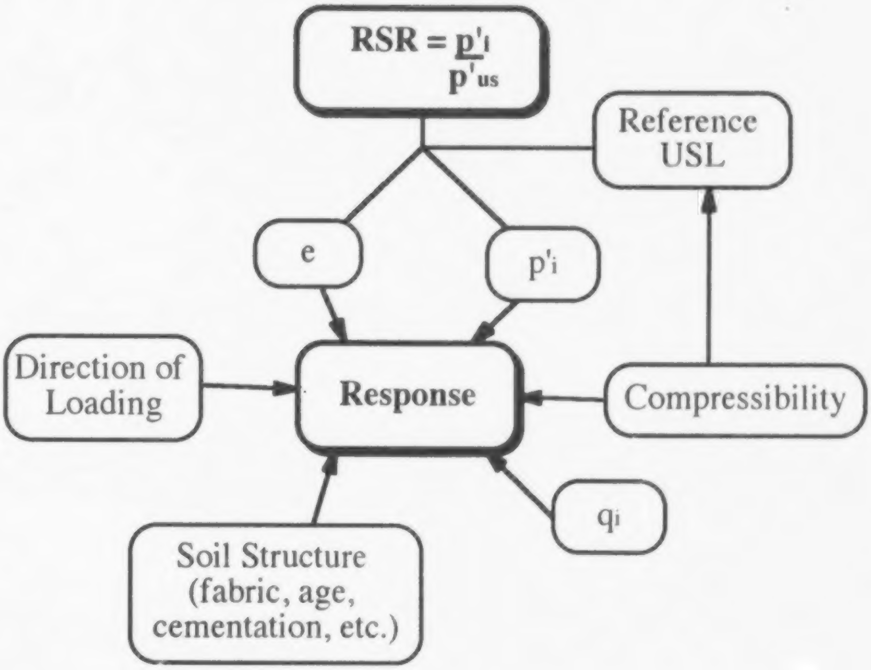

RSR = $\frac{p'_i}{p'_{us}}$
Reference USL
e
p'i
Direction of Loading
Response
Compressibility
qi
Soil Structure (fabric, age, cementation, etc.)

Figure 4-8 Factors influencing response of sandy soils in undrained monotonic testing.

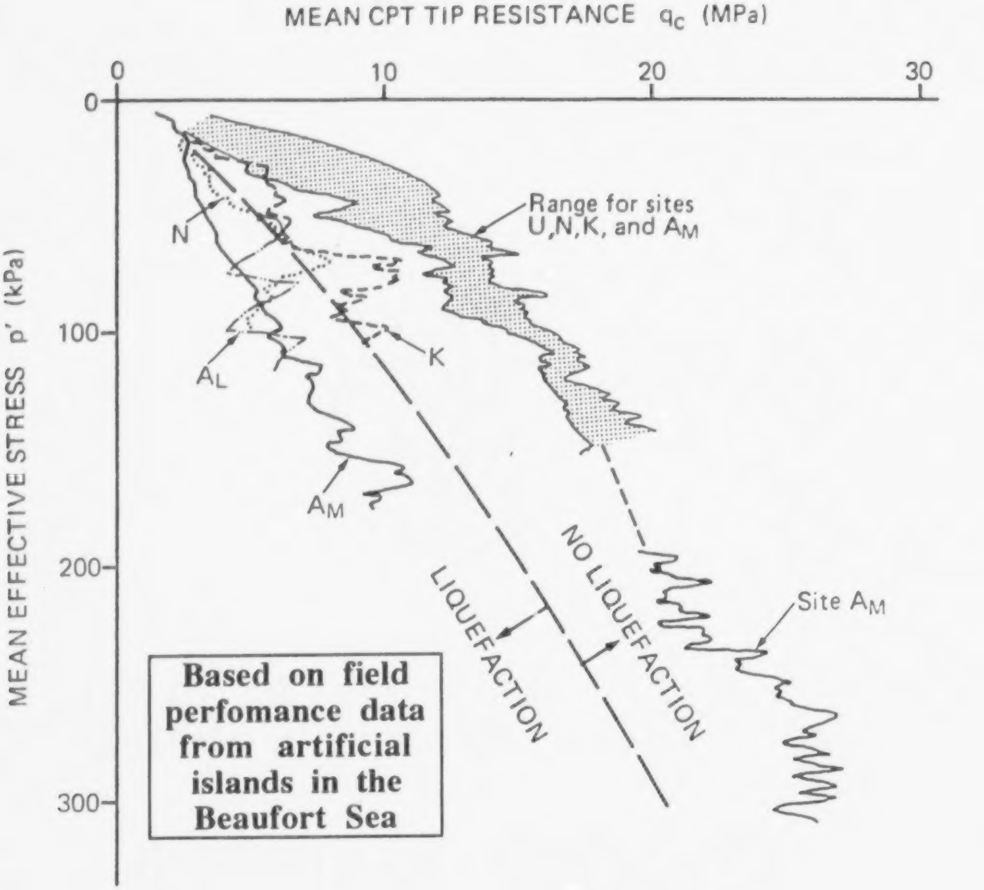

SYMBOL	SITES	PLACEMENT	LIQUEFACTION	SAND
▨--	U,N,K,A_M	Hopper	No	Ukalerk
----------	K	Pipeline	No	Ukalerk
…………	N	Pipeline	Yes	Nerlerk
———	A_M	Pipeline	Yes	Ukalerk
—··—··—	A_L	Pipeline	Yes	Local Borrow

Figure 4-9 CPT liquefaction/nonliquefaction dividing line based on field observations (modified from Sladen and Hewitt, 1989).

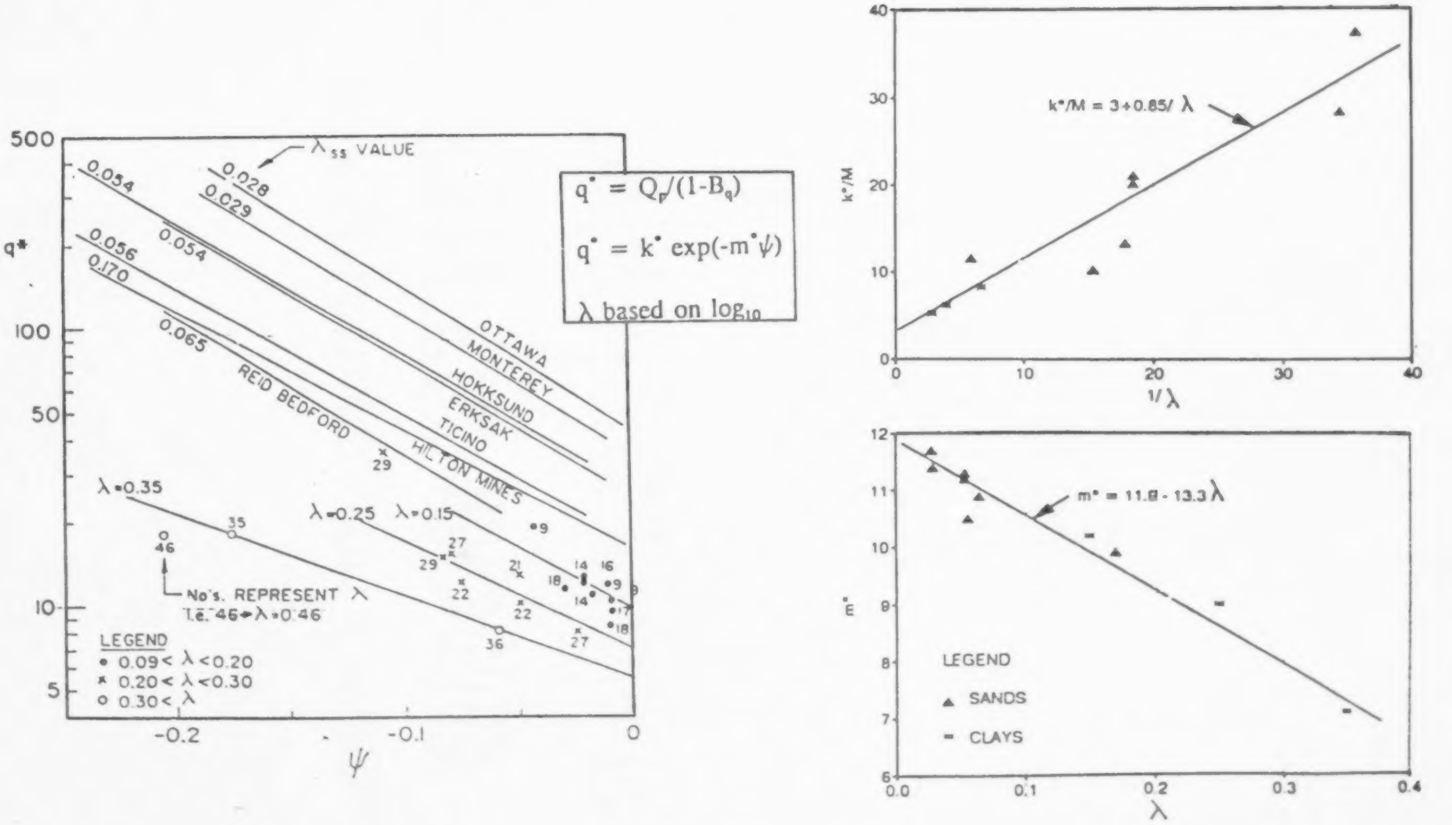

Figure 4-10 Unified relationship of $Q_p(1-B_q)$ to state parameter and critical state parameters M and λ_{log} (modified from Been and Jefferies, 1992).

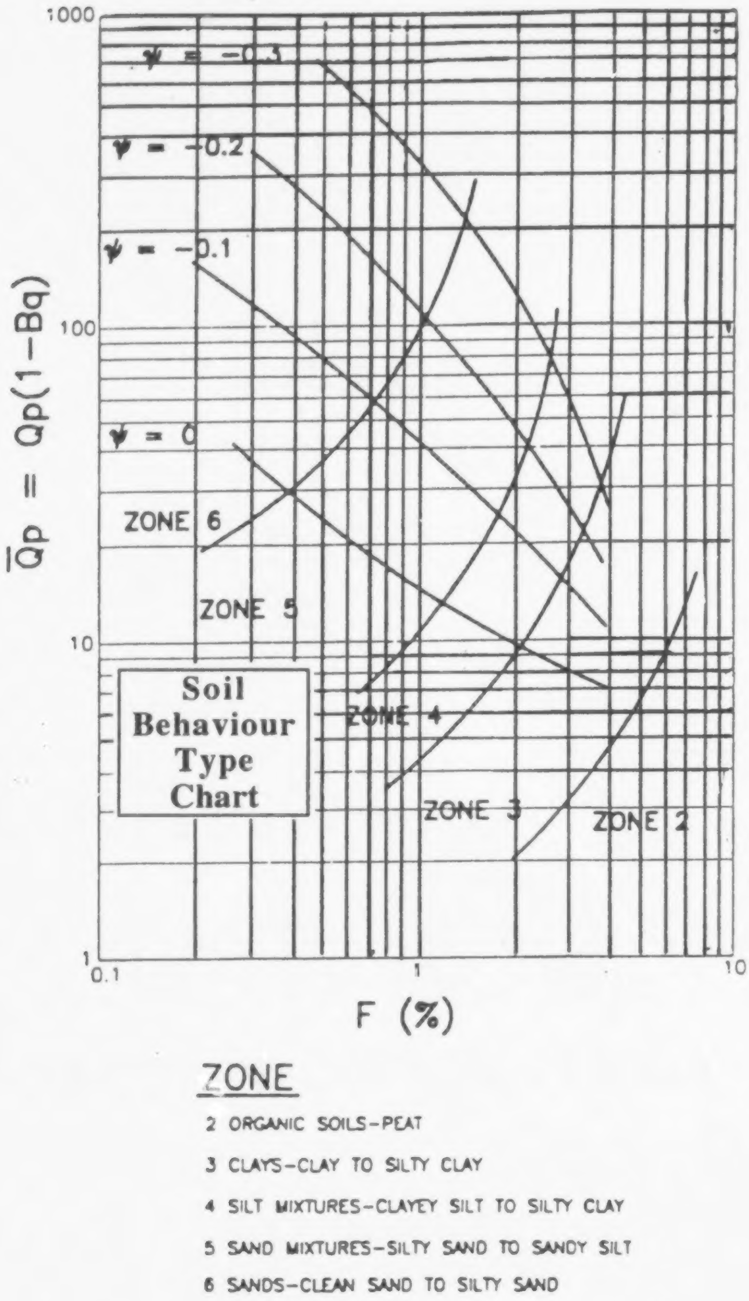

Figure 4-11 Contours of estimated state parameter on soil type behaviour classification chart (modified from Plewes et al., 1992).

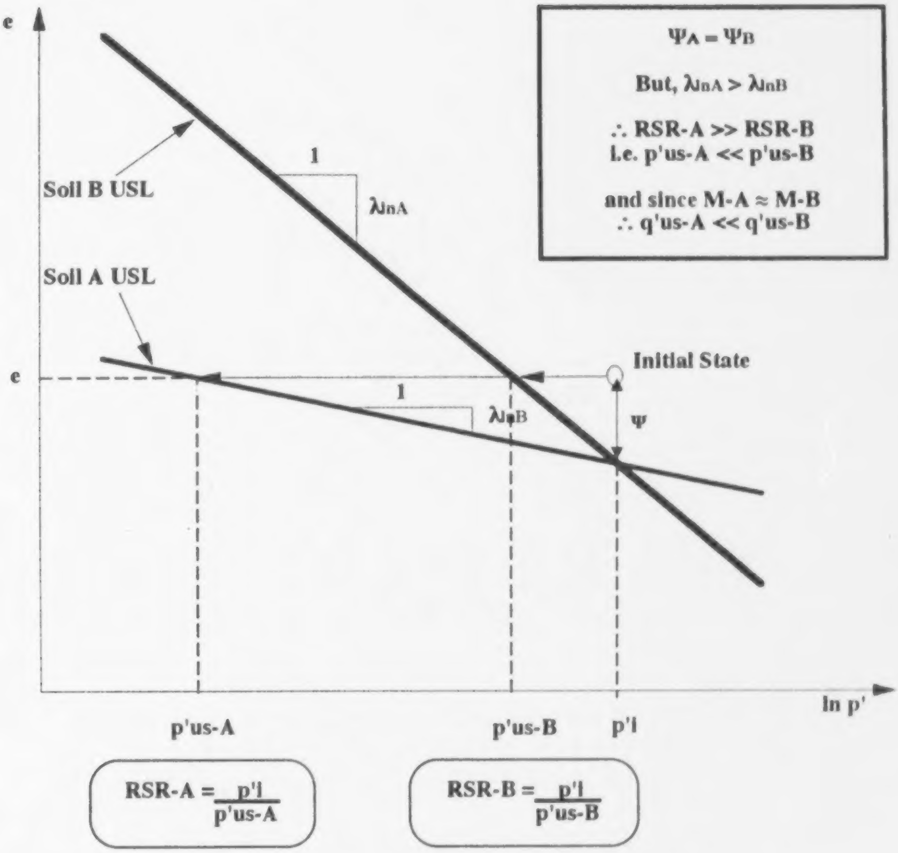
e
$\Psi_A = \Psi_B$
But, $\lambda_{lnA} > \lambda_{lnB}$
$\therefore$ RSR-A >> RSR-B
i.e. p'us-A << p'us-B
and since M-A ≈ M-B
$\therefore$ q'us-A << q'us-B
1
Soil B USL
λ_{lnA}
Soil A USL
Initial State
e
1
λ_{lnB}
ψ
ln p'
p'us-A
p'us-B
p'i
RSR-A = $\frac{p'i}{p'us-A}$
RSR-B = $\frac{p'i}{p'us-B}$

Figure 4-12 Effects of λ_{ln} on undrained response for the same value of state parameter.

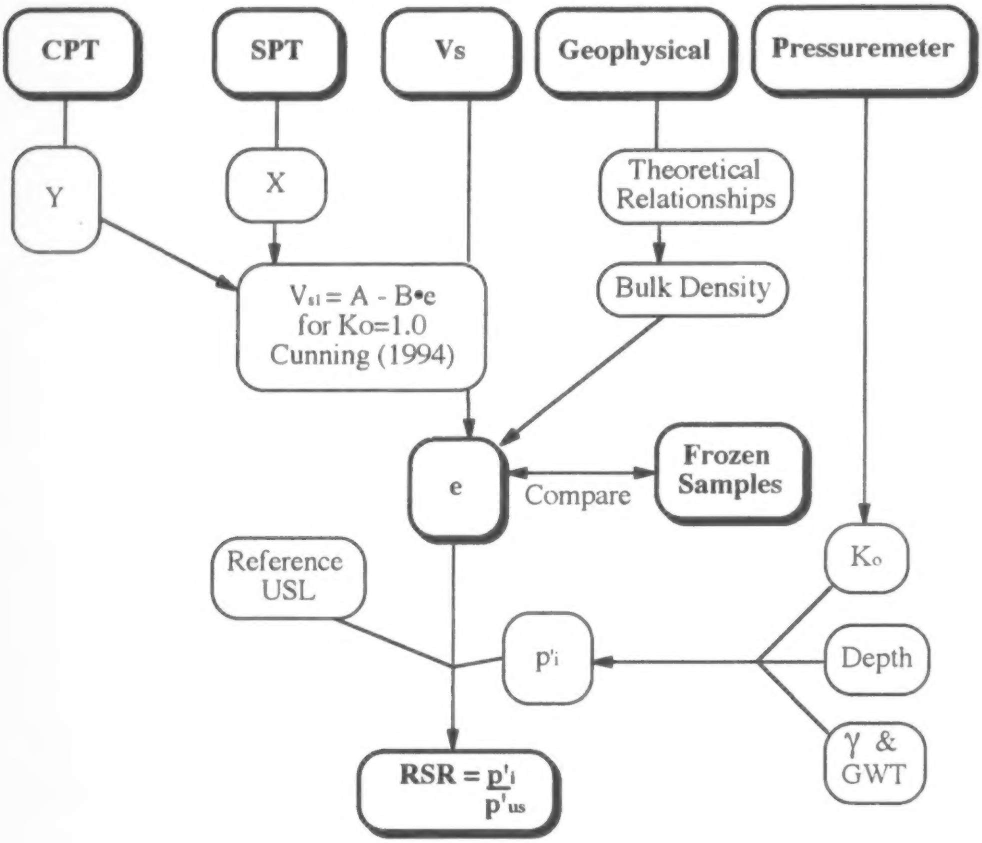
CPT
SPT
Vs
Geophysical
Pressuremeter
Y
X
Theoretical Relationships
Bulk Density
V_s1 = A - B•e
for Ko=1.0
Cunning (1994)
e
Compare
Frozen Samples
Reference USL
Ko
p'i
Depth
γ &
GWT
RSR = p'i / p'us

Figure 4-13 Flowchart for estimating RSR from in-situ testing.

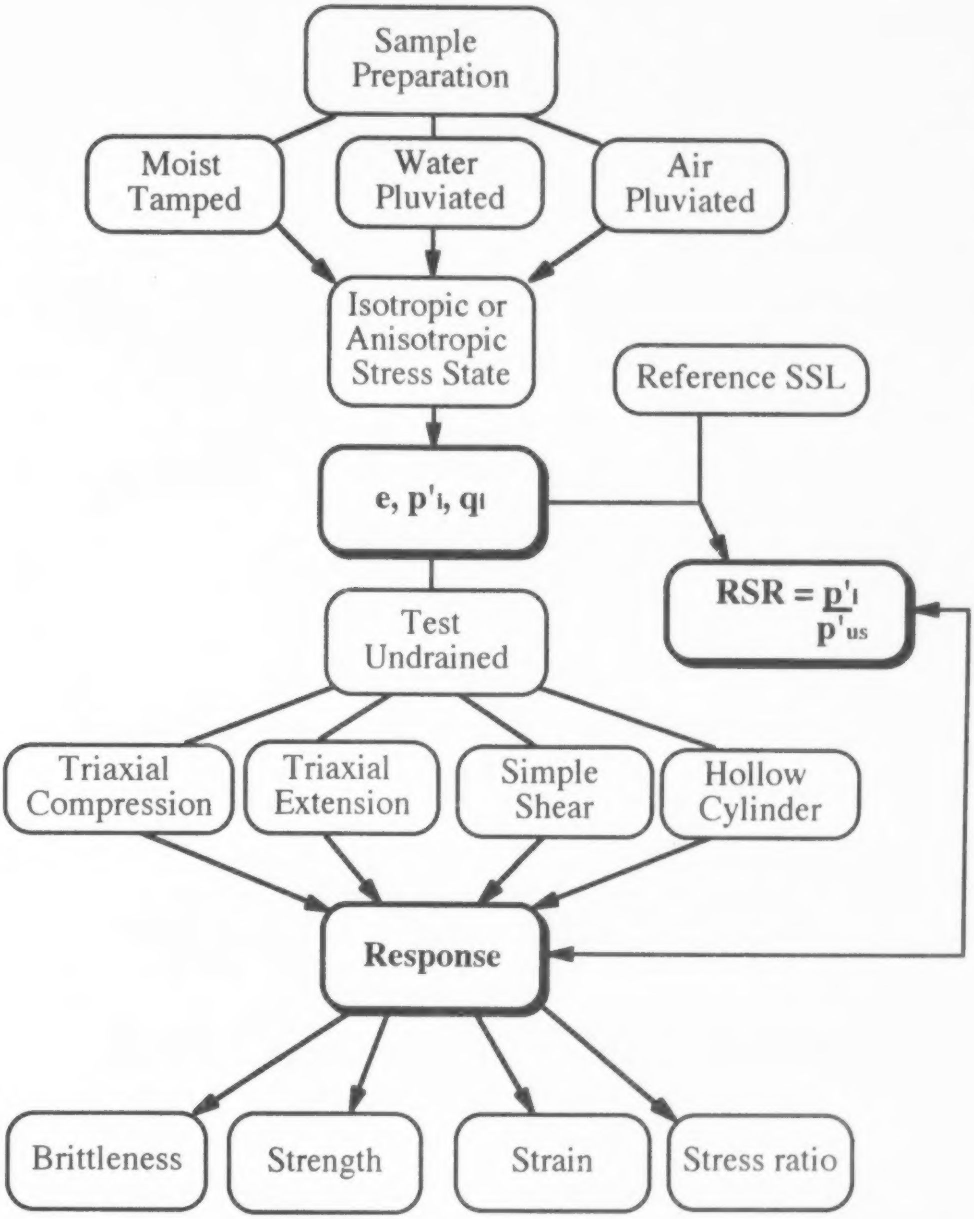
Sample Preparation
Moist Tamped
Water Pluviated
Air Pluviated
Isotropic or Anisotropic Stress State
Reference SSL
e, p'i, qi
RSR = p'i / p'us
Test Undrained
Triaxial Compression
Triaxial Extension
Simple Shear
Hollow Cylinder
Response
Brittleness
Strength
Strain
Stress ratio

Figure 4-14 Flowchart for measuring undrained response from laboratory testing.

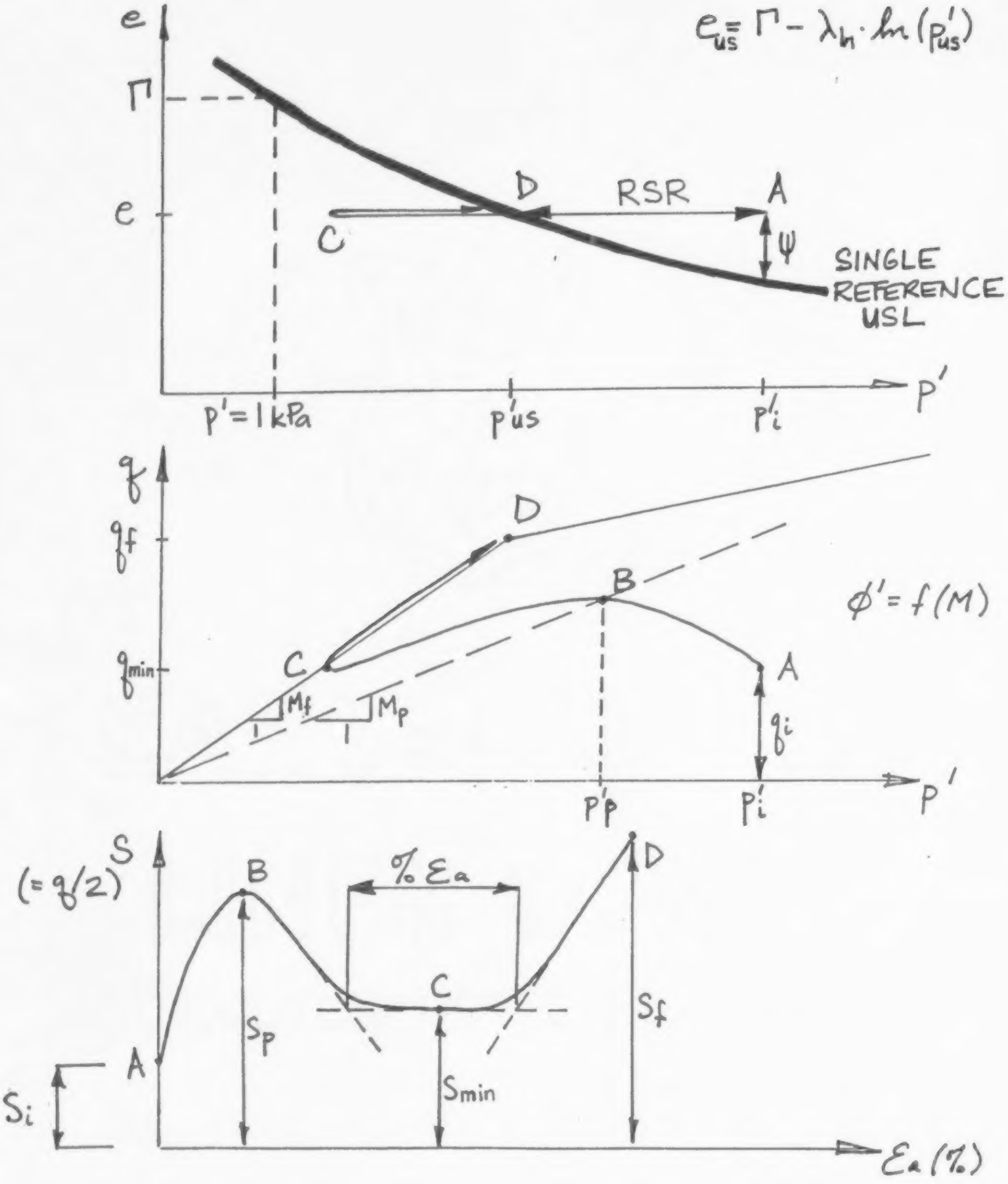

$e_{us} = \Gamma - \lambda_h \cdot \ln(p'_{us})$
e
Γ
e
C
D
RSR
A
ψ
SINGLE REFERENCE USL
p' = 1 kPa
p'us
p'i
p'
q
qf
D
B
$\phi' = f(M)$
qmin
C
A
Mf
1
Mp
1
qi
p'p
p'i
p'
S (= q/2)
B
% εa
D
C
Sf
Sp
A
Si
Smin
εa (%)

Figure 4-15 Components of undrained response for triaxial compression loading.

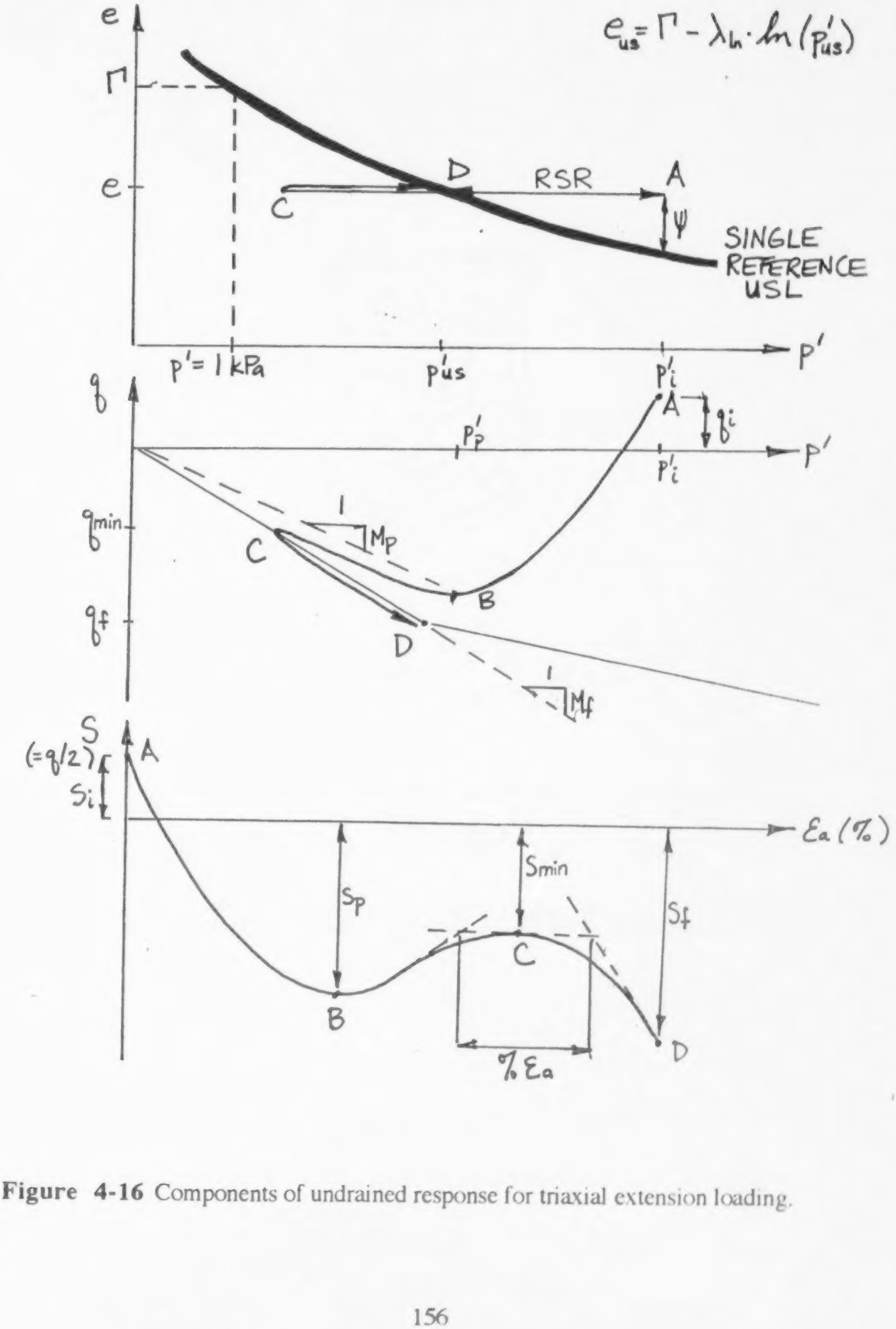

$e_{us} = \Gamma - \lambda_{ln} \cdot \ln(p'_{us})$
e
Γ
e
C
D
RSR
A
ψ
SINGLE REFERENCE USL
p' = 1 kPa
p'us
p'i
p'
q
p'p
A
qi
p'
p'i
1
Mp
qmin
C
B
qf
D
1
Mf
S (=q/2)
A
Si
εa (%)
Sp
Smin
Sf
C
B
D
% εa

Figure 4-16 Components of undrained response for triaxial extension loading.

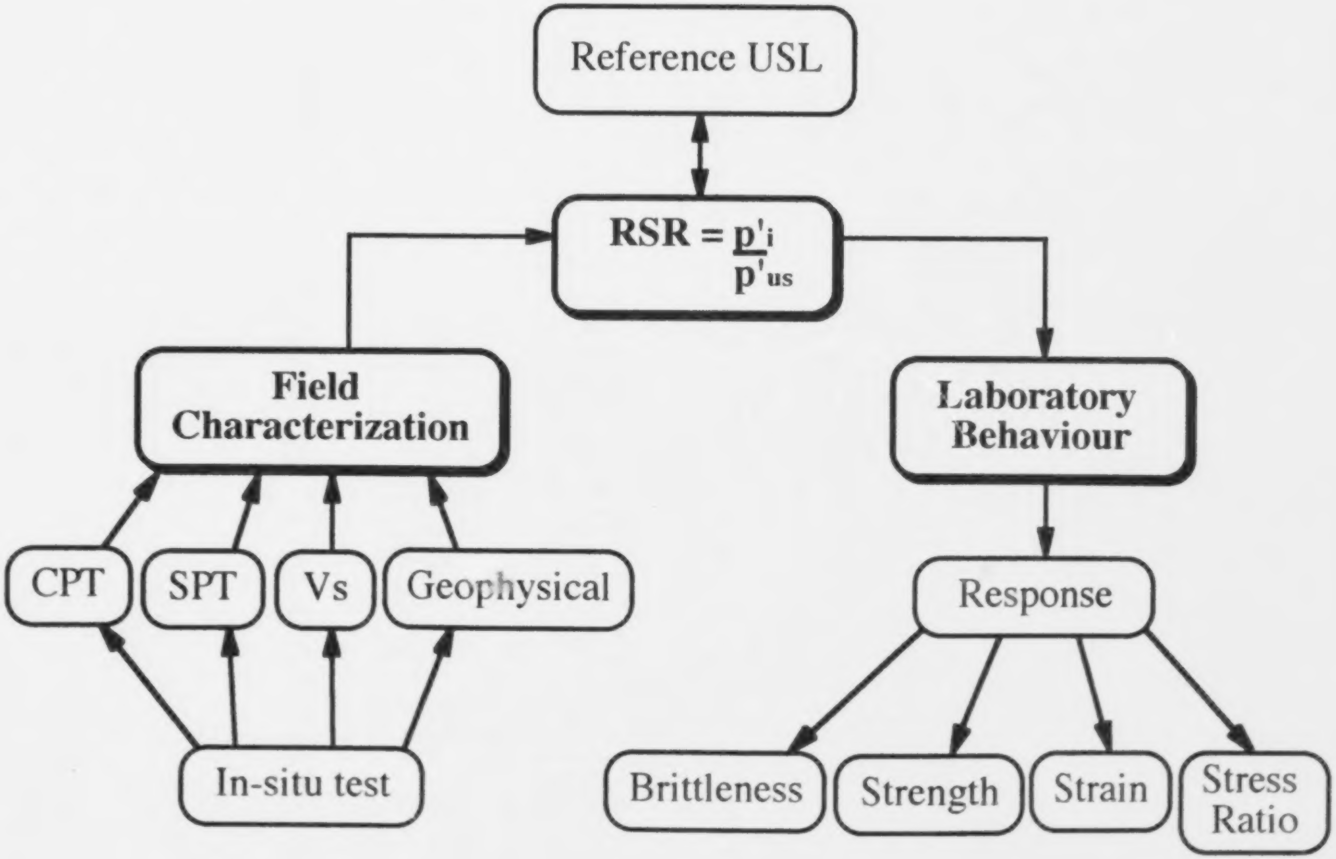
Reference USL
RSR = $\frac{p'_i}{p'_{us}}$
Field Characterization
Laboratory Behaviour
CPT
SPT
Vs
Geophysical
In-situ test
Response
Brittleness
Strength
Strain
Stress Ratio

Figure 4-17 Suggested interaction between field characterization and in-situ response from laboratory testing.

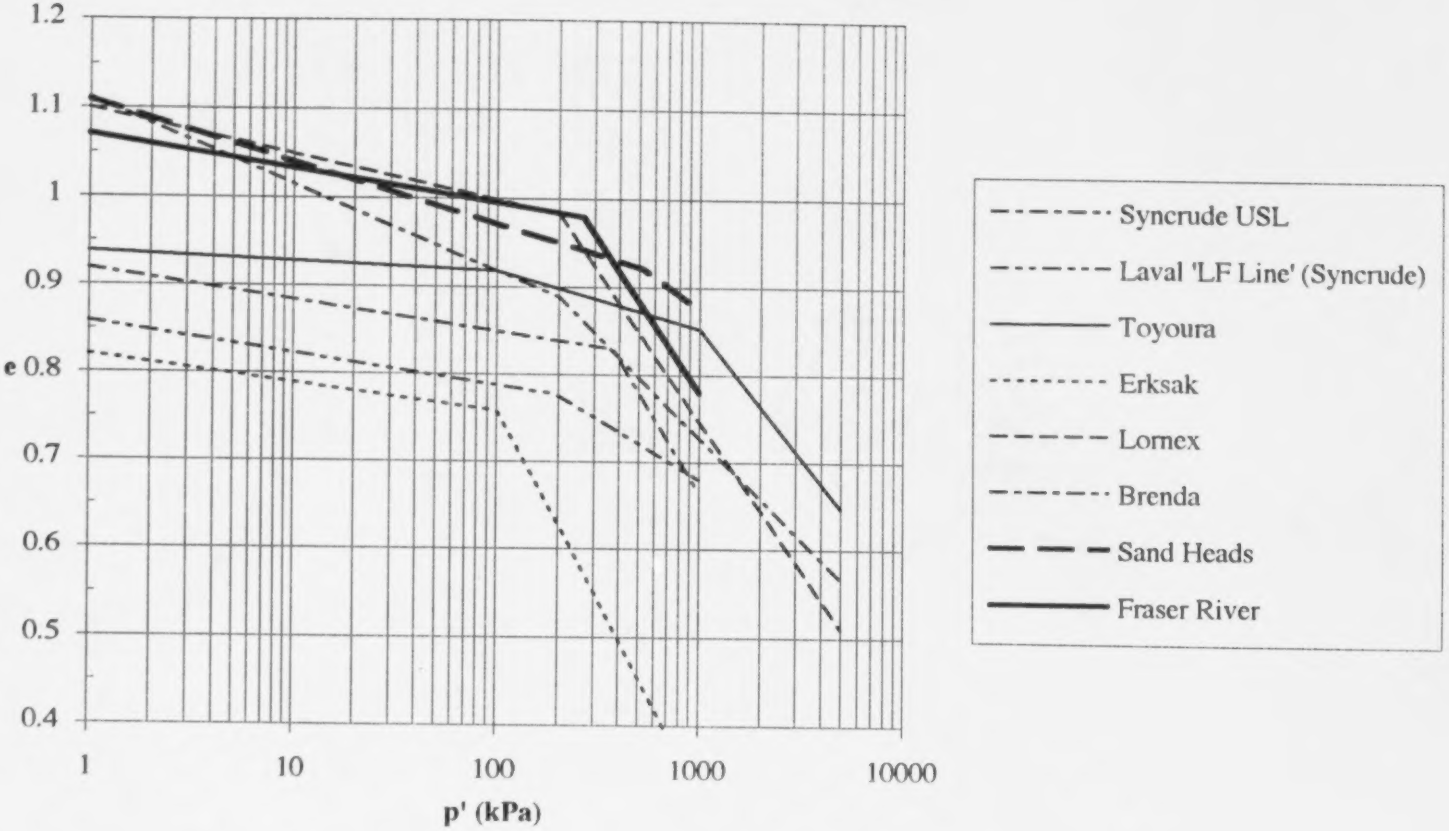

Figure 4-18 Ultimate state lines (USLs) for a variety of sands (based on data tabulated by Sasitharan et al., 1994); also shown are selected reference USLs for Sand Heads sand (after Chillarige et al., 1995) and Fraser River sand.

References

Arthur, J.R.F., and Menzies, B. 1972. Inherent anisotropy in a sand. *Géotechnique*, 22(1): 115-128.

Atkinson, J.H. 1993. *The mechanics of soils and foundations*, McGraw-Hill, London.

Baldi, G. et al. 1986. Interpretation of CPT's and CPTU's, II Part: Drained penetration on sands. *Proc. IV Int. Geotech. Seminar on Field Instrumentation and In Situ Measurements*, Nanyang Tech. Inst., Singapore.

Been, K., and Jefferies, M.G. 1985. A state parameter for sands. *Géotechnique*, 35(2): 99-112.

Been, K., and Jefferies, M.G. 1992. Towards systematic CPT interpretation. *Proceedings of the Wroth Symposium*, 44-55.

Been, K., Jefferies, M.B., Crooks, J.H.A., and Rothenburg, L., 1987. The cone penetration test in sands, Part 2: General inference of state. *Géotechnique*, 37(3): 285-299.

Been, K., Jefferies, M.G., and Hachey, J. 1991. The critical state of sands. *Géotechnique*, 41(3): 365-381.

Bishop, A.W. 1971. Shear strength parameters for undisturbed and remoulded soil specimens. *Roscoe Memorial Symposium*, Cambridge University, 3-58.

Casagrande, A. 1975. Liquefaction and cyclic deformation of sands, a critical review. *Proceedings of the 5th Pan American Conference on Soil Mechanics and Foundation Engineering*, Buenos Aires, 5, 80-133.

Castro, G. 1969. Liquefaction of sands, Harvard Soil Mechanics Series No. 81.

Chillarige, A.R.V. 1995. Liquefaction and seabed instability in the Fraser River Delta. *Ph.D. Thesis*, Department of Civil Engineering, University of Alberta, Edmonton, Alberta, Canada.

Coop, M.R., Atkinson, J.H., and Taylor, R.N. 1995. Strength and stiffness of structured and unstructured soils. *Proceedings of the 11th European Conference on Soil Mechanics and Foundation Engineering*, Copenhagen, 1: 1.55-1.62.

Cuccovillo, T., and Coop, M.R. 1993. The influence of band strength on the mechanics of carbonate soft rocks. *Geotechnical Engineering of Hard Soils - Soft Rocks*, Balkema, Rotterdam, 447-455.

Cunning, J.C. 1994. Shear wave velocity measurement of cohesionless soils for the evaluation of in-situ state. *M.Sc. Thesis*, Department of Civil Engineering, University of Alberta, Edmonton, Alberta, Canada.

Cunning, J.C., Robertson, P.K., and Sego, D.C. 1995. Shear wave velocity to evaluate in-situ state of cohesionless soils. *Canadian Geotechnical Journal*, 32(5): 848-858.

Fear, C.E., and Robertson, P.K. 1995. Estimating the undrained strength of sand: a theoretical framework. *Can. Geotech. J.*, 32(4).

Georgiannou, V.N., Burland, J.B. and Hight, D.W. 1990. The undrained behaviour of clayey sands in triaxial compression and extension, Géotechnique, 40(3): 431-449.

Ishihara, K. 1993. Liquefaction and flow failure during earthquakes. The 33rd Rankine Lecture, *Géotechnique*, 43(3): 351-415.

Jefferies, M.G. and Davies, M.P. 1991. Discussion on soil classification by the cone penetration test. *Canadian Geotechnical Journal*, 28(1): 173-176.

Kulhawy, F.M., and Mayne, P.W. 1990. Manual on estimating soil properties for foundation design. Cornell University, EL-6800, *Research Project 1493-6*, prepared for Electric Power Research Institute.

McRoberts, E.C., and Sladen, J.A. 1992. Observations on static and cyclic sand liquefaction methodologies. *Canadian Geotechnical Journal*, 29(4): 650-665.

Plewes, H.D., McRoberts, E.C., and Chan, W.K. 1988. Downhole nuclear density logging in sand tailings. *Proceedings of ASCE Specialty Conference on Hydraulic Fill Structures*, Fort Collins, Colorado, 290-309.

Plewes, H.D., Davies, M.P, and Jefferies, M.G. 1992. CPT based screening procedure for evaluating liquefaction susceptibility. *Proceedings of the 45th Canadian Geotechnical Conference*, Toronto, Ontario, 4:1-4:9.

Robertson, P.K. 1990. Soil classification using the CPT. *Canadian Geotechnical Journal*, 27(1): 151-158.

Robertson, P.K., Fear, C.E., Woeller, D.J., and Weemees, I. 1995. Estimation of sand compressibility from seismic CPT. *Proceedings of the 48th Canadian Geotechnical Conference*, Vancouver, 1, 441-448.

Robertson, P.K., Woeller, D.J., Kokan, M., Hunter, J., and Luternauer, J. 1992. Seismic techniques to evaluate liquefaction potential. *Proceedings of the 45th Canadian Geotechnical Conference*, 5:1-5:9.

Sasitharan, S. 1994. Collapse behaviour of very loose sand. *Ph.D. Thesis*, Department of Civil Engineering, University of Alberta, Edmonton, Alberta, Canada.

Sasitharan, S., Robertson, P.K., Sego, D.C., and Morgenstern, N.R. 1994. State boundary surface for very loose sand and its practical implications. *Can. Geotech. J.*, 31(3): 321-334.

Skempton, A.W. 1986. Standard penetration test procedures and the effects in sands of overburden pressure, relative density, particle size, ageing and overconsolidation. *Géotechnique*, 36(3): 425-447.

Skirrow, R. 1995. The effects of fines content on the monotonic triaxial testing of cohesionless soils for evaluation of in-situ state. *M.Sc. Thesis*, Department of Civil Engineering, University of Alberta, Edmonton, Alberta.

Sladen, J.A. 1989. Problems with interpretation of sand state from cone penetration test. *Géotechnique*, 39(2): 323-332.

Sladen, J.A., D'Hollander, R.D., and Krahn, J. 1985a. The liquefaction of sands, a collapse surface approach. *Can. Geotech. J.*, 22: 564-578.

Sladen, J.A., D'Hollander, R.D., Krahn, J., and Mitchell, D.E. 1985b. Back analysis of the Nerlerk berm liquefaction slides. *Canadian Geotechnical Journal*, 22: 579-588.

Sladen, J.A., and Hewitt, K.J. 1989. Influence of placement method on the in situ density of hydraulic sand fills. *Canadian Geotechnical Journal*, 26: 453-466.

Vaid, Y.P., Chung, E.K.F., and Kuerbis, R.H. 1990. Stress path and steady state. *Can. Geotech. J.*, 27: 1-7.

Vaid, Y.P., Sivathayalan, S., Uthayakumar, M., and Eliadorani, A. 1995. Liquefaction potential of reconstituted Syncrude sand. *Proceedings of the 48th Canadian Geotechnical Conference*, Vancouver, B.C., 1, 319-330.

Wood, D.M. 1990. *Soil behaviour and critical state soil mechanics*. Cambridge University Press, Cambridge, pp. 179-188.

Wroth, C.P., and Bassett, R.H. 1965. A stress-strain relationship for the shearing behaviour of a sand. *Géotechnique*, 15(1): 32-56.

Yoshida, Y., Ikemi, M., and Kokusho, T. 1988. Empirical formulas of SPT blow-counts for gravely soils. *Proceedings of Penetration Testing*, Balkema, Rotterdam, 1: 381-387.

CHAPTER 5

A FRAMEWORK FOR ESTIMATING UNDRAINED SHEAR STRENGTH BASED ON IN-SITU TESTING[1]

5.1 Introduction

As outlined in Chapter 4, one of the most important response parameters for flow liquefaction considerations is the undrained shear strength of the sand. Conducting an undrained stability analysis of sand, such as for post-liquefaction conditions, requires a knowledge of the undrained ultimate state shear strength (S_u). Provided that liquefaction will be triggered in a sandy slope, the great difficulty lies in deciding what value of S_u will best represent the particular conditions in the field. Current practice makes use of correlations between S_u and Standard Penetration Test (SPT) or Cone Penetration Test (CPT) resistance (Seed and Harder, 1990; Robertson, 1990; Stark and Mesri, 1992).

This study presents a framework for estimating S_u, combining critical state soil mechanics and shear wave velocity measurements, assuming undrained loading with no pore pressure redistribution. Shear wave velocity measurements are also converted to equivalent SPT and CPT penetration resistance. As a result, the uniqueness of each of the current empirical methods for estimating S_u using field penetration tests is critically examined and the factors that play a major role in the potential correlations between S_u and penetration resistance are investigated. In this chapter, S_u is estimated based on the ultimate state line (USL) for a given sand and undrained monotonic loading in triaxial compression; however, the same framework can be used to estimate quasi-steady-state (QSS) strengths or strengths under other directions of loading (e.g. triaxial extension), as already explained in Chapter 4. In addition, the same S_u will correspond to a given initial state of a soil if flow liquefaction is triggered by other means, such as by undrained cyclic loading. The term ultimate state is used in this study; this is synonymous with the terms critical state or steady state, which are interchangeable, after Been et al. (1991). Note that S_u is only applicable to the analysis of stability related to the phenomenon of flow liquefaction; it is not relevant to the analysis of deformations resulting from cyclic softening (liquefaction).

---

[1] *A version of this chapter has been published. Fear, C.E. and Robertson, P.K. 1995. Estimating the undrained strength of sand: a theoretical framework. Canadian Geotechnical Journal, 32(5): 859-870.*

5.2 Current Methods for Estimating S_u using Penetration Tests

Figure 5-1 presents the empirical correlation proposed by Seed and Harder (1990), based on the original work by Seed (1987), which involved 17 case histories and provided a relationship between S_u and equivalent normalized Standard Penetration Test (SPT) resistance, $(N_1)_{60}$, in clean sand. As Figure 5-1 indicates, this relationship consists of upper and lower bound lines which present a dilemma to the geotechnical engineer. It is not uncommon to find that the upper bound line will suggest an apparently acceptable factor of safety whereas the lower bound line will suggest a potentially unstable condition. Conservative practice often leads engineers to use the lower bound line to assess overall slope stability which may result in unnecessary site remediation and expenditures.

Stark and Mesri (1992) provided an alternative approach to estimating S_u, and presented a relationship between undrained strength ratio and equivalent $(N_1)_{60}$ in clean sand, as shown in Figure 5-2. The undrained strength ratio is defined as the mobilized S_u, divided by the initial vertical effective stress, σ_v'. The idea was that expressing undrained strength in terms of the ratio S_u/σ_v' would lead to a method that would be easier to apply in practice. This relationship is based on the Seed and Harder (1990) case histories plus three additional ones. The Stark and Mesri (1992) relationship also consists of upper and lower bound lines. The work by Stark and Mesri (1992) followed the approach taken by Jefferies et al. (1990), which suggested that the shear strength ratio was a function of normalized CPT resistance. This idea was based on the view that shear strength ratio is a function of state parameter (Ψ) and the previous work by Been and Jefferies (1986 and 1987) which proposed that state parameter was a function of normalized CPT resistance.

Robertson (1990) presented a review of the relationship between S_u and normalized penetration resistance for four sands using relative density correlations with SPT $(N_1)_{60}$, correlations between normalized CPT q_{c1} and SPT $(N_1)_{60}$, published data on steady state relationships, field studies and large calibration chamber test results. The resulting relationships are presented in Figure 5-3. Robertson (1990) found that Ottawa sand appeared to provide the minimum steady state strength correlation and that the correlation by Seed (1987) represented a conservative lower bound correlation, especially at large values of $(N_1)_{60}$. The other sands that were studied (Monterey, Ticino and Hilton Mines) all possessed much higher values of S_u at a given penetration resistance than the Seed (1987) correlation would suggest, thus indicating that there appears to be no unique relationship between S_u and penetration resistance for all sands.

Figure 5-4 presents the results of Robertson's (1990) additional investigation into the correlation between normalized ultimate undrained strength (S_u/p') and normalized CPT resistance $(q_c-p)/p'$, based on state parameter, as suggested by Been and Jefferies (1985). Robertson (1990) recognized that these correlations were approximate in nature due to limited test data, but the results clearly suggested the lack of a unique relationship for all sands, with Ottawa sand representing the minimum relationship when compared with the other sands (Reid Bedford, Hilton Mines, Oilsand, Ticino and Monterey).

The approach used to estimate S_u at Duncan Dam (Byrne et al., 1994) was an alternative to the in-situ penetration methods discussed above. High quality undisturbed samples of sand were obtained at Duncan Dam using ground freezing and subsequent coring. These undisturbed samples were then tested in the laboratory to directly determine S_u of the sand. Although attractive, this approach can be expensive and is usually limited to high risk projects which have a sufficiently large scope and budget and for which the consequences of failure can be enormous.

5.3 Framework for Estimating S_u from Shear Wave Velocity Measurements

5.3.1 Determining S_u from critical state soil mechanics

As reviewed in Chapter 4, based on a critical state soil mechanics framework, the ultimate state line (USL) for a given sand and a given direction of loading (e.g. triaxial compression or triaxial extension) can be plotted in p'-q-e space (see Figure 5-5a), where e is void ratio and p' and q are defined as follows:

[5-1] $$p' = \frac{1}{3}(\sigma_1' + 2\,\sigma_3')$$

[5-2] $$q = \sigma_1' - \sigma_3'$$

The USL is controlled by the grain characteristics of the soil. Along the USL, q and p' are related by M, which is a function of friction angle and direction of loading. Theoretical values of M for triaxial compression (M_C) and triaxial extension (M_E) are given by the following equations (Wood, 1990):

[5-3] $$M_C = (q_{us}/p'_{us})_C = \frac{6\sin\phi'_{us}}{3 - \sin\phi'_{us}}$$

[5-4] $$M_E = (q_{us}/p'_{us})_E = \frac{6\sin\phi'_{us}}{3 + \sin\phi'_{us}}$$

In theory, these lines in p'-q-e space project onto a single USL in e-p' space, since ultimate state is independent of the stress path followed to reach it (Been et al., 1991). When the p' axis is plotted on a logarithmic scale, the true USL is curved, as explained in Chapter 4. However, the USL can be approximated as a bi-linear relationship; i.e. as a straight line over a given stress range (see straight line shown in Figure 5-5b for a particular stress range). The USL in the e-p' plane can therefore be defined over a given stress range by two parameters, Γ and λ_{ln}. Γ is the void ratio of the portion of the USL at p'=1 kPa and λ_{ln} is the slope of the portion of the USL when the p' axis is plotted on a natural logarithm scale. Each straight line portion of the USL in e-ln p' space is therefore defined as follows:

[5-5] $$e = \Gamma - \lambda_{ln} \ln (p')$$

Within the critical state soil mechanics framework, it is possible to calculate S_u for a soil with a given void ratio when loaded in undrained shear, assuming no pore pressure redistribution and therefore no change in void ratio. The concept (shown in Figure 5-5) is that a sand which has an initial state given by (p'_i, q_i, e) and is loaded in undrained shear will reach the same S_u as the point on its USL with the same void ratio (p'_{us}, q_{us}, e). Therefore, S_u can be determined as follows:

[5-6] $$S_u = \frac{1}{2} M \left(\frac{p'_i}{\exp\left(\frac{\Psi}{\lambda_{ln}}\right)} \right)$$

where:

M = M_C or M_E , depending on the direction of loading (see Equations 5-3 and 5-4)

[5-7] Ψ= initial state parameter = e - e_{us} (Been and Jefferies, 1985)

e = initial void ratio

e_{us} = void ratio of the point on the USL with the same p' as the initial state

Each straight line portion of the USL is defined by both a range in stress (p') and a range in void ratio. Over the applicable range in void ratio, Ψ is related to the reference stress ratio

(RSR, as defined in Chapter 4) by the slope of that portion of the USL, λ_{ln}, as follows:

[5-8] Reference Stress Ratio (RSR) = $\frac{p'_i}{p'_{us}} = \exp\left(\frac{\Psi}{\lambda_{ln}}\right)$

RSR is a better measure of initial state because it incorporates the effects of an USL that has a changing slope. It can therefore be used to estimate S_u over a wider range of void ratio (or stress). RSR is also a better parameter for comparing sands of different compressibilities, and which, therefore, have different values of λ_{ln}. Combining Equation 5-6 and Equation 5-8 gives the following equation for determining S_u:

[5-9] $S_u = \frac{1}{2} M \left(\frac{p'_i}{RSR}\right)$

For a given sand (i.e. constant M and λ_{ln}), S_u is a function of both RSR and p'_i because defining these two parameters for a given USL determines the void ratio of the sand. Rearranging Equation 5-6 produces the following equation for the strength ratio S_u/p'_i in terms of Ψ:

[5-10] $\frac{S_u}{p'_i} = \frac{1}{2} M \exp\left(-\frac{\Psi}{\lambda_{ln}}\right)$

In terms of RSR, Equation 5-10 can be expressed as follows:

[5-11] $\frac{S_u}{p'_i} = \frac{1}{2} \frac{M}{RSR}$

For a given sand under a particular direction of undrained loading, S_u/p'_i is solely a function of RSR. The maximum value of S_u/p'_i for a contractant soil (i.e. RSR ≥ 1) occurs when RSR=1 and has a value equal to 0.5 M. On a site-specific basis, a constant S_u/p'_i ratio applies only if the in-situ consolidation line for the deposit is parallel to the USL on an e-ln p' plot, resulting in constant RSR. In this sense, sand differs from clay. For clay, it is reasonable to assume that the virgin compression line (i.e. normally consolidated clay) and the USL are relatively straight and parallel in e-ln p' space (Wood, 1990). As a result, all points on the virgin compression line have the same OCR (related to RSR, as explained in Chapter 4) and, therefore, a constant value of S_u/p'_i can be used for a particular normally consolidated clay. Sand, on the other hand, can be deposited in numerous ways, each producing a different consolidation line which may or may not be parallel to the USL. However, experience with reconstituted sand samples in the laboratory indicates that the consolidation line for very loose sands can be approximately parallel to the USL (Cunning, 1994). Therefore, a constant value of S_u/p'_i may be reasonable for very loose sands.

5.3.2 Estimating soil state from shear wave velocity measurements

Drawing on the work by Robertson et al. (1995), Cunning et al. (1995) demonstrated that soil state can be estimated from shear wave velocity measurements over a given range in void ratio using the following formula:

$$[5\text{-}12] \qquad \Psi = \left(\frac{A}{B} - \Gamma\right) - \left(\frac{V_{s1}}{B\ (K_o)^{na}} - \lambda_{ln} \ln\left[\frac{\sigma_{vi}'}{3}(1 + 2K_o)\right]\right)$$

where:

V_{s1} = normalized shear wave velocity, in m/s

$$[5\text{-}13] \qquad = V_s \left(\frac{P_a}{\sigma_v'}\right)^{na+nb}$$

P_a = 100 kPa and na=nb=0.125, typically
A and B = constants for a given sand, both in m/s
K_o = ratio of horizontal to vertical stresses
σ_{vi}' = initial vertical effective stress

State parameter is therefore a function of soil type (A, B, Γ and λ_{ln}), K_o, σ_{vi}', and V_{s1}. Over a given void ratio, this estimated Ψ can be converted to RSR using the corresponding value of λ_{ln} and Equation 5-8. This results in the following equation to estimate RSR:

$$[5\text{-}14] \qquad RSR = \frac{\frac{\sigma_{vi}'}{3}(1 + 2K_o)}{\exp\left(\dfrac{\Gamma - \frac{A}{B} + \frac{V_{s1}}{BK_o^{na}}}{\lambda_{ln}}\right)}$$

5.3.3 Estimating S_u from shear wave velocity measurements

Combining Equations 5-9 and 5-14 results in the following equation relating S_u to V_{s1}:

$$[5\text{-}15] \qquad S_u = \frac{M}{2}\exp\left[\frac{1}{\lambda_{ln}}\left(\frac{V_{s1}}{B\ (K_o)^{na}} - \left(\frac{A}{B} - \Gamma\right)\right)\right] \qquad \text{(kPa)}$$

where V_{s1} is in m/s.

Similarly, combining Equations 5-11 and 5-14 results in the following equation relating S_u/p'_i to V_{s1}:

$$[5\text{-}16] \qquad \frac{S_u}{p'_i} = \frac{M}{2}\,\frac{\exp\left[\dfrac{V_{s1}}{B\ (K_o)^{na}} - \lambda_{ln}\ \ln\left(\dfrac{\sigma_{vi}'}{3}(1+2K_o)\right)\right]}{\exp\left(\dfrac{A}{B} - \Gamma\right)}$$

Replacing p'_i in the left side of Equation 5-16 by the expression given in Equation 5-1 (substituting σ_{vi}' and $K_o \bullet \sigma_{vi}'$ for σ_1' and σ_3', respectively) results in a similar equation relating S_u/σ_{vi}' to V_{s1}:

$$[5\text{-}17] \qquad \frac{S_u}{\sigma_{vi}'} = \frac{M}{6}\left(\frac{\exp\left[\dfrac{V_{s1}}{B\ (K_o)^{na}} - \lambda_{ln}\ \ln\left(\dfrac{\sigma_{vi}'}{3}(1+2K_o)\right)\right]}{\exp\left(\dfrac{A}{B} - \Gamma\right)}\right)(1+2K_o)$$

Examining Equation 5-15, it is clear that for a given material under a particular direction of undrained loading (constant A, B, na, M, Γ and λ_{ln}) and for a given K_o, S_u is uniquely a function of V_{s1}. However, Equations 5-16 and 5-17 show that neither S_u/p'_i nor S_u/σ_{vi}' is a unique function of V_{s1}, even for a given material and K_o. Rather, S_u/p'_i and S_u/σ_{vi}' remain a function of σ_{vi}' as well.

5.4 Application of the Proposed Approach to Two Sands

5.4.1 Test program

Ottawa sand and a compressible tailings sand from Alaska (herein referred to as Alaska sand) were selected for use in this study as they appeared to represent two extremes encompassing most sands that could be encountered in practice. Laboratory data were available for both sands (Sasitharan, 1994; Cunning, 1994) and field data (SPT, CPT and V_s logs) were available for Alaska sand. Ottawa sand is a clean, uniform, subrounded quartz sand that is relatively incompressible. Alaska sand contains approximately 30% fines (passing the No. 200 sieve), composed of a large amount of carbonate shell material which significantly increases the compressibility of the sand.

Table 5-1 presents the material properties for Ottawa and Alaska sand, together with the values for other sands tabulated by Sasitharan et al. (1994). Note that the parameters Γ and λ_{ln} are significantly different for Ottawa and Alaska sand, reflecting the major differences in fabric and compressibility in hydrostatic loading (p'), respectively. Figure 5-6(a) presents the USLs for both Ottawa sand and Alaska sand on an e-ln p' plot, relative to the USLs for the other sands from Sasitharan et al. (1994). It can be seen that Alaska sand clearly represents an upper bound USL up to a p' approximately equal to 55 kPa (at which point, Lornex sand becomes the upper bound), while Ottawa sand is one of the lower bound USLs.

Table 5-1 also contains the material properties for clean Ottawa sand with various amounts of added kaolinite fines from Skirrow (1995) and for kaolin (i.e. fines content of 100%), based on Atkinson (1993). Skirrow (1995) found that the USL became steeper (i.e. larger λ_{ln}) as the fines content was increased from 0% to 10%, but that the value of Γ remained relatively similar to that for clean Ottawa sand. This can be seen in Figure 5-6(b). Pitman (1993) noted that the position of the USL for a particular initial stress (p'=350 kPa) moved downwards as the percentage of fines added was increased up to 20%; however, the USL moved back upwards as the fines content was increased above 20%. The position of the USL for kaolin (100% fines) in Figure 5-6(b), which is well above that for Alaska sand, is consistent with this finding.

Note that the USLs for the various sands in Figure 5-6 are shown up to only p'=200 kPa. For all sands, the USL curves at high stresses (Ishihara, 1993; also see Chapter 4). When the USL is represented by a bi-linear line, the breakpoint in slope generally occurs at a value of p' in the range of 100 to 500 kPa (see Chapter 4, Figure 4-18). Estimating S_u is of particular importance for sands that strain-soften to ultimate state in undrained loading. A sand must have a state loose of the USL in order to strain-soften to ultimate state. Sands that have a state loose of the USL will strain-soften to the flatter portion of the USL if the in-situ void ratio is greater than the void ratio defining the breakpoint in the USL. Sands that strain-soften to the steeper portion of the USL must have lower void ratios and initially be under very high in-situ stresses. Sands that strain-harden or experience limited strain-softening and then dilate will strain-harden to either the flat or steep portion of the USL, depending on the initial in-situ void ratio.

The values of Γ and λ_{ln} given in Table 5-1 for each sand are for the flatter portion of the USL (i.e. $p' < 200$ kPa). The figures presented in the remainder of this chapter are determined using these values of Γ and λ_{ln}. Consequently, the values of S_u in subsequent figures correspond to the flatter portion of each USL. Sands that have an initial void ratio less than the USL breakpoint void ratio will reach an ultimate state on the steeper portion of the USL and will possess higher ultimate undrained strengths. Since the breakpoint in each USL occurs at approximately $p'=200$ kPa and typical values of M_C for sands range from 1.2 to 1.5 (see Table 5-1), these sands will have values of S_u greater than approximately 120 to 150 kPa (based on Equation 5-9 using RSR=1). Although not shown here, for sands having an initial void ratio in the appropriate range (i.e. less than the USL breakpoint void ratio), the same framework as is presented here could be combined with Γ and λ_{ln} associated with the steeper portion of each USL to estimate the corresponding values of S_u. Note that the USL breakpoint void ratio can be converted to a breakpoint V_{s1}, based on A and B for a particular sand. Only soils with measured values of V_{s1} greater than the breakpoint V_{s1} will have ultimate states along the steeper portion of the USL.

When testing the two sands, Cunning (1994) found that the best fit values for (na+nb) were 0.266 for Ottawa sand and 0.260 for Alaska sand. Although it appears that the stress exponents are dependent on the type of sand, this study adopted the historical value for (na+nb) of 0.25 as representing a generalized value that could be applied to all sands. This was divided equally with na and nb assigned equal values of 0.125. The values of A and B for Ottawa and Alaska sand given in Table 5-1 are based on this assumption and therefore differ from the values given by Cunning et al. (1995) which were based on the sand-specific values of (na+nb). Specific values of A and B were not available for the various sands tabulated by Sasitharan et al. (1994), Ottawa sand with added fines, or kaolin. However, global values of A and B were used for these sands (see Table 5-1) since Cunning (1994) showed that most sands tend to fall within a certain band on a V_{s1}-e plot. These global values are also based on the assumption that (na+nb) has a value of 0.25.

5.4.2 Results

Figure 5-7a presents the relationship between S_u/p'_i and state parameter in triaxial compression for both sands, based on Equation 5-10. This is a unique relationship for a given sand and is independent of both stress level and K_o. The curve for Ottawa sand is much steeper, due to the flatness of the USL. Alaska sand, on the other hand, exhibits a more gradual decrease in shear strength ratio with increasing state parameter. Figure 5-7a indicates that S_u/p'_i decreases with increasing Ψ. However, for each type of sand, there is likely a maximum value of Ψ beyond which the sand cannot exist. This would correspond to a minimum possible value of S_u/p'_i.

For comparison, Figure 5-7b presents the relationship between S_u/p'_i and RSR, based on Equation 5-11. The relationship is still unique for a given sand, because it is dependent on the value of M_C. However, M_C for most sands falls within a small range; consequently, the relationships between S_u/p'_i and RSR for both Ottawa and Alaska sands are much more similar than the relationships between S_u/p'_i and Ψ, despite the wide range in soil behaviour type. Figure 5-7b indicates that S_u/p'_i decreases with increasing RSR. However, for each type of sand, there is likely a maximum value of RSR beyond which the sand cannot exist. This would correspond to a minimum possible value of S_u/p'_i.

Figures 5-8(a) and (b) present plots of V_s versus σ_v' at a K_o of 0.4 for Ottawa sand and Alaska sand, respectively. Also shown on these plots are contours of V_{s1} and, hence, contours of S_u in triaxial compression. These figures clearly indicate that the value of V_{s1} that acts as a dividing line between contractant and dilatant behaviour (i.e. RSR = 1) is not constant with σ_v' (or depth). Rather, the dividing value of V_{s1} increases with depth for either sand. Except at low values of σ_v', the dividing values, especially for Ottawa sand, agree well with the values of 140 m/s to 160 m/s suggested by Robertson et al. (1992a). Shear wave velocity profiles from the field could be superimposed over Figures 5-8(a) and (b) in order to evaluate the in-situ state and estimate the range of S_u that could be expected in-situ.

Figure 5-9 presents a plot of S_u versus V_{s1} in triaxial compression for both Ottawa and Alaska sand. For a given sand and a given K_o, S_u is a unique function of V_{s1}. As K_o increases, the S_u-V_{s1} line moves to the right as higher values of K_o will result in higher values of measured shear wave velocity. The shapes and locations of the lines for Ottawa sand and Alaska sand are quite different. This is due to the differences between the USLs, reflected in λ_{ln} and Γ. For a given state (Ψ), a soil with a flat USL (i.e. low value of λ_{ln}) will have a lower value of S_u and be more brittle in undrained shear since RSR will be higher. The S_u-V_{s1} relationship for Ottawa sand is sharper and divides more distinctly between sand with very little undrained strength and sand with high strength. The relationship for Alaska sand is more gradual, indicating a slower, steadier increase in strength as V_{s1} increases. Thus, λ_{ln}, Γ, and K_o are three major factors affecting the S_u-V_{s1}

relationship.

Figure 5-10 compares the S_u-V_{s1} relationships in triaxial compression for Ottawa and Alaska sand to the other sands tabulated by Sasitharan et al. (1994), for K_o equal to 0.4. These figures illustrate that Ottawa and Alaska sand encompass most of the other sands on a plot of S_u versus V_{s1}. In addition, it is clear that most of the other sands have sharp S_u-V_{s1} relationships, similar to or sharper than that for Ottawa sand. Alaska sand has a more gradual relationship than any of the other sands. This is because most of the other sands plotted here have λ_{ln} values similar to that for Ottawa sand whereas the value for Alaska sand is an order of magnitude greater. Comparing Leighton Buzzard and Ottawa sand, which have similar values of λ_{ln} and ϕ'_{us} (see Table 5-1), it can be seen that Leighton Buzzard sand, which has a higher value of Γ, plots to the left of Ottawa sand, although the lines for both sands have similar shapes. The relative shapes and positions of the S_u-V_{s1} relationships for the various sands parallels the relative slopes and positions of the USLs in e-p' space for the various sands (see Figure 5-5a).

Figure 5-11 illustrates the effect of adding fines to clean Ottawa sand on the relationship between S_u and V_{s1} in triaxial compression, relative to clean Ottawa sand and Alaska sand for Ko equal to 0.4. Also included in Figure 5-11 is the relationship for kaolin. It can be seen that increasing the percent kaolinite from 0% to 10% moves the S_u-V_{s1} relationship to the right of the line for clean Ottawa sand. However, if larger percentages of kaolinite were added (greater than 20%) the USL moves upward to higher void ratios (Pitman, 1993) and it would be reasonable to expect that the S_u-V_{s1} relationship would move back to the left and eventually, at 100% kaolinite, to approximately the location of the relationship for kaolin. This would be consistent with the observation made earlier that the S_u-V_{s1} plot parallels the USL plot in e-p' space (see Figure 5-5b).

5.4.3 Conversion of V_{s1} to SPT $(N_1)_{60}$ and CPT q_{c1}

In order to compare the proposed shear wave velocity method of estimating S_u, S_u/p'_i and S_u/σ_{vi}' with existing methods, V_{s1} must be converted to equivalent values of SPT $(N_1)_{60}$ and equivalent CPT q_{c1}. As outlined in Chapter 4, the following equations can be used:

[5-18] $$(N_1)_{60} = (\frac{V_{s1}}{X})^4$$

[5-19] $$q_{c1} = \left(\frac{V_{s1}}{Y}\right)^{4.35}$$

where:
V_{s1} is in units of m/s and q_{c1} is in MPa.

Note that in Chapter 4, the exponent in Equation 5-19 was approximated as a value of 4, for ease of calculation. However, the work in this chapter was completed previously and used an exponent of 4.35 to determine the value of Y.

For clean, unaged, uncemented, relatively incompressible, predominantly silica sands (of which Ottawa sand is one), $X \approx 89.8$ (based on a modification of work by Yoshida (1988)) and $Y \approx 102$ (Robertson et al., 1992b). Equations 5-18 and 5-19 can be combined with Equation 5-15 to produce equations for estimating S_u from $(N_1)_{60}$ and q_{c1} for such sands, as follows:

[5-20] $$S_u = \frac{M}{2} \exp\left[\frac{1}{\lambda_{ln}}\left(\frac{X\ (N_1)_{60}{}^{0.25}}{B\ (K_o)^{na}} - \left(\frac{A}{B} - \Gamma\right)\right)\right] \qquad \text{(kPa)}$$

and:

[5-21] $$S_u = \frac{M}{2} \exp\left[\frac{1}{\lambda_{ln}}\left(\frac{Y\ q_{c1}{}^{0.23}}{B\ (K_o)^{na}} - \left(\frac{A}{B} - \Gamma\right)\right)\right] \qquad \text{(kPa)}$$

where q_{c1} is in MPa.

Similarly, the relationships can be combined with Equations 5-16 or 5-17 to produce equations for estimating S_u/p'_i or S_u/σ_v' from $(N_1)_{60}$ and q_{c1}.

5.4.4 The effect of compressibility on V_{s1}-$(N_1)_{60}$ and V_{s1}-q_{c1} correlations

Compressibility will have little effect on the measured shear wave velocity since shear waves do not compress the sand, but it can greatly affect the SPT and CPT penetration resistance since the more compressible the sand, the lower the penetration resistance, even at the same relative density (Robertson and Campanella, 1983). Shear wave velocity, SPT and CPT profiles were available from the tailings sand site in Alaska. Examining these profiles, it was found that $X \approx 113$ and $Y \approx 135$ were more appropriate value for linking shear wave velocity to SPT and CPT penetration resistance in Alaska sand. The increased values of these constants, as compared to the values for Ottawa sand, reflect the higher compressibility of the sand. Examining Equations 5-18 and 5-19, it is clear that the values of X and Y for Alaska sand will give lower values of penetration resistance than for Ottawa sand for the same value of V_{s1}. Using the Alaska site-specific values of X and Y in Equations 5-20 and 5-21 allows S_u to be predicted from $(N_1)_{60}$ and q_{c1}, respectively, in Alaska sand.

5.4.5 Sensitivity of the proposed method to the input parameters

The discussion presented thus far revolves around the assumption that K_o and the soil parameters ϕ'_{us}, Γ, λ_{ln}, A and B can be determined with certainty. However, in reality, although each parameter will have a "best-fit" value, it will also have a possible range of values due to the uncertainty associated with estimating its true value. Careful laboratory testing and good field estimates of K_o can minimize uncertainties. All of the graphs presented thus far have only shown the results based on the "best-fit" values of ϕ'_{us}, Γ, λ_{ln}, A and B for the two particular sands. However, the possible degrees of inaccuracy associated with these parameters will translate into bands rather than unique lines on the various plots relating S_u to shear wave velocity and penetration resistance. As an example, Figure 5-12 presents the bands of uncertainty in the correlation between S_u and V_{s1} associated with the parameter A for both Ottawa and Alaska sand. The average, upper bound and lower bound relationships between S_u and V_{s1} are shown for each sand, corresponding to the average and potential range in the value of A (see Table 5-1).

As shown in Figure 5-9, for sands with flat USLs, such as Ottawa sand, the S_u-V_{s1} relationship based on the best-fit values is already relatively sensitive. As shown in Figure Figure 5-12 for the parameter A, any degree of uncertainty associated with the input parameters will only serve to accentuate this sensitivity. Clearly, the upper and lower bound lines shown in Figure 5-12 give very different estimates of S_u for sands such as Ottawa sand. The best that can be achieved for these sands is to determine whether the field profiles fall below or above the band (in terms of V_{s1}) in order to determine whether or not undrained stability will be an issue. The effects will be less significant for sands with steep USLs, such as Alaska sand, which have a less sensitive S_u-V_{s1} relationship in the first place. A significant range in S_u (which increases as V_{s1} increases) is still predicted, using the upper and lower bound lines shown in Figure 5-12 for Alaska sand, but the range is generally smaller than for Ottawa sand.

5.5 Other Considerations

This study has considered S_u for triaxial compression loading and has presented a framework to estimate the magnitude of S_u from the USL using shear wave velocity measurements. The USL and S_u in triaxial compression are independent of initial fabric since the soil is remoulded by the time steady state is reached. Some argue that the quasi-steady state (QSS) strength is more critical for stability analyses than the steady state strength (Ishihara, 1993). Some research has also suggested that the USL may be lower and hence S_u would be significantly smaller in triaxial extension than triaxial compression (Vaid et al., 1990; Negussey and Islam, 1994).

Nevertheless, the framework presented here is still valid. If one were interested in QSS or S_u in extensional loading, the same procedure could be used to estimate the undrained strength, given that the parameters Γ, λ_{ln}, and ϕ'_{us} were determined for the quasi steady state line (QSSL) in compression or either the USL or QSSL in extension. Note that the value of M is a function of the direction of loading and that lower ultimate strengths will be predicted for loading in extension than in compression even for the same USL in e-p' space. As indicated in Chapter 4, for typical values of ϕ', the value of M_C is typically 1.4 to 1.5 times the value of M_E. This translates into theoretical ultimate strengths in triaxial compression being generally about 40% to 50% higher than theoretical ultimate strengths in triaxial extension. Chapter 4 also presented a method for estimating the minimum undrained strength at QSS in a particular sand deposit having a uniform soil fabric, based on estimated ΔRSR between the USL and the (approximately parallel) QSSL. This method is applied to one of the CANLEX sites in Chapter 8. Ishihara (1993) demonstrated that the QSS is a function of soil fabric, while ultimate state is not.

5.6 Comparison with the Current Methods of Estimating S_u

Figure 5-13 presents the results of S_u in triaxial compression versus equivalent $(N_1)_{60}$ determined using the results of Figure 5-9 together with X=89.8 for clean Ottawa sand and both X=89.8 (the incompressible correlation, referred to as Alaska (I)) and X=113 (accounting for compressibility, referred to as Alaska (C)) for Alaska sand. The other sands tabulated by Sasitharan et al. (1994) and Ottawa sand with the various percentages of kaolinite cannot be included here since no data are available to allow for a conversion from V_{s1} to $(N_1)_{60}$ in such materials. However, it would seem reasonable to hypothesize that the S_u-$(N_1)_{60}$ lines for Ottawa sand plus kaolinite would plot to the left of clean Ottawa sand since one would expect to record lower blowcounts in soil with a higher fines content.

Results from the investigation into the stability of Duncan Dam are also shown in Figure 5-13. The site investigation results for Duncan Dam indicated an increase in $(N_1)_{60}$ with increasing vertical effective stress in the sand zone in which liquefaction was predicted to be triggered by the design earthquake (Pillai and Stewart, 1994). Post-cyclic undrained monotonic simple shear testing of frozen undisturbed samples of this sand indicated that a constant ratio of S_u/σ_{vi}' of 0.21 was applicable (Pillai and Salgado, 1994). Combining the field and lab results allowed for the relationship between S_u and $(N_1)_{60}$ to be plotted as shown in Figure 5-13. Although the testing involved a different direction of loading than is considered here, the relationship for Duncan Dam is clearly similar to the results of this study, having a similar shape and location on the plot and, in particular, showing S_u to increase with increasing $(N_1)_{60}$ at a similar rate as the triaxial compression relationships for Ottawa and Alaska sand.

Superimposed on Figure 5-13, for purpose of comparison, are the upper and lower bound lines relating S_u to $(N_1)_{60}$ from Seed and Harder (1990), as shown in Figure 5-1. There is a relationship between S_u and $(N_1)_{60}$, as Seed and Harder were suggesting; however, this relationship is unique only for a given sand and a given K_o-condition. This study has shown that K_o plays an important role in the S_u-$(N_1)_{60}$ relationship for any given sand and that the differences in compressibility and fabric between Ottawa sand and Alaska sand result in very different relationships. The empirical plot by Seed and Harder (1990) incorporates 17 case histories involving different types of sand and likely involving different conditions of K_o. Hence, the framework presented in this study can account for the scatter in the Seed and Harder (1990) plot by attributing it in part to variations in compressibility, fabric and K_o amongst the various case histories. The Seed and Harder (1990) lines appear much flatter than both the results from this study and those for Duncan Dam, thereby predicting much lower strengths for high values of $(N_1)_{60}$. It is possible that other factors which have not been taken into account in this study, such as pore pressure redistribution or the effects of other directions of loading, may be responsible for the differences between the Seed and Harder (1990) lines derived from case histories and the results of this study. The case histories forming the Seed and Harder (1990) empirical chart may have actually suffered failures due to a combination of undrained strengths in different directions of loading (e.g. triaxial compression, triaxial extension and simple shear). The single back-calculated value of S_u for each case history likely represents the overall average slope behaviour. In addition, some of the case histories in the Seed and Harder (1990) database appear to be cases of cyclic softening for which an estimate of S_u is not applicable (see Chapter 7).

The plot by Seed and Harder (1990) is for the equivalent SPT $(N_1)_{60}$ in clean sand. Thus, for the case histories in sand with fines, a fines content correction was applied to increase the value of the measured $(N_1)_{60}$ to reflect what the equivalent $(N_1)_{60}$ would be in clean sand. The fines content corrections (ΔN_1) suggested by Seed (1987) were $\Delta N_1 = 1, 2, 4$ and 5 for fines contents of 10%, 25%, 50% and 75%, respectively. Seed (1987) explained that these were tentative values, but that judgement should be exercised in applying the corrections due to differences between different soils. Although not explained as such by Seed (1987), it is felt by the authors that these correction factors were an attempt to account for the increased compressibility of sand with fines relative to clean sand. Looking at the results of this study for Alaska sand which has a fines content of about 31%, it can be seen that the difference between the Alaska (I) results and the Alaska (C) results varies with $(N_1)_{60}$ and K_o, but has an average $\Delta(N_1)_{60}$ of approximately 3. This is consistent with the correction factors suggested by Seed (1987). Note that, although fines content may be an indirect measure of compressibility, clean sands may also be compressible. For these sands, such as clean carbonate sands, Seed (1987) would not recommend a correction factor, whereas the method followed here would directly incorporate the compressibility of the sand into the relationship between S_u and $(N_1)_{60}$.

Figure 5-14 presents the results of S_u/σ_{vi}' in triaxial compression versus equivalent $(N_1)_{60}$ determined by combining Equation 5-17 with Equation 5-18, using X=89.8 for clean Ottawa sand and both X=89.8 (the incompressible correlation, referred to as Alaska (I)) and X=113 (accounting for compressibility, referred to as Alaska (C)) for Alaska sand. For the reasons explained above, the other sands from Sasitharan et al. (1994) and Ottawa sand plus kaolinite are not included on this figure. Superimposed on Figure 5-14, for purpose of comparison, are the upper bound, lower bound and average lines relating S_u/σ_{vi}' to $(N_1)_{60}$ from Stark and Mesri (1992), as shown in Figure 5-2. It can be seen that, contrary to the suggestion by Stark and Mesri, there is no unique relationship between S_u/σ_{vi}' and $(N_1)_{60}$. Although the 20 case histories in Stark and Mesri's plot appear to follow a trend, there is a lot of scatter. This is likely due to differences in compressibility, fabric and K_o between case histories, as in the Seed and Harder plot, but is also compounded by the fact that S_u/σ_{vi}' and $(N_1)_{60}$ are not related by a unique relationship, even for a given sand and K_o-condition. Two case histories involving similar types of sands and K_o-conditions, would not plot in the same place on the plot if the stress levels were different. As for the Seed and Harder (1990) plot, Stark and Mesri's (1992) plot is for the equivalent $(N_1)_{60}$ in clean sand. The same comments, outlined above, regarding the relationship between compressibility and fines content also apply here.

Figure 5-15 presents the results of S_u in triaxial compression versus equivalent q_{c1} using the results of Figure 5-9 and Y=102 for clean Ottawa sand and Y=135 for Alaska sand. The other sands from Sasitharan et al. (1994) and Ottawa sand with the various percentages of kaolinite cannot be included here since no data are available to allow for conversions from V_{s1} to q_{c1} in such materials. However, it would seem reasonable to hypothesize that the S_u-q_{c1} lines for Ottawa sand plus kaolinite would plot to the left of clean Ottawa sand since one would expect to record lower cone tip resistances in a material with a higher fines content. Superimposed on Figure 5-15 are the results from Robertson (1990), as shown in Figure 5-3, which he suggested were approximate in nature due to the limited test data and the complex series of assumptions required. The results of this study and from Robertson (1990) both indicate that there is a unique relationship between S_u and q_{c1} for a given sand at a given Ko. The lines for Ottawa sand from this study and from Robertson (1990) are both lower bounds for the given sands; however, there is some difference. The line for Alaska sand falls in the range of other compressible sands such as Hilton Mines tailings.

Figure 5-16 presents S_u/p'_i in triaxial compression versus normalized CPT penetration resistance, $(q_c\text{-}p)/p'$ for both Ottawa sand and Alaska sand calculated for K_o=0.5, since Robertson's (1990) results which are superimposed on this figure were for a K_o of 0.5 (see Figure 5-4). In general, Ottawa sand and Alaska sand encompass several other types of sands and therefore represent two extremes of the types of sands that are likely to be encountered in practice. Robertson's (1990) unique lines for each sand are based on the proposal by Been and Jefferies (1987) that there is a unique relationship between state parameter and normalized CPT penetration resistance. The fact that the results of this study indicate a dependency on stress for the relationship between S_u/p'_i and normalized CPT suggests that the relationship between state parameter and normalized CPT resistance is not unique. Sladen (1989) also questioned the uniqueness of the relationship proposed by Been and Jefferies (1987).

Figure 5-17 compares the results of this study with those by Baziar and Dobry (1995).

Baziar and Dobry (1995) compiled a database of liquefaction case histories consisting of lateral spreads and failures of slopes or embankments in saturated silty sands and sandy silts. These case histories are shown as points on a plot of $(N_1)_{60}$ versus vertical effective stress in Figure 5-17. Also shown in Figure 5-17 is the upper boundary for large deformation potential in saturated silt-sand deposits that Baziar and Dobry (1995) drew based on these case histories. This line is essentially a dividing line between contractant and dilatant behaviour. Superimposed on Figure 5-12 are the dividing lines (i.e. RSR=1) that would be predicted for Ottawa sand (using X=89.8) and Alaska sand (using X=113) for a K_o of 0.5, based on the framework presented earlier. The results of this study appear to be consistent with the findings by Baziar and Dobry (1995), as their upper boundary line (for silt-sands) falls between the lines for Ottawa sand (with no fines) and Alaska sand (very compressible with approximately 30% fines), at $\sigma_{vi}' < 100$ kPa.

At higher stresses, the Baziar and Dobry (1995) line is controlled by one case history (the Upper San Fernando Dam) which had an average in-situ measured $(N_1)_{60}$ of 13, as reported by Seed and Harder (1990). In fact, this case record did not represent a slope failure, as did most of the other slope or embankment case records. Rather, the dam suffered only limited deformations which were relatively small compared to the overall size of the dam. Therefore, if this case record is disregarded or if a lower $(N_1)_{60}$ (closer to the minimum measured value) controlled the observed deformations (see Chapter 7), the Baziar and Dobry (1995) line would remain between the lines for Alaska and Ottawa sand up to approximately 200 kPa.

5.7 Comparison with Laboratory Testing Results

The predictions of S_u based on in-situ testing using the framework proposed here can be compared to laboratory testing results on undisturbed samples of sand from deposits which have been characterized using in-situ testing. The earlier discussion regarding Duncan Dam provided a comparison between the framework suggested here and the combination of available SPT data and laboratory results. A comparison between laboratory test results and undrained strengths predicted using the framework suggested here and CPT data is illustrated in Chapter 8 for one of the CANLEX sites.

5.8 Conclusions

This study has combined critical state soil mechanics and shear wave velocity measurements in order to develop a framework which can be used to estimate the in-situ undrained ultimate state shear strength of a sand. In the process, the range of values that can be expected to encompass most sands on plots of S_u in triaxial compression versus V_{s1}, q_{c1} or $(N_1)_{60}$ has been shown and has been attributed primarily to the location of the USL in terms of Γ and λ_{ln} as well as K_o. More compressible sands tend to have larger values of λ_{ln}. In this chapter, S_u was estimated based on the ultimate state line for very loose samples tested in triaxial compression for each sand; however, the framework developed here can also be used to estimate undrained strengths at quasi-steady-state or in other directions of loading (see Chapter 4). The plot of S_u versus $(N_1)_{60}$ by Seed and Harder (1990) appears conservative when compared with the results of this study, especially for compressible sands with high values of λ_{ln} and Γ and for site conditions producing low values of K_o. However, other factors such as other directions of loading and pore pressure redistribution may have affected some of the case histories used to produce the Seed and Harder (1990) correlation. In addition, some of the case histories in the Seed and Harder (1990) database appear to be cases of cyclic softening for which an estimate of S_u is not applicable (see Chapter 7).

This study has also demonstrated that it is unlikely to have a unique relationship between S_u/σ_{vi}' and $(N_1)_{60}$, as suggested by Stark and Mesri (1992) or between S_u/p'_i and normalized CPT resistance, as suggested by Jefferies et al. (1990). The empirical case histories do suggest such a relationship, in that the general trend is an increase in S_u/σ_{vi}' or S_u/p'_i as $(N_1)_{60}$ or normalized CPT resistance increases. However, encompassed in the empirical case histories is the fact that the relationships are stress level dependent for a given sand, in addition to being dependent on compressibility and differences in K_o between sands. A constant S_u/p'_i or S_u/σ_{vi}' ratio can only be used on a site-specific basis for a particular direction of loading when RSR is a constant.

Finally, the application of the proposed method relies on laboratory work to determine the parameters of the USL (ϕ'_{us}, Γ, λ_{ln}) and the parameters relating V_{s1} to e for a particular sand (A and B). Although the method appears quite promising, it is not without drawbacks. The level of accuracy in estimating S_u using shear-wave velocity may present significant problems and should be considered when applying the method. If the USL of a sand is relatively flat ($\lambda_{ln} < 0.035$), it will not be possible to accurately determine S_u using shear wave velocity measurements or in-situ penetration testing. Note that this is the case for the flat portion of the USL for most of the uniform, clean silica sands included in this study. In fact, one of the most important findings of this study is that for most sands, S_u appears to be a very sensitive parameter and, therefore, very difficult to accurately estimate using any method, including the one investigated here. However, for such sands, it will be possible to estimate the dividing line, in terms of V_{s1}, $(N_1)_{60}$, or q_{c1}, between soil conditions that will exhibit essentially little or no strength when loaded undrained and soil conditions that will be able to fully mobilize the steady state drained friction angle. A further complication when estimating S_u from in-situ tests is the possible effects of pore pressure redistribution after cyclic (earthquake) loading.

Table 5-1: Material properties for (a) Ottawa and Alaska sand (Cunning, 1994); Ottawa sand with added kaolinite fines (Skirrow, 1995) and (b) other sands (Sasitharan et al., 1994)

(a) Sand	ϕ'_{us}	M_C	M_E	Γ^*	λ_{ln}^*	A	B
Ottawa	30.5	1.22	0.87	0.926	0.032	385.5[a]	261.8
Alaska	36.5	1.48	0.99	1.485	0.117	319.5[b]	178.7
Ottawa+5% fines	29.5	1.18	0.84	0.809	0.029	*c*	*c*
Ottawa+7.5% fines	29.6	1.18	0.85	0.835	0.052	*c*	*c*
Ottawa+10% fines	29.4	1.17	0.84	0.930	0.103	*c*	*c*
Kaolin[d]	25	0.98	0.74	1.92	0.181	*c*	*c*

(b) Sand	ϕ'_{us}	M_C	M_E	Γ^*	λ_{ln}^*	A	B
Erksak	30.9	1.24	0.88	0.82	0.013	*c*	*c*
Toyoura(p'us<100kPa)	30.9	1.24	0.88	0.938	0.004	*c*	*c*
Lornex	35	1.42	0.96	1.1	0.022	*c*	*c*
Brenda	35.9	1.46	0.98	1.112	0.042	*c*	*c*
Syncrude	29.8	1.19	0.85	0.847	0.017	*c*	*c*
Nerlerk	30	1.20	0.86	0.885	0.014	*c*	*c*
Leighton Buzzard	29.8	1.19	0.85	1	0.035	*c*	*c*

Notes:

* Γ and λ_{ln} apply to the flat portion of the USL for each soil (i.e. p'<200 kPa, unless noted otherwise)

a range = 371 to 397 m/s

b range = 314 to 326 m/s

c use global values of A = 363 m/s (range = 340 to 380 m/s) and B = 235 m/s

d ϕ'_{us} cited by Atkinson (1993); λ_{ln} & Γ based on PI=32%, Gs=2.70, and formulae in Atkinson (1993)

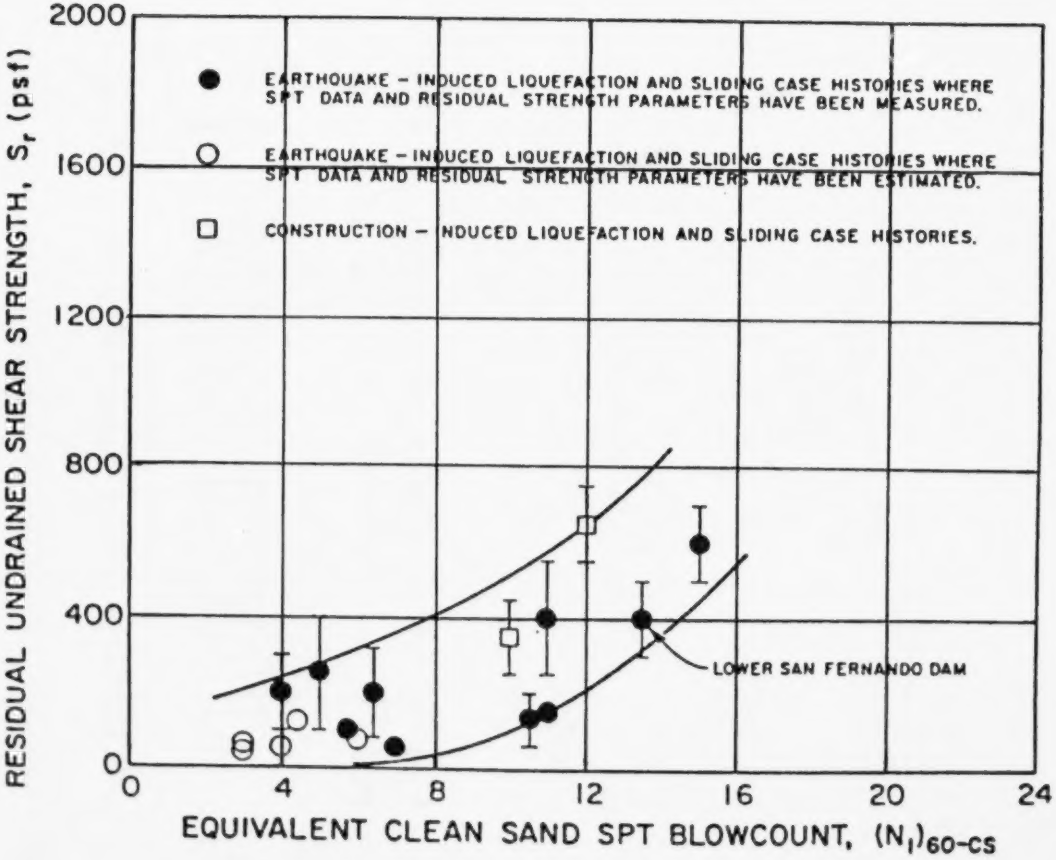

Figure 5-1 Relationship between clean sand equivalent SPT blowcount, $(N_1)_{60}$-cs, and undrained residual strength (S_u) from case studies (modified from Seed and Harder, 1990).

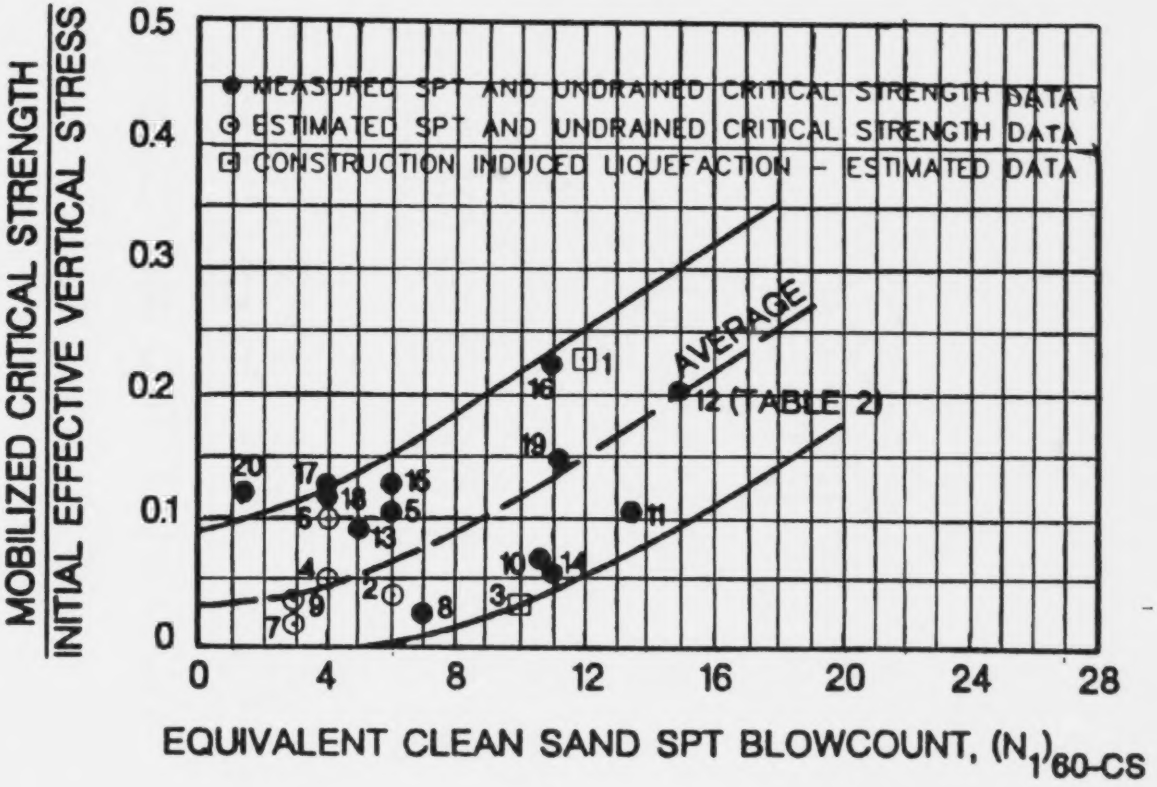

Figure 5-2 Relationship between clean sand equivalent SPT blowcount, $(N_1)_{60\text{-cs}}$ and undrained strength ratio, S_u/σ_v' (modified from Stark and Mesri, 1992).

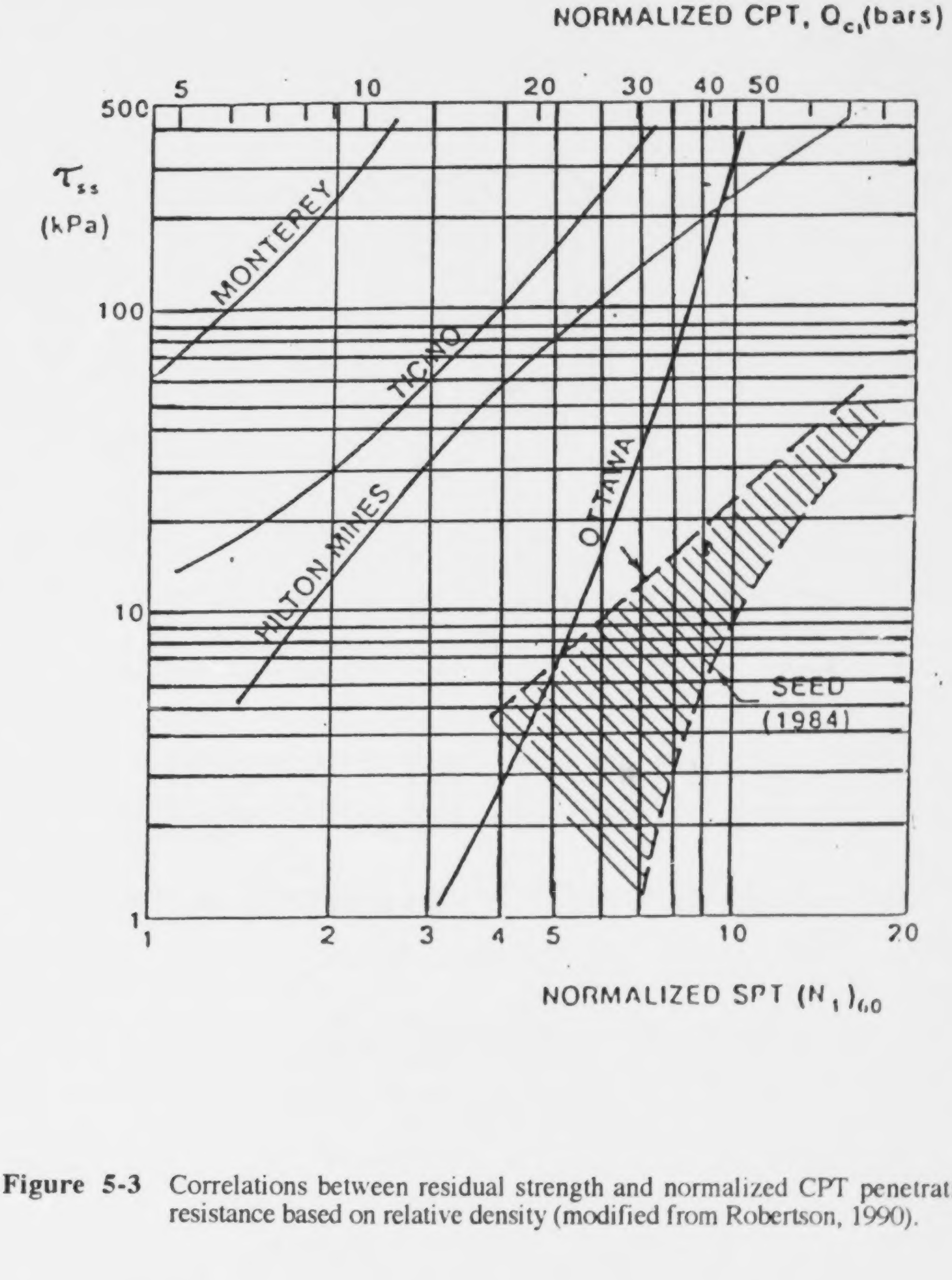

Figure 5-3 Correlations between residual strength and normalized CPT penetration resistance based on relative density (modified from Robertson, 1990).

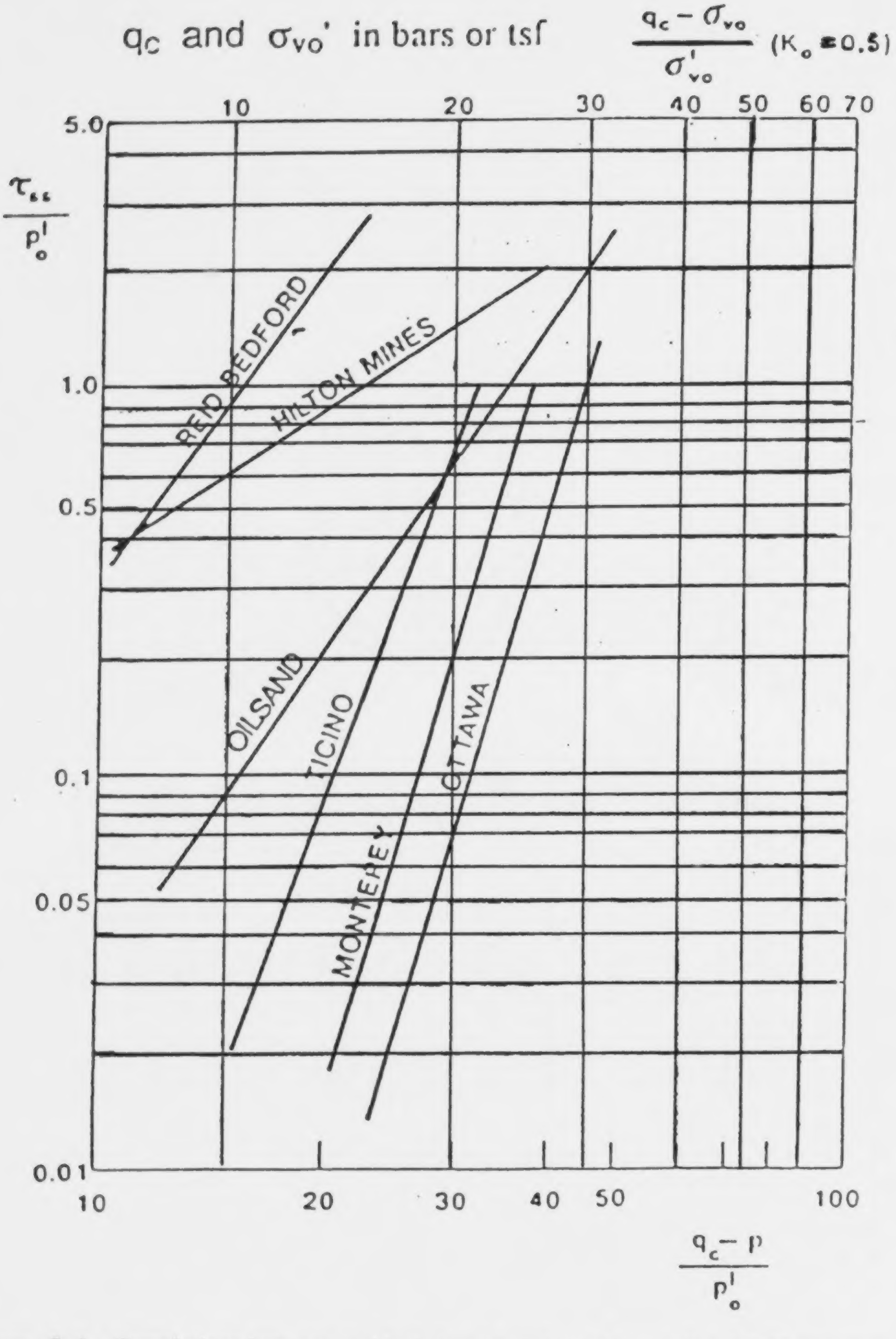

Figure 5-4 Correlations between residual strength ratio and normalized CPT penetration resistance based on state parameter (modified from Robertson, 1990).

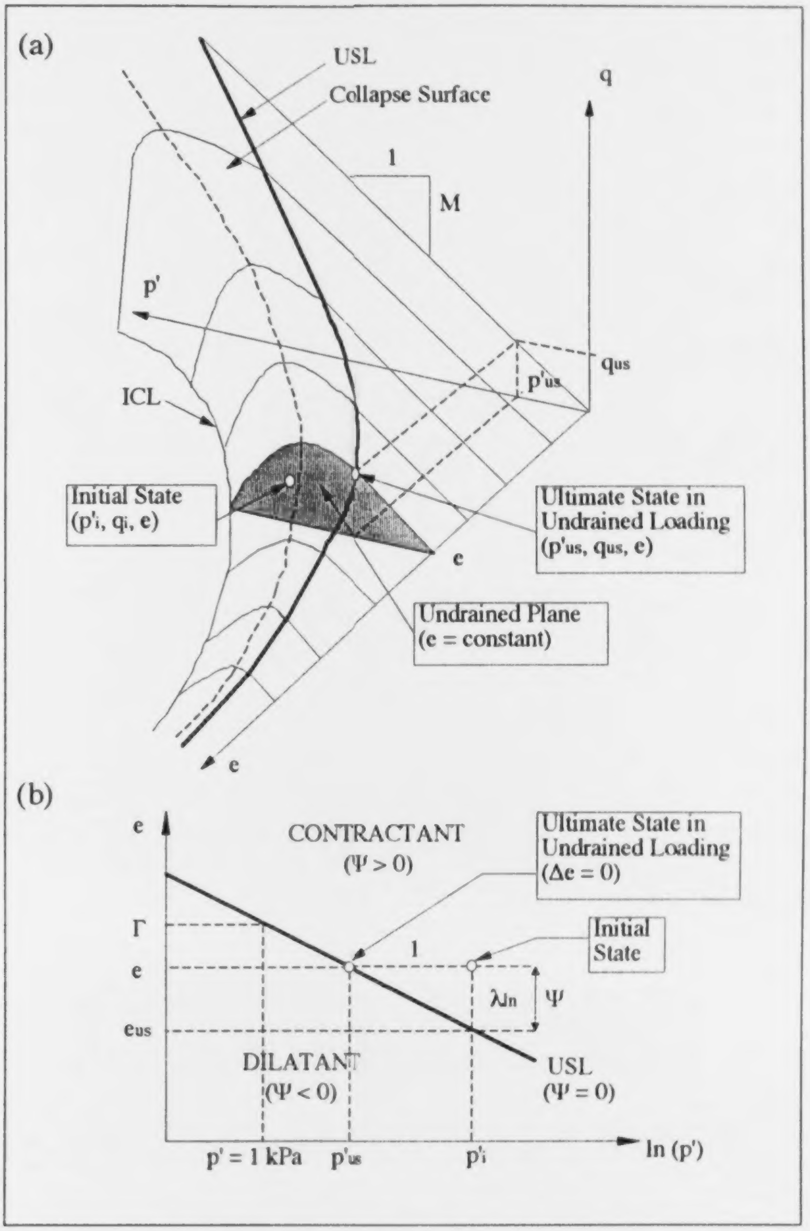
(a)
USL
Collapse Surface
q
1
M
p'
q_us
p'_us
ICL
Initial State (p'i, qi, e)
Ultimate State in Undrained Loading (p'us, qus, e)
e
Undrained Plane (e = constant)
e
(b)
e
CONTRACTANT (Ψ > 0)
Ultimate State in Undrained Loading (Δe = 0)
Γ
e
Initial State
1
λln
Ψ
eus
DILATANT (Ψ < 0)
USL (Ψ = 0)
p' = 1 kPa
p'us
p'i
ln (p')

Figure 5-5 Critical state soil mechanics concepts illustrated by (a) e-p'-q diagram with (b) projections onto the e-ln(p') plane.

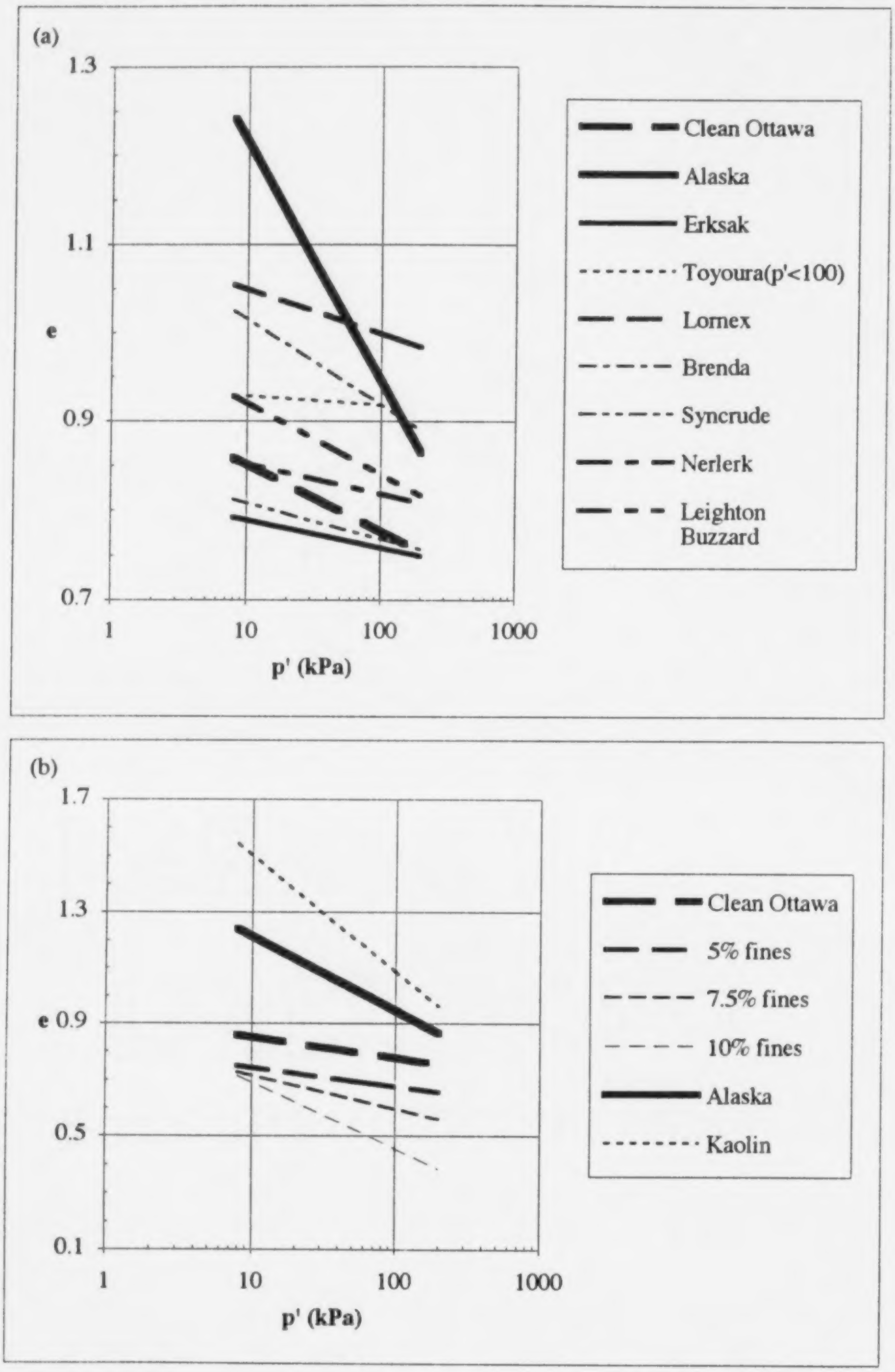

Figure 5-6 Steady state lines for Ottawa sand and Alaska sand compared with (a) other sands and (b) Ottawa sand with fines and kaolin.

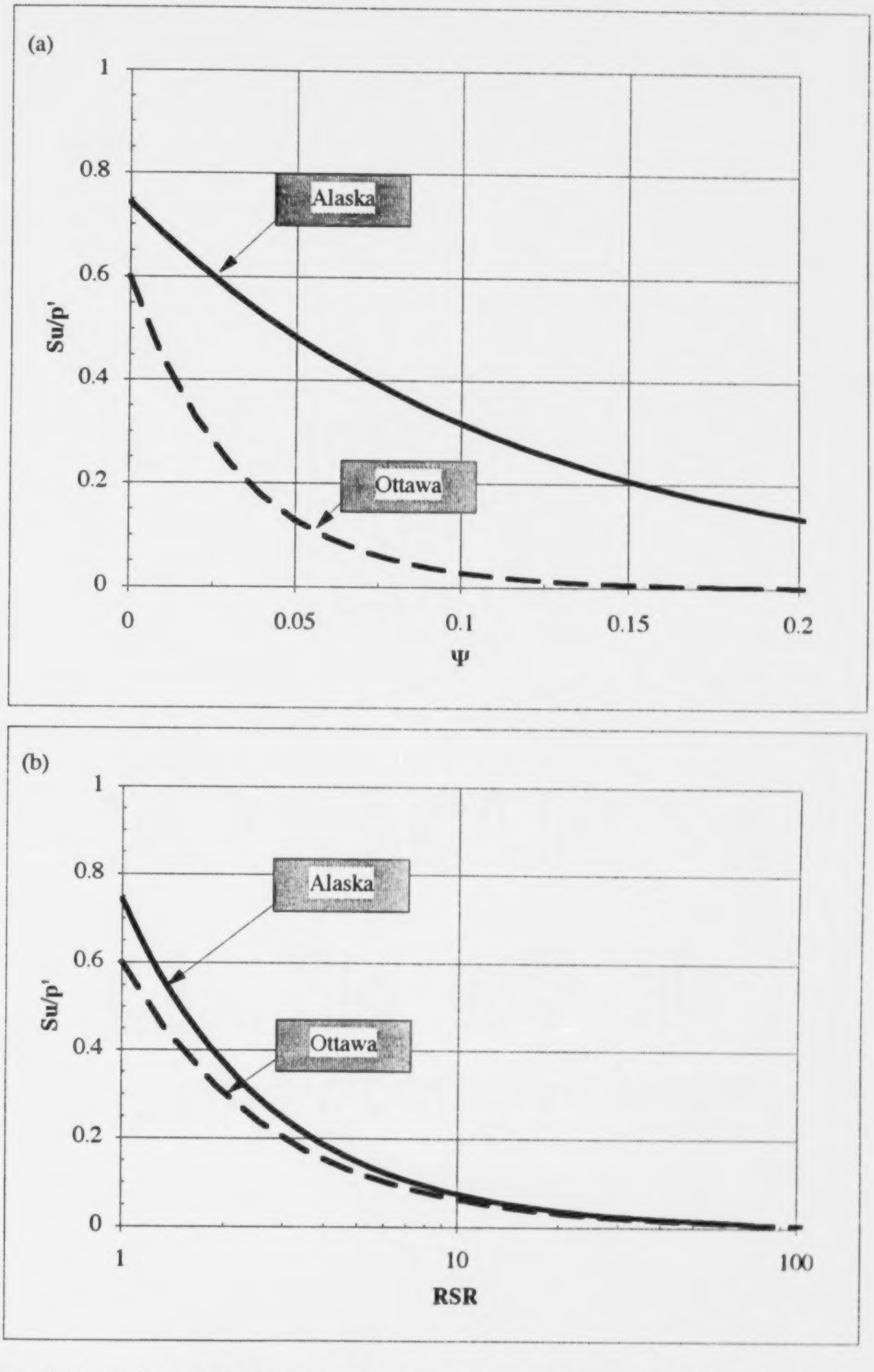

Figure 5-7 Relationship between S_u/p' and (a) state parameter (Ψ) and (b) reference stress ratio (RSR) in triaxial compression for Ottawa sand and Alaska sand.

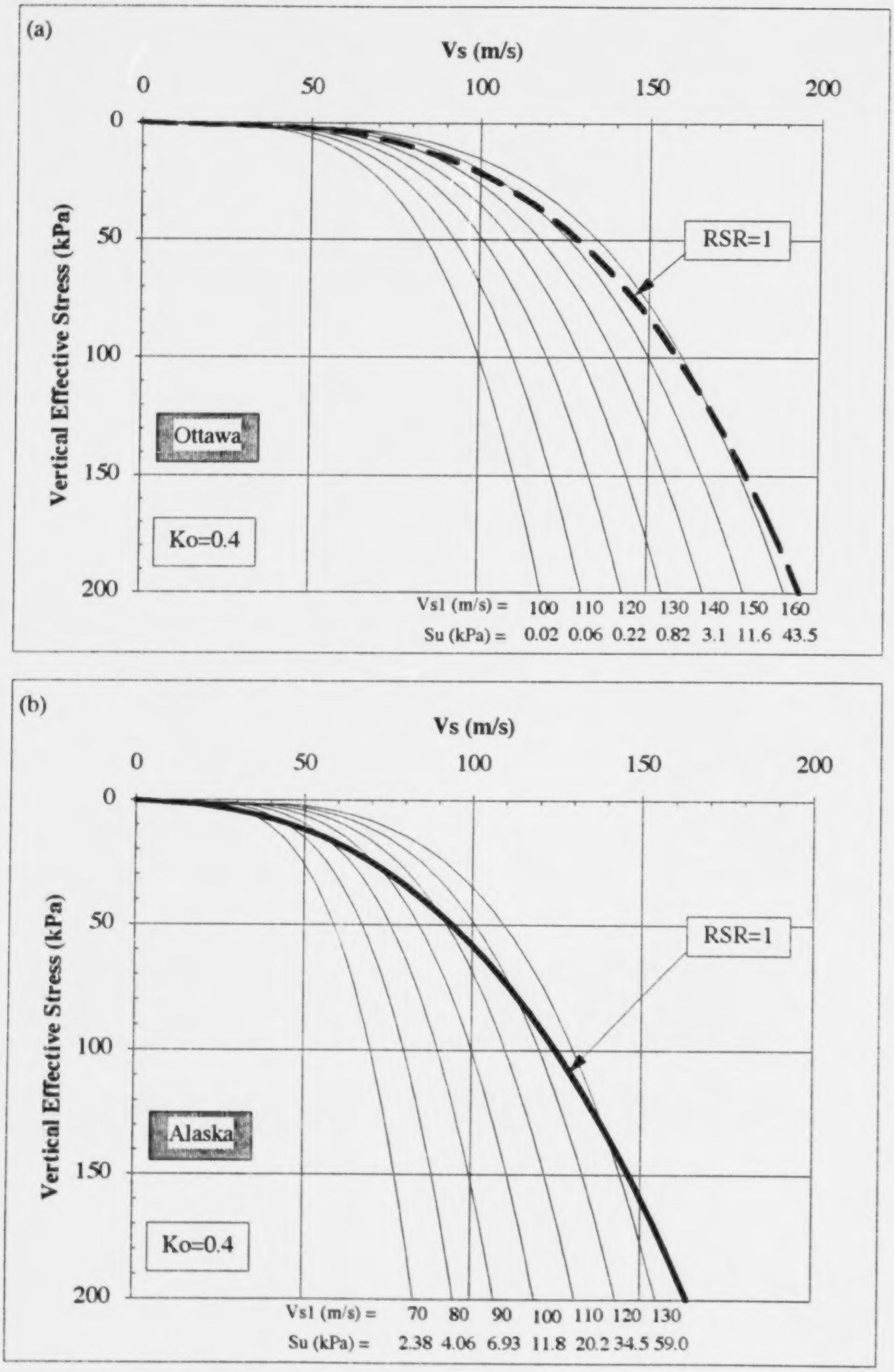

Figure 5-8 Contractant-dilatant boundary (RSR=1 or $\Psi=0$) compared with contours of V_{s1} (or S_u in triaxial compression) for (a) Ottawa sand and (b) Alaska sand.

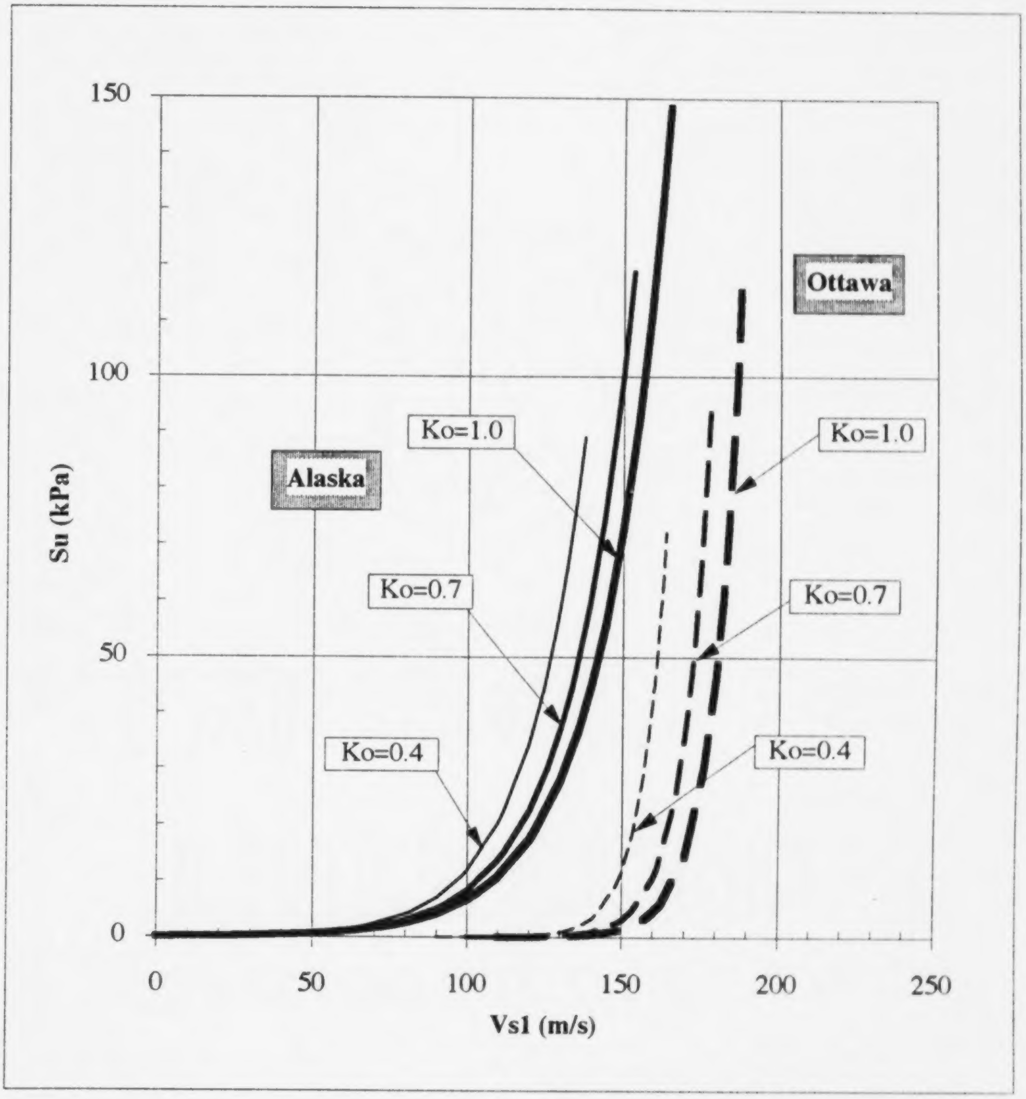

Figure 5-9 Relationship between S_u in triaxial compression and V_{s1} for Ottawa sand and Alaska sand for a range in K_o.

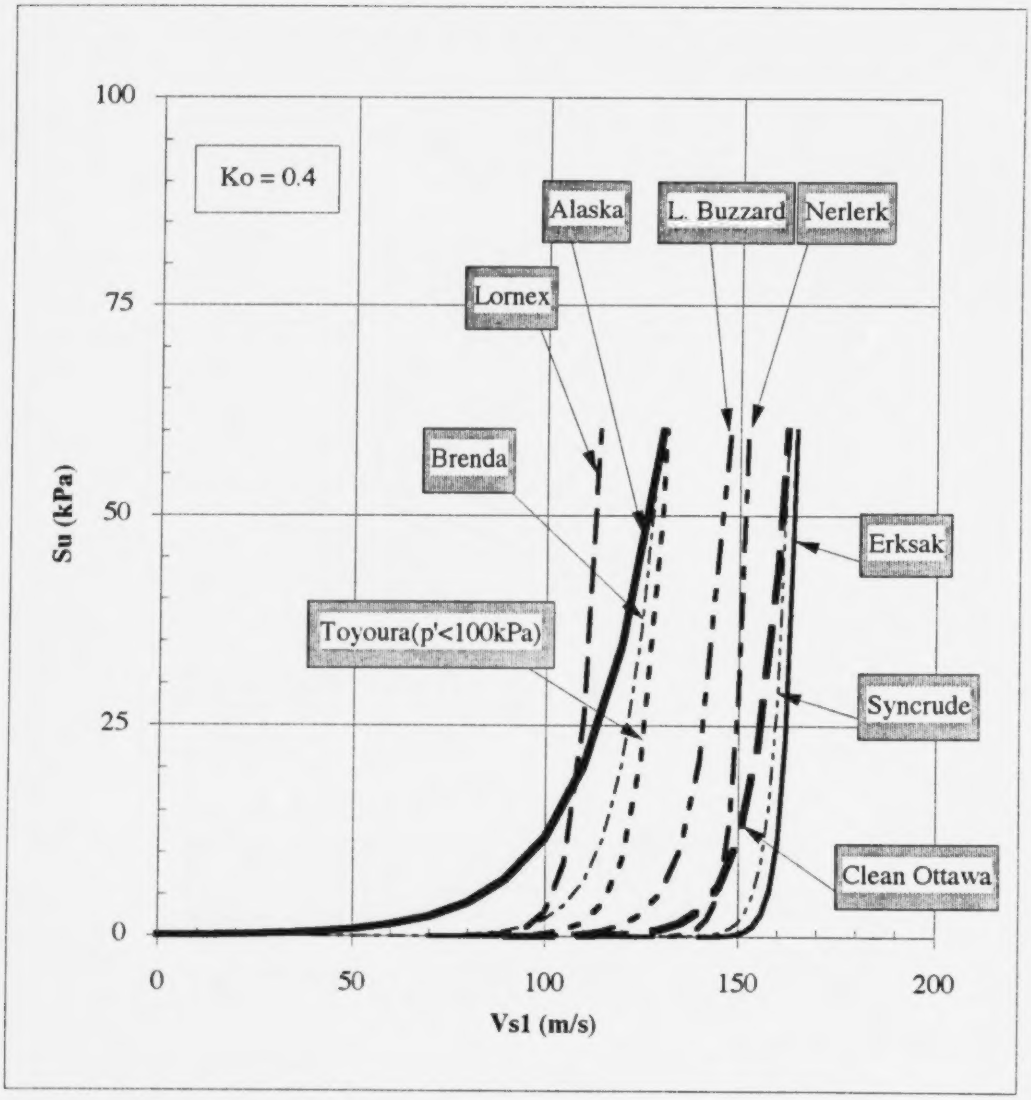

Figure 5-10 Relationship between S_u in triaxial compression and V_{s1} for other sands compared with Ottawa sand and Alaska sand.

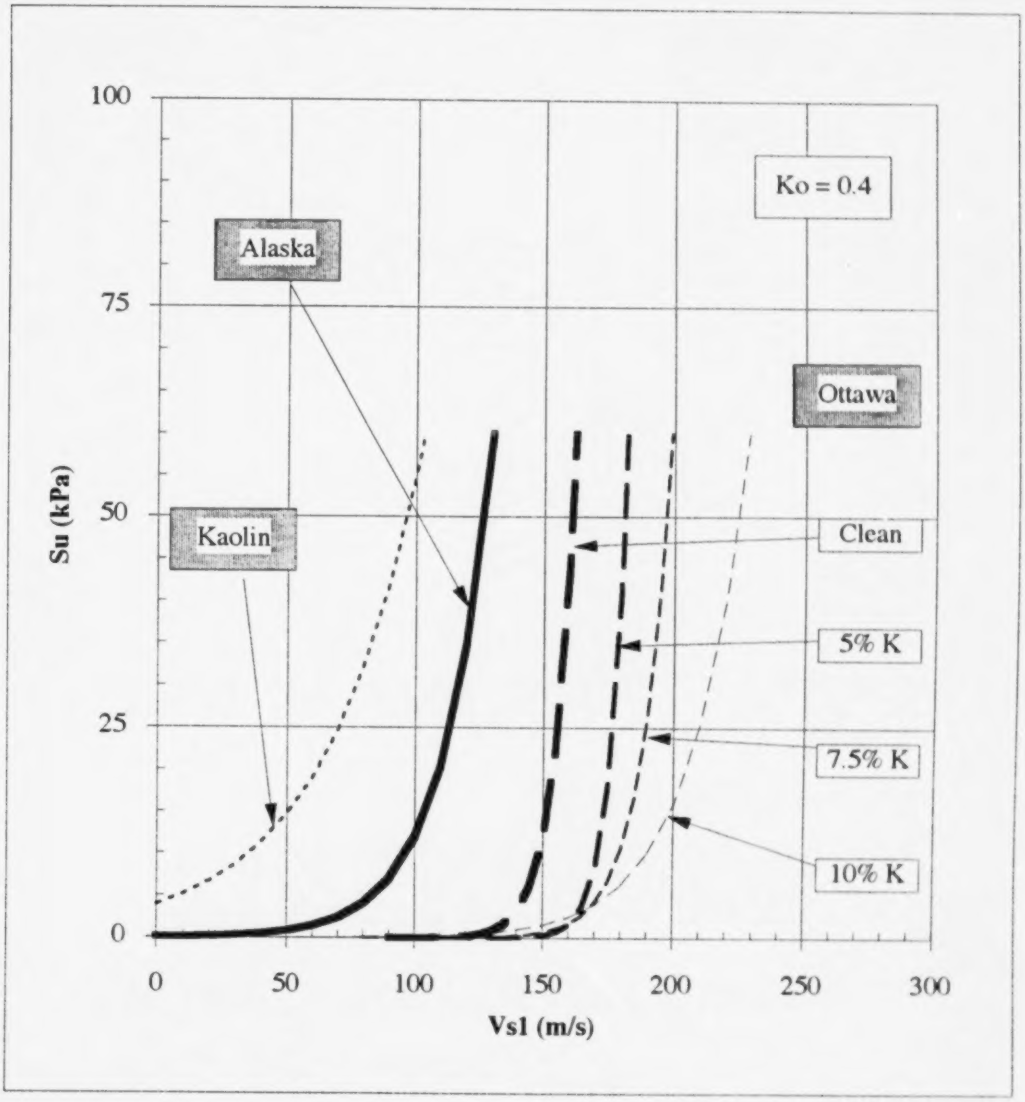

Figure 5-11 Relationship between S_u in triaxial compression and V_{s1} for Ottawa sand with fines and kaolin compared with Ottawa sand and Alaska sand.

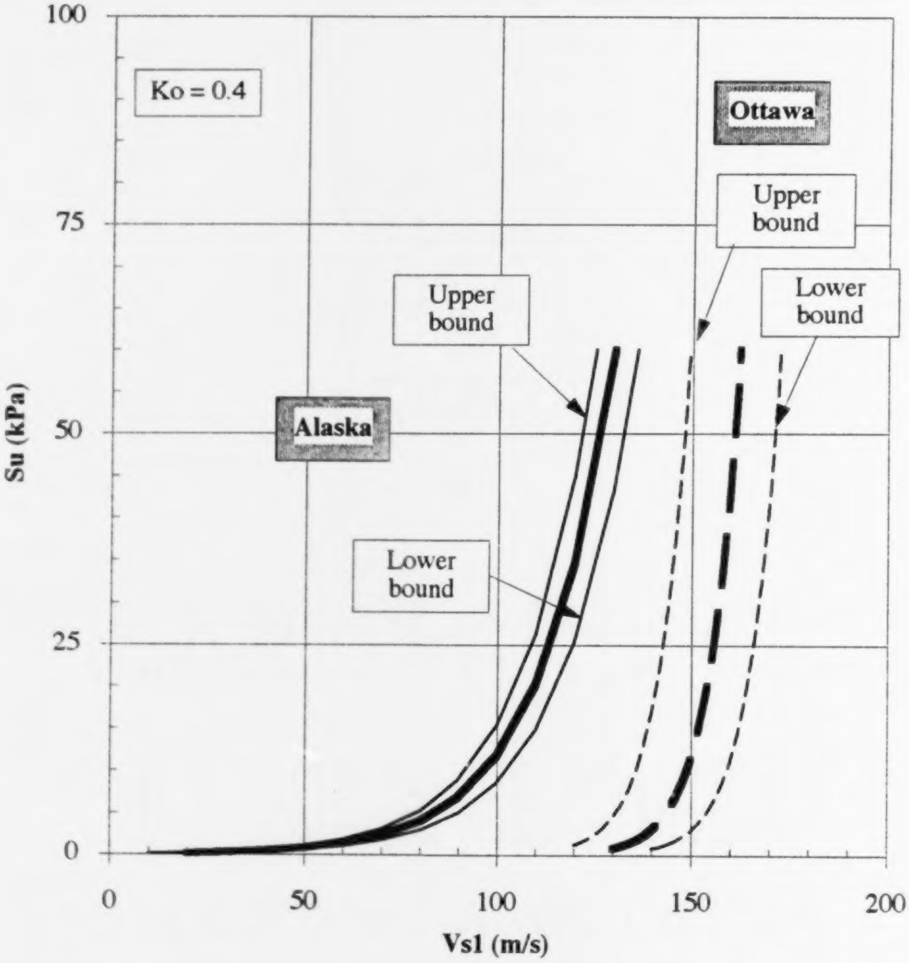

Figure 5-12 Illustration of the sensitivity of S_u-V_{s1} relationship in triaxial compression associated with the range in possible values for the parameter A for Ottawa sand and Alaska sand and K_o=0.4.

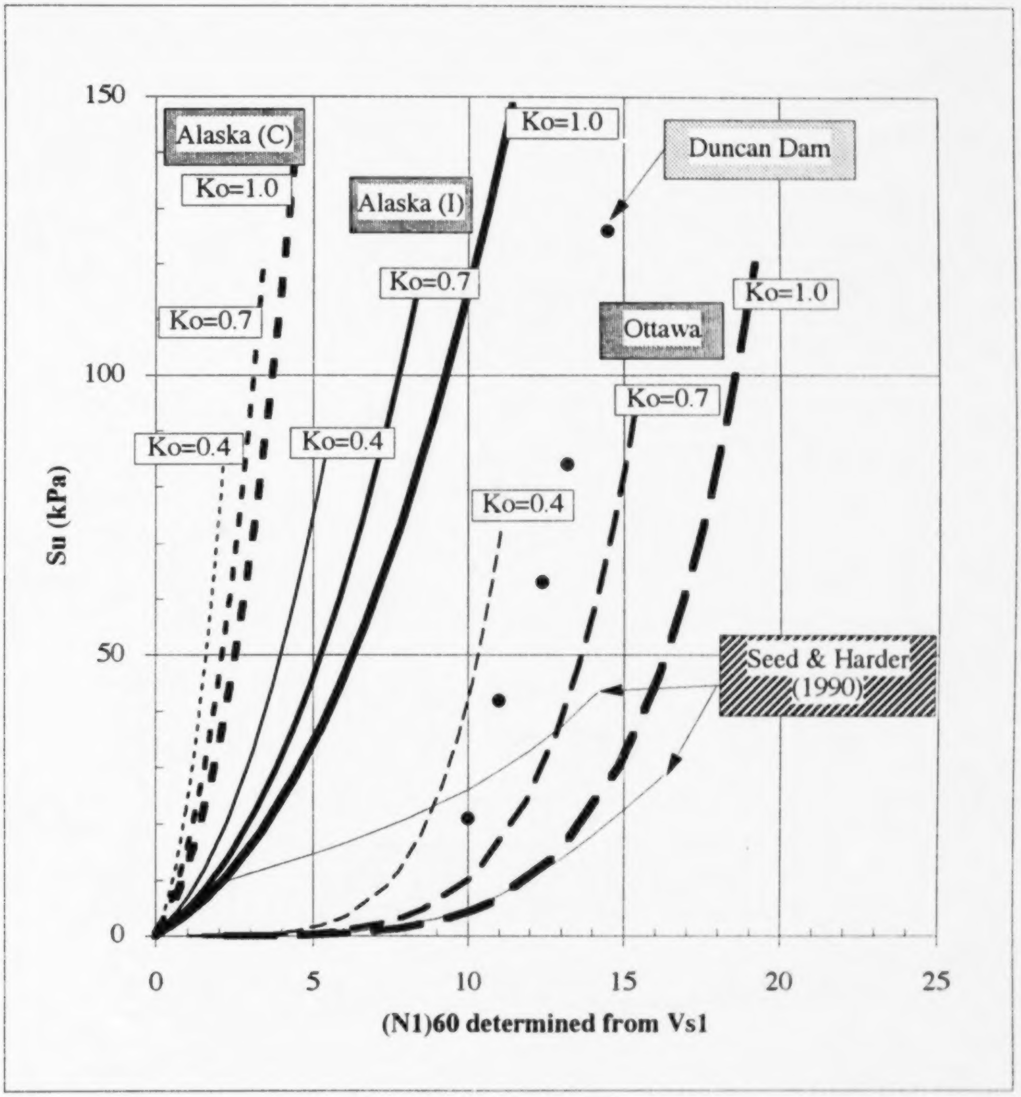

Figure 5-13 Relationship between S_u in triaxial compression and $(N_1)_{60}$ for Ottawa sand and Alaska sand compared with data from Duncan Dam and results from Seed and Harder (1990).

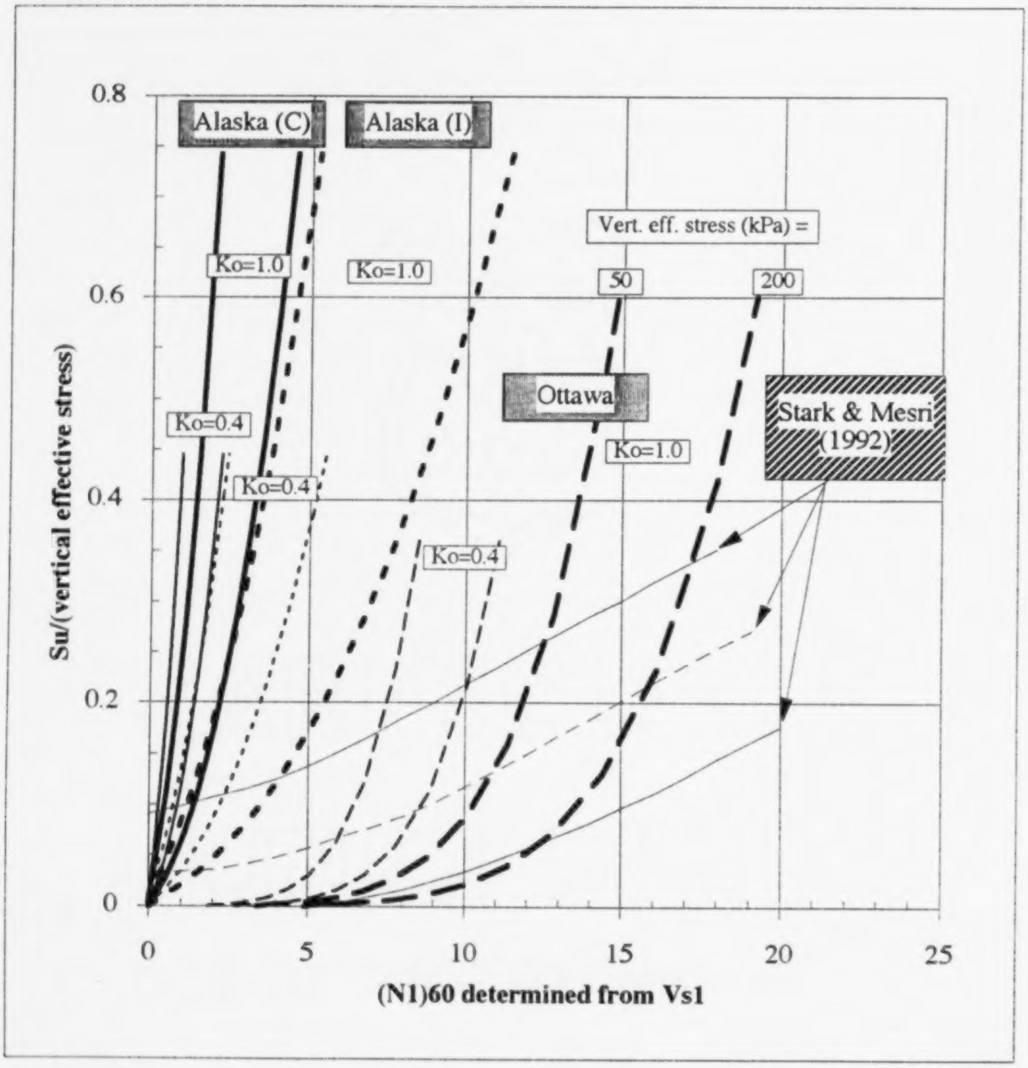

Figure 5-14 Relationship between S_u/σ_v' in triaxial compression and $(N_1)_{60}$ for Ottawa sand and Alaska sand compared with results from Stark and Mesri (1992).

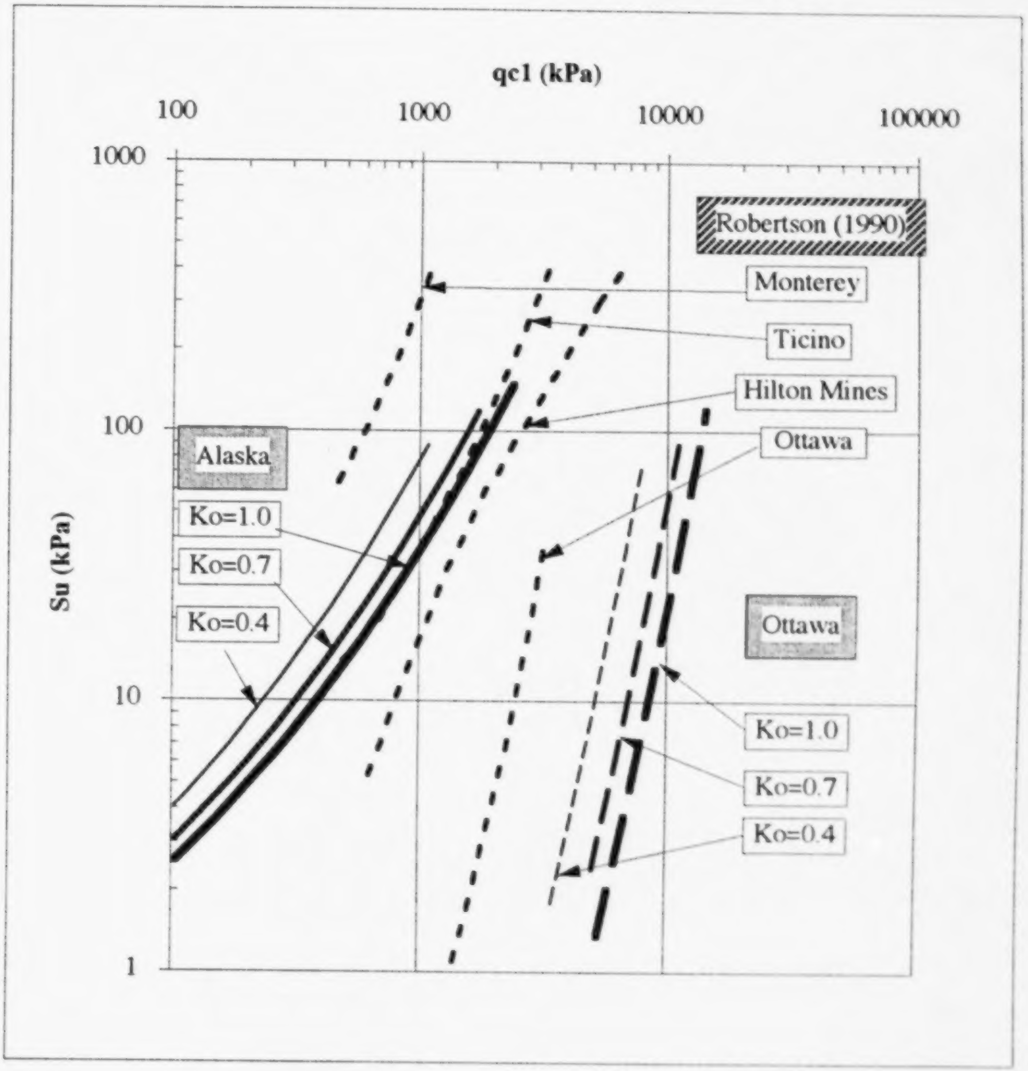

Figure 5-15 Relationship between S_u in triaxial compression and q_{c1} for Ottawa sand and Alaska sand compared with results from Robertson (1990).

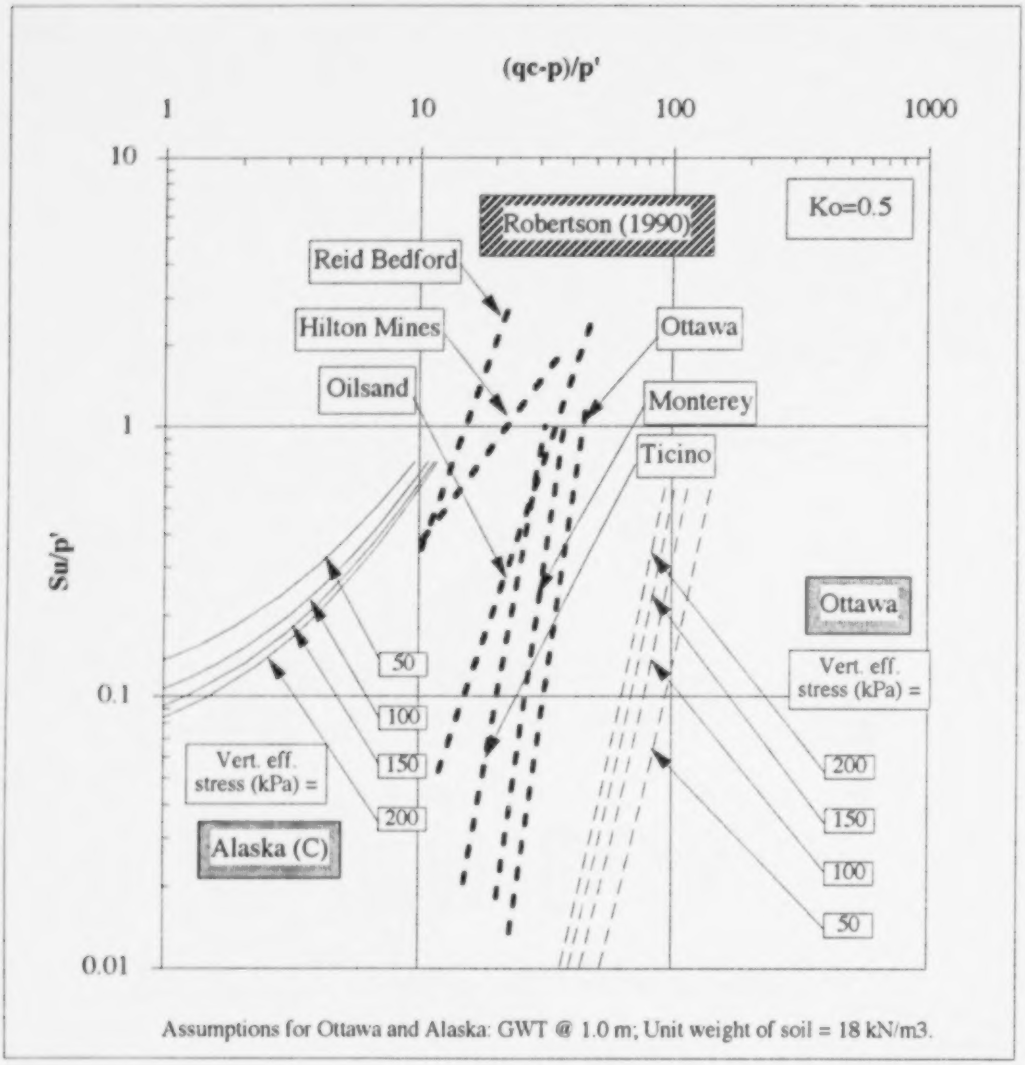

Figure 5-16 Relationship between S_u/p' in triaxial compression and $(q_c-p)/p'$ for Ottawa sand and Alaska sand compared with results from Robertson (1990).

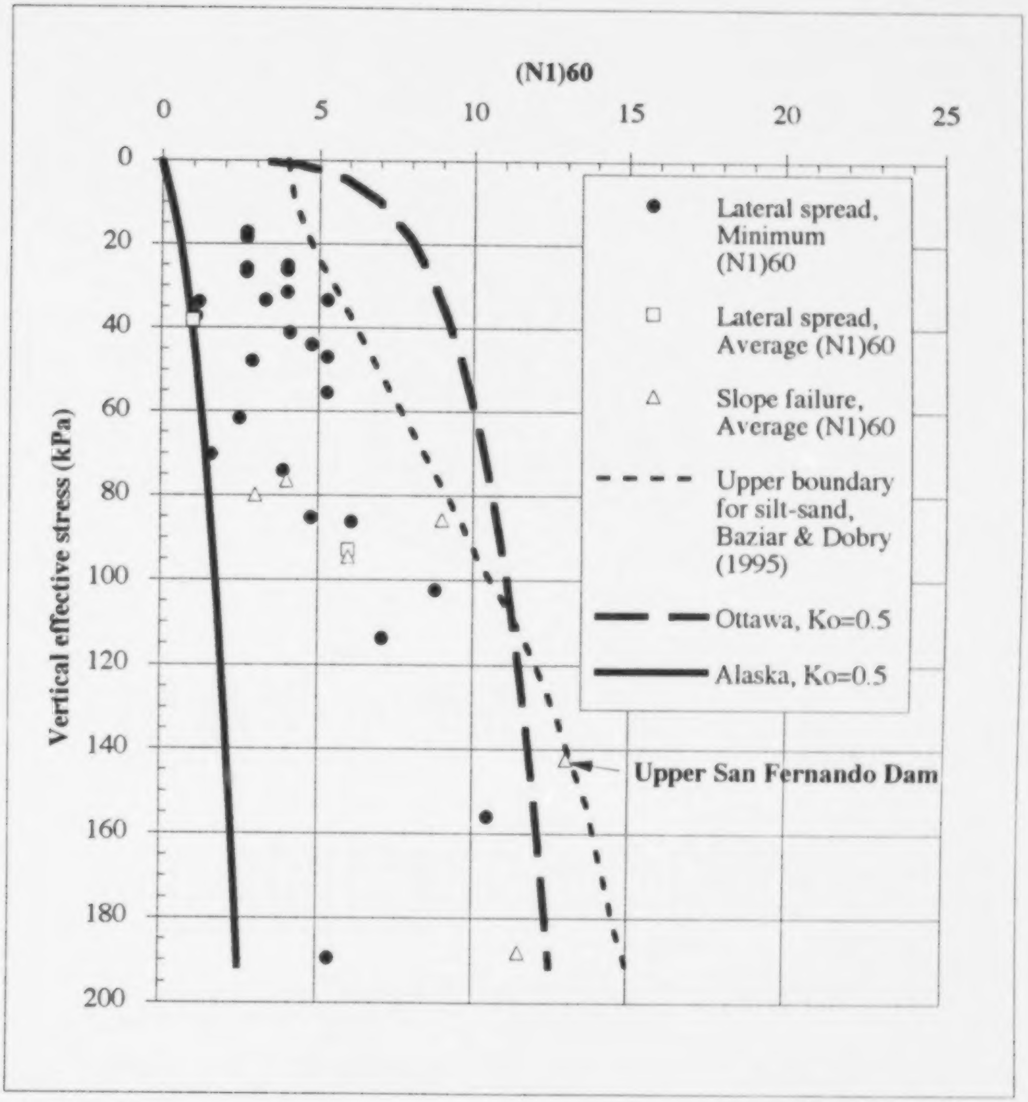

Figure 5-17 Contractant-dilatant boundary lines for Ottawa sand and Alaska sand compared with results from Baziar and Dobry (1995).

References

Atkinson, J. 1993. *An introduction to the mechanics of soils and foundations*, McGraw-Hill, London, pp. 103-123.

Baziar, M.H., and Dobry, R. 1995. Residual strength and large-deformation potential of loose silty sands. *Journal of Geotechnical Engineering*, ASCE 121(12): 896-907.

Been, K., and Jefferies, M.G. 1985. A state parameter for sands. *Géotechnique*, 35(2): 99-112.

Been, K., Crooks, J.H.A., Becker, D.E., and Jefferies, M.G. 1986. The cone penetration test in sands: part I, state parameter interpretation. *Géotechnique*, 36(2): 239-249.

Been, K., Jefferies, M.G., Crooks J.H.A., and Rothenburg, L. 1987. The cone penetration test in sands: part II, general inference of state. *Géotechnique*, 37(3): 285-299.

Been, K., Jefferies, M.G., and Hachey, J. 1991. The critical state of sands. *Géotechnique*, 41(3): 365-381.

Byrne, P.M., Imrie, A.S., and Morgenstern, N.R. 1994. Results and implications of seismic performance studies for Duncan Dam. *Canadian Geotechnical Journal*, 31(6): 979-988.

Cunning J.C. 1994. Shear wave velocity measurement of cohesionless soils for evaluation of in-situ state, *M.Sc. Thesis*, Department of Civil Engineering, University of Alberta at Edmonton, Alberta.

Cunning, J.C., Robertson, P.K., and Sego, D.C. 1995. Shear wave velocity to evaluate in-situ state of cohesionless soils, *Canadian Geotechnical Journal*, 32(5): 848-858.

Ishihara, K. 1993. Liquefaction and flow failure during earthquakes. The 33rd Rankine Lecture, *Géotechnique*, 43(3): 351-415.

Jefferies, M.G., Been, K., and Hachey, J.E. 1990. Influence of scale on the constitutive behaviour of sand. *Proceedings of the 43rd Canadian Geotechnical Conference*, Laval University, 1: 263-273.

Negussey D. and Islam, M.S. 1994. Uniqueness of steady state and liquefaction potential. *Canadian Geotechnical Journal*, 31(1): 132-139.

Pillai, V.S. and Salgado, F.M. 1994. Post-liquefaction stability and deformation analysis of Duncan Dam. *Canadian Geotechnical Journal*, 31(6): 967-978.

Pillai, V.S. and Stewart, R.A. 1994. Evaluation of liquefaction potential of foundation soils at Duncan Dam. *Canadian Geotechnical Journal*, 31(6): 951-966.

Pitman, T.D. 1993. Effect of fines and gradation of the collapse surface of a loose saturated soil. *M.Sc. thesis*, Department of Civil Engineering, University of Alberta, Edmonton, Alberta.

Robertson, P.K. 1990. Evaluation of residual shear strength of sands during liquefaction from penetration tests. *Proceedings of the 43rd Canadian Geotechnical Conference*, Laval University, 1: 257-262.

Robertson, P.K., and Campanella, R.G. 1983. Interpretation of cone penetration tests. Part I: sand. *Canadian Geotechnical Journal*, 20(4): 718-733.

Robertson, P.K., Woeller, D.J., and Finn, W.D.L. 1992a. Seismic cone penetration test for evaluation liquefaction potential under cyclic loading. *Canadian Geotechnical Journal*, 29: 686-695.

Robertson, P.K., Woeller, D.J., Kokan, M., Hunter, J., and Luternauer, J. 1992b. Seismic techniques to evaluate liquefaction potential. *Proceedings of the 45th Canadian Geotechnical Conference*, 5:1-5:9.

Robertson, P.K., Sasitharan, S., Cunning, J.C., and Sego, D.C. 1995. Shear wave velocity to evaluate in-situ state of Ottawa sand. *Journal of Geotechnical Engineering*, ASCE, 121(3): 249-261.

Sasitharan, S. 1994. Collapse behaviour of very loose sand. *Ph.D. Thesis*, Department of Civil Engineering, University of Alberta, Edmonton, Alberta.

Sasitharan, S., Robertson, P.K., Sego, D.C., and Morgenstern, N.R. 1994. State boundary surface for very loose sand and its practical implications. *Canadian Geotechnical Journal*, 31(3): 321-334.

Seed, H.B. 1987. Design problems in soil liquefaction. *Journal of Geotechnical Engineering*, 113(8): 827-845.

Seed, R.B., and Harder, L.F. 1990. SPT-based analysis of cyclic pore pressure generation and undrained residual strength. *Proceedings of the H. Bolton Seed Memorial Symposium*, 2: 351-376.

Skirrow, R. 1995. The effects of fines content on the monotonic triaxial testing of cohesionless soils for evaluation of in-situ state. *M.Sc. Thesis*, Department of Civil Engineering, University of Alberta, Edmonton, Alberta.

Sladen, J.A. 1989. Problems with interpretation of sand state from cone penetration test. *Géotechnique*, 39(2): 323-332.

Stark, T.D., and Mesri, G. 1992. Undrained shear strength of liquefied sands for stability analysis. *Journal of Geotechnical Engineering*, ASCE 118(11): 1727-1747.

Vaid, Y.P., Chung, E.K.F., and Kuerbis, R.H. 1990. Stress path and steady state. *Canadian Geotechnical Journal*, 27: 1-7.

Wood, D.M. 1990. *Soil Behaviour and Critical State Soil Mechanics*. Cambridge University Press, pp. 179-188.

Yoshida, Y., Ikemi, M., and Kokusho, T. 1988. Empirical formulas of SPT blow-counts for gravely soils. ***Proceedings of Penetration Testing***, Balkema, Rotterdam, 1: 381-387.

CHAPTER 6

EMPIRICAL ESTIMATION OF UNDRAINED SHEAR STRENGTH BASED ON DOWNHOLE PLATE LOAD TESTS[1]

6.1 Introduction

The previous chapter has illustrated the difficulty in estimating undrained shear strengths from conventional penetration testing in sand. In clay, plate load testing is a method that is often used to estimate undrained shear strengths. This chapter reports on an experimental program that was developed to investigate the potential of using rapid downhole plate load testing as an alternative method for estimating undrained shear strengths in sand. The goal of the plate load testing was to push the plates as rapidly as possible in an attempt to load the sand in an undrained manner and, therefore, to be able to estimate the undrained shear strength of the loose sand from the measured bearing stress on the plate.

The experimental program consisted of a series of downhole plate load tests that were conducted at radii of approximately 5 to 9 m (in plan) from the location of in-situ freezing and sampling in J-pit at Syncrude, in conjunction with the Canadian Liquefaction Experiment (CANLEX) Phase III site investigation activity. This phase of the CANLEX project consisted of filling an old borrow pit (J-pit) at Syncrude, in Ft. McMurray, Alberta, with tailings to create a relatively loose sand deposit with a groundwater table at a depth of approximately 0.5 m.

The experimental program was preliminary in nature; however the results appear promising. This chapter describes the test program, presents the measured results from testing using both 4" (10 cm) and 6" (15 cm) diameter plates, provides a basic interpretation of the results and makes recommendations for future studies. Ideally, it would be desirable to compare the undrained strengths predicted using the plate load tests with undrained strengths measured in the laboratory by testing undisturbed samples. However, to date only very limited testing on undisturbed samples of Phase III sand has been conducted by the CANLEX project. Therefore, comparisons of the results of the plate load testing with the results of laboratory testing on undisturbed samples from the site will be possible at a future date once additional laboratory testing is performed and the overall Phase III data review activity is completed.

---

[1] *An abstract for a version of this chapter has been accepted for publication. Fear, C.E., Cyre, G., Robertson, P.K., and Morgenstern, N.R. 1996. Proceedings of the 49th Canadian Geotechnical Conference, St. John's, Newfoundland, September 23-25.*

6.2 Test Program and Equipment[2]

Figure 6-1 presents a plan view of the detailed test site at J-pit. Indicated on Figure 6-1 are the locations of in-situ freezing and sampling, locations of conventional in-situ testing (SPT, CPT, geophysical logging) and the approximate locations of the plate load tests that were conducted at the site. 4" diameter plates were used in boreholes PL1, PL2, FS5 and FS52. Note that the abbreviation FS indicates a frozen sampling borehole; testing in these boreholes was conducted in the unfrozen soil beneath the frozen target zone after sampling of the frozen soil was completed. 6" diameter plates were used in boreholes PL4, PL5 and PL6, with the exception of one test using a seven inch diameter plate (the first test in borehole PL4).

6.2.1 Basic equipment for initial 4" diameter plate load tests

From June 27 to 29, 1995, a total of sixteen plate load tests were carried out using a 4" diameter steel plate (3/4 inch thick) that could be screwed onto the end of a drill stem. A load cell was constructed to fit between the drill head and the top of the drill stem and a displacement transducer that could measure the displacement of the drill head was mounted on the drill rig. Figure 6-2 illustrates the configuration of the overall test setup. Figure 6-3 illustrates the details of the plate system, the load cell and the displacement transducer. The data acquisition system that was in place to monitor the instrumentation for the planned CANLEX static liquefaction event was used to take and record readings from both the load cell and the displacement cell every tenth of a second. The average rate of penetration was approximately 30 cm/s, using a hydraulic drill rig from Mobile Augers.

Table 6-1 summarizes the details of each individual 4" diameter plate load test. The tests were carried out at a variety of depths in four boreholes, two of which were sampling holes through the frozen target zone (plate load tests in these holes were carried out in the unfrozen soil below the frozen target zone). The plate was displaced anywhere from 20 cm to 120 cm during a given test.

---

[2] *The plate load test equipment was all designed and built by Gerry Cyre of the University of Alberta. The detailed figures illustrating the specifics of the equipment configuration in the following section were also produced by Gerry Cyre.*

The data acquisition system was turned on before each test was started and was kept running until the test was completed. The load cell and displacement cell readings were recorded automatically on a continuous basis. It was therefore very important to correctly identify the start of the test within a large data file and "zero" the initial readings accordingly. Figure 6-4 presents calibration charts for the load cell and the displacement cell that were used in this stage of plate load testing. Both of these charts were determined in the laboratory prior to conducting the plate load tests in the field.

The start of each test was identified as the point at which the displacement cell readings began to quickly change. At this point, the initial displacement was set equal to zero. Subsequent displacements were determined from the change in voltage and the displacement cell calibration chart given in Figure 6-4. The corresponding load measured by the load cell was set equal to zero. Additional loads were determined by the change in voltage and the load cell calibration chart given in Figure 6-4. The total initial load on the plate was determined by adding the weight of the rods and plate system to the load measured by the load cell, accounting for the correct number of rods that were added as the borehole advanced. The bearing stress on the plate was then determined by dividing the total load by the plate area.

6.2.2 Advanced equipment for 6", 7" or 8" diameter plate load tests

As will be explained in subsequent sections of this chapter, it appeared that the 4" diameter plate load testing did not create undrained conditions in the sand. Therefore, from August 21 to 22, 1995, a second stage of testing was conducted. This consisted of five plate load tests in 3 boreholes using larger diameter plates (i.e. with longer drainage paths), to try to ensure undrained conditions. Three of these tests were carried out continuously over several metres, stopping only to attach additional lengths of drillstem. A more sophisticated system consisting of a downhole load cell and a steel plate with a built-in pore pressure transducer was designed and built. The advantages of this system were that more reliable measurements of bearing stress on the downhole plate and an indication of the effects of loading on pore pressures could be obtained. If undrained conditions could be produced with sufficiently rapid loading, one would expect to see increases in pore pressure measured by the pore pressure transducer. Figure 6-5 illustrates the configuration of the overall test setup for the second stage of plate load testing.

Three plates of different diameters (6", 7" and 8") were constructed, each with a pore pressure transducer. Figure 6-6 illustrates the details of the downhole plate, load cell and pore pressure transducer configuration. The location of the pore pressure transducer is such that it may not correctly measure the actual pore pressures; however, the relative increase or decrease in observed pore pressure response can be meaningful. The same displacement transducer was used as for the 4" plate load tests. Again, readings were taken and recorded every tenth of a second, using the on-site data acquisition system. The average rate of penetration was slower, at approximately 5 to 7 cm/s, using a hydraulic drill rig from Elgin.

Table 6-2 summarizes the details of each individual 6" diameter plate load tests. The 8" plate would have been difficult to use because it would have been too tight a fit in the 8" borehole that the rig could drill. The first test was carried out starting at a depth of 10 ft (3 m) using the 7" diameter plate, but could not be pushed more than 10 inches because the bearing stress exceeded the capacity of the drill rig. The set-up was therefore switched to the 6" plate, which was used for the rest of the tests in this second stage of plate load testing. The first 6" plate load test at a depth of 15 ft (4.6 m) also exceeded the capacity of the drill rig after a small displacement. However, at a greater depth (starting at 20 ft (6.1 m)), the 6" plate advanced easily and a continuous plate load test was performed with a total displacement of approximately 6 m, at which point the drill rig's capacity was exceeded. Subsequently, in two other boreholes, continuous plate load tests were also performed using the 6" plate, starting at depths of 20 ft (6.1 m) and 17 ft (5.2 m), respectively, with each test advancing a total of 5 to 6 m before refusal.

As for the 4" diameter plate load tests, the data acquisition system was turned on before each test was started and was kept running until the test was completed and the load cell and displacement cell readings were recorded automatically on a continuous basis. Again, it was very important to correctly identify the start of the test within a large data file and "zero" the initial readings accordingly. Figure 6-7 presents the calibration charts for the load cell and displacement cell that were used during this stage of plate load testing. The load cell calibration was carried out in the laboratory after completion of the fieldwork. The displacement cell calibration was carried out while in the field. Figure 6-8 presents the calibration chart for the pore pressure transducer that was built into the downhole plate system. The pore pressure calibration was performed in the laboratory prior to conducting the plate load tests.

The start of the test was identified as the point at which the displacement cell readings began to quickly change. At this point, the initial displacement was set equal to zero. Subsequent displacements were determined from the change in voltage and the displacement cell calibration chart given in Figure 6-7. Since the load cell in this configuration was a downhole load cell, it essentially measures the total load on the plate. The total initial load measured by the load cell corresponding to zero displacement was set equal to the weight of the rods acting on the load cell before plate was advanced. Additional loads were determined by the change in voltage and the load cell calibration chart given in Figure 6-7. Since the load cell was part of the downhole plate system, any additional rods that were added as the plate was advanced would be felt by the load cell and be incorporated into the observed change in voltage relative to the initial zero value. The bearing stress on the plate was then determined by dividing the total load by the plate area. It was difficult to zero the pore pressure readings since no reference pressure was available. Pore pressure was therefore calculated directly by combining the measured voltage from the pore pressure transducer with the pore pressure calibration chart presented in Figure 6-8.

6.3 General Plate Load Test Theory

Conventional bearing capacity theory used to estimate the undrained strength of clay from plate load tests can be used to interpret undrained strengths in sand if the plate load test is performed with a big enough diameter plate and occurs rapidly enough to promote undrained conditions. The following section outlines conventional theory for estimating the undrained strength of a soil from plate load tests.

Assuming that undrained conditions apply, and that the soil is rigid, perfectly plastic in nature, the ultimate bearing capacity (q_f) of an infinite strip footing located on the ground surface is related to the undrained strength of the soil (S_u) by the following exact solution based on classical plasticity theory:

[6-1] $$q_f = (2 + \pi)\,S_u$$

Skempton (1951) modified this equation to account for the effects of footing shape (e.g. circular or square versus strip) and the depth below ground surface, provided that locating the plate at depth provides a confining effect to the soil beneath the plate. The resulting equation is:

[6-2] $$q_f = N_c S_u + \gamma D$$

where:
N_c = bearing capacity factor
γ = unit weight of soil
B = width of plate
L = length of footing
D = depth of footing

The bearing capacity factor, N_c, is a function of both the shape of the footing (defined by the ratio B/L) and the depth of the footing (defined by the ratio D/B). The chart proposed by Skempton (1951) for estimating N_c is given in Figure 6-9 and applies to soils that are rigid, perfectly plastic, as indicated. For infinite strip footings (i.e. B/L=0) located at the ground surface (i.e. D/B=0) the chart in Figure 6-9 gives an N_c of 5.14 corresponding to the value given in Equation 6-1 (i.e. $2 + \pi$).

The plate load tests conducted in this study were all circular plates; therefore the ratio B/L has a value of 1. In addition, the plate diameter (B) ranged from 4" to 6" (10 cm to 15 cm) and the depths that the tests were conducted at ranged from approximately 2.5 ft to 25 ft (0.8 to 8 m), giving ratios of D/B greater than 5 (the maximum value shown in Figure 6-9). For most of the tests, D/B was much greater than 5 since many of the tests were conducted at depths of more than 10 ft (3.3 m). Therefore, based on Skempton's (1951) chart shown in Figure 6-9, an N_c of 9 is appropriate for an initial interpretation of the downhole plate load tests, assuming that the soil is rigid, perfectly plastic in nature and that locating the plate at depth provides confinement.

Rearranging Equation 6-2 gives the following equation to theoretically estimate undrained shear strengths (S_u) in sand from the measured bearing stress (q_f) during rapid downhole circular plate load tests, assuming undrained conditions are induced:

[6-3] $$S_u = \frac{q_f - \sigma_v}{N_c}$$

where:
σ_v = total overburden stress at the depth of the test = γD
N_c = 9 for a test at depth (with confinement) in a rigid, perfectly plastic material

This formula is based on classical plasticity theory for a general shear model. However, many of the plate load tests that were conducted as part of this study (particularly during the second stage of testing) were continuous tests over a range in depth of up to several metres. The only pauses were to attach additional lengths of drillstem. Therefore, many of the tests were somewhat like a large CPT test. Note that the conventional CPT has a tip area of approximately 10 cm^2, while the 4" and 6" diameter plates used in this study had much larger areas of approximately 80 cm^2 and 180 cm^2, respectively. An additional complicating factor with the plate load tests, as compared to the CPT, is the geometry of the plate and rod system being pushed continuously into the soil. Since the plate diameter is larger than the drillstem diameter (see Figures 6-3 and 6-6) soil will be pushed around the plate and behind it as the plate is advanced into the soil. This may decrease the measured bearing stress on the plate, due to the lack of confinement of the soil.

CPT testing in fine grained soil has been used to estimate the undrained strength of the soil (Robertson and Campanella, 1988/89). The same formula as given by Equation 6-3 can been used, except that the term N_c is replaced by an empirical cone bearing factor, N_k. Various studies comparing the estimated undrained shear strengths with other methods of estimating undrained strengths in clay (e.g. the field vane test), as summarized by Robertson and Campanella (1988/89) have shown that N_k is in the order of 15 ± 5. In clay, the factor N_k is a function of OCR, sensitivity and soil stiffness; studies also show that in sensitive clays, N_k may have a value less than 10 (Robertson and Campanella, 1988/89).

In this study, N_c was assigned a value of 9 for an initial interpretation of the downhole plate load tests. Based on the earlier discussion, this value may not be appropriate if the soil is strain-softening in nature (i.e. not rigid, perfectly plastic) or if there is a lack of confinement at depth. Studies (e.g. Chan, 1986) indicate that Skempton's (1951) N_c values may underpredict the peak undrained strength in strain-softening soil from the measured bearing stress on the plate (particularly if the rate of strain-softening is high), while providing a reasonable estimate of the residual undrained strength. When the soil is at residual strength, it is closer to a rigid, perfectly plastic material. The soil beneath the plate may actually consist of a combination of elements at peak strength and elements at residual strength. Lack of confinement at depth (e.g. as soil squeezes around the advancing plate) may create a condition closer to a plate load test at the ground surface. Hence N_c values lower than 9 should be used, even in a rigid, perfectly plastic material.

6.4 Interpretation of Results

In the following section, the results of each stage of downhole plate load testing are compared with the results of adjacent CPT testing at the site (see Figure 6-1). Four CPTs were conducted at a 5 m radius from the zone of frozen sampling: CPT-20, CPT-21, CPT-22 and CPT-23. In addition, two nearby CPTs (CPT-26 and CPT-27) which were seismic CPTs were included in the CPT results.

Figure 6-10 presents the complete set of results for one CPT (CPT-21), which is typical for all six of the CPTs in the vicinity. Pore pressure measurements during CPT penetration indicate that the local groundwater table was located at approximately 0.5 m depth and that, relative to the hydrostatic line, some excess pore pressures were noted as each additional length of cone push rod was added. However, this excess was generally small relative to the hydrostatic pressure and the CPTs can be considered to be essentially drained penetration tests. Slightly larger pore pressures during cone penetration were observed for CPT-23 (see Figure 6-1) than for the other CPTs in the area.

Figure 6-11 compares the profiles of CPT cone tip resistance from the six CPTs in the vicinity of the plate load testing. The thick horizontal lines at 3 m and 7 m indicate the extent of the target zone for freezing, sampling and other in-situ testing at the site. With the exception of two denser zones within the target zone indicated by CPT-21, the six CPTs all give reasonably consistent results over the depth range, particularly below 3 m. Figure 6-12 plots the CPT results in the target zone on the soil classification chart proposed by Robertson (1990) which was presented in Chapter 3 (see Figure 3-6). Most of the data fall within zone 5, classifying the soil as a sand mixture, ranging from a silty sand to a sandy silt. Some of the data fall into zone 6 (sands: clean sand to silty sand) and zone 4 (silt mixtures: clayey silt to silty clay). A few datapoints fall into zone 3 (clays). In addition, the data generally fall within the normally consolidated region (see Chapter 3, Figure 3-6), which is to be expected for such a young deposit (approximately one month old).

For each plate load test, loads and displacements were recorded. The measured load during each test was converted to bearing stress on the plate. The measured displacement was converted to an actual depth, using the starting depth of each test as a reference. Put together, the stress and depth measurements result in a profile of bearing stress with depth through the soil deposit. These profiles of measured bearing stress for the plate load tests can be compared with the profiles of measured CPT cone tip resistance (bearing stress). If the results are similar, it would seem logical to conclude that the plate load tests were essentially drained. However, if the plate load tests give much lower bearing stresses that the CPT, the plate load tests may be at least partially undrained. Further details are given in the subsequent sections. The second stage of testing had the advantage that pore pressure measurements were recorded during the plate load tests. These results can be used as an independent assessment of whether the tests were drained or undrained.

6.4.1 Four inch diameter plate load tests

Figures 6-13 to 6-16 present the profiles of measured bearing stress with depth in the individual boreholes PL1, PL2, FS5 and FS52, respectively, during the first stage of downhole plate load testing using the 4" diameter plate. Superimposed on each of these figures are the measured average and range (minimum and maximum) of the six adjacent CPT profiles of cone tip resistance (see Figure 6-11). The thick horizontal lines at 3 m and 7 m indicate the extent of the target zone for freezing, sampling and other in-situ testing as part of the CANLEX project at the Phase III site.

In general, each test was conducted by first advancing the borehole to a new depth, placing the plate at the bottom of the borehole and then rapidly pushing the plate into the soil (see Figure 6-2). The starting depths of tests in the same borehole were typically at 1.5 m (5 ft) intervals from each other. It is interesting to note that a sharp peak in measured bearing stress occurred at the start of most of the tests. Although the presence of these peaks may be a consequence of the variability of the deposit, as indicated by the CPT profile (see Figure 6-11), it appears coincidental that virtually every plate load test captured a dense layer of sand at the beginning of the test. It is possible that initially, each test was drained and then became at least partially undrained, resulting in an initially high bearing stress following by a decrease in bearing stress as the plate advanced and the process became undrained. However, the measured bearing stress on the plate during each test was generally similar to the CPT cone tip resistance. Another explanation may be that stress concentrations formed at the bottom of the borehole such that high initial stresses were required to start pushing the plate into the soil below. Once the plate continued to advance, any end-of-borehole stress effects would become less of a factor.

In general, the measured bearing stress on the plate appears to coincide with the minimum to average CPT cone tip resistance profiles. This suggests that the combination of plate size and rate of penetration was not sufficient to create undrained conditions. It would, therefore, not be appropriate to estimate undrained strengths from the profile of bearing stress on the plate using Equation 6-3 which requires undrained conditions to be present. Although it is possible that portions of one or two tests which had lower bearing stresses than the CPT profiles (e.g. the last test in borehole PL1; see Figure 6-13) caused at least partially undrained conditions, there was no independent means of confirming this, such as having pore pressure measurements indicating excess pore pressures.

An interesting feature to note is the results of the first test in borehole FS52 which are not shown in Figure 6-15. As indicated in Table 6-1, a lot of slough (drill cuttings) was present in the borehole; although the borehole had been advanced to a depth of 18 ft (5.5 m), the top of the slough was at about 14.5 ft (4.4 m). The drillers moved the rods up and down to break through the slough, but the result was that the rods sank under their own weight from about 18 ft (5.5 m), eventually stopping at a depth of almost 25' (7.6 m). Perhaps some cyclic softening was induced in the sand.

6.4.2 Six inch diameter plate load tests

The second stage of plate load testing involved the more sophisticated system of a downhole load cell and a plate with a built-in pore pressure transducer (see Figure 6-5).

a) Raw field data versus time

Figures 6-17 and 6-18 present the measured displacements, pore pressures and bearing stress versus time for the first two tests in borehole PL4. The first test was performed starting at a depth of 10 ft (3.0 m) with a 7" diameter plate (see Figure 6-17). Figure 6-18 presents the results of the second test in borehole PL4, the first test with the 6" diameter plate, which started at a depth of 15 ft (4.6 m). Again, the drill rig reached its load capacity without pushing the plate very far. This test was done in two stages (hence the pause in the profiles versus time); the test was stopped momentarily as the rods were bending. Figures 6-17 and 6-18 indicate that the pore pressures in these first two tests decreased while the plate was being advanced (i.e. the observed excess pore pressure was negative). This could be indicative of a dense sand.

The borehole was then advanced to a depth of 19.5 ft (5.9 m) and the third test in borehole PL4 was performed (see Figure 6-19). This time, the plate advanced easily. The test was therefore continued for several metres, stopping only to attach additional lengths of drillstem. The plate was pushed for three complete intervals of approximately 150 cm before finally reaching the load capacity of the drill rig towards the end of the fourth interval. Figure 6-19 clearly indicates that the average rate of penetration for each interval was approximately 5 cm/s and that with each interval of pushing the plate, pore pressures measured by the built-in pore pressure transducer increased. In addition, in between intervals of advancing the plate, the pore pressures clearly dissipated.

Figures 6-20 and 6-21 present similar results as Figure 6-19, but for continuous plate load tests conducted in boreholes PL5 and PL6, respectively. As a result of the high bearing stresses measured at depths less than 15 ft (4.6 m) in borehole PL4 (see Figures 6-17 and 6-18), the tests in boreholes PL5 and PL6 were started at depths of 20 ft (6.1 m) and 17 ft (5.2 m) respectively. Again, four intervals of advancing the plate were conducted in each borehole with the load capacity of the drill rig being reached at some point in the last interval. Slightly higher average penetration rates of approximately 6 cm/s were reached in both boreholes PL5 and PL6. Again, clear increases in pore pressures were measured by the built-in pore pressure transducer. The excess pore pressures in borehole PL6 were similar to those in borehole PL4 (see Figure 6-19), increasing as the plate was advanced and dissipating while the plate was stopped and additional lengths of drillstem were attached. However, in borehole PL5, the pore pressures appeared to rapidly reach a peak and then dissipate very rapidly while the plate was still being advanced. In fact, the trends of the pore pressure profile in PL5 are somewhat similar to the trends of the bearing stress profile, whereas in PL4 and PL6 the pore pressure profiles had trends opposite to the bearing stress profiles. Therefore, it is possible that the pore pressure transducer was not correctly measuring pore pressures during this test. However, the measured pore pressure profiles in boreholes PL4 and PL6 seem reasonable; this is shown more clearly in subsequent figures (Figures 6-26 to 6-28) which compare the measured pore pressures to the estimated hydrostatic line.

In Figures 6-19 to 6-21, it is interesting to note that although the bearing stress was set equal to the initial weight of the rods in each borehole, such that the initial value was slightly greater than zero on the scale shown, the measured bearing stress appears to go slightly negative in the intervals of time in which additional rods were being added and the plate was stationary. While there may be some small errors in the "zeroing" of the load on the plate or the calibration of the load cell, a more likely explanation for this observation may be the method used by the drillers to attach additional lengths of drillstem. The drillstem is often lifted up slightly and clamped before the next rod is added. This may result in a slight tension on the drillstem because of the displaced soil around the plate and the portion of the drillstem below the bottom of the augered borehole. A slight tension would translate to a negative load on the load cell and, would appear as a negative bearing stress when divided by the plate area.

b) Bearing stress profiles

Figures 6-22 to 6-24 present the profiles of measured bearing stress with depth in the individual boreholes PL4, PL5 and PL6, respectively. Superimposed on each of these figures are the measured average and range (minimum and maximum) of the six adjacent CPT profiles of cone tip resistance. The thick horizontal lines at 3 m and 7 m indicate the extent of the target zone for freezing, sampling and other in-situ testing at the site.

Clearly the first two tests in borehole PL4 had bearing stresses in the range of the minimum to average CPT cone tip resistance (see Figure 6-22). However, much of the continuous third test had bearing stresses that were smaller than the range in CPT cone tip resistance. In particular, low bearing stresses were measured in the region of 7 m depth and 9.5 m depth. Similar observations could be made in both boreholes PL5 and PL6 (see Figures 6-23 and 6-24, respectively). It appears likely that the plate load tests may be at least partially undrained, particularly in the two zones of low measured bearing stresses.

Figure 6-25 summarizes the measured bearing stresses from the three boreholes, PL4, PL5 and PL6 and compares the results to the CPT profiles of cone tip resistance. The zones of low bearing stress appear to coincide in all three plate load test boreholes and have values significantly lower than the measured CPT cone tip resistance. Borehole PL4 extends to a greater depth than the other two boreholes. At depths greater than 11 m, the bearing stress on the plate in PL4 appears to be within the range of measured CPT values, as both the plate load test and the CPT detected the layer of clay shale at the base of J-pit.

c) Processed field data versus depth

Figures 6-26 to 6-28 present profiles of bearing stress versus depth, pore pressure versus depth, time versus depth and estimated undrained shear strength versus depth for the 6" plate load tests in boreholes PL4, PL5 and PL6, respectively. The profiles of bearing stress are identical to those in Figures 6-22 to 6-24. Superimposed over the pore pressure profiles for each test as a reference line is the approximate hydrostatic line based on a groundwater table located at a depth of 0.5 m. The profiles of estimated undrained shear strength were calculated by combining the profiles of bearing stress with Equation 6-3 (based on an N_c of 9). Although this equation is only applicable to undrained conditions, it was applied to the entire profile from each test to see what the results would be. Clearly the most likely areas to be considered as possibly undrained during testing are the two zones of low measured bearing stress as indicated in the previous section.

As explained earlier, the first (7" diameter plate) and second tests in borehole PL4 caused the load capacity of the drill rig to be met without much displacement of the plate. The pore pressures during these two tests decreased to values less than the hydrostatic reference line while the plate was being pushed (see Figure 6-26).

As outlined previously, the third test in PL4 (Figure 6-26) and the tests in PL5 (Figure 6-27) and PL6 (Figure 6-28) were continuous over several metres. As discussed previously, the pore pressure measurements in PL4 and PL6 demonstrated similar trends, while in PL5, the pore pressures behaved somewhat differently. In PL4 and PL6, pore pressures increased in excess of the hydrostatic reference line every time the plate was advanced and dissipated while the plate was stopped. The points of lowest measured bearing stress coincided with the highest measured excess pore pressures in both profiles. Towards the bottom of PL4, the excess pore pressures are a function of encountering fine-grained material (clay shale). At depths of 6 m to 11 m, however, it is likely that the high pore pressures are a result of at least partially undrained conditions being created in the sand. This is probably a combination of plate size, rate of loading and amount of fines in the sand. As discussed earlier, in PL5, the measured pore pressure profile appear to be inconsistent with the bearing stress profile, as compared to the results in PL4 and PL6. It is unclear whether the pore pressure measurements truly reflect the pore pressures in the ground during the test in this borehole or whether they are partially linked with the bearing stress on the plate.

d) Estimated undrained strength profiles

Figures 6-26 to 6-28 also present the estimated profiles of undrained strength based on combining the profiles of measured bearing stress with Equation 6-3. A groundwater table located at approximately 0.5 m and average unit weights of 18.5 kN/m^3 and 19.5 kN/m^3 for the soil above and below the groundwater table, respectively, were used to compute the total stress term in Equation 6-3. Zones of low estimated undrained strength occurred when the measured bearing stress was low, which as explained above, generally occurred when excess pore pressures were high. Based on an N_c of 9, undrained strengths less than 50 kPa are predicted in these zones. However, for reasons outlined earlier, an N_c less than 9 may be more appropriate; this would result in higher estimated undrained strengths.

In a couple of locations, slightly negative undrained shear strengths were calculated when Equation 6-3 was used to interpret the bearing stress data. This can not be correct and would only result if the estimated total stress was larger than the measured bearing stress (see Equation 6-3). Some uncertainty in either term may be the cause of this error in the calculated undrained shear strength. The likely lack of confinement as some soil squeezed around the advancing plate may have decreased the measured bearing stress on the plate in these regions. In addition, if there were a lack of confinement, the plate load test should have been interpreted as if it were at the ground surface (i.e. with lower N_c values and without subtracting the total stress term). In general, in the regions of low strength, the values of estimated undrained shear strength using an N_c of 9 are within the range conventionally applied to liquefied sand (see the plot by Seed and Harder (1990) for estimating undrained shear strengths from the SPT; Chapter 5, Figure 5-1). However, for reasons explained above, the actual undrained strengths may be significantly larger.

Figure 6-29 summarizes the estimated undrained strengths from PL4, PL5 and PL6 over a depth range of 6 m to 12 m. The lowest undrained strengths are predicted to occur from 6.5 m to 8 m , 9 to 10 m and in the region of 11 m. Using an Nc of 9, the lowest strengths are generally estimated to be in the order of 10 kPa; however, the actual values may be significantly higher. The variation in estimated undrained strengths may reflect the fact that the plate load testing appeared to be a mixture of undrained and drained penetration, as indicated by the increase and decrease of measured pore pressures relative to the hydrostatic reference line. However, the natural variability of the deposit (as reflected by the CPT testing) is likely another contributing factor. Even if the plate load tests were all completely undrained, variability in the estimated undrained strength profile would be expected as a result of the inherent variability of the sand deposit. Chapter 5 illustrated that undrained strength of a sandy soil can be very sensitive to its in-situ state. Consequently, it would not be surprising to find that the profile of undrained strength in a sandy deposit would be variable in nature. In addition, pre-peak estimates of strength are likely not reliable.

All of the estimated undrained strength profiles in Figure 6-29 were estimated using

Equation 6-3. This involved assuming an N_c of 9. Traditionally, the undrained shear strengths associated with N_c=9 have been in rigid, perfectly plastic materials. However, if a sand has a sufficiently loose state and is susceptible to flow liquefaction, it will be strain-softening in its response to undrained loading. Insufficient testing and analysis has been carried out at the Phase III site to investigate whether or not the sand is indeed strain-softening. If it is strain-softening, the simple interpretation used here may not be applicable.

Figures 6-30 and 6-31 present the profiles of S_u/σ_v' and S_u/p', respectively. In the zones of low estimated undrained strength, the ratio S_u/σ_v' has a typical value of about 0.2, based on an N_c of 9. The profile of S_u/p' was determined from the profile of S_u/σ_v' assuming that K_o at the site has a value of 0.5. Therefore, the zones of minimum $S_u/\sigma_v' \approx 0.2$ correspond to values of $S_u/p' \approx 0.3$. Chapter 5 explained that, based on critical state soil mechanics, the theoretical maximum Su/p' for a sand that strain-softens to ultimate state is given by 0.5M. For typical soils M_C can range from 1.2 to 1.5 and M_E can range from 0.9 to 1.0. These ranges correspond to a range in maximum S_u/p' of 0.6 to 0.75 in triaxial compression and 0.45 to 0.5 in triaxial extension. Therefore, the low points in the estimated undrained strength profiles give strength ratios in the range typically considered to apply to potentially liquefiable soils once they are triggered in flow liquefaction. However, as discussed above, the interpretation applied here (using N_c=9) may not be appropriate if the material is strain-softening or if a lack of confinement arises during the plate load test.

6.5 Comparison with Other Measures of Undrained Shear Strength

Unfortunately, it is not possible at this time to compare the estimates of undrained shear strength from the second stage of rapid downhole plate load tests with other measures of undrained shear strength at the site. Once the CANLEX project laboratory work and analysis of the Phase III site is completed, such a comparison will be made. This may help establish the appropriate N_c values for the sand deposit.

To date, only limited testing of undisturbed (frozen) samples of sand from the site has been performed. The few samples that have been tested strain-hardened in triaxial compression and demonstrated limited strain-softening (to a QSS) in triaxial extension before strain-hardening to ultimate state. Even when the testing of Phase III undisturbed samples is complete, a direct comparison with the second stage of plate load tests will not be possible. The frozen samples were all obtained in the 3 m to 7 m target zone (see Figure 6-11), while the region in which the second stage of plate load testing appeared to be possibly undrained was from 6 m to 12 m.

The flow liquefaction framework described in Chapter 4 will eventually be applied to the laboratory and field data from the Phase III site. The results can then be compared with the estimated undrained shear strengths from the second stage of downhole plate load testing. However, an added complication at the Phase III site is that the results of the data review for the Phase III site so far suggest that this sand is unusual, as compared to the other CANLEX sites. The average values of $(N_1)_{60}$, q_{c1} and V_{s1} are all significantly smaller than the values at the Phase I and Phase II sites. The integrated CPT method outlined in Chapter 3 predicts a higher fines content at the Phase III site than at the other sites. Limited laboratory testing to date supports this conclusion. Conventional or shear wave velocity based interpretations of the $(N_1)_{60}$, q_{c1} or V_{s1} profiles would predict significantly higher void ratios than suggested by the undisturbed samples available to date. However, geophysical logging predicts an average void ratio similar to the average void ratio of the undisturbed samples available to date.

A possible explanation for the discrepancy in results at the Phase III site is that the SPT, CPT and shear wave velocity measurements were strongly influenced by the high fines content and, hence, were controlled more by the skeletal void ratio at the Phase III site. The void ratios estimated for the undisturbed samples and predicted by the geophysical logging are total void ratios. When the undisturbed sample total void ratios were corrected to approximate equivalent skeletal void ratios based on the average fines content in the target zone, the void ratio interpretations of the SPT, CPT and shear wave velocity measurements had much better agreement with the undisturbed samples. The results seem to indicate that skeletal void ratio may be a factor for sands with a high fines content. Scanning electron microscopy has also shown that at least some of the undisturbed samples from the Phase III site appear to have an unusual fabric due to the high fines content (Hofmann, 1996). It will be interesting to carefully examine the results of testing undisturbed samples to see if their response appears to be linked to skeletal or total void ratios. It is unclear at this point whether skeletal or total void ratios would affect the results of the plate load tests.

6.6 Conclusions and Recommendations

The experimental program described in this chapter was clearly preliminary in nature. The above discussion indicates that interpreting results and estimating undrained shear strengths from downhole plate load tests can be complicated, particularly if, as for this study, the tests are not conventional plate load tests, but continuous penetration tests. If the soil is strain-softening in nature and/or a lack of confinement arises during the plate load test, the interpretation procedure becomes more challenging. However, a simple analysis of the results using Skempton's bearing capacity formula indicates that the downhole plate load test appears promising as a potential in-situ test for estimating undrained strengths in sandy soils. However, the undrained strengths can only be estimated using this formula when the combination of rate of loading and the size of the plate is sufficient to produce undrained loading and the soil behaves as a rigid, perfectly plastic material. Pore pressure measurements are useful as an independent means of assessing whether a given plate load test was drained or undrained. Studies by Charlie et al. (1993) investigating the potential of the Piezovane™ for identifying sands that are susceptible to liquefaction have led to similar conclusions; i.e. estimating the undrained strength of the sand is difficult, but the type of soil (susceptible to liquefaction or not) can be identified based on an observed increase or decrease in pore pressure during shear.

It would be interesting to conduct additional plate load tests in sandy deposits for which other methods of estimating or directly measuring the undrained strength have been applied; e.g. any of the CANLEX sites. However, based on the conclusions of Chapter 5, undrained strength is a response parameter that can be very sensitive to variability within a deposit. Consequently, the resulting estimates of undrained strength from rapid downhole plate load tests may be no better than estimates of undrained strength from other in-situ tests using methods described in Chapter 5. What might be the most worthwhile test to investigate in future studies is a large diameter CPT that can create undrained loading in a sandy deposit. The effects of sand squeezing around the plate in a plate load test would not be a factor in such a test. However, the loads required to push such a probe into the ground may pose difficulties to conventional drill rigs.

Table 6-1: Summary of 4" (10 cm) plate load testing

Borehole	Test No.	No. Rods*	Start Depth (ft)	Total Displacement (cm)	Total Time (s)	Comments
PL1	1	1	2.5	≈60	< 5	•no data available§
	2	2	7.5	≈60	< 5	•no data available§
	3	3	12.5	≈60	2.67	•no data available§
	4	4	17.5	≈65	1.91	
	5	5	22.5	≈60	1.86	
	6	6	24.5	≈60	--	•plate was advanced for about 2', then unloaded
		7		≈60	--	•plate was reloaded and advanced another 2'
	7	8	28.5	≈120	≈ 3.8	•plate was advanced continuously for about 4'
PL2	1	1	2.5	≈50	≈2	
	2	2	5	--	--	•system buckled out and load cell was dislodged; test was restarted 8" deeper (see test no. 3)
	3	2	5.67	≈40	1.81	
	4	3	10	≈65	≈2	
	5	4	15	≈20	≈2	•plate advanced 8"; then test stopped to prevent buckling and restarted
		4	15.67	≈45	--	
	6	5	20	≈20	2.1	•plate was loaded and advanced for about 8", then unloaded
		5	20.67	≈45	--	•plate was reloaded and advanced about 1.5'
FS52	1	5	18	≈208	--	•slough into borehole; depth to top of slough was about 14.5'; moved rods up and down to break through slough; rods sank under their own weight from about 18' to 24'; rods continued to slowly sink to a depth of 24'10"
	2	6	25	≈55	1.89	•added another rod, loaded and advanced the plate; slough in borehole; depth to top of slough was about 15'
FS5	1	6	24.17	≈30	1.14	•plate was advanced for about 1', then unloaded
		6	25.17	≈120	≈ 2 or 3	•plate was reloaded and advanced about 4'

Notes:

* Weight of one rod ≈ 13.64 kg
Weight of 4" plate + short attachment rod + screws = 6.4 kg

§ Data for these tests were lost because the data acquisition system was not recording information from the load and displacement cells at a sufficiently frequent rate; this was corrected for subsequent tests

Table 6-2: Summary of 6" (15 cm) plate load testing

Borehole	Test No.	No. Rods*	Start Depth (ft)	Total Displacement (cm)	Total Time (s)	Comments
PL4	1**	4	10	≈25	--	•hollow stem auger to depth; pulled auger out and filled hole with water •approx. 2' of slough below 10' depth; advanced plate about 10" before meeting load capacity of drill rig
	2	5	15	≈25	--	•hollow stem auger to depth; pulled auger out and filled hole with mud •advanced plate a bit, but seemed to be bending rods; stopped and then pushed a bit more; met load capacity of drill rig
	3					•hollow stem auger to depth; pulled auger out and filled borehole with mud
		6	19.5	≈150	--	
		7		≈150	32.25	
		8		≈150	20.5	
		9		≈150	25	•load capacity of drill rig reached during last interval
PL5	1					•hollow stem auger to depth; pulled auger out and filled borehole with mud
		5	19.6	≈25	12	
		6		≈150	23.75	
		7		≈150	28.6	
		8		≈50	--	•load capacity of drill rig reached during last interval
PL6	1					•hollow stem auger to depth; pulled auger out and filled borehole with mud
		5	17.2	≈60	22.79	
		6		≈150	19.75	
		7		≈150	18.57	
		8		≈125	≈22	•load capacity of drill rig reached during last interval

Notes:

* Weight of one rod ≈ 13.64 kg

** Test performed with 7" (18 cm) diameter plate

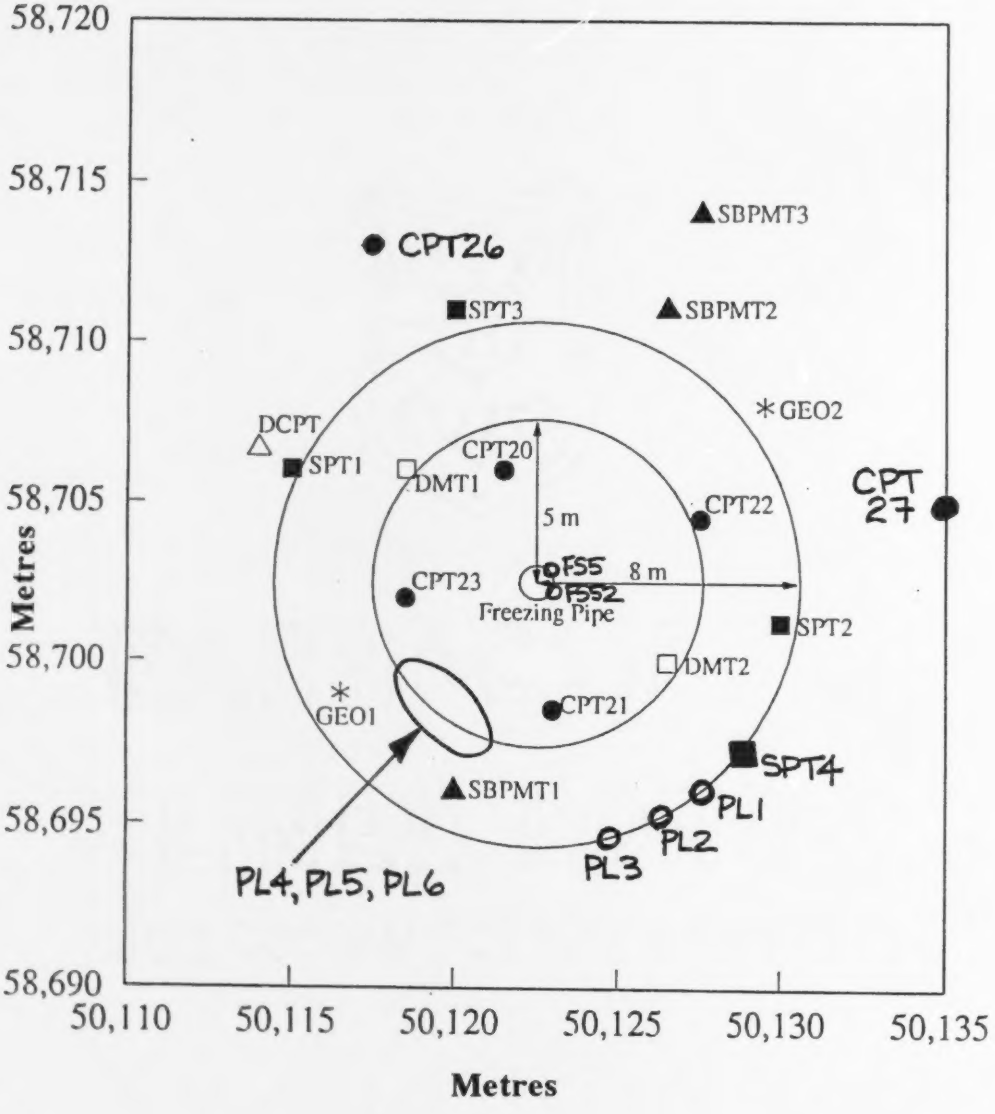

Figure 6-1 Plan of the detailed test site area at the CANLEX Phase III site (J-pit) (modified from Iravani et al., 1996).

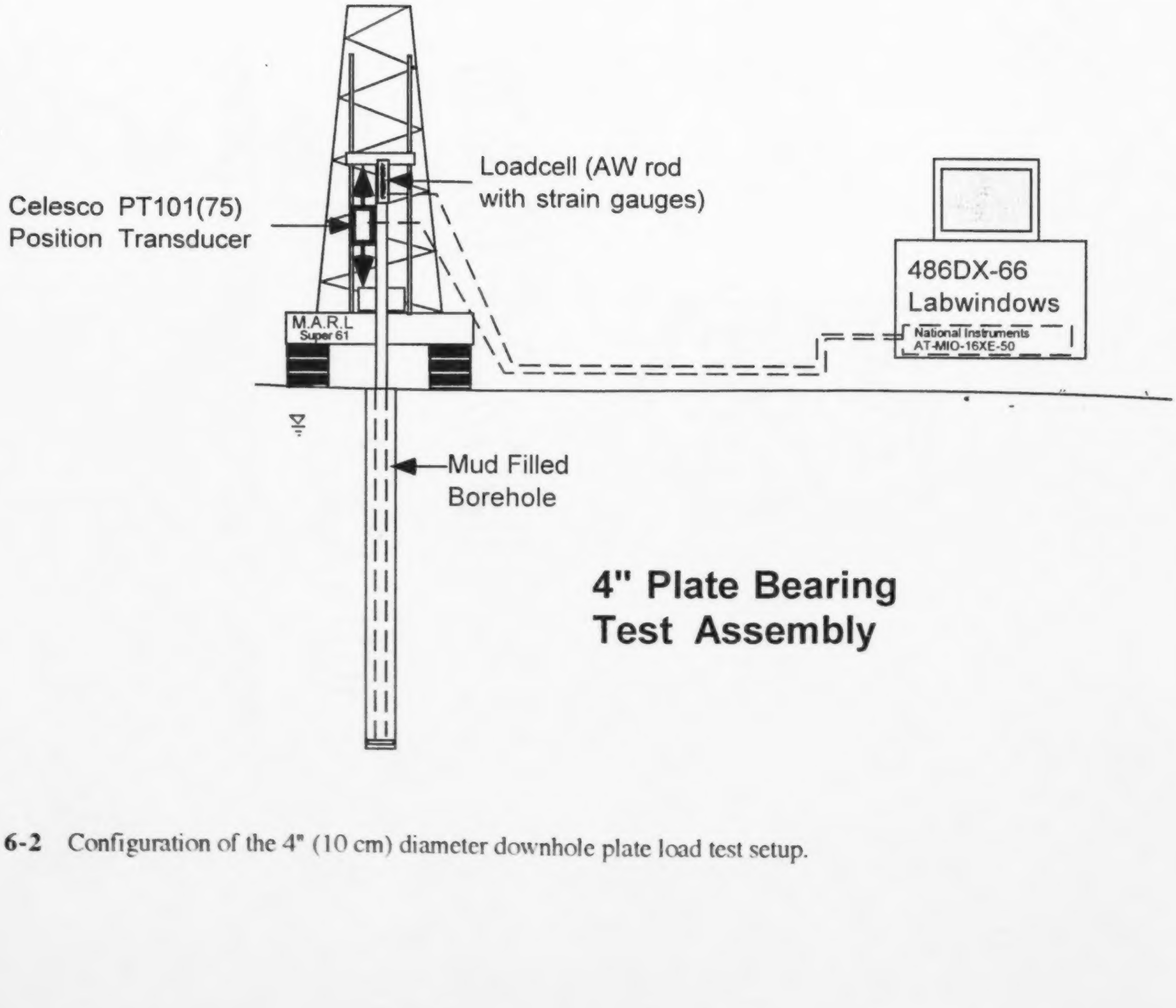
Loadcell (AW rod
with strain gauges)
Celesco PT101(75)
Position Transducer
486DX-66
Labwindows
National Instruments
AT-MIO-16XE-50
M.A.R.L
Super 61
Mud Filled
Borehole
4" Plate Bearing
Test Assembly

Figure 6-2 Configuration of the 4" (10 cm) diameter downhole plate load test setup.

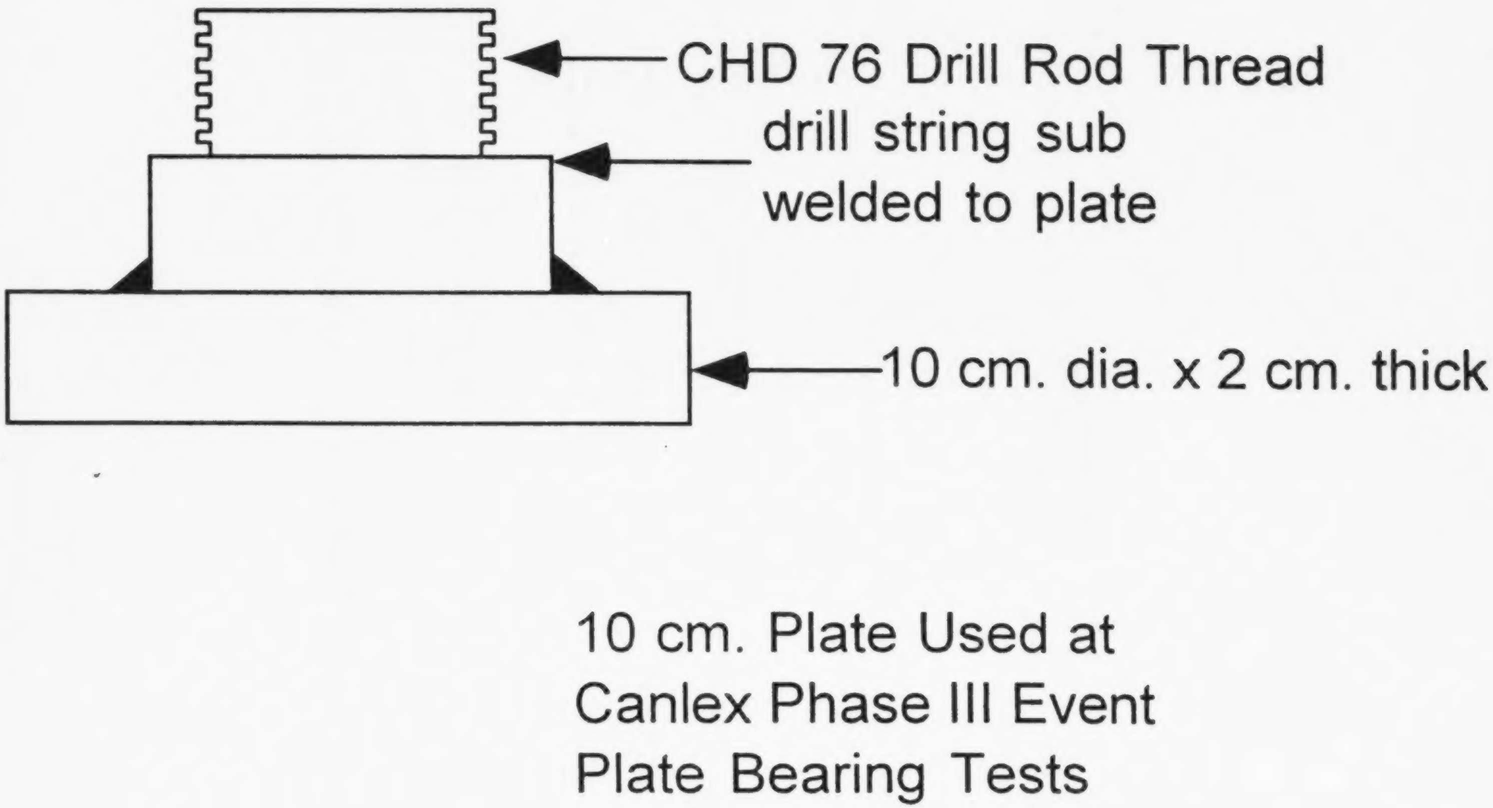
CHD 76 Drill Rod Thread
drill string sub
welded to plate
10 cm. dia. x 2 cm. thick
10 cm. Plate Used at
Canlex Phase III Event
Plate Bearing Tests

Figure 6-3 Schematic outlining the details of the 4" (10 cm) diameter downhole plate assembly.

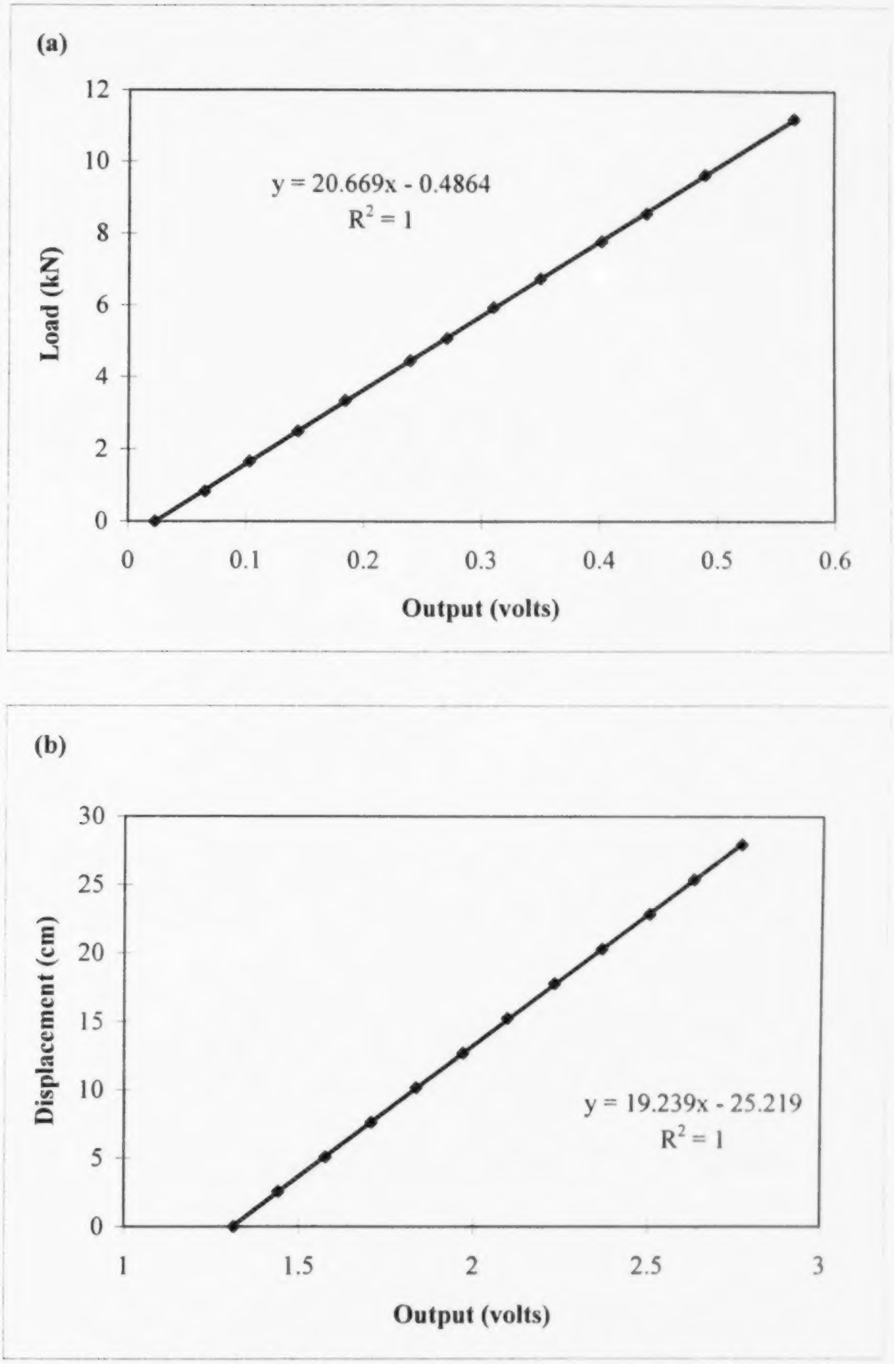

Figure 6-4 Calibration charts for the 4" (10 cm) plate load tests for (a) the load cell and (b) the displacement cell.

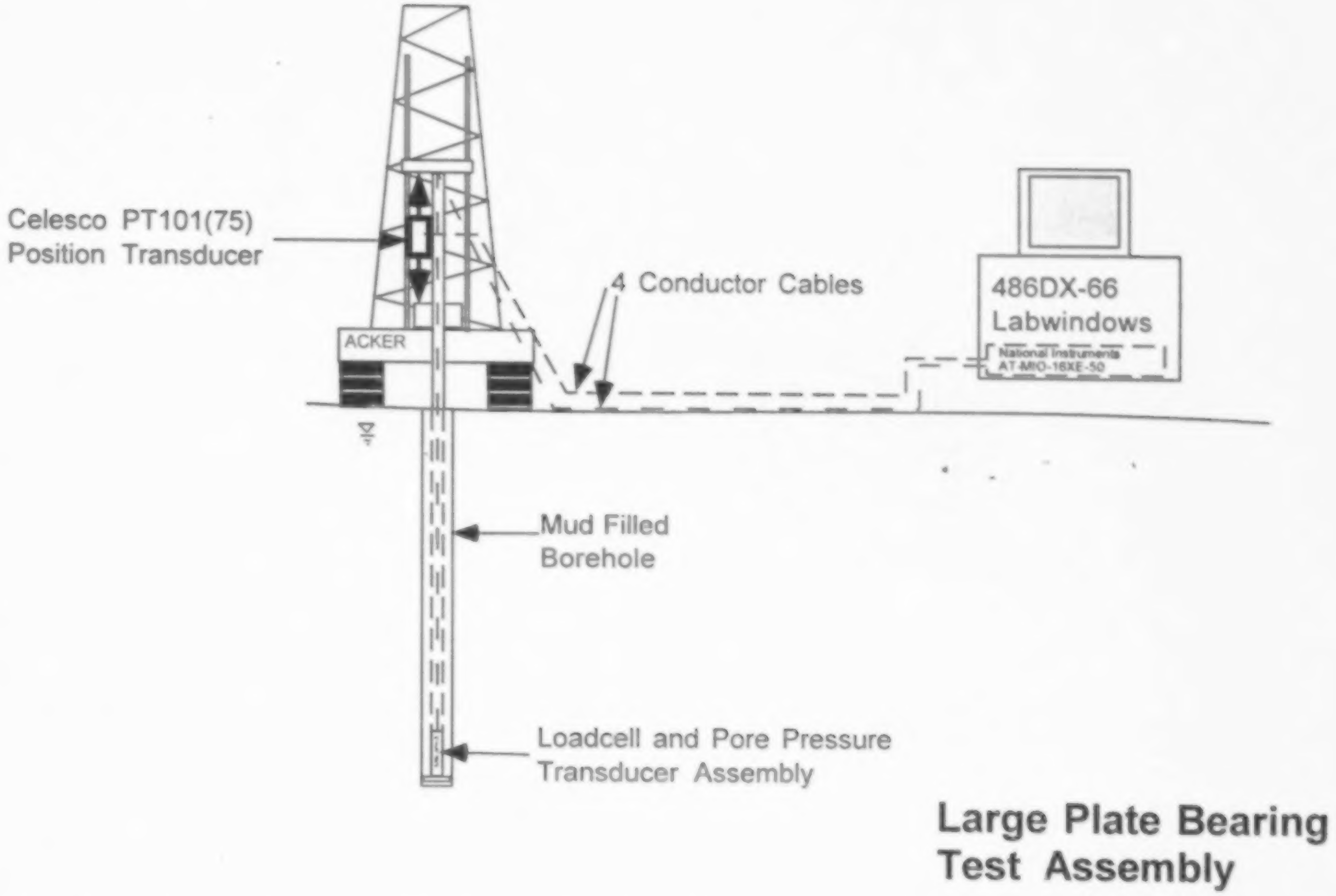
Celesco PT101(75)
Position Transducer
4 Conductor Cables
486DX-66
Labwindows
National Instruments
AT-MIO-16XE-50
ACKER
Mud Filled
Borehole
Loadcell and Pore Pressure
Transducer Assembly
Large Plate Bearing
Test Assembly

Figure 6-5 Configuration of the large diameter downhole plate load test setup, with downhole load cell and pore pressure transducer.

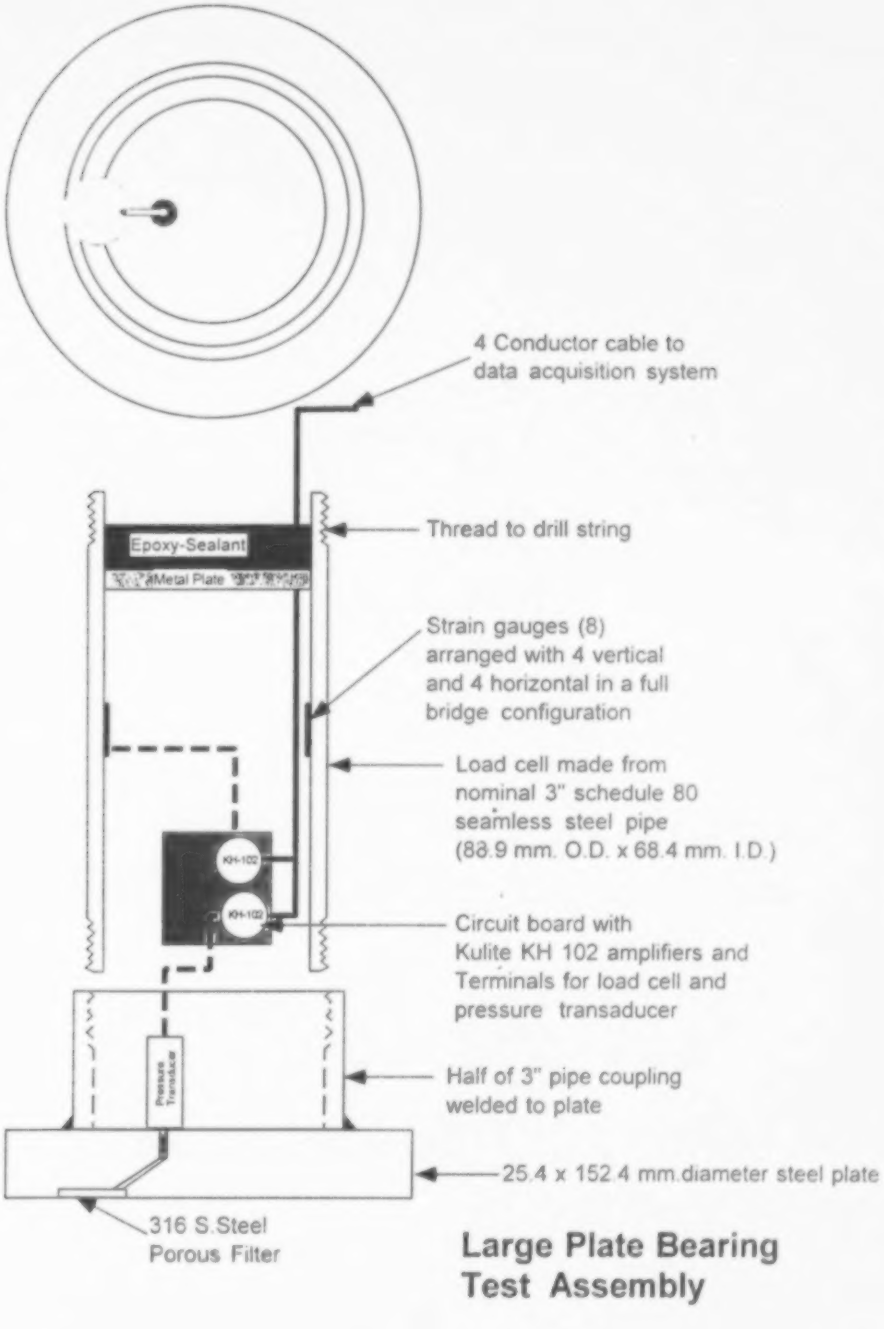
4 Conductor cable to data acquisition system
Thread to drill string
Epoxy-Sealant
Metal Plate
Strain gauges (8) arranged with 4 vertical and 4 horizontal in a full bridge configuration
Load cell made from nominal 3" schedule 80 seamless steel pipe (88.9 mm. O.D. x 68.4 mm. I.D.)
KH-102
KH-102
Circuit board with Kulite KH 102 amplifiers and Terminals for load cell and pressure transaducer
Pressure Transducer
Half of 3" pipe coupling welded to plate
25.4 x 152.4 mm.diameter steel plate
316 S.Steel Porous Filter
Large Plate Bearing Test Assembly

Figure 6-6 Schematic outlining the details of the large diameter downhole plate assembly, with built-in load cell and pore pressure transducer.

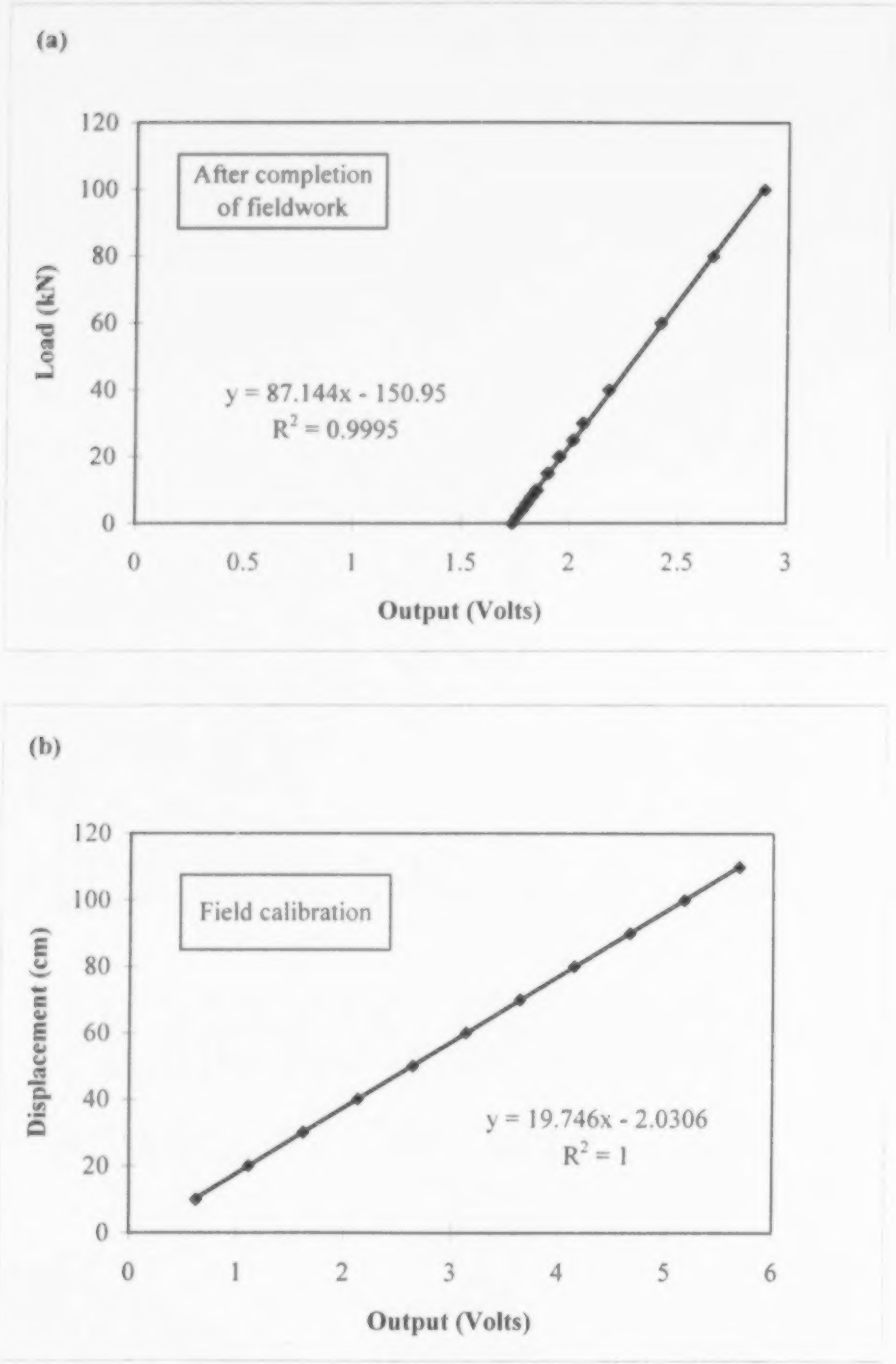

Figure 6-7 Calibration charts for the large diameter plate load tests for (a) the load cell and (b) the displacement cell.

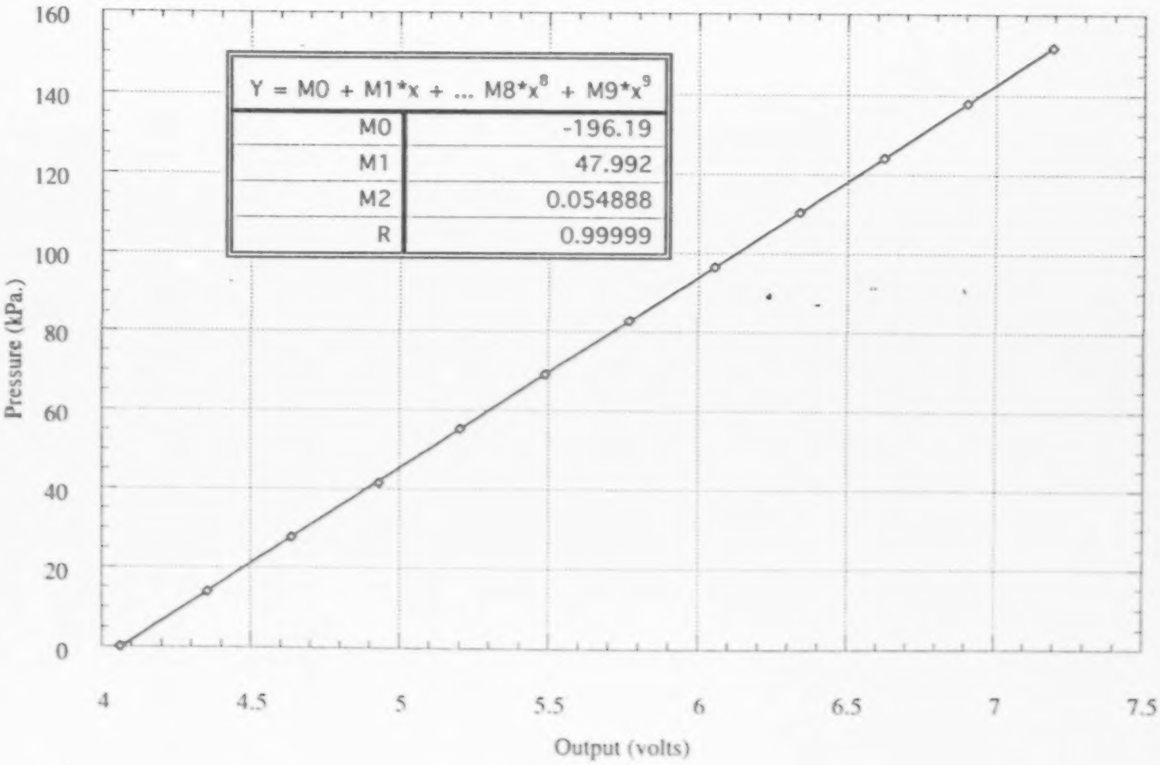

Figure 6-8 Calibration chart for the large diameter plate load tests for the pore pressure transducer.

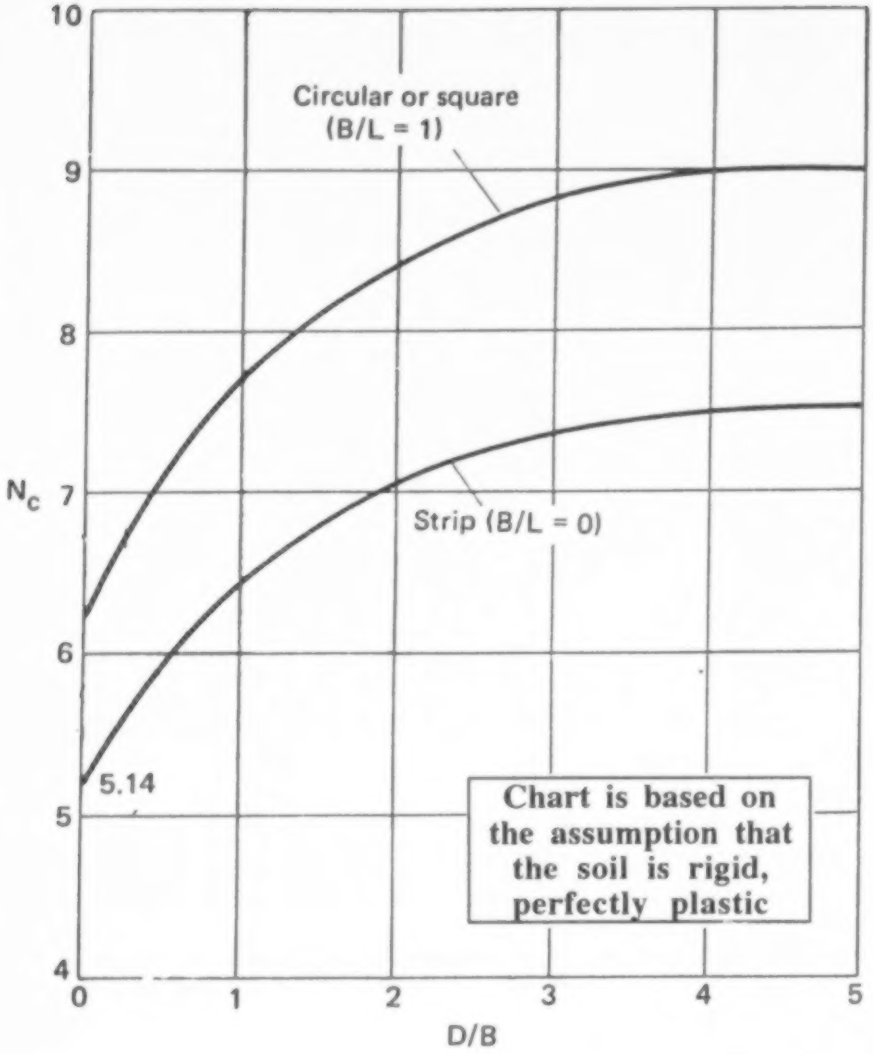

Figure 6-9 Recommended values of N_c for undrained loading in saturated clays (modified from Skempton, 1951).

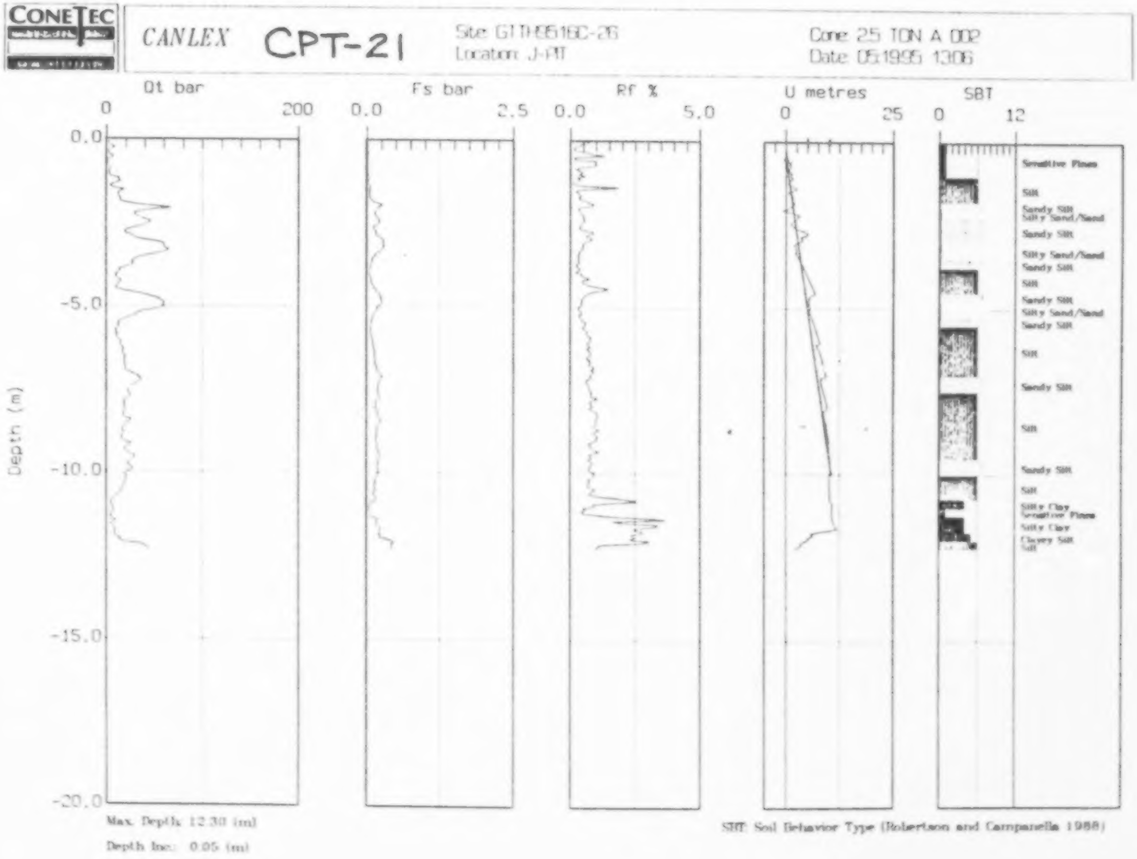

Figure 6-10 Typical CPT results (CPT-21) in the detailed test site area at the CANLEX Phase III site (J-pit) (modified from ConeTec, 1995).

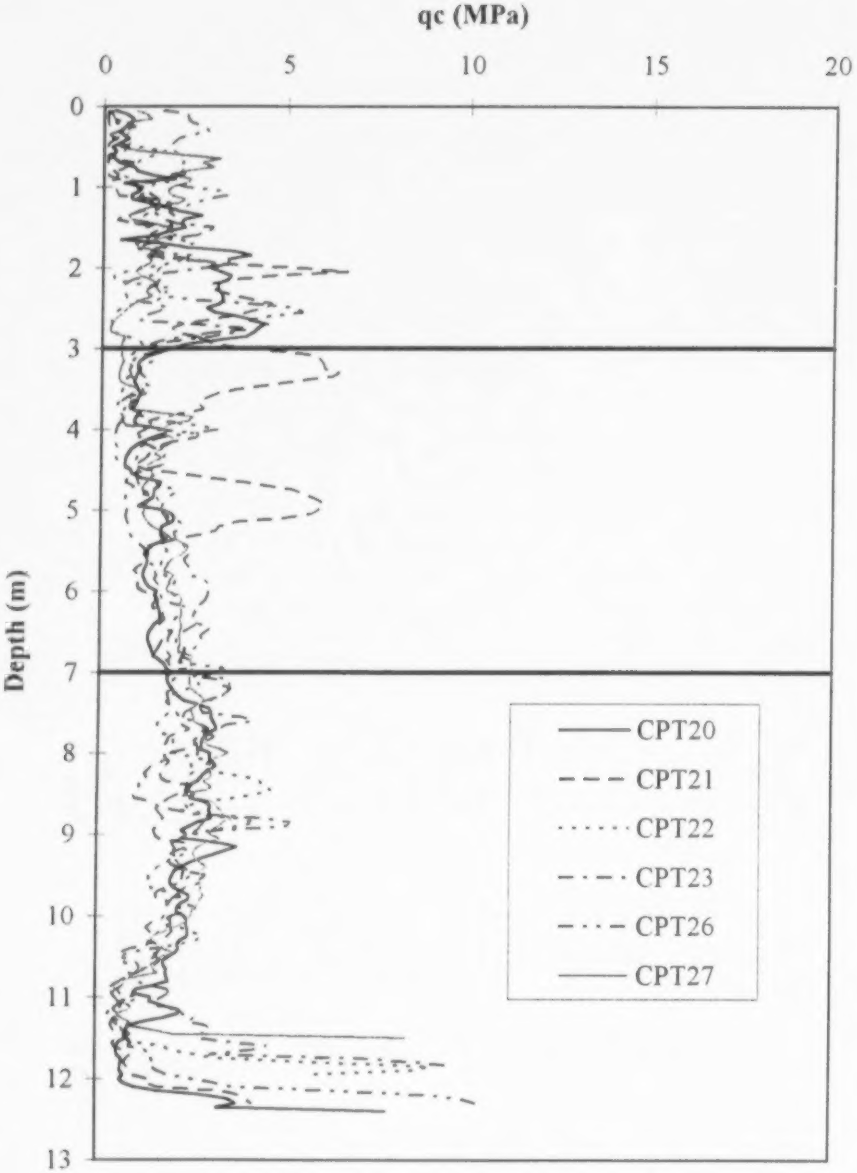

Figure 6-11 Summary of corrected CPT cone tip resistance profiles from all CPTs in and near the detailed test site area at the CANLEX Phase III site (J-pit); test site target zone for testing and sampling located from 3 m to 7 m, as indicated.

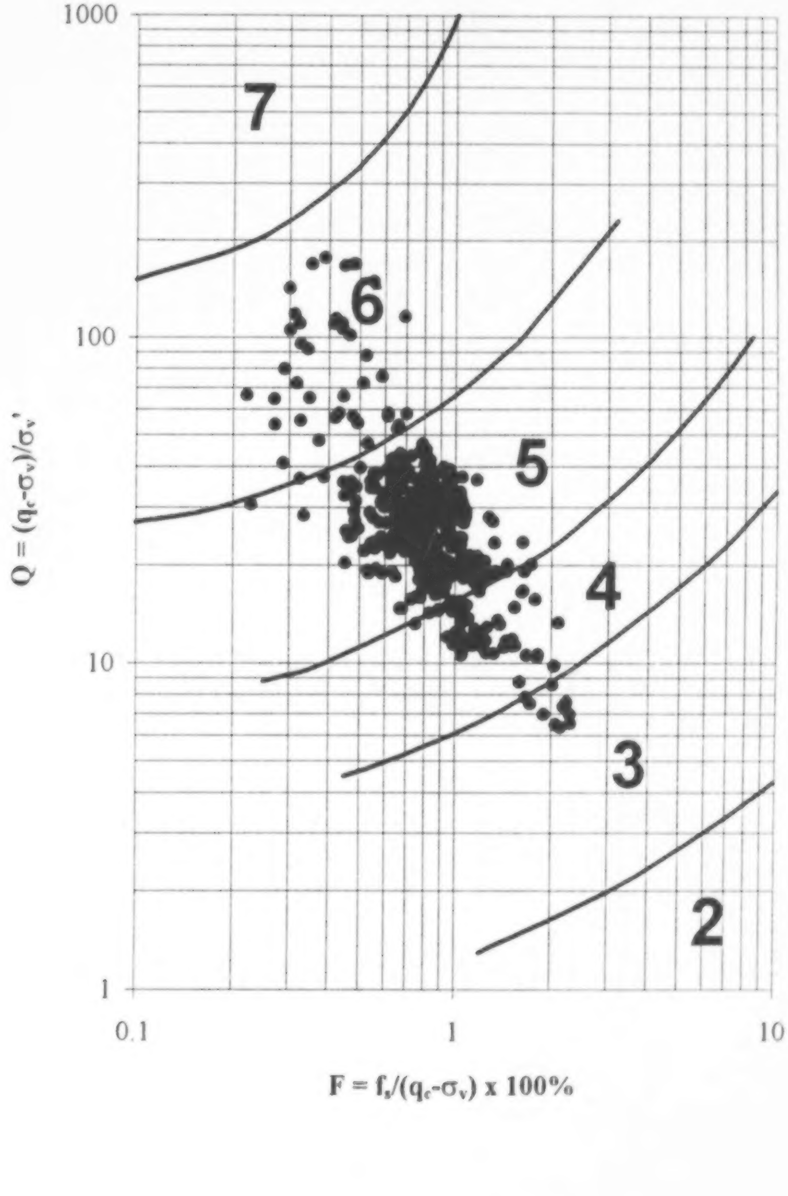

Figure 6-12 Plot of the CPT data in the target zone at CANLEX Phase III site (J-pit) on the soil behaviour type classification chart by Robertson (1990).

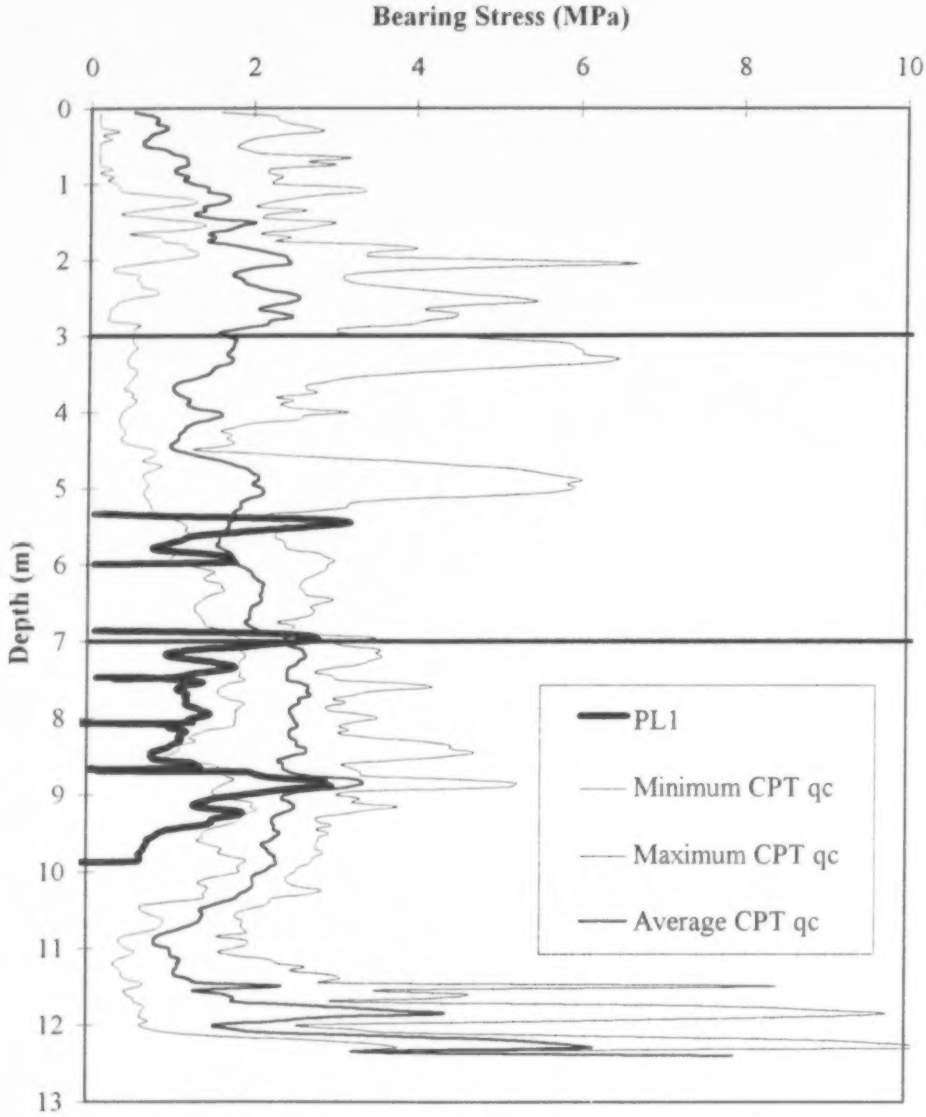

Figure 6-13 Bearing stress versus depth measured during 4" (10 cm) diameter plate load tests in borehole PL1.

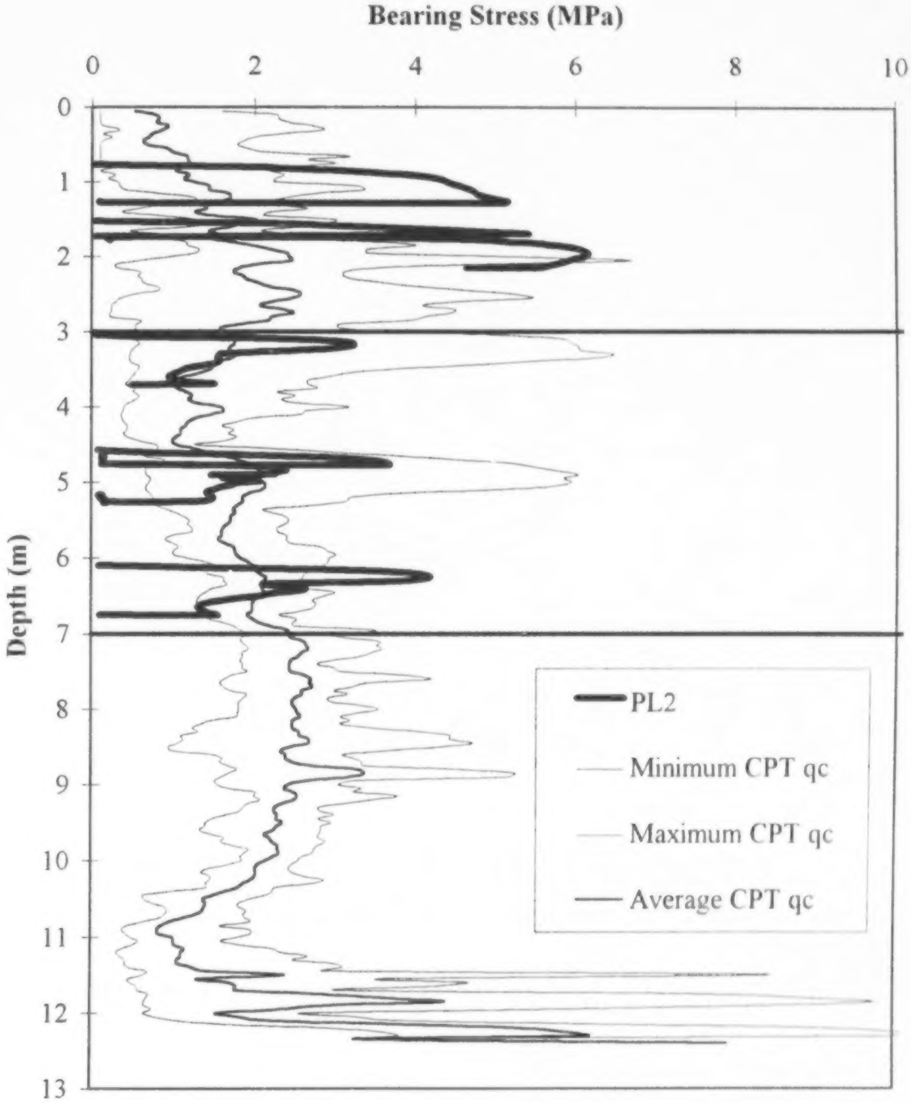

Figure 6-14 Bearing stress versus depth measured during 4" (10 cm) diameter plate load tests in borehole PL2.

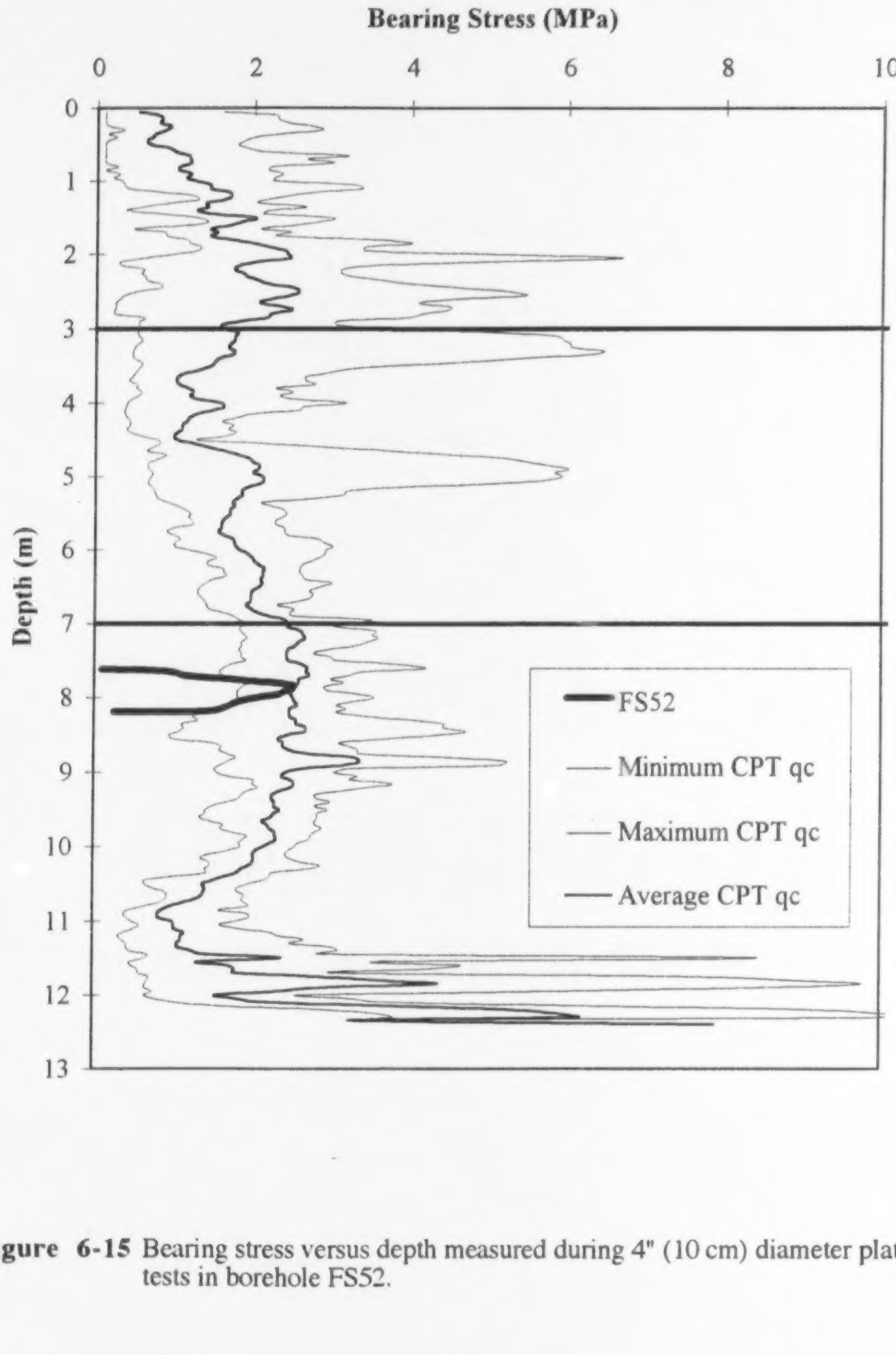

Figure 6-15 Bearing stress versus depth measured during 4" (10 cm) diameter plate load tests in borehole FS52.

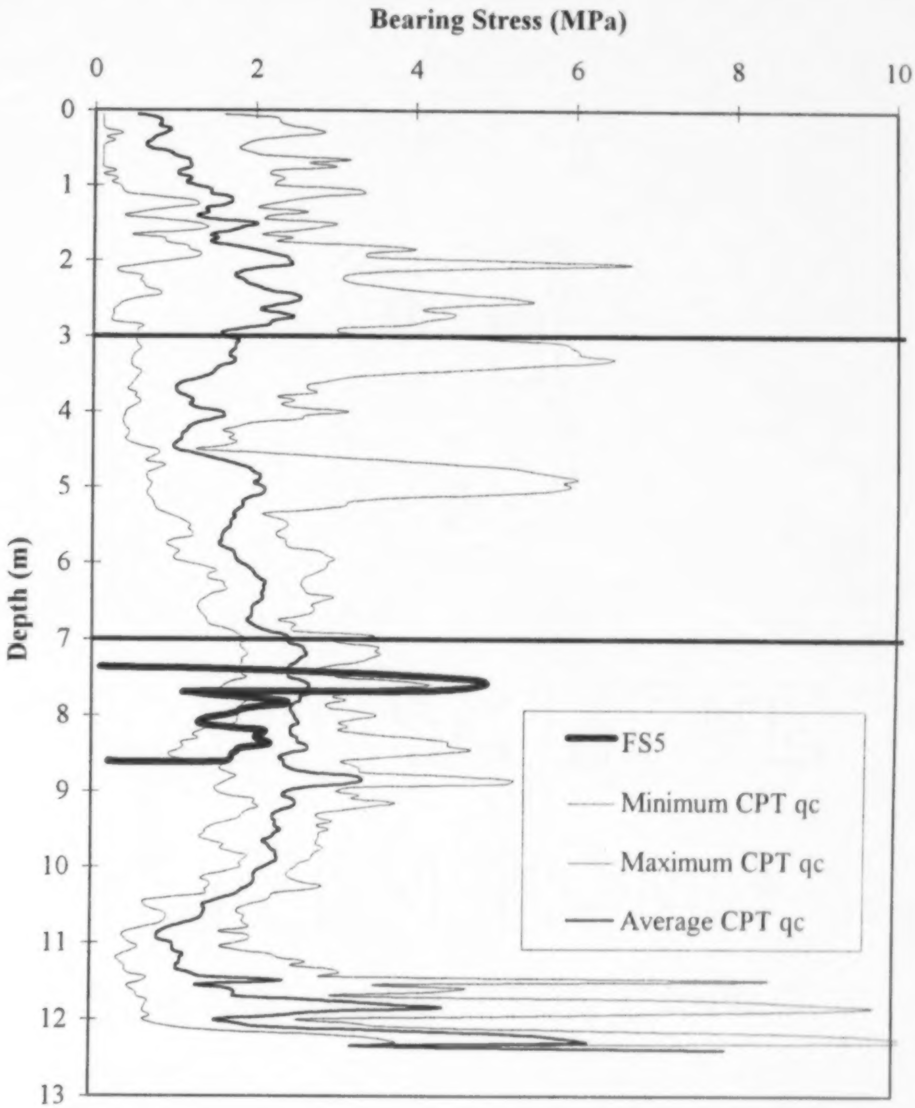

Figure 6-16 Bearing stress versus depth measured during 4" (10 cm) diameter plate load tests in borehole FS5.

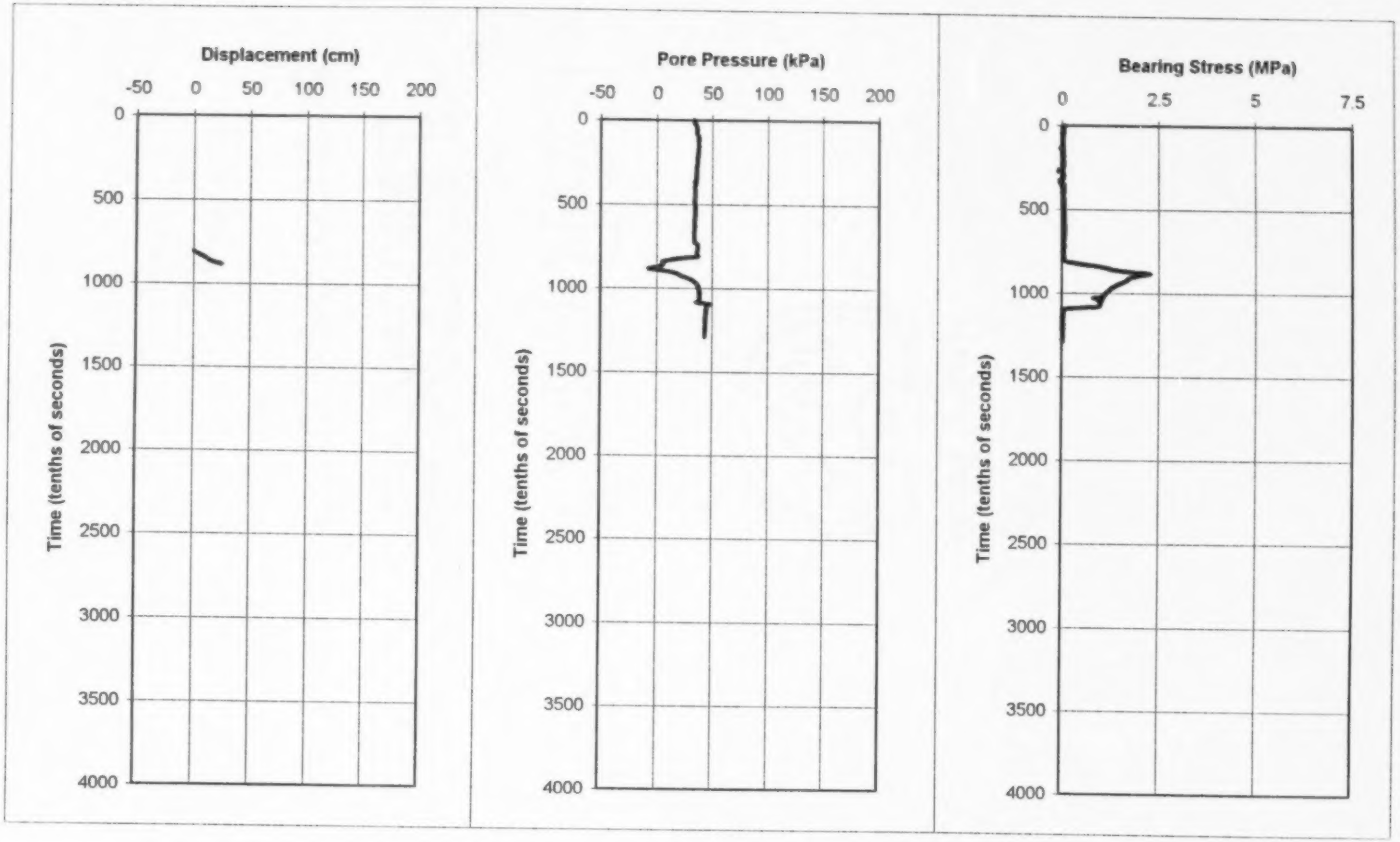

Figure 6-17 Results of 7" (18 cm) plate load test PL4-1 in terms of (a) displacement versus time, (b) pore pressure measurements versus time and (c) bearing stress measurements versus time.

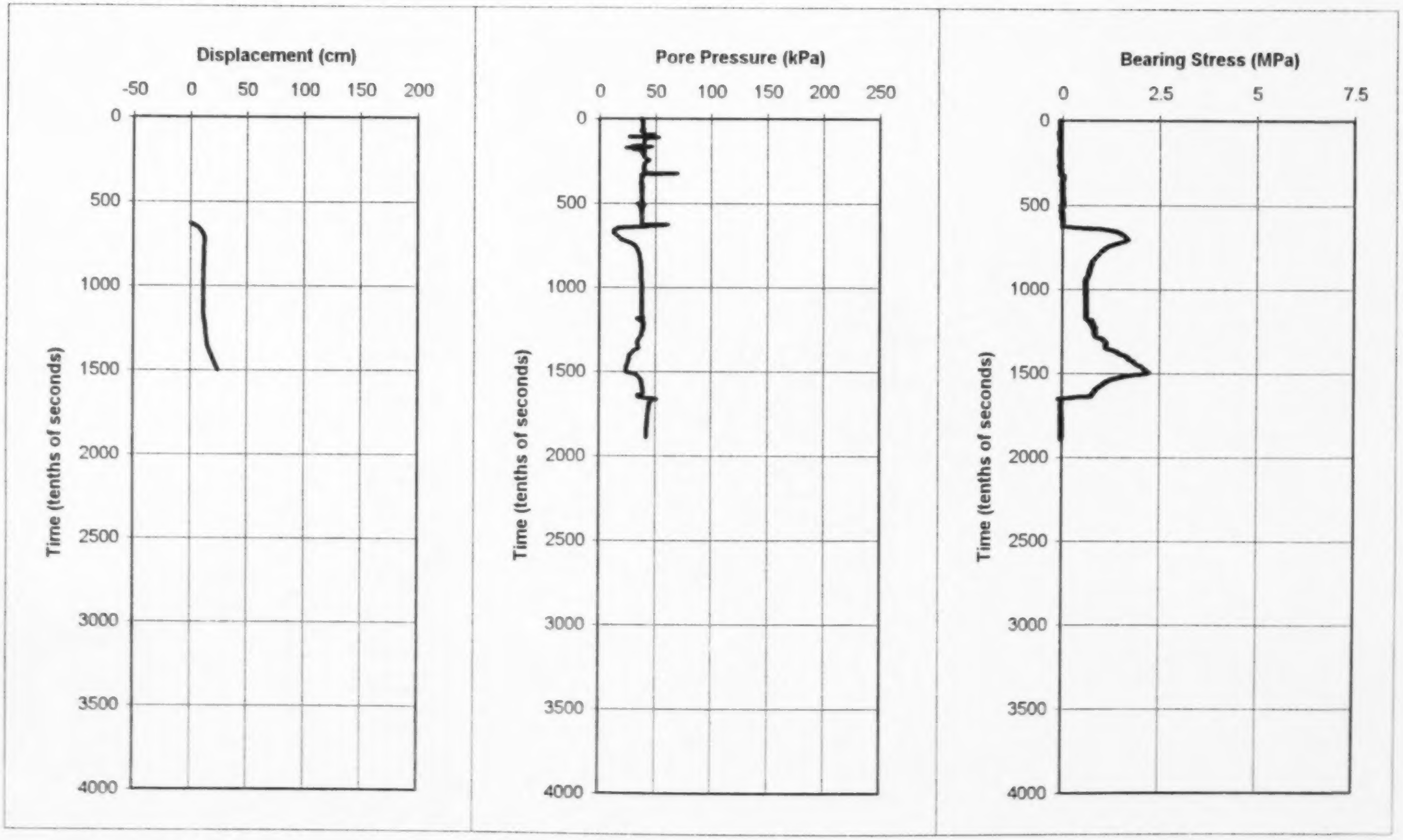

Figure 6-18 Results of 6" (15 cm) plate load test PL4-2 in terms of (a) displacement versus time, (b) pore pressure measurements versus time and (c) bearing stress measurements versus time.

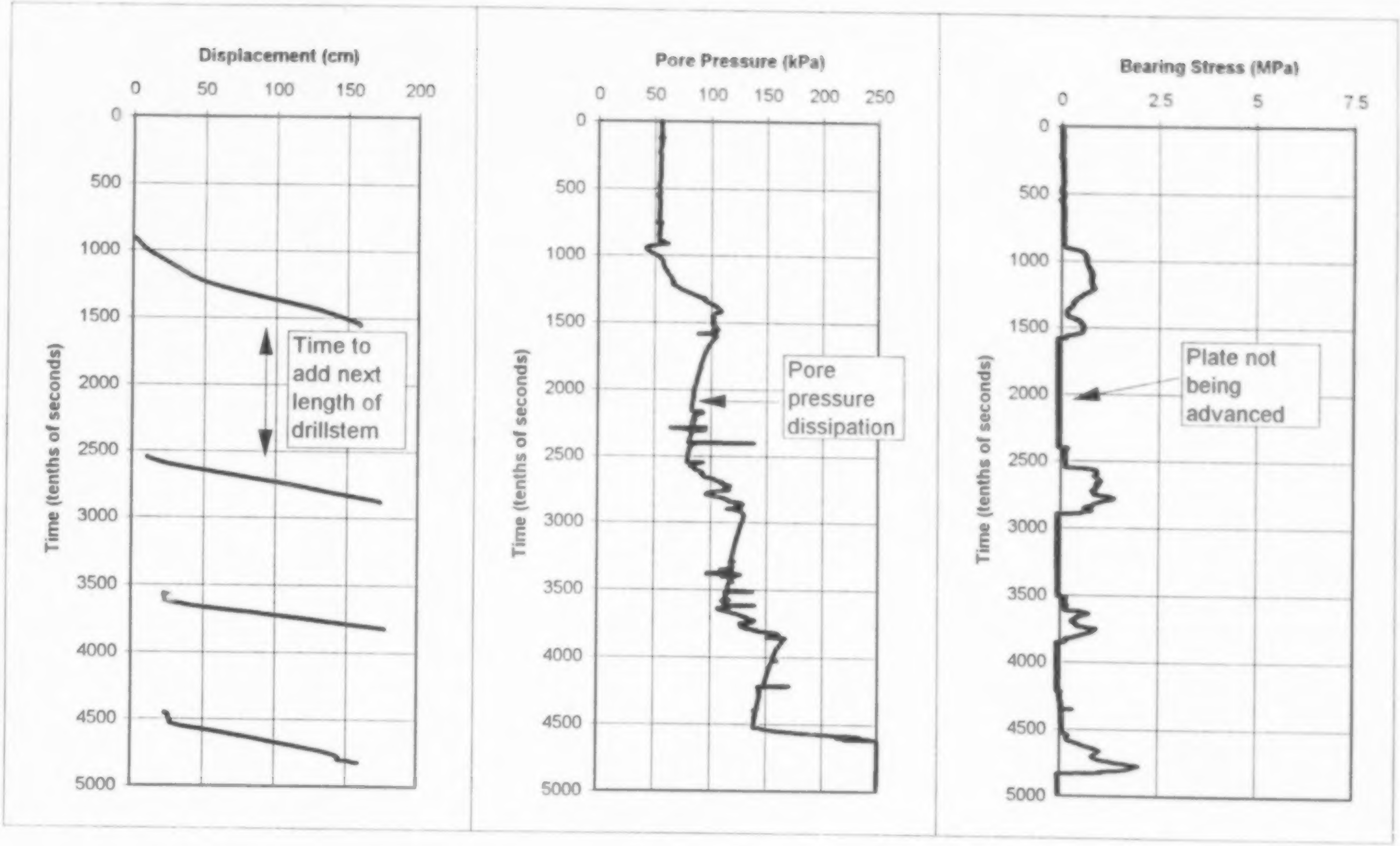

Figure 6-19 Results of 6" (15 cm) plate load test PL4-3 in terms of (a) displacement versus time, (b) pore pressure measurements versus time and (c) bearing stress measurements versus time.

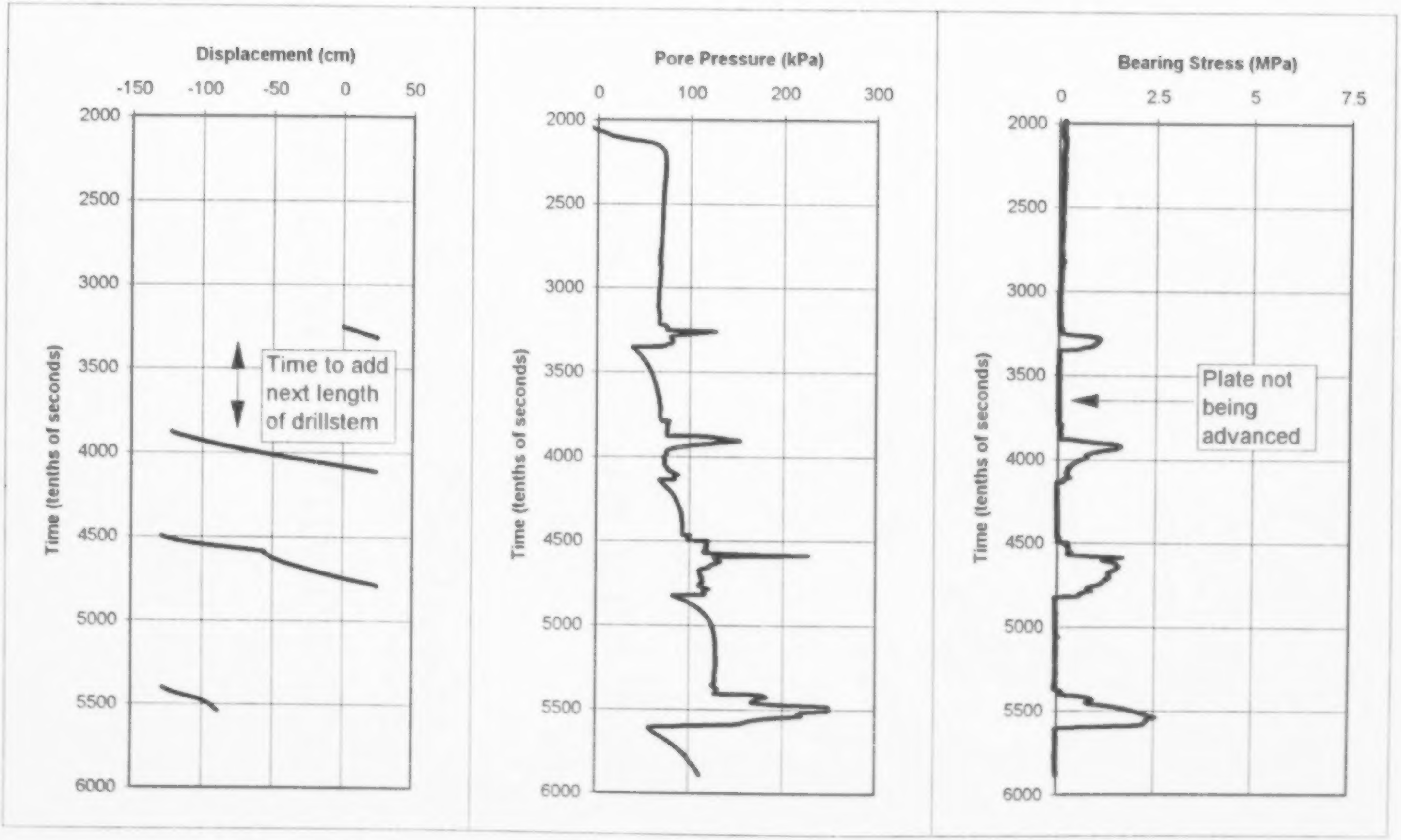

Figure 6-20 Results of 6" (15 cm) plate load test PL5-1 in terms of (a) displacement versus time, (b) pore pressure measurements versus time and (c) bearing stress measurements versus time.

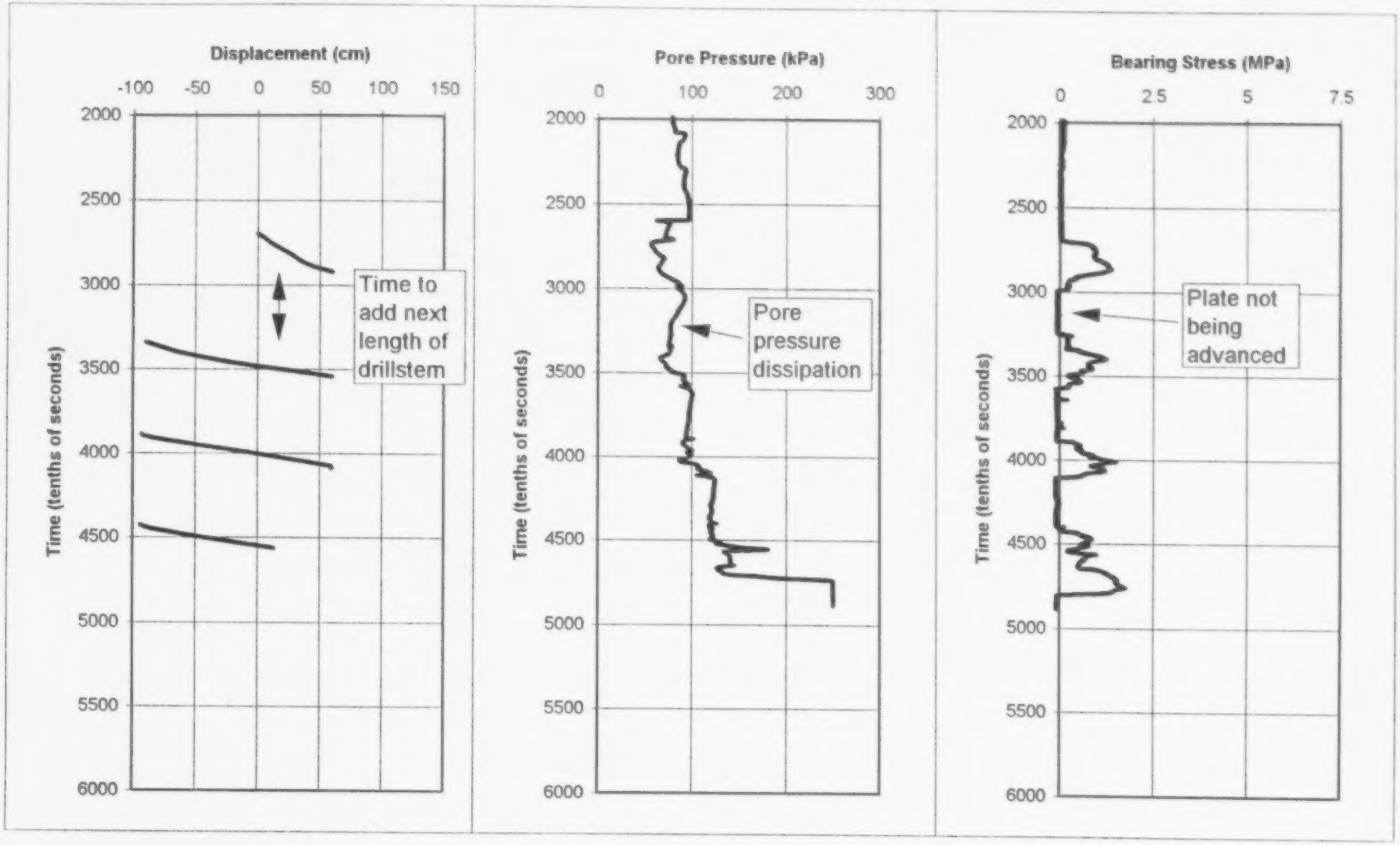

Figure 6-21 Results of 6" (15 cm) plate load test PL6-1 in terms of (a) displacement versus time, (b) pore pressure measurements versus time and (c) bearing stress measurements versus time.

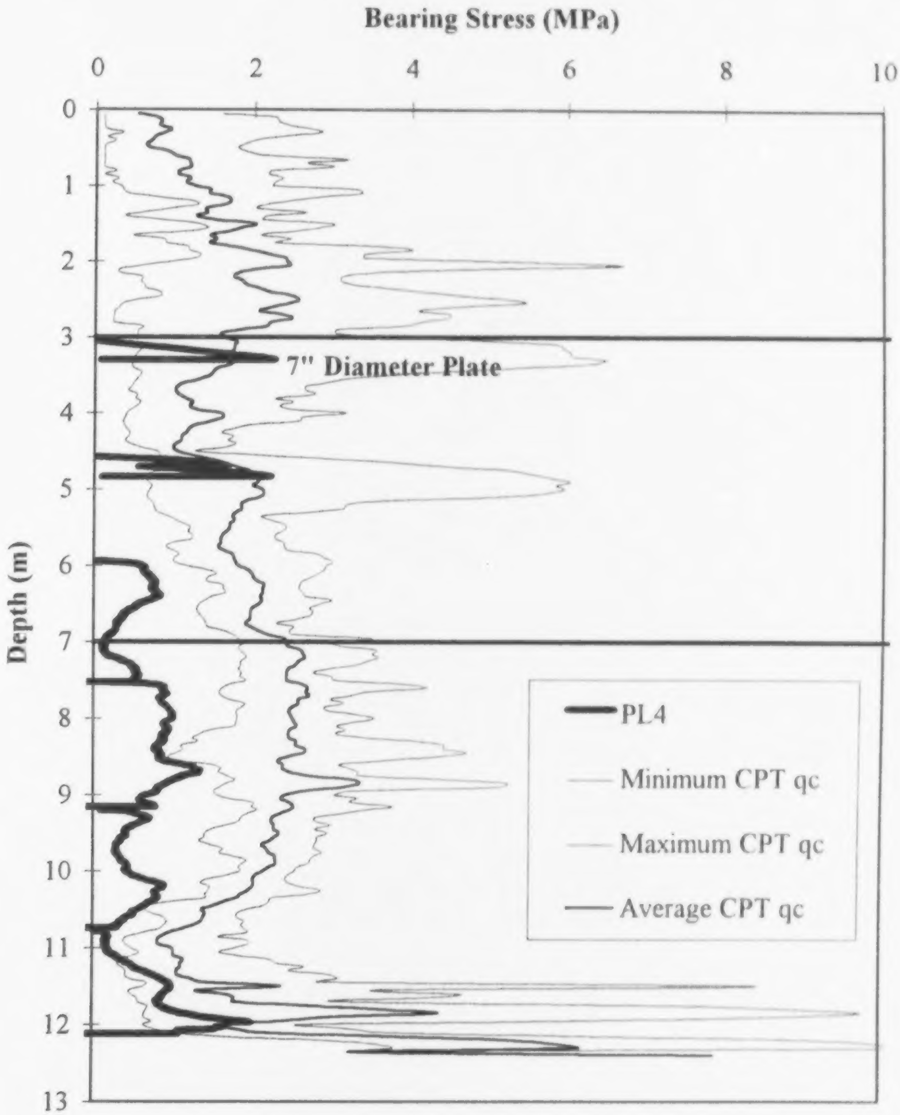

Figure 6-22 Bearing stress versus depth measured during 6" (15 cm) diameter plate load tests in borehole PL4; note the first test used a 7" (18 cm) diameter plate.

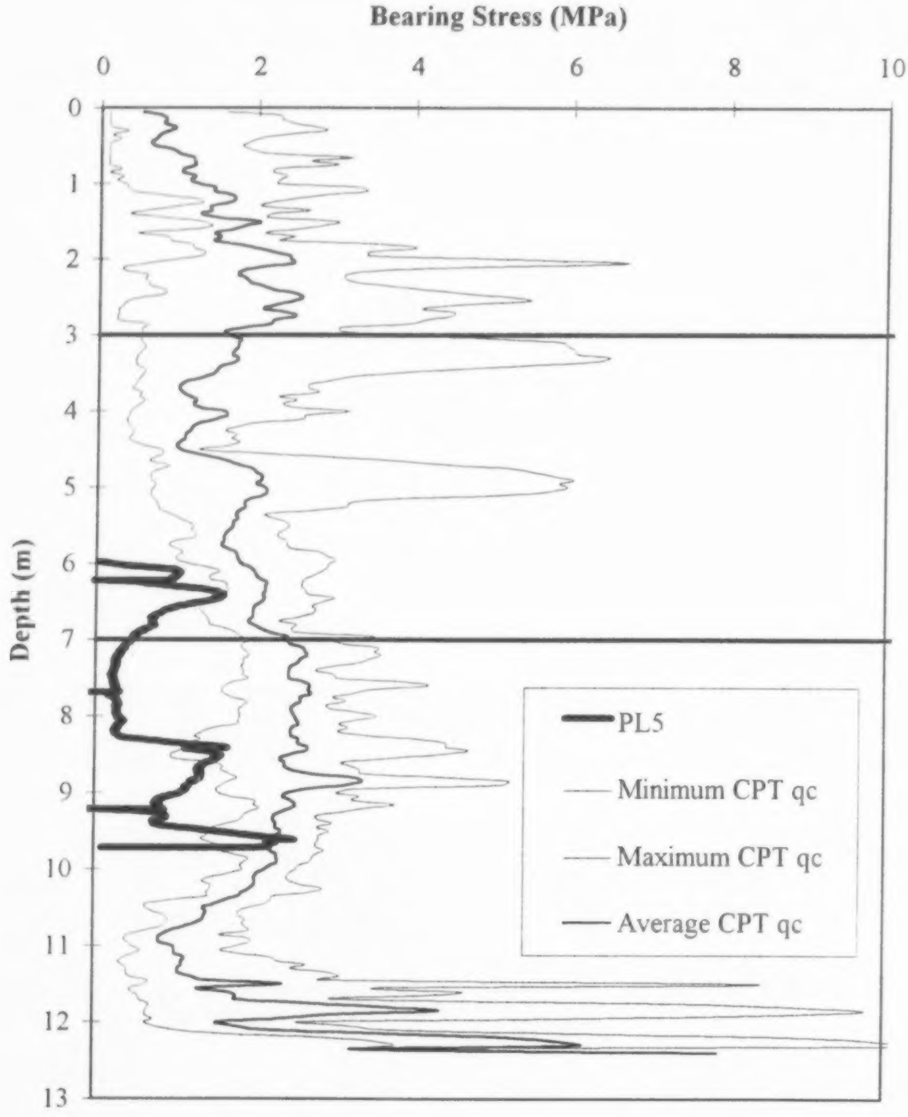

Figure 6-23 Bearing stress versus depth measured during 6" (15 cm) diameter plate load tests in borehole PL5.

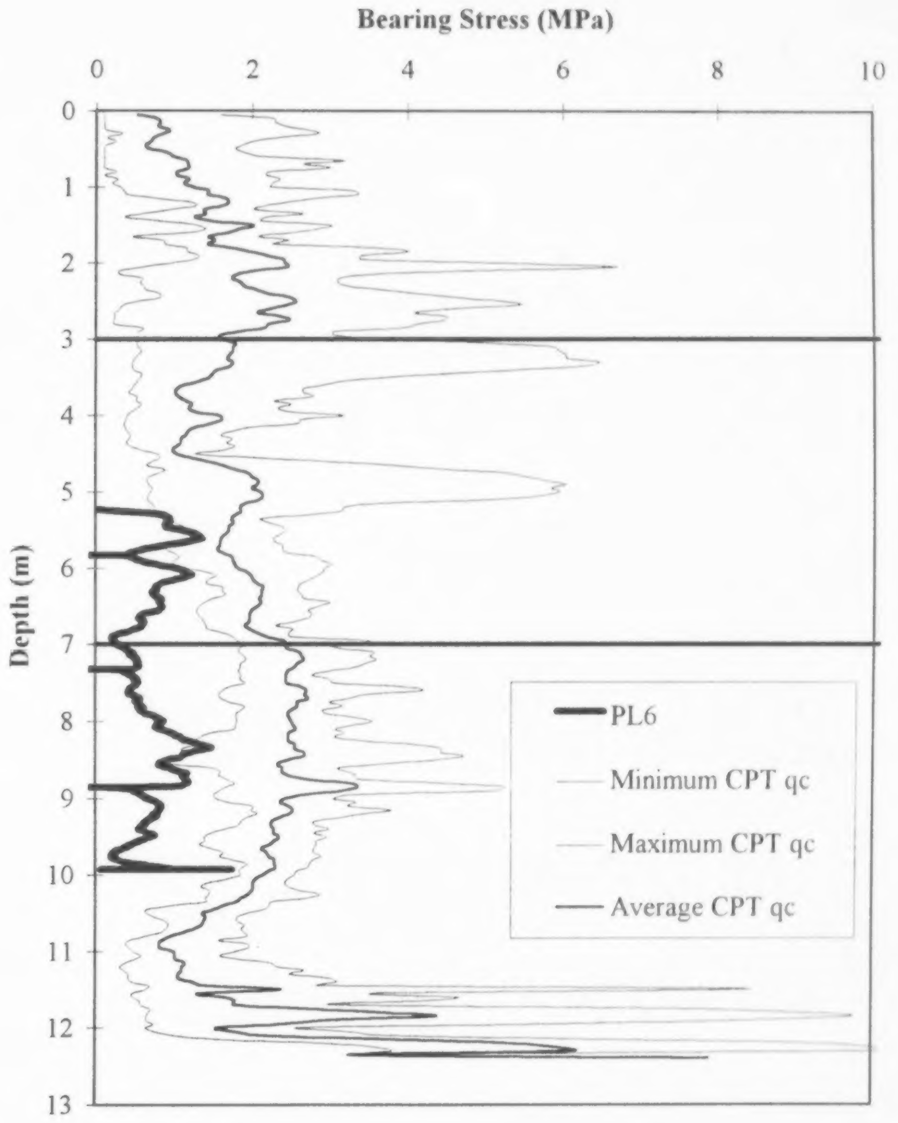

Figure 6-24 Bearing stress versus depth measured during 6" (15 cm) diameter plate load tests in borehole PL6.

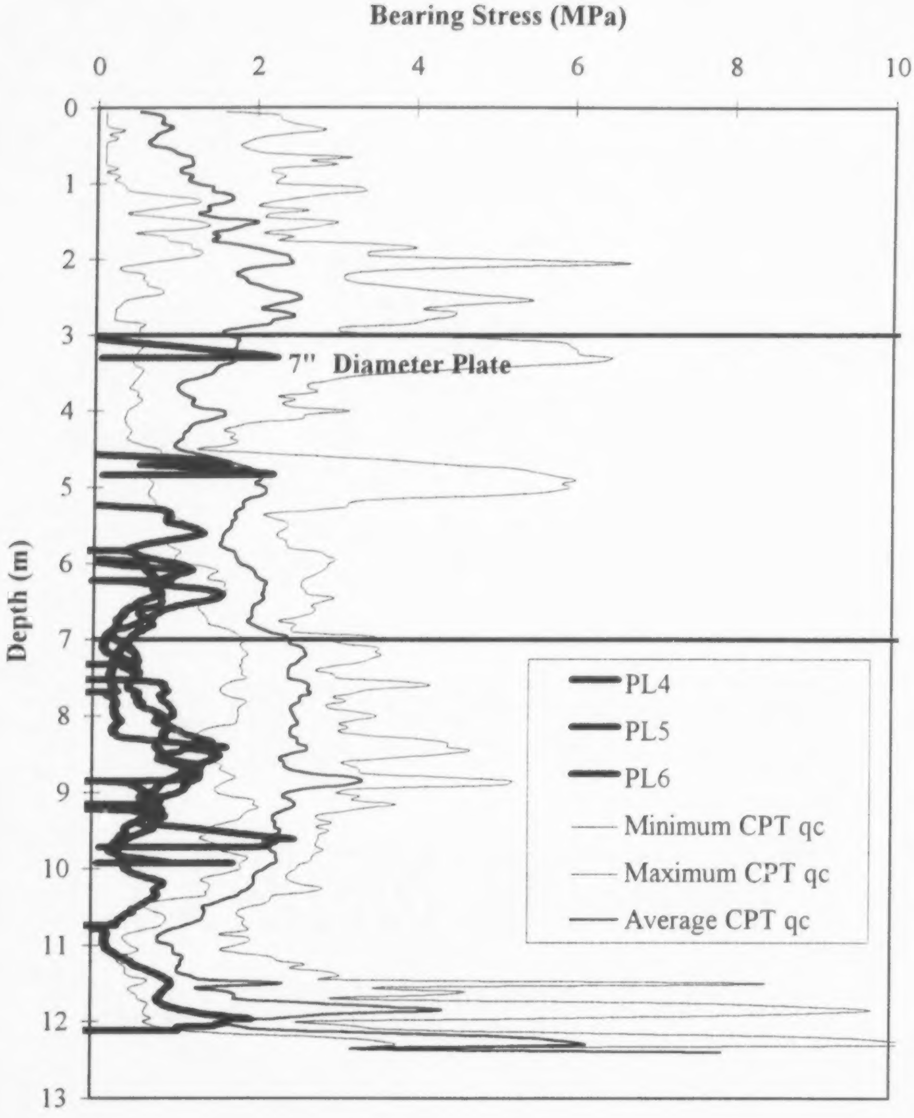

Figure 6-25 Summary of bearing stress versus depth measured during 6" (15 cm) diameter plate load tests in boreholes PL4, PL5 and PL6.

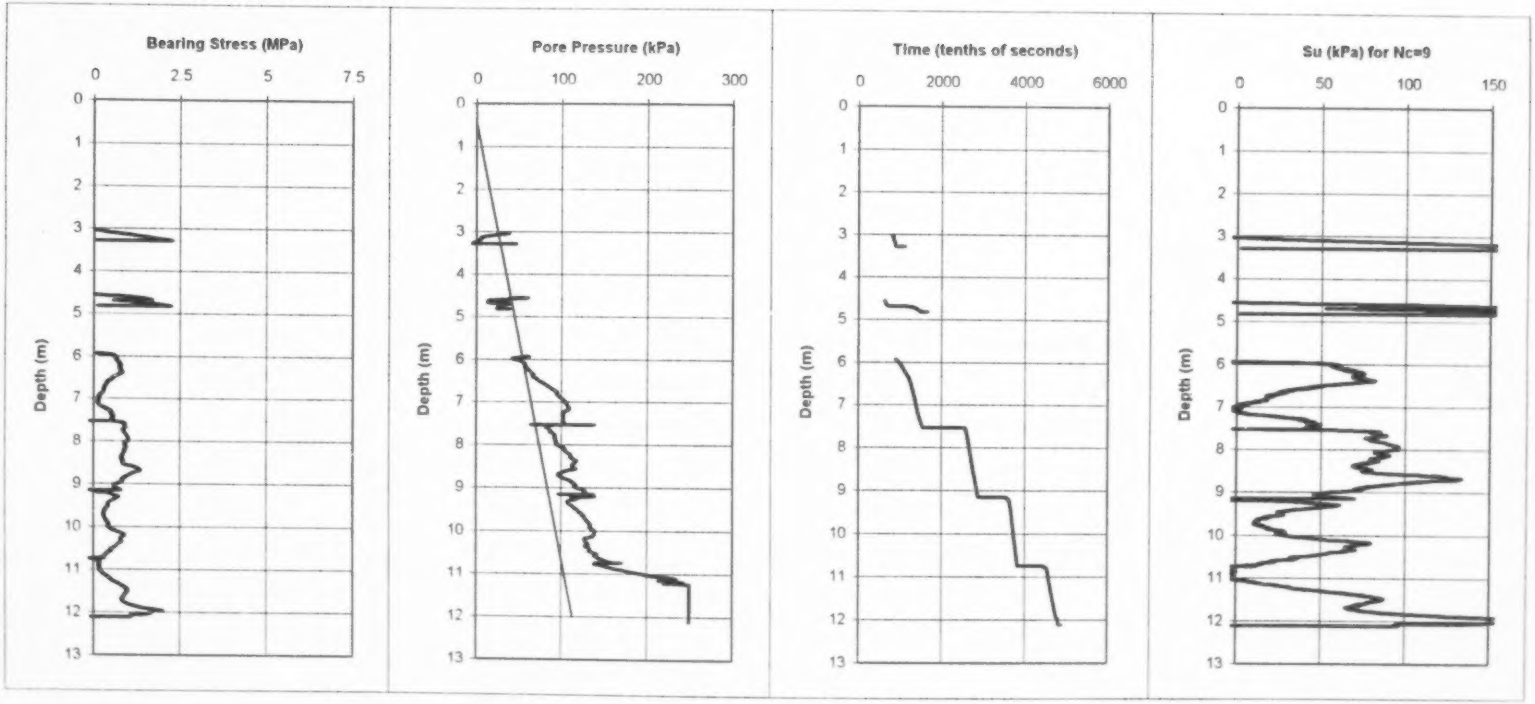

Figure 6-26 Profiles of 6" (15 cm) plate load test results versus depth in borehole PL4 in terms of (a) bearing stress, (b) pore pressure compared to hydrostatic, (c) time, and (d) estimated undrained shear strength (S_u) based on N_c=9.

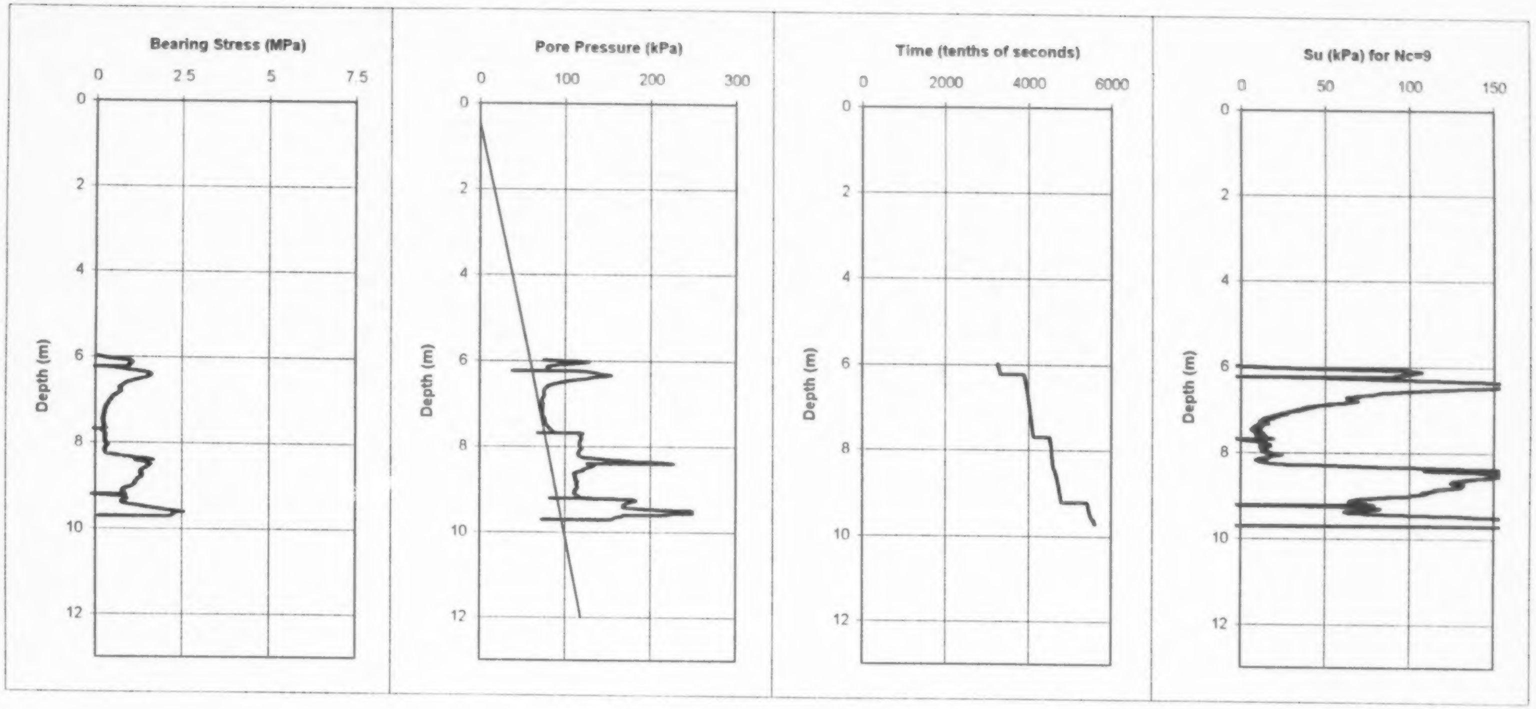

Figure 6-27 Profiles of 6" (15 cm) plate load test results versus depth in borehole PL5 in terms of (a) bearing stress, (b) pore pressure compared to hydrostatic, (c) time, and (d) estimated undrained shear strength (S_u) based on N_c=9.

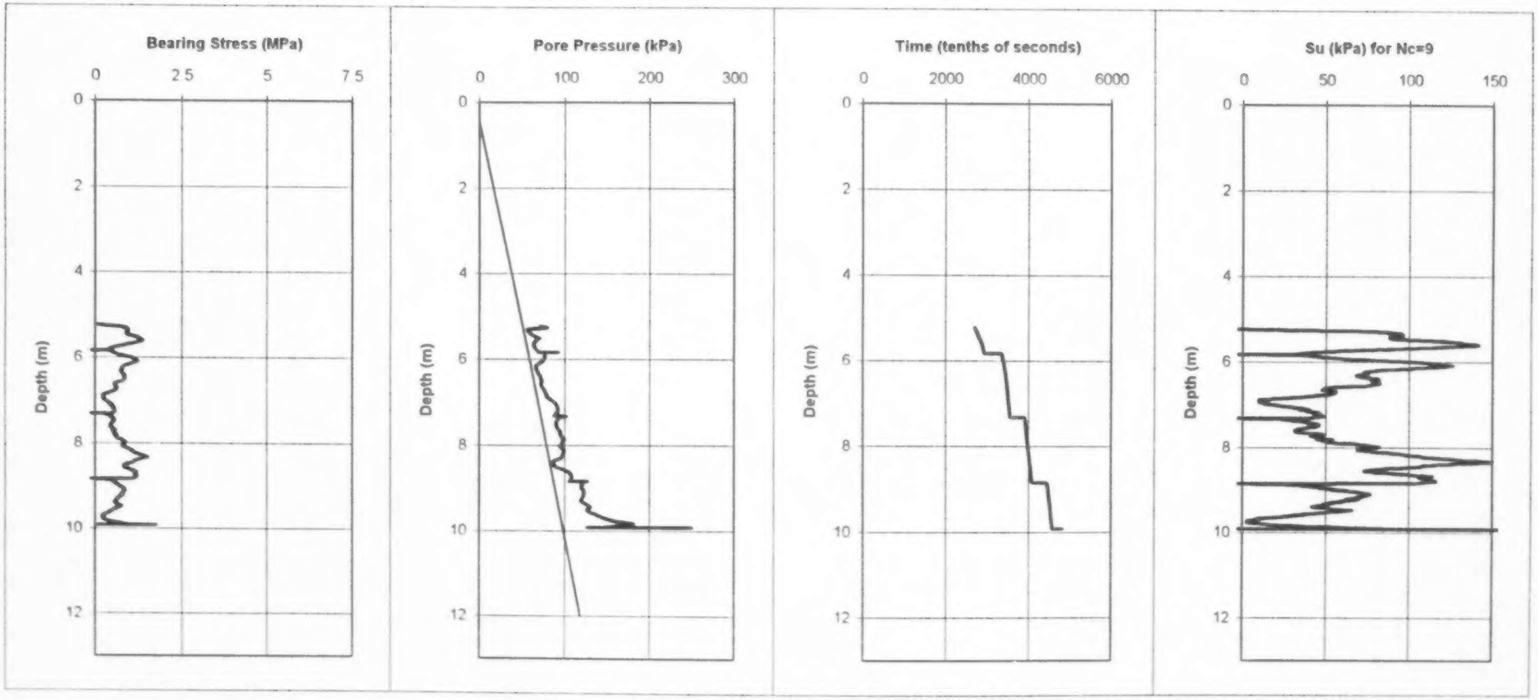

Figure 6-28 Profiles of 6" (15 cm) plate load test results versus depth in borehole PL6 in terms of (a) bearing stress, (b) pore pressure compared to hydrostatic, (c) time, and (d) estimated undrained shear strength (S_u) based on N_c=9.

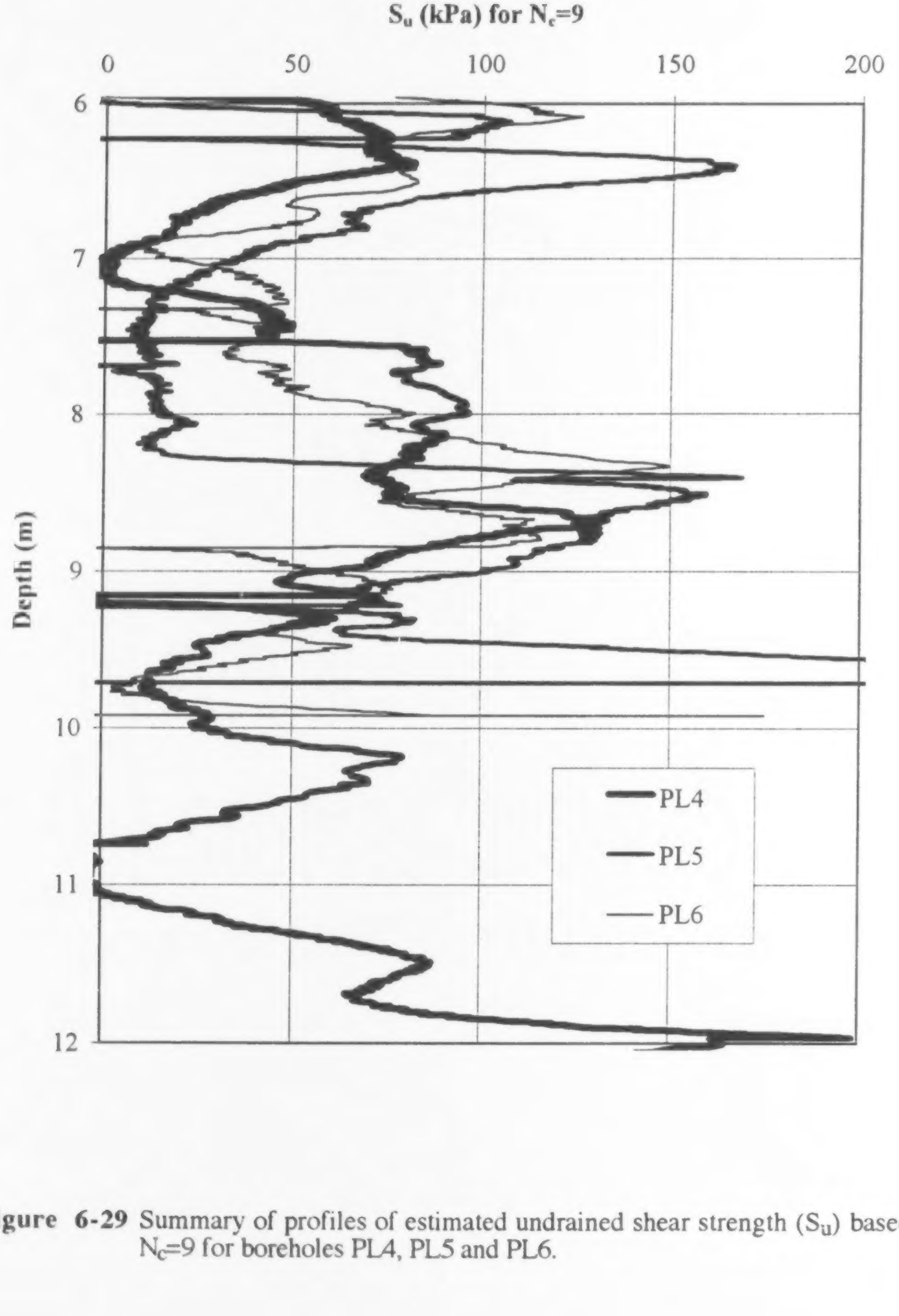

Figure 6-29 Summary of profiles of estimated undrained shear strength (S_u) based on N_c=9 for boreholes PL4, PL5 and PL6.

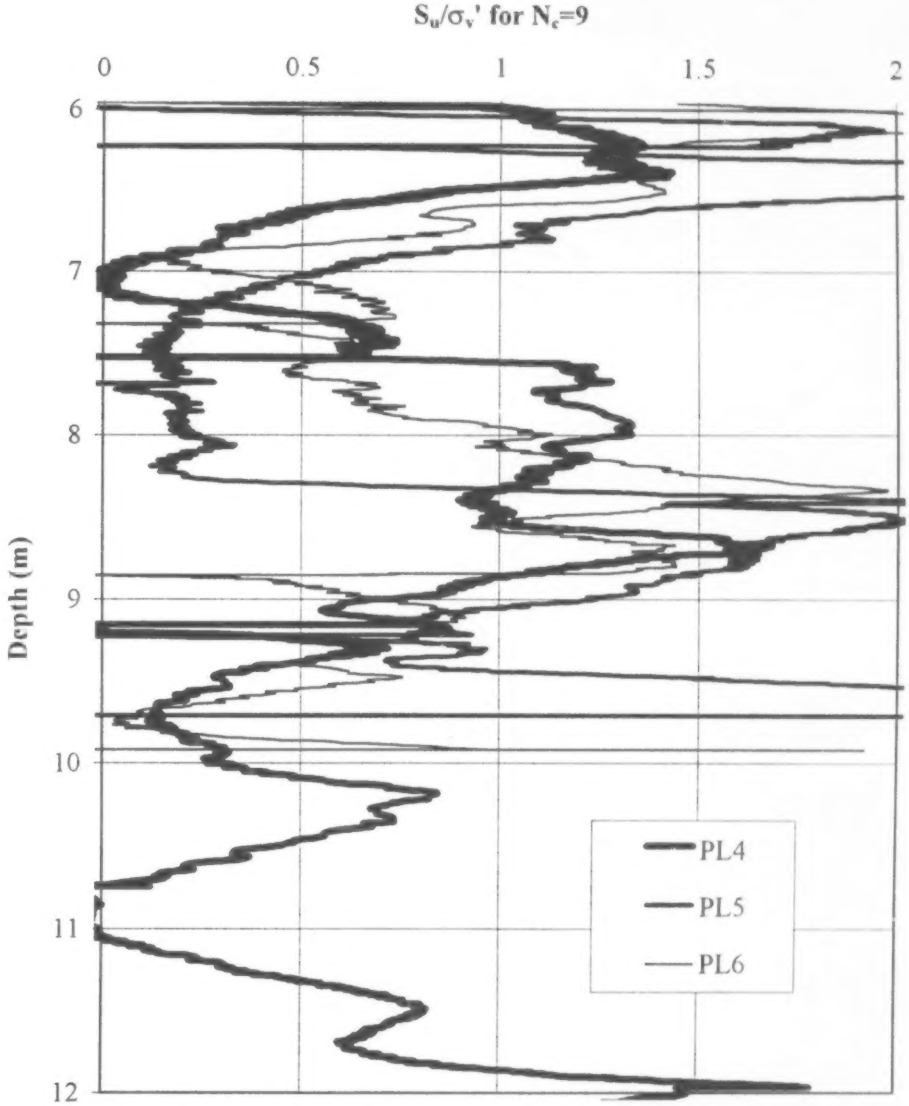

Figure 6-30 Summary of profiles of estimated ratio of undrained shear strength to vertical effective stress (S_u/σ_v') based on N_c=9 for boreholes PL4, PL5 and PL6.

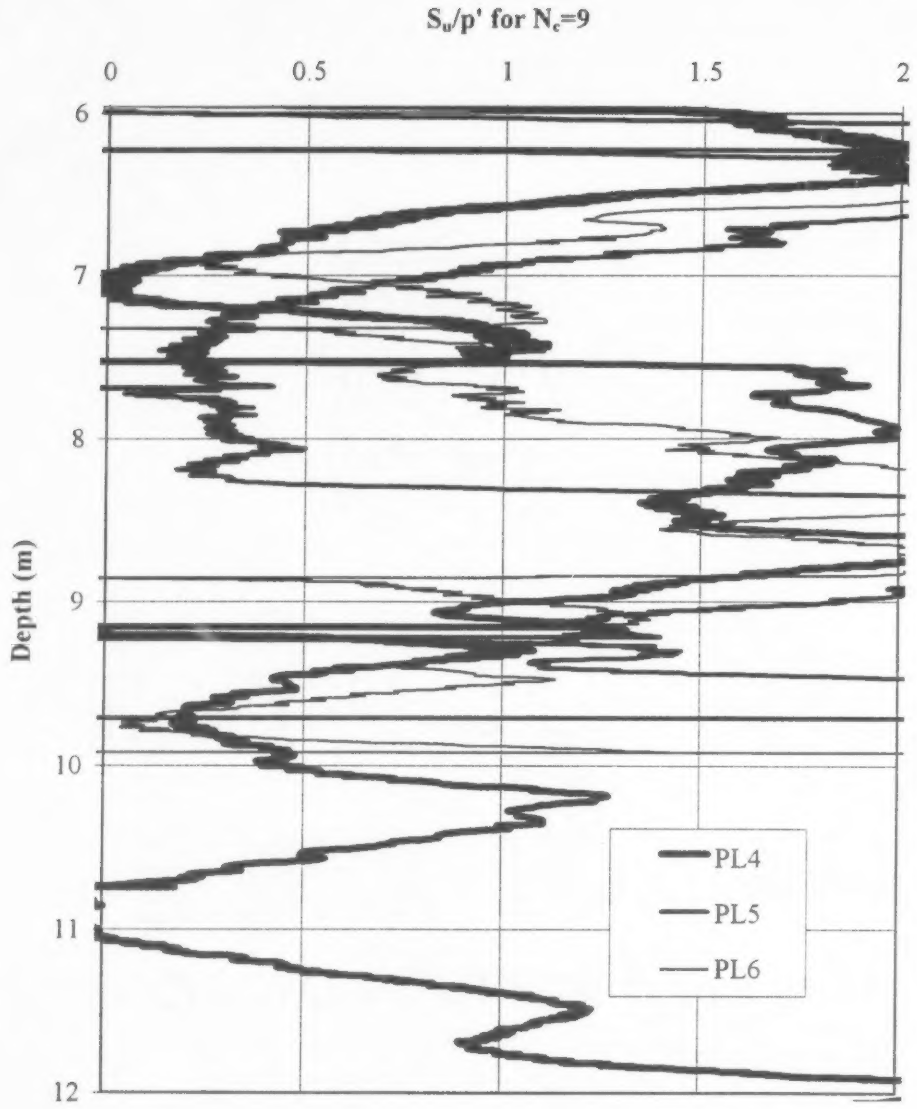

Figure 6-31 Summary of profiles of estimated ratio of undrained shear strength to mean normal effective stress (S_u/p') based on N_c=9 and K_o=0.5 for boreholes PL4, PL5 and PL6.

References

Chan, D. 1986. Finite element analysis of strain softening material. *Ph.D. Thesis*, Department of Civil Engineering, University of Alberta, Edmonton, Alberta, Canada.

Charlie, W.A., Doehring, D.O., Brislawn, J.P., Scott, C.E., and Butler, L.W. 1993. Piezovane™ evaluation of liquefaction of pile foundations. *Proceedings of the 46th Canadian Geotechnical Conference*, Saskatoon, Saskatchewan, 29-33.

ConeTec. 1995. Field report prepared for University of Alberta, CANLEX in-situ testing program. *Report on CANLEX Phase III (J-pit) In-situ Testing*, Included as Chapter 3 in the CANLEX report by Iravani et al. (1995).

Hofmann, B.A. 1996. Personal communication.

Iravani, S., Hofmann, B.A., Fear, C., Cyre, G., Lefebvre, M.E., Natarajan, S., Stahl, R., and Robertson, P.K. 1995. General Site Characterization of J-pit Site - Syncrude Canada Ltd., *CANLEX Phase III Activity 3A (General Site Characterization)*, University of Alberta.

Robertson, P.K. 1990. Soil classification using the CPT. *Canadian Geotechnical Journal*, 27(1): 151-158.

Robertson, P.K., and Campanella, R.G. 1988/89. *Guidelines for geotechnical design using the cone penetrometer test and CPT with pore pressure measurement.* Hogentogler & Company, Inc., 4th edition.

Seed, R.B., and Harder, L.F. 1990. SPT-based analysis of cyclic pore pressure generation and undrained residual strength. *Proceedings of the H. Bolton Seed Memorial Symposium*, 2: 351-376.

Skempton, A.W. 1951. The bearing capacity of clays. *Proceedings Building Research Congress*, 1.

CHAPTER 7

A RECONSIDERATION OF CASE HISTORIES USED TO EMPIRICALLY ESTIMATE UNDRAINED SHEAR STRENGTH[1]

7.1 Introduction

As Chapters 4, 5 and 6 have explained, if a sand is considered to be susceptible to flow liquefaction, an estimation of the resulting undrained shear strength (S_u) is required for any stability analysis. As mentioned in Chapter 5, one of the most commonly used methods for estimating the undrained strength of liquefied sand is the SPT-based chart by Seed and Harder (1990), based on earlier work by Seed (1987). The chart is based on 17 case histories and provides a relationship between S_u and equivalent normalized Standard Penetration Test (SPT) resistance, $(N_1)_{60}$, in clean sand. Figure 7-1 presents a version (converted to metric units) of the Seed and Harder (1990 chart), identifying the case histories by number. Table 7-1 summarizes the data presented in Figure 7-1, in tabular form. As explained already in Chapter 5, the Seed and Harder (1990) relationship consists of upper and lower bound lines which present a dilemma to the geotechnical engineer. It is not uncommon to find that the upper bound line will result in an acceptable factor of safety whereas the lower bound line will suggest a potentially unstable condition. Conservative practice often leads engineers to use the lower bound line which may result in unnecessary expenditures.

The Seed and Harder (1990) chart, as presented in Figure 7-1 is in terms of equivalent clean sand (i.e. $FC \leq 5\%$) values of $(N_1)_{60}$, denoted in this chapter as $(N_1)_{60}$-cs. For each case history, the $(N_1)_{60}$ measured in the field (denoted in this chapter as $(N_1)_{60}$-in-situ) was converted to a clean sand equivalent value using the following equation:

[7-1] $$(N_1)_{60}\text{-cs} = (N_1)_{60}\ \text{in-situ} + \Delta(N_1)_{60}$$

where the correction factor, $\Delta(N_1)_{60}$ is dependent on fines content (after Seed, 1987), as follows:

---

[1] *Much of the work contained in this chapter was done in conjunction with Dr. E.C. McRoberts, Chief Technical Officer, AGRA Earth & Environmental, Edmonton, Alberta, Canada.*

[7-2] $FC = 10\%$ $\Delta(N_1)_{60} = 1$
$FC = 25\%$ $\Delta(N_1)_{60} = 2$
$FC = 50\%$ $\Delta(N_1)_{60} = 4$
$FC = 75\%$ $\Delta(N_1)_{60} = 5$

In addition to $(N_1)_{60}$-cs, Table 7-1 presents the estimated fines content for each case history and the $(N_1)_{60}$ in-situ (Seed and Harder, 1990). Figure 7-2 presents S_u versus $(N_1)_{60}$ in-situ based on these data. As expected, the spread of the data increases, as compared to Figure 7-1, reflecting the fact that some soils (with higher fines contents) are more compressible than others giving lower penetration resistance. Note that the Seed and Harder (1990) boundary lines are not shown in Figure 7-2 because they apply only when data are plotted in terms of clean sand equivalent values of $(N_1)_{60}$. Note that, as indicated in Table 7-1, no fines content data were available for case histories 1 to 4 and 6 to 9 from Seed and Harder (1990). However, based on data from Poulos (1988), approximate fines contents for case histories 1, 3 and 4 were >60%, 30% and <5%, respectively. These fines contents were used to estimate $\Delta(N_1)_{60}$ in order to plot case histories 1, 3 and 4 in Figure 7-2. Fines contents of 25% and 20% were estimated for case histories 2 and 8, respectively. Case histories 6, 7 and 9 were assumed to consist of clean sand. Further discussions of the individual case histories are given later in this chapter.

Two uncertainties arise upon examining the database of case histories used in the Seed and Harder (1990) chart. First, it appears that some of the case histories are cases of true flow liquefaction for which S_u is meaningful; however, some of the case histories appear to be cases of cyclic liquefaction for which deformations can be associated with a loss in stiffness rather than strength (see terminology section in Chapter 1). Secondly, as was the case with the SPT-based cyclic liquefaction trigger chart by Seed et al. (1984) that was reviewed in Chapter 2, there is uncertainty over the choice of representative $(N_1)_{60}$ for each of the case histories. The intent of this chapter is to raise potential questions about the database of case histories (in order to caution the geotechnical engineer as to when and how to apply such an empirical chart), but not necessarily to answer all of the questions. The review of the database presented in this chapter assesses the case histories on a somewhat qualitative basis. Further studies into each of the individual case histories would be both interesting and useful in an attempt to answer some of the questions that are raised in this chapter and to assess the case histories in a more quantitative manner.

7.2 Historical Information about the Case Histories

The following provides a listing of some of the essential details regarding each of the case histories in the Seed and Harder (1990) chart. Also included in this listing are three case histories added to the database by Stark and Mesri (1992), and some remarks about the detailed site investigation carried out at Duncan Dam (Byrne et al., 1994). The case histories are identified by both name and number (in brackets). The numbers are used to identify individual case histories in Figures 7-1 and 7-2 presented earlier and in subsequent figures throughout this chapter.

7.2.1 Calaveras Dam (1)

Calaveras Dam is an hydraulic fill dam constructed early this century near San Francisco. The upstream shell of the dam failed on March 24, 1918, while the dam was under construction (Hazen and Metcalf, 1918; Hazen, 1918), having reached a height of approximately 61 m, with an upstream slope angle of 18.4°. The failure was not associated with any earthquake loading. Upstream movements extended 183 m beyond the original toe of the upstream slope (giving a runout to original height ratio of 3.0) and resulted in a post-failure slope angle of approximately 5.7°. Hazen and Metcalf (1918) noted that "the dam moved more rapidly on the east end and so revolved as it moved. When it stopped it had turned something like 30° from its original direction. The movement was something like the opening of a door". The dam had experienced some problems with upstream movements between June 18, 1917 and March 24, 1918, but the "final movement at the time of failure ... was very rapid. The greater part of it probably took place within a space of not more than five minutes" (Hazen and Metcalf, 1918).

The upstream shell was comprised of light porous weathered sandstone steam-shovel fill that was placed in thick lifts and, thus, was not well compacted. The dam core consisted of sluiced fill with a high clay content (silty clay with 100% passing the 0.02 mm size) and was in a semi-liquid state at failure. The question arises as to what really liquefied: the upstream shell or perhaps the core itself? No SPTs were performed at Calaveras Dam and thus values of $(N_1)_{60}$ can only be estimated. Seed (1987) estimated an $(N_1)_{60}$-cs of 12 as a typical value for the hydraulic sand fill in the original structure, based on "tests performed in recent years". This value was also adopted by Seed and Harder (1990) and Stark and Mesri (1992). Poulos (1988) adopted a much lower value of 2 for N_1, noting a degree of compaction of approximately 76% and a fines content of more than 60%. If this is assumed to be the in-situ N_1 at 60% energy, it becomes an $(N_1)_{60}$-cs of 7, using the Seed (1987) correction factor for fines, based on a fines content of greater than or equal to 60%.

Seed (1987) assigned an S_u of 750 psf, based on the post-failure configuration of the slide mass. No specific details are given as to how this value was calculated. Poulos (1988) incorporated the effects of energy and the dynamics of the failure into the calculation of S_u, resulting in calculated values of 1500 psf for the pre-failure driving stress, 250 psf for the post-failure driving stress, and 600 to 1100 psf for the mobilized undrained shear strength, with a recommendation to use an S_u of 700 psf. The same results are given by Davis et al. (1988). Seed and Harder (1990) adopted an S_u of 650 ± 50 psf, as did Stark and Mesri (1992). Although not stated by Seed and Harder (1990), it appears that this represents the range from the minimum value of 600 psf to the recommended value of 700 psf, given by Poulos (1988).

7.2.2 Sheffield Dam (2)

Sheffield Dam in California was approximately 7.6 m in height, with a downstream slope angle of 21.8° when it experienced a downstream failure as a result of cyclic loading by the 1925 Santa Barbara earthquake (Seed, 1969). The earthquake was Magnitude 6.3 and the maximum acceleration at the dam was approximately 0.15g. The downstream movements extended 30 m beyond the original toe of the downstream slope (giving a runout to original height ratio of 3.95). There was not enough information given by Seed (1969) to estimate the post-failure slope angle. It is interesting to note that the nature of the failure was similar to that of the Calaveras Dam. There were no eye-witnesses to the failure, but in summarizing the findings of the post-failure inspection, Seed (1969) referred to one of the reports which said that "the foundations of the dam had become saturated and the rise of the water as the ground was shaken formed a liquid layer of sand under the dam, on which it floated out, swinging about as if on a hinge".

The failure was attributed to liquefaction of the 5 to 6 foot thick saturated silty sand foundation underlying the base of the dam (Seed, 1969; Seed, 1987). No SPTs were performed at Sheffield Dam and thus values of $(N_1)_{60}$ can only be estimated. Seed (1969) estimated that the upper 1 to 1.5 feet of the foundation sand had a degree of compaction of approximately 76%, which corresponded to a relative density of about 35 to 40%. The rest of the foundation sand was denser. Seed (1987) estimated $(N_1)_{60}$-cs to be 6 to 8, based on an estimated relative density of 40 to 50%. It appears that this estimation was based on the type of correlations found in Skempton (1986). Seed and Harder (1990) adopted the lower value of 6 for $(N_1)_{60}$-cs, as did Stark and Mesri (1992).

Finite element analysis (Seed, 1969) indicated that the base of the dam likely failed in a progressive nature, with liquefaction occurring in elements beneath the crest first and then progressing out toward the toes. Seed (1987) assigned an S_u of 50 psf, based on a simple calculation which assumed that the entire base liquefied and acted as the slip surface with the thrust leading to failure being a result of the 15 ft deep reservoir on the upstream side of the dam. With no explanation, Seed and Harder (1990) adopted a value of 75 ± 25 psf, as did Stark and Mesri (1992).

7.2.3 Fort Peck Dam (3)

Fort Peck Dam is a hydraulic fill dam in Montana which experienced a major upstream failure on September 22, 1938, during its original construction (US Army Corps of Engineers, 1939). At the time of failure, the dam had reached a height of approximately 61 m, with a upstream slope angle of 14°. The failure was not associated with any earthquake loading. Upstream movements extended 457 m beyond the original toe of the upstream slope (giving a runout to original height ratio of 7.49) and resulted in a post-failure slope angle of approximately 2.9°. It is interesting to note that the nature of the failure was similar to that of both Calaveras Dam and Sheffield Dam in that "... the moving portion of the slope started to swing in a rotational movement as if hinged at the abutment. Through this gap the core pool drained with enormous speed. The western portion which was moving out faster and further, broke into several large blocks and came to rest in [a] fan-shaped pattern" (Casagrande, 1965). In fact, Casagrande (1965) himself noted the striking similarities between the failures of Fort Peck Dam and Calaveras Dam.

In the literature, discussion of the failure at Fort Peck Dam revolves around what actually caused the failure (Middlebrooks, 1940; Casagrande, 1965). To this day, it remains somewhat unresolved as to whether failure was a result of shear failure in the shale foundation or liquefaction of the dam. The majority of the Board investigating the failure concluded the former and did not feel that liquefaction was a major factor (Casagrande, 1965). It is plausible that a combination of the two mechanisms resulted in failure. Movement in the shale foundation due to shear failure could have produced large enough strains to trigger liquefaction in the dam above, resulting in the extensive observed failure. This theory was put forward by G. Gilboy (see discussion in Middlebrooks, 1940), who suggested that some liquefaction occurred in the dam, particularly in the transition zone (fine sand zone of the shell, next to the core). Casagrande (1965) agreed with this conclusion. A similar mechanism was noted at Nerlerk (see case history 19 described later in this chapter). It should also be noted that no berm had been built in the failure area, but that a berm was built elsewhere, where no failure occurred (Casagrande, 1965; Figure 3).

A site investigation was carried out in 1976 as a part of a re-evaluation of the dam (Marcusen and Krinitzsky, 1976). The resulting report gave relative densities of 40 to 50% in the shell material and 55% in the foundation sands. The boreholes presented in the report indicate values of $(N_1)_{60}$ greater than or equal to about 7. No other SPTs were performed at Fort Peck Dam and thus values of $(N_1)_{60}$ were only estimated by other authors. Seed (1987) estimated that the foundation sands had a relative density of 45 to 50%, based on the work by Marcusen and Krinitzsky (1976), and stated that this corresponded to an $(N_1)_{60}$-cs of 11 to 12. Poulos (1988) adopted a much lower value of 5.3 for N_1, noting a fines content of 30%. If this is assumed to be the in-situ N_1 at 60% energy, it becomes an $(N_1)_{60}$-cs of 7.3, using the Seed (1987) correction for fines, based on the fines content of 30%.

Lucia (1981, 1982) assigned an S_u of 250 psf, based on the post-failure configuration of the slide mass. With no specific explanations, Seed (1987) stated that "other studies indicate a pre-sliding driving stress of about 700 psf; a reasonably conservative value [for S_u] is probably 600 psf". Poulos (1988) incorporated the effects of energy and the dynamics of the failure into the calculation of S_u, resulting in calculated values of 1 800 psf for the pre-failure driving stress, 50 psf for the post-failure driving stress, and 500 to 1 100 psf for the mobilized undrained shear strength, with a recommendation to use an S_u of 700 psf. The same results are given by Davis et al. (1988). Seed and Harder (1990) adopted an S_u of 350 ± 100 psf, as did Stark and Mesri (1992).

7.2.4 Solfatara Canal Dike (4)

Solfatara Canal Dike refers to the north levee of the Solfatara Canal, which originally was approximately 2.1 m in height, sloping away from the canal at an angle of approximately 27°. The levee experienced a failure away from the canal as a result of cyclic loading by the 1940 Imperial Valley earthquake (Ross, 1968). The levee on the other side of the canal (the south levee) did not fail, although it did experience some deformations. The earthquake was Magnitude 7.1 and the maximum accelerations at the levee were approximately 0.1g to 0.33g. The downstream movements of the north levee extended 23 m beyond the original toe of the downstream slope (giving a runout to original height ratio of 10.95) and resulted in a post-failure slope angle of approximately 3.6°.

The north levee was comprised of very loose clean uniform fine sand. No SPTs were performed at Solfatara Canal Dike and thus values of $(N_1)_{60}$ can only be estimated. In 1967, a site investigation was conducted, consisting of one boring in what remained of the north levee and one in the south levee (Ross, 1968). Ross (1968) noted that the original north levee could be considered to have had a similar relative density to the existing south levee, which was estimated from the borings to be about 32%. Seed (1987) adopted a relative density of 30% for the dike and estimated a corresponding $(N_1)_{60}$-cs of 5. Poulos (1988) adopted a much lower value of 0 for N_1, noting a fines content of less than 5% and a relative density of about 32%. If this is assumed to be the in-situ N_1 at 60% energy, the equivalent $(N_1)_{60}$-cs would also be 0 as there is no correction to blowcount for sands with fines contents less than or equal to 5% according to Seed (1987).

Seed (1987) assigned an S_u of 130 psf, representing "the average shear stress at the base of the dike". Further details as to how this value was calculated were not given. Poulos (1988) incorporated the effects of energy and the dynamics of the failure into the calculation of S_u, resulting in calculated values of 105 psf for the pre-failure driving stress and 0 psf for the post-failure driving stress. Poulos (1988) did not calculate a specific value for the mobilized undrained shear strength, but concluded that it would have to be greater than 0 psf. Seed and Harder (1990) adopted an S_u of 50 ± 25 psf, as did Stark and Mesri (1992). No explanation was given as to the choice of this range.

7.2.5 Lake Merced Bank (5)

Lake Merced Bank refers to a fill embankment built along the edge of Lake Merced during road construction in the 1930's. It was originally approximately 9.8 m high with a slope into the lake of approximately 34°. The embankment failed into the lake as a result of cyclic loading by the 1957 San Francisco earthquake (Ross, 1968). The earthquake was Magnitude 5.3 and the maximum acceleration at the embankment was approximately 0.12g. Two major slides occurred, referred to as Slide 1 and Slide 2 by Ross (1968). Slide 1 experienced movements into the lake extending at least 18 m beyond the original toe of the slope (giving a runout to original height ratio of at least 1.84) and resulted in a post-failure slope angle of approximately 24°.

The embankment consisted of fine sand fill (termed unit C) over natural saturated surficial uniform fine sand (termed unit B). Ross (1968) felt that unit B liquefied and led to the failure. Two boreholes were drilled in 1967 as part of the site investigation reported by Ross (1968). One borehole (BH 1) was located behind the scarp of Slide 1 (i.e. in unfailed material), while the other (BH 2) was located just within the failed zone of Slide 2. Ross (1968) reported a range in raw N from 4 to 21, with an average value of 11, in unit B. For unit C, Ross (1968) reported a range in raw N from 8 to 24, with an average value of 16. However, these ranges combine the result of both boreholes, without considering that only BH2 was located within the slide area; BH 1 was outside the failure zone. Looking at the boreholes individually, one finds for unit B a range in raw N of 4 to 21 (average of 16) in BH1 (unfailed zone) and 4 to 10 (average of 7) in BH2 (failed zone). Using the results from BH2 and normalizing the data leads to a minimum $(N_1)_{60}$-in-situ of 7. Seed (1987) adopted an $(N_1)_{60}$-cs of 5, and an estimated relative density of 40%. Seed and Harder (1990) adopted an $(N_1)_{60}$-cs of 6, as did Stark and Mesri (1992), who also noted a fines content of 3%. Upon reviewing the cross-sections and results of the site investigations reported by Ross (1968), this study concluded that the soil mass that played the predominant role in the Lake Merced failures was the underwater fill. This soil was not tested as a part of the site investigation since neither of the boreholes reported by Ross (1968) penetrated the fill area. BH 1 was located well outside of the fill, through natural soil, and BH 2 was located just on the outside edge of the cut/fill boundary of the highway, again, through natural soils. The SPT results in the natural soil do not have any meaning for the fill material. Although the discussion above would suggest an $(N_1)_{60}$ of 5 to 7, this is for unit B, not the fill material, which may well have been less dense since it was placed mostly by dumping into Lake Merced. The questionable validity of the SPT data for this case history suggests that perhaps it should be removed from the database.

Seed (1987) noted that "since the duration of shaking was only about 4 seconds, it seems clear that most of the slide movements (about 100 ft) must have occurred after the earthquake motions had stopped." Seed (1987) estimated an S_u of 100 psf for the slide mass, although no explanation was offered as to how this value was calculated. Seed and Harder (1990) and Stark and Mesri (1992) also adopted an S_u of 100 psf.

7.2.6 Kawagishi-Cho Building (6)

This case history differs from all of the other case histories in the database since it involves a building located on level ground. The other case histories all involved some type of slope, from gentle slopes to steep slopes, with no overlying superstructure. The Kawagishi-Cho Building, located in Japan, experienced a foundation failure in 1964 as a result of cyclic loading from the Niigata earthquake (Seed, 1987). The earthquake was Magnitude 7.5, but it was not clear what the estimated maximum acceleration was at the site. The 4-storey building overturned as a result of what was thought to be liquefaction of the foundation sand (Seed, 1987).

Seed (1987) estimated that the $(N_1)_{60}$-cs would probably not be less than 4. The only reference that was given in Seed (1987), Seed and Harder (1990) or Stark and Mesri (1992) for this case history was a paper by Yamada (1966). This study obtained the Yamada (1966) paper, but found that it did not specifically discuss the Kawagishi-Cho Building. It did, however, refer to the Niigata Railway Station Building which was founded on piles and did not fail during the earthquake. Yamada (1966) noted that "a four-storied building which had been constructed under these considerations [i.e. the Railway Station] suffered no damage due to liquefaction while neighboring buildings without piles foundation[s] suffered severe unequal settlement or tipping". This suggests that the foundation conditions below Kawagishi-Cho Building may have been similar to those below the Railway Station. The Railway Station was located over about 12 m of loose sand overlying dense sand. Some silt zones and silty sand regions were noted. Low blowcounts of 2 to 4.5 (raw N) were recorded in the upper sand layer. Assuming similar soil conditions beneath the Kawagishi-Cho Building, an $(N_1)_{60}$ of 4 is probably a reasonable value for the foundation sand.

Seed (1987) assigned an S_u of 120 psf to this case history. This value was calculated as the average shear stress in the foundation, based on an estimated average base pressure from the building of 600 psf. Thus, it appears that S_u was calculated using the plasticity theory undrained foundation failure equation of $q_f = 5.14\ S_u$, where q_f is the base pressure from the building. Seed and Harder (1990) and Stark and Mesri (1992) also adopted an S_u of 120 psf.

7.2.7 Uetsu Railway Embankment (7)

Uetsu Railway Embankment in Japan was approximately 10 m high, with a slope angle of 29° (on the side of the embankment where failure occurred), when it failed as a result of cyclic loading by the 1964 Niigata earthquake (Yamada, 1966). The earthquake was

Magnitude 7.5, but it was not clear what the estimated maximum acceleration was at the site. The railway line embankment collapsed (in one direction only) over a 150 m length of embankment. The movements extended up to 115 m beyond the original toe of the slope (giving a runout to original height ratio of 11.5) and resulted in a post-failure slope angle of approximately 4°. Yamada (1966) noted that "a farmer who worked near the fill at a time of the earthquake recognized that the middle part of slope broke out initially and flowed over the ground surface at relatively high speed. The upper part of roadbed with ballast fell down vertically and track became like a ladder. It is recognized that only fill itself flow-slided, because the ground surface at both sides and below fill had no mark of sliding".

The railway embankment was comprised of uniform fine sand fill which was saturated at the base because it had been placed over a foundation of peat and rice fields (possibly containing swamps), which, in turn, was underlain by a clay layer with sand seams (Yamada, 1966). As a result, pore pressures may have been prevented from dissipating away from the sand fill. The ground over which the soil flowed was sloping at approximately 2° (Lucia, 1981 and 1982). No SPTs were performed at Uetsu Railway Embankment and thus values of $(N_1)_{60}$ could only be estimated. Seed (1987) felt that "since the embankment had performed satisfactorily under train loadings before the earthquake, it [was] unlikely that the [equivalent clean sand] $(N_1)_{60}$-value for the sand was less than about 3". Seed and Harder (1990) and Stark and Mesri (1992) also adopted this value.

Lucia (1981, 1982) assigned an S_u of 35 psf, based on the post-failure configuration of the slide mass. Seed (1987) adopted this value from the work of Lucia (1981, 1982). Seed and Harder (1990) adopted a value of 40 psf, with no specific explanation, as did Stark and Mesri (1992). This study indicated a range in reported values of S_u from 35 psf to 40 psf (midpoint = 37.5 psf). However, it is possible that the calculated mobilized S_u would have been larger if energy effects had been taken into account as done by Poulos (1988) and Davis et al. (1988) for some of the case records.

7.2.8 Snow River Bridge Fill (8)

The Snow River Bridge Fill case history refers to the Snow River river bed in Alaska which experienced lateral spreading as a result of cyclic loading by the 1964 Alaska earthquake (Ross et al., 1969). In particular, this case history refers to the movements and damage that occurred at Bridge 605A, crossing the Snow River, which was under construction at the time of the earthquake. The river bed had a slope of approximately 1.25°. The earthquake was Magnitude 9.2, but it was not clear as to what the estimated maximum acceleration was at the site. The lateral spreading resulted in downstream movements of the river bed of approximately 3 m. The Snow River bridges were built for the Seward Highway to cross the Snow River valley where it forms a delta at the south end of Kenai Lake. These bridges suffered extensive damage as a result of the earthquake and the lateral spreading that occurred. Bridge foundations experienced downstream movements, while the piers rotated and tilted in an upstream direction.

The river bed was comprised of glacial and fluvial sediments which consisted of medium to fine sands with thin silt lenses and fine gravel stringers. Four bridges (No. 603, 604, 605 and 606), all founded on timber bents, were in service across the river bed prior to the earthquake. Bridges 603 and 604 both suffered some damage, but remained in service following the earthquake. Bridge 606 suffered significant damage and bridge 605 was destroyed by the earthquake. Beside bridge 605 was a replacement bridge (No. 605A), which was under construction at the time of the earthquake. It too suffered significant damage, with large downstream displacements (up to 8 ft) and tilting (up to 15° in an upstream direction) of the foundations under construction. Observers noted "that 'mud' oozed up in cracks and that the 10-ft high road embankment was reduced to the level of the flood plain" (Ross et al, 1969). Ross et al. (1969) concluded that "the preferred downstream movement of the footings and upstream tilt of the pier shafts indicate liquefaction at a depth below footing level possibly accompanied by a lakeward flow along a zone that was well below the ground surface". It should be noted that the earthquake occurred in March and thus frozen ground and ice was prevalent in Alaska (Ross et al., 1969). Perhaps the frozen crust contributed to the buildup of pore pressures.

A site investigation had been carried out, prior to constructing the new bridge, 605A. The resulting boreholes are presented in Ross et al. (1969). The investigation found that the river bed consisted of interbedded fluvial soil with raw blowcounts of approximately 5 to 10 in the upper 40 to 50 feet, and increasing to about 30 at the tips of the deepest piles (about 60 feet). Seed (1987) noted that the soil involved in the lateral slide was a gravelly sand and assigned an $(N_1)_{60}$-cs of 7 in the text, but only 5 in the summary table presented in the paper. Seed and Harder (1990) adopted the higher value of 7 for $(N_1)_{60}$-cs. Stark and Mesri (1992) reported a fines content of 10 to 30% and assigned an $(N_1)_{60}$-in-situ of 5 and corrected this to an $(N_1)_{60}$-cs of 7 to 10, depending on the type of fines content correction factor that was used. The logs presented by Ross et al. (1969) suggest that an $(N_1)_{60}$-in-situ of 5 is reasonable as a lower bound value.

Seed (1987) concluded that "the residual strength of the liquefied sand was very low, probably about 50 psf, for movements of about 10 ft to have occurred". No further explanation was given as to how this value was calculated, but it is possible that something like a Newmark sliding block analysis was used. Seed and Harder (1990) and Stark and Mesri (1992) also adopted an S_u of 50 psf.

7.2.9 Koda Numa Railway Embankment (9)

Koda Numa Railway Embankment in Japan was actually a small highway embankment (Mishima and Kimura, 1970), not a railway embankment as stated by Lucia (1981, 1982) and Seed (1987). Seed and Harder (1990) and Stark and Mesri (1992) also used the term "railway embankment". From here on in, this study will use the name "Koda Numa Embankment" for this case history.

Koda Numa Embankment was approximately 3 m high, with a slope angle of 30°, when it failed as a result of cyclic loading by the 1968 Tokachioki earthquake (Mishima and Kimura, 1970). The earthquake was Magnitude 8.1, but it was not clear what the estimated maximum acceleration was at the site. The embankment moved in both directions from the centreline. The movements extended approximately 18 m beyond the original toes of the slopes (giving a runout to original height ratio of 6.0) and resulted in post-failure slope angles of approximately 4°.

The embankment consisted of fine to medium sand (Lucia, 1982) situated over clayey soil underlain by sand (Mishima and Kimura, 1970) and was only one of many embankments that failed due to the Tokachioki earthquake. In general, most of the embankments that were damaged during the earthquake were made of volcanic ashes or fine sands with low coefficients of uniformity (Mishima and Kimura, 1970). The embankments were saturated due to infiltration of rain prior to the earthquake, which may have also increased pore water pressures in the embankments (Mishima and Kimura, 1970). Most of the failures that were observed, including Koda Numa Embankment, were slope failures, not base failures, and thus were a result of the embankment itself failing, rather than the underlying foundation (Mishima and Kimura, 1970). No SPTs were performed at Koda Numa Embankment and thus values of $(N_1)_{60}$ could only be estimated. Seed (1987) felt that the $(N_1)_{60}$-cs "is not likely to be less than about 3 or 4 in a railway embankment of this type" since the embankment had performed satisfactorily under loadings prior to the earthquake, similar to Uetsu Railway Embankment. Seed and Harder (1990) and Stark and Mesri (1992) also adopted an $(N_1)_{60}$-cs of 3.

Lucia (1981, 1982) assigned an S_u of 25 psf, based on the post-failure configuration of the slide mass which flowed out over level ground. Referring to the work by Lucia (1981, 1982), Seed (1987) assigned an S_u of 25 psf in the text, but, without any explanation, adopted a value of 50 psf in the summary table presented in the paper. It is plausible that the calculated mobilized S_u would be larger than the 25 psf calculated by Lucia (1981, 1982) since energy effects were not taken into account as done by Poulos (1988) and Davis et al. (1988) for some of the case records. However, it is still not clear how the value of 50 psf was calculated. Seed and Harder (1990) and Stark and Mesri (1992) also adopted an S_u of 50 psf.

7.2.10 San Fernando Juvenile Hall (10)

San Fernando Juvenile Hall refers to a large area of very gently sloping ground located between Upper Van Norman Lake and the San Fernando Juvenile Hall facilities (Bennett, 1989). This large soil mass experienced lateral spreading towards Upper Van Norman Lake as a result of cyclic loading by the 1971 San Fernando earthquake, but no stability failure. The ground had a slope of approximately 1.5°. The lateral spread was approximately 1.2 km long and thus there was a 30 m height difference between the toe and head of the slide mass area. The earthquake was Magnitude 6.4 and the maximum acceleration at the site was estimated as 0.5g. The lateral spreading resulted in average downslope movements of the ground of approximately 0.75 m (giving a runout to original height ratio of 0.03). The overall movement was tongue-shaped in appearance, with ground ruptures defining the extent of the lateral spread. The head of the sliding mass area was located behind Juvenile Hall and the toe at the shoreline of Upper Van Norman Lake. The lateral spreading resulted in significant damage to facilities crossing the spread area. Many sand boils were observed in and near the area of the spread.

The results of investigations into the ground conditions in the spread area were reported and summarized by Bennett (1989). Both SPTs and CPTs were conducted. In general, the subsurface soils in the area originated as alluvial fan sediments and could be divided into four units: A (poorly sorted loose to medium-dense silty sand), underlain by B (very loose to loose, poorly sorted silty sand to silt), underlain by C (medium dense to dense poorly sorted silty sand), underlain by D (stiff clayey silt). Unit A was subdivided into A1 (poorly sorted loose to medium dense silty sand and medium dense sandy silt) and A2 (poorly sorted silty sand; channel deposit of fluvial origin, rather than of alluvial fan-origin like the other soil units). Unit B was subdivided into B1 (poorly sorted loose sandy silt and silty sand) and B2 (very loose poorly sorted sandy silt and silt). The groundwater table was located within unit B1. Bennett (1989) concluded that the saturated portion of unit B1 liquefied and caused the lateral spread.

Seed (1987) assigned an $(N_1)_{60}$-in-situ of 2 for the saturated sandy silt and stated that this would correspond approximately to an $(N_1)_{60}$-cs of 6. Davis et al. (1988) reported an $(N_1)_{60}$-in-situ of 4 and noted a fines content of 50 to 75% for the liquefied soil. Bennett (1989) reported a range in $(N_1)_{60}$-in-situ for unit B1 from 3.7 to 11.2 (average 7.9). Seed and Harder (1990) adopted an $(N_1)_{60}$-in-situ of 6 and corrected it based on a fines content of 65% to an $(N_1)_{60}$-cs of 10. Stark and Mesri also adopted an $(N_1)_{60}$-in-situ of 6 and corrected it based on a fines content of 65% to an $(N_1)_{60}$-cs of 10.5 to 13.0, depending on the type of correction used. It appears that the resulting values of $(N_1)_{60}$-cs reported by Seed and Harder (1990) and Stark and Mesri (1992) have been double corrected for fines content since the value that they assumed as the in-situ $(N_1)_{60}$ was 6. However, this was the equivalent clean sand value reported by Seed (1987), having already been corrected for fines content from the in-situ $(N_1)_{60}$ of 2.

Seed (1987) adopted an S_u of 140 psf. This was based on a Newmark-type deformation analysis for a maximum ground surface acceleration of 0.6g and the 5 ft of observed surface displacements. Seed (1987) noted that "the shear stress on the base of the sliding mass was only about 55 psf, and, even over a length of 800 ft, this would not be sufficient to overcome passive pressure acting on the end of the slide mass and the residual strength of the soil along the base. Apparently, sliding could only occur when the inertia forces induced by the earthquake motions were operative in the downslope direction". Davis et al. (1988) incorporated the effects of energy and the dynamics of the failure into the calculation of S_u, using a Newmark-type analysis, resulting in calculated pre- and post-failure driving stresses of 55 psf, and a mobilized undrained shear strength of 50 to 450 psf, with a recommendation to use an S_u of 200 psf. Seed and Harder (1990) assigned an S_u of 130 ± 70 psf. No explanation is given, but the upper end of the given range (200 psf) coincides with the value recommended by Davis et al. (1988). Stark and Mesri (1992) also adopted this range in S_u.

7.2.11 Lower San Fernando Dam (11)

Lower San Fernando Dam was a hydraulic fill dam in California which experienced an upstream failure as a result of cyclic loading by the 1971 San Fernando earthquake (Seed et al., 1975). The dam was fully constructed and operational at the time of the earthquake, with a height of approximately 43 m and an upstream slope angle of 21.4°. The earthquake was Magnitude 6.5 and the maximum ground acceleration at the dam was estimated as 0.5g to 0.55g. Upstream movements extended 61 m beyond the original toe of the upstream slope (giving a runout to original height ratio of 1.42) and resulted in a post-failure slope angle of approximately 8.1°. It is important to note that "the slide had already occurred when a caretaker inspected the dam crest about 5 min after the earthquake" (Seed, 1979). In fact, it appears that the slide occurred "some 30 seconds after the main shaking stopped" (Seed, 1979). Therefore, although the earthquake likely increased pore pressures, the static gravity stresses appear to be what drove the failure. "The slide nearly caused a major, uncontrolled release of the reservoir" (Davis et al., 1988).

Lower San Fernando Dam stands out as possibly being different from some of the other case histories in that it was shown to be highly stratified with interbedded silty sand and sandy silt. Borings were drilled in the downstream shell of the dam (which did not fail) after the earthquake. In those borings, Seed (1987) noted that the average $(N_1)_{60}$ for the shell material was about 16 and the relative density was about 50 to 55%. It was assumed that the pre-earthquake values would be lower and thus, Seed (1987) assigned an estimated pre-earthquake $(N_1)_{60}$-cs of 15, based on a pre-earthquake relative density of 50%. Seed et al. (1988) summarized the results of the previous investigation (1971) and investigated the soil conditions further (based on an additional site investigation in 1985) while re-evaluating the failure. "The [previous] field investigation showed that the slide occurred due to liquefaction of a zone of hydraulic sand fill near the base of the upstream shell" (Seed et al., 1988). This zone, located from elevation 1023 to 1000 feet (McRoberts and Sladen, 1992) and termed Zone 5 in the 1971 and 1985 borehole logs presented by Seed et al. (1988), consisted of stratified silty sands and sandy silts. All of the boreholes were drilled in the downstream side of the dam, which did not fail.

In Zone 5, the mean $(N_1)_{60}$-in-situ was found to be 16 from the 1971 logs and 14.5 from the 1985 logs. Seed et al. (1988) suggested that an average $(N_1)_{60}$-in-situ of 14.5 was representative of the post-earthquake Zone 5 in the downstream side of the dam. Seed et al. (1988) then estimated an average $(N_1)_{60}$-in-situ of 12.5 as representative of the pre-earthquake Zone 5 in the downstream side of the dam. The difference in $(N_1)_{60}$ of 2 between the pre- and post-earthquake conditions was based on assuming a change in void ratio from before to after the earthquake of 0.020 due to settlement, giving a change in relative density of 4% and assuming that $(N_1)_{60}/Dr^2=50$ in Zone 5. Seed et al. (1988) then went on to estimate an average pre-earthquake $(N_1)_{60}$-in-situ of 11.5 for Zone 5 upstream. The difference in $(N_1)_{60}$ of 1 between the upstream and downstream sides of the dam was based on assuming that the void ratio in the upstream side could be as much as 0.011 higher than in the downstream side. The $(N_1)_{60}$-in-situ was converted to an $(N_1)_{60}$-cs of 13.5 by Seed et al. (1988) based on a fines content of 25 to 30%.

Poulos (1988) noted an N_1 of 8.5 and a fines content of 50% for Lower San Fernando Dam, without indicating whether this was for the upstream or downstream, pre- or post-earthquake conditions. Davis et al. (1988) assigned an $(N_1)_{60}$ of 8.5 to the downstream side of Lower San Fernando Dam and noted a fines content of 50%. If this is assumed to be the in-situ $(N_1)_{60}$ in the downstream side after the earthquake, it becomes an upstream, pre-earthquake $(N_1)_{60}$-in-situ of 5.5, using the $\Delta(N_1)_{60}$ values applied by Seed et al. (1988), as outlined above. This would convert to an $(N_1)_{60}$-cs of 9.5, based on a fines content of 50%. However, if Davis et al. (1988) had used a fines content of 25 to 30%, as reported by Seed et al. (1988) for Zone 5, this would convert to an $(N_1)_{60}$-cs of 7.5.

Seed and Harder (1990) adopted the same values for $(N_1)_{60}$-in-situ and $(N_1)_{60}$-cs as Seed et al. (1988). Stark and Mesri (1992) adopted the same value of $(N_1)_{60}$-in-situ as Seed et al. (1988), but converted it to an $(N_1)_{60}$-cs of 13.5 to 17.5, depending on the type of correction factor used, based on a fines content of 25 to 30%. McRoberts and Sladen (1992) reviewed the 1985 SPT logs from Lower San Fernando Dam and found that a post-earthquake downstream $(N_1)_{60}$-in-situ of 8 would be a sensible lower bound for Zone 5. Once corrected using the corrections by Seed et al. (1988) outlined above, this would give a pre-earthquake upstream lower bound $(N_1)_{60}$-cs of 7. McRoberts and Sladen (1992) go on to say that "if such lower density weaker zones were continuous over sufficient distances, then the impact on the generalization of the case record is significant".

McRoberts and Sladen (1992) also examined the CPT logs from the 1985 field investigation. They suggested a lower bound post-earthquake downstream tip resistance of 24 bar (25 tsf) and converted this to a post-earthquake downstream $(N_1)_{60}$-cs of 7, or a pre-earthquake upstream $(N_1)_{60}$-cs of 4. However, the CPT is much more continuous than the SPT and will reflect the interbedded nature of the hydraulic fill, while the SPT will give a smoother, averaged profile. The low tip resistance of 25 tsf may well be due to the more compressible silt layers and one must be careful in converting these values to equivalent SPT $(N_1)_{60}$. The original SPT and CPT logs from the 1985 field investigation are given in a report by GEI Consultants (1988).

Seed (1987) assigned an S_u of 750 psf as the residual strength of the zone of liquefied sand in Lower San Fernando Dam. This was estimated based on the pre-failure slope configuration and by assigning known strengths to the non-liquefied zones at the toe and crest of the slope. Seed et al. (1988) re-evaluated the Lower San Fernando Dam and calculated pre-earthquake driving stresses of 850 psf. They also estimated the S_u of the hydraulic fill in question based on steady-state strength test results from the laboratory. The steady-state line was determined for post-earthquake samples from the downstream side of the dam. The pre-earthquake upstream state was estimated based on the estimated void ratio changes due to differences between pre- to post-earthquake conditions, differences between upstream and downstream conditions, sampling and handling of the downstream samples, and the assumption that the soil followed a consolidation line parallel to the steady state line. The pre-earthquake upstream strength could then be estimated by combining the pre-earthquake estimated state with the steady-state line strength results. The resulting analysis gave a pre-earthquake downstream S_u of 1050 psf and a pre-earthquake upstream S_u of 850 psf. Seed et al. (1988) recommended a more conservative interpretation of steady-state strength and suggested using the 35-percentile strength. For the upstream slope of the dam, this resulted in an S_u of 580 psf. In addition, Seed et al. reported that the "actual residual shear strength determined from configuration when slide mass stopped moving" was 400 ± 100 psf. The lower bound of this range was calculated "knowing that sliding would stop when the factor of safety attained a value of unity" and "based on the configuration of the slide mass at the end of sliding" (Seed et al., 1988). The upper bound was calculated by allowing for "the inertia effects associated with the rate of movement and a possible 70% reduction in strength of the liquefied soil as it moves into the reservoir" (Seed et al, 1988).

Davis et al. (1988) incorporated the effects of energy and the dynamics of the failure into the estimation of S_u and calculation a pre-failure driving stress of 950 psf and a mobilized undrained shear strength of 510 psf. Poulos (1988) also incorporated the effects of energy and the dynamics of the failure into his analysis and calculated a pre-failure driving stress of 1 000 psf and a range in mobilized undrained shear strength of 500 to 1 000 psf, with a recommendation to use 750 psf. Based on the findings of Seed et al. (1988), Seed and Harder assigned an S_u of 400 ± 100 psf, as did Stark and Mesri (1992).

Gu (1992) conducted finite element post-earthquake deformation analyses, based on collapse mechanics and ultimate state strengths, investigating stress redistribution at the Lower San Fernando Dam and found that the observed progressive failure would be predicted if the ultimate state strength in the hydraulic fill were lower than the average value based on laboratory tests reported by Seed et al. (1988), as described above. However, the analyses predicted that no failure would occur if the ultimate state strength were higher than the average laboratory testing value reported by Seed et al. (1989). The analyses also showed that the liquefied zone after stress redistribution may be more extensive that the initial liquefied zone directly due to earthquake shaking. This observation could explain the time delay between the end of the earthquake and the observed failure.

A final note about characterization of the Lower San Fernando Dam stems from the work by McRoberts and Sladen (1992) who stated that "an additional complication at the Lower San Fernando Dam is that the characteristic blowcounts for the failed upstream sections are based on the stable downstream sections. The hydraulic fill in Zone 5 at the Lower San Fernando Dam had fines contents of up to 90 percent (mean 50 percent) and clay contents of up to 25 percent. The clay zones were normally consolidated as was the clay core. The potential role of the clay zones and the clay core in the failure perhaps deserves further study and the relevance of this case history to clean sands can be questioned".

7.2.12 Upper San Fernando Dam (12)

Upper San Fernando Dam was also a hydraulic fill dam in California which was affected by cyclic loading from the 1971 San Fernando earthquake. The dam was fully constructed and operational at the time of the earthquake, with a height of approximately 17.6 m and a downstream slope angle of 21.8°. Although evidence indicates that pore pressures in the dam increased, the dam did not loose stability and fail. Rather, it experienced limited deformations in the downstream direction. Downstream movements were about 1.5 m (giving a runout to original height ratio of 0.09) and were damaging, but not extensive, compared to the size of the structure. In addition, the dam experienced settlements up to 1.0 m. The dam had a 100 ft (30.5 m) berm on the downstream side, which broke the otherwise continuous downstream slope into two portions. This berm may have contributed to limiting the observed deformations.

Upper San Fernando Dam also stands out as possibly being different from some of the other case histories in that it was also shown to be highly stratified. Trenches dug after the earthquake indicated that, away from the core, the hydraulic fill consisted of alternating layers of clean sand, silty sand and sandy silt (Lee et al., 1975). Borings were drilled in the dam as part of a post-earthquake site investigation and the SPT results are presented by Dept. of Water Resources (1989). These authors explained that pre-earthquake values of $(N_1)_{60}$ could be estimated by subtracting 4.5 blows from the post-earthquake measured values. This was based on an estimated relative density change of 12%, based on an estimated void ratio change of 0.08 from before to after the earthquake. Dept. of Water Resources (1989) concluded that in the hydraulic fill, the average post-earthquake $(N_1)_{60}$-in-situ was equal to 13.5 from Elevation 1170 to 1195 and 17.5 from Elevation 1145 to 1170. These corresponded to pre-earthquake average $(N_1)_{60}$-in-situ values of 9 and 13, respectively. Dept. of Water Resources (1989) concluded that the sliding occurred through the lower elevations of the hydraulic fill and that, therefore, an average $(N_1)_{60}$-in-situ of 13 was applicable. Based on a fines content of 25%, Dept. of Water Resources (1989) corrected the average $(N_1)_{60}$-in-situ of 13 to an average $(N_1)_{60}$-cs of 15. It appears that Seed and Harder (1990) referred to the work by the Dept. of Water Resources (1989) and assigned an $(N_1)_{60}$-in-situ of 13, converting this to an equivalent $(N_1)_{60}$-cs of 15, based on a fines content of 25%. Stark and Mesri (1992) also adopted an $(N_1)_{60}$-in-situ of 13, but converted it to an $(N_1)_{60}$-cs of 15 to 19, depending on the type of correction factor used, based on a fines content of 25%.

Dept. of Water Resources (1989) estimated an S_u for the liquefied soil ranging from 500 psf to 700 psf. The liquefied zone (identified as Zone IV) was predicted to have occurred in the bottom half of the hydraulic fill, based on earthquake-induced compressive strain potential analysis. The S_u values were calculated based on having a factor of safety of one for a circular failure surface through the pre-failure dam configuration and assuming strength parameters for the other, non-liquefied zones. The range in values was a function of the strength parameters assigned to the partially liquefied zone of hydraulic fill (Zone III) surrounding Zone IV. It appears that Seed and Harder (1990) referred to the Dept. of Water Resources (1989) and assigned a range in S_u of 600 ± 100 psf to the Upper San Fernando Dam, as did Stark and Mesri (1992).

7.2.13 Mochi-Koshi Tailings (13)

Mochi-Koshi Tailings refers to a tailings pond from a gold mine in Japan, which was impounded by three dams, all constructed using the upstream construction method (Marcusen et al., 1979; Ishihara, 1984). Dams 1 and 2 failed downstream as a result of cyclic loading from the 1978 Near Izu Oshima earthquake. It was not clearly stated which of the two dams Seed (1987) was referring to for this case history, but it appears from the estimated values of S_u (discussed below) that it was Dam 2. This study will include both Dam 2 (referred to as case history 13a) and Dam 1 (referred to as case history 13b). Dam 1 failed during the main shock of the earthquake (the starter dike was stable, but the additional lifts failed), while Dam 2 failed later, after a series of aftershocks, while no shaking was occurring (Marcusen et al., 1979). Accounts by eyewitnesses indicate that Dam 1 failed within 10 seconds of the main shock, while Dam 2 likely failed in a progressive manner over a much longer period of time (Marcusen et al., 1979). Dam 2 and Dam 1 had pre-failure heights of approximately 20 m and 30 m, respectively. Both dams had pre-failure slope angles of approximately 20.1°. In Dam 2, downstream movements extended 240 m beyond the original toe of the downstream slope (giving a runout to original height ratio of 12.0) and resulted in a post-failure slope angle of approximately 4.5°. In Dam 1, downstream movements extended 500 m beyond the original toe of the downstream slope (giving a runout to original height ratio of 16.7) and resulted in a post-failure slope angle of 4.5°. In both cases, the ground over which the failed material flowed was a mountainside with a slope greater than 20°. Thus, the runouts were much larger than they might have been if the ground downstream from the dams had been flatter. In fact, the tailings flowed so far that they polluted a river at the base of the slope and then were carried by the river as far as a bay about 30 km from the tailings pond.

Ishihara (1984) reports the results of a site investigation that was conducted after the two dams failed. Twelve borings were drilled in and around the tailings pond in order to examine the soil profile and conduct SPTs. The investigation found that in the tailings pond, a raw N of zero existed down to about 15 m, upon which depth the material had been consolidated to a raw N of about 3 to 7. In the starter dikes (which did not fail) and the bulldozer-rolled fills of the containment dikes, the raw N was about 5. Ishihara (1984) also noted a fines content of 85%. Seed (1987) assigned an $(N_1)_{60}$-cs of 6, based on an in-situ $(N_1)_{60}$ of about 1 in very fine-grained (silt sized) material. The larger correction to $(N_1)_{60}$ is justified because the gold tailings were probably very compressible compared to most clean sands. Poulos (1988) and Davis et al. (1988) assigned an $(N_1)_{60}$-in-situ of 0 and noted that the fines content was greater than 60%. Seed and Harder (1990) adopted an $(N_1)_{60}$-cs of 5, based on an $(N_1)_{60}$-in-situ of 0 and a fines content of 80%. Stark and Mesri (1992) also adopted an $(N_1)_{60}$-in-situ of 0 and a fines content of 80%, but calculated an $(N_1)_{60}$-cs from 5 to 7, depending on the type of fines content correction that was used.

Lucia (1981, 1982) assigned an S_u of 210 psf, based on the post-failure configuration of the tailings remaining in the tailings pond. Referring to the work by Lucia (1981, 1982), Seed (1987) assigned an S_u of 210 psf in the text, but, without any explanation, adopted a value of 250 psf in the summary table presented in the paper. For Dam 2, Poulos (1988) incorporated the effects of energy and the dynamics of the failure into the calculation of S_u, resulting in calculated values of 390 psf for the pre-failure driving stress, 100 psf for the post-failure driving stress, and 75 to 200 psf for the mobilized undrained shear strength, with a recommendation to use an S_u of 130 psf. For Dam 1, Poulos (1988) calculated 540 psf for the pre-failure driving stress, less than 50 psf for the post-failure driving stress, and 50 to 110 psf for the mobilized undrained shear strength, with a recommendation to use an S_u of 60 psf. The same results are given by Davis et al. (1988). From the results of Poulos (1988), it appears that both Lucia (1981, 1982) and Seed (1987) were referring to Dam 2 at Mochi-Koshi Tailings pond. Seed and Harder (1990) and Stark and Mesri (1992) both adopted an S_u of 250 ± 150 psf. It is not clear as to how this range was estimated, but it is assumed that this is for Dam 2, since it draws on the original work by Seed (1987).

A final note is that there is an argument for removing this case history from the database altogether, as was done by Baziar and Dobry (1995). They argued that an $(N_1)_{60}$ of zero was inconsistent with the significant back-calculated strength of 250 ± 150 psf reported by Seed and Harder (1990). They pointed out that "the SPT measurements giving this zero value were made after the failure when the soil was still very soft, with high excess pore pressures present in the silt down to a significant depth" and that "a higher blowcount would have been measured if the SPT test had been performed, either before the earthquake or long after it, as done for the other case histories".

7.2.14 Whiskey Springs Fan (14)

Whiskey Springs Fan is a gently sloping alluvial fan located in the Thousand Springs Valley in central Idaho (Harder, 1988). This soil mass experienced lateral spreading as a result of cyclic loading by the 1983 Borah Peak, Idaho earthquake, but no stability failure.

The ground was sloping at approximately 5° at the time of the earthquake. The lateral spread was approximately 60 m long and thus the height difference between the toe and head of the slide mass area was approximately 9.1 m. The earthquake was Magnitude 6.9 and the maximum acceleration at the site was estimated as 0.4g. The lateral spreading resulted in downslope movements of approximately 1.2 m and caused damage to Highway 93 which traversed the spread area near the toe of the spread. Fissures were noted at the head of the spread and buckled sod at the toe. Sand boils were observed in and near the spread area.

A site investigation was conducted in 1985, as summarized by Harder (1988). The initial field reconnaissance by Youd et al. (1985) and Andrus et al. (1986, 1987) concluded that a weak silty gravel "liquefied" as a result of the earthquake and caused the lateral spread. SPTs were performed, but the gravelly nature of the soil may have affected the results, giving high blowcounts. Therefore, Becker penetration tests (BPT) were also performed and reported by Harder (1988). When converted to equivalent SPT, the BPT results gave an $(N_1)_{60}$-in-situ of 8 and an $(N_1)_{60}$-cs of 10, based on 20% total fines content (Harder, 1988). Seed and Harder (1990) also adopted an $(N_1)_{60}$-in-situ of 8, but corrected it to an $(N_1)_{60}$-cs of 11, based on 40% fines in the sand matrix alone. Stark and Mesri (1992) also assigned an $(N_1)_{60}$-in-situ of 8, but corrected it to an $(N_1)_{60}$-cs of 11 to 15, depending on the type of fines content correction used, based on the sand matrix fines content of 40%. Andrus and Youd (1989) concluded that "the lateral spread was caused by liquefaction and shear deformation within unit C1" which was a loose silty gravel underlying the dense to very dense silty sandy gravel cap at Whiskey Springs Fan. SPT and CPT results are reported by Andrus and Youd (1989). The CPT results were converted to equivalent $(N_1)_{60}$, giving average values of $(N_1)_{60}$-in-situ of 6 to 12 for unit C1 in the various boreholes. The equivalent $(N_1)_{60}$-in-situ proposed by Harder (1988) based on the BPT logs appear to be an average value for the silty gravel layer.

Harder (1988) assigned a range in S_u to the lateral spread at Whiskey Springs Fan of 130 to 160 psf. The lower bound value was estimated using a stability analysis under static loading conditions and determining S_u for a factor of safety of one. The upper bound value was estimated using the 1978 Makdisi-Seed modification of Newmark's sliding block double integration method, based on the fact that the slide moved 1.2 m downslope. Referring to Harder (1988), Seed and Harder (1990) adopted an S_u of 150 ± 10 psf, a slightly narrower range. Stark and Mesri (1992) also adopted an S_u of 150 ± 10 psf.

7.2.15 La Marquesa Dam - Upstream Slope (15)

La Marquesa Dam was a operational small storage reservoir dam which experienced both upstream and downstream failures as a result of cyclic loading by the 1985 Central Chile earthquake (De Alba et al., 1988). This case history refers to the upstream failure; the downstream failure is addressed in case history 16. The earthquake was Magnitude 8.0 and the maximum ground acceleration at the site was estimated as 0.6g. The failures led to a loss of freeboard in the middle of the dam and necessitated an emergency draining of the reservoir after the earthquake. The upstream slope was approximately 7.9 m high with a slope of 27° at the time of failure. The upstream movements extended 11 m beyond the original toe of the slope (giving a runout to original height ratio of 1.39) and resulted in a post-failure slope angle of approximately 12.5°.

La Marquesa Dam was comprised of silty and clayey sand with a sandy clay core, founded on a layer of silty sand (referred to as "contact silty sand") over a sandy clay base. Site investigations were carried out in 1985 and 1986, as summarized in De Alba et al. (1988). Based on this information, De Alba et al. (1988) concluded that the contact silty sand liquefied during the earthquake, a major flow of this material occurred and the rest of the dam slid down and out over the liquefied layer. De Alba et al. (1988) also concluded that the average $(N_1)_{60}$-in-situ for this material under the upstream slope was estimated to be 4 with a corresponding $(N_1)_{60}$-cs of 6, based on a fines content of 30% and the blowcount correction suggested by Seed (1987). Seed and Harder (1990) also used an $(N_1)_{60}$-in-situ of 4 and an $(N_1)_{60}$-cs of 6. Stark and Mesri (1992) adopted an $(N_1)_{60}$-in-situ of 4 as well, but calculated an $(N_1)_{60}$-cs of 6 to 10, depending on the type of fines content correction used and based on a fines content of 30%. However, it is very important to note that only 5 boreholes were drilled in the zone of major damage at La Marquesa Dam: 1 at the crest, 1 roughly midway along each slope, and 1 just beyond the toe of each slope. One borehole was drilled outside the area of major damage. In the damaged area of the upstream slope, the only blowcounts measured in the contact silty sand were one blowcount in the crest borehole and one blowcount in the borehole located just beyond the toe of the slope. Thus, the available information regarding the soil layer of interest is limited. The two available blowcounts in the contact silty sand are approximately 3 and 5 (actual values were not given in the SPT logs presented by De Alba et al., 1988).

De Alba et al. (1988) estimated a range in S_u from 76 psf to 340 psf. The lower bound value was estimated based on the post-failure configuration and equals the post-failure driving stress. The upper bound value was based on the initial configuration of the slope, including horizontal stresses from the core plus inertia effects. Based on De Alba et al. (1988), Seed and Harder (1990) adopted a similar range in S_u of 200 ± 120 psf, as did Stark and Mesri (1992).

7.2.16 La Marquesa Dam - Downstream Slope (16)

The downstream slope of La Marquesa Dam was approximately 7.0 m high with a slope of 34° at the time of failure. The upstream movements extended 6.5 m beyond the original toe of the slope (giving a runout to original height ratio of 0.93) and resulted in a post-failure slope angle of approximately 18.0°.

As explained for case history 15, La Marquesa Dam was comprised of silty and clayey sand with a sandy clay core, founded on a layer of silty sand (referred to as "contact silty sand") over a sandy clay base. Site investigations were carried out in 1985 and 1986, as summarized in De Alba et al. (1988). Based on this information, De Alba et al. (1988) concluded that the contact silty sand liquefied during the earthquake, a major flow of this material occurred and the rest of the dam slid down and out over the liquefied layer. De Alba et al. (1988) also concluded that the average $(N_1)_{60}$-in-situ for this material under the downstream slope was estimated to be 9 with a corresponding $(N_1)_{60}$-cs of 11, based on a fines content of 20% and the blowcount correction suggested by Seed (1987). Seed and Harder (1990) also used an $(N_1)_{60}$-in-situ of 9 and an $(N_1)_{60}$-cs of 11. Stark and Mesri (1992) adopted an $(N_1)_{60}$-in-situ of 9 as well, but calculated an $(N_1)_{60}$-cs of 11 to 14, depending on the type of fines content correction used and based on a fines content of 20%. This study concluded that, for the upstream slope at La Marquesa Dam, a lower bound $(N_1)_{60}$-in-situ of 5.5 could be used, thus giving an $(N_1)_{60}$-cs of 7.5 for 20% fines. Again, it is very important to note that only 5 boreholes were drilled in the zone of major damage at La Marquesa Dam: 1 at the crest, 1 roughly midway along each slope, and 1 just beyond the toe of each slope. One borehole was drilled outside the area of major damage. In the damaged area of the downstream slope, the only blowcounts measured in the contact silty sand were one blowcount in the crest borehole, one blowcount in the borehole midway along the slope, and three blowcounts in the borehole located just beyond the toe of the slope. Thus, the available information regarding the soil layer of interest is limited. The $(N_1)_{60}$-in-situ of 9 reported by De Alba et al. (1988), and adopted by the other authors, appears to be the single blowcount in the contact silty sand in the borehole midway along the slope. The single blowcount in the crest borehole and the minimum value in the borehole beyond the toe are lower values.

De Alba et al. (1988) estimated a range in S_u from 266 psf to 580 psf. The lower bound value was estimated based on the post-failure configuration and equals the post-failure driving stress. The upper bound value was based on the initial configuration of the slope, including horizontal stresses from the core plus inertia effects. Based on De Alba et al. (1988), Seed and Harder (1990) adopted a similar range in S_u of 400 ± 150 psf, as did Stark and Mesri (1992).

7.2.17 La Palma Dam (17)

La Palma Dam was another operational small storage reservoir dam which failed as a result of cyclic loading by the 1985 Central Chile earthquake (De Alba et al., 1988). Major sliding occurred in the upstream slope whereas the downstream slope suffered very little damage. La Palma Dam was approximately 11 m high with an upstream slope angle of 34° at the time of failure. The earthquake was Magnitude 8.0 and the maximum ground acceleration at the site was estimated as 0.46g. Upstream movements extended 5 m beyond the toe of the original upstream slope (giving a runout to original height ratio of 0.45) and resulted in a post-failure slope angle of 17°. The reservoir was not full at the time of failure, but it was drained after the earthquake in order to prevent any further failure.

La Palma Dam was comprised of clayey silty sand (with a sandy clay core), founded on a thin loose silty sand layer (mostly under the upstream slope) underlain by a base of sandy clay and clayey sand. On the upstream side, there was also a layer of silt and silty sand between the thin loose silty sand layer and the base soil. Site investigations were carried out in 1986, as summarized by De Alba et al. (1988). Based on this information, De Alba et al. (1988) concluded that the thin saturated loose silty sand layer under the upstream portion of the dam liquefied during the earthquake and that the rest of the dam moved down and out over the liquefied layer. In addition, De Alba et al. (1988) hypothesized that liquefaction did not occur beneath the downstream slope because the loose silty sand layer was above the groundwater table and thus not saturated at this location. De Alba et al. (1988) also concluded that the $(N_1)_{60}$-in-situ for the loose silty sand layer beneath the upstream shell was about 3 and that this would correspond to an $(N_1)_{60}$-cs of 4, based on a fines content of 15% and the blowcount correction proposed by Seed (1987). Seed and Harder (1990) adopted the same values as De Alba et al. (1988). Stark and Mesri also adopted an $(N_1)_{60}$-in-situ of 3, but calculated an $(N_1)_{60}$-cs ranging from 4 to 7, depending on the type of fines content correction used and based on 15% fines. It is important to note that only 4 boreholes were drilled in the major damage area at La Palma Dam: 2 in the crest area (one on each side of the core) and 2 located midslope. One borehole was drilled towards the right abutment, outside the area of major damage. In the damaged area of the upstream slope, the only blowcounts measured in the loose silty sand layer were one blowcount in each of the two boreholes located midslope. Thus, the available information regarding the soil layer of interest is limited. The two available blowcounts in the loose silty sand layer are approximately 2 and 3.

De Alba et al. (1988) estimated a range in S_u from 120 psf to 300 psf for the upstream slope of La Palma Dam. The lower bound value was based on the post-failure configuration and equals the post-failure driving stress. The upper bound value was based on the initial configuration of the slope, including horizontal stresses from the core plus inertia effects. Based on De Alba et al. (1988), Seed and Harder (1990) adopted a similar range in S_u of 200 ± 100 psf, as did Stark and Mesri (1992).

7.2.18 Lake Ackerman (18)

Lake Ackerman is a case history added to the Seed and Harder (1990) database by Stark and Mesri (1992). Lake Ackerman refers to a hydraulic fill road embankment, which was constructed in the 1950's, oriented in an east-west direction across the north end of Lake Ackerman in Michigan. It was originally about 6.4 m high with a slope into the lake of approximately 26.6°. The embankment failed into the lake as a result of cyclic loading from six 22-ton seismic trucks generating seismic signals for a deep reflection survey to map potential deep oil-bearing formations (Hryciw et al., 1990). The estimated average cyclic stress ratio generated by the seismic trucks was 0.12. A 91 m long section of the embankment failed and took three trucks with it as it moved into the lake. Fortunately there were no fatalities. The movements into the lake extended approximately 12 m beyond the original toe of the slope (giving a runout to original height ratio of 1.88) and resulted in a post-failure slope angle of approximately 7.5°. It is interesting to note that "the embankment did not fail until the trucks had vibrated across half of the embankment over liquefaction-prone soil" (Hryciw et al, 1990). Investigations after the failure revealed that "an intact section of the embankment was found submerged in the lake" (Hryciw et al., 1990), having moved significantly outward relative to its initial position.

The road embankment at Lake Ackerman was comprised of medium to fine sand fill which had been placed by end-dumping into the lake and was therefore very loose. The lake bottom originally consisted of peat and "muck", but this was removed prior to construction of the embankment. The fill which had been placed above lake level was moderately compacted and covered with a layer of compacted gravel followed by the roadway bitumen. The road rose from west to east with a 3% grade. A site investigation was carried out after the failure, as reported by Hryciw et al. (1990). Tests (SPT, DMT, Push-auger) were conducted both within and outside the failure area. The results of the SPT indicated value of $(N_1)_{60}$ of 6 to 8 in the failed section, but only 1 to 4 in the unfailed section. Hryciw et al. (1990) believed that these apparently inconsistent results could be explained as follows: "the soil tested [in the failure zone] may have originally been the denser sand above the ground water that had dropped into the void left by the liquefied soil" and "it is believed that the soil [in the unfailed zone] liquefied but did not flow. Therefore, Hryciw et al. (1990) concluded that an $(N_1)_{60}$-in-situ of 3 was representative of the original pre-failure density of the loose sand fill. Stark and Mesri (1992) also assigned an $(N_1)_{60}$-in-situ of 3, but corrected it to an $(N_1)_{60}$-cs of 4, based on a fines content of 0 to 5%.

Hryciw et al. (1990) assigned a range in S_u of 170 psf to 260 psf to the embankment at Lake Ackerman. Both strengths were estimated using two-dimensional stability analyses, one in the failed zone and one in the zone that had not failed, although the seismic trucks had passed over it. Analysis for failure to have occurred (i.e. factor of safety equal to one) in the unfailed zone gives the lower bound value of 170 psf. The upper bound value of 260 psf is given by analysis for failure to have occurred (i.e. factor of safety equal to one) in the failed zone. The analysis appears to have assumed a single S_u throughout both the loose sand fill and the denser sand above the groundwater table. As a result, it may overpredict the range in S_u.

7.2.19 Nerlerk Embankment (19)

Nerlerk embankment is a case history added to the Seed and Harder (1990) database by Stark and Mesri (1992). Nerlerk embankment was an oval-shaped (in plan) subsea hydraulic fill berm intended to support an offshore drilling platform in the Canadian Beaufort Sea. While under construction, Nerlerk embankment experienced 5 separate failures in various directions in 1983 (Sladen et al., 1985a). In addition, the embankment had experienced a previous failure in 1982 (Rogers et al., 1990). The failures were not associated with any earthquake loading. At the times of failure in 1983, the embankment had reached a height of about 24 m with a slope angle of approximately 12.65°.

Movements of the largest slide in 1983 (Slide 3) extended 100 m beyond the original toe of the embankment slope (giving a runout to original height ratio of 4.17) and resulted in a post-failure slope angle of 1.5°.

As for Fort Peck Dam, there are conflicting views in the literature as to whether or not Nerlerk Embankment actually liquefied. Sladen and Hewitt (1989) felt that the placement techniques used at Nerlerk (involving hopper dredges) resulted in very loose hydraulic fills which, with additional placement of fill, were triggered to liquefy. Been et al. (1987) concluded that the slides were a result of a translational failure through the 1 to 2 metres of soft clay beneath the berm. Sladen et al. (1987) disagreed with this analysis. Been et al. (1987) also concluded that the sand fill could not have liquefied because most of the sand state was inferred to be dilatant, based on CPT-state parameter correlations proposed by Been and Jefferies (1986, 1987). However, as shown later by Sladen (1989a, 1989b), the correlations did not correctly account for the effects of stress level and, therefore, they may not have correctly estimated state parameter from the CPT results. Upon revisiting the slides in Nerlerk Embankment, Rogers et al. (1990) concluded that the mechanism leading to failure likely involved both the underlying clay and the loose sand fill. Strains in the underlying weak clay may have provided the trigger for failure of the loose sand fill. Note that a similar phenomenon may have occurred at Fort Peck Dam, in that strains in the underlying weak shale may have triggered the failure of the cohesionless soil above. Finally, evidence such as bowl-shaped crests and narrower-necked portions below the bowl (Sladen et al., 1985a) indicated that the failure was of a progressive nature. Sladen et al. (1985a) remarked that "failures started at locally oversteepened side slopes and retrogressed to form bowl-shaped crests". Sladen et al. (1987) provide a good description of the features of the embankment failures and note that the failures were very brittle in nature, similar to other previous flow slides in sand.

Nerlerk Embankment was comprised of hydraulic fill placed by hopper dredges. In 1982, a layer of Ukalerk sand was placed on the seabed, followed by a layer of Nerlerk sand. At the time of failure in 1983, an additional layer of Nerlerk sand was being placed. Nerlerk sand had about 10% fines, while Ukalerk sand had about 2% fines (Sladen et al, 1985a). There is some argument over the appropriate fines content for Nerlerk sand; Rogers et al. (1990) suggest a lower fines content of 2%. None of the slides involved the underlying Ukalerk sand (Sladen et al, 1985a). No SPTs were conducted at Nerlerk Embankment. The primary in-situ test used to investigate the site was the CPT. CPT profiles are given by Sladen et al. (1985a) and Rogers et al. (1990). Jefferies et al. (1990) presented the Nerlerk

Embankment case history on a plot of S_u/σ_{vo}' versus $(N_1)_{60}$-cs inferred from the CPT results, with an $(N_1)_{60}$-cs of approximately 11. Referring to Jefferies et al. (1990), Stark and Mesri assigned an $(N_1)_{60}$-in-situ of 10 to 11 to Nerlerk Embankment and estimated that the $(N_1)_{60}$-cs would be 10 to 12.5, depending on the type of correction used, based on 0 to 10% fines.

Sladen et al. (1985a) assigned an S_u of less than 2 kPa (42 psf) for all slides in Nerlerk Embankment. This represented the steady state strength required for limiting equilibrium of an infinite slope, based on the ranges in post-failure slope angles and thicknesses of the failed soil masses. However, remembering the work by Poulos (1988) and Davis et al. (1988), this S_u may be lower than the actual mobilized undrained strength because the method of analysis was based on the post-failure configurations and did not take into account the dynamics of the failures. On the plot of S_u/σ_{vo}' versus $(N_1)_{60}$-cs inferred from the CPT results presented by Jefferies et al. (1990), S_u/σ_{vo}' was shown to be approximately 0.15. Jefferies et al. (1990) also took K_o to be 0.7. There is also some argument over what K_o is appropriate for Nerlerk embankment; Rogers et al. (1990) estimated K_o to be 0.8, while conventional studies would often use a K_o of about 0.4. Stark and Mesri (1992) did not give a value of S_u; rather, they gave a strength ratio, S_u/σ_{vo}', of 0.148 in the embankment, based on Jefferies et al. (1990). Based on an average embankment height of about 12 m (=24/2) and a estimated unit weight of soil of about 18 kN/m^3, this strength ratio translates into an average S_u of approximately 14.4 kPa (300 psf).

7.2.20 Heber Road (20)

Heber Road is a case history added to the Seed and Harder (1990) database by Stark and Mesri (1992). Heber Road refers to gently sloping ground between Heber Road and a canal in the Imperial Valley in Southern California. This mass of soil underwent lateral spreading as a result of cyclic loading by the 1979 Imperial Valley earthquake, but did not experience a stability failure (Davis et al., 1988). The ground was essentially level ground (i.e. with a slope angle of 0°) and thus there was essentially no height difference between the toe and head of the spread area. The earthquake was Magnitude 6.55 and the maximum ground acceleration at the site was estimated to be greater than 0.8g. The overall movement was from behind Heber Road towards the free-face at the canal. Horizontal displacements ranged from 4 ft to 7 ft, at the road and canal, respectively, with an average horizontal displacement of 5.5 ft (or 1.65 m). The spread caused significant damage to the paving over a 160 m long section of Heber Road (Youd and Bennett, 1983). Sand boils were noted in and near the spread area and cracking delineated the extent of the spread (Youd and Bennett, 1983). The head of the spread was located behind Heber Road and the toe was located beyond the canal.

A site investigation was carried out in 1979, as reported by Youd and Bennett (1983). SPT and CPT logging was performed. The results indicated that beneath a cap of sandy fill (0.9 to 1.5 m thick) lay a 3.4 to 4.0 m thick layer of fluvial sand deposits which could be dividing into three distinct units (A1, A2 and A3), located side by side. Beneath this thick sand layer were "alternating, continuous layers of medium-stiff lacustrine clays and dense channel or deltaic sands" (Youd and Bennett, 1983). Unit A1 was a dense fine point-bar sand. Unit A2 was a natural channel deposit of loose, very fine sand and silty sand. Unit A3 was a moderately dense sand and silty sand overbank deposit. Youd and Bennett (1983) concluded that "surficial effects of liquefaction were concentrated over Unit A2 (the old channel), the loosest, saturated sand in the section" and that "clearly, this [was] the unit that liquefied during the 1979 earthquake". Raw N-values in Unit A2 were reported as 1 to 7 (safety hammer) or 2 to 4 (donut-hammer) by Youd and Bennett (1983). Davis et al. (1988) reported an $(N_1)_{60}$-in-situ of 1.4 for Heber Road, based on a raw N of 1 over a depth of 6 to 11 ft, and noted a fines content of 15%. Stark and Mesri (1992) reported an $(N_1)_{60}$-in-situ of 1 and estimated an equivalent $(N_1)_{60}$-cs of 1.5 to 5, depending on the type of fines correction used, based on a fines content of 15%. This case history was also included in the cyclic softening (liquefaction) trigger plot by Seed et al. (1984), reviewed in Chapter 2.

Davis et al. (1988) analyzed Heber Road, incorporating the effects of energy and the dynamics of the lateral spread, using a Newmark-type analysis to match the observed movements. The results indicated both pre- and post-failure driving stresses of 40 psf and a mobilized S_u of 100 psf. Stark and Mesri (1992) referenced the work by Davis et al. (1988) and also used an S_u of 100 psf.

7.2.21 Duncan Dam (21)

Duncan Dam is a hydroelectric dam located on the Duncan River, about 8 km upstream from Kootenay Lake in southeastern British Columbia, Canada. The dam itself has never experienced a liquefaction failure; however, a recent dam safety review by B.C. Hydro (Little et al., 1994) investigated the seismic resistance of the dam, with liquefaction resistance of primary concern. Duncan Dam is a zoned earthfill embankment approximately 39 m high with a downstream slope angle of approximately 11.3°. The design earthquake for the dam is Magnitude 6.5 with a maximum firm ground acceleration of 0.12g.

In-situ testing and sampling (Sego et al., 1994; Plewes et al., 1994), laboratory testing of undisturbed frozen samples (Pillai and Stewart, 1994) and subsequent analysis (Pillai and Salgado, 1994) indicated that the soil unit of greatest concern was Unit 3-c, which is located under the downstream side of the right half of Duncan Dam. Unit 3-c consists of uniform fine sand with approximately 5% fines. The sand is composed of angular to subangular grains of quartz, plagioclase, K-feldspar and calcite-dolomite. Both conventional and laboratory-based design approaches were used to analysis the liquefaction resistance of Duncan Dam. Both conventional triggering analysis (Seed and Harder, 1990) and results from laboratory testing of the undisturbed frozen samples predicted that cyclic softening (liquefaction) of Unit 3-c could be triggered by the design earthquake (Pillai and Stewart, 1994). However, the predicted zone of liquefied soil was more extensive using the conventional approach. In addition, conventional undrained shear strength analysis (Seed and Harder, 1990) predicted lower strengths than indicated by the results of the lab testing, particularly at higher confining stresses (Pillai and Salgado, 1994). The difference in strengths was large enough that the conventional approach would predict a flow slide and release of the reservoir whereas the laboratory-base approach would only predict small, tolerable deformations of the dam. Therefore, the conventional approach produced much more conservative predictions than the direct, laboratory-based approach (Byrne et al., 1994). The implications of this difference were significant because, "based on the direct approach no remediation of Duncan Dam for liquefaction was deemed necessary. This has resulted in the savings of tens of millions of dollars for the owner, B.C. Hydro" (Byrne et al., 1994).

The in-situ site investigation found the SPT $(N_1)_{60}$ to increase non-linearly with increasing overburden stress. The reported values of $(N_1)_{60}$ in Unit 3-c sand were 10, 11, 12.4, 13.2, 14.5, 15.7, 17.3, and 18.5 for overburden pressures (in kPa) of 100, 200, 300, 400, 600, 800, 1000, and 1200, respectively (Plewes et al, 1994; Pillai and Stewart, 1994). When converted to imperial units, these overburden pressures correspond to (in psf) pressures of 2088, 4177, 6266, 8354, 12 531, 20 886, and 25 063. Laboratory testing of undisturbed frozen samples concluded that an undrained residual shear strength ratio, S_u/σ_{vo}', of 0.21 was applicable to Unit 3-c sand (Pillai and Salgado, 1994). This ratio was based on postcyclic undrained monotonic simple shear test results.

As indicated in Chapter 5 (see Figure 5-13), the site investigation and lab testing results can be combined, in order to correlate values of S_u with values of $(N_1)_{60}$ for given values of overburden pressure. Therefore, Duncan Dam could be characterized by values of S_u (in psf) of 439, 877, 1 316, 1 754, 2 631, 4 386, and 5 263 for $(N_1)_{60}$ equal to 10, 11, 12.4, 13.2, 14.5, 15.7, 17.3, and 18.5, respectively. These datapoints can be plotted and compared with the other empirical case histories discussed above, keeping in mind that this case history did not fail.

7.3 Classification of the Case Histories

7.3.1 Summary of case history statistics

Based on the discussion in the previous section, Table 7-2 summarizes various details for each of the individual case histories. Included in Table 7-2 for each case history are the initial height and slope angle, the type of trigger mechanism, the earthquake (EQ) magnitude and acceleration (if applicable), the nature of the observed failure, the runout distance and the post-failure slope angle. Runout was defined as the horizontal distance from the toe of the original slope to the toe of the post-failure slope. Based on the details in Table 7-2 and the detailed information presented earlier, the case histories can be classified into various categories in an attempt to ultimately distinguish between cases of flow liquefaction and cyclic liquefaction. Of the 21 case histories listed in Table 7-2, three case histories were statically triggered failures, while 17 case histories suffered some type of deformations as a result of cyclic loading. The cyclic loading was predominantly earthquake loading, but one case history (18, Lake Ackerman) was triggered by cyclic loading related to a seismic exploration, as explained previously. The type of failure assigned to each case history in Table 7-2 will be discussed below.

7.3.2 Comparison of initial conditions

Figure 7-3 summarizes the initial slope geometry for all of the case histories listed in Table 7-2 and clearly indicates that the database contains a wide range of initial slope height and angle combinations. The initial slope height was defined as the vertical distance from the toe to the crest of the pre-failure slope. If a slope was stepped, the initial slope angle represents most of the slope. Five case histories had initial slope angles less than 5°

(this includes case history 6, which was not a slope, but a building on level ground). Of these five case histories, only case history 10 (San Fernando Juvenile Hall) is shown to have a large slope height (i.e. > 10 m). As explained previously, this is a result of the fact that the lateral spread at the site was approximately 1.2 km long and thus there was a 30 m height difference between the toe and head of the slide mass area. Eight case histories had initial slope angles greater than 25°, but all of these case histories had initial slope heights of less than 11 m. Nine case records had initial slope angles ranging from approximately 11° to 22°. One of these case records (2, Sheffield Dam) had an initial slope height of 7.6 m, but the other eight had much higher initial slope heights ranging from 17.6 to 61 m.

7.3.3 Comparison of observed deformations

Drawing on the information in Tables 7-1 and 7-2, Table 7-3 provides a summary of the general deformation analysis carried as part of this study for each of the case histories. For each of the case histories, several terms have been computed to help quantify the observed deformations relative to those experienced by the other case histories in the database.

The observed runouts for the various case histories cannot be compared directly because of the wide range in initial slope height (see Table 7-2 and Figure 7-3). It is logical to conclude that as the initial slope height increases, observed runouts could increase as a result of the higher driving stresses and the additional momentum that the material will gather as it fails. Dividing the observed runout by the initial slope height provides a simple way of comparing relative runouts between various case histories. Table 7-3 indicates that nine of the case histories had relative runouts of 3 or greater. The remaining case histories had relative runouts ranging from zero to 2. A related term to the relative runout ratio is the amount of horizontal strain that occurred. This was defined by dividing the observed runout by the initial slope length and expressing the result in percent. The initial slope length was defined as the horizontal distance from the toe of the slope to the point immediately below the crest of the slope (i.e. it was calculated from the initial slope height and angle). Eleven of the case histories had strains greater than 90%. Four of the case histories had strains less than 4%.

Another simple measure for comparing the deformations of the various case histories is the relative slope ratio. This is defined as the ratio of the post-failure slope angle to the initial slope angle. Table 7-3 indicates that four of the case histories had relative slope ratios of 1.0; i.e. no significant change in slope was observed from before to after the failure.

Ten case histories had relative slope ratios of less than 0.40.

Figure 7-4 indicates that there is a clear relationship between relative runout and relative slope angle for all of the case histories. This is to be expected because a slope that runs out further relative to its initial height would obviously have a lower ratio of its post-failure slope angle to its initial slope angle. However, as will be discussed further in later sections of this chapter, what is of most interest is where the various case histories happen to plot in Figure 7-4 .

As was proposed in Chapter 4 and will be illustrated in Chapter 8, the brittleness index of a soil in undrained loading appears to be related to RSR. Sladen et al. (1987) suggested that for slides that do not involve toe erosion, brittleness index can be estimated by comparing initial and post-failure slope profiles using the following formula:

$$[7\text{-}3] \qquad I_B = \frac{\tan\beta_i - \tan\beta_f}{\tan\beta_i}$$

where:
β_i = initial slope angle
β_f = post-failure slope angle

This term is a related term to the relative slope ratio discussed above. Note that the maximum possible value for I_B using Equation 7-3 is 1.0; this differs from the equations given in Chapter 4, which indicate that anisotropically consolidated soils can have values of I_B greater than 1.0. Table 7-3 indicates that ten of the original Seed and Harder (1990) case histories have values of I_B greater than or equal to 0.64.

Estimating the average RSR for each case history is difficult. The best that can be done is to calculate an approximate value. The average value of p'_i was estimated based on the average value of σ_{vo}' given by Stark and Mesri (1992) for the middle of the liquefied layer and assuming a K_o of 0.5. The average value of p'_{us} was estimated (see Equation 4-15 in Chapter 4) by assuming an average M of 1.2 and assuming that $q_{us} = 2S_u$, using the mean value of S_u in the Seed and Harder (1990) database. Clearly, the resulting value of average RSR may be inaccurate. Nevertheless, it is interesting to compare the relationship between I_B and estimated RSR for the case histories in the original Seed and Harder (1990) database (with the exception of case history 2, for which the post-failure angle was not available, and case history 6, which was not a slope failure) with that suggested by Sladen et al.

(1985b), as presented in Figure 7-5. Despite some scatter, there is definitely an observable increase in I_B with increasing RSR, similar to that suggested by Sladen et al. (1985b). The only exceptions to this are the lateral spread case histories (8, 10, and 14), which have zero brittleness irrespective of the estimated RSR because no significant change in slope angle occurred as a result of each lateral spread.

7.3.4 Classification based on deformation characteristics

In general, as outlined in Table 7-2, all of the case histories in the database can be divided into three types of failures: flow failures, slump failures and lateral spreads. The category that a given case history falls into depends on its deformation characteristics as quantified by the various terms in Table 7-3. Case histories in the database classified as flow failures have large relative runouts (and large strains) and small slope angle ratios (and large values of I_B). Figure 7-6 illustrates the flow failure at the Calaveras Dam (case history 1). Case histories in the database classified as lateral spreads have small relative runouts (and small strains), slope angle ratios of 1.0 (and I_B values of zero) and occur in gently sloping ground (i.e. initial slope angle ≤ 5°). Figure 7-7 illustrates the lateral spread at Whiskey Springs Fan (case history 14). Slump failures have deformation characteristics in between those of flow failures and those of lateral spreads. Case histories in the database classified as slump failures have smaller relative runouts (and smaller strains) and larger slope angle ratios (and smaller values of I_B) than the flow failures, but have large enough deformations in steeply sloping ground that they cannot be considered to be lateral spreads. Figure 7-8 illustrates the upstream and downstream slump failures at La-Marquesa Dam (case records 15 and 16, respectively). However, the large deformations could have resulted from cyclic liquefaction combined with large earthquake motions.

This study has classified flow failures as those failures which had a relative runout of 2 or greater and a slope angle ratio of less than 0.4. Thus, case histories 1, 3, 4, 7, 9, 13a &b, and 19 (Calaveras Dam, Fort Peck Dam, Solfatara Canal Dike, Uetsu Embankment, Mochi-Koshi Tailings, and Nerlerk Embankment, respectively) would be classified as flow failures (see Figure 7-4). Case histories 8, 10, and 14 (Snow River Bridge Fill, San Fernando Juvenile Hall, and Whiskey Springs Fan, respectively) would be classified as lateral spreads because they all had a relative runout less than 2, a slope angle ratio of 1 and occurred in gently sloping ground (initial slope angle ≤ 5°). Case histories 5, 12, 15, 16 and 17 (Lake Merced Bank, Upper San Fernando Dam, La Marquesa Dam - Upstream and Downstream, and La Palma Dam, respectively) would be classified as slump failures because they had relative runouts less than 2 and slope angle ratios greater than 0.4. Case histories 11 and 18 (Lower San Fernando Dam and Lake Ackerman, respectively) can be considered as borderline between the flow and slump categories.

The dividing line between a flow failure and a slump failure, as described above, is obviously somewhat subjective. It would be reasonable to expect some transition zone between flow and slump type failure deformation characteristics. Examining Figure 7-5, the dividing line between flow and slump failures in terms of brittleness index is an I_B of about 0.6. It is interesting to note that the classification of the individual case histories is similar to that by Baziar and Dobry (1995) who divided the database into flow slides, lateral spreads and major slides.

7.4 Flow Liquefaction versus Cyclic Softening

It is often difficult, if not impossible, to distinguish between flow liquefaction and cyclic softening (liquefaction) phenomena in the field after a failure has occurred. Both types of liquefaction can result in large deformations. Ideally, instrumentation during and after a failure together with comprehensive site characterization would be required to correctly identify which phenomenon occurred. However, such information is not available for the case histories being discussed here. The best that can be done is to make an estimate of which phenomenon controlled which case history, based on the terminology definitions adopted in Chapter 1 and the observed deformation characteristics of each case history.

7.4.1 Statically triggered slope failures

Case histories 1 (Calaveras Dam), 3 (Fort Peck Dam), and 19 (Nerlerk Embankment) suffered failures as a result of static triggers. All three of these case histories have been classified as flow failures. Provided that failure truly occurred in the sand within each slope, these three case histories would have to be classified as cases of flow liquefaction, because the trigger was static. As the discussion above mentioned briefly, there is some ongoing debate over the influence of other factors such as weak clay shale or clay layers influencing the failure. However, it is possible that although strains may have first occurred in these weak layers, they may have been sufficiently large to trigger flow liquefaction in the strain-softening sand above, such that the overall failure was a result of the phenomenon of flow liquefaction.

7.4.2 Cyclically loaded case histories

Of the case histories in Table 7-2, one case history (21, Duncan Dam) did not fail, but consisted of field and laboratory studies investigating what conditions could lead to failure. Case history 6 (Kawagishi-Cho Building) differed from all of the other cyclically loaded case histories in that it consisted of the failure of a building foundation rather than deformations or failure of a slope. However, the remaining 16 case histories suffered some type of slope deformation as a result of cyclic loading. As discussed in the previous section, these case histories have been subdivided as to the nature of the deformation that occurred (see Table 7-2).

a) Lateral spreads

Four of the cyclically loaded case histories (8, 10, 14 and 20; Snow River Bridge Fill, San Fernando Juvenile Hall, Whiskey Springs Fan, and Heber Road, respectively) were lateral spreads, rather than severe slope failures. All four of these case histories had initial slope angles less than or equal to 5° and suffered no significant change in slope angle after failure. Each of these case histories suffered lateral deformations ("runout") of less than or equal to 3 m. Youd (1993), based on earlier work by Bartlett and Youd (1992) included all four of these case histories within a database of lateral spread case histories.

Since these lateral spreads occurred in level to gently sloping ground, it is reasonable to conclude that shear stress reversal did occur during the earthquake loading. Consequently, these lateral spreads are all likely deformations that are predominantly a result of of cyclic softening (liquefaction).

b) Flow failures

Case histories 4, 7, 9, and 13a &b (Solfatara Canal Dike, Uetsu Embankment, Mochi-Koshi Tailings Dam 2 and Dam 1, respectively) were all cyclically loaded case histories that were classified as flow failures (see Figure 7-4).

It is likely that these case histories suffered such large runout ratios and responded in such a brittle manner because they contained a sufficiently large mass of potentially strain-softening material that was triggered to strain-soften by the cyclic loading. Once triggered, the driving stresses were higher than the undrained shear strength and the material flowed significantly relative to the size of the slope or embankment. Thus, these case records are likely all cases of flow liquefaction. They can be grouped together with the statically triggered cases of flow liquefaction discussed earlier.

c) Slump failures

The slump failures are more difficult to classify as being controlled primarily by either flow liquefaction or cyclic softening (liquefaction). The observed slumping deformation pattern could be due to either type of liquefaction. If flow liquefaction occurred within the soil structure, there must have been an insufficient quantity of strain-softening material relative to strain-hardening material to result in a true flow failure. However, if shear stress reversal was able to occur within the soil structure, cyclic liquefaction with deformations accumulating during cyclic loading may have caused the observed deformations. In particular, if cyclic liquefaction occurred in the level ground at the toe of a slope, the slumping deformation pattern may have been a result of the soil structure moving into the zone of softened soil. Further studies into all of the failures would be required to clearly identify what happened at each site. However, for interest, this study attempts to distinguish between possible flow liquefaction and possible cyclic softening.

Using the results by Pando and Robertson (1995) as a guide, it is possible that shear stress reversal may have occurred within the slope of case histories 5, 15, 16 and 17 (Lake Merced Bank, La Marquesa Dam - Upstream and Downstream, and La Palma Dam, respectively) because they were all relatively short steep structures (see Figure 7-3). In particular, shear stress reversal may have occurred in the level ground in the toe region of each slope, causing a loss in soil stiffness and resulting in the embankment slumping into the surrounding ground. Case record 6 (Kawagishi-Cho Building) may have been affected by a similar phenomenon.

Case history 12 (Upper San Fernando Dam) was a large enough structure that it is possible that shear stress reversal may not have occurred throughout the structure. A more probable explanation is that the dam consisted of a small portion of strain-softening or limited strain-softening material such that it suffered damaging, but limited deformations, rather than a catastrophic flow failure. The presence of the downstream berm may have also contributed to limiting the deformations that occurred.

Case histories 11 and 18 (Lower San Fernando Dam and Lake Ackerman, respectively) which were considered as borderline between the flow and slump categories, may have contained more strain-softening material than case history 12, but still had an insufficient amount to result in relative runouts as high as most of the flow failure case histories. Also the approximate RSR for the Lower San Fernando Dam was smaller than the approximate values of RSR calculated for the other case histories classified as flow failures (see Table 7-3). Nevertheless, these two case histories will be included with the flow failure group of case histories because the deformations were fairly large and their slope angle ratios were low. The observation of a time delay between the end of the earthquake and the failure of the Lower San Fernando Dam supports the classification of the case history as flow liquefaction. However, the zone of material that suffered flow liquefaction was limited in size relative to the overall size of the dam, resulting in the borderline flow/slump deformations.

7.4.3 S_u versus $(N_1)_{60}$ for flow liquefaction case histories

Figure 7-9 presents a similar plot to that by Seed and Harder (1990) given in Figure 7-1, but includes only the case histories in the database which were classified as flow failures or borderline flow/slump failures. These case histories are considered most likely to be cases of flow liquefaction, for which estimating an undrained strength is appropriate. Clearly, the data still falls within the Seed and Harder (1990) boundary lines because the values of Su and $(N_1)_{60}$-cs have not been changed. Superimposed on Figure 7-9 are theoretical lines for clean Ottawa sand for both K_o=0.5 and K_o=1.0, based on the results of Chapter 5. With the exception of case history 13a (Mochi-Koshi Tailings Dam 2), which was considered questionable by Baziar and Dobry (1995), as explained previously, the limited data in Figure 7-9 could also be said to follow the trend of the clean Ottawa sand lines.

Figure 7-10 presents the same data as in Figure 7-9, but with the $(N_1)_{60}$ values equal to the in-situ values rather than the clean sand equivalent values. Also superimposed on Figure 7-10 are the results from the detailed site investigation and laboratory testing for case record 21 (Duncan Dam), as summarized in Table 7-5. The Seed and Harder (1990) boundary lines cannot be shown on this figure because they only apply to clean sand equivalent values of $(N_1)_{60}$. However, the theoretical lines for clean Ottawa sand are shown. Again, it is difficult to draw any definite conclusions because the case history data are limited. The data for Duncan Dam (which did not fail) certainly appear to follow the trend of the theoretical lines. With the exception of case record 13a (Mochi-Koshi Tailings

Dam 2), which could be left out of the database, as discussed previously, the remaining data could be said to agree with the trends of the theoretical lines. Since the theoretical lines that are shown are for clean Ottawa sand, it is reasonable to expect that some data in more compressible material will plot to the left of the lines. Note that case records 1 and 3 (Calaveras Dam and Fort Peck Dam, respectively) were assigned fines contents of >60% and 30% respectively, based on data by other authors (see Tables 7-1 and 7-4). In general, as fines content increases, so does the compressibility of a soil, resulting in a lower measured SPT penetration resistance. As presented in Chapter 5, the theoretical lines relating S_u to $(N_1)_{60}$ in-situ will move to the left for more compressible materials with steeper ultimate state lines (e.g. Alaska sand; see Chapter 5).

7.5 Representative Values of $(N_1)_{60}$ and S_u

7.5.1 Range of data reported in the literature

Table 7-1 summarized the values of $(N_1)_{60}$ (in-situ and clean sand equivalent) and S_u used by Seed and Harder (1990). However, the discussion of the individual case histories earlier in this chapter indicates that there is considerable uncertainty in selected values and there appears to be a wide range of reported representative values of $(N_1)_{60}$ and S_u for each case history.

It is important to note, as outlined earlier in the descriptions of the case histories, that several of the case histories in the Seed and Harder (1990) database had representative $(N_1)_{60}$ values selected based on no or little SPT data. In particular, case histories 1 and 3 (Calaveras Dam and Fort Peck Dam), which are two of the case histories with higher representative values of $(N_1)_{60}$ (see Figure 7-1), had $(N_1)_{60}$ values assigned based on relative density type estimates. Case history 16 (La Marquesa Dam, Downstream Slope), which was also one of the higher $(N_1)_{60}$ case histories (see Figure 7-1), appears to have a representative $(N_1)_{60}$ selected based on a single blowcount in the layer that appeared to have liquefied. Uncertainties also arise for case histories 11 and 12 (Lower and Upper San Fernando Dams, respectively) which had the highest representative $(N_1)_{60}$ values in the Seed and Harder (1990) database (see Figure 7-1). The selected values were extrapolated from post-earthquake conditions to pre-earthquake conditions and in the case of the Lower San Fernando Dam, from downstream conditions to upstream conditions. Some of the uncertainties associated with the selection of representative values of S_u are discussed later in this chapter.

Drawing on the details given earlier in this chapter, Table 7-4 presents a summary of the range in reported values of $(N_1)_{60}$ in-situ, S_u and estimated fines content by various authors. Based on the estimated fines content, the values of $(N_1)_{60}$ in-situ could be converted to equivalent clean sand values of $(N_1)_{60}$-cs using Equation 7-2. It is important to also note that there is a considerable uncertainty with the fines content corrections using Equation 7-2.

Figure 7-11 presents a plot of S_u versus $(N_1)_{60}$ in-situ based on the range of values given in Table 7-4. The solid dot plotted for each case history represents the midpoint between the maximum and minimum S_u in Table 7-4 plotted against the midpoint between the maximum and minimum $(N_1)_{60}$ in-situ in Table 7-4. The error bars indicate the range from minimum to maximum for both S_u and $(N_1)_{60}$. The data presented for the case histories in Figure 7-11 clearly cover a wider range than in Figure 7-2, based on the Seed and Harder (1990) data alone.

7.5.2 A minimum $(N_1)_{60}$ approach

In general, the values of $(N_1)_{60}$ in the Seed and Harder (1990) chart appear to be average representative values for each case history. Experience has shown that the Seed and Harder (1990) chart often gives conservative estimates of S_u (e.g. Byrne et al., 1994), particularly when applied to all points in an SPT profile, including any low values. Based on the discussion in Chapter 2, it is likely the weakest link in the chain or minimum $(N_1)_{60}$ that can result in either cyclic softening (liquefaction) or flow liquefaction being triggered at a particular site. Likewise, it could be argued that the estimated undrained shear strength for a liquefied soil deposit should be correlated with the minimum representative $(N_1)_{60}$, rather than the average value.

Table 7-6 presents a summary of the revised values of S_u and $(N_1)_{60}$ chosen to represent each case history, based on the minimum $(N_1)_{60}$ viewpoint.[2] A reasonable lower bound $(N_1)_{60}$ in-situ was selected and the clean sand equivalent value was estimated based on the fines content and the SPT corrections proposed by Seed (1987), in Equation 7-2. Table 7-6 provides comments regarding the selection of both S_u and $(N_1)_{60}$ for each case history.

---

[2] *The data presented in Table 7-6 were selected in a joint effort by the author and Dr. E.C. McRoberts after carefully reviewing all of the case histories.*

When possible, the value of S_u was selected as one which incorporated energy effects (Poulos, 1988; Davis et al., 1988), as this was felt to be closer to the "true" value of S_u. Conducting this exercise led to the conclusion that it is very difficult to represent a complex slope failure by a single S_u and a single $(N_1)_{60}$.

Table 7-6 presents the revised selections of S_u and $(N_1)_{60}$ for each of the case histories in the database. However, based on the discussion earlier in this chapter, an undrained shear strength is really only appropriate for cases of flow liquefaction. While cases of cyclic softening (liquefaction) will likely experience deformations related to the minimum $(N_1)_{60}$, the earlier discussion led to the conclusion that undrained shear strengths are not appropriate to analysis of such a site. At best, they can give equivalent values of S_u that would predict similar deformations as those caused by the loss in soil stiffness. However, these values of S_u may not be appropriate for analyzing sites outside of the database.

Figure 7-12 presents the revised selection of S_u and $(N_1)_{60}$-cs in Table 7-6 for the case histories in the Seed and Harder (1990) database that were classified as flow failures and borderline flow/slump failures. Also shown in Figure 7-12 are two of the three case histories added by Stark and Mesri (1992) that were classified as these type of failures (case histories 18 and 19, Lake Ackerman and Nerlerk Embankment, respectively). Superimposed on Figure 7-12 are the Seed and Harder (1990) boundary lines and the K_o=0.5 theoretical line for clean Ottawa sand (see Chapter 5). The general trend of the data appears to be more similar to the clean Ottawa sand line than the Seed and Harder (1990) boundary lines. However, the data are fairly limited and contain considerable scatter.

Figure 7-13 presents the same data as in Figure 7-12, except that $(N_1)_{60}$ in-situ is given instead of $(N_1)_{60}$-cs. The Seed and Harder (1990) boundary lines cannot be shown in this figure as they only apply to equivalent clean sand values of $(N_1)_{60}$. Superimposed on Figure 7-13 are the K_o=0.5 theoretical lines for both clean Ottawa sand and Alaska sand (see Chapter 5). The data do tend to fall within the two lines; however, the range in $(N_1)_{60}$ between the two lines is large and is a function of compressibility of the soil. It is difficult to draw any further conclusions regarding the trend of the data.

7.5.3 Uncertainty with S_u

In reviewing the case histories in the Seed and Harder (1990) and Stark and Mesri (1992) combined database, it soon becomes clear that there is considerable uncertainty in the selection of a representative value of S_u for an individual case history. Many of the case histories appeared to involve "liquefaction" of a soil mass, while some (case histories 2, 10, 15, 16, 17 18 and 20) involved "liquefaction" of a particular soil layer. For those case histories that involved failure of a soil mass, the zone occupied by the mass within the soil structure was sometimes limited in extent (e.g. case histories 11 and 12). Different assumptions were made by various authors as to the mechanics of failure in calculating a single representative S_u for each case history, resulting in the range of reported values presented in Table 7-4. For example, Lucia (1981, 1982) calculated S_u based on the post failure slope configuration, while Poulos (1988) and Davis et al. (1988) noted that the pre-failure and post-failure driving stresses would bracket the actual mobilized undrained shear strength and attempted to account for energy effects associated with the dynamics of failure when calculating S_u.

In actual fact, a single value of S_u may reflect only the overall failure, but not apply everywhere within the failing soil mass or layer. Different directions of loading may occur at different points within a soil structure such that various elements reach different values of S_u. However, many authors assume a single S_u along a failure surface. In addition, variability in soil state within the soil mass could result in different elements of soil having different values of S_u. Some failures (e.g. 19, Nerlerk embankment) were progressive in nature. If this is not accounted for, undrained strengths may not be properly estimated. Newmark type deformation analyses were often used to estimate the S_u that would result in the observed accumulated deformations during cyclic loading for the lateral spreading type case histories. However, the previous discussion has suggested that these deformations are generally due to a loss in soil stiffness during cyclic loading. While a value of S_u estimated using this method may match the observed deformations at a particular site, it is really only an equivalent S_u because the physics leading to failure did not necessarily involve a loss in strength. Extrapolating such results to other sites is not appropriate.

7.6 Conclusions

The empirical SPT-based chart by Seed and Harder (1990) is one of the most commonly used methods for estimating the undrained shear strength of sand following liquefaction. This chapter has illustrated that the database of case histories on which the chart is based contains a wide range of deformation characteristics and may actually contain a variety of flow liquefaction and cyclic softening (liquefaction) case histories. However, for some case histories, after the failure has occurred, it is very difficult to correctly identify which phenomenon controlled the observed deformations. In addition, the detailed summaries provided for each case history illustrate the difficulty in assigning a single S_u and a single $(N_1)_{60}$ to a complex slope failure.

Previous studies (see Chapter 5) have indicated that the undrained shear strength of sand is a flow liquefaction response parameter that is very sensitive to variability in a soil deposit as well as the direction of loading. Plotting from the database only the case histories which were considered to be flow failures or borderline flow/slump failures, a similar trend can be seen, although the data are limited. As a result, assigning undrained shear strengths to a variable soil deposit for post flow liquefaction stability calculations can be difficult. The original relationships proposed by Seed and Harder (1990) appear to be conservative. They appear to be based on average representative $(N_1)_{60}$ values for each case history. As a result, they may be overly conservative for low points in any SPT $(N_1)_{60}$ profile in a soil deposit. For low risk projects, the Seed and Harder (1990) chart may be useful as a preliminary guide, providing flow liquefaction is considered possible. However, for high risk projects, for which the consequences of failure can be enormous, site specific investigations are recommended.

Deformations that result from the phenomenon of cyclic softening (liquefaction) should not be analyzed using an undrained shear strength in a stability analysis. Although the magnitude of the deformations that may occur will depend on the density of the soil (as indicated by $(N_1)_{60}$ values), they will also depend on the size and duration of cyclic loading. Other methods such as that developed by Youd (1993) should be used to estimate deformations associated with potential lateral spreads. Sloping ground that is not considered to be susceptible to flow liquefaction based on site specific testing should be carefully evaluated for the potential of cyclic softening (liquefaction) and resulting deformations. In such cases, it is important to carefully evaluate the level ground at the toe of the slope, in order to examine the effect that cyclic liquefaction and loss in stiffness within zone may have on overall deformations of the slope. Similar investigations should be carried out for buildings located on level ground.

This chapter has served to illustrate the complexity and range of liquefaction failures contained within the combined Seed and Harder (1990) and Stark and Mesri (1992) database, whether they result from flow liquefaction or cyclic softening phenomena. Many factors other than soil state (as reflected by $(N_1)_{60}$ measurements) can also influence the deformation characteristics of sloping ground, particularly when the soil is non-uniform in nature. The charts in Figures 7-9, 7-10, 7-12 and 7-13 were produced in order to investigate how the data would plot if only the flow failures are considered and/or if a minimum $(N_1)_{60}$ approach were taken. These figures were shown solely for illustrative purposes. It is not recommended that they be used for design against flow liquefaction, particularly in the case of high risk projects.

Table 7-1: Summary of data by Seed and Harder (1990)

Case History		S_u				$(N_1)_{60}$		FC
No.	Name	mean (psf)	mean (kPa)	+/- (psf)	+/- (kPa)	in-situ	clean sand equivalent	(%)
1	Calaveras Dam	650	31.1	50	2.4	7	12	>60*
2	Sheffield Dam	75	3.6	25	1.2	4	6	25*
3	Fort Peck Dam	350	16.8	100	4.8	8	10	30*
4	Solfatara Canal Dike	50	2.4	25	1.2	4	4	<5*
5	Lake Merced Bank	100	4.8	0	0.0	6	6	3
6	Kawagishi-Cho Building	120	5.7	0	0.0	4	4	
7	Uetsu Railway Embankment	40	1.9	0	0.0	3	3	
8	Snow River Bridge Fill	50	2.4	0	0.0	5.5	7	15*
9	Koda Numa Embankment	50	2.4	0	0.0	3	3	
10	San Fernando Juvenile Hall	130	6.2	70	3.4	6	10.5	65
11	Lower San Fernando Dam	400	19.2	100	4.8	11.5	13.5	25
12	Upper San Fernando Dam	600	28.7	100	4.8	13	15	25
13a	Mochi-Koshi Tailings -Dam 2	250	12.0	150	7.2	0	5	80
13b	-Dam 1	--	--	--	--	--	--	--
14	Whiskey Springs Fan	150	7.2	10	0.5	8	11	40
15	La Marquesa Dam - U/S Slope	200	9.6	120	5.7	4	6	30
16	La Marquesa Dam - D/S Slope	400	19.2	150	7.2	9	11	20
17	La Palma Dam	200	9.6	100	4.8	3	4	15

Notes: * estimated for this study

Table 7-2: Summary of case history statistics

Case History		Initial Slope Geometry		Type of Trigger	EQ Magnitude	a_{max} (in g)	Type of Failure	Post-failure Geometry	
No.	Name	Height (m)	Angle (°)					Runout (m)	Angle (°)
1	Calaveras Dam	61	18.4	construction	N/A	N/A	flow	183	5.71
2	Sheffield Dam	7.6	21.8	EQ	6.3	0.15	flow	30	--
3	Fort Peck Dam	61	14	construction	N/A	N/A	flow	457	2.86
4	Solfatara Canal Dike	2.1	27	EQ	7.1	0.1 - 0.33	flow	23	3.6
5	Lake Merced Bank	9.8	34	EQ	5.7	0.12	slump	18	24
6	Kawagishi-Cho Building	0	0	EQ	7.5	--	building foundation	0	N/A
7	Uetsu Railway Embankment	10	29	EQ	7.5	--	flow	115	4
8	Snow River Bridge Fill	3	1.25	EQ	9.2	--	lateral spread	3	1.25
9	Koda Numa Embankment	3	30	EQ	8.1	--	flow	18	4
10	San Fernando Juvenile Hall	30	1.5	EQ	6.5	0.5	lateral spread	0.75	1.5
11	Lower San Fernando Dam	43	21.8	EQ	6.5	0.5 - 0.55	flow/slump	61	8.13
12	Upper San Fernando Dam	17.6	21.8	EQ	6.5	0.5 - 0.6	slump	1.5	21.8
13a	Mochi-Koshi Tailings -Dam 2	20	20.1	EQ	7	0.1 - 0.25	flow	240	4.5
13b	-Dam 1	30	20.1	EQ	7	0.1 - 0.25	flow	500	4.5
14	Whiskey Springs Fan	9.1	5	EQ	6.9	0.4	lateral spread	1.2	5
15	La Marquesa Dam - U/S Slope	7.9	27	EQ	8	0.6	slump	11	12.5
16	La Marquesa Dam - D/S Slope	7	34	EQ	8	0.6	slump	6.5	18
17	La Palma Dam	11	34	EQ	8	0.46	slump	5	17
18	Lake Ackerman	6.4	26.6	seismic explor.	N/A	CSR = 0.12	flow/slump	12	7.5
19	Nerlerk Embankment	24	12.65	construction	N/A	N/A	flow	100	1.5
20	Heber Road	0	0	EQ	6.55	>0.8	lateral spread	1.65	0
21	Duncan Dam	39	11.3	N/A	N/A	0.12	N/A	N/A	N/A

Table 7-3: Summary of deformation analysis

Case History No.	Case History Name	Runout Height (m/m)	Strain (%)	Post angle / Pre angle	Brittleness Index $I_B = \frac{\tan\beta_i - \tan\beta_f}{\tan\beta_i}$	σ'_{vi} (Stark & Mesri, 1992) (psf)	σ'_{vi} (Stark & Mesri, 1992) (kPa)	Approx. RSR (p'_i/p'_{ss})
1	Calaveras Dam	3.0	99.8	0.31	0.70	2855	136.7	1.8
2	Sheffield Dam	3.9	157.9	--	--	1975	94.6	10.5
3	Fort Peck Dam	7.5	186.8	0.20	0.80	10815	517.8	12.4
4	Solfatara Canal Dike	11.0	558.1	0.13	0.88	955	45.7	7.6
5	Lake Merced Bank	1.8	123.9	0.71	0.34	950	45.5	3.8
6	Kawagishi-Cho Building	--	--	--	--	1225	58.7	4.1
7	Uetsu Railway Embankment	11.5	637.5	0.14	0.87	2690	128.8	26.9
8	Snow River Bridge Fill	1.0	2.2	1.00	0.00	2100	100.5	16.8
9	Koda Numa Embankment	6.0	346.4	0.13	0.88	1550	74.2	12.4
10	San Fernando Juvenile Hall	0.0	0.1	1.00	0.00	1940	92.9	6.0
11	Lower San Fernando Dam	1.4	56.7	0.37	0.64	3930	188.2	3.9
12	Upper San Fernando Dam	0.1	3.4	1.00	0.00	2975	142.4	2.0
13a	Mochi-Koshi Tailings -Dam 2	12.0	439.1	0.22	0.78	2715	130.0	4.3
13b	-Dam 1	16.7	609.9	0.22	0.78	4072.5	195.0	--
14	Whiskey Springs Fan	0.1	1.2	1.00	0.00	2630	125.9	7.0
15	La Marquesa Dam - U/S Slope	1.4	70.9	0.46	0.56	1600	76.6	3.2
16	La Marquesa Dam - D/S Slope	0.9	62.6	0.53	0.52	1790	85.7	1.8
17	La Palma Dam	0.5	30.7	0.50	0.55	1670	80.0	3.3
18	Lake Ackerman	1.9	93.9	0.28	0.74	1845	88.3	--
19	Nerlerk Embankment	4.2	93.5	0.12	0.88	--	--	--
20	Heber Road	--	--	--	--	800	38.3	--
21	Duncan Dam	N/A	N/A	N/A	N/A	--	--	--

Table 7-4: Summary of range in data reported by various authors

Case History		S_u								$(N_1)_{60}$ in-situ				FC	
No.	Name	Minimum		Maximum		Avg. of Max/Min		+/- for Max/Min		Minimum	Maximum	Avg. of Max/Min	+/- for Max/Min	Minimum (%)	Maximum (%)
		(psf)	(kPa)	(psf)	(kPa)	(psf)	(kPa)	(psf)	(kPa)						
1	Calaveras Dam	600	28.7	750	35.9	675	32.3	75	3.6	2	7	4.5	2.5		>60
2	Sheffield Dam	50	2.4	100	4.8	75	3.6	25	1.2	4	6	5	1		25*
3	Fort Peck Dam	250	12.0	700	33.5	475	22.7	225	10.8	5.3	10	7.65	2.35		30
4	Solfatara Canal Dike	0	0.0	130	6.2	65	3.1	65	3.1	0	4	2	2		<5
5	Lake Merced Bank	100	4.8	100	4.8	100	4.8	0	0.0	5	7	6	1	3	3
6	Kawagishi-Cho Building	120	5.7	120	5.7	120	5.7	0	0.0	4	4	4	0		
7	Uetsu Railway Embankment	35	1.7	40	1.9	38	1.8	3	0.1	3	3	3	0		
8	Snow River Bridge Fill	50	2.4	50	2.4	50	2.4	0	0.0	5	5.5	5.25	0.25		
9	Koda Numa Embankment	25	1.2	50	2.4	38	1.8	13	0.6	3	4	3.5	0.5		
10	San Fernando Juvenile Hall	60	2.9	200	9.6	130	6.2	70	3.4	2	6	4	2	50	65
11	Lower San Fernando Dam	300	14.4	750	35.9	525	25.1	225	10.8	5.5	11.5	8.5	3	25	25
12	Upper San Fernando Dam	500	23.9	700	33.5	600	28.7	100	4.8	13	13	13	0	25	>60
13a	Mochi-Koshi Tailings -Dam 2	100	4.8	400	19.2	250	12.0	150	7.2	0	1	0.5	0.5	>60	80
13b	-Dam 1	50	0.0	110	0.0	80	3.8	30	1.4	0	1	0.5	0.5	>60	80
14	Whiskey Springs Fan	130	6.2	160	7.7	145	6.9	15	0.7	6	12	9	3	40	40
15	La Marquesa Dam - U/S Slope	76	3.6	340	16.3	208	10.0	132	6.3	4	4	4	0	30	30
16	La Marquesa Dam - D/S Slope	266	12.7	580	27.8	423	20.3	157	7.5	9	9	9	0	20	20
17	La Palma Dam	100	4.8	300	14.4	200	9.6	100	4.8	3	3	3	0	15	15
18	Lake Ackerman	170	8.1	260	12.4	215	10.3	45	2.2	3	3	3	0	0	5
19	Nerlerk Embankment	42	2.0	300	14.4	171	8.2	129	6.2	10	11	10.5	0.5	2	12
20	Heber Road	100	4.8	100	4.8	100	4.8	0	0.0	1	1	1	0		29

__Notes__: * estimated for this study

Table 7-5: Duncan Dam results (Byrne et al., 1994)

σ_v' (kPa)	σ_v' (psf)	$S_u=0.21\sigma_v'$ (kPa)	S_u (psf)	$(N_1)_{60}$ in-situ
100	2089	21	439	10
200	4177	42	877	11
300	6266	63	1316	12.4
400	8354	84	1754	13.2
600	12531	126	2632	14.5
800	16708	168	3509	15.7
1000	20886	210	4386	17.3
1200	25063	252	5263	18.5

Notes: $S_u=0.21\sigma_v'$ is based on undrained monotonic direct simple shear testing of undisturbed samples

Table 7-6: Summary of minimum (N1)60 approach

Case History		Type of Failure	S_u mean		$(N_1)_{60}$		FC	Comments
No.	Name		(psf)	(kPa)	in-situ	clean sand equivalent	(%)	
1	Calaveras Dam	flow	700	33.5	2	7	>60	Minimum N_1 and S_u from Poulos (1988); assumed $N_1=(N_1)_{60}$ (i.e. ER=60%)
2	Sheffield Dam	flow	75	3.6	4	6		Used lowest stated D_r=35% and $(N_1)_{60}/D_r^2$=48 for clean sand equivalent and =34 for in-situ
3	Fort Peck Dam	flow	700	33.5	5	7	30	S_u from Davis et al. (1988); N_1 from Poulos (1988); assumed $N_1=(N_1)_{60}$ (i.e. ER=60%)
4	Solfatara Canal Dike	flow	50	2.4	0	0	<5	N_1 from Poulos (1988); assumed $N_1=(N_1)_{60}$ (i.e. ER=60%)
5	Lake Merced Bank	slump	100	4.8	5	5	3	Case record validity doubtful, no data from fill in lake, data from natural ground behind failure zone
6	Kawagishi-Cho Building	building foundation	120	5.7	4	4		Case record is different from all other cases because it was not a slope
7	Uetsu Railway Embankment	flow	80	3.8	3	3		Original S_u based on runout; doubled to account for energy effects
8	Snow River Bridge Fill	lateral spread	50	2.4	5	6.5		
9	Koda Numa Embankment	flow	50	2.4	3	3		
10	San Fernando Juvenile Hall	lateral spread	200	9.6	2	6	65	S_u from Davis et al. (1988); original Seed (1987) $(N_1)_{60}$=2; Seed & Harder (1990) applied ΔN twice
11	Lower San Fernando Dam	flow/slump	500	23.9	6	8	25	$(N_1)_{60}$ from lower bound assessment of sandy SPTs in GEI (1988) and S_u from Davis et al. (1988)
12	Upper San Fernando Dam	slump	600	28.7	5.5	7.5	25	Department of Water Resources (1989) Figure 432 data corrected to pre-event
13a	Mochi-Koshi Tailings -Dam 2	flow	130	6.2	0	5	80	S_u from Davis et al. (1988) and Poulos (1988); $(N_1)_{60}$ from Ishihara (1984)
13b	-Dam 1	flow	60	0.0	0	5	80	As above
14	Whiskey Springs Fan	lateral spread	150	7.2	5	8	40	$(N_1)_{60}$ from Andrus and Youd (1989) from Becker equivalents
15	La Marquesa Dam - U/S Slope	slump	200	9.6	4	6	30	
16	La Marquesa Dam - D/S Slope	slump	400	19.2	5.5	7.5	20	
17	La Palma Dam	slump	200	9.6	3	4	15	
18	Lake Ackerman	flow/slump	215	10.3	3	3	0	
19	Nerlerk Embankment	flow	315	15.1	3	4	10	Lower bound $(N_1)_{60}$ based on Sladen et al. (1985) CPT data and $q_{c1}/(N_1)_{60}$=0.5
20	Heber Road	lateral spread	100	4.8	1	3	29	Spread for soil A2 also in Seed et al. (1985) trigger database; see Fear & McRoberts (1993, 1995)

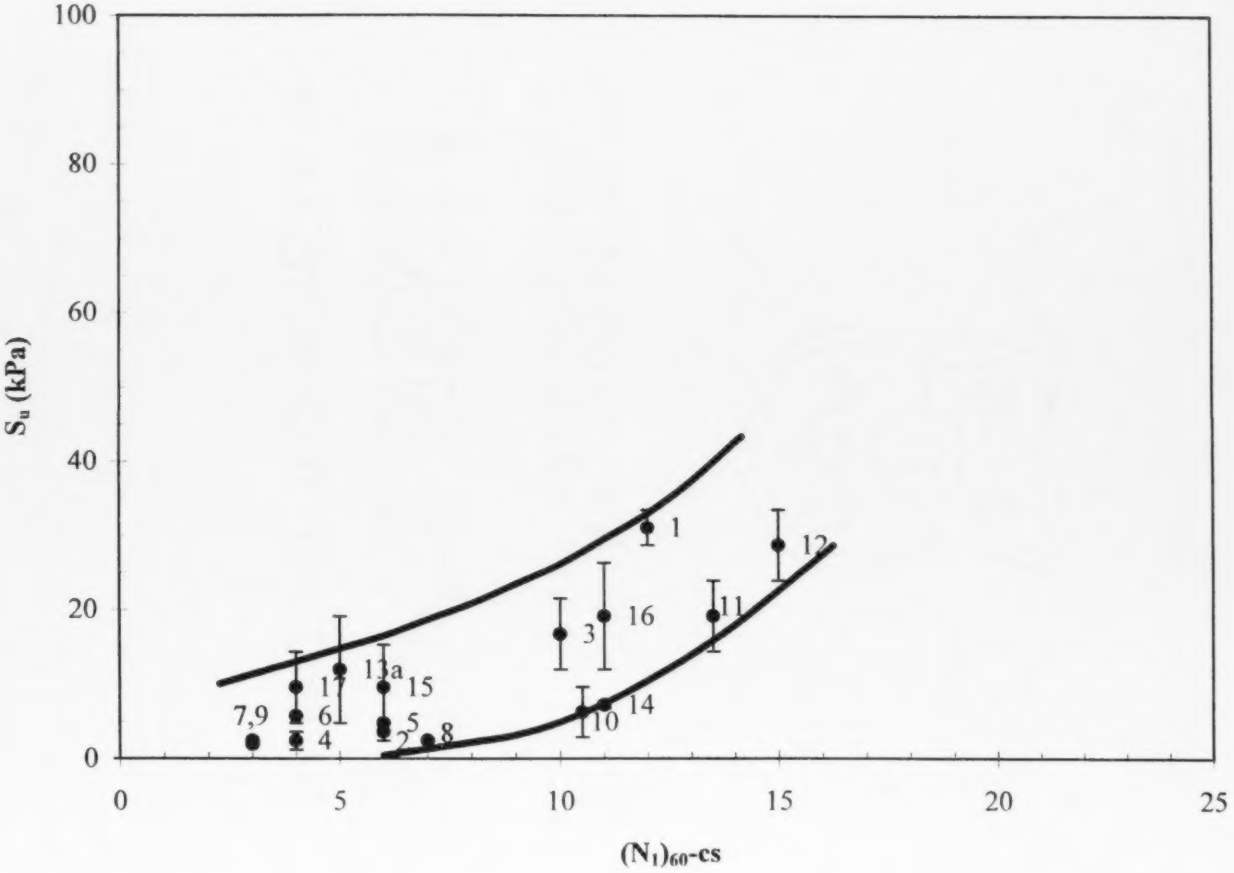

Figure 7-1 Relationship between clean sand equivalent SPT blowcount, $(N_1)_{60}$-cs, and undrained residual strength (S_u) from case histories (after Seed and Harder, 1990).

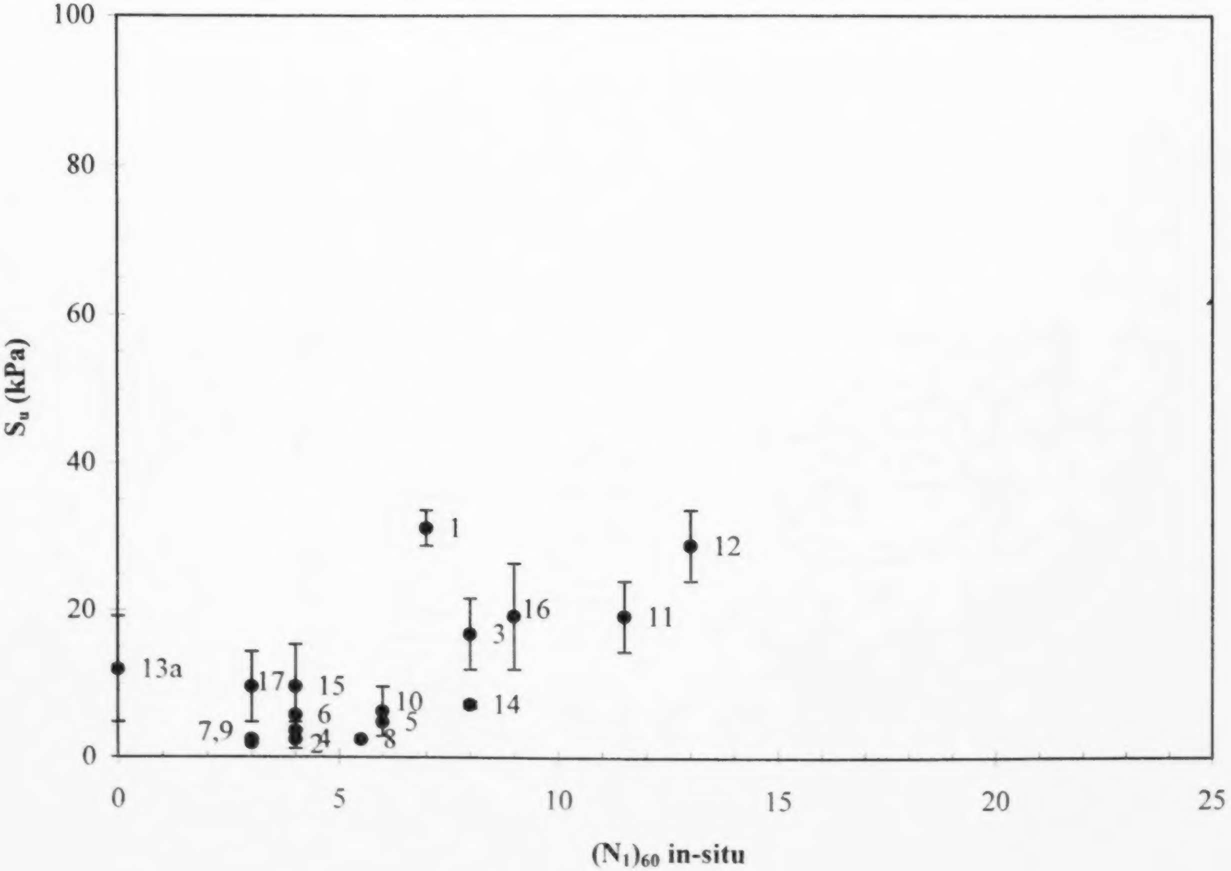

Figure 7-2 Relationship between field SPT blowcount, $(N_1)_{60}$ in-situ, and undrained residual strength (S_u) from case histories (after Seed and Harder, 1990).

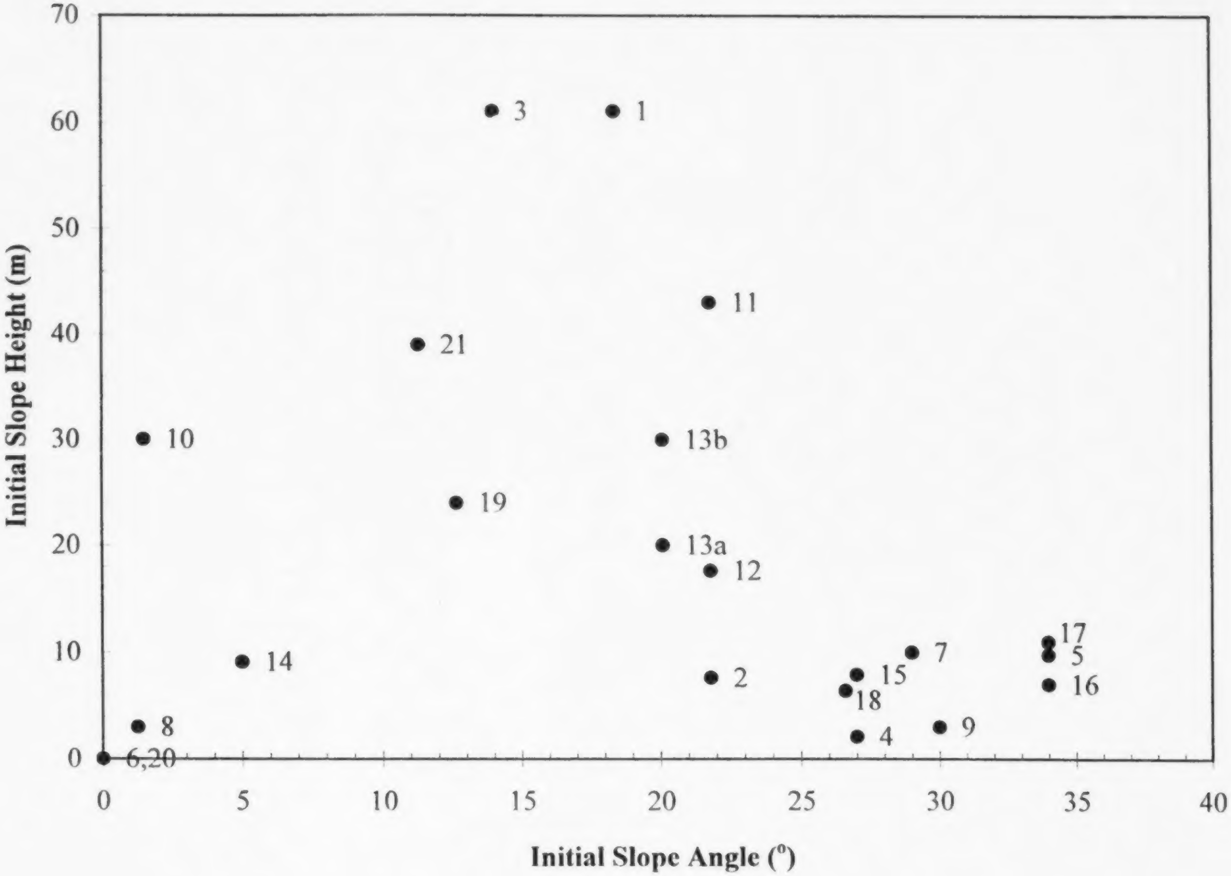

Figure 7-3 Case histories from Seed and Harder (1990) and Stark and Mesri (1992) plotted in terms of initial slope height and initial slope angle.

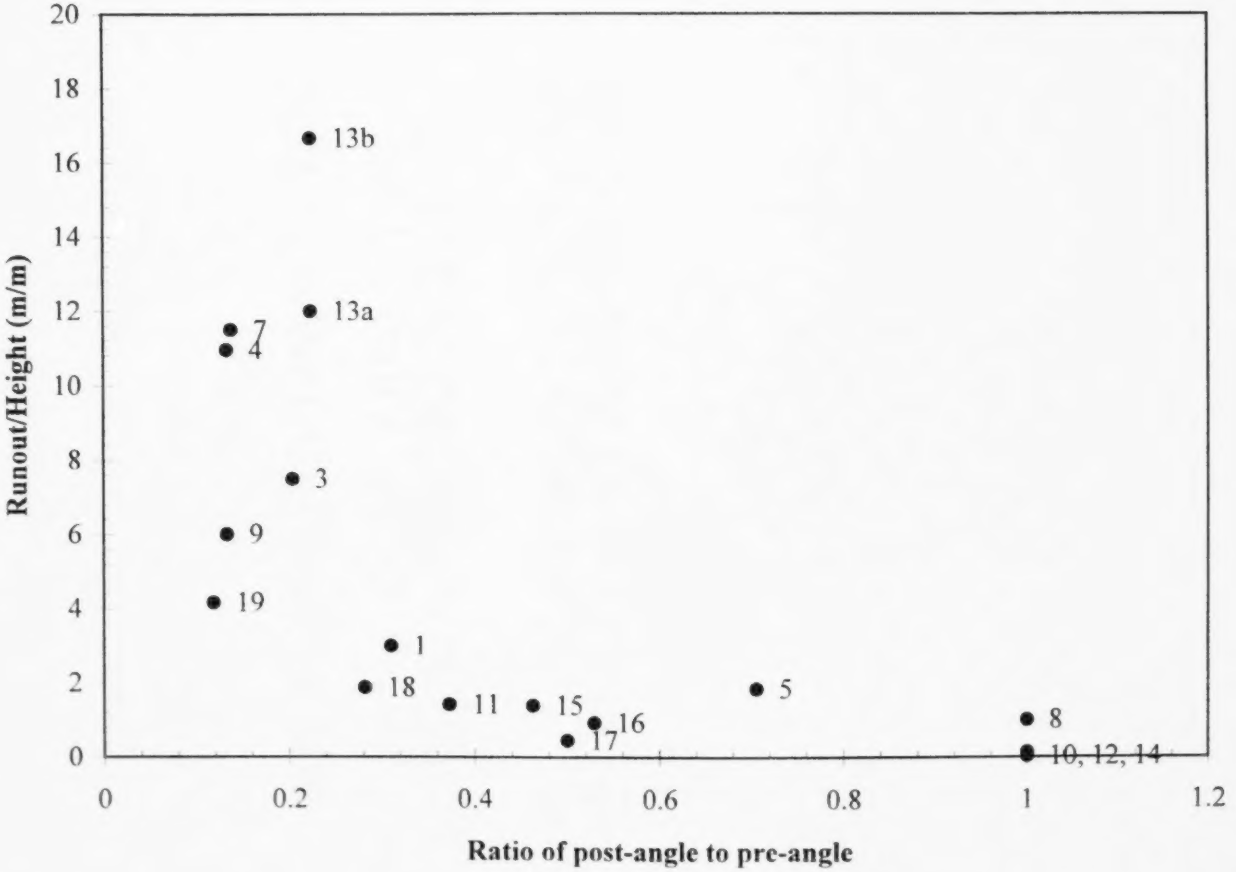

Figure 7-4 Case histories from Seed and Harder (1990) and Stark and Mesri (1992) plotted in terms of relative runout (runout/initial height) and slope angle ratio (ratio of post-failure slope angle to initial slope angle).

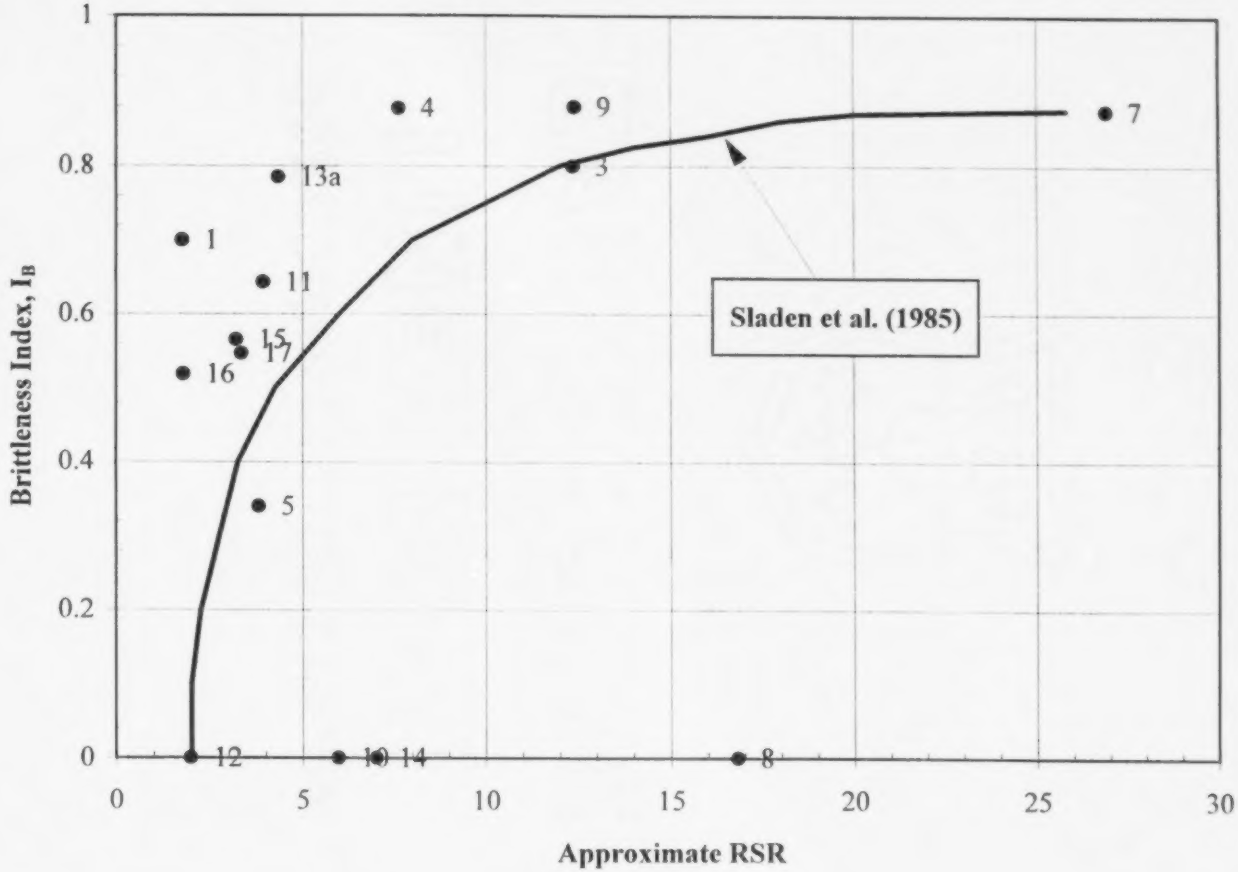

Figure 7-5 Case histories from Seed and Harder (1990) and Stark and Mesri (1992) plotted in terms of brittleness index (see Equation 7-3) and approximate RSR; the relationship suggested by Sladen et al. (1985) is also shown.

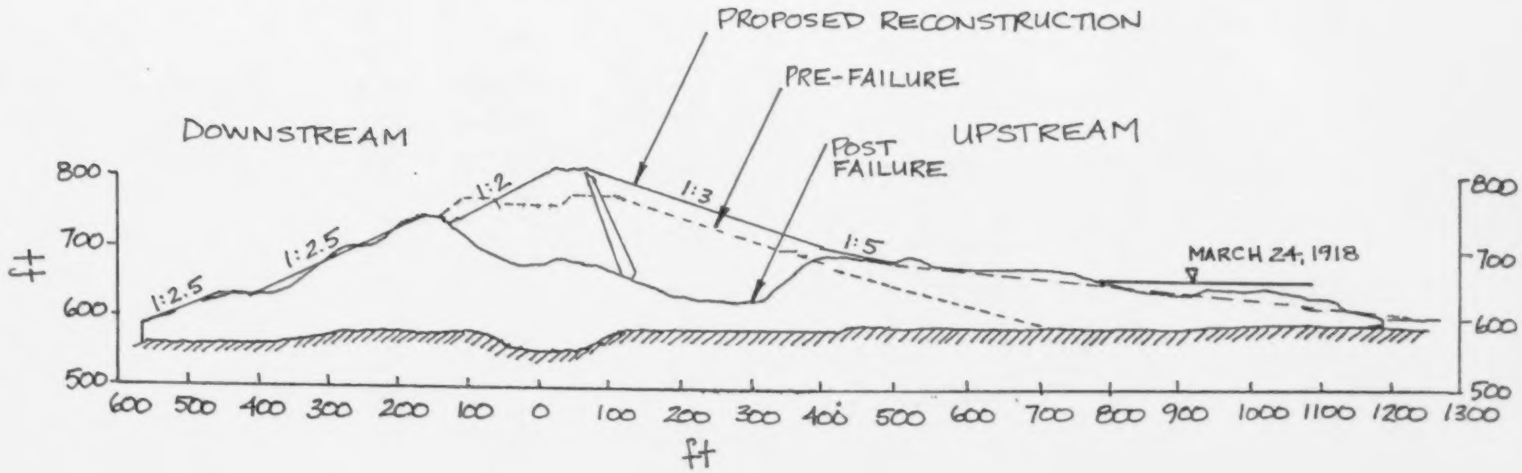
PROPOSED RECONSTRUCTION
PRE-FAILURE
POST FAILURE
DOWNSTREAM
UPSTREAM
1:2.5
1:2.5
1:2
1:3
1:5
MARCH 24, 1918
ft
800
700
600
500
600
500
400
300
200
100
0
100
200
300
400
500
600
700
800
900
1000
1100
1200
1300
ft
800
700
600
500

Figure 7-6 Example of a flow failure: cross-section of pre-failure and post-failure geometry of Calaveras Dam (case record 1), modified from Hazen (1918).

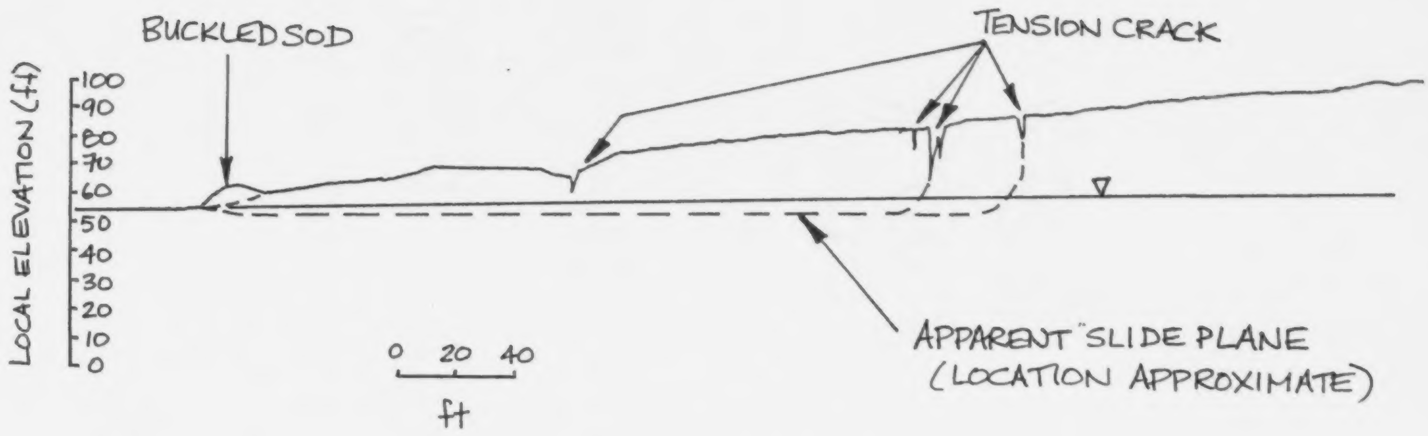
BUCKLED SOD
TENSION CRACK
LOCAL ELEVATION (ft)
100
90
80
70
60
50
40
30
20
10
0
0
20
40
ft
APPARENT "SLIDE PLANE
(LOCATION APPROXIMATE)

Figure 7-7 Example of a lateral spread: cross-section of pre-failure and post-failure geometry of Whiskey Springs Fan (case record 14), modified from Harder (1988).

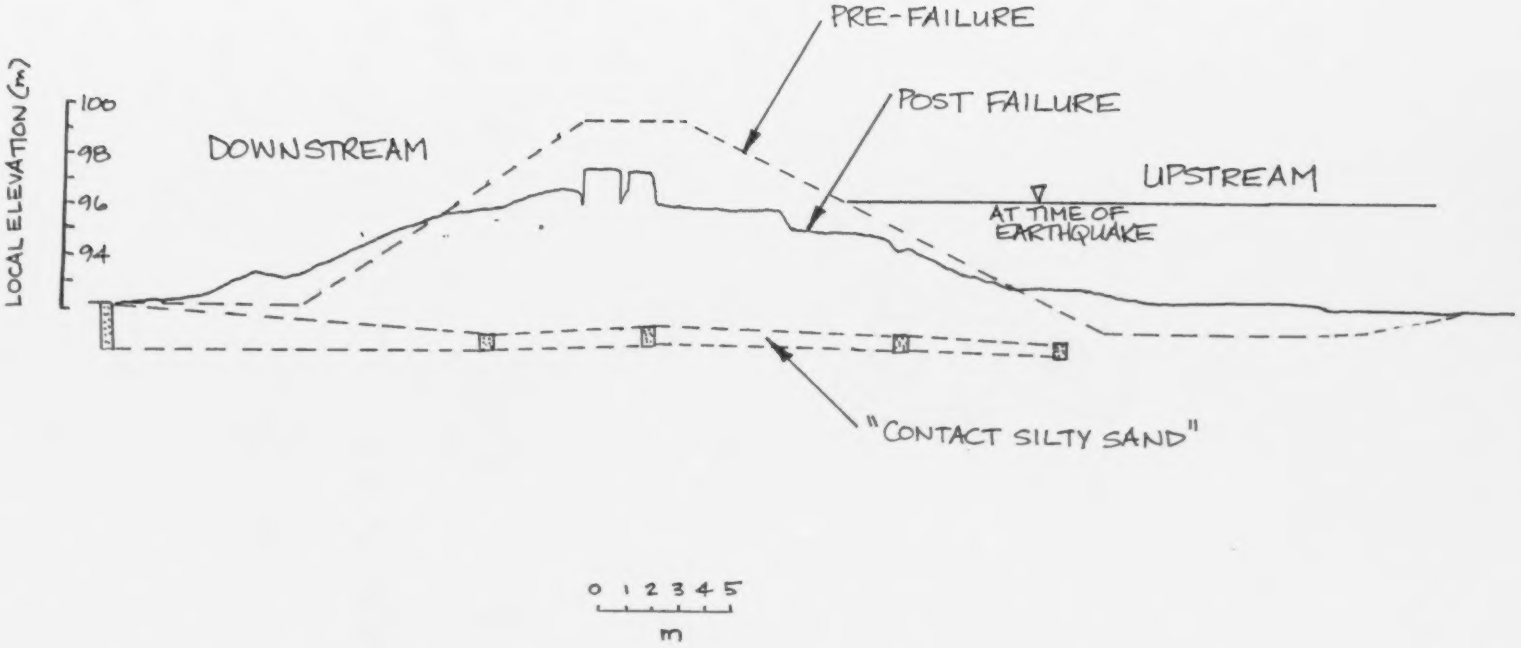
LOCAL ELEVATION (m)
100
98
96
94
DOWNSTREAM
PRE-FAILURE
POST FAILURE
UPSTREAM
AT TIME OF EARTHQUAKE
"CONTACT SILTY SAND"
0 1 2 3 4 5
m

Figure 7-8 Example of a slump failure: cross-section of pre-failure and post-failure geometry of La Marquesa Dam Upstream and Downstream (case records 15 and 16), modified from De Alba et al. (1988).

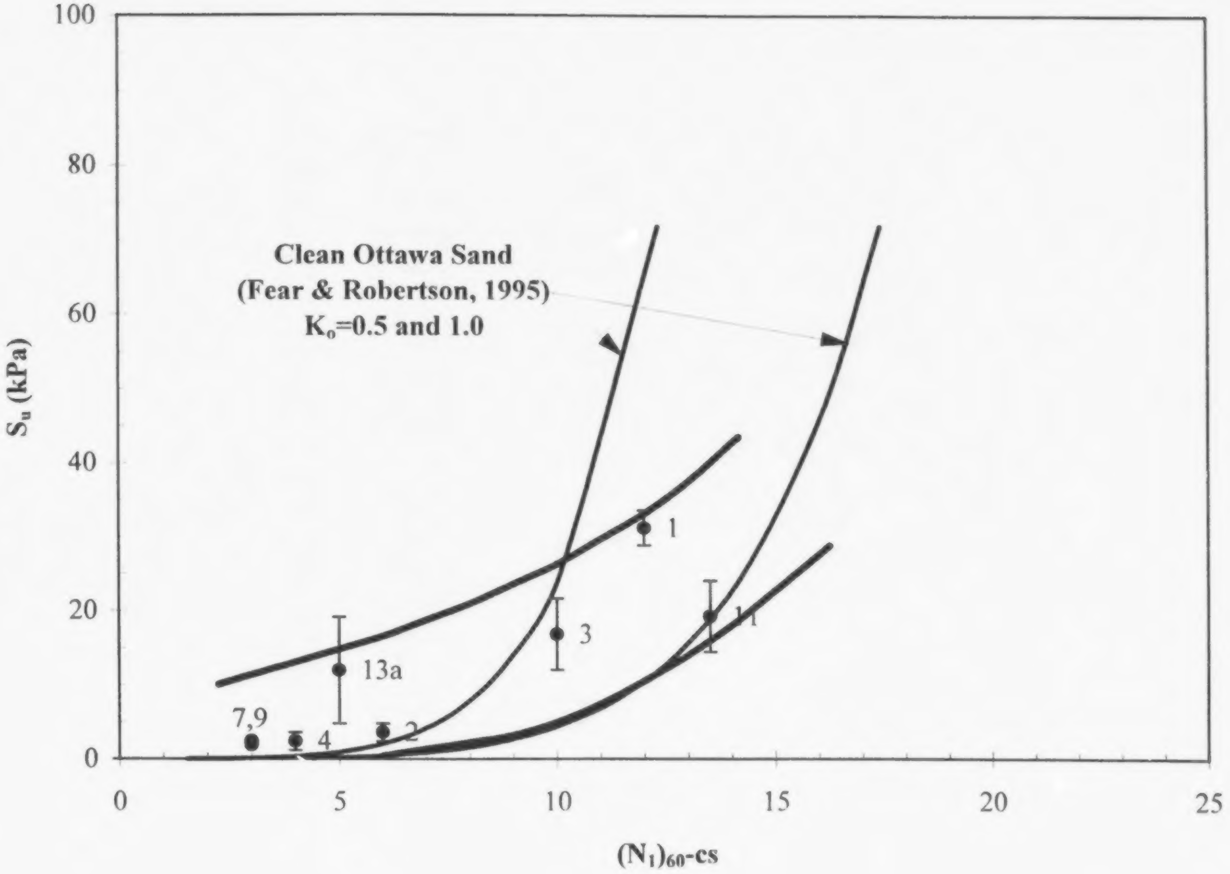

Figure 7-9 Plot of S_u versus clean sand equivalent SPT blowcount, $(N_1)_{60}$-cs, after Seed and Harder (1990) for those case histories classified as flow failures; theoretical clean Ottawa sand lines (see Chapter 5) shown for comparison.

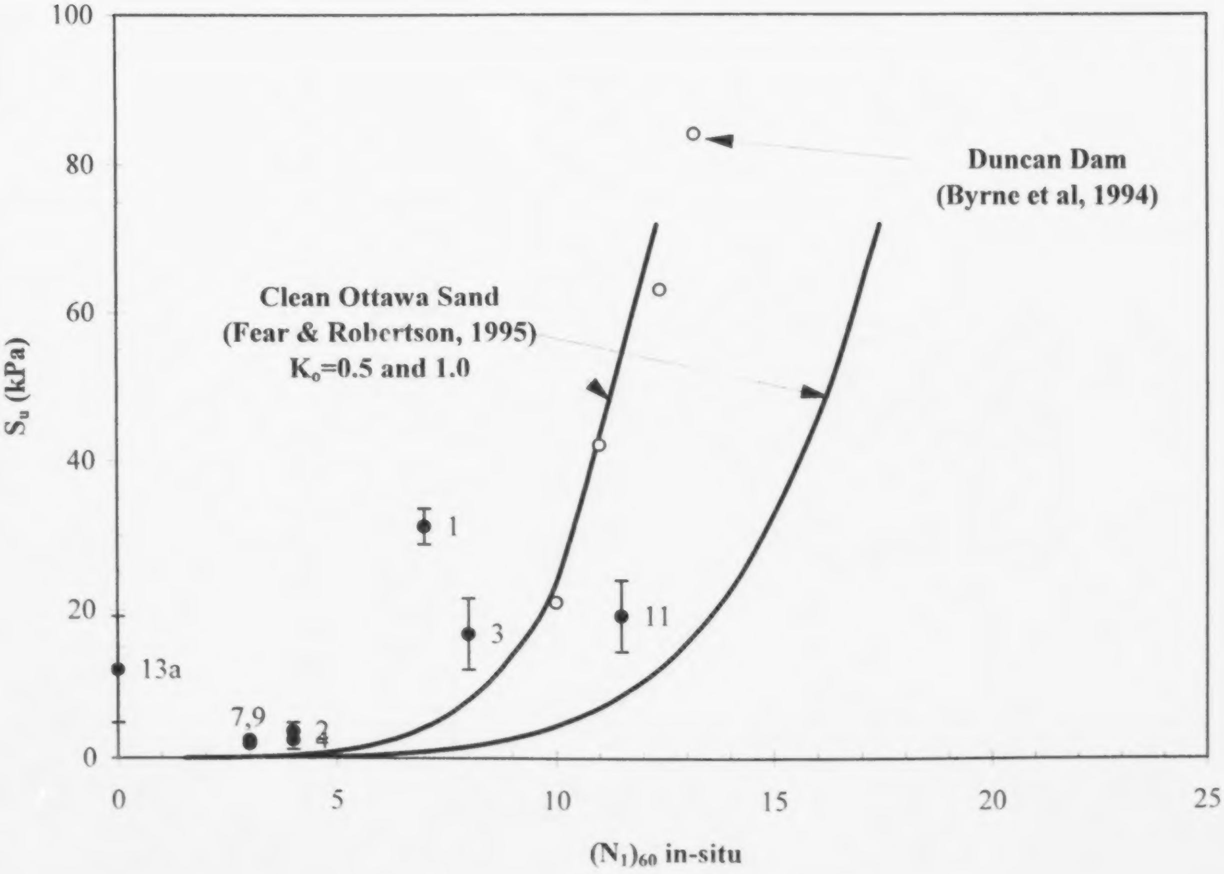

Figure 7-10 Plot of S_u versus field SPT blowcount, $(N_1)_{60}$ in-situ, after Seed and Harder (1990) for those case histories classified as flow failures; theoretical clean Ottawa sand lines (see Chapter 5) and Duncan Dam (21) results shown for comparison.

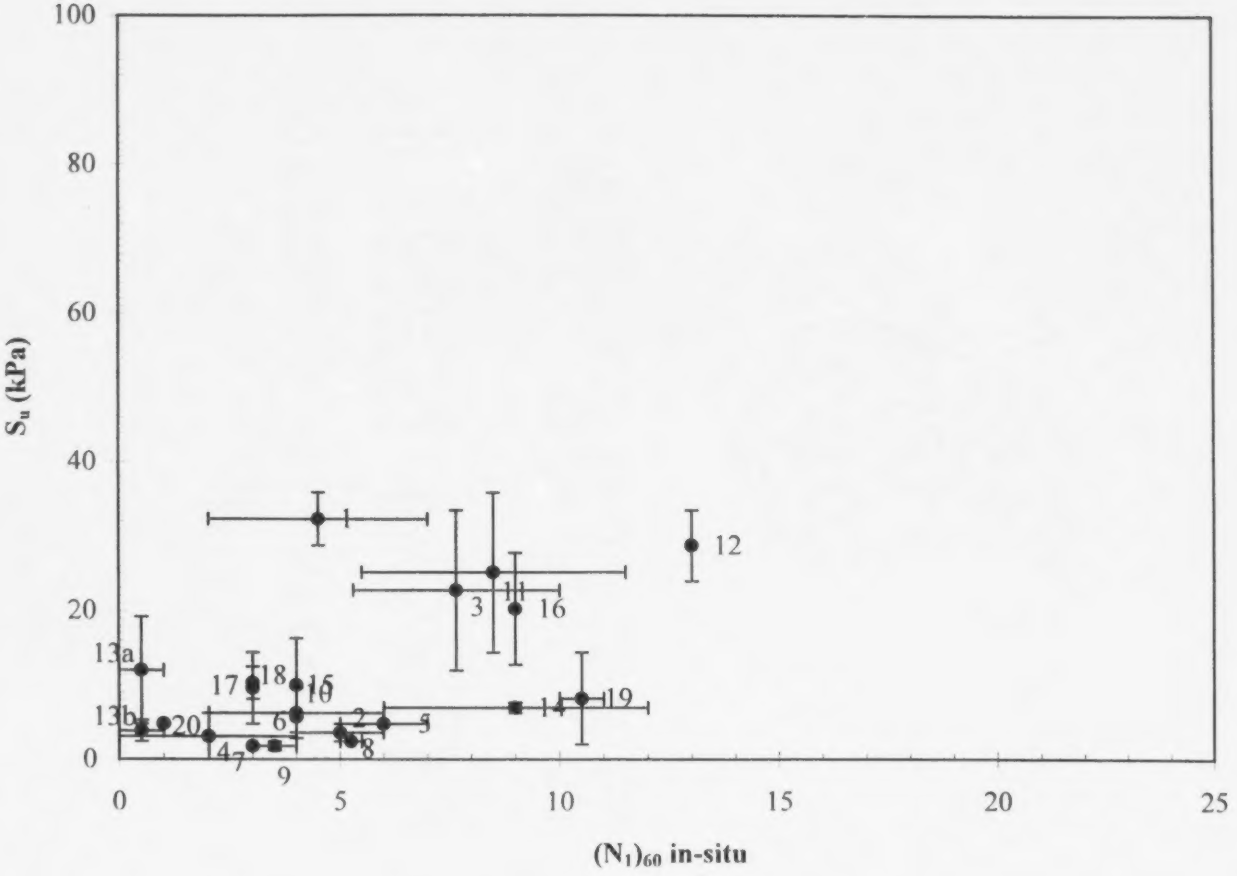

Figure 7-11 Range in S_u and $(N_1)_{60}$ in-situ reported by various authors (see Table 7-4) for the case histories in the Seed and Harder (1990) and Stark and Mesri (1992) database.

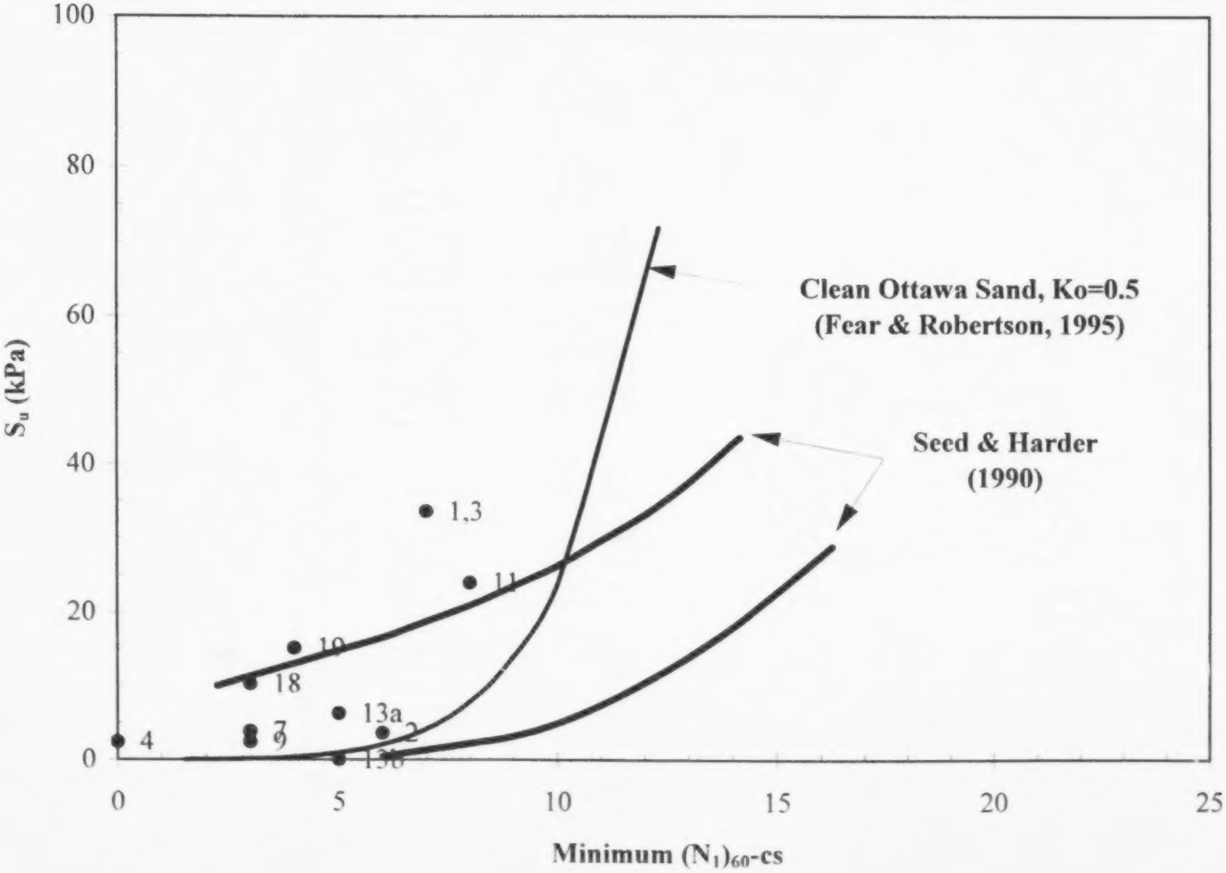

Figure 7-12 Plot of S_u versus minimum clean sand equivalent SPT blowcount, $(N_1)_{60}$-cs, for those case histories classified as flow failures; Seed and Harder (1990) lines and theoretical clean Ottawa sand line (see Chapter 5) shown for comparison.

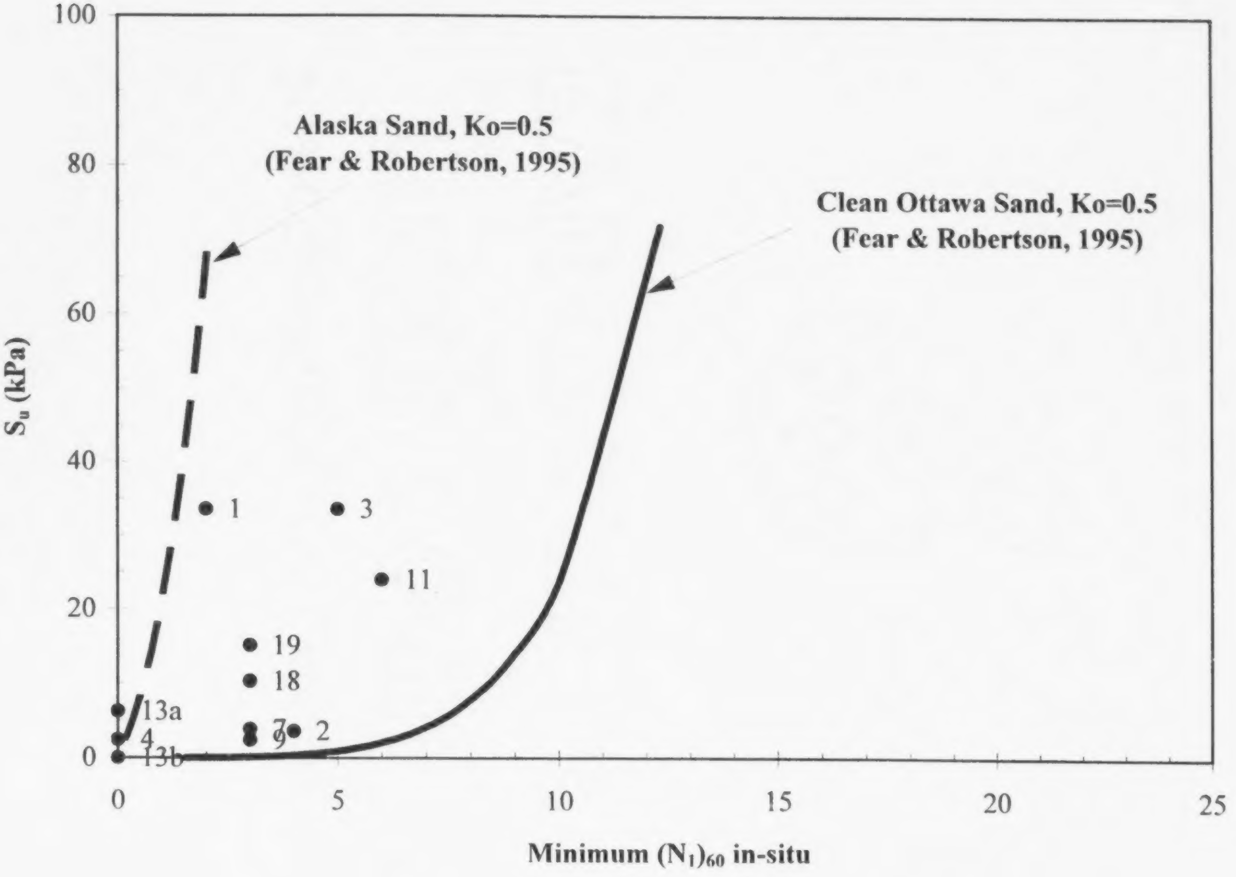

Figure 7-13 Plot of S_u versus minimum field SPT blowcount, $(N_1)_{60}$ in-situ, for those case histories classified as flow failures; Seed and Harder (1990) lines and theoretical clean Ottawa sand and Alaska sand lines (see Chapter 5) shown for comparison.

References

Andrus, R.D., Youd, T.L., and Carter, R.R. 1986. Geotechnical evaluation of a liquefaction induced lateral spread, Thousand Springs Valley Idaho. *Proceedings of the 22nd Annual Symposium on Engineering Geology and Soils Engineering*, Boise, ID, February 24-26, 1984.

Andrus, R.D. and Youd, T.L. 1987. Subsurface investigation of a liquefaction induced lateral spread - Thousand Springs Valley, Idaho. *Report prepared for the U.S. Army Corps of Engineers (miscellaneous paper GL-87-8)*, Dept. of Civil Engineering, Brigham Young University, Provo, Utah.

Andrus, R.D., and Youd, T.L. 1989. Penetration tests in liquefiable gravels. *Proceedings of the 12th International Conference on Soil Mechanics and Foundation Engineering*, Rio de Janeiro, 1: 679-682.

Bartlett, S.F., and Youd, T.L. 1992. Empirical analysis of horizontal ground displacement generated by liquefaction-induced lateral spread. *National Center for Earthquake Engineering Research, Technical Report NCEER-92-0021*.

Baziar, M.H., and Dobry, R. 1995. Residual strength and large-deformation potential of loose silty sands. *Journal of Geotechnical Engineering*, ASCE 121(12): 896-907.

Been, K., Conlin, B.H., Crooks, J.H.A., Fitzpatrick, S.W., Jefferies, M.G., Rogers, B.T., and Shinde, S. 1987. Back analysis of the Nerlerk berm liquefaction slides (Discussion). *Canadian Geotechnical Journal*, 24: 170-179.

Been, K., Crooks, J.H.A., Becker, D.E., and Jefferies, M.G. 1986. The cone penetration test in sands: part I, state parameter interpretation. *Géotechnique*, 36(2): 239-249.

Been, K., Jefferies, M.G., Crooks J.H.A., and Rothenburg, L. 1987. The cone penetration test in sands: part II, general inference of state. *Géotechnique*, 37(3): 285-299.

Bennett, M.J. 1989. Liquefaction analysis of the 1971 ground failure at the San Fernando Valley Juvenile Hall, California. *Bulletin of the Association of Engineering Geologists*, 26(2): 209-226.

Byrne, P.M., Imrie, A.L., and Morgenstern, N.R. 1994. Results and implications of seismic performance studies for Duncan Dam. *Canadian Geotechnical Journal*, 31:-979-988.

Casagrande, A. 1965. Role of the 'calculated risk' in earthwork and foundation engineering. The Terzaghi Lecture, *Journal of the Soil Mechanics and Foundations Division*, Proceedings of the ASCE, 91(SM4): 1-40.

Davis, Jr., A.P., Castro, G. and Poulos, S.J. 1988. Strengths backfigured from liquefaction case histories. *Proceedings of the Second International Conference on Case Histories in Geotechnical Engineering*, St. Louis, Mo., Paper No. 4.35, 1693-1701.

De Alba, P.A., Seed, H.B., Retamal, E., and Seed, R.B. 1988. Analysis of dam failures in 1985 Chilean earthquake. *Journal of Geotechnical Engineering*, ASCE, 114(12): 1414-1434.

Department of Water Resources 1989. Examination of the performance of Upper San Fernando Dam during the earthquake of February 9, 1971. *Addendum F of Bulletin 203-88 (The August 1, 1975, Oroville Earthquake Investigation, Supplement to Bulletin 203-78)*, The Resources Agency, State of California.

GEI Consultants 1988. Re-evaluation of the Lower San Fernando Dam, an investigation of the February 9, 1971 slide. *Submitted to U.S. Army Corps of Engineers, Waterways Experiment Station*, 2 Volumes.

Gu, W.H. 1992. Liquefaction and post-earthquake deformation analysis. *Ph.D. Thesis*, University of Alberta, Edmonton, Alberta, Canada.

Harder, L.F. 1988. Use of penetration tests to determine the cyclic loading resistance of gravelly soils during earthquake shaking. *Ph.D. Thesis*, Department of Civil Engineering, University of California, Berkeley.

Hazen, A. and Metcalf, L. 1918. Middle section of upstream side of Calaveras Dam slips into reservoir. *Engineering News-Record*, 80(14): 679-681.

Hazen, A. 1918. A study of the slip in the Calaveras Dam. *Engineering News-Record*, 81(26): 1158-1164.

Hryciw, R.D., Vitton, S., and Thomann, T.G. .1990. Liquefaction and flow failure during seismic exploration. *Journal of Geotechnical Engineering*, 116 (12): 1881-1899.

Ishihara, K. 1984. Post-earthquake failure of a tailings dam due to liquefaction of the pond deposit. *Proceedings of the International Conference on Case Histories in Geotechnical Engineering*, St. Louis, Mo, May 6-11, 3: 1129-1146.

Jefferies, M.G., Been, K., and Hachey, J.E. 1990. Influence of scale on the constitutive behaviour of sand. *Proceedings of the 43rd Canadian Geotechnical Conference, Laval University*, 1: 263-273.

Lee, K.L., Seed, H.B., Idriss, I.M., and Makdisi, F.I. 1975. Properties of soil in the San Fernando hydraulic fill dams. *Journal of Geotechnical Engineering*, ASCE, 101(GT8): 801-821.

Little, T.E., Imrie, A.S., Psutka, J.F. 1994. Geologic and seismic setting pertinent to dam safety review of Duncan Dam. *Canadian Geotechnical Journal*, 31: 919-926.

Lucia, P.C. 1981. Review of experiences with flow failures of tailings dams and waste impoundments. *Ph.D. Thesis*, University of California, Berkeley.

Lucia, P.C., Duncan, J.M. and Seed, H.B. 1982. Summary of research on case histories of flow failures of mine tailings impoundments. *Proceedings of the Workshop on Mine Waste Disposal Technology*, Denver, Colorado, Bureau of Mines Information Circular 8857.

Marcusen, W.F. III, Ballard, R.F., Jr., and Ledbetter, R.H. 1979. Liquefaction failure of tailings dams resulting from the near Izu Oshima earthquake, 14 and 15 January, 1978. *Proceedings, 6th Pan-American Conference on Soil Mechanics and Foundations Engineering*, Lima, Peru.

Marcusen, W.F. III, and Krinitzsky, E.L. 1976. Dynamic analysis of Fort Peck Dam. *Technical Report S-76-1*, U.S. Army Engineer Waterways Experiment Station, Vicksburg, Miss.

McRoberts, E.C., and Sladen, J.A. 1992. Observations on static and cyclic sand liquefaction methodologies. *Canadian Geotechnical Journal*, 29, 4.

Middlebrooks, T.A. 1940. Fort Peck slide (with discussions by Messrs. J. Field, J.D. Justin, W. Gerig, A.J. Ryan, G. Gilboy, F.E. Fahlquist, I.B. Crosby and T.A. Middlebrooks). *ASCE Transactions*, Paper No. 2144, 723-764.

Mishima, S., and Kimura, H. 1970. Characteristics of landslides and embankment failures during the Tokachioki earthquake. *Soils and Foundations*, 10(2): 39-51.

Pando, M., and Robertson, P.K. 1995. Evaluation of shear stress reversal due to earthquake loading for sloping ground, *Proceedings of the 48th Canadian Geotechnical Conference*, Vancouver, B.C., 2: 955-962.

Pillai, V.S., and Salgado, F.M. 1994. Post-liquefaction stability and deformation analysis of Duncan Dam. *Canadian Geotechnical Journal*, 31: 967-978.

Pillai, V.S., and Stewart, R.A. 1994. Evaluation of liquefaction potential of foundation soils at Duncan Dam. *Canadian Geotechnical Journal*, 31: 951-966.

Plewes, H.D., Pillai, V.S., Morgan, M.R., and Kilpatrick, B.L. 1994. In situ sampling, density measurements, and testing of foundation soils at Duncan Dam. *Canadian Geotechnical Journal*, 31: 927-938.

Poulos, S.J. 1988. Liquefaction and related phenomena. A*dvanced Dam Engineering for Design, Construction, and Rehabilitation*, R.B. Jansen (ed.), Van Nostrand Reinhold, New York, 292-320.

Rogers, B.T., Been, K., Hardy, M.D., Johnson, G.J., and Hachey, J. 1990. Re-analysis of Nerlerk B-67 berm failures. *Proceedings of the Canadian Geotechnical Engineering Conference*, Laval University, 1, 227-237.

Ross, G.A. 1968. Case studies of soil stability problems resulting from earthquakes. *Ph.D. Thesis*, University of California at Berkeley.

Ross, G.A., Seed, H.B., and Migliaccio, R.R. 1969. Bridge foundations in Alaska earthquake. *Journal of Soil Mechanics and Foundations Division*, ASCE, 95(4): 1007-1036.

Seed, H.B. 1969. Analysis of Sheffield Dam failure. *Journal of the Soil Mechanics and Foundations Division*, Proceedings of the ASCE, 95(SM 6): 1453-1490.

Seed, H.B. 1979. Considerations in the earthquake-resistant design of earth and rockfill dams. The Rankine Lecture, *Géotechnique*, 29(3): 215-263.

Seed, H.B. 1987. Design problems in soil liquefaction. *Journal of Geotechnical Engineering*, ASCE 113(8): 827-845.

Seed, R.B., and Harder, L.F. 1990. SPT-based analysis of cyclic pore pressure generation and undrained residual strength. *Proceedings of the H. Bolton Seed Memorial Symposium*, 2, 351-376.

Seed, H.B., Idriss, I.M., Lee, K.L., and Makdisi, F.I. 1975. Dynamic analysis of the slide in the lower San Fernando Dam during the earthquake of February 9, 1971. *Journal of the Geotechnical Engineering Division*, ASCE, 101(GT9): 889-912.

Seed, H.B, Tokimatsu, K., Harder, L.F., and Chung, R.M. 1984. The influence of SPT procedures in soil liquefaction resistance evaluations. *Earthquake Engineering Research Center Report No. UCB/EERC-84/15*, College of Engineering, University of California, Berkeley, California.

Seed, H.B., Seed, R.B., Harder, L.F., and Jong, H-L. 1988. Re-evaluation of the slide in the Lower San Fernando dam in the earthquake of Feb. 9, 1971. *Report No. UCB/EERC-88/04, Earthquake Engineering Research Center*, University of California, Berkeley.

Sego, D.C., Robertson, P.K., Sasitharan, S., Kilpatrick, B.L., and Pillai, V.S. 1994. Ground freezing and sampling of foundation soils at Duncan Dam. *Canadian Geotechnical Journal*, 31: 939-950.

Skempton, A. W. 1986. Standard penetration test procedures and the effects in sands of overburden pressure, relative density, particle size, ageing and overconsolidation. *Geotechnique*, 36(3): 425-447.

Sladen, J.A. 1989a. Cone penetration test calibration for Erksak (Beaufort Sea) sand: Discussion. *Canadian Geotechnical Journal*, 26: 173-177.

Sladen, J.A. 1989b. Problems with interpretation of sand state from cone penetration test. *Géotechnique*, 39(2): 323-332.

Sladen, J.A., D'Hollander, R.D., Krahn, J. and Mitchell, D.E. 1985a. Back analysis of the Nerlerk berm liquefaction slides. *Canadian Geotechnical Journal*, 22: 579-588.

Sladen, J.A., D'Hollander, R.D., and Krahn, J. 1985b. The liquefaction of sands, a collapse surface approach. *Can. Geotech. J.*, 22: 564-578.

Sladen, J.A., D'Hollander, R.D., Krahn, J. and Mitchell, D.E. 1987. Back analysis of the Nerlerk berm liquefaction slides: Reply. *Canadian Geotechnical Journal*, 24: 179-185.

Sladen, J.A., and Hewitt, K.J. 1989. Influence of placement method on the in situ density of hydraulic sand fills. *Canadian Geotechnical Journal*, 26: 453-466.

Stark, T.D., and Mesri, G.M. 1992. Undrained shear strength of liquefied sands for stability analysis. *Journal of Geotechnical Engineering*, ASCE, 118 (11): 1727-1747.

U.S. Army Corps of Engineers 1939. *Report on the slide of a portion of the upstream face of the Fort Peck Dam, Fort Peck, Montana.* U.S. Government Printing Office, Washington.

Yamada, G. 1966. Damage to earth structure and foundations by the Niigata earthquake June 16, 1964, in JNR. *Soils and Foundations*, 6(1): 1-13.

Youd, T. L. 1993. Liquefaction-induced lateral spread displacement. *Technical Note N-1862*, Naval Civil Engineering Laboratory, Port Hueneme, California.

Youd, T.L. and Bennett, M.J. 1983. Liquefaction sites, Imperial Valley, California. *Journal of Geotechnical Engineering*, ASCE, 109(3): 440-457.

Youd, T.L., Harp, E.L., Keefer, D.K., and Wilson, R.C. 1985. The Borah Peak, Idaho Earthquake of Oct. 28, 1983 -- liquefaction. *Earthquake Spectra*, Earthquake Engineering Research Institute, 2(1).

CHAPTER 8

WORKED EXAMPLE[1]

8.1 Introduction

Chapters 3 and 4 presented frameworks for evaluating cyclic softening (liquefaction) potential and flow liquefaction potential, respectively, at a given site. This chapter presents a worked example for the CANLEX Phase II Massey site, with occasional references to the other Phase II site (Kidd site) to illustrate the application of the proposed methods for evaluating cyclic softening potential and flow liquefaction potential. Some comparisons are also made between the Massey and Kidd sites and the Phase I and Phase III sites, which were both located at Syncrude, just outside of Fort McMurray, Alberta. Both in-situ testing and ground freezing and sampling were conducted at each of the four sites. The frozen (undisturbed) samples were then subjected to a variety of tests in the laboratory to determine their response to both monotonic and cyclic undrained loading.

The Massey and Kidd sites are situated in the Fraser River Delta, outside of Vancouver, B.C. and were initially selected as a result of the CANLEX Phase II site selection activity (Stewart, 1993). The Massey site is situated near the south end of the Massey Tunnel (see Figure 8-1) and consists of naturally deposited sands that are approximately 200 years old (Monahan et al., 1995). The Kidd site is also indicated in Figure 8-1. The Kidd site is situated next to the B.C. Hydro Kidd 2 Substation and consists of naturally deposited sands that are approximately 4000 years old (Monahan et al., 1995).

8.2 Soil Parameters for the Massey Site

8.2.1 Index parameters

Index parameters for the Massey site are given in Table 8-1 and can be compared with those for the other CANLEX sites (Phases I to III) and for Ticino sand, which are also given in Table 8-1. Details of the data review results for each of the CANLEX sites will be eventually be presented in CANLEX project final reports. Table 8-1 indicates that the

---

[1] *A version of this chapter is contained in a Canadian Liquefaction Experiment (CANLEX) Report. Fear, C.E. and Robertson, P.K. 1996. CANLEX Phase II data review report.*

Phase II sites (Massey and Kidd) which consist of natural sand deposits in the Fraser River Delta of B.C., are significantly older than the deposits at the other test sites, which are artificially placed sand deposits as a result of the mining industry. Table 8-1 also indicates that the target zones at the Phase II sites are significantly shallower than at the Phase I site and, thus, the sand deposits are at much lower effective overburden stresses. The Phase III site has the shallowest target zone of all of the sites.

8.2.2 Choice of reference ultimate state line (USL)

Prior to obtaining samples from the Phase II sites, Chillarige et al. (1995) conducted monotonic triaxial compression tests on isotropically consolidated samples of reconstituted sand from Sand Heads in the Fraser River Delta. The index parameters for the Fraser River sand from Sand Heads are similar to those for the Massey and Kidd sites. Both moist tamping and water pluviation techniques were used to prepare the samples. Drained and undrained tests were performed. By plotting the ultimate state (end of test) points from all of the tests on an e-p' plot, the USL was estimated. The USL was found to be bi-linear in nature, with a break occurring at a value of p' of approximately 530 kPa. This is consistent with non-linear USLs reported in the literature for other sands, as summarized by Sasitharan et al. (1994) and shown in Chapter 4 (see Figure 4-18). The sand at the Phase II sites is similar to that from Sand Heads and, therefore, the USL reported by Chillarige et al. (1995) was initially adopted as the reference USL for this study.

However, with additional testing of Fraser River sand from both the Massey and Kidd sites, it was found that the Sand Heads USL did not fit all of the Fraser River sand data well. Figure 8-2 presents the results of testing both undisturbed and reconstituted samples of Fraser River sand, in terms of the state at the end of each test on an e-p' plot. Results of testing undisturbed samples from both the Kidd and Massey sites under anisotropic stress states are presented (tested at the University of British Columbia (UBC), Université Laval (Laval) and the University of Alberta (U. of A.)). Test results are also presented for reconstituted samples, as follows: anisotropically consolidated samples of Massey sand prepared by moist tamping (Ayoubian, 1995) and Fraser River sand prepared by water pluviation (Thomas, 1992); the isotropically consolidated Sand Heads samples by Chillarige et al. (1995); and isotropically consolidated samples of Massey sand prepared by moist tamping (Pouliot and Konrad, 1995). Superimposed on Figure 8-2 is the selected reference USL which has a break at approximately p'=260 kPa and associated values of Γ and λ_{ln} as given in Table 8-2. The choice of the steeper portion of the reference USL was driven by the results of tests on undisturbed samples. All of these tests, particularly the triaxial extension tests, were still dilating to some extent at the end of the test; consequently, the true USL at high stresses may be located slightly further to the right. The choice of the flatter portion of the reference USL was driven by the results of Chillarige et al. (1995) and Ayoubian (1995) for moist-tamped samples which strain-softened to ultimate state. The resulting reference USL is consistent with the non-linear USLs reported in the literature for other sands, as summarized by Sasitharan et al. (1994) and shown in Chapter 4 (see Figure 4-18). In fact, the Fraser River reference USL selected here is more consistent with the historical data for other sands, particularly at high stresses, than the USL chosen by Chillarige et al. (1995), based on Sand Heads data alone.

Figure 8-3 presents the quasi-steady-state (QSS) conditions on an e-p' plot for the Fraser River samples shown in Figure 8-2 that experienced a QSS. Typically, only samples tested in triaxial extension experienced a true QSS; the triaxial compression samples tended to continuously dilate throughout a test. Superimposed on Figure 8-3 is the approximate QSSL for both the Massey and Kidd sites, corresponding to a shift in the reference USL of approximately ΔRSR=26. Obviously, the data available at present is limited; however, the data from the two Phase II sites does appear to follow a similar trend, suggesting that soil fabric at the two sites may be similar. The scatter of data around the approximate QSSL is to be expected, following the findings by Ishihara (1993). It is interesting to note that the water pluviated samples of Fraser River sand tested by Thomas (1992) have significantly different QSS points than the Phase II undisturbed samples; this is likely due to differences in soil fabric (Ishihara, 1993). As more laboratory test data become available, the selected QSSL may be modified and further comments may be made concerning the uniqueness of the line for the Phase II sites.

8.2.3 Grain characteristic parameters

Various parameters must be estimated to be input into the proposed framework for evaluating flow liquefaction potential outlined in Chapter 4. These grain characteristic parameters for the Phase II sites are presented in Table 8-2. Grain characteristic parameters for the Phase I and Phase III sites are also presented for comparison. The sand at the Phase II sites appears to be slightly more compressible, having a slightly steeper reference USL at low stresses (i.e. slightly larger value of λ_{ln}). The reference USL also falls above that for Syncrude sand (based on testing of Phase I Syncrude sand; Phase I and Phase III are assumed to have the same USL until further test results are available from Phase III) on an e-ln p' plot, indicating that it is possible for the Fraser River sand to have looser void ratios (at the same stress level) than Syncrude sand without being more contractant in nature. At the Phase II sites, the parameter A (linking V_{s1} to e) requires a correction for aging, reflecting the fact that the deposits are significantly older than the Phase I and Phase III deposits. A larger correction is required at the Kidd site (approx. 4000 years old) than at the Massey site (approx. 200 years old).

8.3 Review of Field Data and Void Ratio Interpretations

The target zone for undisturbed sampling and in-situ testing at the Massey site was selected from 8 to 13 m depth, based on initial site screening. Figure 8-4 shows a detailed site plan of the testing area, indicating the locations of the various in-situ tests relative to the freezepipe and sampling boreholes. Detailed logs and interpretations for all of the in-situ tests are presented in the CANLEX report by Fear and Robertson (1996).

Six CPTs, identified as M9401 through to M9407, were conducted through the target zone at the Massey site (Campanella, 1995). Two SPTs, identified as SPT1 and SPT2, were conducted through the target zone at the Massey site (Campanella, 1995).

Six of the CPTs were seismic CPTs and thus, six shear wave velocity logs, identified as M9401 through to M9406, were conducted at the Massey site (Campanella, 1995). Only two of the shear wave velocity logs (M9401 and M9402) pass through the entire target zone. For some unknown reason, the other shear wave velocity logs start approximately midway through and extend beyond the specified target zone.

Two geophysical logs, identified as MTH1 and MTH2, were conducted through the target zone at the Massey site (Lawrence et al., 1995). Each geophysical hole was run four times and the results were subjected to a 5 filter point smoothing (Lawrence et al., 1995). Lawrence et al. (1995) regarded the first run in each hole as being unreliable; therefore, the average interpreted void ratio profiles based on the last three runs in each borehole were used in this study.

Pressuremeter testing was also carried out in the target zone at the Massey Site (Campanella, 1995). This study adopted an average K_o of 0.5 for interpretation of the Massey Site.

8.3.1 In-situ testing results

Figures 8-5a to c present the in-situ test signatures, corrected for effective overburden stress (and energy effects, in the case of the SPT profiles), for each of the shear wave velocity logs, CPTs and SPTs at the Massey site. The thick solid horizontal lines at 8 m and 13 m in these figures and in subsequent figures in this chapter indicate the extent of the target zone at the Massey site. In Figure 8-5a, the shear wave velocity profiles are shown as step functions, indicating that the shear wave velocity is measured (using a method of differences), as an average value over a given interval (typically about 1 m). In Figure 8-5b, the CPT profiles are shown as continuous profiles, since measurements are typically taken every few centimetres. In Figure 8-5c, the SPT profiles are shown as discrete points, corresponding to the midpoint of the 30 cm over which the value of N was measured. The bars attached to each point indicate the 30 cm range over which N was determined.

The six V_{s1} and seven q_{c1} profiles are very consistent with little scatter. The $(N_1)_{60}$ profile from SPT2 is fairly constant, but SPT1 shows considerable scatter and, hence, the two $(N_1)_{60}$ profiles are not very consistent. The CPT profiles, however, do show that there is some variability in the deposit. In the target zone, the overall average measured values and standard deviations (SD) are as follows: V_{s1}=168.2 m/s (SD=6.4 m/s), q_{c1}=5.34 MPa (SD=1.00 MPa), and $(N_1)_{60}$=10.3 (SD=3.8).

8.3.2 Conventional void ratio interpretations

Figures 8-6a to d presents the estimated void ratio profiles at the Massey site, based on conventional interpretations of the CPT and SPT, interpretations of the shear wave velocity measurements and interpretations of the geophysical logs. The solid dots that are superimposed on Figures 8-6a to d represent the void ratios of the undisturbed frozen samples. At present, all of the in-situ void ratios are based on volume calculations made at U. of A. prior to sending out the samples to the various laboratories (Hofmann, 1995). Void ratios of the samples obtained using a large diameter sampler from Laval were determined in the same way and are shown on Figures 8-6a to d for comparison, as indicated by the open dots. The void ratios for both the undisturbed and Laval sampler samples are summarized in Table 8-3. Note that void ratio axes in Figures 8-6a to d have been plotted from 0.70 to 1.1, corresponding approximately to e_{min} and e_{max} for the sand at the Massey site (see Table 8-1). Thus approximate relative densities for the soil samples (D_r) can be computed directly.

For the samples tested to date, the average void ratio for the undisturbed samples is 0.976 (SD=0.046) ($Dr \approx 31\%$; SD=11.5%) and for the samples obtained using the Laval large diameter sampler is 0.942 (SD=0.077). It is important to note that the actual average in-situ void ratio in the target zone is likely slightly less than 0.976 because the undisturbed samples tested to date were selected in attempt to test the loosest samples first. As a result, the undisturbed void ratios are likely biased towards higher than average values. As more testing is conducted, further comments can be made about the actual average and range in void ratio in-situ. The void ratios of the Laval sampler samples appear to agree with the undisturbed void ratios except for the two samples at about 9.25 m, which appear to have significantly lower void ratios. As void ratios from additional samples become available, further conclusions regarding the Laval sampler samples can be made.

The thick semi-vertical line superimposed on each of Figures 8-6a to d represents the void ratios corresponding to an RSR of 1 over the depth of the target zone, based on the selected Fraser River reference USL (see Figure 8-2 and Table 8-2). The RSR=1 line corresponds to a relative density (D_r) of approximately 25%. Most of the undisturbed samples tested to date have void ratios less than the RSR=1 line (i.e. $D_r > 25\%$), although some of the samples have higher void ratios, particularly between 10 and 11 m.

Figure 8-6a presents the results of the conventional void ratio interpretation of the CPT, based on applying the method by Baldi et al. (1986) described in Chapter 4 (see Equations 4-1 and 4-2) to the maximum, minimum and average boundaries of all of the CPT cone tip resistance, q_c, profiles. Figure 8-6b presents the results of the conventional void ratio interpretation of the SPT, based on the method by Skempton (1986), as described in Chapter 4 (see Equations 4-2 and 4-3). Figure 8-6c presents the results of the void ratio interpretation of the shear wave velocity, as described in Chapter 4 (see Equation 4-4) and the values of A and B given in Table 8-2. Figure 8-6d presents the results of the void ratio interpretation of the geophysical logs as given by Lawrence et al. (1995), but with the value of G_s changed to 2.68 from the value of 2.74 used in the Lawrence et al. (1995) report (see Equation 4-6 in Chapter 4). According to Hofmann (1995), this is the correct value of G_s for the sand at the Massey site and was the value used to estimate the void ratios of the frozen samples.

The interpreted void ratio profiles from the geophysical logs seem to best capture the overall trend and range of the frozen sample void ratios in the target zone at the Massey site, predicting an average void ratio of 0.991 (SD=0.071). This is higher than the average of the void ratios of the undisturbed samples tested to date. The greatest differences between the undisturbed void ratios and the geophysical predicted void ratios appears to occur between approximately 11.5 and 12.5 m, at which depths the geophysical method predicts significantly higher void ratios. The two geophysical profiles are generally consistent, but indicate a rapid variation in void ratio with depth at the site. The interpreted void ratio profiles from the shear wave velocity measurements reasonably capture the trend and range of the frozen sample void ratios at the Massey site, predicting an average void ratio of 0.934 (SD=0.048). This is not surprising, because the value of A was adjusted from the value measured in the laboratory on young reconstituted Fraser River sand to correct for aging effects (see Table 8-2) and produce a reasonable fit. Correcting the factor A for aging is a trial and error process at present, because the corrections suggested by Robertson et al. (1995) and described in Chapter 4 (see Figure 4-5) were only estimates. What appeared to be little scatter in the V_{s1} profile converts to more significant scatter in the void ratio profile predicted by shear wave velocity, due to the sensitivity of the method. However, unfortunately, much of the shear wave velocity testing at the Massey site was conducted outside the target zone (at greater depths) where there are no frozen samples available for reference. The maximum and minimum boundaries to void ratio based on the conventional method of interpreting the CPT at the Massey site do not fully capture the range of void ratios for the frozen samples, although the average void ratio profile appears to generally follow the trend of the frozen samples. The overall predicted average void ratio in the target zone using this method is 0.944. In general, the conventional interpretation of the SPT at the Massey site appears to underpredict the undisturbed void ratios, giving an average void ratio of 0.909 (SD=0.035). Corrections for aging should also be applied to the CPT and SPT data.

8.3.3 Correlations between in-situ tests

Figures 8-5a to c showed that, in the target zone at Massey, reasonably constant values of both Vs1 and qc1 were measured, while the measured $(N_1)_{60}$ appeared to be more scattered. The effects of these trends are illustrated in Figures 8-7a to c, which compare the CPT, SPT and shear wave velocity logs at the Massey site .

In order to compare the CPT and the SPT, the closest pairs of test types were determined by examining the detailed site plan (see Figure 8-4). SPT1 and CPT M9401 were paired together, as were SPT2 and CPT M9406. Based on the comparison between these two pairs of tests, Figure 8-7a shows that the value of $q_{c1}/(N_1)_{60}$ is rather scattered in the target zone, but has an average value of 0.58 (SD=0.17). This value is within the historical range for a sand. The scatter is predominantly due to the scatter in the SPT $(N_1)_{60}$ values (see Figure 8-5c).

Comparing the CPT and shear wave velocity was straightforward because each CPT and shear wave velocity pair are conducted in the same hole and are directly comparable. However, unfortunately, many of the seismic measurements were made beyond the extent of the target zone (at greater depths). At Massey site, as shown in Figure 8-7b, the value of Y was found to be fairly consistent, with an average value of 110.2 (SD=4.6) in the target zone. This would correspond to a moderately compressible sand. In general, the value of Y appears to gradually increase with depth within the target zone. Robertson et al. (1995) suggested that Y should increase with age for a given sand type.

In order to compare the SPT and shear wave velocity, the closest pairs of test types were determined by examining the detailed site plan (see Figure 8-4). SPT1 and seismic CPT M9401 were paired together, as were SPT2 and seismic CPT M9406. Based on these two pairs of tests, Figure 8-7c shows that the value of X in the target zone is scattered, but has an average value of 94.7 (SD=7.7). The scatter is again due to the scatter in the SPT $(N_1)_{60}$ values.

8.3.4 Shear wave velocity based estimations of void ratio

Figures 8-8a to d compare the shear wave velocity based method of interpreting void ratio from the CPT and the SPT with the direct interpretations of void ratio from the shear wave velocity logs and the geophysical logs at the Massey site. The average value of Y in the target zone (110.2) was used to interpret the CPT profiles using the method described in Chapter 4 (see Equation 4-11). The average value of X in the target zone (94.7) was used to interpret the SPT profiles using the method described in Chapter 4 (see Equation 4-12). As a result, the void ratio estimations outside of the target zone are not reliable. However, it is only within the target zone that frozen samples are available for comparison. To be absolutely correct (particularly if applying this method for design purposes), even within the target zone, values of Y and X that vary with depth should be used to interpret the CPT and SPT using the shear wave velocity based method. However, this study has used a single average value of both Y and X, for ease of calculation. The values of A and B that were used for the shear wave velocity based interpretations of void ratio from the CPT and SPT are given in Table 8-2.

In Figures 8-8a to d, as in Figures 8-6a to d, the solid dots represent the void ratios of the undisturbed frozen samples obtained at the Massey site and the open dots represent the void ratios of the samples obtained using the Laval large diameter sampler. The void ratios for both the undisturbed and Laval sampler samples are summarized in Table 8-3. Again, as in Figures 8-6a to d, the RSR=1 ($D_r \approx 25\%$) reference line is shown superimposed on Figures 8-8a to d.

Based on the frozen void ratios for undisturbed samples available to date, and comparing Figure 8-8a with Figure 8-6a, the shear wave velocity based method of interpreting the CPT appears to be better than the conventional method at capturing the trend and range of void ratios over the target zone at the Massey site. In particular, the shear wave velocity based interpretation appears to be better than the conventional method at predicting the zones in which the undisturbed sample void ratios are greater than the RSR=1 line. The shear wave velocity based method of interpreting the CPT predicts an average void ratio of 0.939 (SD=0.062) in the target zone. Note that CPT M9407 has not been included in Figure 8-8a. It was not a seismic CPT log and, as a result, there was not a borehole-specific average Y value to process the log using the shear wave velocity based method.

Comparing Figure 8-8b with Figure 8-6b, it is difficult to comment on which method is better for interpreting the SPT. Although the conventional method underpredicts the actual void ratios (which could be dangerous), the shear wave velocity based method still does not capture the actual range of void ratios very accurately. The most significant reason for this is likely the fact that a single value of X was used in the target zone to interpret the SPT, but in actual fact (see Figure 8-7c) the value of X is quite variable throughout the deposit. The shear wave velocity based method of interpreting the SPT predicts an average void ratio of 0.938 (SD=0.112) in the target zone, but with wide scatter.

8.3.5 Soil behaviour type

Figure 8-9 presents all of the Massey site CPT data in the target zone (8 to 13 m) on a soil classification chart using the method by Robertson (1990). The data has an average Q of

49.4 (SD=9.9) and an average F of 0.398 (SD=0.089). The majority of the data falls into Zone 6 (having an average I_c of 1.962; SD=0.085) and would be classified as a sand, ranging from a clean sand to a silty sand (see Chapter 3, Table 3-1). Small amounts of the data fall into Zone 5 and would be classified as a sand mixture, ranging from a silty sand to a sandy silt. The data falls close to, but slightly to the left of the region considered to correspond to normally consolidated soils. Based on where the data plots on the soil classification chart in Figure 8-9, it would be expected that the soil does not contain a large amount of fines. This will be expanded upon in a later section of this chapter. Note that the data fall within a small range of friction ratio (F).

8.4 Interpretations of State

8.4.1 Sladen and Hewitt (1989)

Based on values of e_{max}, e_{min}, G_s, average FC, D_{50} and D_{10}, Fraser River sand at the Massey site (see Table 8-1) initially appears to be somewhat similar to Nerlerk and Ukalerk sands (see Chapter 4), although both e_{max} and e_{min} are larger at the Massey site (approximately 1.1 and 0.7 at the Massey site, respectively; approximately 0.8 and 0.6 at Ukalerk, respectively).

As described in Chapter 4, field observations in the Nerlerk and Ukalerk sands were used to develop the relationship proposed by Sladen and Hewitt (1989) to determine whether or not a material is susceptible to flow liquefaction. Chapter 4 suggested that this relationship is only applicable in similar sands and that the best method of estimating if the response of two sands will be similar is to examine their ultimate state lines. The USL for Fraser River sand is presented in Figure 8-2. The USL for Nerlerk sand was presented earlier, in Chapter 5 (Figure 5-6 and Table 5-1). At low stresses ($p' < 200$ kPa) although the USL for each sand has a similar slope, λ_{ln}, (0.0165 at Fraser River; 0.014 at Nerlerk), the value of Γ is quite different (1.071 at Fraser River; 0.885 at Nerlerk), with the result being that the Massey USL would be located at higher void ratios than the Nerlerk USL on an e-ln p' plot. Consequently, if applying the Sladen and Hewitt (1989) dividing line to the CPT data from the target zone at the Massey Site, this difference in the USLs must be kept in mind.

Based on a groundwater table at a depth of 1.5 m and the unit weights of soil given in Table 8-1, the Sladen and Hewitt (1989) relationship given in Chapter 4 (see

Equation 4-19) can be converted to a liquefaction/non-liquefaction dividing line in terms of q_c versus depth. This dividing line is shown superimposed over CPT data from the target zone at the Massey site in Figure 8-10. In the target zone (8 to 13 m), if directly applied as shown in Figure 8-10, the field observation method by Sladen and Hewitt (1989) would predict that, on average, the material at Massey Site could be susceptible to flow liquefaction and that from approximately 9.5 to 10.5 m, the material could be considered as borderline. However, as pointed out above, the USL for Fraser River sand is different than that for Nerlerk sand. To move from the Nerlerk USL to the Fraser River USL on an e-ln p' plot would require an upward shift in void ratio. This would translate into a significant shift to the left in the Sladen and Hewitt (1989) dividing line shown in Figure 8-10, resulting in a different evaluation of flow liquefaction potential in the Massey site target zone. Although the exact size of the corresponding shift is not clear at this point, it is likely to be large enough that the target zone would be predicted to have no flow liquefaction potential, with perhaps some zones being borderline.

8.4.2 Been and Jefferies (1992)

Also shown on Figure 8-10 is the dividing line (Ψ=0) determined for Fraser River sand using the method proposed by Been and Jefferies (1992), based on correlating CPT results with state parameter for various soils. The dividing line was determined using Equations 4-20 to 4-24 in Chapter 4, assuming B_q=0 in sandy deposits. The measured CPT profiles confirm that B_q=0. M was assigned a value of 1.5, the approximate average laboratory measured value for triaxial compression tests (M_C) on undisturbed samples from the Massey site, presented later in this chapter; the corresponding friction angle, ϕ'_{us}, is approximately 37°, based on Equation 4-15 in Chapter 4. Since the range of stresses in the target zone at Massey are low, the flatter part of the bi-linear USL can be used to estimate the state dividing line. This part of the USL has a λ_{ln} of 0.0165 (see Table 8-2) which corresponds to a λ_{log} of 0.038. Combining the Been and Jefferies (1992) equations, using the groundwater table depth and unit weights given in Table 8-1, and setting Ψ equal to zero results in the dividing line in terms of q_c versus depth as indicated in Figure 8-10. Also shown in Figure 8-10 are the lines for Ψ= -0.05 and Ψ= -0.1.

In the target zone (8 to 13 m), the Been and Jefferies (1992) method would predict that none of the sand is liquefiable because the entire deposit is denser than the Ψ=0 dividing line. The average predicted state is approximately Ψ= -0.05. Based on the undisturbed samples, the estimated mean in-situ state parameter is Ψ= -0.024. However, the Been and

Jefferies (1992) approach appears to predict a slightly denser state.

8.4.3 Plewes et al. (1992)

Figure 8-11 shows the CPT data from the target zone at the Massey site plotted on the soil classification chart after Jefferies and Davies (1991), as proposed by Plewes et al. (1992) for estimating contours of state parameter. On this soil classification chart, the material in the target zone (8 to 13 m) plots almost entirely in Zone 6 and would be classified as a sand, ranging from a clean sand to a silty sand. The method by Plewes et al. (1992) would predict an approximate range in state parameter from $\Psi = -0.02$ to $\Psi = -0.15$, with an average of $\Psi = -0.08$. This would suggest that the material is dense of ultimate state and would not be susceptible to flow liquefaction. The fact that this conclusion agrees with the prediction using the Been and Jefferies (1992) methodology is logical since the Plewes et al. (1992) method draws on earlier work by Been and Jefferies, as explained previously.

At an average vertical effective stress of approximately 115 kPa and a K_o of 0.5, the Kidd site has an average mean normal effective stress, p', of approximately 76.7 kPa. Given that the reference USL in this stress range has been defined by $\Gamma=1.071$ and $\lambda_{ln}=0.0165$, the range in Ψ predicted by the method by Plewes et al. (1992) can be converted into a range in void ratio of 0.839 to 0.979, with an average of 0.919. This tends to underestimate the void ratios of the undisturbed samples tested to date which have an average value of 0.976 (SD=0.046).

8.5 Review of Laboratory Data

Figure 8-12 presents an enlarged version of Figure 8-8a, comparing the shear wave velocity based interpretation of void ratio from the CPT with the void ratios of the undisturbed and Laval sampler samples. Different symbols are used in Figure 8-12 for each undisturbed sample (FS) indicating to which laboratory it was sent and the type of test that was performed. Unfortunately, it appears that the majority of the loosest samples (i.e. with void ratios higher than the RSR=1 reference line) were not subjected to triaxial compression (TC) or extension (TE) tests, but rather to simple shear (SS) tests (which are more difficult to interpret) or cyclic simple shear (CSS) tests (which do not apply to flow liquefaction considerations). It is interesting to note, however, that of the five undisturbed samples that have been tested to date under simple shear (see Fear and Robertson (1996) for stress-strain curves), three samples demonstrated strain-hardening while two samples (one from 9.3 m and one from 10.8 m) demonstrated limited strain-softening (one more significantly than the other). However, based on the void ratio estimates by Hofmann (1995), it was not the loosest sample at each of the two depths that exhibited some strain-softening. Three triaxial tests (TC) were carried out on undisturbed samples with void ratios above the RSR=1 by Laval. The label "D" for two of the samples tested by UBC (one TC and one TE) indicate a drained test. The rest of the triaxial tests were undrained.

The complete stress-strain response curves for all of the laboratory tests are presented in the CANLEX report by Fear and Robertson (1996) (tests performed at the U. of A., UBC and Laval). Results from triaxial (compression and extension), simple shear and cyclic simple shear tests on undisturbed samples of Fraser River sand from the Massey site are presented. In addition, the results of testing reconstituted samples of Fraser River sand by Thomas (1992), Ayoubian (1995), and Pouliot and Konrad (1995) are included. Note that the tests by Thomas (1992) and Ayoubian (1995) were on anisotropically consolidated samples which are directly relevant to field conditions, while the tests by Pouliot and Konrad (1995) were all essentially isotropically consolidated.

8.5.1 Flow liquefaction response

a) Undisturbed samples

Table 8-4 summarizes the undrained triaxial compression and extension test results for all of the undisturbed samples of Fraser River sand from the Massey site tested to date. The individual tests are identified by the laboratory that conducted the testing as well as the sampling identification number assigned by Hofmann (1995). The results of testing each sample in undrained monotonic loading is broken down into the individual components of response, as outlined in Chapter 4. Based on the definitions of response in Chapter 4 (see Figures 4-15 and 4-16), each undrained TC and TE stress-strain curve (see CANLEX report by Fear and Robertson, 1996) has been divided into four main points: (A) the initial state, (B) the peak (or yield) state, (C) the minimum state and (D) the ultimate state.

i) Initial state

The initial state of each sample is defined by its void ratio after thaw and consolidation (e_c) and the vertical and horizontal effective stresses (σ'_{vi} and σ'_{hi}) placed on it. The value of

e_c is generally less than the void ratio of the sample in-situ (see Table 8-3), as estimated by Hofmann (1995), as a result of small volume changes that occur during thaw and consolidation. The difference between the in-situ void ratio and e_c will be discussed later in this chapter. When examining the response of a sample in the laboratory, it is important to define RSR for the sample based on e_c and the laboratory applied stresses. It is this combination that defines the state of the sample immediately prior to testing and influences how it will respond to undrained loading. RSR is defined relative to the appropriate section of the bi-linear reference USL shown in Figure 8-2 (see Table 8-2), depending on the value of e_c (i.e. whether it is greater than or less than the breakpoint void ratio of 0.979).

(ii) Stress-strain response

None of the Massey undisturbed samples tested to date strain-softened directly to their ultimate state during a triaxial test. Most of the samples strain-hardened towards their ultimate state. The three undisturbed samples that were subjected to triaxial extension demonstrated limited strain-softening in that they strain-softened to a quasi-steady state (QSS) before eventually, at large enough strains, strain-hardening towards ultimate state (see CANLEX report by Fear and Robertson, 1996).

For samples that strain-hardened to their ultimate state without demonstrating any limited strain-softening (all of the triaxial compression tests), the peak and minimum values of p' and q were taken as equal to the end-of-test values of p' and q. Consequently, the peak and minimum strengths were taken as equal to the end-of-test strength (which can be generally considered to be close to the ultimate state strength). These samples responded to undrained triaxial compression loading in a non-brittle manner and were assigned $I_B=0$ (see Chapter 4, Equation 4-27). These samples were also assigned an axial strain at minimum strength of zero because there was no minimum condition during the stress-strain curve.

For the three samples that were tested in triaxial extension, a QSS point occurred. The corresponding stress-strain curves (see CANLEX report by Fear and Robertson, 1996) had distinct peak, minimum and ultimate points since the samples demonstrated limited strain-softening. For each test, the values of p' and q (and, hence, the values of strength) were determined for each of the three individual points along the stress-strain curve. The values of I_B for these samples were still small (maximum of 0.11) because the samples were anisotropically consolidated to approximate the level ground in-situ stress state and were therefore preloaded in compression. Significant unloading had to occur before the samples experienced limited strain-softening. Axial strains that occurred while at the QSS point (i.e. at the point of minimum strength) were also fairly small, ranging from approximately 3% to 8%. The minimum strengths of these samples were significantly smaller than the end-of-test strengths ($S_{min} \approx 0.20$ to 0.30 of S_f).

b) Reconstituted samples

(i) Initial conditions

Included in Table 8-4 are the results by Ayoubian (1995) for tests (one TC and one TE) on anisotropically consolidated reconstituted samples of Fraser River sand from the Massey site (prepared by moist tamping) and the results by Thomas (1992) for tests (one TC and one TE) on anisotropically consolidated reconstituted samples of Fraser River sand (prepared by water pluviation). The reconstituted samples of Fraser River sand tested by Chillarige et al. (1995) and Pouliot and Konrad (1995) are not included because they were isotropically consolidated. Anisotropically consolidated reconstituted samples (with $K_o \approx 0.5$) more closely represent the in-situ stress state and, as discussed previously, produce a response that can be directly linked with the expected in-situ response under level ground conditions. The anisotropically consolidated reconstituted samples can be thought of as being preloaded in compression.

Moist tamping allows for a much looser state to be reached than water pluviation. Thus, the combination of moist tamped and water pluviated reconstituted samples span a large range of RSR and would be expected to span a large range in observed response to undrained loading. The moist tamped samples prepared by Ayoubian (1995) had values of RSR of about 12, significantly greater than 1 and approximately 7 to 8 times those of the water pluviated samples prepared by Thomas (1992). The initial void ratios for the water pluviated samples prepared by Thomas (1992) were not directly available, but were estimated based on consolidation data also presented by Thomas (1992); thus the values of RSR are approximate.

(ii) Stress-strain response

Both the triaxial compression and extension tests by Thomas (1992) experienced a QSS and demonstrated limited strain softening with little brittleness; however, the triaxial compression test was more brittle than the triaxial extension test. At the QSS point of each test, fairly small axial strains occurred, ranging from approximately 1% (TC) to 6% (TE).

The triaxial extension test by Ayoubian (1995) essentially strain-softened directly to ultimate state. The test did experience a QSS, but it was located very close to the end of test state and both the QSS and end-of-test strengths were smaller than the peak strength. The response was not very brittle, but 11% axial strain occurred at the minimum point. On the other hand, the triaxial compression test by Ayoubian (1995) strain-softened directly to ultimate state and required very little additional load to trigger the strain-softening response. Consequently, the response was very brittle, with I_B=4.1. In addition, the axial strain at minimum (ultimate) strength was large, accumulating to approximately 23% by the end of the test. The differences in brittleness between the TC and TE tests illustrates the effects of preloading a sample in compression as it could be under level ground conditions in-situ.

c) Link between RSR and response

Figures 8-13 and 8-14 present the various components of response of all of the undrained triaxial tests on anisotropically consolidated undisturbed Massey site samples and reconstituted Fraser River samples tested to date versus the individual RSR of each sample. In addition, Figure 8-13a presents the initial conditions of each sample relative to the selected Fraser River reference USL and Figure 8-14a presents the end-of-test conditions of each sample relative to the same USL. The undisturbed samples were tested at an average initial p' of about 75 kPa which is approximately equal to the average in-situ p' in the target zone at the Massey site. The reconstituted samples were tested at significantly higher initial values of p', but with similar values of K_o (≈ 0.5).

Figures 8-13b to d and 8-14b to d present the components of response as follows: brittleness index (I_B), minimum strength ratio (S_{min}/p'_i), axial strain at minimum strength (ε_a), end-of-test strength ratio (S_f/p'_i), peak stress ratio (M_p) and end-of-test stress ratio (M_f). It is clear that, for a given direction of loading (i.e. TC or TE) each component of response appears to be a function of RSR.

Superimposed on the plots of S_{min}/p'_i versus RSR (Figure 8-13b) and S_f/p'_i (Figure 8-14b) versus RSR are the theoretical predictions of strength ratio based on the methods outlined in Chapters 4 and 5. The values of S_{min}/p'_i and $Sf/p'i$ are equal for most of the triaxial compression tests. The undisturbed sample tested by Ayoubian (1995) experienced a QSS and had an S_{min}/p'_i less than its S_f/p'_i. The water pluviated reconstituted sample by Thomas (1992) had an S_{min}/p'_i slightly less than its S_f/p'_i. The values of S_{min}/p'_i for the triaxial extension tests correspond to the QSS, while the values of S_f/p'_i correspond to the end-of-test conditions. As RSR decreases, the difference between these two values becomes larger. In general, for most samples, the theoretical relationship between the ultimate state S/p'i and RSR for triaxial compression (indicated by TC-USS) agrees well with the test results. There is clearly a certain amount of scatter to the data around the theoretical relationship, but the trend of the data to increase with decreasing RSR is captured well by the theoretical line. The two samples which appear to disagree with the theoretical line the most were tested by Laval in triaxial compression. One of the samples had an estimated RSR of about 1.1, while the other had an estimated RSR of about 14.3 (i.e. in Figure 8-13a, these two samples have initial conditions plotting above the Fraser River reference USL). For the samples tested in triaxial extension, the estimated relationship between S/p'_i at QSS and RSR, based on ΔRSR=26 (indicated by TE-QSS), agrees well with the test results. At low values of RSR (i.e. less than 1), it is impossible to compare the theoretical relationship between the ultimate state S/p'_i and RSR for triaxial extension (indicated by TE-USS) with the results of lab testing because the samples were all still dilating towards ultimate state at the end of the test.

Figure 8-13c presents brittleness index (I_B) versus RSR. In general, I_B increases as RSR increases, but the effect at high RSR is much more significant for triaxial compression. Approximate relationships between I_B and RSR for triaxial compression and triaxial extension are shown on Figure 8-13c and can be expressed as follows:

[8-1a] $I_B = 0.1\mathrm{RSR} + 0.02\mathrm{RSR}^2$ for triaxial compression

[8-1b] $I_B = 0.05 + 0.001\mathrm{RSR}$ for triaxial extension

Clearly, these relationships are strongly influenced by the results of the moist tamped, anisotropically consolidated samples tested by Ayoubian (1995) and should be considered as tentative until further data are available. The undisturbed samples generally have RSR<1 and respond in either a non-brittle or a slightly brittle fashion (i.e. I_B is equal to or close to zero). Again, the sample which tends to deviate from the proposed relationships the most is the undisturbed sample with an RSR of approximately 14.3 tested under triaxial compression by Laval. If RSR were overestimated for this sample (e.g. the void ratio was overpredicted), the discrepancy in the results could be explained.

Figure 8-13d presents axial strain at minimum strength (ε_a) versus RSR. In general, ε_a increases as RSR increases. Approximate relationships between ε_a and RSR for triaxial compression and triaxial extension are shown on Figure 8-13e and can be expressed as follows:

[8-2a] $\varepsilon_a = 0.15\mathrm{RSR}^2$ for triaxial compression

[8-2b] $\varepsilon_a = 6.6\mathrm{RSR}^{0.25}$ for triaxial extension

Clearly, these relationships are strongly influenced by the results of the moist tamped, anisotropically consolidated samples tested by Ayoubian (1995) and should be considered as tentative until further data are available. The triaxial extension test by Ayoubian (1995) experienced large strains because the sample essentially strain softened directly to ultimate state. The triaxial compression test by Ayoubian (1995) strain softened directly to ultimate state and experienced even larger strains. However, the undisturbed samples generally have RSR<1 and have ε_a at S_{min} of zero for triaxial compression tests (because, in general, no QSS was experienced) and ε_a at S_{min} ranging from 2% to 8% for triaxial extension tests. Again, the sample which tends to deviate from the proposed relationships the most is the undisturbed sample with an RSR of approximately 14.3 tested under triaxial compression by Laval. As previously mentioned, if RSR were overestimated for this sample, the discrepancy in the results could be explained.

The purpose behind extending the I_B-RSR and ε_a-RSR relationships beyond the range of RSR in which the undisturbed samples exist (with the exception of the one sample noted above) is to provide a global approach to evaluating flow liquefaction. At the Massey site, the undisturbed samples tested to date tend to generally have RSR<1, responding with little brittleness, always eventually strain-hardening to ultimate state, and only experiencing small axial strains if the stress-strain curve passes through a QSS (typically only extension tests demonstrate a true QSS). However, at another site, similar Fraser River sand may exist with RSR>1. This may occur possibly due to processes such as light cementation or in soils deposited under unsaturated conditions which later become saturated. Should such deposits be loaded undrained, they may respond in a brittle manner, strain-softening directly to ultimate state and experiencing large strains at minimum strength. These soils are the ones which are most susceptible to flow liquefaction and, provided a kinematically admissible mechanism can develop, may lead to catastrophic failures. The case history at Sand Heads, as reported by Chillarige et al. (1995) is an example of such Fraser River sand. Therefore, the intent of the framework proposed here is to cover a wide range of conditions that may exist in nature. Obviously, in-situ conditions with RSR significantly greater than 1 are probably less common, but they may exist, given the right environment.

Figure 8-14d presents the end-of-test values of M (which can be considered approximately equal to the ultimate values since the samples were all dilating towards or at ultimate state when the tests were stopped) versus RSR. Despite some scatter, over a large range of RSR, the triaxial compression tests (undisturbed and reconstituted) almost all resulted in similar values of M_C. With the exception of one sample (one of the undisturbed samples tested by Laval) which had an unusually high value of $M_C=1.78$, the triaxial compression samples had an average M_C of 1.49 (SD=0.06). Likewise, over a range of RSR, most of the triaxial extension tests (undisturbed and reconstituted) resulted in similar values of M_E. With the exception of one sample (the Ayoubian (1995) moist tamped sample) which had an unusually high value of $M_E=1.28$, the triaxial extension samples had an average M_E of 0.96 (SD=0.04). Using Equations 4-15 and 4-16 in Chapter 4, the observed M_C correlates to an average friction angle, ϕ'_{us}, of 36.6° (SD=1.5°) and the observed M_E correlates to an average friction angle, ϕ'_{us}, of 35.0° (SD=2.0°). Therefore, both the triaxial compression and triaxial extension tests appear to have approximately the same ultimate state friction angle.

Figure 8-14c presents the peak values of M versus RSR. Despite a fair amount of scatter, the triaxial compression tests appear to demonstrate that $(M_p)_C$ tends to decrease with increasing RSR. Again, the sample which tends to deviate from this overall trend the most is the undisturbed sample with an RSR of approximately 14.3 tested under triaxial compression by Laval. As previously mentioned, if RSR were overestimated for this sample, the discrepancy in the results could be explained. Comparing the peak values of $(M_p)_C$ in Figure 8-14c to the ultimate values of M_C in Figure 8-14d, it appears (with the exception of the one sample just mentioned) that for RSR less than about 1, $(M_p)_C=M_C$, but for higher value of RSR, $(M_p)_C$ is significantly less than M_C. Samples with high values of RSR tend to strain-soften directly to US (or, at least to a QSS that is very close to the US) and, when the stress-strain curve is plotted in q-p' space, it seems logical that the peak point would have a lower q/p' ratio (i.e. M) than the point at ultimate state. However, samples with small values of RSR (i.e. typically less than 1) tend to strain harden to ultimate state and, therefore, the peak point and the ultimate state point are essentially the same.

The triaxial extension tests in Figure 8-14c appear to demonstrate that $(M_p)_E$ also tends to decrease with increasing RSR. However, fewer samples have been tested in triaxial extension and they have more scatter than exhibited by the triaxial compression data. Therefore, it is more difficult to draw any definite conclusions.

8.5.2 Cyclic softening response

a) Undisturbed samples

Table 8-5 summarizes the results of cyclic simple shear testing to date on undisturbed samples of Fraser River sand from the Massey site. All of the testing was conducted at UBC; the individual tests are identified by the sampling identification number assigned by Hofmann (1995). The detailed stress-strain curves are presented in the CANLEX report by Fear and Robertson (1996). The state of each sample is defined by its void ratio after thaw and consolidation (e_c). As for the triaxial samples, the value of e_c is generally less than the void ratio of the sample in-situ, as estimated by Hofmann (1995), as a result of small volume changes that occur during thaw and consolidation. The difference between the in-situ void ratio and e_c will be discussed later in this chapter. It is the void ratio immediately prior to testing that will affect the response of the sample to undrained cyclic loading. The samples that have been tested to date had an average e_c of 0.953 (SD=0.062).

Table 8-5 summarizes the test results in terms of the applied cyclic stress ratio ($CSR=\tau_{cy}/\sigma'_{vc}$) and the measured number of cycles, N, required to cause uncontrolled deformations. Using Equation 3-7 in Chapter 3, the equivalent earthquake magnitude, M, was calculated. The correction ($1/r_m$) proposed by Tokimatsu and Yoshimi (1983) for estimating the equivalent CSR for a Magnitude M=7.5 earthquake from the CSR for a given magnitude earthquake, based on the work by Seed et al. (1985), was then calculated using Equation 3-6 in Chapter 3. Multiplying the applied CSR by the appropriate correction factor gives the equivalent cyclic resistance ratio (CRR) for a Magnitude M=7.5 earthquake, considered to have N=15 uniform cycles of loading. The samples tested to date have an resulting average equivalent CRR for M=7.5 (or N=15 cycles) of 0.101 (SD=0.018).

8.6 Link between Field and Laboratory Data

Testing undisturbed samples in the laboratory under suitable stress conditions is the most reliable method of estimating in-situ response. However, the scope of many projects does not allow for expensive in-situ freezing and sampling. In-situ testing is a convenient and less expensive alternative provided that the results can be meaningfully interpreted. For high risk projects, undisturbed sampling may be necessary and be within the project budget. However, for linking the results from a limited area of undisturbed sampling and testing with in-situ testing, it is necessary to extrapolate the results across the site. In-situ testing is also a useful tool for initial site screening of a high risk project, again provided the results can be meaningfully interpreted.

8.6.1 Flow liquefaction

The proposed link between laboratory testing and in-situ testing for flow liquefaction considerations is the parameter RSR. Since response of undisturbed samples in the laboratory have been shown to be a function of RSR, the in-situ response can be estimated by first estimating profiles of RSR in-situ. These estimated profiles can be compared to the response of the undisturbed samples. Table 8-3, which summarizes the in-situ void ratios for each of the undisturbed and Laval sampler samples, also summarizes the in-situ RSR and the individual components of response observed in the laboratory for each sample.

a) Estimated in-situ profiles of reference stress ratio (RSR)

Figure 8-15a to d present estimated profiles of RSR based on the CPT, SPT, shear wave velocity measurements and geophysical logging. These profiles were determined by combining the void ratio profiles in Figures 8-8a to d with Equations 4-18 and 4-25 in Chapter 4. Note that Figure 8-8 used the shear wave velocity based method of estimating void ratio for the CPT and SPT. This is for illustrative purposes only. Any method to estimate state (either void ratio or state parameter) could be used. The value of RSR was referenced to either the flat or steep portion of the Fraser River reference USL shown in Figure 8-2 (see values of Γ and λ_{ln} in Table 8-2), depending on whether the estimated void ratio at any given depth was above or below the void ratio defining the breakpoint in the reference USL. Since the average values of Y and X were used to estimate the void ratio profiles from the CPT and SPT, respectively, the RSR estimations outside of the target zone are not reliable. RSR in Figures 8-15 a to d is plotted on a scale from 0.01 to 100.

Relative to the flat portion of the Fraser River reference USL (λ_{ln}=0.0165), this would correspond to a range in state parameter of Ψ= - 0.076 to Ψ= + 0.076. However, the estimated void ratio is often less than the breakpoint void ratio and therefore RSR is referenced to the steep portion of the reference USL.

Superimposed on Figures 8-15 a to d are solid dots representing the RSR values of the undisturbed frozen samples obtained at the Massey site and open dots representing the RSR values of the samples obtained using the Laval large diameter sampler (see Table 8-3). The RSR values of the samples were determined by combining the estimates of in-situ void ratio for each samples (Hofmann, 1995) with the Equations 4-18 and 4-25 in Chapter 4. Again, the value of RSR was referenced to either the flat or steep portion of the Fraser River reference USL shown in Figure 8-2 (see values of Γ and λ_{ln} in Table 8-2), depending on whether the estimated void ratio of a particular sample was above or below the void ratio defining the breakpoint in the reference USL.

Comparing RSR estimated from the in-situ tests with RSR of the undisturbed samples in Figure 8-15 is the same as comparing void ratio estimated from the in-situ tests with void ratio of the undisturbed samples in Figure 8-8, because void ratio was converted to RSR using the same method for both in-situ testing and the undisturbed samples. Therefore, as for the void ratio comparison in Figure 8-8, the range in undisturbed sample RSR seems to be captured by all of the methods, but the CPT (interpreted using the shear-wave velocity based method) and the geophysical logging appear to best capture the detailed variability of RSR in the target zone at the Massey site. Although there are definitely regions in the target zone where RSR>1 would be estimated, the undisturbed and Laval samples tested to date seem to indicate that over a large portion of the target zone, the in-situ RSR ranges between approximately 0.1 and 0.3. The interpretations of the in-situ testing, particularly the CPT, shear wave velocity and geophysical logs predict a similar conclusion.

b) Estimated in-situ profiles of response to undrained monotonic loading

Based on the profiles of estimated RSR from in-situ testing as shown in Figure 8-15, profiles of response to undrained monotonic loading can be estimated using the relationships between individual components of response and RSR, as observed in the laboratory. Since the CPT profiles appear to be one of the better methods at estimating the variability and range in void ratio (and hence, RSR) in the target zone at the Massey site, the CPT will be used to illustrate how in-situ response can be estimated.

(i) Comparison of void ratio and RSR in the laboratory and in the field

In order to check the accuracy of the CPT at predicting in-situ response, the predicted profiles of individual components of response can be compared with the response of the undisturbed samples, when tested in the laboratory, plotted at the appropriate depths. However, the response in the laboratory is linked to the RSR of the sample immediately prior to shearing; i.e. at the void ratio after thaw and consolidation and under the anisotropic stress state imposed in the laboratory. Based on the relationships between response and RSR in the laboratory, the true in-situ response at the depth at which the sample was obtained would only be equal to the response of the sample if the in-situ RSR is the same as the RSR of the sample. Figure 8-16a compares the estimated in-situ void ratio of each undisturbed sample (Hofmann, 1995) with the void ratio immediately before testing in the laboratory. Likewise, Figure 8-16b compares the estimated in-situ RSR of each undisturbed sample with the RSR immediately before testing in the laboratory. Both the laboratory and estimated field values of void ratio and RSR for each sample are summarized in Table 8-3.

Figure 8-16a shows that most undisturbed samples only experienced a small change in void ratio during thaw and consolidation, with the void ratio immediately prior to testing (e_{lab}) being generally smaller than the estimated in-situ void ratio (e_{field}). The exception is one sample tested by Laval, which had a higher e_{lab} than e_{field}. This is the same sample which always appeared to disagree with the general trend of the data in the laboratory response curves in Figures 8-13 and 8-14. In general, the samples tested by UBC experienced smaller decreases in void ratio during thaw and consolidation than the samples tested by Laval. One sample tested by Laval had a decrease in void ratio during thaw and consolidation that was significantly greater than for any of the other samples.

Figure 8-16b shows that for most of the undisturbed samples, the RSR immediately prior to testing (RSR_{lab}) was approximately equal to the estimated in-situ RSR (RSR_{field}), with RSR_{field} generally being slightly larger than RSR_{lab}. The exception is the one sample tested by Laval which has been discussed several times and appeared to have a much higher RSR_{lab} than RSR_{field}. However, if its actual RSR_{lab} were closer to RSR_{field} (i.e. 0.33 instead of 14.3), its response would fit the trend of the data on the laboratory response curves much better. In general, the samples tested by UBC have values of RSR_{lab} that more closely match RSR_{field} than the samples tested by Laval. Two of the samples tested by Laval had values of RSR_{lab} that were significantly smaller than RSR_{field}. It is important to note that the relationship between RSR_{lab} and RSR_{field} for any given sample is not directly equivalent to the relationship between e_{lab} and e_{field} for the same sample because RSR is influenced by both void ratio and mean normal effective stress state. The mean normal effective stresses placed on the sample in the laboratory (used to calculate RSR_{lab}) may not be exactly the same as those estimated in-situ when estimating RSR_{field}, although, in general, the laboratories attempted to simulate the in-situ stresses quite closely.

In addition, although one Laval sample had e_{lab} significantly less than e_{field}, the difference between RSR_{lab} and RSR_{field} was less significant and comparable to other samples; however two other Laval samples that had similar values of e_{lab} and e_{field}, had more significant differences between RSR_{lab} and RSR_{field}. The explanation for these differences is that for void ratios above the breakpoint void ratio of the Fraser River reference USL (i.e. 0.979), small difference in void ratio can translate into large differences in RSR because RSR is referenced to the flatter portion of the USL. For void ratios less than the breakpoint value, for which RSR is references to the steeper portion of the USL, differences in void ratio can be larger before resulting in significant differences in RSR.

Based on the above observations, it would be reasonable to conclude that the response of some of the undisturbed samples in the laboratory would likely differ slightly from the in-situ material located at the same depths from which the undisturbed samples were obtained. This must be kept in mind when comparing the response of the undisturbed samples with the estimated average in-situ response profiles presented in the following section of this chapter. This applies particularly to the one Laval sample with RSRlab>>RSRfield, which was obtained from a depth of 10.73 m, and to the two Laval samples with RSRlab<<RSRfield, which were obtained from depths of 10.95 m and 12.62 m.

(ii) CPT-based average estimated response profiles

Figures 8-17 and 8-18 present average estimated response profiles based on combining the interpretations of RSR from the CPT with the relationships between response and RSR in the laboratory, presented in Figures 8-13 and 8-14.

Profiles of average estimated brittleness index for both triaxial compression and triaxial extension are given in Figure 8-17a. The profiles were determined by combining the average RSR from CPT profiles M9401 to M9406 (see Figure 8-15a) with Equations 8-1a and b, which describe the tentative relationships between I_B and RSR for triaxial compression and extension, respectively, as given in Figure 8-13c. The profiles of estimated brittleness index are unreliable outside of the target zone since the average Y in the target zone was used to estimate void ratio (and, hence, RSR) from the CPT profiles. The scale for I_B is shown from zero to 5 to reflect the range in I_B that could occur, given a large enough range of RSR. Throughout the target zone (8 to 13 m), the CPT predicts, on average, essentially non-brittle behaviour for both triaxial compression and extension. Testing on undisturbed samples to date confirms this. More triaxial compression testing, particularly between 8 and 9 m, near 11 m and near 12.5 m would be useful to investigate the comparison between the response of undisturbed samples and the average CPT predicted response profile for triaxial compression which indicates the possibility of higher brittleness zones.

Profiles of average estimated axial strain (in percent) at minimum strength for both triaxial compression and triaxial extension are given in Figure 8-17b. The profiles were determined by combining the average RSR from CPT profiles M9401 to M9406 (see Figure 8-15a) with Equations 8-2a and b which describe the tentative relationships between ε_a and RSR for triaxial compression and extension, respectively, as given in Figure 8-13d. The profiles of estimated axial strain at minimum strength are unreliable outside of the target zone since the average Y in the target zone was used to estimate void ratio (and, hence, RSR) from the CPT profiles. The scale for ε_a is shown from zero to 20% to reflect the range in εa that could occur, given a large enough range of RSR. Throughout the target zone (8 to 13 m), the CPT predicts, on average, essentially zero strain for triaxial compression; this is because the material would generally be predicted to strain-harden in triaxial compression such that no point of minimum strength occurs. For triaxial extension loading, the CPT predicts, on average, about 5% axial strain at minimum strength (i.e. during the condition of QSS). Testing on undisturbed samples to date appears to agree with these conclusions. More triaxial testing, particularly between 8 and 9 m, near 11 m and near 12.5 m would be useful to investigate the comparison between the response of undisturbed samples and the average CPT predicted response profiles which indicate the possibility of higher axial strains at minimum strength, particularly in triaxial compression.

Figures 8-17c and 8-18a present profiles of average estimated minimum strength ratio and ultimate strength ratio, respectively, for both triaxial compression and triaxial extension. Figure 8-13b and 8-14b showed that the theoretical relationships between strength ratio and RSR given by Equations 4-28 and 4-29 in Chapter 4 provided a fairly good fit to S_{min}/p'_i at QSS for triaxial extension tests and that for both triaxial compression and triaxial extension tests, the samples all appeared to be continuing to head towards the theoretical ultimate S/p'_i at the end of the test. Therefore, the profiles in Figures 8-17c and 8-18a were determined by combining the average RSR from CPT profiles M9401 to M9406 (see Figure 8-15a) with the theoretical relationships between strength ratio and RSR. Approximate average values of M_C=1.5, M_E=1.0 and ΔRSR=26 were used in these equations. The profiles of estimated strength ratio are unreliable outside of the target zone since the average Y in the target zone was used to estimate void ratio (and, hence, RSR) from the CPT profiles. The scale for strength ratio is shown from zero to 9 to capture the range in strength ratio that was observed for the undisturbed samples. Throughout the target zone (8 to 13 m), the CPT predicts, on average, very low minimum strength ratios in triaxial extension (see Figure 8-17c). However, on average, the CPT predicts significantly higher ultimate strength ratios of about 2 in the target zone. Triaxial extension testing to date appears to agree with these conclusions; the end-of-test strength ratios for the undisturbed samples will be smaller than their expected ultimate values since, in general, the samples were not at ultimate state when the tests were stopped. Strain ratios of this type, that have temporarily low values before ultimately reaching much higher values, are indicative of material that can experience limited strain softening under the right type of loading (i.e. triaxial extension loading). For triaxial compression loading, the CPT predicts, on average, equal minimum and ultimate strength ratios (because, on average, no strain-softening would be predicted) of about 3. Triaxial compression testing on undisturbed samples to date appears to agree with these conclusions. Strength ratios of this magnitude are clearly indicative of strain-hardening material that is not susceptible to flow liquefaction. Note that in Figure 8-18a, the average predicted ultimate strength ratio in triaxial extension is about 40-50% less than in compression; this is a result of the difference between M_E and M_C, as discussed previously. More triaxial testing, particularly between 8 and 9 m, near 11 m and near 12.5 m would be useful to investigate the comparison between the response of undisturbed samples and the average CPT predicted response profiles which indicate the possibility of low strength ratios, even in triaxial compression.

Figures 8-18 b and c present the peak and end-of-test values of M for both triaxial extension and triaxial compression tests on undisturbed samples. Superimposed on both of these plots as a reference are the approximate ultimate values of M for triaxial extension (M_E=1.0) and compression (M_C=1.5), as determined from laboratory testing to date.

These lines correspond to a friction angle, ϕ'_{us}, of approximately 37°. It is clear that more testing is required, particularly in triaxial extension, to confirm the average ultimate values and, especially to make more definitive statements about the peak values of M.

The estimated average response profiles shown in Figures 8-17 and 8-18 are primarily shown for illustrative purposes. While the magnitudes predicted for the various individual components of response profiles can be sensitive to the relationships both to estimate RSR from the CPT and to link RSR with response, these profiles can be useful as a guide in deciding which layers could be susceptible to flow liquefaction and what the relative response of various layers may be. The relationships linking brittleness index and axial strain at minimum strength to RSR, as shown in Figure 8-13 and given by Equations 8-1 and 8-2, are tentative in nature and will be modified if necessary, once further testing on Fraser River sand is completed. Further testing on other sands is also required to investigate if the suggested relationships are general in nature. Obviously, the reference USL for each type of sand has to be carefully chosen first, before such conclusions could be made. The interpretation of void ratio (and hence RSR) from the CPT is a function of several factors. Ranges of uncertainty in these factors will translate into ranges of uncertainty on the response profiles.

Overall, the Fraser River sand in the target zone at the Massey site appears to be generally non-brittle in triaxial compression and slightly brittle in triaxial extension. On average, it appears that the sand would strain harden to high strength ratios under undrained triaxial compression, but would demonstrate limited strain softening in undrained triaxial extension, reaching a low strength ratio temporarily before strain hardening to a high strength ratio. Axial strains while at the low strength ratio (i.e. QSS) would be expected to be less than 5%, on average. On average, the material appears to have ultimate friction angles ranging from 34° to 37°.

The figures in the proceeding sections have not included simple shear testing results, although the complete stress-strain curves for simple shear testing to date on Massey Site samples are presented in the CANLEX report by Fear and Robertson (1996). As previously mentioned, it is interesting to note that of the five undisturbed samples that have been tested in simple shear, three samples demonstrated strain-hardening while two samples (one from 9.3 m and one from 10.8 m) demonstrated limited strain-softening (one more significantly than the other). However, based on the void ratio estimates by Hofmann (1995), it was not the loosest sample at each of the two depths that exhibited some strain-softening.

Therefore, on average, the material in the target zone would not be susceptible to flow liquefaction, given a suitable trigger mechanism. However, it is often not the average properties of a soil mass that govern the overall response; the presence of a particular weak layer may provide the weak-link-in-the-chain that controls the response. The initial attempt at producing CPT-based predicted response profiles do indicate that various layers within the target zone may respond in a much more brittle manner, with lower strengths and higher strains. These zones should be investigated in greater detail, first by conducting more tests on undisturbed samples from these depths and secondly, by checking the interpretations of average void ratio and hence RSR from the CPT at these locations. The six CPTs show little or no evidence of a continuous loose sand layer within the target zone of the small test area (having a diameter of approximately 10 m).

8.6.2 Cyclic softening

The integrated CPT method for estimating cyclic resistance ratio (CRR) can be applied at the Massey site in order to estimate the profile of CRR throughout the target zone. This profile can be compared with the results of the cyclic simple shear tests on undisturbed samples from the Massey site. Table 8-3, which summarizes the in-situ void ratios for each of the undisturbed samples, also summarizes the CRR observed in the laboratory for each sample tested in cyclic simple shear.

a) Estimated in-situ profiles of CRR

Figure 8-19a presents the corrected CPT cone tip resistance (q_{c1}) profile. The average q_{c1} profile based on CPT M9401 to M9407 is shown. The maximum and minimum boundaries to CPT M9401 to M9407 are also shown. Note that the overall average q_{c1} in the target zone is 5.34 MPa (SD=1.00 MPa).

Previously, Figure 8-9 showed that interpreting all of the CPT profiles in the target zone using the soil classification chart by Robertson (1990) concluded that the target zone material is primarily a sand, ranging from a clean sand to a silty sand, with an average soil behaviour type index, I_c, of 1.962 (SD=0.085). Small amounts of the target zone material would be classified as a sand mixture, ranging from a silty sand to a sandy silt. Using

Equation 3-5 in Chapter 3, an average fines content of 6.8 % would be predicted, on average, in the target zone. Limited data is available at present regarding the grain size distributions of the undisturbed samples. A comparison can be made once this information becomes available. Preliminary information indicates that in-situ fines contents could be slightly smaller, in the order of 2% to 5%. The maximum, minimum and average predicted fines content profiles based on the CPT are shown in Figure 8-19b. It is interesting to note that these profiles predict a reasonably uniform fines content (indicating a reasonably uniform material) in the target zone.

Based on Equation 3-3 in Chapter 3, the average fines content of 6.8% would lead to, on average, a very small recommended correction of Δq_{c1}=0.3 MPa to the q_{c1} profile to produce a clean sand equivalent profile of cone tip resistance, $(q_{c1})_{cs}$. Combining the resulting clean sand equivalent profile with Equation 3-2 in Chapter 3, leads to the estimated CRR profile, as shown in Figure 8-19c. Again, the maximum, minimum and average profiles of estimated CRR are given. Superimposed on Figure 8-19c are solid dots representing the results of cyclic simple shear testing on undisturbed samples from the Massey site target zone. Both the estimated profile of CRR and the undisturbed sample CRR values are for Magnitude M=7.5 earthquakes (N=15 cycles). The estimated profile of CRR agrees well with the undisturbed samples tested to date, indicating a reasonably uniform average CRR of approximately 0.1 in the target zone. The standard deviation of 1.00 MPa for qc1 measurements in the target zone translates into a fairly small range in estimated CRR of approximately ± 0.01.

The soil classification data presented in Figure 8-9 can be compared with the soil classification chart methods of predicting CRR by Olsen and Koester (1995) and by Suzuki et al. (1995), as described in Chapter 3 (see Figures 3-14 and 3-15, respectively). Each of the three soil classification charts normalize cone tip resistance in a different manner, but for vertical effective stresses close to the reference atmospheric pressure of 100 kPa (as is the case at the Massey site), the three methods are very similar. The values on the cone tip resistance axis on the Robertson (1990) chart and the Olsen and Koester (1995) chart will be approximately equal (both axes are dimensionless). However, the values on the cone tip resistance axis on the Suzuki et al. (1995) will be approximately one tenth of the values on the Robertson (1990) chart, due to differences in units (the Suzuki et al. (1995) axis is in units of MPa, while the Robertson (1990) axis is dimensionless). The Olsen and Koester (1995) method would predict a similar average CRR of about 0.1 in the Massey site target zone. The Suzuki et al. (1995) method would probably also predict an average CRR of about 0.1 in the target zone (only contours of CRR=0.15 and CRR=0.25 are given on the Suzuki et al. (1995) plots, so some judgement is required).

For design purposes, the expected earthquake-induced cycle stress ratio (CSR) profile could be superimposed over Figure 8-19e. If there were large zones over which CSR is significantly larger than CRR, potential deformations could be estimated by predicting post cyclic liquefaction shear and volumetric strains using the method by Ishihara (1993), as described in Chapter 3 (see Figure 3-10). If there were only limited zones over which CSR>CRR, these zones should be investigated in greater detail because the CPT methods of predicting CRR likely contains some conservatism due to the selection of average values to produce the correlations.

The in-situ CRR can also be estimated from the SPT data in the target zone at the Massey site. The average $(N_1)_{60}$ in the target zone was 10.3 (SD=3.8). The estimated fines content at Massey of 6.8% is such that the sand is close to being classified as a clean sand ($FC \leq 5\%$) by the Seed et al. (1985) methodology (i.e. the recommended correction to $(N_1)_{60}$ would be small). The clean sand relationships between CRR and SPT $(N_1)_{60}$ by both Seed et al. (1985) and Fear and McRoberts (1995) described in Chapter 2 (see Figures 2-1 and 2-8, respectively) would predict an average CRR slightly greater than 0.10 based on the average $(N_1)_{60}$ of 10.3 in the target zone at Massey. However, the standard deviation of 3.8 for $(N_1)_{60}$ measurements in the target zone translates to a large range in predicted CRR of at least ± 0.05.

The shear wave velocity measurements in the target zone at the Massey site can also be used to estimate the in-situ CRR. The average V_{s1} in the target zone was 168 m/s (SD=6.4 m/s). The relationship between CRR and V_{s1} by Robertson et al. (1992) described in Chapter 3 (see Figure 3-17a) would predict an average CRR of approximately 0.19 based on the average V_{s1} of 168.2 m/s; this is significantly higher that the results of laboratory testing on undisturbed samples. However, the shear wave velocity correlation based on the recent NCEER Workshop (1996) discussions, as described in Chapter 3 (see Figure 3-17b), gives an estimated CRR of approximately 0.1, agreeing much better with the results of laboratory testing. The standard deviation of 6.4 m/s for V_{s1} measurements in the target zone translates into a much smaller range in predicted CRR (approximately ± 0.02) than the standard deviation in $(N_1)_{60}$ does.

8.7 Discussion

8.7.1 Data review results compared with other CANLEX sites

Table 8-6 compares the results of the data review at the Massey and Kidd sites with the data review that has been performed at Phase I and Phase III of the CANLEX project. Detailed descriptions of the Phase I and Phase III data reviews, as well as the detailed data review of the Kidd site will be contained in CANLEX Project final reports. All of the values in Table 8-6 are given as the overall average in the target zone at each site; for some parameters, the overall standard deviation is also given. Index parameters for the four sites were given in Table 8-1. Grain characteristic parameters for the four sites were given in Table 8-2.

Overall, the target zone at the Kidd site had higher average values of $(N_1)_{60}$, q_{c1}, and V_{s1} than the target zone at the Massey site. This is likely partially due to aging effects. The scatter in SPT, CPT and shear wave velocity data (as represented by the standard deviations) was similar at the two sites. The Massey and Kidd sites had similar average values of Y, while both the average X and the average qc1/(N1)60 were smaller at Kidd than at Massey. Similar average fines contents were predicted at each site using the integrated CPT method described in Chapter 3. Actual fines content data from undisturbed samples are still required to check the accuracy of these predictions. The average void ratio predicted by the geophysical logs is closer to the average of the undisturbed samples tested to date at the Massey site. At the Kidd site, the geophysical logging appears to significantly underpredict the average void ratio. However, as reported by Lawrence et al. (1995), the geophysical logs at Kidd were not of the same quality as at Massey. The average void ratio at Massey appears to be higher than the average void ratio at Kidd. However, additional undisturbed samples at both sites, particularly Kidd (at which only six sample void ratios are available to date) are required to confirm the average values. Since samples were initially selected with the goal of attempting to test the loosest samples first, the actual average void ratio at each site may be slightly less than the average value to date, as given in Table 8-6.

The data review results for the Phase I (Syncrude) site are also presented in Table 8-6. The target zone at the Phase I site was located at a much greater depth than the target zone at either of the Phase II sites. The average $(N_1)_{60}$ and q_{c1} were higher than either of the Phase II sites. However, the average V_{s1} was lower than either of the Phase II sites. The scatter in SPT and CPT data at the Phase I site was similar to the scatter at both of the

Phase II sites. The shear wave velocity data, however, was much more scattered than the shear wave velocity data at either of the Phase II sites, with the standard deviation being in the order of 20 m/s compared to 5 to 6 m/s at the Phase II sites (see Table 8-6). This suggests that the shear wave velocity measurements at the Phase I site either have more variation or are less reliable than at the Phase II sites. The fact that the standard deviations for the CPT are similar at both the Phase I and II sites suggests the latter. The average value of $q_{c1}/(N_1)_{60}$ at the Phase I site was similar to that at the Kidd site, while the average values of both Y and X at the Phase I site were much smaller than at either of the Phase II sites. In addition, the values of Y and X were more scattered at the Phase I site (indicated by the larger standard deviations). Both Y and X at the Phase I site were likely strongly influenced by the lower values of shear wave velocity which high a high degree of scatter. Geophysical logging at the Phase I site predicted a similar average void ratio to the average of the undisturbed samples available to date. As for the Phase II sites, the actual average void ratio at each site may be slightly less than the average value to date shown in Table 8-6, because samples were initially selected with the goal of attempting to test the loosest samples first. An average fines content of 12.4% was predicted at the Phase I site, using the integrated CPT method described in Chapter 3. To date, grain size distributions for undisturbed samples have indicated a smaller average fines content in the order of 5%. However, more data is required before any firm conclusions can be made. In addition, the method outlined in Chapter 3 proposed tentative relationships to estimate fines content. The method will be updated as additional data become available; in addition, Chapter 3 recommended that the equations given in the method were general and might require site specific modifications.

Table 8-6 also presents the summarized data review results available to date from the Phase III (J-pit) site. The target zone at the Phase III site is shallower than the target zones at the Phase I and II sites. The Phase III site is also the youngest deposit of the four sites, consisting of freshly placed (< 1 month old) Syncrude sand tailings. The results of the data review for the Phase III site suggest that this sand is unusual, as compared to the other sites. The average values of $(N_1)_{60}$, q_{c1} and V_{s1} are all significantly smaller than the values at the Phase I and Phase II sites. In general, the SPT, CPT and shear wave velocity measurements also appear to be more consistent (i.e. less scattered) that at the other sites. The average values of Y, X and $q_{c1}/(N_1)_{60}$ do not appear unusual and are in the same range as the values for the other sites. The integrated CPT method described in Chapter 3 predicts a higher fines content at the Phase III site than at the other sites. However, actual fines content data from undisturbed samples are required to check the accuracy of these predictions. Conventional or shear wave velocity based interpretations of the $(N_1)_{60}$, q_{c1} or V_{s1} profiles would predict significantly higher void ratios than suggested by the undisturbed samples available to date. However, geophysical logging predicts an average void ratio similar to the average void ratio of the undisturbed samples available to date.

A possible explanation for the discrepancy in results is that the SPT, CPT and shear wave velocity measurements were strongly influenced by the high fines content and, hence, possibly the skeletal void ratio at the Phase III site. The void ratios estimated for the undisturbed samples and predicted by the geophysical logging are total void ratios. When the undisturbed sample total void ratios were corrected to approximate equivalent skeletal void ratios based on the average fines content in the target zone, the void ratio interpretations of the SPT, CPT and shear wave velocity measurements had much better agreement with the undisturbed samples. Further details of this analysis will be provided the Phase III data review report. The results seem to indicate that skeletal void ratio may be a factor for sands with a high fines content. Scanning electron microscopy has also shown that at least some of the undisturbed samples from the Phase III site appear to have an unusual fabric due to the high fines content (Hofmann, 1995). It will be interesting to carefully examine the results of testing undisturbed samples to see if their response appears to be linked to skeletal or total void ratios.

8.7.2 Estimated response

a) Flow liquefaction

Table 8-7 summarizes the average state of Fraser River sand in the target zone at the Massey site, based on the undisturbed samples available to date. The average RSR of 0.29 was estimated by combining the average effective stresses at the mid-depth of the target zone at each site and the overall average void ratio of all undisturbed samples available to date, as summarized in Table 8-6. In general, as discussed previously, interpretation of the in-situ testing signatures appears to predict similar average states over most of the target zone at each site. However, both in-situ testing and undisturbed samples have indicated that there may be layers with the target zone having significantly higher values of RSR (i.e. looser). Based on the average predicted RSR at the Massey site, Table 8-7 presents the corresponding estimated values for the various components of response described in Chapter 4 (see Figures 4-15 and 4-16), for triaxial compression and extension, respectively.

Brittleness index (I_B) and axial strain at minimum strength (ε_a) were estimated based on Equations 8-1 and 8-2, respectively; i.e. the laboratory based relationships based on testing at the Massey site. The ultimate values of M were assumed to be approximately $(M_f)_C=1.5$ and $(M_f)_E=1.0$, for triaxial compression and extension, respectively, based on the results of the laboratory testing at the Massey site, discussed previously. Based on the limited testing to date on undisturbed samples of Fraser River sand, $I_B \approx 0$ for triaxial compression loading indicates that the material would strain-harden in triaxial compression. Consequently, S_{min}, S_p and S_f will all be equal and can be estimated by combining Equation 4-28 in Chapter 4, which estimates the theoretical S_f/p_i', with the average $(M_f)_C$ and p'_i. The value of p'_f can be estimated by combining S_f and M_f (see Equation 4-15 in Chapter 4) and will be equal to both p'_{min} and p'_p. Axial strain at minimum strength is not applicable for strain hardening material. In triaxial extension, S_{min} can be estimated by combining Equation 4-29 in Chapter 4, which estimates the theoretical S_{min}/p'_i, with the average p'_i. S_p can be estimated by combining the estimated I_B and S_{min} with the average S_i ($=q_i/2$) and the triaxial extension formula for brittleness index (see Equation 4-27a in Chapter 4). S_f can be estimated by combining Equation 4-28 in Chapter 4, which estimates the theoretical S_f/p_i', with the average $(M_f)_E$ and p'_i. The value of p'_{min} can be estimated by combining S_{min} and M_{min} (see Equation 4-16 in Chapter 4), assuming that $M_{min}=M_f$. The value of p'_p can be estimated by combining S_p and M_p. Using the plots of M_p versus RSR for Massey as a reference (see Figure 8-14c), an average M_p of 0.75 was selected for triaxial extension based on the average RSR values of 0.24 to 0.29 calculated for the Phase II sites. The value of p'_f can be estimated by combining S_f and M_f.

Included in Table 8-7 are the average corrected values of SPT and CPT penetration resistance and shear wave velocity measurements. The correlation parameters between the three tests (i.e. Y, X and $q_{c1}/(N_1)_{60}$) are also given. As a guide to estimating in-situ response to undrained monotonic loading, the average values of $(N_1)_{60}$, q_{c1} and V_{s1} can be linked to the average response in triaxial compression and triaxial extension at each site. The averaged values of $(N_1)_{60}$, q_{c1} and V_{s1} were all higher at Kidd than at Massey; this is likely partially a result of aging. The average RSR at the two sites are reasonably similar; consequently, the estimated components are somewhat similar, although higher strengths are predicted at Kidd because RSR is slightly smaller. The methods of estimating the undrained strength are sensitive to RSR, as is indicated by this comparison. However, the methods can be useful in estimating the overall average and general range in response at a given site.

Based on the summary presented in Table 8-7, Figure 8-20 illustrates how average q-p' stress paths and S_u-ε_a stress-strain curves for Fraser River sand in the target zone at each Phase II site can be back-calculated by combining the individual components of response estimated from the average state in the target zone at each site. Average stress paths and stress-strain curves are shown for both triaxial compression and triaxial extension directions of loading. The stress path curves were estimated by sketching a line through the points (p'_i, q_i), (p'_p, q_p), (p'_{min}, q_{min}), and (p'_f, q_f), as summarized in Table 8-7, using, as a reference, some of the actual stress paths plotted for undisturbed samples with similar values of RSR tested in the laboratory. Obviously some artistic licence has been used to create these figures and they are shown primarily for illustrative purposes. The stress-strain curves were estimated by sketching a line through the points (S_i, $(\varepsilon_a)_i=0$), (S_p, $(\varepsilon_a)_p$), (S_{min}, $(\varepsilon_a)_{min}$), and (S_f, $(\varepsilon_a)_f$), as summarized in Table 8-7. The triaxial compression stress-strain curves are shown to strain-harden directly to ultimate state; the shapes of the curves were drawn using, as a reference, some of the actual stress-strain curves plotted for undisturbed samples with similar values of RSR tested in the laboratory. For the triaxial extension stress-strain curves, $(\varepsilon_a)_p$ was estimated to have a value of approximately 0.25%, based on laboratory results. The value of $(\varepsilon_a)_{min}$ for the triaxial extension stress-strain curves was estimated by adding half of the axial strain estimated to occur while at minimum strength to the value of $(\varepsilon_a)_p$. For both triaxial compression and extension tests, $(\varepsilon_a)_f$ was set equal to 20%. This is typically the limit to which laboratory tests are taken; however, the actual ultimate strength likely occurs at larger strains, as indicated by the fact that many of the undisturbed samples were still strain-hardening towards their respective ultimate states when the triaxial tests were stopped.

b) Cyclic softening

Included in Table 8-7 is a summary of the integrated CPT method for estimating CRR, described in Chapter 3, as applied to the average CPT data in the target zone at each of the Phase II sites. The average I_c classifies the soil in the target zone at the Massey site as a sand (clean sand to silty sand) since $1.31 < I_c < 2.05$ (see Chapter 3, Table 3-1). The standard deviation is small, indicating a fairly uniform target zone, in terms of soil classification. Similar average fines contents of approximately 7% are predicted for the target zone at the Massey site. The resulting average recommended correction to CPT penetration resistance, Δq_{c1}, is very small. In the target zone, when the average Δq_{c1} is added to the average corrected q_{c1}, an average CRR of approximately 0.10 is estimated.

Since the Massey soil deposit is considered to be fairly uniform in the target zone, a fairly uniform average CRR of 0.10 would be expected throughout much of the target zone at each site. This was clearly shown in Figures 8-19.

Included in Table 8-7 are the average corrected values of SPT and CPT penetration resistance and shear wave velocity measurements. The correlation parameters between the three tests (i.e. Y, X and $q_{c1}/(N_1)_{60}$) are also given. As a guide to estimating in-situ response to undrained cyclic loading, the average values of $(N_1)_{60}$, q_{c1} and V_{s1} can be linked to the average estimated CRR at each site. It is of interest to compare the value of CRR that other existing methods would predict from the average in-situ testing with the average value estimated using the integrated CPT approach. The estimated fines content at Massey of 6.8% is such that the sand is close to being classified as a clean sand (FC ≤ 5%) by the Seed et al. (1985) methodology (i.e. the recommended correction to (N1)60 would be small). The clean sand relationships between CRR and SPT $(N_1)_{60}$ by both Seed et al. (1985) and Fear and McRoberts (1995), as described in Chapter 2 (see Figures 2-1 and 2-8), would predict an average CRR slightly greater than 0.10 based on the average $(N_1)_{60}$ of 10.3 in the target zone at Massey. However, the relationship between CRR and Vs1 by Robertson et al. (1992), described in Chapter 3 (see Figure 3-17a), would predict a higher average CRR of approximately 0.19 based on the average V_{s1} of 168.2 m/s. However, as discussed earlier, the shear wave velocity correlation based on the recent NCEER Workshop (1996) discussions, as described in Chapter 3 (see Figure 3-17b), gives an estimated CRR of approximately 0.1, agreeing much better with the results of laboratory testing. As previously discussed, for the average values of Q and F at both Phase II sites, the soil classification based method by Olsen and Koester (1995), described in Chapter 3 (see Figure 3-14), would predict an average CRR of approximately 0.075, similar to the value of 0.10 predicted by the integrated CPT method.

8.8 Summary and Conclusions

Consistent frameworks for evaluating the potential for both cyclic softening and flow liquefaction have been proposed in Chapters 3 and 4 as a means of interpreting and comparing various field and laboratory data and linking the observed response in the laboratory to in-situ test results. The suggested framework for evaluation of flow liquefaction potential is based on estimating values of RSR for laboratory samples and in-situ field conditions, relative to a reference USL established by laboratory testing, as described in Chapter 4. RSR provides the link between in-situ testing signatures and response to undrained monotonic loading observed in the laboratory. The suggested framework for evaluating cyclic softening potential is based on an integrated CPT approach described in Chapter 3.

Applying the two frameworks to the Massey site in this chapter has led to the general conclusion that in the target zone the site is, on average, essentially non-susceptible to flow liquefaction. If a suitable trigger resulted in undrained monotonic loading, most of the target zone at the site would respond in a non-brittle, strain-hardening manner in triaxial compression and could exhibit a temporary loss in strength with minimum associated axial strains in triaxial extension before strain-hardening. Some specific zones at the Massey site would require further investigation for design purposes to evaluate the continuity of the looser layers. When subjected to cyclic loading, the target zones at the Massey site would have an average M=7.5 equivalent CRR of approximately 0.1. Cyclic liquefaction and subsequent deformations would only be a problem if the earthquake induced CSR exceeded this resistance.

Table 8-1: Index parameters for CANLEX sites

Parameter	**Phase I**	**Phase II (Fraser River Sand)**		**Phase III**	**Ticino Sand***
	Syncrude	**Massey**	**Kidd**	**J-pit**	
Approx. age of deposit	30 years	200 years **	4 000 years **	1 month	< 1 week
Target Zone Depth (m)	27 to 37 (Elev. 325 m to 315 m)	8 to 13	12 to 17	3 to 7	-
Depth to GWT (m)	21	1.5	1.5	0.5	-
γ (kN/m^3) above GWT below GWT	18.5 19.5	18.5 19.5	18.5 19.5	18.5 19.5	-
Mineralogy (of silt size fraction of soil)	90% quartz 5% feldspar 5% kaolinite	70% quartz 15 % feldspar 5% mica 5% kaolinite 5% chlorite & smectite	70% quartz 15 % feldspar 5% mica 5% kaolinite 5% chlorite & smectite	assumed to be the same as Phase I	95% quartz 5% feldspar
Grain Size Cu (D_{60}/D_{10})	2.22 (0.2/0.09)	2.14 (0.30/0.14)	2.5 (0.35/0.14)	not presently available	1.13 (0.65/0.40)
Average FC (%) from SPT	12	3	6.8	10	< 5%
e_{max}§	0.958	1.102	1.077	0.901 (FC=4%-10%) 0.986 (FC=10%-40%)	0.89
e_{min}§	0.668	0.715	0.715	0.579 (FC=4%-10%) 0.461 (FC=10%-40%)	0.52
G_s	2.66	2.68	2.72	2.62	2.67
K_o***	0.5	0.5	0.5	0.5	-

Notes:

* Calibration chamber studies (Baldi et al., 1986)

** Monahan et al. (1995)

*** estimated from pressuremeter testing results

§ all values of e_{max} and e_{min} were determined by U. of A., except those for Phase I which were determined by UBC

Table 8-2: Grain characteristic parameters for CANLEX sites

Parameter	Phase I	Phase II (Fraser River Sand)		Phase III
	Syncrude	Massey	Kidd	J-pit
Γ	0.919 ($e>0.829$) 1.920 ($e<0.829$)	1.071 ($e>0.979$) 1.80 ($e<0.979$)	1.071 ($e>0.979$) 1.80 ($e<0.979$)	0.919 ($e>0.829$) 1.920 ($e<0.829$)
λ_{ln}	0.015 ($e>0.829$) 0.182 ($e<0.829$)	0.0165 ($e>0.979$) 0.1477 ($e<0.979$)	0.0165 ($e>0.979$) 0.1477 ($e<0.979$)	0.015 ($e>0.829$) 0.182 ($e<0.829$)
A*	311 (311 + 0)	317 (295 + 22)	325 (295 + 30)	311 (311 + 0)
B	188	143	143	188

Notes:

* a (b + c), where a = estimated value for the deposit in-situ; b = value determined from testing young reconstituted samples in the laboratory; c = correction to account for aging effects in-situ, based on the work by Robertson et al. (1995)

Table 8-3: Summary of data for Massey frozen samples tested to date

Massey Tunnel		Pa	100	(kPa)		e>0.979	e<0.979
Gs	2.68	γ water	9.8	(kPa)	Γ	1.071	1.8
GWT (m)	1.5	γ dry	18.5	(kN/m3)	λ	0.0165	0.1477
Ko	0.5	γ sat.	19.5	(kN/m3)	Breakpoint void ratio		0.979

FROZEN SAMPLES Sample No.	Average Depth (m)	Average σv' (kPa)	Void Ratio	RSR	Source of e S=sent R=received	Lab sent to	T=triaxial (C,E) SS=simple shear CSS=cyclic SS	Fines Content (% passing No. 200 sieve)	Lab e	Lab RSR	IB	Smin/p1	% εa at Smin	Sf/p1	Mp	Mf	CRR (M=7.5)
M94F6 C2B	9.155	102.0	0.9788	0.262	S	UBC	TE - DRAINED										
M94F4 C4-2	10.425	114.3	0.9793	0.294	S	UBC	TE		0.982	0.333	0.106	0.050	8.0	0.273	1.47	0.92	
M94F6 C7A	11.85	128.1	0.9299	0.236	S	UBC	TE		0.914	0.205	0.000	0.181	3.3	0.665	0.99	0.94	
M94F2 C2B-1	9.005	100.5	0.9129	0.165	S	UBC	TE		0.910	0.158	0.021	0.135	2.3	0.683	0.68	1.01	
M94F2 C7B-1	10.685	116.8	0.9852	0.430	S	UBC	TC - DRAINED										
M94F4 C4-1	10.255	112.7	0.9928	0.657	S	UBC	TC		0.990	0.531	0.000	1.960	0.0	1.960	1.38	1.38	
M94F4 C4-3	10.605	116.1	0.9803	0.317	S	UBC	TC		0.983	0.360	0.000	2.133	0.0	2.133	1.55	1.55	
M94F6 C4-2	10.375	113.8	0.9473	0.236	S	UBC	TC		0.942	0.220	0.000	2.727	0.0	2.727	1.42	1.42	
M94F4 C3A	9.33	103.7	1.0188	2.922	S	UBC	SS										
M94F6 C3-1	9.31	103.5	1.0025	1.066	S	UBC	SS										
M94F6 C3-2	9.33	103.7	0.9855	0.388	S	UBC	SS										
M94F2 C7B-2	10.78	117.8	1.0319	7.341	S	UBC	SS										
M94F2 C7B-3	10.81	118.1	1.0189	3.347	S	UBC	SS										
M94F2 C2B-2	9.545	105.6	0.8788	0.138	S	UBC	CSS		0.809								0.144
M94F2 C2B-3	10.03	110.5	0.9041	0.171	S	UBC	CSS		0.862								0.099
M94F5 C3C-1	10.47	114.8	1.0327	7.509	S	UBC	CSS		1.005								0.098
M94F5 C3C-2	10.5	115.1	0.9854	0.428	S	UBC	CSS		0.968								0.080
M94F2 C11B-1	12.75	136.9	1.025	5.617	S	UBC	CSS		0.995								0.111
M94F2 C11B-2	12.78	137.2	1.0287	6.239	S	UBC	CSS		0.997								0.089
M94F6 C4B-1	10.53	115.3	1.0241	4.482	S	UBC	CSS		0.998								0.094
M94F6 C4B-2	10.55	115.5	1.0257	4.946	S	UBC	CSS		0.986								0.093
M94F6 C6-1	11.19	121.7	0.9766	0.308	S	UBC	CSS		0.958								0.112
M94F6 C6-2	11.22	122.0	0.9697	0.294	S	UBC	CSS		0.953								0.084
M94F6 C6-3	11.25	122.3	0.9705	0.297	S	UBC	CSS		0.957								0.111
M94F4 C2B	9.075	101.2	0.9065	0.159	S	Laval - VA01	TC		0.909	0.140	0	4.502	0	4.502	1.57	1.57	
M94F6 C2A	8.775	98.3	0.8706	0.121	S	Laval - VA02	TC		0.853	0.094	0	8.246	0	8.246	1.54	1.54	
M94F4 C4	10.2362	112.5	0.9733	0.278	S	Laval - VA12	TC		0.962	0.251	0	2.825	0	2.825	1.78	1.78	
M94F4 C4-4	10.73	117.3	0.9808	0.330	S	Laval - VA13	TC		1.043	14.293	0	1.370	0	1.370	1.47	1.47	
M94F2 C11B	12.62	135.6	1.0285	6.880	S	VA14 (M94F2C	TC		1.000	1.193	0	2.160	0	2.160	1.47	1.47	
M94F2 C7B-1	10.84	118.3	0.9146	0.197	S	Laval - VA15	TC		0.810	0.094	0	7.104	0	7.104	1.52	1.52	
M94F2 C7B-2	10.95	119.4	1.0149	2.657	S	Laval - VA16	TC		0.983	0.370	0	3.105	0	3.105	1.51	1.51	
M94F6 C4-1	10.5	115.1	0.9831	0.373	S	Laval -VA17	TC		0.968	0.268	0	3.146	0	3.146	1.52	1.52	
M94F4 C1B	7.87	89.5	1.0512	17.979	S	Laval											
M94F2 C3A-1	8.18	92.5	0.9379	0.180	S	Laval											
M94F2 C3A-2	8.29	93.6	0.9378	0.182	S	Laval											
M94F2 C10-1	12.19	131.4	0.9504	0.278	S	Laval											
M94F2 C10-2	12.3	132.5	0.976	0.334	S	Laval											
M94F4 C6-4	12.6	135.4			S	UofA											
LAVAL LARGE DIAMETER SAMPLES																	
MT 1-1 (Samp#1Tu	8.12	92.0	1.033	6.128	S	Laval - VA04											
MT 1-2 (Samp#1Tu	8.12	92.0	1.0376	8.099	S	Laval - VA05											
MT 3-1 (Samp#1Tu	8.12	92.0	1.0435	11.580	S	Laval - VA03											
MT 3-2 (Samp#1Tu	8.12	92.0	1.0141	1.949	S	Laval - VA06											
Tube#2 A-1	8.85	99.0	0.9515	0.211	S	Laval											
Tube#2 A-2	8.85	99.0	0.9426	0.199	S	Laval											
Tube#2 A-4	8.85	99.0	0.974	0.246	S	Laval											
Tube#2 B-1	8.95	100.0	0.9513	0.213	S	Laval											
Tube#2 B-2	8.95	100.0	0.9438	0.202	S	Laval											
Tube#2 B-3	9.01	100.6	0.9017	0.153	S	Laval											
Tube#2 B-4	9.01	100.6	0.891	0.142	S	Laval											
Tube#2 C-1	9.125	101.7	0.8909	0.144	S	Laval											
Tube#2 D-1	9.22	102.6	0.8015	0.079	S	Laval											
Tube#2 D-2	9.22	102.6	0.8162	0.088	S	Laval											

Table 8-4: Summary of undrained monotonic test results for Massey site

Lab.	Test No.	INITIAL STATE									RSR	PEAK or YIELD						
		(e)c	σvi'	σhi'	p'i	qi	Si	ess	Ψ	Ψ/λ	p'i/p'ss	(q)p		(S)p		(p')p	Mp	Peak
												Δ	total	Δ	total		total q/p'	φ'
UBC	M94 F4 C41 (TC)	0.99	108	54	72.0	54	27	1.000	-0.010	-0.632	0.531	228.3	282.3	114.2	141.2	204.8	1.38	34.1
UBC	M94 F4 C43 (TC)	0.983	112	56	74.7	56	28	1.000	-0.017	-1.020	0.360	262.5	318.5	131.3	159.3	206.1	1.55	37.9
UBC	M94 F6 C42 (TC)	0.942	110	55	73.3	55	27.5	1.166	-0.224	-1.514	0.220	345.0	400.0	172.5	200.0	282.2	1.42	35.0
U of A	FS-UT-TAC	0.963	135.6	76.2	96.0	59.4	29.7	1.126	-0.163	-1.103	0.332	92.6	152.0	46.3	76.0			
UBC	M94 F4 C42 (TE)	0.982	110	55	73.3	55	27.5	1.000	-0.018	-1.099	0.333	69.8	14.8	34.9	7.4	10.1	1.47	75.8
UBC	M94 F6 C7A (TE)	0.914	124	62	82.7	62	31	1.148	-0.234	-1.584	0.205	92.0	30.0	46.0	15.0	30.2	0.99	36.5
UBC	M94 F2 C2B1 (TE)	0.91	98	49	65.3	49	24.5	1.183	-0.273	-1.846	0.158	68.0	19.0	34.0	9.5	28.1	0.68	22.4
U of A	FS-MT-TAC (T1)	1.01	643.7	328.9	433.8	314.8	157.4	0.971	0.039	2.376	10.758	71.4	386.2	35.7	193.1	430.0	0.90	23.0
U of A	FS-MT-TAE (T4)	1.013	638.4	322.8	428.0	315.6	157.8	0.971	0.042	2.544	12.730	449.1	133.5	224.6	66.8	180.0	0.74	25.0
UBC - Thomas	FS-WP-TAC	0.934	791.0	409.0	536.3	382	191	0.872	0.062	0.421	1.524	84.2	466.2	42.1	233.1	465.5	1.00	25.4
UBC - Thomas	FS-WP-TAE	0.934	791.0	409.0	536.3	382	191	0.872	0.062	0.421	1.524	512.0	130.0	256.0	65.0	136.5	0.95	34.5
Laval - VA01	M94F4 C2B	0.909	87.47	43.57	58.2	43.90	21.95	1.200	-0.291	-1.969	0.140	480.1	524.0	240.1	262.0	332.8	1.57	38.6
Laval - VA02	M94F6 C2A	0.853	84.77	43.27	57.1	41.50	20.75	1.203	-0.350	-2.367	0.094	900.2	941.7	450.1	470.9	611.6	1.54	37.8
Laval - VA12	M94F4 C4	0.962	113.20	53.20	73.2	60.00	30.00	1.166	-0.204	-1.380	0.251	353.6	413.6	176.8	206.8	231.8	1.78	43.4
Laval - VA13	M94F4 C4-4	1.043	121.00	56.50	78.0	64.50	32.25	0.999	0.044	2.660	14.293	149.2	213.7	74.6	106.9	145.7	1.47	36.1
Laval - VA14	M94F2 C11B	1.000	131.27	66.67	88.2	64.60	32.30	0.997	0.003	0.177	1.193	316.5	381.1	158.3	190.6	260.1	1.47	36.1
Laval - VA15	M94F2 C7B-1	0.810	115.13	57.03	76.4	58.10	29.05	1.160	-0.350	-2.367	0.094	1027.4	1085.5	513.7	542.8	714.7	1.52	37.3
Laval - VA16	M94F2 C7B-2	0.983	114.57	57.77	76.7	56.80	28.40	0.999	-0.016	-0.993	0.370	419.5	476.3	209.8	238.2	316.4	1.51	37.0
Laval - VA17	M94F6 C4-1	0.968	112.53	55.93	74.8	56.60	28.30	1.163	-0.195	-1.318	0.268	414.1	470.7	207.1	235.4	309.1	1.52	37.4

Lab.	Test No.	MINIMUM								ULTIMATE (End of test)							
		(q)qss		(S)min		Smin/p'o	p'min	% axial strain at Smin	IB	(q)uss		Sf		Sf/p'i	p'f	Mf	USS
		Δ	total	Δ	total	total			Δ	Δ	total	Δ	total	total		total q/p'	φ'
UBC	M94 F4 C41 (TC)	228.3	282.3	114.2	141.2	1.96	204.8	0	0.00	228.3	282.3	114.2	141.2	1.96	204.8	1.38	34.1
UBC	M94 F4 C43 (TC)	262.5	318.5	131.3	159.3	2.13	206.1	0	0.00	262.5	318.5	131.3	159.3	2.13	206.1	1.55	37.9
UBC	M94 F6 C42 (TC)	345.0	400.0	172.5	200.0	2.73	282.2	0	0.00	345.0	400.0	172.5	200.0	2.73	282.2	1.42	35.0
U of A	FS-UT-TAC	80.1	139.5	40.1	69.8	0.73		4	0.14								
UBC	M94 F4 C42 (TE)	62.4	7.4	31.2	3.7	0.05	10.1	8	0.11	95.0	40.0	47.5	20.0	0.27	43.4	0.92	33.0
UBC	M94 F6 C7A (TE)	92.0	30.0	46.0	15.0	0.18	30.2	3.3	0.00	172.0	110.0	86.0	55.0	0.67	117.5	0.94	33.7
UBC	M94 F2 C2B1 (TE)	66.6	17.6	33.3	8.8	0.13	16.1	2.3	0.02	138.2	89.2	69.1	44.6	0.68	88.1	1.01	37.5
U of A	FS-MT-TAC (T1)	-222.5	92.3	-111.3	46.2	0.11	60.0	23	4.12	-222.5	92.3	-111.3	46.2	0.11	60	1.54	37.7
U of A	FS-MT-TAE (T4)	422.9	107.3	211.4	53.6	0.13	80.0	11	0.06	430.6	115.0	215.3	57.5	0.13	90	1.28	54.3
UBC - Thomas	FS-WP-TAC	55.6	437.6	27.8	218.8	0.41	327.1	1.2	0.34	95.6	477.6	47.8	238.8	0.45	343.1	1.39	34.4
UBC - Thomas	FS-WP-TAE	469.6	87.6	234.8	43.8	0.08	82.1	5.5	0.08	515.3	133.3	257.7	66.7	0.12	136.5	0.98	35.7
Laval - VA01	M94F4 C2B	480.1	524.0	240.1	262.0	4.50	332.8	0	0.00	480.1	524.0	240.1	262.0	4.50	332.8	1.57	38.6
Laval - VA02	M94F6 C2A	900.2	941.7	450.1	470.9	8.25	611.6	0	0.00	900.2	941.7	450.1	470.9	8.25	611.6	1.54	37.8
Laval - VA12	M94F4 C4	353.6	413.6	176.8	206.8	2.83	231.8	0	0.00	353.6	413.6	176.8	206.8	2.83	231.8	1.78	43.4
Laval - VA13	M94F4 C4-4	149.2	213.7	74.6	106.9	1.37	145.7	0	0.00	149.2	213.7	74.6	106.9	1.37	145.7	1.47	36.1
Laval - VA14	M94F2 C11B	316.5	381.1	158.3	190.6	2.16	260.1	0	0.00	316.5	381.1	158.3	190.6	2.16	260.1	1.47	36.1
Laval - VA15	M94F2 C7B-1	1027.4	1085.5	513.7	542.8	7.10	714.7	0	0.00	1027.4	1085.5	513.7	542.8	7.10	714.7	1.52	37.3
Laval - VA16	M94F2 C7B-2	419.5	476.3	209.8	238.2	3.10	316.4	0	0.00	419.5	476.3	209.8	238.2	3.10	316.4	1.51	37.0
Laval - VA17	M94F6 C4-1	414.1	470.7	207.1	235.4	3.15	309.1	0	0.00	414.1	470.7	207.1	235.4	3.15	309.1	1.52	37.4

Notes: Tests are anisotropically consolidated triaxial compression and extension tests on Massey undisturbed and reconstituted sand; tests by Thomas are on reconstituted Fraser River sand

Table 8-5: Summary of undrained cyclic simple shear test results for Massey site

Depth (m)	Sample No.	e_c	τ_{cy}/σ'_{vc}	N	M	Correction $\frac{CRR_M}{CRR_{M=7.5}}$	CRR (M=7.5)
9.55	M94 F2 C2B2	0.809	0.123	30	8.61	0.854	0.144
10.02	M94 F2 C2B3	0.862	0.123	7	6.23	1.244	0.099
10.46	M94 F5 C3C1	1.005	0.09	20	8.07	0.920	0.098
10.49	M94 F5 C3C2	0.968	0.1	7	6.23	1.244	0.080
12.74	M94 F2 C11B1	0.995	0.095	31	8.62	0.853	0.111
12.77	M94 F2 C11B2	0.997	0.107	8	6.41	1.201	0.089
10.52	M94 F6 C4B1	0.998	0.109	9	6.59	1.162	0.094
10.54	M94 F6 C4B2	0.986	0.108	9	6.59	1.162	0.093
11.18	M94 F6 C61	0.958	0.098	25	8.43	0.874	0.112
11.21	M94 F6 C62	0.953	0.108	6	6.03	1.292	0.084
11.24	M94 F6 C63	0.957	0.105	18	7.87	0.946	0.111

Table 8-6: Summarized results of data review: average values of soil parameters in the target zone at CANLEX sites

Parameter	Phase I	Phase II		Phase III
	Syncrude	Massey	Kidd	J-pit
Target Zone Depth (m)	27 to 37 (Elev. 325-315)	8 to 13	12 to 17	3 to 7
In-situ testing results:				
$(N_1)_{60}$	18.2 (SD=3.0)	10.3 (SD=3.8)	17.2 (SD=4.8)	3.4 (SD=2.0)
q_{c1} (MPa)	7.46 (SD=1.69)	5.34 (SD=1.00)	6.53 (SD=1.82)	2.35 (SD=1.53)
V_{s1} (m/s)	156.4 (SD=20.1)	168.2 (SD=6.4)	177.4 (SD=5.4)	127.1 (SD=3.0)
Y	95.5 (SD=12.1)	110.2 (SD=4.6)	110.8 (SD=5.0)	101.1 (SD=5.9)
X	75.0 (SD=8.6)	94.7 (SD=7.7)	88.4 (SD=6.1)	88.0 (SD=5.6)
$q_{c1}/(N_1)_{60}$	0.42 (SD=0.15)	0.58 (SD=0.17)	0.45 (SD=0.07)	0.51 (SD=0.25)
e predicted by geophysical	0.787 (SD=0.052)	0.991 (SD=0.071)	0.776 (SD=0.064)	0.736 (SD=0.091)
FC (%) predicted by CPT	12.4	6.8	6.7	14.9
Frozen samples tested to date:				
FC (%)	5.1 (range: 1.8 to 11.1)	≈ 2 to 8	≈ 3 to 8	≈ 10 to 15
e	0.769 (SD=0.036)	0.976 (SD=0.046)	0.908 (SD=0.040)	0.761 (SD=0.059)
D_r (%) *	65	31	48	43
Ψ**	- 0.063	- 0.024	- 0.086	- 0.104
RSR***	0.59	0.29	0.24	0.06

Notes:

Values for parameters are shown as the average in the target zone (SD= standard deviation)

* calculated using e_{max} and e_{min} in Table I-3 (FC=10-40% used for Phase III)

** relative to the flat portion of the appropriate reference USL; see Table I-4

*** relative to the appropriate reference USL (see Table I-4); calculated from average e of frozen samples and average estimated p' in target zone

Table 8-7: Predicted average response at the Massey site based on average values of soil parameters in the target zone

Parameter	Average value at Massey Site	
Flow liquefaction		
Depth (m)	10.5	
GWT(m)	1.5	
Unit weight of soil (kN/m^3)	18.5 (above GWT) 19.5 (below GWT)	
in-situ σ'_{vi} (kPa)	115	
in-situ K_o	0.5	
in-situ σ'_{hi} (kPa)	57.5	
in-situ p'_i (kPa)	76.7	
in-situ q_i (kPa)	57.5	
in-situ e	0.976	
in-situ p'_{us}	264.8	
in-situ RSR	0.29	
Average Response	**Compression**	**Extension**
I_B	0.03	0.05
S_{min}/p'_i	2.6	0.02
ε_a (%) at S_{min}	N/A	4.8
S_f/p'_i	2.6	1.7
M_p	1.5	0.75
M_f	1.5	1.0
S_{min} (kPa)	199.4	1.5
p'_{min} (kPa)	265.9	3.0
S_p (kPa)	199.4	3.09
p'_p (kPa)	265.9	8.2
S_f (kPa)	199.4	130.4
p'_f (kPa)	265.9	260.8
In-situ Testing		
$(N_1)_{60}$	10.3 (SD=3.8)	
q_{c1} (MPa)	5.34 (SD=1.00)	
V_{s1} (m/s)	168.2 (SD=6.4)	
Y	110.2 (SD=4.6)	
X	94.7 (SD=7.7)	
$q_{c1}/(N_1)_{60}$	0.58 (SD=0.17)	
Cyclic liquefaction		
Q	49.4 (SD=9.9)	
F	0.398 (SD=0.089)	
I_c	1.962 (SD=0.085)	
Soil behaviour type	clean to silty sand	
FC (%)	6.8	
Δq_{c1} (MPa)	0.30	
CRR (M=7.5; N=15 cycles)	0.10	

Note:
Values for parameters are shown as the average in the target zone (SD=standard deviation)

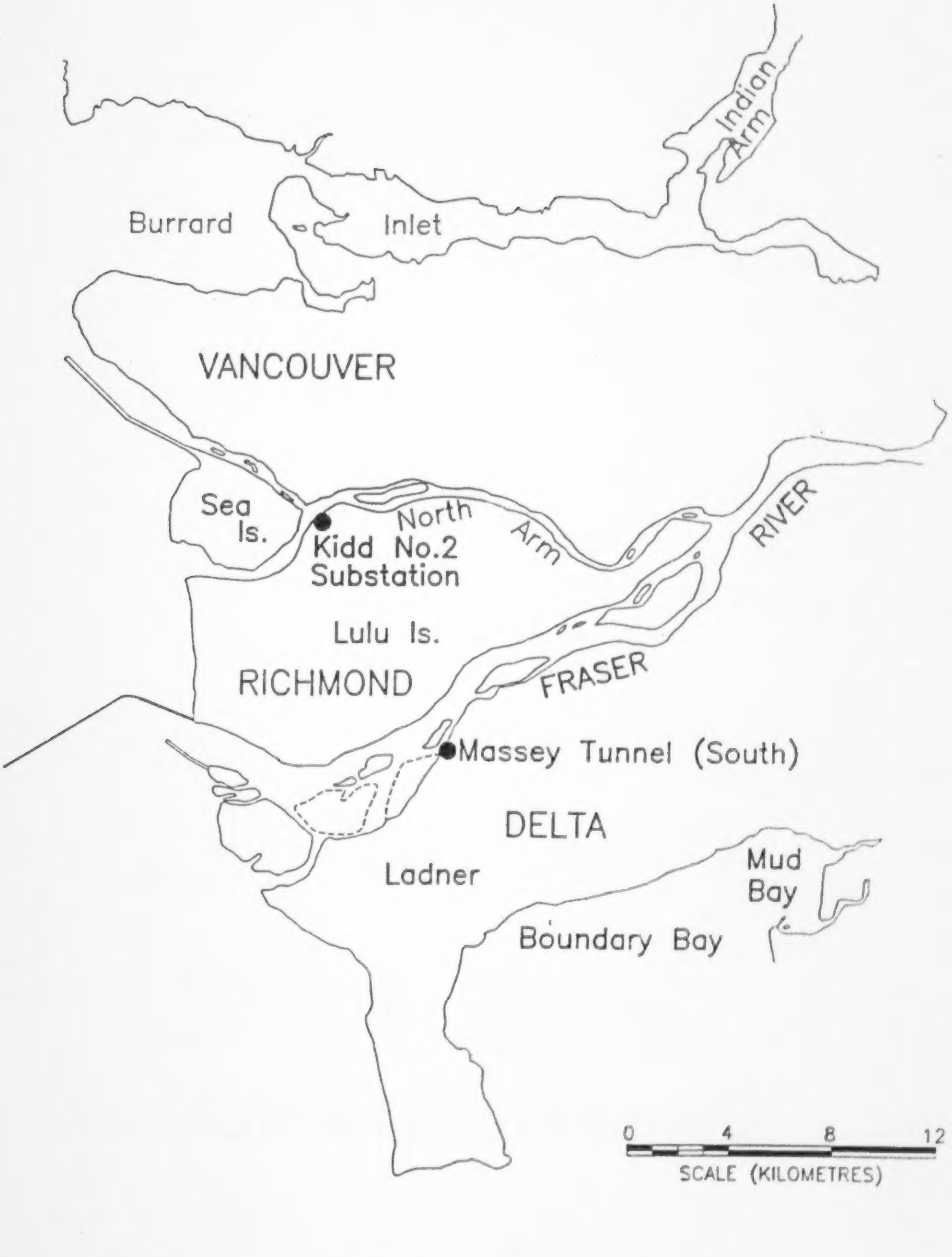
Burrard
Inlet
Indian Arm
VANCOUVER
Sea Is.
North Arm
Kidd No.2 Substation
Lulu Is.
RICHMOND
FRASER
RIVER
Massey Tunnel (South)
DELTA
Ladner
Mud Bay
Boundary Bay
0
4
8
12
SCALE (KILOMETRES)

Figure 8-1 Location of CANLEX Phase II Massey and Kidd sites in the Fraser River Delta, B.C. (modified from Lawrence et al., 1995).

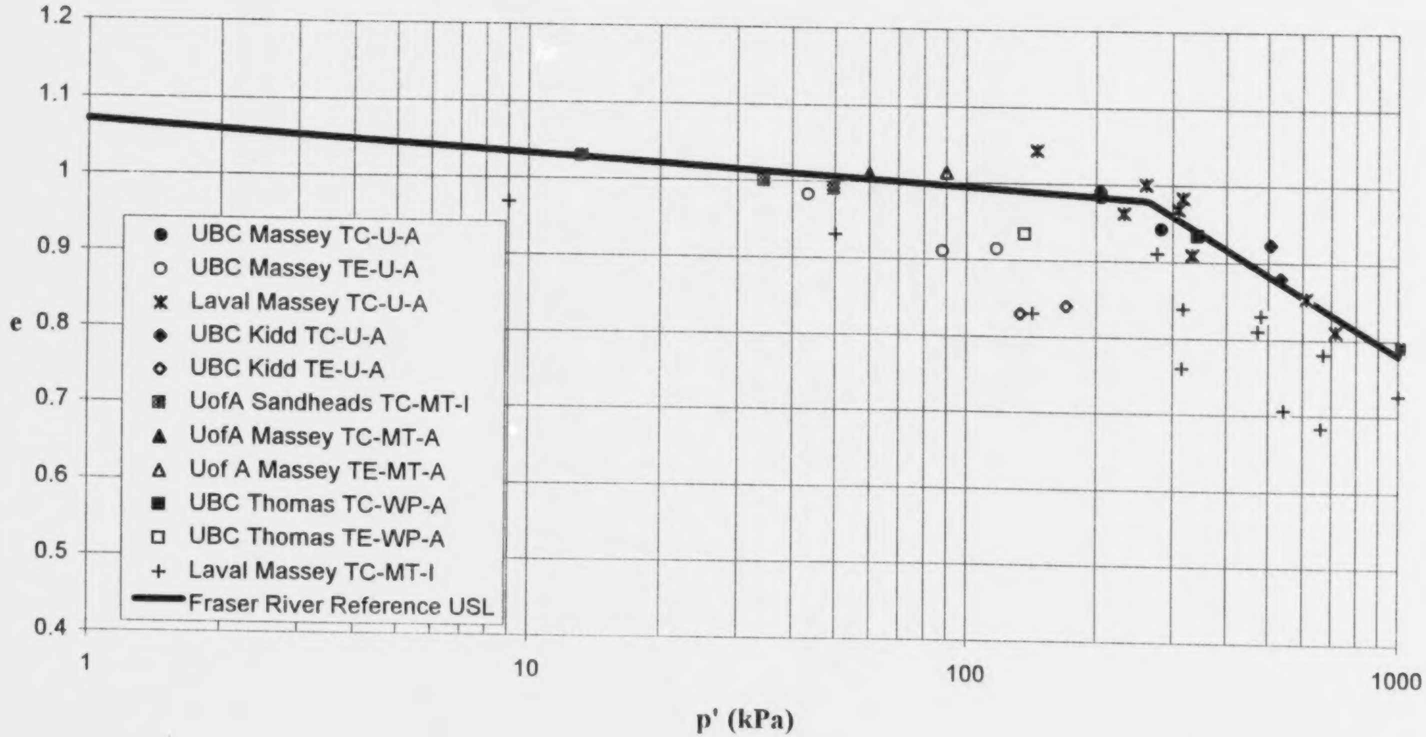

Figure 8-2 End of test conditions for all Fraser River reconstituted and undisturbed triaxial samples; selected reference ultimate state line (USL) for Fraser River sand is indicated.

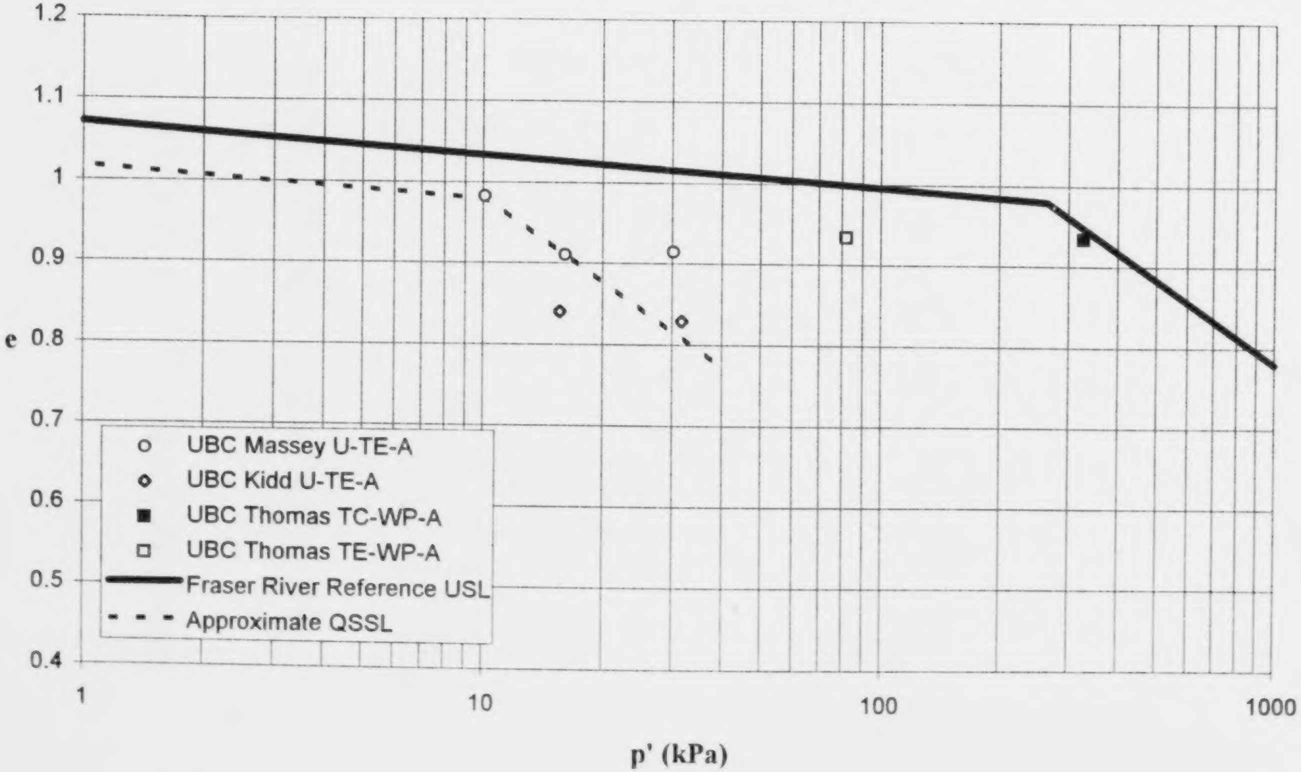

Figure 8-3 Quasi-steady state (QSS) conditions for any of the Fraser River samples in Figure 8-2 that had a QSS; selected approximate QSS line (QSSL) is indicated; selected reference USL is shown for comparison.

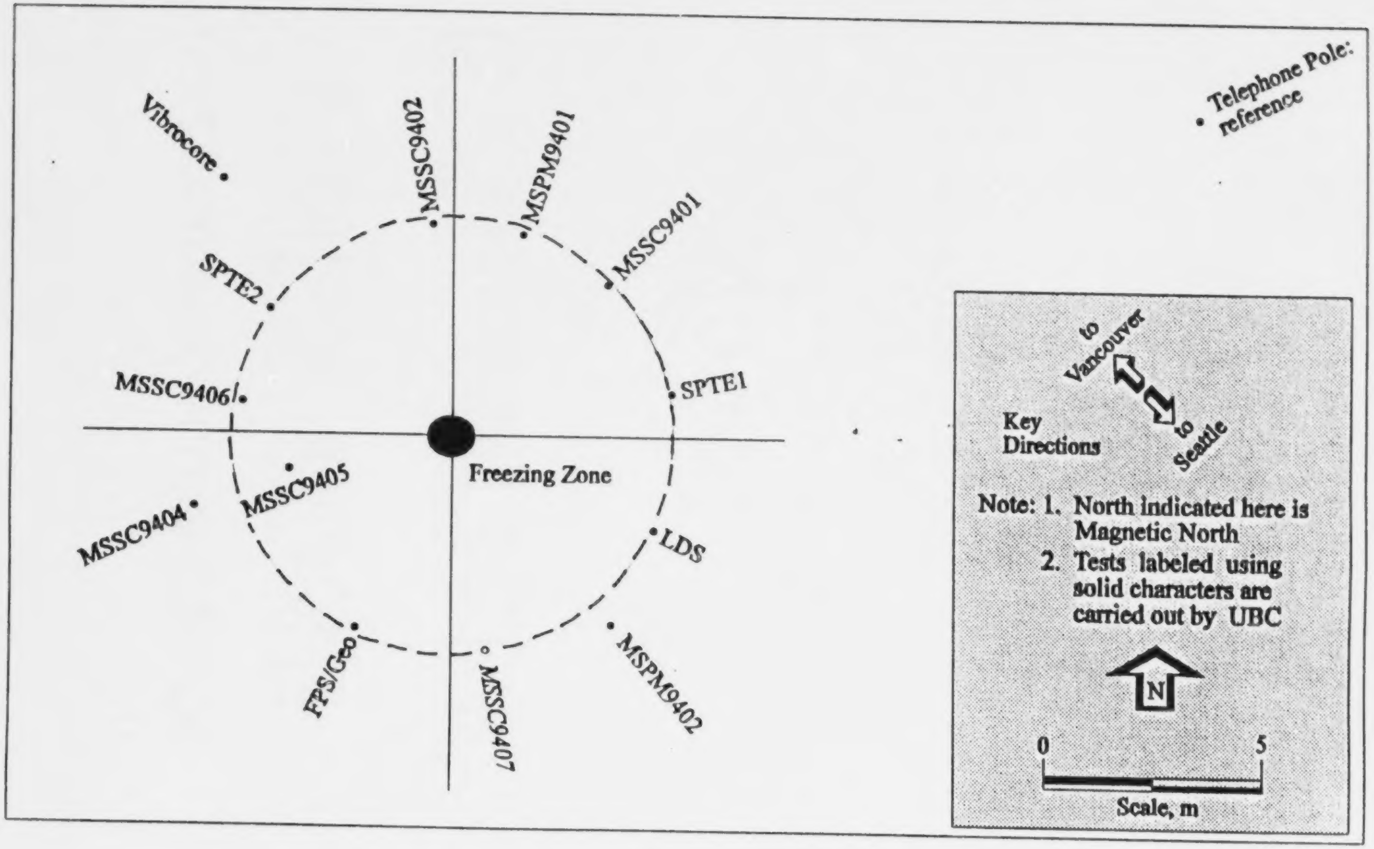
Vibrocore
MSSC9402
MSPM9401
MSSC9401
SPTE2
SPTE1
MSSC9406
Freezing Zone
MSSC9405
MSSC9404
LDS
FPS/Geo
MSSC9407
MSPM9402
Telephone Pole: reference
Key Directions
to Vancouver
to Seattle
Note: 1. North indicated here is Magnetic North
2. Tests labeled using solid characters are carried out by UBC
N
0
5
Scale, m

Figure 8-4 Plan of the detailed test site at the CANLEX Phase II Massey site (modified from Campanella, 1995).

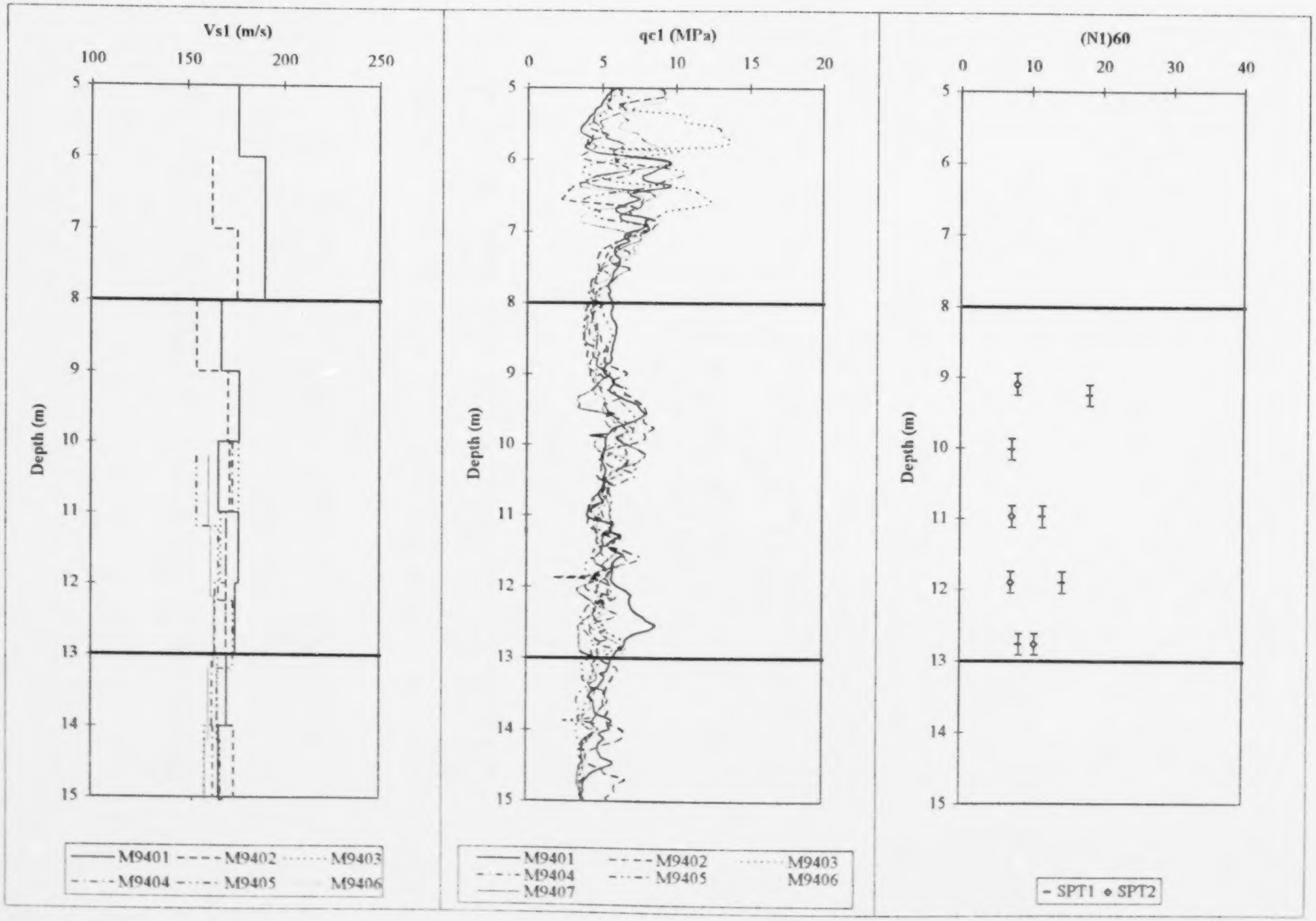

Figure 8-5 Corrected profiles of (a) shear wave velocity, V_{s1}, (b) CPT cone tip resistance, q_{c1}, and (c) SPT blowcount, $(N_1)_{60}$, at the Massey site; test site target zone for testing and sampling located from 8 m to 13 m, as indicated.

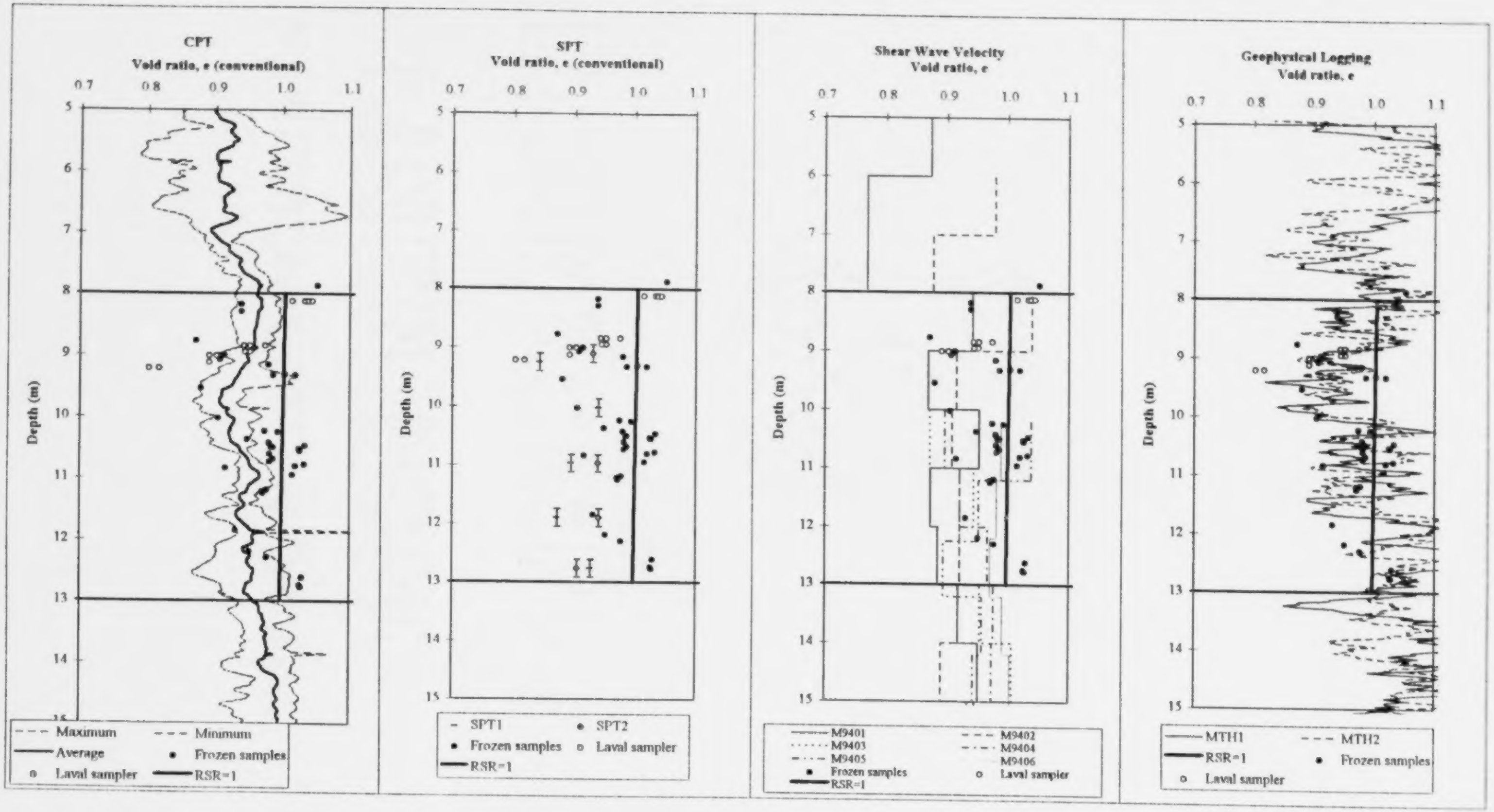

Figure 8-6 Conventional void ratio interpretations for (a) CPT, (b) SPT, (c) V_s measurements, and (d) geophysical logging; void ratios of frozen samples and Laval sampler samples are shown for comparison; RSR=1 line based on selected reference Fraser River USL is also shown.

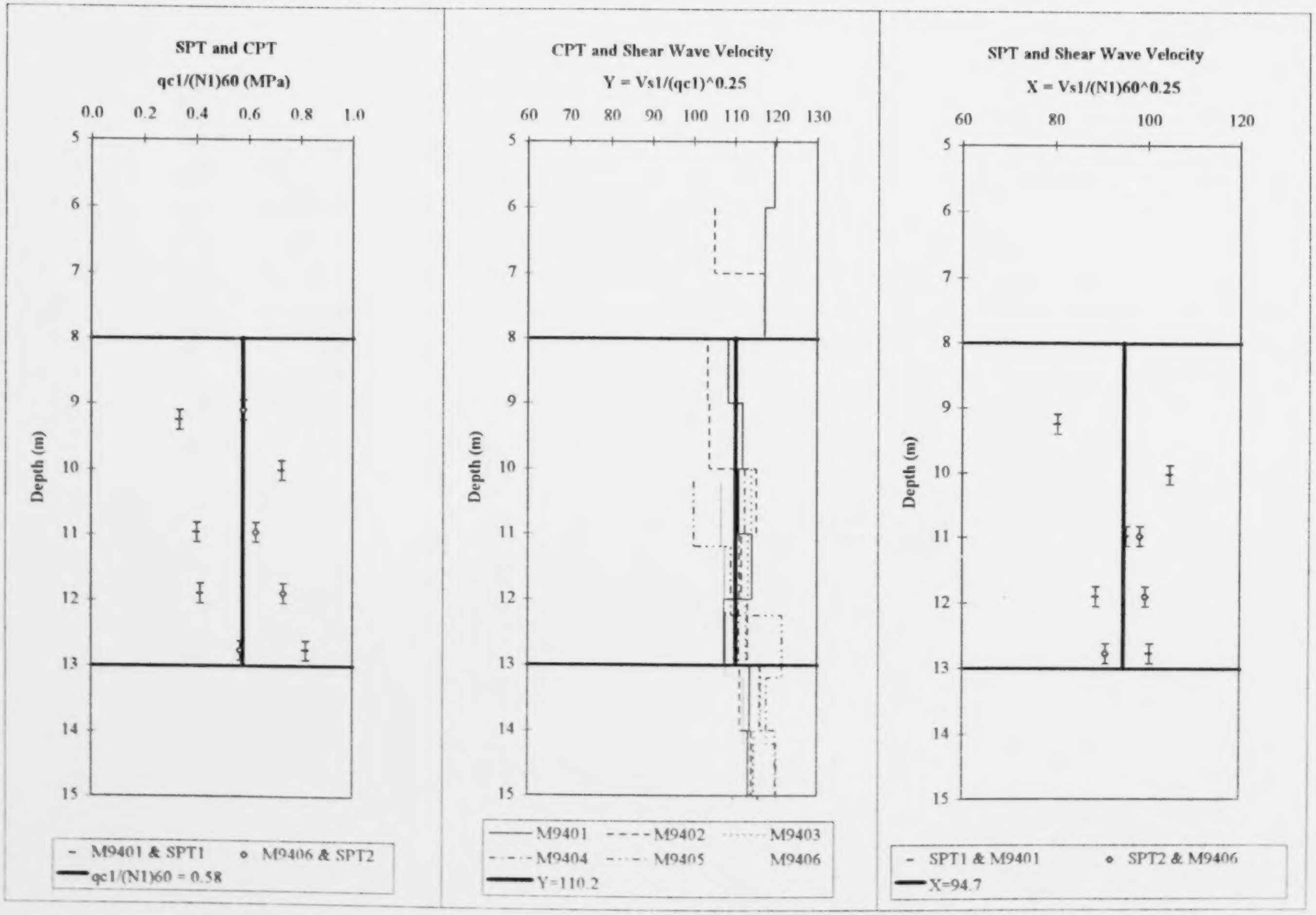

Figure 8-7 Correlations between in-situ tests: (a) comparison of CPT and SPT in terms of $q_{c1}/(N_1)_{60}$, (b) comparison of CPT and V_s in terms of Y, (c) comparison of SPT and shear wave velocity in terms of X.

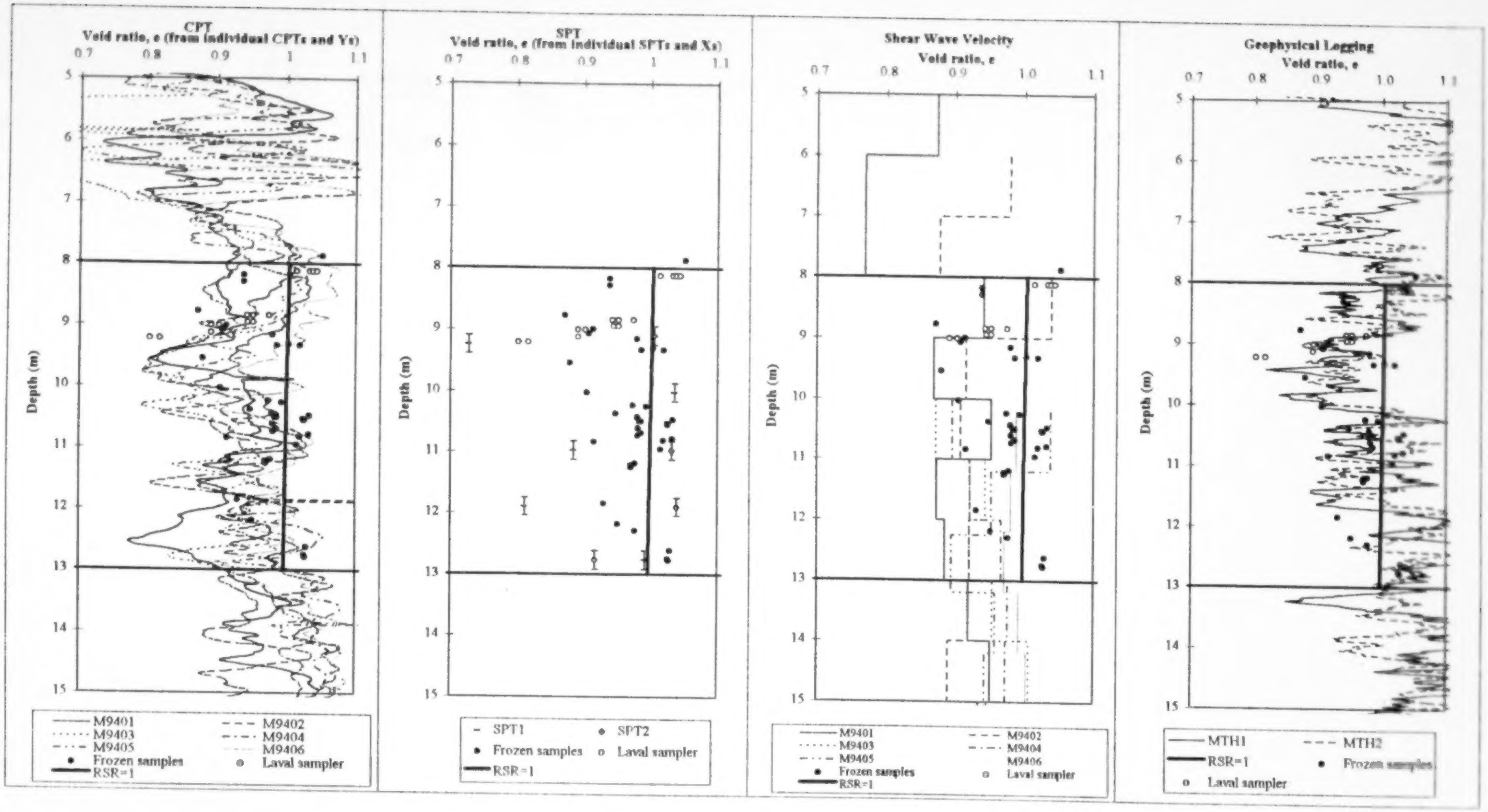

Figure 8-8 Direct void ratio interpretations for (a) CPT, (b) SPT, (c) V_s measurements, and (d) geophysical logging; void ratios of frozen samples and Laval sampler samples are shown for comparison; RSR=1 line based on selected reference Fraser River USL is also shown.

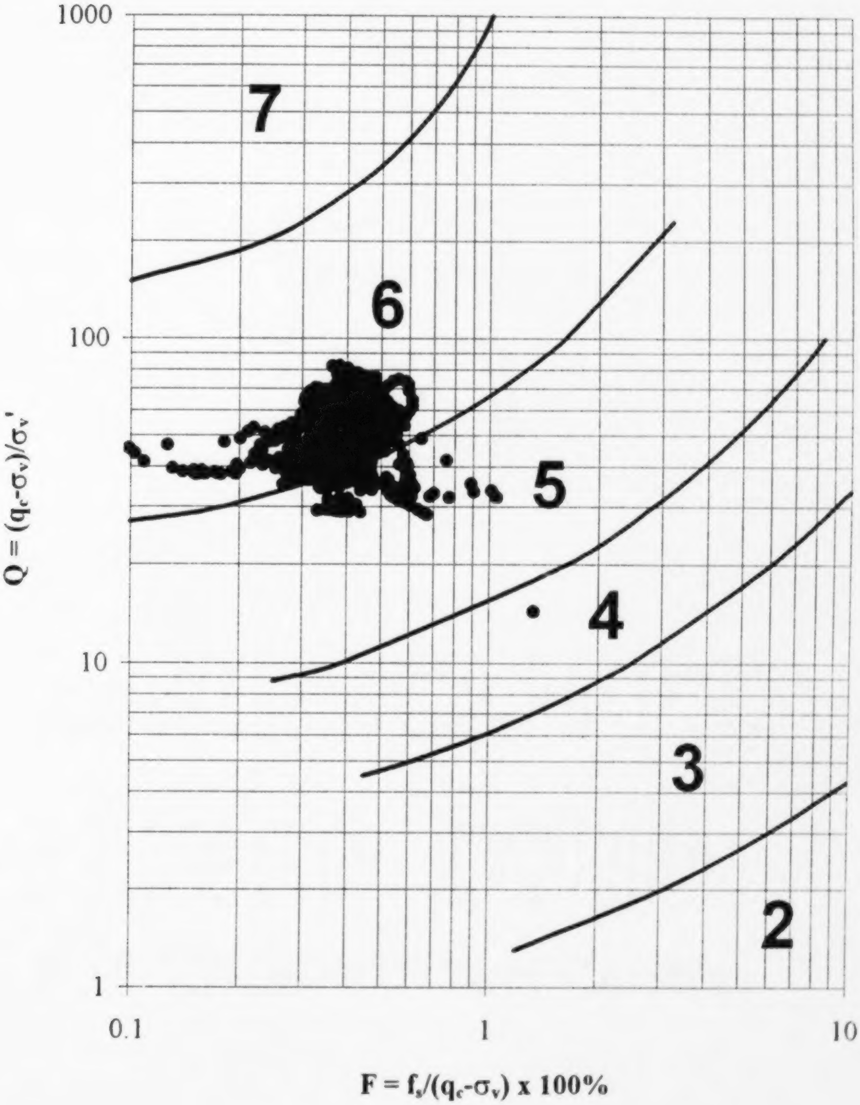

Figure 8-9 Plot of the CPT data in the target zone at the Massey site (8 m to 13 m) on the soil behaviour type classification chart by Robertson (1990).

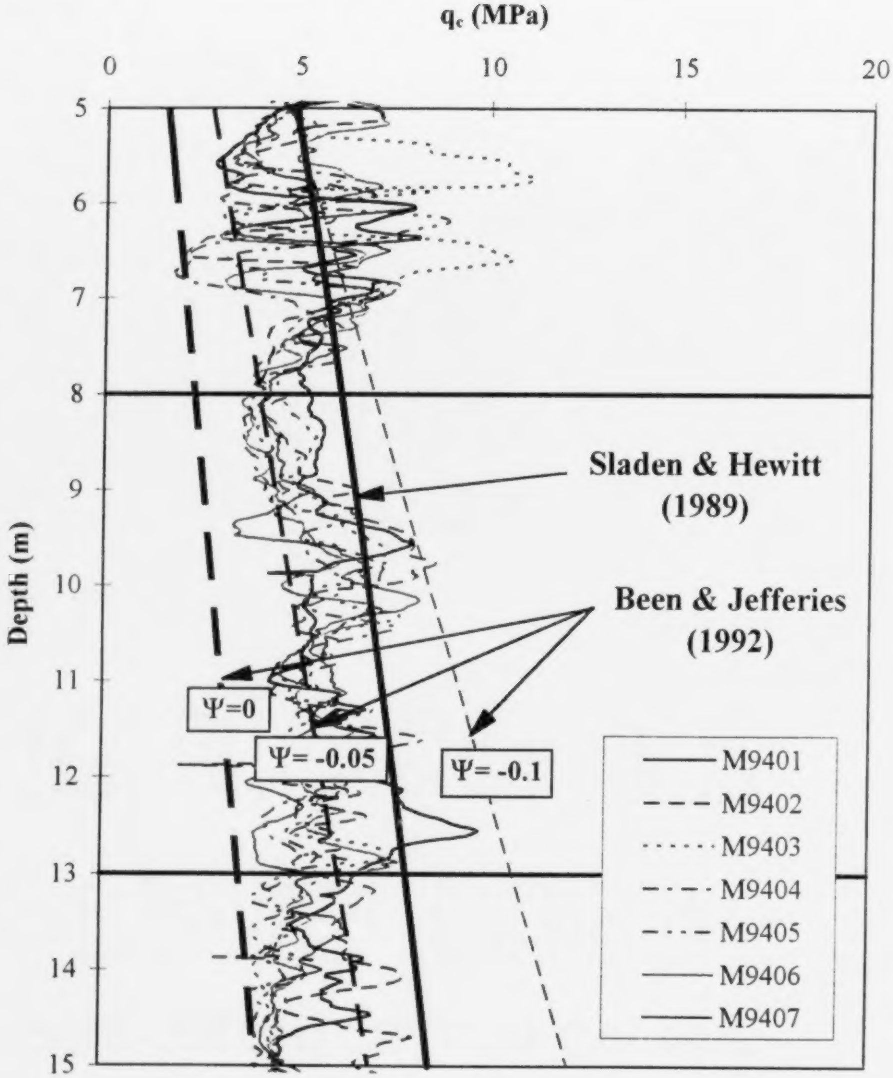

Figure 8-10 Comparison at the Massey site of the state parameter method by Been and Jefferies (1992) and the field observation method by Sladen and Hewitt (1989) for estimating flow liquefaction potential based on CPT results.

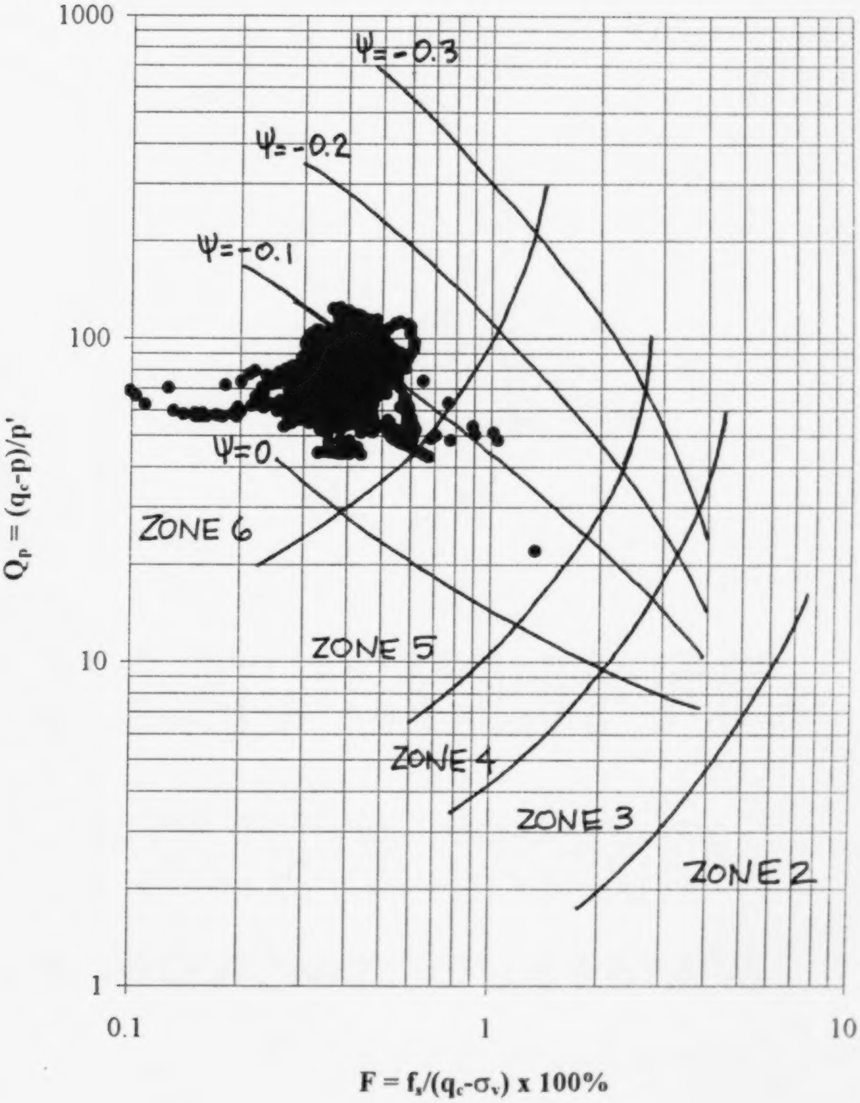

Figure 8-11 Estimation of state parameter in the target zone at the Massey site using the method by Plewes et al. (1992) based on estimated contours of state parameter on a soil behaviour type classification chart.

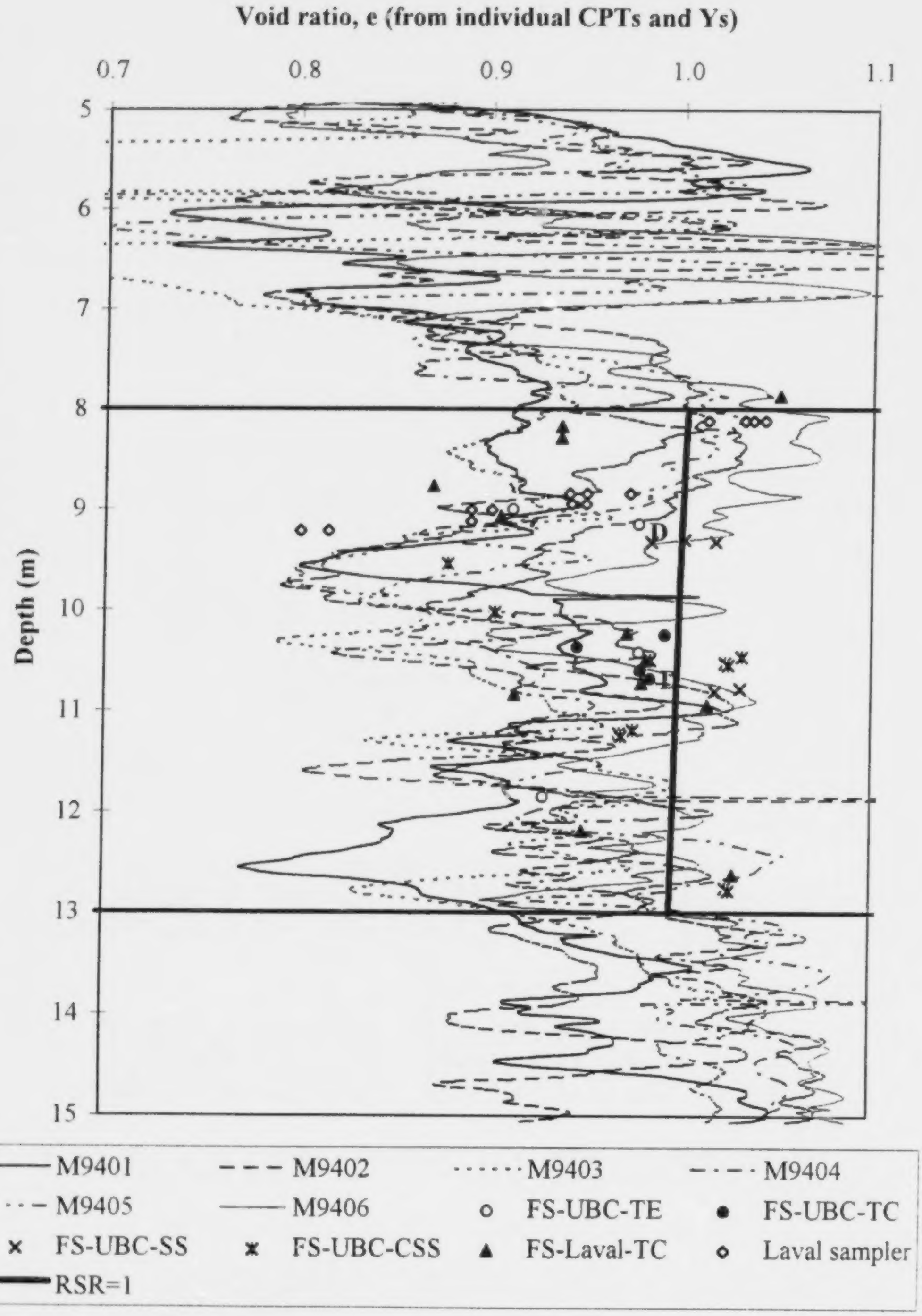

Figure 8-12 Enlarged plot of shear wave velocity based interpretation of void ratio from the CPT from Figure 8-8(a) illustrating the types of laboratory tests that were conducted on frozen samples from the Massey site (D=drained test).

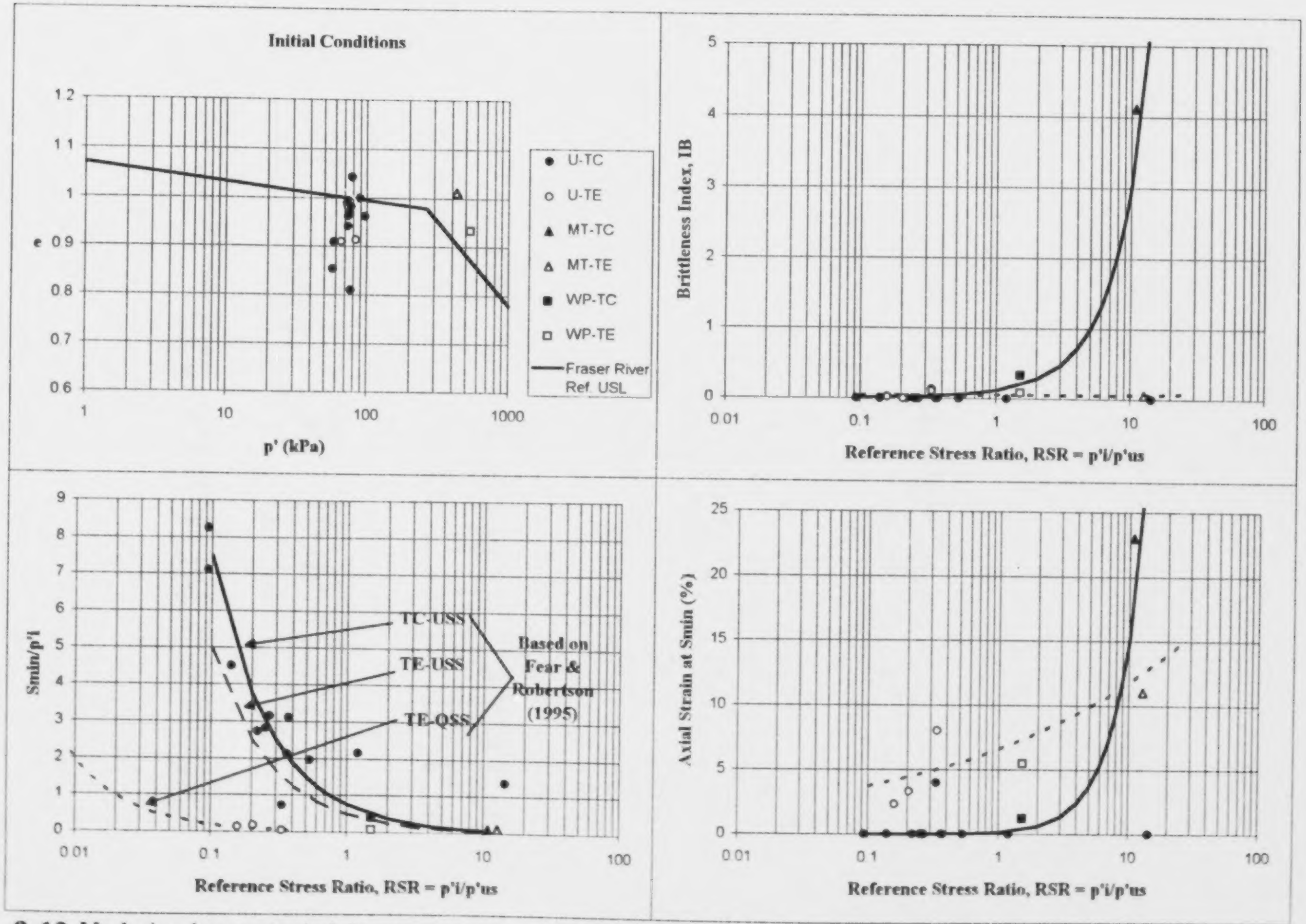

Figure 8-13 Undrained monotonic laboratory response of anisotropically consolidated Massey triaxial samples: (a) initial conditions, (b) brittleness index, I_B, (c) minimum strength ratio, S_{min}/p'_i, and (d) axial strain (ε_a) at S_{min}.

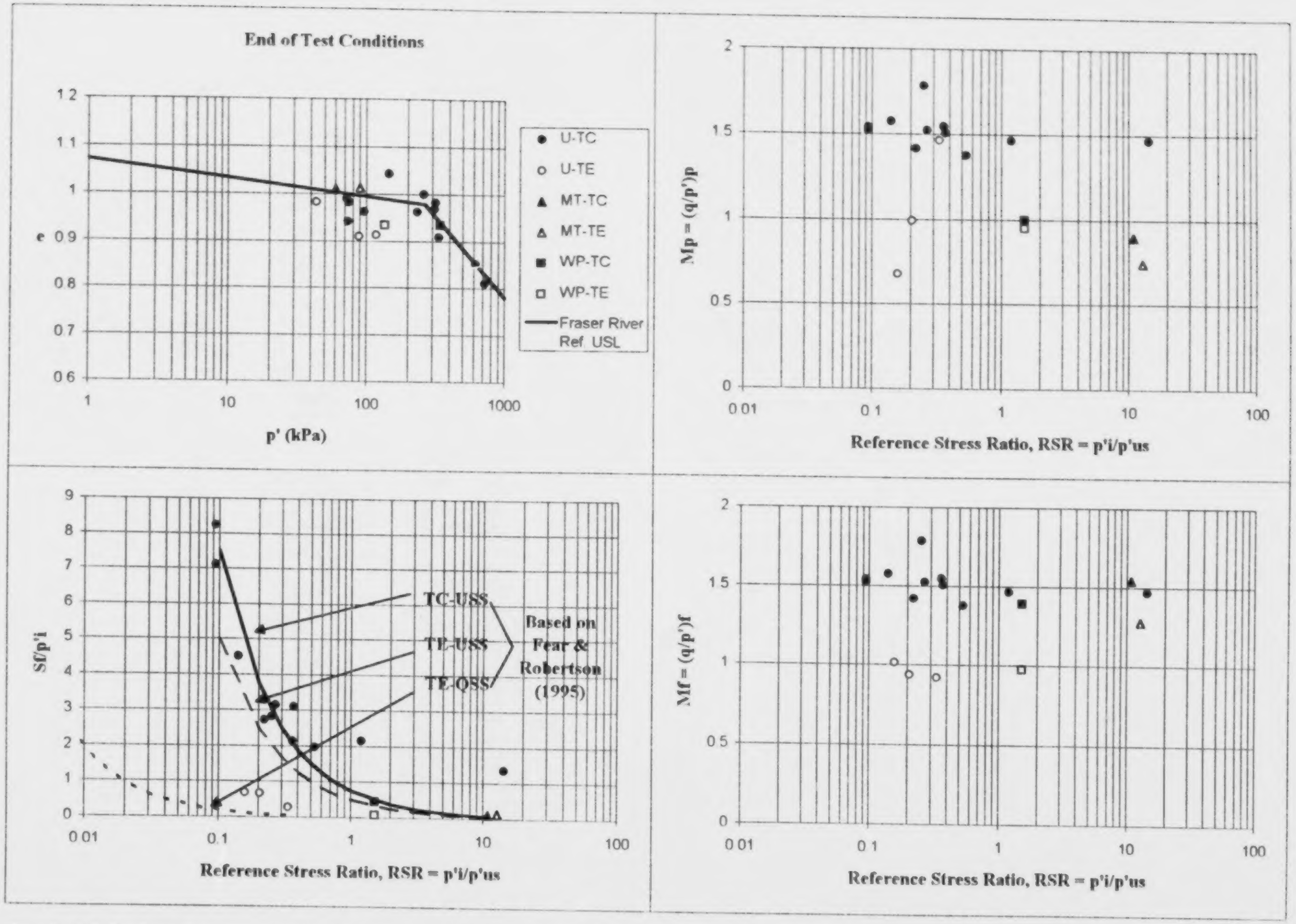

Figure 8-14 Undrained monotonic laboratory response of anisotropically consolidated Massey triaxial samples: (a) end-of-test conditions, (b) end-of-test strength ratio, S_f/p'_i, (c) peak stress ratio, M_p, and (d) end-of test stress ratio, M_f.

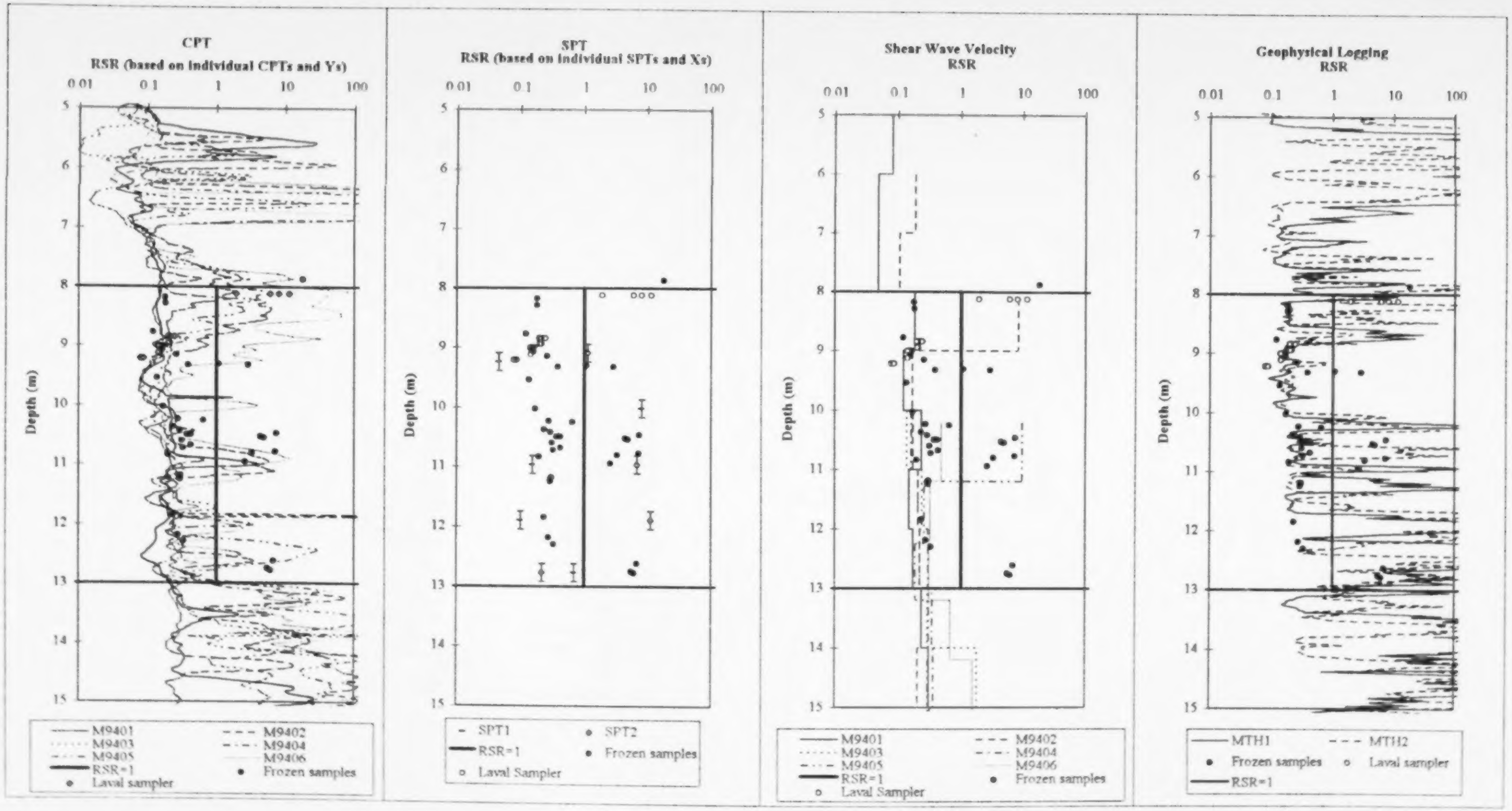

Figure 8-15 Profiles of estimated RSR in-situ at the Massey site relative to the reference Fraser River USL for (a) CPT, (b) SPT, (c) Vs, and (d) geophysical logging.

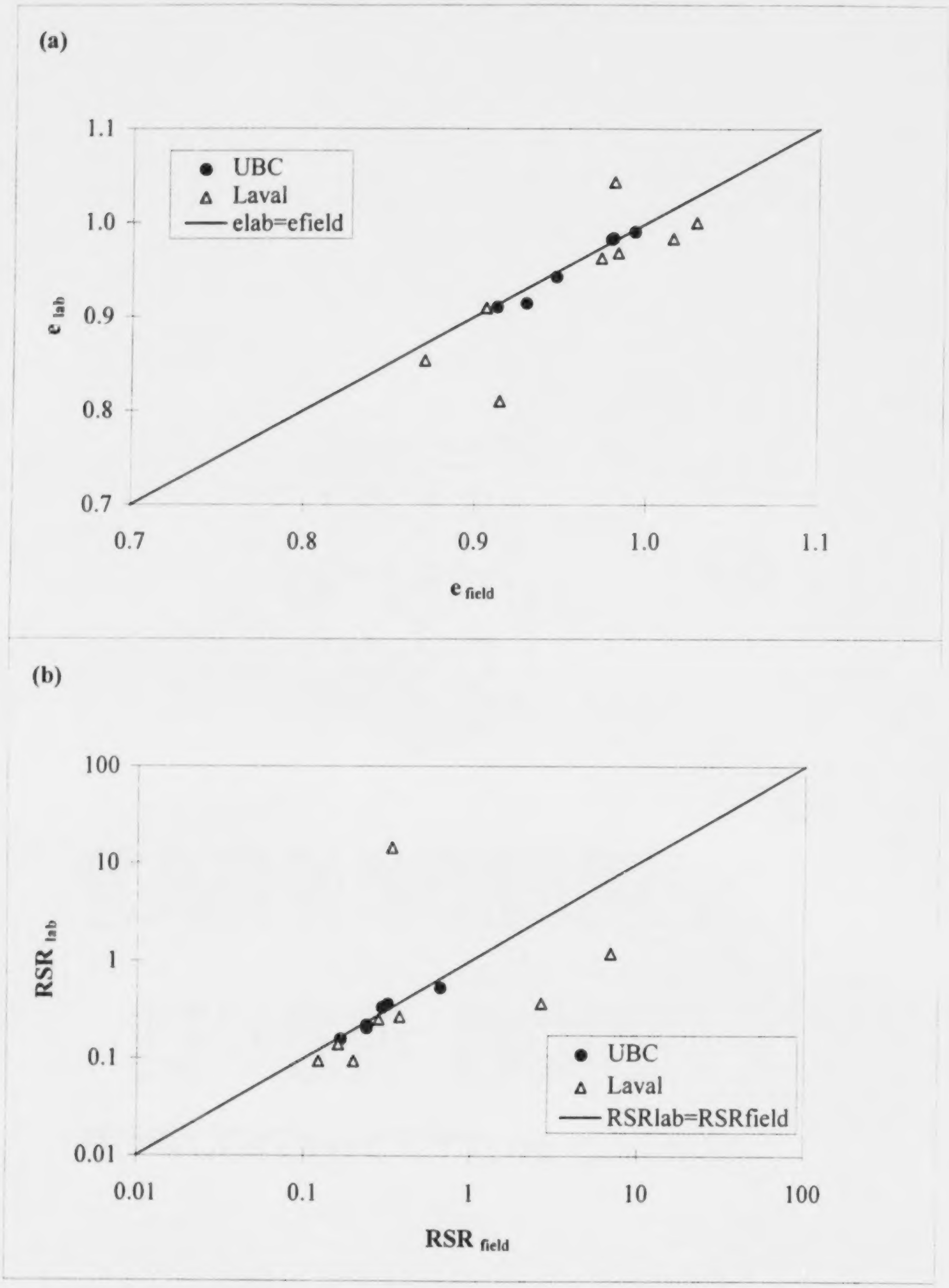

Figure 8-16 Comparison between laboratory conditions (termed lab) and estimated in-situ conditions (termed field) for frozen samples from the Massey site: (a) comparison of e_{lab} and e_{field}, (b) comparison of RSR_{lab} and RSR_{field}.

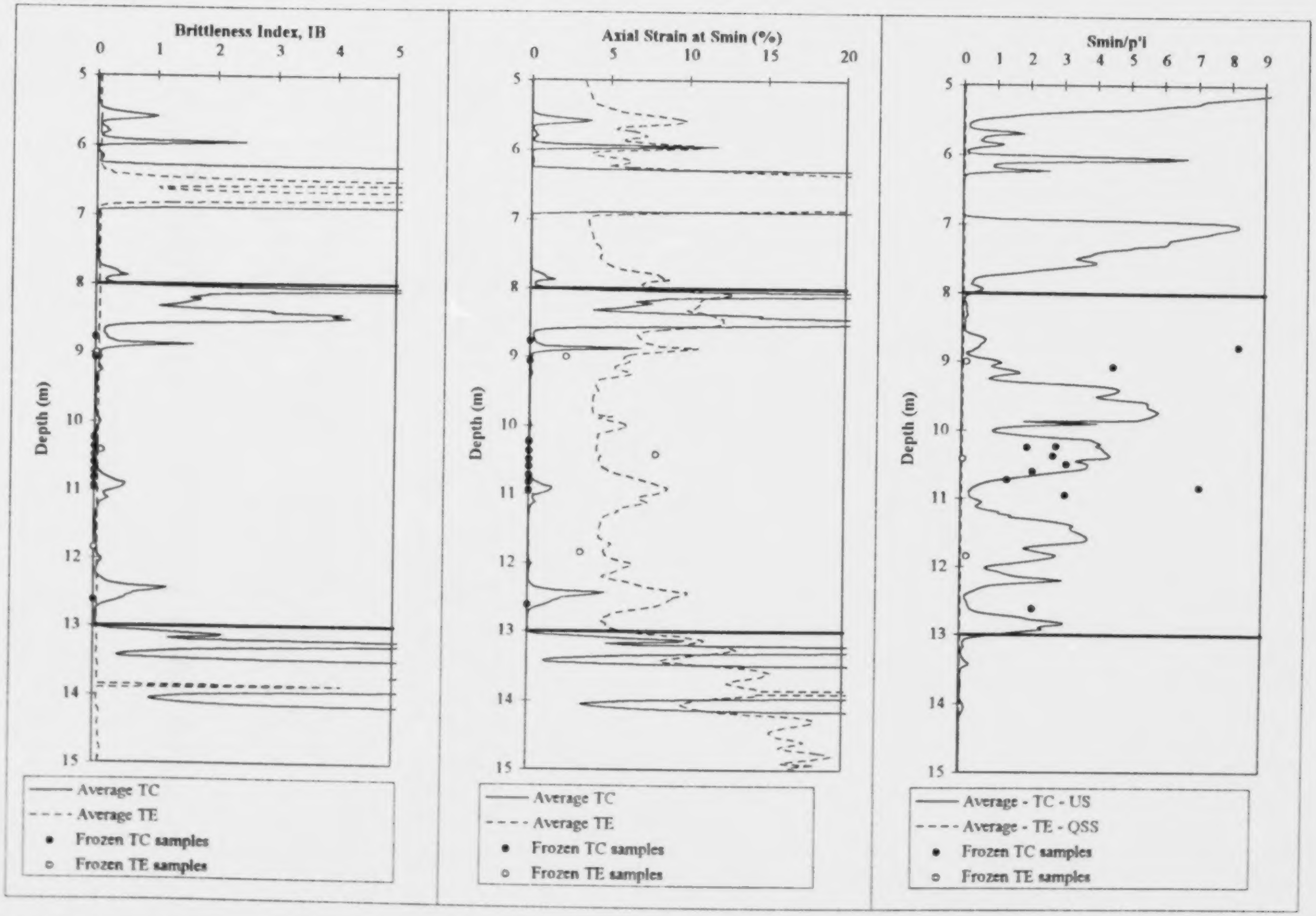

Figure 8-17 Estimated average profiles of undrained triaxial compression and extension response in-situ at the Massey site based on interpretation of the CPT compared with results of testing frozen samples: (a) brittleness index, I_B, (b) axial strain (ε_a) at minimum strength, and (c) minimum strength ratio, S_{min}/p'_i.

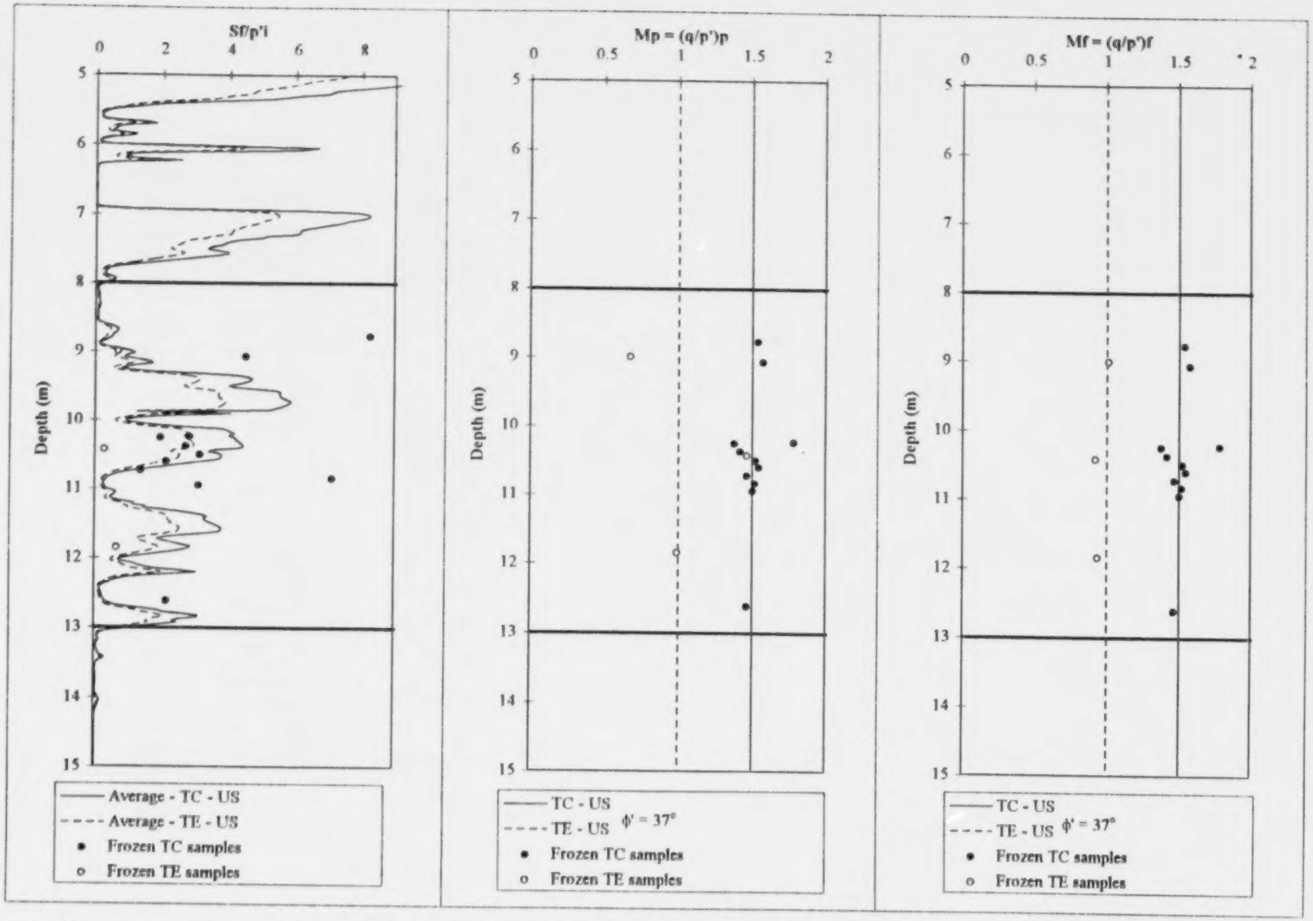

Figure 8-18 Estimated average profiles of undrained triaxial compression and extension response in-situ at the Massey site based on interpretation of the CPT compared with results of testing frozen samples: (a) end-of-test strength ratio, S_f/p'_i, (b) peak stress ratio, M_p, and (c) end-of-test stress ratio, M_f.

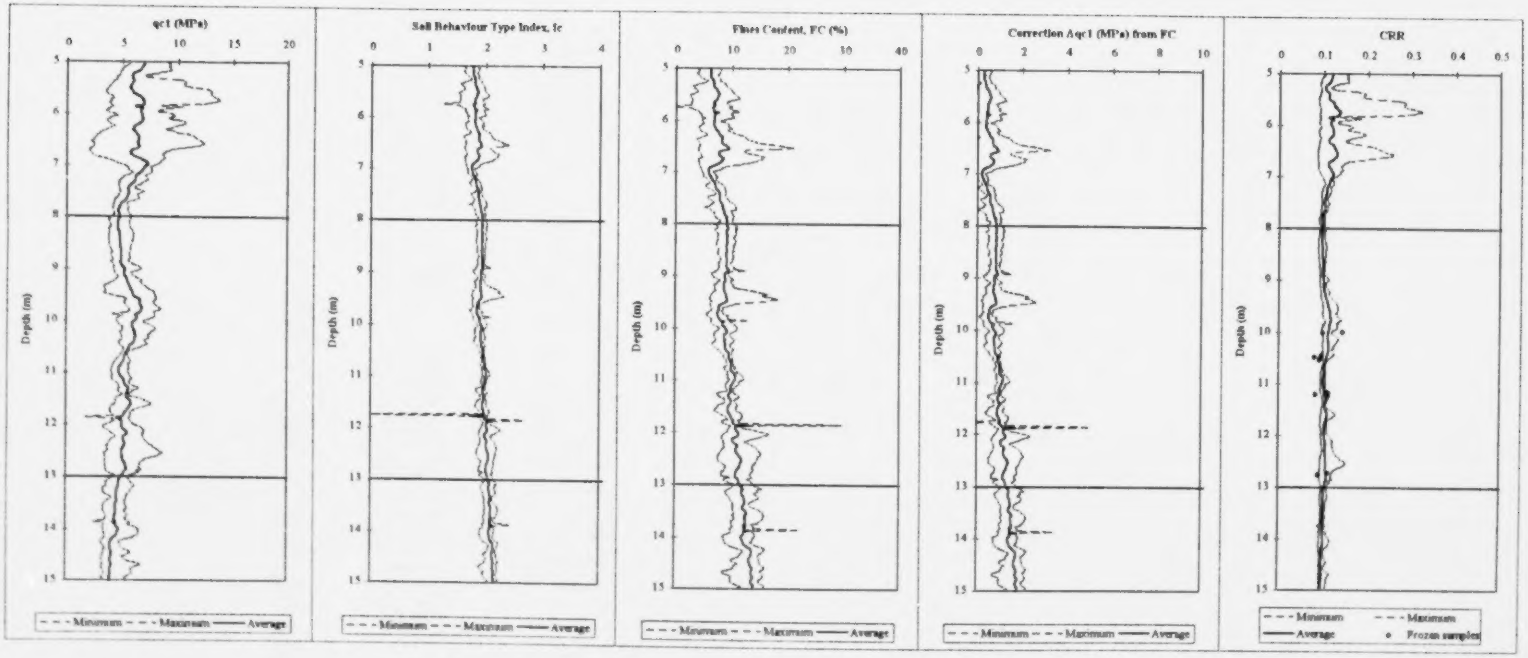

Figure 8-19 Application of the integrated CPT method to the Massey site: (a) CPT q_{c1} results, (b) interpreted soil behaviour type index, I_c, (c) estimated fines contents (FC), (d) recommended fines content based correction to q_{c1} to obtain clean sand equivalent value, and (e) estimated cyclic resistance ratio (CRR) profile compared with results of testing frozen samples.

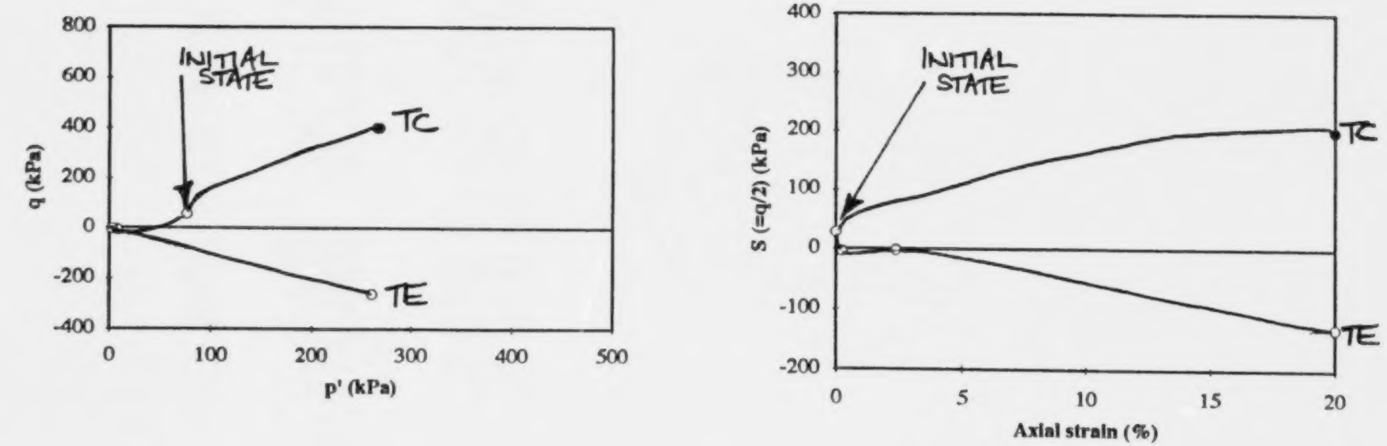

Figure 8-20 Illustration of how typical undrained triaxial compression and triaxial extension (a) stress paths and (b) stress strain curves can be estimated by combining individual estimated components of response corresponding to the average estimated RSR in the Massey site target zone (see Table 8-7).

References

Ayoubian, A. 1995. Triaxial testing on very loose sands for flow liquefaction analyses. *M.Sc. Thesis*, University of Alberta.

Baldi, G. et al. 1986. Interpretation of CPT's and CPTU's. II Part: Drained penetration on sands. *Proc. IV Int. Geotech. Seminar on Field Instrumentation and In Situ Measurements, Nanyang Tech. Inst.*, Singapore.

Been, K., and Jefferies, M.G. 1992. Towards systematic CPT interpretation. *Proceedings of the Wroth Symposium*, 44-55.

Campanella, R.G. 1995. General site characterization of Massey Tunnel north end at Deas Island, Highway 99, Ministry of Transportation and Highways right-of-way. *CANLEX Phase II Activity 3A Report*, In-situ Testing Group, The University of British Columbia.

Chillarige, A.R.V., Morgenstern, N.R., Robertson, P.K., and Christian, H. 1995. Characterization of Fraser River Delta sand. *Proceedings of the 48th Canadian Geotechnical Conference*, Vancouver, B.C., 2: 711-720.

Fear, C.E., and McRoberts, E.C. 1995. Reconsideration of initiation of liquefaction in sandy soils. *Journal of Geotechnical Engineering*, ASCE 121(3): 249-261.

Fear, C.E., and Robertson, P.K. 1996. CANLEX Phase II data review report. CANLEX Project Report, University of Alberta.

Hofmann, B.A. 1995. Personal communication.

Ishihara, K. 1993. Liquefaction and flow failure during earthquakes. The 33rd Rankine Lecture, *Géotechnique*, 43(3): 351-415.

Jefferies, M.G. and Davies, M.P. 1991. Discussion on soil classification by the cone penetration test. *Canadian Geotechnical Journal*, 28(1): 173-176.

Lawrence, M.S., Shelbourn, M.A.B., and Howie, J.A. 1995. Geophysical logging of Phase II sites. *CANLEX Phase II Activity 4A (Conventional Sampling and Logging) Report*, AGRA Earth & Environmental Limited.

Monahan, P.A., Luternauer, J.L., and Barrie, J.V. 1995. The geology of the CANLEX Phase II sites in Delta and Richmond British Columbia. *Proceedings of the 48th Canadian Geotechnical Conference*, Vancouver, B.C., 59-68.

NCEER Workshop 1996. Proceedings to be published at a subsequent date by Youd et al. (1996).

Olsen, R.S., and Koester, J.P. 1995. Prediction of liquefaction resistance using the CPT. *Proceedings of the International Symposium on Cone Penetration Testing, CPT '95*, Linkoping, Sweden.

Plewes, H.D., Davies, M.P, and Jefferies, M.G. 1992. CPT based screening procedure for evaluating liquefaction susceptibility. *Proceedings of the 45th Canadian Geotechnical Conference*, Toronto, Ontario, 4:1-4:9.

Pouliot, N. and Konrad, J.-M. 1995. Laboratory testing of reconstituted and of in-situ frozen specimens, Massey Tunnel Sand. *CANLEX Phase II Report*, Université Laval.

Robertson, P.K. 1990. Soil classification using the CPT. *Canadian Geotechnical Journal*, 27(1): 151-158.

Robertson, P.K., Fear, C.E., Woeller, D.J., and Weemees, I. 1995. Estimation of sand compressibility from seismic CPT. *Proceedings of the 48th Canadian Geotechnical Conference*, Vancouver, 1: 441-448.

Robertson, P.K., Woeller, D.J., and Finn, W.D.L. 1992. Seismic cone penetration test for evaluating liquefaction potential under cyclic loading. *Canadian Geotechnical Journal*, 29: 686-695.

Sasitharan, S., Robertson, P.K., Sego, D.C., and Morgenstern, N.R. 1994. State boundary surface for very loose sand and its practical implications. *Can. Geotech. J.*, 31(3): 321-334.

Seed, H.B., Tokimatsu, K., Harder, L.F., and Chung, R. 1985. Influence of SPT procedures in soil liquefaction resistance evaluations. *Journal of Geotechnical Engineering*, ASCE 111(12): 1425-1445.

Skempton, A.W. 1986. Standard penetration test procedures and the effects in sands of overburden pressure, relative density, particle size, ageing and overconsolidation. *Géotechnique*, 36(3): 425-447.

Sladen, J.A., and Hewitt, K.J. 1989. Influence of placement method on the in situ density of hydraulic sand fills. *Canadian Geotechnical Journal*, 26: 453-466.

Stewart, R.A. 1993. Site selection - Phase II. *CANLEX Phase I Activity 7 Report*, B.C. Hydro.

Suzuki, Y., Tokimatsu, K., Taye, Y. and Kubota, Y. 1995. Correlation between CPT data and dynamic properties of in-situ frozen samples. *Proceedings of the 3rd International Conference on Recent Advances in Geotechnical Earthquake Engineering and Soil Dynamics*, St. Louis, U.S.A., 1.

Thomas, J. 1992. Static, cyclic and post liquefaction undrained behaviour of Fraser River sand. *M.Sc. Thesis*, University of British Columbia.

Tokimatsu, K., and Yoshimi, Y. 1983. Empirical correlation of soil liquefaction based on SPT N-value and fines content. *Soils and Foundations*, 23(4): 56-74.

CHAPTER 9

GENERAL DISCUSSION AND CONCLUSIONS

9.1 Overview

As described in Chapter 1, liquefaction of sandy soils can have significant financial, environmental and human impacts. Observable surface features can range from sand boils to catastrophic flow failures, depending on the type and extent of liquefaction that occurs. Liquefaction phenomena have been divided into two main types, after Robertson (1994) and Robertson and Fear (1995), as defined in Chapter 1. Cyclic softening (liquefaction) generally occurs in level to gently sloping ground in which shear stress reversal can occur, but may also occur in and around soil structures and buildings. Deformations associated with cyclic softening occur only during the cyclic loading and accumulate with additional cycles of loading as a consequence of a loss in soil stiffness. Flow liquefaction occurs only in strain-softening soil, provided that a trigger mechanism (static or cyclic) causes the soil to strain-soften. Flow liquefaction generally occurs in sloping ground in which the driving stresses are larger than the resulting ultimate or minimum undrained shear strength of the soil. Deformations can be catastrophic (i.e. flow failures) if the soil structure contains sufficient strain-softening material relative to strain-hardening material and if the geometry is such that a kinematically admissible mechanism can develop.

9.2 Evaluation of Cyclic Softening Potential

The most reliable method of estimating cyclic resistance of sandy soils in the laboratory is by testing high quality undisturbed samples under the appropriate cyclic loading. In-situ ground freezing and subsequent coring has recently been successful in obtaining such samples at several sites as part of the CANLEX project (Hofmann et al., 1994; 1995). However, in-situ ground freezing technology is expensive and would typically be limited to high risk projects for which the consequences of failure can be enormous and large financial decisions must be made. Consequently, methods for estimating cyclic resistance based on less expensive in-situ tests are required. Conventionally, SPT-based methods have been used; recently, CPT and shear wave velocity based methods have been developed. Seismic CPT probes provide shear wave velocity measurements in addition to conventional CPT data. Thus, the seismic CPT provides a useful technique for evaluating cyclic softening (liquefaction) potential based on two independent profiles. If there is not consistency in the evaluation of cyclic softening (liquefaction) potential, soil samples should be obtained to evaluate grain characteristic parameters. Whether or not a sandy soil deposit is susceptible to cyclic softening (liquefaction) is a function of both the sand characteristics (such as density, stresses, amount of fines, plasticity of fines) and the size and duration of cyclic loading.

9.2.1 Simplified "Seed" methodology

The late Professor H.B. Seed and other researchers at the University of California, Berkeley, developed a simplified method for evaluating cyclic softening (liquefaction) potential of sandy soils based on SPT in-situ testing (Seed et al., 1985; Seed and Harder, 1990). The primary advantage of this method is that it is easy to understand and relatively easy to apply. At the time that the method was developed, there was a large database of SPT data and, hence, the SPT was the best in-situ test to use to estimate the cyclic resistance of a sandy soil. Various corrections were proposed by Seed (1987), Seed et al. (1985) and Seed and Harder (1990) for fines content, sloping ground conditions and high overburden stress stresses.

As illustrated in Chapter 2, the Seed methodology generally provides a conservative estimate of cyclic softening (liquefaction) potential because the case records in the database were generally assigned average representative $(N_1)_{60}$ values; however, the method is typically applied to the entire $(N_1)_{60}$ profile at a site. The revised database presented in Chapter 2, based on a minimum representative $(N_1)_{60}$ approach for each case record gives less conservative correlations, particularly at higher values of $(N_1)_{60}$. The resulting correlations (see Figure 2-8 in Chapter 2) are more similar to the limiting shear strain values associated with liquefaction, developed by Seed et al. (1985) and shown in Figure 2-11 in Chapter 2. A very important point to reiterate is that the database of case records was developed based on Holocene age deposits, level to gently sloping ground, equivalent magnitude M=7.5 earthquakes, and depths ranging from 1 to 14 m (3 to 47 ft), but generally (i.e. 90% of the case records) less than 10 m (32 ft). Hence, caution should be exercised when extrapolating the correlation to conditions outside of this range. Experience has shown that the corrections for sloping ground and high overburden stress conditions are not always reliable; e.g. at Duncan Dam (Byrne et al., 1994). In addition, the phenomenon of flow liquefaction is often of greater concern in large sloping structures and the resulting deformations can be more catastrophic. Therefore, extrapolation of the correlations based on cyclic softening (liquefaction) in level ground to the evaluation of large sloping structures does not seem appropriate.

For low risk, small scale projects in level to gently sloping ground, the SPT-based simplified Seed methodology is useful and generally conservative. The SPT sampler provides soil samples which can be used to estimate fines content and apply the fines content corrections recommended by Seed (1987). However, many factors can affect the measured SPT penetration resistance (Skempton, 1986; Robertson et al., 1983). The two most important factors are effective overburden stress and the energy delivered to the SPT sampler, expressed in terms of rod energy ratio (ER), in percent. A vertical effective stress of 100 kPa and an ER of 60% are generally accepted as the reference values to use to correct the measured blowcount to an $(N_1)_{60}$ value (Seed et al., 1985; Robertson and Fear, 1995). It is very important to carefully measure the ER during the actual site investigation, if possible, in order to obtain a reliable measure of corrected SPT penetration resistance. Global values of ER are available for various SPT hammer/anvil systems and methods of hammer release and ER at a site is often assumed based on these global values (Seed et al., 1985). However, these values are only a guide and site specific values may differ significantly from the global values.

9.2.2 Integrated CPT approach

The SPT has many inherent difficulties and often poor repeatability. Consequently, CPT-based methods of estimating cyclic resistance have been developed and the database of available case records is continually growing. The CPT has the advantage that, not only is it generally more repeatable and reliable than the SPT, but it also provides a continuous profile of soil stratigraphy. Chapter 3 presented a new, integrated CPT method for evaluating the cyclic softening (liquefaction) potential of a sandy soil deposit. Although the CPT does not provide soil samples like the SPT does, the integrated method demonstrates that grain characteristics such as fines content can be estimated from the CPT data in order to correct the measured penetration resistance for fines content. Increasing fines content is generally associated with increasing compressibility and, therefore, decreasing penetration resistance. Once the in-situ penetration resistance is corrected for overburden effects and fines content, the corrected clean sand equivalent penetration resistance can be used to estimate the cyclic resistance of a soil, based on the modified Robertson and Campanella (1985) correlation proposed by the recent NCEER Workshop (1996), as described in

Chapter 3.

The integrated CPT method proposed in Chapter 3 is broken down into its individual components such that site specific modifications can be made, if necessary. The integrated CPT method is easily applied to CPT results using a spreadsheet. The equations representing the various components of the method can be used and can be easily modified to suit any site specific conditions that differ from the recommended relationships. For high risk projects, both the fines content and cyclic resistance estimations can be checked on a site specific basis by obtaining and testing undisturbed samples under the appropriate cyclic loading. For moderate risk projects, the fines content estimations based on the CPT can be checked on a site specific basis from bulk samples. The various components of the integrated CPT method proposed here can be combined and summarized on a CPT based soil classification chart, as demonstrated in Chapter 3 (see Figure 3-16). Thus, for low risk projects, the method can be applied directly.

The integrated CPT method is also based around the simplified Seed methodology. The original Robertson and Campanella (1985) method of estimating cyclic resistance from the CPT was based on SPT-CPT conversions, although the proposed correlation is now based on extensive field observations. Thus, an important feature to recognize is that, as for the Seed et al. (1985) SPT method, the correlation given in Chapter 3 appears to be based on average values of q_{c1}. However, the correlation is often applied to the entire CPT profile at a site. Consequently, the integrated CPT method may provide a conservative estimate of cyclic softening (liquefaction) potential and caution should be applied in variable deposits in which a small part of the CPT data could indicate possible cyclic softening (liquefaction). Although not carried out in this study, it would be interesting to revisit the CPT case records in detail from a minimum q_{c1} approach similar to the review of the SPT case records presented in Chapter 2. Chapter 3 also illustrated a method for correcting the measured penetration resistance in thin sand layers embedded in thick soft clay layers. A very important point to reiterate is that, similar to the SPT database, the database of CPT case records was developed based on Holocene age deposits, level to gently sloping ground, equivalent magnitude M=7.5 earthquakes, and depths ranging from 1 to 15 m (3 to 45 ft), but generally (i.e. 84% of the case records) less than 10 m (32 ft). Hence, as for the SPT method, caution should be exercised when extrapolating the CPT correlations to conditions outside of this range. In addition, as for the SPT method, extrapolation of the CPT correlations based on cyclic softening (liquefaction) in level ground to the evaluation of large sloping structures does not seem appropriate.

9.3 Evaluation of Flow Liquefaction Potential and Subsequent Response

Flow liquefaction occurs in strain-softening soils if a suitable trigger mechanism can develop. The trigger mechanism can be static or cyclic and undrained or drained in nature. Once such material is triggered, undrained strain-softening occurs. Flow liquefaction can occur rapidly, with little warning, and if sufficient strain-softening material liquefies, catastrophic deformations can result. As for the evaluation of cyclic softening, the seismic CPT provides a useful technique for evaluating flow liquefaction potential based on two independent profiles. If there is not consistency in the evaluation of flow liquefaction potential, soil samples should be obtained to evaluate grain characteristic parameters. Whether or not a sand deposit is susceptible to flow liquefaction is a function of the sand characteristics in terms of density, stresses, grain characteristics and soil structure.

9.3.1 Empirical approach

Conventionally, the simplified Seed methodology described above has been used to predict liquefaction potential in general for a given cyclic (earthquake) loading. It has been used as a design tool in both level to gently sloping ground and in large, steeply sloping soil structures. However, as discussed previously, experience (e.g. Byrne et al, 1994) has shown that the correction factors to account for sloping ground and high overburden stresses (Seed and Harder, 1990) are questionable. In addition, flow liquefaction resulting from a static trigger can not be evaluated using the Seed methodology since it only incorporates cyclic (earthquake) loading conditions. Therefore, extrapolating the empirical methods for evaluating cyclic softening (liquefaction) potential to evaluating the potential of flow liquefaction resulting from either static or cyclic triggers is not appropriate. As outlined in Chapter 1, when describing the terminology adopted in this thesis, the two phenomena involve different physics; therefore, it is more logical to evaluate the potential of the two phenomena using different methods.

Sladen and Hewitt (1989), Been and Jefferies (1992) and Plewes et al. (1992) all developed various methods of estimating soil state (and therefore flow liquefaction potential) from CPT results. The Sladen and Hewitt (1989) method was based on field observations of cases of flow failures and cases of no failure in the Beaufort Sea for which CPT data was available. The Been and Jefferies (1992) and Plewes et al. (1992) methods involved estimating state parameter as a measure of flow liquefaction potential from the CPT based on calibration chamber studies.

9.3.2 Simplified reference stress ratio (RSR) approach

The conventional CPT empirical methods described above are suitable for evaluating flow liquefaction potential, but are not capable of estimating the undrained response of a sand over a large stress range or when comparing different sands. In addition, the state parameter method by Been and Jefferies (1992) is much less conservative than the Sladen and Hewitt (1989) field observation based method. Therefore, the geotechnical engineer may be uncertain if a soil deposit is susceptible to flow liquefaction if the two methods give conflicting predictions.

Chapter 4 proposed a new method of evaluating flow liquefaction potential based on the term reference stress ratio (RSR) which provides an alternate measure of soil state and is related to state parameter by the slope of the ultimate state line (USL). The framework incorporates critical state soil mechanics and provides a link between in-situ testing results and observed undrained response when soil samples are tested in the laboratory. Not only does the proposed framework provide an estimate of flow liquefaction potential, but it is capable of estimating undrained response under different directions of loading (i.e. triaxial compression or triaxial extension) over a range in RSR (i.e. a range in void ratio and initial stress conditions).

To apply the proposed framework directly requires various input parameters, in particular an estimate of the void ratio profile and the location and slope of the USL in e-p' space for a given soil deposit. The void ratio profile can be estimated from the SPT, CPT, shear wave velocity measurements or geophysical logging using any of the conventional or new methods discussed in Chapter 4. The shear wave velocity based method of interpreting seismic CPT results or direct interpretations of geophysical results appear to be best at capturing the range in void ratio on a continuous basis in a given soil deposit, at least for young, uncemented loose sands. If the project is of low risk in nature, the USL parameters can be estimated based on the results of testing other, but similar, sands. The database of USLs for various types of sands is growing and can be used as a reference. The seismic CPT is especially useful as it allows for estimations of the compressibility of a soil by comparing the measured cone tip resistance with the shear wave velocity measurements. Soil compressibility in turn can be used to estimate the slope of the USL, as proposed by

Robertson et al. (1995). It is also possible to estimate USL parameters (namely, λ_{ln}) directly from CPT soil classification charts (Been and Jefferies, 1992).

By combining the estimated void ratio profile in a soil deposit with the estimated USL parameters, it is possible to make an estimation of RSR throughout the deposit. A profile of RSR can be used to estimate soil response to undrained loading, based on the type of RSR based laboratory response curves presented in Chapter 8 for the CANLEX Phase II Massey site. Although data are preliminary and, therefore, at present the resulting response curves are only applicable to Fraser River sand, they may prove to be general in nature as additional data becomes available from other CANLEX sites. The proposed framework illustrated that undrained response can be divided into various components. Once these components are estimated for a particular soil deposit, they can be combined to estimate stress-strain curves, as illustrated in Chapter 8.

The method for evaluating flow liquefaction potential proposed in Chapter 4 requires some knowledge or estimate of the USL. However, as a very preliminary site screening approach, single valued criteria in terms of $(N_1)_{60}$, q_{c1} or V_{s1} can be used as a guide to evaluate flow liquefaction potential. Typical values that are often used are $(N_1)_{60} \approx 10$, $q_{c1} \approx 5$ MPa and $V_{s1} \approx 150$ m/s. However, it is extremely important to note that these values are not applicable to all sandy soils. The values of $(N_1)_{60}$ and q_{c1}, in particular, are influenced by the compressibility of a soil (of which fines content can help provide a measure), whereas the value of V_{s1} is little affected. The method proposed by Plewes et al. (1992) recognizes this effect in that the value of the normalized cone tip resistance defining the $\Psi=0$ contour (i.e. the USL) is a function of friction ratio (see Figure 4-11 in Chapter 4). More compressible soils tend to have higher friction ratios for the same cone tip resistance.

9.3.3 Site specific approach

Clearly, the flow liquefaction framework proposed in Chapter 4 is best applied on a detailed site specific basis such that the individual parameters such as the location and slope of the USL can be determined with greater certainty. If the shear wave velocity based method is to be used to interpret void ratios, the parameters A and B (linking shear wave velocity to void ratio) and X and Y (linking shear wave velocity to the SPT and CPT, respectively) can be determined better on a site specific basis. Void ratio estimates based on the CPT or geophysical logging appear to be the most promising methods, particularly as they are capable of providing detailed continuous profiles through a given soil deposit.

A detailed site specific approach also allows for obtaining and testing undisturbed samples. The framework can then be fine-tuned and modified to link the in-situ test results with the laboratory results via RSR on a site specific basis. The worked example in Chapter 8 illustrates how the proposed framework can be applied to a specific site (the CANLEX Massey site), how site specific relationships between various components of response and RSR can be estimated, and how site specific methods of estimating RSR from in-situ tests can be developed.

9.4 Risk Assessment: A Family of Solutions

Various methods have been reviewed and proposed for evaluating both cyclic softening (liquefaction) and flow liquefaction in sandy soils, based on in-situ testing. Figure 9-1 provides a conceptual illustration of how, for a given in-situ test (e.g. the CPT), the described methods can be used to estimate a dividing line in terms of the test's measured parameter (e.g. cone tip resistance, q_c) for evaluating flow liquefaction potential or cyclic softening (liquefaction) potential. The dividing line for evaluating flow liquefaction potential is a function of sand characteristics, while the dividing line for evaluating cyclic softening (liquefaction) potential depends on both sand characteristics and the size and duration of the expected cyclic loading. In general, very loose, strain-softening sand will be susceptible to both flow liquefaction and cyclic softening, loose to medium dense sand may be susceptible to cyclic softening (depending on the size and duration of the cyclic loading), but not to flow liquefaction, and denser sands will not be susceptible to either type of liquefaction.

Figure 9-2 presents a flowchart summarizing the recommended procedure for evaluating the liquefaction potential of a sandy soil deposit. This chart can be used in conjunction with the flowchart explaining liquefaction terminology (modified from Robertson, 1994) presented in Chapter 1 (see Figure 1-1). Since flow liquefaction can generally lead to larger deformations and, thus, greater risk to human safety, the given soil deposit should first be evaluated for flow liquefaction potential. The framework proposed in Chapter 4 can be applied as illustrated in the worked example at the Massey site in Chapter 8. If some material is found to be susceptible to flow liquefaction, response to undrained loading should be estimated using the framework. A stability analysis should then be performed based on the estimated response to determine whether or not the combination of site geometry and type of soil are such that a kinematically admissible mechanism can form and lead to a flow failure. If the soil structure is found to be stable, a deformation analysis should be carried out. Deformations may arise if there is a mixture of strain-softening or limited strain-softening material and strain-hardening material present. The direction of loading that will occur in-situ must be carefully considered when performing such stability and deformation evaluations. Triaxial extension and triaxial compression loading, which appear to represent the two loading extremes (Vaid et al., 1995) may lead to very different responses to undrained loading. Undrained response in simple shear would be predicted to be somewhere in between the two extremes (Vaid et al., 1995).

If a material is not susceptible to flow liquefaction, it may still be susceptible to cyclic softening (liquefaction) depending on the sand characteristics and the size and duration of cyclic loading (typically associated with a design earthquake). The integrated CPT method proposed in Chapter 3 should be used to estimate the cyclic softening (liquefaction) potential of the soil. If the soil is found to be susceptible to this type of liquefaction, a deformation analysis should be performed. In level ground, for example, horizontal displacements and settlements can be estimated using methods proposed by Ishihara (1993), as described in Chapter 3 (see Figure 3-10). In gently sloping ground, methods such as that by Youd (1993) can be used to evaluate expected deformations associated with lateral spreading. More complex methods using finite element analysis, for example, may be required to evaluate the extent of deformations in sloping ground as a result of a loss in soil stiffness during cyclic loading. If a soil is found to be susceptible to cyclic softening and drainage paths are restricted by overlying less permeable layers, the soil should be re-evaluated for flow liquefaction potential because pore water redistribution may lead to loosening of the soil.

If the analyses described above indicate a stability problem or excessive deformations resulting from either flow liquefaction or cyclic softening, site remediation may be required. Depending on the type of liquefaction that is of concern, either the framework proposed for evaluating flow liquefaction or the integrated CPT method for evaluating cyclic softening (liquefaction) can be used as a quality control measure to evaluate the effectiveness of any site remediation that is performed.

Figures 9-3 and 9-4 present flowcharts outlining the recommended methods for evaluating cyclic softening (liquefaction) and flow liquefaction, respectively, based on in-situ testing in sandy soils. Each figure indicates that the recommended procedure is a function of the risk level associated with a particular project. Ideally, a complete field investigation and laboratory testing of undisturbed samples would be carried out at a given site. However, such a comprehensive method of evaluation of liquefaction potential is often beyond the budget and scope of many projects. The higher the risk level associated with a given project, the more important it is to strive towards the ideal comprehensive investigation. The following sections describe the recommended procedures for various levels of risk.

9.4.1 Low risk projects

In general terms, low risk projects are ones for which the consequences of failure will have an extremely low probability of impacting human safety, have little effect on the environment and for which the financial implications will not be significant. Consequently large financial decisions do not need to be made for these types of projects. As a result, the project scope and budget is often fairly restrictive in the amount of in-situ testing and laboratory testing that can be performed.

For such projects, cyclic softening (liquefaction) can be evaluated using penetration tests such as the SPT or CPT. Figure 9-3 indicates that the CPT is the preferred method because it is generally more reliable and provides a continuous profile of soil stratigraphy. The integrated CPT method proposed in Chapter 3 can be used directly to evaluate the cyclic softening (liquefaction) potential of low risk projects.

Figure 9-4 indicates that various types of in-situ testing to estimate soil state can be used to evaluate flow liquefaction potential for low risk projects. The CPT and geophysical logging are preferable because they generally give more reliable continuous profiles. The shear wave velocity based method of estimating void ratio from the seismic CPT appears to be better than conventional methods, at least for young, uncemented loose sands. Interpretations of void ratio from whatever type of in-situ testing is selected can be combined with an estimate of the USL for the soil (based on other similar soils or via compressibility estimated by the seismic CPT) to evaluate flow liquefaction potential.

9.4.2 Moderate risk projects

Moderate risk projects have higher probabilities of affecting human safety and the environment and have larger financial consequences associated with failure. For such projects, both Figures 9-3 and 9-4 illustrate that some site specific modifications to the simplified methods of evaluating either cyclic softening (liquefaction) or flow liquefaction should be made. In the case of cyclic softening (liquefaction) evaluation, Figure 9-3 indicates that components of the integrated CPT method can be modified based on site specific fines contents (from bulk samples) and measured cyclic resistance of reconstituted samples at similar void ratios and fabric to those in-situ. Shear wave velocity measurements can be used to check that the reconstituted samples are as similar as possible to the in-situ conditions (Tokimatsu and Hosaka, 1986). Additional in-situ testing such as geophysical logging or shear wave velocity measurements can be conducting to provide independent means of evaluating cyclic resistance.

In the case of flow liquefaction evaluation, Figure 9-4 indicates that laboratory testing of reconstituted samples can be used to better estimate a site specific USL in order to estimate RSR from in-situ tests. Conducting shear wave velocity measurements and determining parameters such as X and Y (linking shear wave velocity measurements to SPT and CPT penetration resistance, respectively) on a site specific basis allows for better interpretation of void ratio from either the SPT or CPT using the shear wave velocity based method of interpreting void ratio. Having shear wave velocity measurements and/or geophysical logging results in addition to CPT results provides independent means of estimating flow liquefaction potential at a given site.

9.4.3 High risk projects

High risk projects are those for which the consequences of failure can be enormous in terms of human safety, environmental impacts and/or financial implications. For such projects, it is essential to conduct a detailed site specific analysis. Both Figures 9-3 and 9-4 indicate that a preliminary site investigation can be carried out first, using the simplified methods of evaluating either cyclic softening (liquefaction) or flow liquefaction. Based on the results of such a preliminary site screening, a detailed investigation including obtaining and testing undisturbed soil samples can be initiated. Self boring pressuremeter testing is useful for estimating horizontal stress conditions and, hence, the value of Ko in-situ. The results of testing undisturbed samples in the laboratory can also be linked to the in-situ testing in order to extrapolate the results from the detailed (frozen) sampling area across the site. Figure 9-3 indicates that for evaluating cyclic softening (liquefaction), this can be done by modifying the integrated CPT method at the site to match the cyclic resistance of undisturbed samples when tested in the laboratory. For evaluating flow liquefaction, Figure 9-4 indicates that RSR, relative to the site specific USL, can be used to link the undrained laboratory response of undisturbed samples to in-situ testing across the site.

9.5 Cautionary Notes and Limitations of the Proposed Methods

The proposed methods for evaluating cyclic softening (liquefaction) or flow liquefaction potential are still somewhat preliminary in nature, but confidence in applying the methods should increase as the methods are applied at additional sites and modified as necessary.

9.5.1 Cyclic softening evaluation

a) Loose clean sand versus sand with fines

Referring to the soil classification chart by Robertson (1990) in Chapter 3 (see Figure 3-6), it is clear that, based on CPT results, loose clean sands may sometimes be confused with somewhat denser sands containing fines. Both materials would have low cone tip penetration resistances. Since the integrated CPT method applies a fines content correction based on fines content, if a loose clean sand is interpreted as having an apparent fines content, the resulting prediction of CRR could be unconservative. However, the friction ratio should increase in the denser sand containing fines. A site specific check of the fines content that the integrated CPT method predicts is useful to avoid this confusion.

b) Minimum versus average design approach

Chapter 2 illustrated the effect of consistently selecting a minimum SPT $(N_1)_{60}$ to represent each case record. If this method is applied to the entire SPT profile, any low points would definitely be considered to be susceptible to cyclic softening (liquefaction). The conventional SPT, CPT and shear wave velocity based methods of evaluating cyclic softening (liquefaction) potential all consist of case records for which the average penetration resistance or measurement was generally used as the representative value. However, when applied in practice, the resulting correlations are often applied quite literally to every point in the in-situ test profile, including low points. Thus, these methods may be overly conservative in some soil deposits.

9.5.2 Flow liquefaction evaluation

a) Grain characteristic and site specific input parameters

The estimation of various aspects of response using the framework proposed in Chapter 4 can be sensitive to some of the input parameters, particularly the parameters defining the reference USL for a particular soil. Site specific testing allows for better estimates of such input parameters. When shear wave velocity measurements are used to interpret void ratio, the parameters A and B must be carefully selected. If SPT or CPT measurements are interpreted using the shear wave velocity based method, site specific values for the parameters X and Y can result in better estimates of void ratio.

b) Total void ratio versus skeletal void ratio effects on response

As briefly outlined in Chapter 8, when comparing the data review of the Massey site to the results of the data reviews at the other CANLEX sites to date, the Phase III site appeared unusual and suggested that skeletal void ratio may have a dominating effect on penetration resistance or shear wave velocity measurements in sands with high fines contents (FC ≥ 10%). It remains unclear at this point whether skeletal void ratio also dominates the undrained response of undisturbed soil samples when tested in the laboratory. Further studies on the Phase III site samples will allow this factor to be investigated further. If skeletal void ratio is found to be a controlling factor at sites with high fines contents, the proposed framework for investigating flow liquefaction potential could still be applied by combining profiles of skeletal void ratio with an USL based on skeletal void ratios. Additional studies would have to be performed to determine whether or not further modifications would have to be made to components of the integrated CPT method for evaluating cyclic softening (liquefaction) potential at such sites.

c) Using undisturbed samples as a reference

Throughout this thesis undisturbed samples are required as a reference for detailed evaluations of both cyclic softening (liquefaction) and flow liquefaction potential and response. Ground freezing and subsequent coring appear to be capable of providing undisturbed samples at a variety of sites (Hofmann, 1994 and 1995). Once undisturbed samples are obtained, changes in void ratio and stresses (i.e. changes in RSR) must be minimized if samples are to be tested and the results compared directly with predictions of undrained response based on in-situ testing and the methods proposed here. Testing undisturbed samples under anisotropic stress states to mimic the in-situ conditions is an essential factor for observing a relevant undrained response in the laboratory. If samples experience small changes in state (ΔRSR) due to disturbance in sampling, handling, thawing, or consolidation, it may be possible to correct the response using the general response curves shown in Chapter 8.

9.6 Recommendations for Future Work

The work presented here serves to illustrate that liquefaction of sandy soils is a complex process. The methods presented in this thesis provide a step in the right direction, but clearly much more research is necessary to better understand how to characterize sandy soils and evaluate liquefaction potential.

9.6.1 Investigating proposed methods of evaluation at other sites

As the CANLEX project continues to process field and laboratory data from other sites, the methods proposed here for evaluating cyclic softening (liquefaction) and flow liquefaction can be further evaluated. Modifications to the methods can be made as necessary and, as the volume of data grows, more definite conclusions can be made about the possible global nature of the proposed methods and correlations.

a) Cyclic softening

Application of the integrated CPT method to a variety of sites (e.g. all of the CANLEX sites) will confirm or help modify the individual components discussed in Chapter 3. In particular, the relationship between soil behaviour type index, I_c, and fines content can be investigated and the resulting estimates of CRR can be compared with the results of testing undisturbed samples at each site.

An additional useful exercise would be to review the database of case histories forming the CRR-CPT correlation to investigate the choice of representative q_{c1} for each case record, similar to the review of the SPT database carried out in Chapter 2. However, this review should include all aspects of the CPT profile, including friction ratio and pore pressure measurements, where available.

b) Flow liquefaction

The issue of quasi-steady state (QSS) is something that needs to be pursued further in future studies. QSS is currently a topic of debate amongst researchers. The framework proposed in this study incorporates QSS; however, in addition to RSR, QSS depends on soil fabric (Ishihara, 1993) and thus may be difficult to estimate in a global manner. Ultimate state, however, may be linked with RSR in a global manner because it is not dependent on soil fabric since the soil becomes completely remoulded by the time ultimate state is reached. The phenomenon of QSS is observed in the laboratory, particularly in triaxial extension tests (see laboratory stress strain curves for the Massey site in Appendix B). Further studies should investigate if QSS actually occurs in the field and if not, if there are mechanisms such as shear banding and internal void ratio changes within the soil sample while being tested in undrained monotonic loading that create a QSS in the laboratory.

The implications of any such findings will be significant because undrained strengths associated with the QSS can be much lower than those associated with ultimate state. To be conservative, many geotechnical engineers may use the QSS strengths rather than ultimate strengths to analyze stability. This can have large financial implications. If a soil has limited strain-softening behaviour, it will demonstrate a QSS. However, after limited straining associated with the point of QSS, the soil will strain-harden to ultimate state. In analyzing a slope stability problem, the question arises as to whether the material will have gained enough momentum during the point of QSS that it cannot stop itself when it would be expected to strain-harden and become stronger.

Further studies are needed to investigate the triaxial extension direction of loading. First to investigate the phenomenon of QSS, as discussed above, but secondly, to investigate when, where and the extent to which a soil actually becomes loaded in triaxial extension in the field. The much lower undrained strengths for soil tested in triaxial extension in the laboratory (as compared to triaxial compression) only apply if a soil becomes loaded to failure in this direction of loading. As Chapter 4 indicated, K_o (K_o<1.0) conditions in-situ will preload elements of soil in compression. As a result, sufficient unloading is first required before an element will become loaded in extension. Extensional loading is typically associated with the toe of a slope. However, additional studies would be useful to examine the extent of possible in-situ extensional loading in greater detail.

9.6.2 Development of a continuous seismic CPT

Chapters 4 and 8 illustrated that shear wave velocity measurements may provide a good method of estimating void ratio (and hence, RSR) in-situ because shear wave velocity measurements are much less affected by factors such as soil compressibility than either SPT or CPT penetration resistance. However, shear wave velocity measurements are typically averaged over 1 m intervals providing a step function rather than a continuous profile. A useful research project would be to develop the technology to perform continuous shear wave velocity measurements in order to obtain a continuous shear wave velocity profile.

Current technology for measuring shear wave velocity that is commonly used consists of stopping the CPT every 1 m, hitting a seismic beam with a sledge hammer at the ground surface and measuring the time the seismic wave takes to reach the geophone located in the CPT probe at depth. Measurements are recorded electronically and the operator checks that a good signal has been obtained. A method of differences is used to average the shear wave velocity over every 1 m interval of depth. In order to continuously record shear wave velocities, a source at the ground surface would provide seismic waves and the interval difference over which the measurements are averaged would need to be decreased to a few centimetres. The electronics and computer system would have to be modified to record measurements continuously together with the CPT measurements, rather than stopping every time a shear wave velocity measurement is required.

Further studies using bender elements to measure shear wave velocities in soil samples of different states in the laboratory should also be carried out to further investigate the relationship between shear wave velocity and void ratio described in Chapter 4. The method outlined in Chapter 4 (see Equation 4-4) is sensitive to the value of the parameters A and B. Additional studies may be able to confirm or modify the relationship between shear wave velocity and void ratio for various sands in an attempt to improve the accuracy of estimating void ratio from shear wave velocity measurements. This could lead to better interpretations of in-situ shear wave velocity profiles. When combined with the possibility of obtaining continuous shear wave velocity profiles, the resulting method may be able to provide fairly accurate detailed estimates of void ratio.

9.6.3 Further testing of downhole plate load tests in loose sand

Using a simple interpretation method, Chapter 6 served to illustrate the promising potential of rapid downhole plate load tests in loose sand for estimating undrained strengths. The experimental program was clearly preliminary in nature and only limited data are available. Further studies would be useful and would need to place more consideration on how the test results are interpreted. Once a sufficient number of undisturbed samples from the site where the plate load tests were performed are tested, comparisons can be made between the interpretation of the plate load tests and the undrained strength of the soil in the laboratory. Due to factors such as soil squeezing around the plate while the plate is being advanced which may complicate the interpretation of the tests, rapid large diameter cone tests may be a better alternative. However, practical difficulties may arise with respect to the load capacity of the drill rig required to push a large cone, particularly in ground conditions having variable soil states.

9.7 Final Remarks

Liquefaction of sandy soils is a complex process which can be affected by a variety of factors including sand characteristics, site geometry and the nature of the undrained loading. A distinction has been made here between cyclic softening and flow liquefaction. However, as illustrated in Chapter 8, after a "liquefaction" induced soil failure has occurred, it is often difficult to establish which phenomenon controlled the observed deformations. Both in-situ testing and laboratory testing are often part of any site investigation. However, this thesis has proposed a framework by which to link the two types of testing together in a meaningful way to better understand the undrained response of sand to both static and cyclic loading.

The integrated CPT method proposed for evaluating cyclic softening potential is an empirical method, whereas the framework for evaluating flow liquefaction potential and response combines both theoretical and empirical aspects. The concept of RSR to characterize the state of a sand for considerations of flow liquefaction has advantages over the state parameter approach as it is more global in nature, relates better to undrained response and is related to OCR which is traditionally used to evaluate clay, it may allow for all soils to be considered in a similar manner. The recommended procedure to follow at any site is a function of the level of risk associated with a particular project. Thus, a family of solutions exist for evaluating either cyclic softening or flow liquefaction, ranging from simple, conservative, empirical methods to fully comprehensive, site specific field and laboratory investigations.

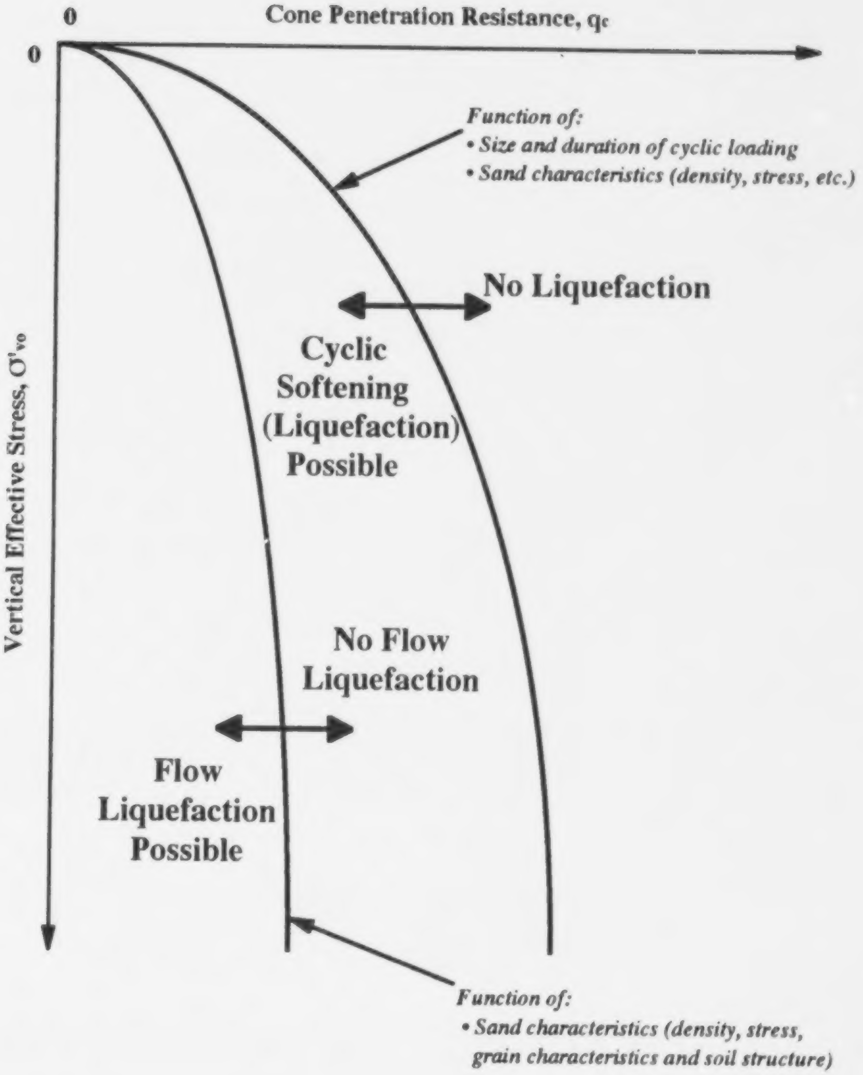

0
Cone Penetration Resistance, q_c
0
Vertical Effective Stress, σ'_{vo}
Function of:
• Size and duration of cyclic loading
• Sand characteristics (density, stress, etc.)
No Liquefaction
Cyclic Softening (Liquefaction) Possible
No Flow Liquefaction
Flow Liquefaction Possible
Function of:
• Sand characteristics (density, stress, grain characteristics and soil structure)

Figure 9-1 Schematic illustrating the concept of dividing lines in terms of CPT penetration resistance, q_c, for both flow liquefaction potential and cyclic softening (liquefaction) potential.

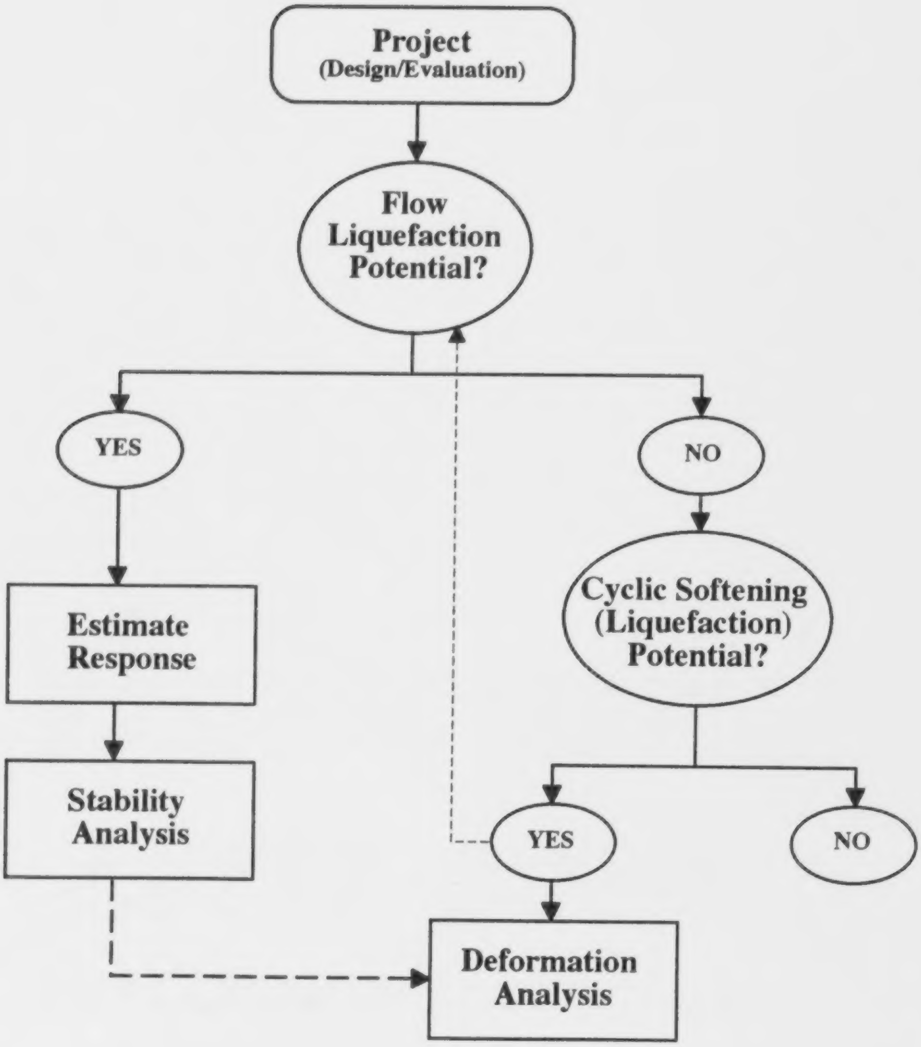
Project
(Design/Evaluation)
Flow Liquefaction Potential?
YES
NO
Estimate Response
Stability Analysis
Cyclic Softening (Liquefaction) Potential?
YES
NO
Deformation Analysis

Figure 9-2 General flowchart for evaluating liquefaction potential at a site.

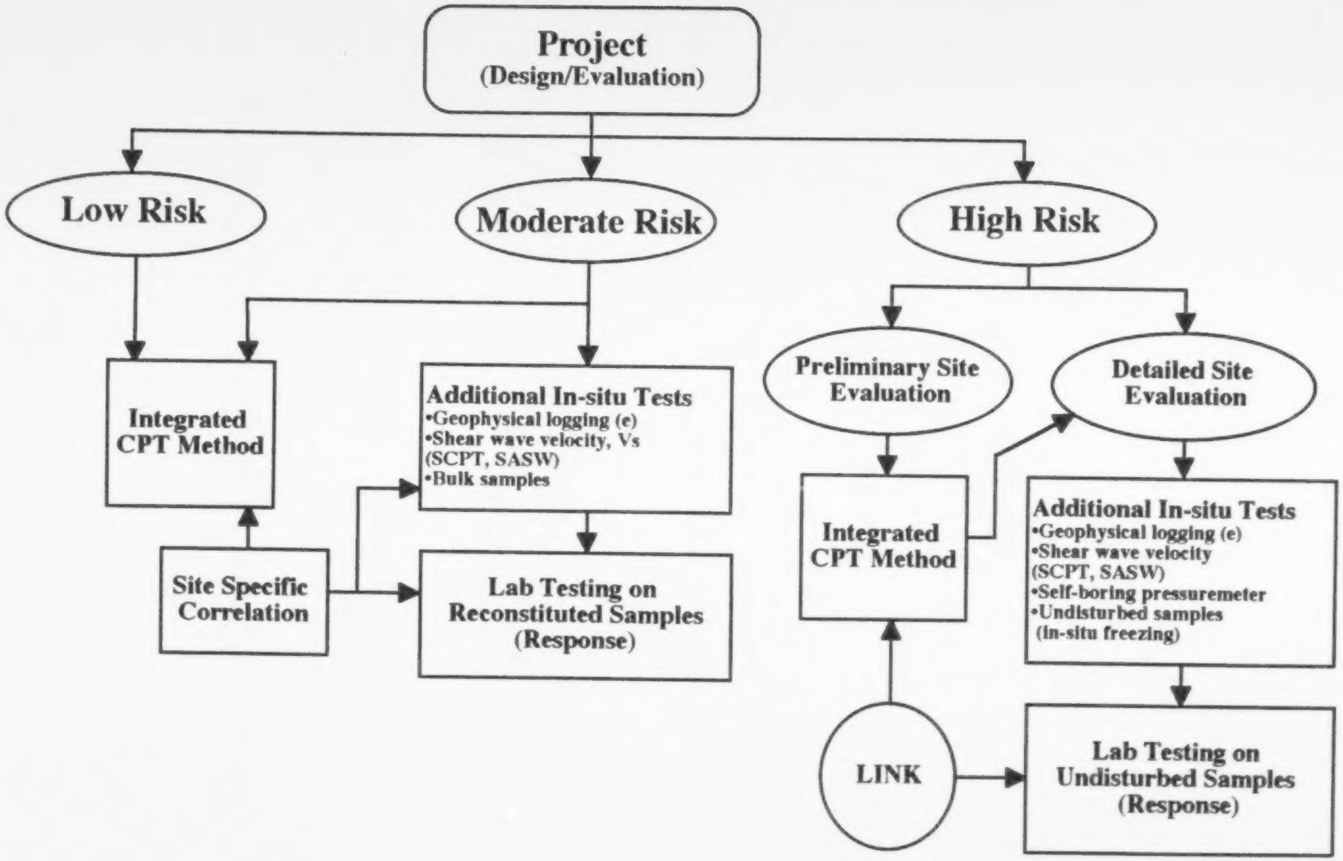
Project
(Design/Evaluation)
Low Risk
Moderate Risk
High Risk
Integrated CPT Method
Site Specific Correlation
Additional In-situ Tests
•Geophysical logging (e)
•Shear wave velocity, Vs (SCPT, SASW)
•Bulk samples
Lab Testing on Reconstituted Samples (Response)
Preliminary Site Evaluation
Detailed Site Evaluation
Integrated CPT Method
Additional In-situ Tests
•Geophysical logging (e)
•Shear wave velocity (SCPT, SASW)
•Self-boring pressuremeter
•Undisturbed samples (in-situ freezing)
LINK
Lab Testing on Undisturbed Samples (Response)

Figure 9-3 Recommended family of solutions for evaluating cyclic softening (liquefaction) potential based on the risk level (i.e. consequences of failure) associated with a particular project.

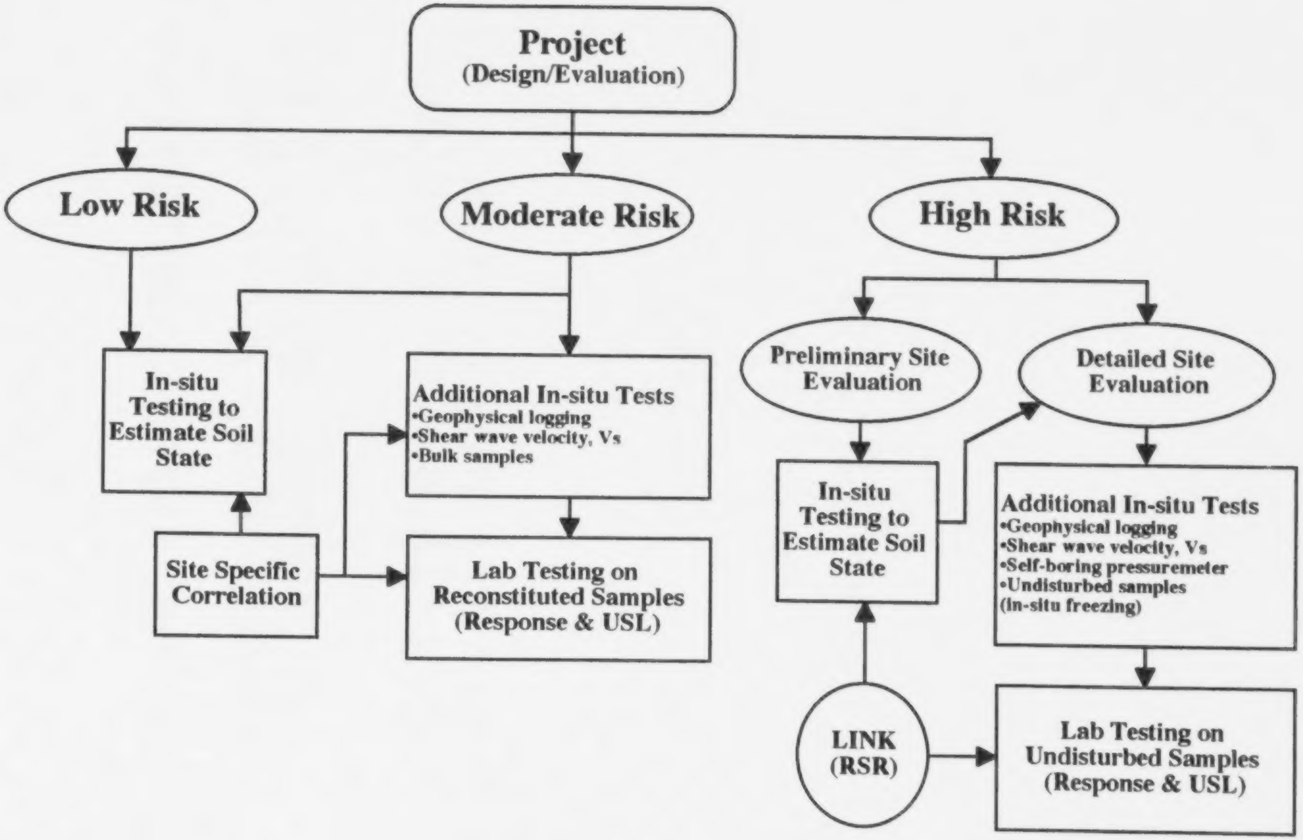
Project
(Design/Evaluation)
Low Risk
Moderate Risk
High Risk
In-situ Testing to Estimate Soil State
Site Specific Correlation
Additional In-situ Tests
•Geophysical logging
•Shear wave velocity, Vs
•Bulk samples
Lab Testing on Reconstituted Samples (Response & USL)
Preliminary Site Evaluation
Detailed Site Evaluation
In-situ Testing to Estimate Soil State
Additional In-situ Tests
•Geophysical logging
•Shear wave velocity, Vs
•Self-boring pressuremeter
•Undisturbed samples
(In-situ freezing)
LINK (RSR)
Lab Testing on Undisturbed Samples (Response & USL)

Figure 9-4 Recommended family of solutions for evaluating flow liquefaction potential based on the risk level (i.e. consequences of failure) associated with a particular project.

References

Been, K., and Jefferies, M.G. 1992. Towards systematic CPT interpretation. *Proceedings of the Wroth Symposium*, 44-55.

Byrne, P.M., Imrie, A.L., and Morgenstern, N.R. 1994. Results and implications of seismic performance studies for Duncan Dam. *Canadian Geotechnical Journal*, 31: 979-988.

Hofmann, B.A., Sego, D.C., and Robertson, P.K. 1994. Undisturbed sampling of a deep loose sand deposit using ground freezing. *Proceedings of the 47th Canadian Geotechnical Conference*, Halifax, Nova Scotia, 287-296.

Hofmann, B.A., and Sego, D.C. 1995. In-situ ground freezing for undisturbed samples of loose sand - Phase II. *Proceedings of the 48th Canadian Geotechnical Conference*, Vancouver, B.C., 197-212.

Ishihara, K. 1993. Liquefaction and flow failure during earthquakes. The 33rd Rankine Lecture, *Géotechnique*, 43(3): 351-415.

NCEER Workshop 1996. Proceedings to be published at a subsequent date by Youd et al. (1996).

Plewes, H.D., Davies, M.P, and Jefferies, M.G. 1992. CPT based screening procedure for evaluating liquefaction susceptibility. *Proceedings of the 45th Canadian Geotechnical Conference*, Toronto, Ontario, 4:1-4:9.

Robertson, P.K. 1990. Soil classification using the CPT. *Canadian Geotechnical Journal*, 27(1): 151-158.

Robertson, P.K. 1994. Suggested terminology for liquefaction. *Proceedings of the 47th Canadian Geotechnical Conference*, Halifax, Nova Scotia, 277-286.

Robertson, P.K. and Fear, C.E. 1995. Liquefaction of sands and its evaluation. *IS Tokyo '95, First International Conference on Earthquake Geotechnical Engineering*, Keynote Lecture.

Robertson, P.K., Campanella, R.G., and Wightman, A. 1983. SPT-CPT correlations. *Journal of Geotechnical Division of ASCE*, 109: 1449-1459.

Robertson, P.K., Fear, C.E., Woeller, D.J., and Weemees, I. 1995. Estimation of sand compressibility from seismic CPT. *Proceedings of the 48th Canadian Geotechnical Conference*, Vancouver, 1, 441-448.

Robertson, P.K. and Campanella, R.G. 1985. Liquefaction potential of sands using the cone penetration test. *Journal of Geotechnical Division of ASCE*, 22(3): 298-307.

Seed, H.B. 1987. Design problems in soil liquefaction. *Journal of Geotechnical Engineering*, ASCE 113(8): 827-845.

Seed, H. B., Tokimatsu, K., Harder, L. F., and Chung, R. 1985. Influence of SPT procedures in soil liquefaction resistance evaluations. *J. Geotech. Engrg.*, ASCE 111(12): 1425-1445.

Seed, R.B., and Harder, L.F. 1990. SPT-based analysis of cyclic pore pressure generation and undrained residual strength. *Proceedings of the H. Bolton Seed Memorial Symposium*, 2: 351-376.

Skempton, A. W. 1986. Standard penetration test procedures and the effects in sands of overburden pressure, relative density, particle size, ageing and overconsolidation. *Geotechnique*, 36(3): 425-447.

Sladen, J.A., and Hewitt, K.J. 1989. Influence of placement method on the in situ density of hydraulic sand fills. *Canadian Geotechnical Journal*, 26: 453-466.

Tokimatsu, K., and Hosaka, Y. 1986. Effects of sample disturbance on dynamic properties of sand. *Soils and Foundations*, 26(1): 53-64.

Vaid, Y.P., Sivathayalan, S., Uthayakumar, M., and Eliadorani, A. 1995. Liquefaction potential of reconstituted Syncrude sand. *Proceedings of the 48th Canadian Geotechnical Conference*, Vancouver, B.C., 1: 319-330.

Youd, T. L. 1993. Liquefaction-induced lateral spread displacement. *Technical Note N-1862*, Naval Civil Engineering Laboratory, Port Hueneme, California.